Evolution des sols à l'échelle du paysage sous des conditions de changements climatique et de structure du paysage.

Marine Lacoste

▶ **To cite this version:**

Marine Lacoste. Evolution des sols à l'échelle du paysage sous des conditions de changements climatique et de structure du paysage.. Sciences du Vivant [q-bio]. AGROCAMPUS OUEST, 2012. Français. NNT : . tel-02809195

HAL Id: tel-02809195
https://hal.inrae.fr/tel-02809195

Submitted on 6 Jun 2020

HAL is a multi-disciplinary open access archive for the deposit and dissemination of scientific research documents, whether they are published or not. The documents may come from teaching and research institutions in France or abroad, or from public or private research centers.

L'archive ouverte pluridisciplinaire **HAL**, est destinée au dépôt et à la diffusion de documents scientifiques de niveau recherche, publiés ou non, émanant des établissements d'enseignement et de recherche français ou étrangers, des laboratoires publics ou privés.

N° ordre : 2012-25
N° Série : D-68

THESE / AGROCAMPUS OUEST

Sous le label de l'Université Européenne de Bretagne

pour obtenir le diplôme de :

DOCTEUR DE L'INSTITUT SUPERIEUR DES SCIENCES AGRONOMIQUES, AGRO-ALIMENTAIRES, HORTICOLES ET DU PAYSAGE

Spécialité : « Sciences de l'Environnement »

Ecole Doctorale : « Vie Agro Santé»

présentée par :

Marine Lacoste

EVOLUTION DES SOLS A L'ECHELLE DU PAYSAGE SOUS DES CONDITIONS DE CHANGEMENTS CLIMATIQUE ET DE STRUCTURE DU PAYSAGE

soutenue le 30 NOVEMBRE 2012 devant la commission d'Examen

Composition du jury :

Rapporteur : Dan Pennock, Professeur, University of Saskatchewan Canada

Rapporteur : Christian Valentin, Directeur de recherche, IRD Bondy

Examinateur : Dominique Arrouays, Ingénieur de recherche, INRA Orléans

Examinateur : Sylvain Charpentier, Professeur, Agrocampus Ouest Angers

Examinateur: Véronique Souchère, Ingénieure de recherche, INRA Grignon

Co-encadrant : Didier Michot, Maître de conférences, Agrocampus Ouest Rennes

Co-encadrant: Valérie Viaud, Chargée de recherche, INRA Rennes

Directeur de thèse : Christian Walter, Professeur, Agrocampus Ouest Rennes

Laboratoire d'accueil :
UMR INRA – Agrocampus Ouest, Sol Agro et hydrosystème Spatialisation (Rennes)

AVANT-PROPOS

Ce mémoire est le résultat d'un travail de trois années (octobre 2009 – novembre 2012), réalisé au sein de l'Unité Mixte de Recherche INRA-Agrocampus Ouest, Sol Agro et hydrosystème Spatialisation de Rennes (UMR SAS). Ce travail a été encadré par Christian Walter, Valérie Viaud et Didier Michot de l'UMR SAS.

Cette thèse a été financée par le projet ANR LandSoil (Structure du paysage et conservation des sols sous des conditions évolutives d'occupation du sol et de climat, ANR-08-VULN-006-01), inscrit dans l'appel d'offre *Vulnérabilité : Environnement, Climat, Sociétés* (*VMCS*) de l'Agence Nationale de la Recherche.

Elle a été suivie par un comité de pilotage composé de Jacques Baudry (SAD-Paysage, Rennes), Françoise Burel (UMR ECOBIO, Rennes), Patrick Durand (UMR SAS, Rennes), Yves Le Bissonnais (UMR LISAH, Montpellier) et Sébastien Salvador Blanes (Université de Tours).

REMERCIEMENTS

Aujourd'hui, une thèse est loin d'être un travail solitaire. J'aimerais donc remercier ici tous ceux qui ont accompagné, de près ou de loin, ces trois années de doctorat.

Je tiens tout d'abord à remercier mes trois encadrants, Christian Walter, Valérie Viaud et Didier Michot pour m'avoir fait confiance pour mener ce travail à bien, pour m'avoir fait partager leur expérience de chercheur et d'enseignant, pour leur soutien, leur grande disponibilité et leurs indéniables qualités humaines.

Je remercie les membres de mon jury de thèse, Dan Pennock (University of Saskatchewan, Canada), Christian Valentin (IRD, Bondy), Dominique Arrouays (US Infosol, Orléans), Sylvain Charpentier (Agrocampus Ouest, Angers) et Véronique Souchère (INRA, Grignon), d'avoir accepté d'évaluer ce travail de thèse et pour l'intéressante discussion que nous avons eu lors de la soutenance. Merci également aux membres du comité de pilotage, Jacques Baudry (SAD Paysage, Rennes), Françoise Burel (UMR ECOBIO, Rennes), Patrick Durand (UMR SAS, Rennes), Yves Le Bissonnais (UMR LISAH, Montpellier) et Sébastien Salvador Blanes (Université de Tours), pour l'intérêt qu'ils ont porté à ce travail.

Merci à tous les membres du projet ANR LandSoil pour les discussions fructueuses que nous avons eu, notamment lors des séminaires LandSoil. Le programme ANR LandSoil a été un cadre de travail privilégié, permettant de partager nos moyens et nos expériences, ce qui a clairement constitué un avantage pour le bon déroulement de mon travail de thèse.

Merci à tous ceux qui ont participé au travail de terrain sur lequel cette thèse s'est appuyée, et sans qui rien n'aurait pu être mené à bien. Je remercie particulièrement Gilles Dutin (UMR SAS), pour m'avoir accompagné pendant de longues journées sur la Zone Atelier Armorique. Merci Gilles pour tout le travail accompli pendant les froides journées d'hivers et pour les bons moments passés ensembles.

Merci à tous ceux qui, par leur collaboration, ont contribué à faire avancer ce travail : Budiman Minasny, Alex McBratney et Brendan Malone (University of Sydney) pour leur accueil au sein de leur équipe à l'Université de Sydney et leur contribution à la cartographie digitale des sols de ma zone d'étude ; Olivier Evrard et Irène Lefèvre (LSCE, Gif-sur-Yvette) pour la réalisation des mesures de ^{137}Cs et leur interprétation ; Chantal Gascuel (UMR SAS, Rennes) pour son aide dans la calibration du modèle LandSoil ; François Pustoc'h (UMR CReAAH, Rennes) et Armelle Racapé (UMR SAS, Rennes) pour leur aide lors des mesures de granulométrie laser et la préparation des échantillons de sol ; Jean Nabucet (LTEG-Rennes Costel), Christophe Codet (SAD Paysage, Rennes) et Nicolas Schermann (SAD Paysage, Rennes) pour nous avoir fourni les données parcellaires de ma zone d'étude ; Odile Quidu (UMR SAS, Rennes) pour la digitalisation du cadastre Napoléonien ; Vincent Hallaire et Yannick Hamon (UMR SAS, Rennes) pour les mesures de conductivité hydraulique ; sans oublier les agriculteurs de la Zone Atelier Armorique qui nous ont accueilli sur leurs parcelles.

Merci à tous les membres de l'UMR SAS pour leur accueil, leur gentillesse et leur bonne humeur. Ça a été un grand plaisir de travailler parmi vous. Merci à mes collègues de bureau, Cyril Benhamou et Rémi Dupas pour leur présence au quotidien, ainsi qu'à Blandine Lemercier, Lionel Berthier, Alice Aubert, Hongtao Hao, Emmanuel Tete, Emmanuelle Guarrigues, Coralie Haese, Virginie Parnaudeau, Aurélie Wilfart… Il faudrait tous vous citer pour être juste ! J'aimerais particulièrement remercier Monique Delabuis pour son aide lors de mes recherches bibliographiques ; Cédric Durand pour son efficacité dans la résolution des problèmes informatiques ; Séverine Renaud, Karine Derrien, Tiphaine Labbé et Maryvonne Pertué pour le traitement efficace (et avec le sourire) des questions administratives et budgétaires.

Merci à ceux qui ont relu avec attention les différentes parties de ce manuscrit, et notamment Elena Robish pour les parties en anglais.

Merci enfin à mes proches et mes amis pour m'avoir soutenu et supporté pendant ces trois années de thèse, et toutes celles qui ont précédées.

RESUME

Les sols constituent une ressource essentielle, rendant de nombreux services écosystémiques, mais sont soumis à de nombreuses dégradations (érosion, diminutions des teneurs en carbone organique…). En vue d'une meilleure gestion, des outils prédictifs intégrant différentes propriétés du sol sont nécessaires pour évaluer l'impact des activités humaines et des changements globaux sur les sols.

L'objectif de la thèse est de développer une démarche de modélisation de l'évolution des sols au sein d'un paysage agricole complexe et sur une durée de quelques décennies, en tenant compte d'évolutions d'occupation des sols et de climat. Deux processus ont été considérés : la redistribution des sols (érosion-dépôt) et la dynamique du carbone organique (C).

La zone d'étude considérée est un paysage agricole bocager de 1 000 ha situé au sein de la Zone Atelier Armorique. L'évolution des sols a été modélisée en couplant deux modèles dynamiques spatialement distribués : (i) le modèle LandSoil simule la redistribution des sols par érosion hydrique et aratoire, (ii) le modèle C simule la dynamique du carbone dans la totalité des horizons organo-minéraux, en tenant compte des variations d'épaisseur de sol. Le modèle LandSoil a été calibré pour être utilisé dans le contexte des sols limoneux bretons, à partir de mesures expérimentales disponibles à l'échelle de la parcelle. L'aptitude de LandSoil à modéliser la redistribution des sols aux abords des haies a été évaluée en comparant les résultats de LandSoil à des estimations par le ^{137}Cs. Pour initialiser les entrées sols des deux modèles, des cartographies 3D à haute résolution spatiale (2 m) ont été réalisée par méthodes d'apprentissage. Des simulations de l'évolution des sols ont été réalisées sur la période 2010 – 2100, pour des scénarios croisant des modalités de structure du paysage (occupation du sol et présence de haies) et de climat (climat stationnaire ou changement climatique).

La comparaison des scénarios montre que le facteur majeur d'évolution des sols à l'échelle du paysage est l'occupation des sols, suivi du changement climatique puis de la présence de haies. La redistribution des sols conduit à une perte nette de C à l'échelle du paysage, surtout due à la perte nette de sol hors du système. Tous les paysages modélisés montrent une sensibilité au changement climatique, mais avec des amplitudes variables, les paysages les plus homogènes (absence de haies) et cultivées intensivement étant les plus sensibles.

La méthode de modélisation mise en place permet de simuler dynamiquement l'évolution couplée de la redistribution des sols et de la dynamique du C à l'échelle du paysage, à haute résolution 3D et sur des temps longs. Son amélioration reposera notamment sur le couplage d'autres processus d'évolution des sols et sur son intégration dans des modèles plus globaux.

Mots clefs : évolution des sols, érosion, carbone organique, modélisation spatiale, haute résolution, paysage, changement climatique.

ABSTRACT

Soils are a natural resource, providing many ecosystem services, but submitted to numerous degradations (erosion, decrease in carbon content…). To achieve a better soil management, predictive tools with an integrative consideration of soil properties are required to evaluate the impact of human activities and global changes on soils.

The objective of this work is to develop a modeling approach of soils evolution within a heterogeneous agricultural landscape, for some decades, and by taking into account land use and climate evolutions. Two processes were considered: soil redistribution (erosion-deposit) and organic carbon (C) dynamic.

The study area is an agricultural hedgerow landscape (1 000 ha) located within the Zone Atelier Armorique. Soils evolution has been modeled by coupling two dynamic and spatially distributed models: (i) the LandSoil model simulates soils redistributions due to water and tillage erosion, (ii) the C model simulates the organic carbon dynamic within the whole organic soil horizons, by taking into account soil thickness variations. The LandSoil model has been calibrated to be used in the context of loamy soils of the French Brittany, based on available field measurements at the field scale. LandSoil ability to model soil redistribution at the hedge vicinity has been evaluated by comparing LandSoil results to soil redistribution estimates from ^{137}Cs. To initialize the two soil evolution models, 3D maps with high spatial resolution (2m) have been produced using machine learning methods. Simulations of soils evolution has been done for the 2010 to 2100 time period, for scenarios based on cross-parameters of landscape structure (considering land use and hedges) and climate (business as usual or climate change).

The scenarios comparison shows that the prevailing factor of soils evolution at the landscape scale is land use, then climate change and finally hedges presence. Soils redistribution leads to a net C loss at the landscape scale, mainly due to a net soil exportation out of the considered area. All the modeled landscapes are sensitive to climate change, but in variable range. The most sensitive landscapes are the most homogeneous ones (no hedges) with intensive cropping.

The developed modeling approach allows simulating in a dynamic way the simultaneous evolution of soil redistribution and C dynamic at the landscape scale, with a high 3D resolution and for long time period. Its improvement could consist in considering other important processes of soil evolution and in its integration to more global modeling.

Keywords: soils evolution, erosion, organic carbon, spatially distributed modeling, landscape, climate change

TABLE DES MATIERES

Introduction générale

Le sol est un système dynamique et complexe, situé à l'interface entre la biosphère, l'atmosphère, l'hydrosphère et la lithosphère. Les sols constituent le support de l'activité humaine et rendent de nombreux services écosystémiques[1]. Ces services ont été classés en quatre groupes par le Millenium Ecosystem Assessment (2005) : services de soutien, qui maintiennent des conditions favorables à la vie sur Terre et sont nécessaires à tout autre service (formation des sols, cycles biogéochimiques, support de la photosynthèse), services d'approvisionnement (support physique de la production agricole et forestière, support du paysage, production de nourriture, d'eau douce, source de matériaux et de biodiversité), services de régulation (régulation du climat, régulation de la qualité de l'air et de l'eau, régulation de l'érosion et des risques naturels, régulation des pathogènes) et services culturels (valeurs religieuses, spirituelles et esthétiques, mémoire du passé et protection de patrimoine archéologique, récréation, tourisme). Les sols sont donc nécessaires au bien-être de l'homme et au bon fonctionnement des écosystèmes[2]. De ce fait, ils sont au cœur de grands enjeux planétaires (sécurité alimentaire, changement climatique, disponibilité en eau potable, préservation de la biodiversité) et leur préservation est essentielle.

La formation des sols résultent d'un ensemble de processus généralement lents, si bien qu'on les considère comme une ressource non renouvelable à l'échelle humaine. Cependant, les sols sont soumis à de nombreuses pressions anthropiques pouvant modifier leur état, leurs fonctions, leurs échanges avec les autres milieux, et donc dégrader leurs services écosystémiques. Parmi les principales formes de dégradation des sols, on répertorie l'érosion, la diminution des teneurs en matières organiques, la salinisation, le tassement, la diminution de la biodiversité, les glissements de terrain et l'inondation (Commission Européenne, 2002). Ces menaces sont intimement liées aux changements globaux[3] consécutifs au développement des populations humaines.

Les dynamiques d'évolution des sols

Les sols et les paysages agricoles évoluent conjointement et en interaction, sous l'effet de facteurs anthropiques et climatiques.

Depuis les années 1950, des changements rapides du contexte agricole (innovations technologiques, modification des modes de consommation et des préoccupations environnementales, mondialisation de l'économie) ont provoqué le développement de nouveaux systèmes agricoles qui ont influé sur l'organisation des paysages, tant au niveau de l'utilisation des terres que de la structure du paysage (Antrop, 2005). Ces changements sont provoqués par des décisions prises à divers niveaux, allant de l'agriculteur aux structures décisionnelles nationales et internationales.

A ces évolutions structurelles se surimposent les effets du changement climatique, maintenant reconnu comme l'un des facteurs majeurs de l'évolution future des paysages agricoles (Alcamo et al., 2007). Les changements de distribution spatiale et temporelle des paramètres climatiques (notamment la pluviométrie et la température) devraient avoir de larges conséquences sur la productivité des écosystèmes cultivés et devraient contraindre les agriculteurs à définir de nouvelles stratégies de gestion des paysages agricoles (FAO, 2012).

[1] Il s'agit des bienfaits que les hommes obtiennent des écosystèmes (Millenium Ecosystem Assessment, 2005).
[2] Système où des organismes vivants interagissent avec leur environnement physique (Millenium Ecosystem Assessment, 2005).
[3] Changements dans les processus chimiques, physiques et biologiques se produisant à l'échelle planétaire (IGPB).

Des stratégies d'adaptation ont été proposées dans le but de conserver les sols dans un contexte de changement global. Ces stratégies s'appuient sur une gestion adaptée des paysages pour accroître leur résilience vis-à-vis du changement climatique (FAO, 2012) et visent notamment à préserver les sols de l'érosion et des pertes en carbone (C), par exemple en favorisant le boisement (GIEC, 2007).

Le bocage[4] est de fait une organisation courante des systèmes agricoles de par le monde (Baudry et al., 2000), même si ce type de paysage a également été affecté par les changements globaux. Si les raisons de leur mise en place, leur développement et leurs modes de gestions diffèrent, ces paysages sont néanmoins reconnus comme étant favorables à la préservation des sols. Différentes études ont notamment montré que ces paysages contribuaient au stockage de C dans les sols (Follain et al., 2007 ; Walter et al., 2003a) et permettaient de limiter l'érosion hydrique et aratoire des sols tout en favorisant leur stockage au sein du paysage plutôt que leur exportation vers les systèmes aquatiques (Carnet et al., 1979 ; Govers et al., 1994 ; Salvador-Blanes et al., 2006 ; Van Oost et al., 2000). Les études existantes ont néanmoins menées sur des secteurs restreints et une approche intégrant une plus grande diversité de situations apparaît nécessaire pour identifier les interactions entre sol et paysage et évaluer le potentiel de l'ingénierie du paysage dans une optique de protection des sols et dans un contexte de changement climatique.

Selon King (2006), « If knowledge about soil resources is poor on a global scale, knowledge on soil evolution is even more reduced ». Or, pour mieux prendre en compte l'effet des activités humaines et du changement climatique sur les sols, il est nécessaire de mieux comprendre les mécanismes de leur évolution. Les sols évoluent à des échelles spatiales allant de la molécule à la région voire au continent, et à des échelles temporelles allant de processus instantané au millénaire. Les modélisations de l'évolution des sols ont jusqu'ici été majoritairement conduites sur des étendues spatiales restreintes (inférieures ou égales au solum), ou au contraire sur de vastes zones (région, pays, continent) (Hoosbeek et al., 2000). Il est en effet plus délicat de prendre en compte la variabilité des sols à des échelles spatiales intermédiaires comme celle du paysage, car elles induisent une grande diversité de combinaisons de facteurs d'évolution des sols, ce qui conduit à une forte hétérogénéité des sols à de courtes distances. L'intérêt de l'échelle du paysage est justement d'intégrer ces hétérogénéités spatiales, alors que l'échelle régionale tend à les gommer. Concernant les évolutions temporelles des sols, les travaux existants ont surtout considéré des durées courtes, du jour à l'année, dans une perspective de gestion ou d'adaptation des techniques, ou à l'inverse des temps longs (du siècle au millénaire) pour modéliser les processus de pédogenèse (Finke and Hutson, 2008 ; Legros, 1982 ; Minasny and McBratney, 2006b). Peu d'études ont été réalisées en combinant des échelles de temps et d'espace intermédiaires, ce qui serait surtout dû au fait que les connaissances sur l'évolution des sols et les données nécessaires à la modélisation de leurs évolutions sont moins disponibles à ces échelles (Kirk, 2006). Finke et Hudson (2008) ont par exemple modélisé la formation des sols à l'échelle du profil pendant l'Holocène, ce qui représente une

[4] Paysage caractérisé par la présence de réseaux de structures linéaires de végétaux ligneux, que ce soient des haies dites traditionnelles, des rideaux brise-vent récents ou des haies spontanées issue de l'absence d'entretien des clôtures Baudry, J. and Jouin, A. (Editors), 2003. De la haie aux bocages. Organisation, dynamique et gestion. INRA, Paris, 431 p. pp. Les haies, quant à elles, sont des éléments linéaires composés de végétaux ligneux, arbres et/ou arbustes. Baudry, J. and Perichon, S., 2007. Les haies et les bocages dans le monde : éléments de comparaison. In: A. Antoine and D. Marguerie (Editors), Bocages et sociétés. Espace et territoires. Presses Universitaires de rennes, Rennes, pp. p. 23-32.

période de 15 000 ans. Montagne et Cornu (2008) ont modélisé l'impact du drainage sur les sols, également à l'échelle du profil, pour des échelles temporelles de l'ordre de la décennie. A l'échelle du paysage, Follain et al. (2006b) ont simulé l'évolution de l'épaisseur du sol sur une période de 1 200 ans et Minasny et al. (2006b) le développement du sol sur 30 000 ans, mais sous des hypothèses très simplificatrices d'occupation des sols, qui rendent les résultats des simulations numériques peu réalistes.

En considérant les changements rapides actuels des facteurs d'évolution des sols (activités humaines sur les sols, changement climatique, etc.), il paraît nécessaire de combiner les différentes échelles temporelles et spatiales de variation des sols et de prendre en compte les échelles intermédiaires qui apparaissent liées aux effets de l'influence humaine : échelle spatiale correspondant au paysage, échelle temporelle allant de la décennie au siècle (Kirk, 2006 ; McKenzie, 2006). Ceci devrait permettre d'intégrer l'accélération supposée des dynamiques d'évolution des sols (Petersen, 2006).

Objectifs de la thèse

L'objectif général de la thèse est de développer une démarche de modélisation représentant l'évolution des sols au sein d'un paysage agricole complexe et sur une durée de quelques décennies, en tenant compte d'évolutions potentielles de l'occupation des sols et du climat.
Cet objectif se décline en trois questions :

1. Comment développer une approche de modélisation dynamique et spatialement distribuée, qui soit sensible aux modifications d'occupation de sol et de climat ?
2. Comment évaluer les impacts futurs de l'occupation du sol et du changement climatique sur l'évolution des sols, en prenant en compte leurs hétérogénéités spatiales et temporelles ?
3. Quelle est la hiérarchie de ces facteurs d'évolution vis à vis de leurs impacts sur les sols ?

Dans ce travail, les évolutions des sols seront étudiées et modélisées à travers deux propriétés : la redistribution des sols en lien avec les processus d'érosion et la dynamique des stocks de C organique. L'approche choisie est une modélisation intégrée, spatialement distribuée à l'échelle du paysage et dynamique, à des pas de temps allant de la décennie au siècle.
Cette approche soulève deux questions méthodologiques :

- Comment définir de manière fine et en trois dimensions l'état initial des sols ?
  A l'échelle du paysage, il est en effet nécessaire de prendre en compte les variations à courtes distances des propriétés des sols (horizontales mais aussi verticales), en relation étroite avec les éléments du paysage.
- Comment modéliser de manière intégrée l'évolution des sols à l'échelle du paysage ? Ceci implique de lier les dynamiques des propriétés des sols à celles de leurs facteurs d'évolution (occupation du sol, structure du paysage, climat, etc.) et ce à différentes échelles spatiales et temporelles.

Enjeux

Sur le plan scientifique, cette thèse s'inscrit dans une démarche de questionnement général sur l'évolution des sols et sur les interactions existant entre le sol, le paysage et le climat. Un des enjeux majeurs dans un contexte de changement climatique est de caractériser la distribution des stocks de C au sein des paysages, en intégrant les stocks profonds, et de déterminer la capacité d'un sol à séquestrer du C.

D'un point de vue méthodologique, cette thèse se situe dans la lignée des travaux menés en cartographie numérique des sols, cherchant à cartographier les sols et à représenter leur variabilité dans l'espace (McBratney et al., 2003). Mais, il s'agit également d'utiliser ces cartographies comme données d'entrées à des modélisations à haute résolution spatiale, dynamiques et spatialement distribuées, intégrant les interactions entre les différentes propriétés du sol, du paysage et du climat ainsi que leurs hétérogénéités spatiales et temporelles.

A terme, l'enjeu est de constituer des outils d'aide à la décision permettant d'évaluer des scénarios d'évolution conjointe des paysages, des occupations du sol et des pratiques agricoles, et donc d'accompagner l'élaboration de stratégies de gestion des paysages pour la préservation des ressources naturelles et des écosystèmes, dans un contexte de changement climatique et d'évolution rapide des activités agricoles.

Structure du mémoire

Ce mémoire s'organise en 6 chapitres :

- le **chapitre 1** est une étude bibliographique portant sur la pertinence de l'échelle du paysage pour l'étude de l'évolution des sols ; les échelles temporelles à considérer pour représenter les dynamiques de différentes propriétés du sol et de leurs facteurs d'évolution ; l'intérêt des méthodes de modélisation pour l'étude de l'évolution des sols à l'échelle du paysage ;
- le **chapitre 2** présente le matériel et les méthodes utilisés pour modéliser l'évolution des sols à l'échelle du paysage, à savoir la zone d'étude considérée, les modèles mis en œuvre et la méthode utilisée pour acquérir les données pédologiques nécessaires à l'initialisation des modèles ;
- le **chapitre 3** expose les méthodes utilisées pour calibrer le modèle de redistribution des sols pour son utilisation dans le contexte de la zone d'étude ; un article porte sur le test du modèle quant à sa capacité à simuler la redistribution des sols aux abords des haies ;
- le **chapitre 4** est consacré à la modélisation de l'organisation spatiale actuelle des sols (stock de C, épaisseur des sols), à haute résolution et en trois dimensions, pour l'initialisation des modèles d'évolution des sols ;
- le **chapitre 5** est dédié la modélisation dynamique spatiale de l'évolution des sols à l'échelle du paysage, sous différents scénarios de paysage et d'évolution du climat ;
- une conclusion générale et des perspectives sont présentées dans le dernier chapitre.

Les chapitres 3, 4 et 5 incluent des articles scientifiques soumis ou en préparation pour des revues internationales à comité de lecture et sont rédigés en anglais. Les références bibliographiques sont regroupées en un seul ensemble en fin de document.

Chapitre 1.
Modélisation de l'évolution des sols à l'échelle du paysage : état de l'art

1.1 Introduction

Depuis les travaux de Dokuchaev (Gennadiyev and Olson, 1998) et de Jenny (1941), il est reconnu que la formation et l'évolution d'un sol sont liées à son environnement et sont contrôlées par les interactions entre des facteurs biotiques (faune, flore, activités humaines) et des facteurs abiotiques (matériau parental, relief, climat).

Etudier l'évolution des sols nécessite de prendre en compte non seulement la variabilité spatiale des sols, mais aussi leur variabilité temporelle. La variabilité des sols dans l'espace, dans les dimensions verticales et horizontales, découle de l'hétérogénéité des facteurs de formation des sols et de leurs interactions spatiales et temporelles. Cette diversité est présente à toutes les échelles spatiales, depuis le profil pédologique jusqu'au continent, en passant par la parcelle, le versant ou encore le bassin-versant. L'estimation et la représentation cartographique de la variabilité spatiale des sols ont fait l'objet de nombreuses études, et constituent un domaine de recherche actif qui a été favorisé par le développement d'outils statistiques, des systèmes d'informations géographiques (SIG) et de méthodes d'acquisition de données comme par exemple la télédétection (McBratney et al., 2003). La cartographie et les outils de spatialisation permettent de caractériser la diversité des sols et de leurs propriétés et fournissent des informations sur la localisation des sols et sur leurs propriétés à un instant donné. La variabilité des sols dans le temps, i.e. leur évolution, résulte de la dynamique des processus de formation et de dégradation se déroulant à différents échelles temporelles et de leurs interactions. L'ambition de ce travail est d'aborder conjointement la variabilité spatiale et temporelle des sols.

Ce chapitre bibliographique a pour objectif de faire la synthèse des connaissances sur la modélisation de l'évolution des sols à l'échelle du paysage. Il s'organise en trois parties :

- nous montrerons en quoi le paysage est une échelle spatiale pertinente pour étudier l'évolution des sols,
- nous discuterons des échelles temporelles à considérer,
- nous montrerons que la modélisation dynamique et spatialisée est un outil adapté pour aborder l'évolution des sols, et ferons la synthèse des approches de modélisation existantes, en nous focalisant sur la redistribution des sols (érosion et accumulation) et sur la dynamique du carbone (C) organique des sols.

1.2 Pertinence de l'échelle du paysage pour l'étude de l'évolution des sols

1.2.1 Définition du paysage et de ses composantes

Le concept de paysage est utilisé dans de nombreuses disciplines (géographie, écologie, aménagement du territoire, etc.) et fait l'objet de différentes définitions. La définition courante du paysage renvoie aux concepts d'espace et de perception : en 2000, la Convention européenne du paysage définit le paysage comme une partie de territoire telle que perçue par les populations, dont le caractère résulte de l'action de facteurs naturels et/ou humains et de leurs interrelations. Nous retiendrons une définition plus fonctionnelle, en relation avec l'étude de processus écologiques, proposée par l'écologie du paysage (Burel and Baudry, 2003 ; Turner, 1989) :

- le paysage correspond à un niveau d'organisation des systèmes écologiques supérieur à l'écosystème ;
- il se caractérise essentiellement par son hétérogénéité et par sa dynamique : il est constitué par un assemblage d'éléments qui interagissent et évoluent à plusieurs échelles

spatiales et temporelles. L'organisation de ces éléments résulte de l'interaction entre le milieu physique, le climat et les activités humaines. Il est également le support de flux de matière, d'énergie et d'organismes vivants ;

- la structure du paysage se définit par sa composition (description des éléments composant le paysage) et par son organisation spatiale (description des interactions entre les éléments et de leur localisation spatiale).

Le paysage correspond à un niveau d'intégration intermédiaire entre la parcelle et la région géographique. Cependant, son extension spatiale et la façon dont il est caractérisé dépendent des processus écologiques étudiés et des facteurs biophysiques et anthropiques qui les contrôlent (Forman, 1995). L'extension spatiale doit être suffisante pour aborder les interactions entre milieu et activité anthropique, qui se déroulent souvent sur des étendues différentes.

L'intérêt de l'échelle du paysage est reconnue lorsqu'il s'agit de traiter de problématiques environnementales et de protection des ressources qui impliquent des flux de matières et d'énergie dans l'espace et dans le temps (Sommer, 2006). Les politiques publiques et les actions d'aménagement des espaces agricoles ciblent de plus en plus des étendues spatiales qui dépassent la parcelle ou le territoire de l'exploitation agricole, pour mieux prendre en compte les interactions entre sources et puits, ainsi que les interactions entre processus biophysiques et processus anthropiques. Cette échelle est utilisée depuis une trentaine d'années pour des problématiques de biodiversité, car elle permet d'intégrer la connectivité spatiale et temporelle des espaces de vie ou de circulation des espèces (Burel and Baudry, 1999). Concernant la qualité de l'eau, l'approche bassin versant est largement utilisée pour les programmes d'étude et de gestion de la qualité de l'eau (Gerrits and Edelenbos, 2004 ; Maxted et al., 2009 ; Merot et al., 2008). Son intérêt est aussi reconnu pour l'étude des transferts atmosphériques (Cellier et al., 2011 ; de Vries et al., 2011).

Concernant l'étude des sols, l'utilisation du concept de paysage est plus récente, même si son intérêt est implicite depuis longtemps. Par exemple, il est sous-jacent dans les approches de l'analyse structurale de la couverture pédologique (Ruellan et al., 1989) ou dans celle "d'agroecosystem" proposée par (Anderson et al., 1983). Ces approches définissent le sol comme un milieu organisé dans les trois dimensions de l'espace et dans la dimension temporelle, et montrent que les propriétés de sol et les processus pédologiques ne peuvent être compris lorsqu'ils sont isolés de leur contexte spatial et/ou temporel. C'est le cas quand des transferts d'eau, de solutés ou de sédiments, passés ou présents, permettent d'expliquer les caractéristiques actuelles d'un sol ou d'un processus dans une situation particulière. Minasny et McBratney (2006b) ont par exemple montré que la modélisation de la pédogénèse à l'échelle du paysage permettait de prendre en compte les interactions, dans l'espace et dans le temps, entre trois grands facteurs de formation des sols : la formation du sol à partir de la dégradation physique du matériau parental, la perte de constituants par altération chimique et le transport de matériaux par érosion. Il a notamment été reconnu qu'il était important de prendre en compte le contexte spatial pour mieux comprendre les processus pédologiques et l'évolution des propriétés des sols (par ex. Delmas et al., 2012 ; Huggett, 1975 ; Lin, 2011 ; Ritchie et al., 2007). Le concept de *Landscape pedology* a été développé pour prendre en compte dans l'étude des sols l'organisation du paysage dans son ensemble et la variabilité spatio-temporelle des processus et des flux y prenant place (Pennock and Veldkamp, 2006 ; Sommer, 2006). Dans ce cadre, différents composants du paysage sont à considérer (Figure 1-1) : le climat, le milieu physique (en relation étroite avec la topographie), les sols dont les propriétés peuvent varier verticalement et horizontalement, la structure du paysage (composition et l'organisation spatiale), et les activités humaines (systèmes d'exploitation, pratiques agricoles). On considère ainsi l'ensemble

des facteurs de contrôle de l'évolution des sols, non seulement les éléments physiques et chimiques, mais aussi anthropiques (Viaud et al., 2010). Sommer (2006) montre ainsi l'intérêt de l'échelle du paysage, non seulement pour considérer des zones ayant des évolutions différentes, mais aussi pour intégrer leurs interactions.

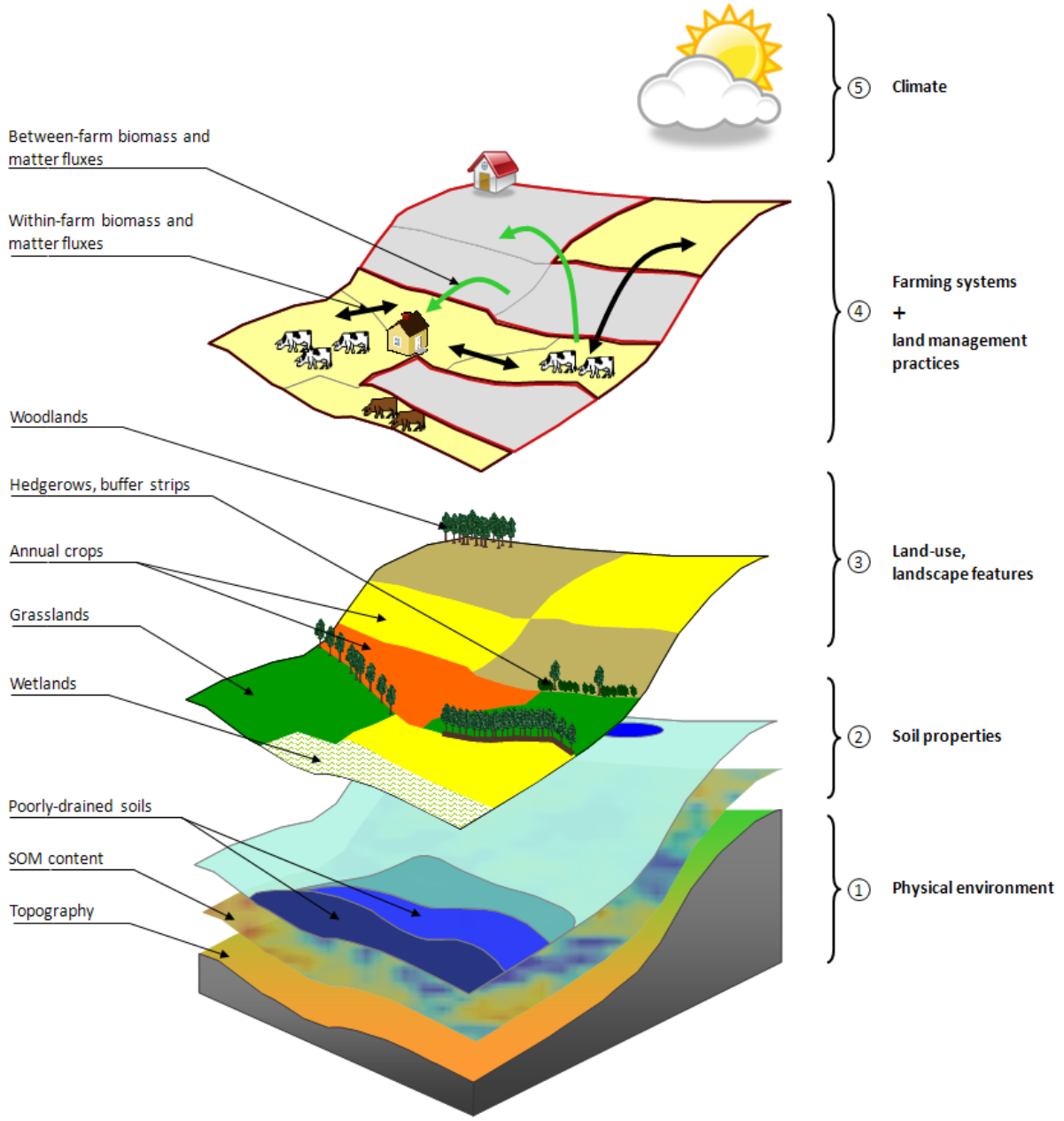

Figure 1-1. Les différents composants d'un paysage agricole à considérer pour l'étude de l'évolution des sols (d'après Viaud et al., 2010).

Les études à l'échelle du paysage permettent également de prendre en compte tous les éléments d'un paysage agricole : non seulement les parcelles cultivées, mais aussi les espaces artificialisés (zones bâties, routes…), les espaces naturels ou semi-naturels (zones humides, friches, espaces forestiers…), et les espaces interstitiels (bandes enherbées, haies…)(Viaud et al., 2010). Ces espaces interstitiels sont courants dans les paysages agricoles. Dans certaines situations, leur présence est historique et fortement liée à l'histoire des populations humaines. C'est par exemple le

cas des réseaux de haies dans les paysages bocagers de l'ouest de l'Europe (Baudry et al., 2000 ; Marguerie et al., 2003). Leur implantation peut également être le résultat de politiques agricoles ou environnementales mises en place dans le but de préserver les ressources naturelles. La préservation et l'implantation des trames vertes en Europe sont par exemple encouragées par des mesures agro-environnementales, établies dans le cadre de la Politique Agricole Commune dans le but de préserver la biodiversité, les ressources en eau et les sols (Berger et al., 2006 ; European Commission, 2005). Au sein de ces éléments du paysage, les processus pédologiques peuvent différer par leur nature ou leur dynamique. Par exemple, selon la zone considérée, les sols peuvent constituer des puits de C organique (prairies permanentes, zones humides, haies…), ou des sources (zones cultivées) (par ex. Follain et al., 2007 ; Viaud et al., 2010 ; Walter et al., 2003a). De la même manière, les éléments du paysage peuvent correspondre à des zones de production de sédiments par érosion hydrique ou aratoire (parcelles cultivées), ou à des zones de capture et d'accumulation de sédiments (haies et bandes enherbées) (Follain et al., 2006b).

Un paysage agricole a donc une hétérogénéité horizontale mais aussi verticale. Les différents éléments qui le composent sont en interaction les uns avec les autres, ce qui engendre des flux de matières et d'énergie, des modifications de structure, des modifications des processus, etc. L'étude des sols à l'échelle du paysage permet d'intégrer ces différents processus et leurs interactions, mais aussi de prendre en compte des processus se déroulant à des échelles spatiales et/ou temporelles différentes (O'Neill et al., 1989).

1.2.2 Effets de la structure du paysage sur le stockage de carbone et l'érosion des sols

De nombreuses études ont cherché à déterminer les impacts des éléments du paysage sur l'évolution des sols, notamment sur le stockage du C et l'érosion, en considérant le milieu physique (climat, propriétés du sol, matériau parental, topographie), les occupations du sol et les pratiques agricoles sur les parcelles, ainsi que les éléments interstitiels des espaces agricoles. Les paragraphes suivants donnent quelques éléments, non exhaustifs, sur les relations établies entre les composants du paysage et l'évolution des sols (érosion, dynamique du C).

1.2.2.1 Milieu physique

Considérant le climat, Raich et Schlesinger (1992) ont montré que, toutes choses égales par ailleurs, une augmentation de la température de 10°C diminue les temps de résidence du C dans le sol par un facteur de 2 à 3. D'après Rodrigo et al. (1997), l'humidité du sol favorise la biodégradation et fait varier les temps de résidence du C dans un rapport de 1 pour un sol sec à 2 pour un sol à la capacité au champ. L'intensité des événements pluvieux est un des facteurs contrôlant l'érosion des sols. Chaplot et Le Bissonnais (2000) ont par exemple montré que la quantité d'eau ruisselée variait de 45 à 85% de la quantité d'eau apportée par la pluie pour des événements pluvieux naturels de 8 mm h^{-1}, et de 75 à 85% pour des événements pluvieux simulés de 50 mm h^{-1}.

En ce qui concerne l'impact du matériau parental sur l'érosion des sols, Cerdan (1999) a observé des taux d'érosion de 0 à 3 720 g m^{-2} h^{-1} pour des sols issus de marnes, de 0 à 131 g m^{-2} h^{-1} pour des sols sur argiles ou calcaires, de 0 à 0,29 g m^{-2} h^{-1} pour des sols issus de grès.

La topographie est également un facteur à prendre en compte. De nombreuses études, parfois contradictoires, ont tenté de quantifier l'effet de la morphologie des versants sur l'érosion des sols. Selon Lal (1997), dans le cas d'un travail du sol conventionnel au Nigeria, l'érosion des sols est multipliée par 4 quand la longueur de pente est augmentée de 10 m à 60 m. Mais dans le cas d'un travail du sol sans labour, la longueur de la pente n'a aucun effet sur l'intensité de l'érosion. D'après

le travail de Chaplot et Le Bissonnais (2000), dans le contexte de sols limoneux en Normandie (France), le ruissellement augmente de 20 à 90% et la concentration en sédiments de 2 à 6 g l^{-1} lorsque la pente augmente de 2 à 8%. L'étude de Gascuel-Odoux et al. (1996), réalisée sur des sols limoneux bretons (France), montre que le ruissellement diminue au niveau des zones concaves, du fait de l'augmentation de l'infiltration. Ces études soulignent qu'il faut considérer l'ensemble des caractéristiques topographiques : longueur et intensité de la pente, mais aussi sa courbure (concavité versus convexité) et la microtopographie, notamment due au travail du sol.

Les propriétés des sols ont également des impacts forts sur la dynamique du C dans les sols. Arrouays et al. (1999) ont observé que la teneur en argile faisait varier les temps de résidence et les stocks de C d'un facteur de 1 à 2,5. L'étude menée par Le Bissonnais et al. (1995) souligne qu'il existe des interactions complexes entre la teneur en C, la texture et l'humidité d'un sol, ces trois propriétés influant sur la désagrégation des agrégats du sol, le ruissellement et l'érosion des sols. Les travaux de Scott et al. (1996) vont dans le même sens : ils démontrent que la texture d'un sol n'a pas d'effet sur la minéralisation du C pour une teneur en eau constante, mais que l'action combinée de la texture et de l'humidité permet d'augmenter la minéralisation pour des sols pour des teneurs en argile et en eau relativement plus importantes.

1.2.2.2 Occupation du sol et pratiques agricoles sur les parcelles

La gestion des terres agricoles donne lieu à de nombreuses combinaisons d'occupation du sol et de pratiques agricoles, influant sur l'évolution des sols.

Le type d'occupation du sol impacte la dynamique du C via les entrées de C au sol par la biomasse racinaire et aérienne (quantité de C apportée, nature de la matière organique (MO), distribution dans le profil). Cet impact ressort dans les inventaires qui permettent de faire le lien entre les grands types d'occupation du sol et les stocks de C. Par exemple, Bradley et al. (2005) ont estimé que les stocks de C sur une profondeur de 1 m dans les sols d'Angleterre et du Pays de Galles étaient de l'ordre de 32 t ha^{-1} pour les espaces semi-naturels, 25 t ha^{-1} pour les forêts, 16 t ha^{-1} pour les prairies pâturées, 12 t ha^{-1} pour les sols cultivés. D'après Cerdan et al. (2010), les taux moyens d'érosion des sols en Europe sont de 15,1 t ha^{-1} an^{-1} pour les sols nus, 4,40 t ha^{-1} an^{-1} pour les parcelles cultivées, 0,14 t ha^{-1} an^{-1} pour les forêts et 0,30 t ha^{-1} an^{-1} pour les prairies.

Le type de travail du sol influence également la dynamique d'évolution du sol. La simplification du travail du sol semble par exemple favoriser le stockage de C dans les sols de 0,2 tC ha^{-1} an^{-1} en moyenne dans le contexte français (Arrouays et al., 2002). Balesdent et al. (2000) indiquent que le labour a pour effet de déstructurer des agrégats du sol, ce qui diminue la protection physique des matières organiques et augmentent leur minéralisation. D'autre part, Van Muysen et al. (2006) estiment que le travail du sol induit des déplacements de sols de l'ordre de 781 kg m^{-1} an^{-1}, dans le cadre d'une agriculture mécanisée. D'une manière générale, les dynamiques des caractéristiques de surface pour un sol donné (couverture, rugosité, faciès) dépendent des pratiques agricoles, et influent fortement sur la genèse du ruissellement et sur l'érosion des sols (Le Bissonnais et al., 2005).

Si l'on considère la gestion des résidus de culture, Plénet et al. (1993) décrivent un stockage de 3 à 4 tC ha^{-1} en 25 ans de pratique de restitution des tiges et feuilles sur monoculture de maïs. Selon Gilley et al. (2000), lorsque la couverture du sol par les résidus de culture augmente de 10 à 83%, les pertes en sol diminuent de 4,26 à 0 t ha^{-1}.

1.2.2.3 Espaces non cultivés du paysage

Différents éléments non cultivés des paysages agricoles, considérés comme des espaces interstitiels, influent sur les stocks de C et l'érosion des sols.

La présence de végétation permanente (ligneuse ou non), induit une augmentation de la production de biomasse, et donc une augmentation des apports de C. Walter et al. (2003a) montrent par exemple que les stocks de C au niveau des haies représentent 13 à 38% du stock de C total au sein d'un paysage agricole bocager.

Les éléments interstitiels ont également un effet reconnu sur les circulations d'eau, que ce soit à l'échelle parcellaire, voire infra-parcellaire, ou à l'échelle du paysage. La présence de bandes enherbées ou de haies perpendiculaires à la pente, permet l'augmentation de l'infiltration de l'eau dans le sol, et donc la diminution du ruissellement de surface. Gilley et al. (2000) observent que, selon les pratiques culturales, une bande enherbée placée en travers de la pente permet de diminuer le ruissellement de 10 à 66%, et les pertes en sols de 17 à 85%. Ces structures ont également pour effet de piéger les particules de sol transportées par ruissellement. Ceci a un effet sur la distribution des sols et de leurs propriétés dans le paysage : des épaississements de sol ont été observés en amont des haies, alors que les zones en aval des haies sont plus susceptibles à l'érosion (Carnet, 1976 ; Layer, 2000 ; Walter et al., 2003a). Salvador-Blanes et al. (2006) estiment par exemple que la présence de haies perpendiculaires à la pente a permis des accumulations de sol de 3 à 7 m^3 par mètre linéaire de haies (Massif Central, France). Cependant, selon sa position dans le paysage, une structure linéaire telle qu'une haie peut également favoriser le ruissellement concentré (Burel et al., 1993).

1.3 Prise en compte de la dimension temporelle pour l'étude de l'évolution des sols

Dans le cadre de l'étude de l'évolution des sols, il est nécessaire de prendre en compte la dimension temporelle des processus d'évolution des sols, celles des facteurs contrôlant les processus pédologiques (climat, pratiques agricoles...) mais aussi le temps de réponse des processus pédologiques au changement des facteurs de contrôle.

1.3.1 Dynamique temporelle du climat

Le climat actuel présente une variabilité intra-annuelle et interannuelle (Belleguic et al., 2012). Dans le contexte d'un climat océanique tempéré par exemple, les mois d'été sont caractérisés par des températures plus élevées et des cumuls pluviométriques plus faibles par rapport aux mois hivernaux. Des années très humides et des années plus sèches se succèdent aléatoirement. Des événements climatiques modérés et fréquents, se produisant plusieurs fois par an, s'opposent à des événements extrêmes à temps de retours plus longs (Figure 1-2). De même, les températures annuelles moyennes fluctuent d'une année à l'autre (Figure 1-3).

A ces variations intra et interannuelles se surimpose une évolution globale du climat. Tout au long de son histoire, la Terre a subi de nombreux changements climatiques, occasionnés par des facteurs externes (changement de l'orbite terrestre, variation de l'énergie émise par le soleil…) ou internes (tectonique des plaques, éruptions volcaniques…). Cependant, des variations rapides du climat ont été observées au cours du $XX^{ème}$ siècle, caractérisées notamment par une augmentation des températures moyennes à l'échelle du globe (Figure 1-3) et une augmentation des fréquences des événements pluvieux extrêmes (GIEC, 2007). Une augmentation moyenne de 0.9°C a par

exemple été mesurée à Rennes entre 1901 et 2000 (Belleguic et al., 2012). Ces variations sont imputées à l'augmentation des concentrations en gaz à effet de serre dans l'atmosphère, provoquée par l'intensification des activités humaines, qu'elles soient agricoles, industrielles, récréatives ou commerciales (GIEC, 2007). Les études sur la variation du climat estiment qu'il est très probable que dans le futur les températures moyennes continuent à augmenter, et que la fréquence de journées froides diminue. A l'échelle globale la sécheresse devrait progresser et la fréquence des événements extrêmes (vagues de chaleur, événements pluvieux, etc.) devrait augmenter.

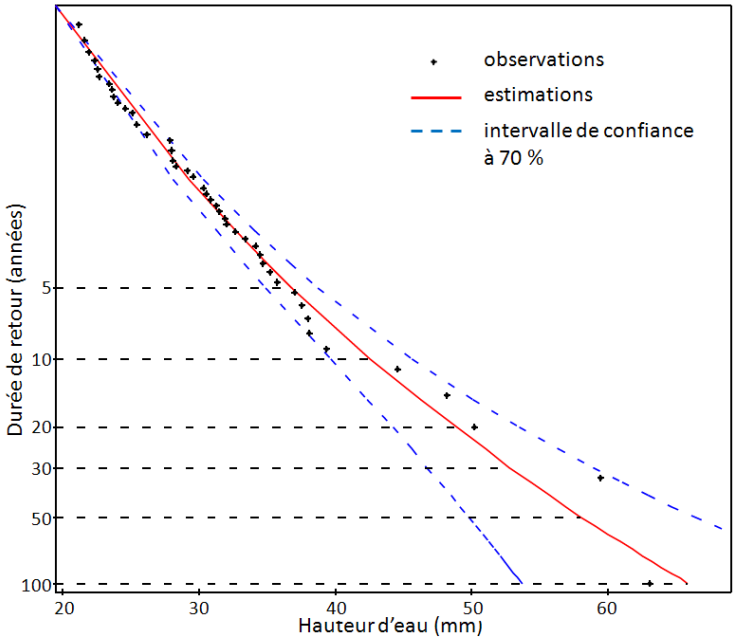

Figure 1-2. Durée de retour des événements pluvieux selon leur cumul pluviométrique (Station de Rennes, Météo-France)

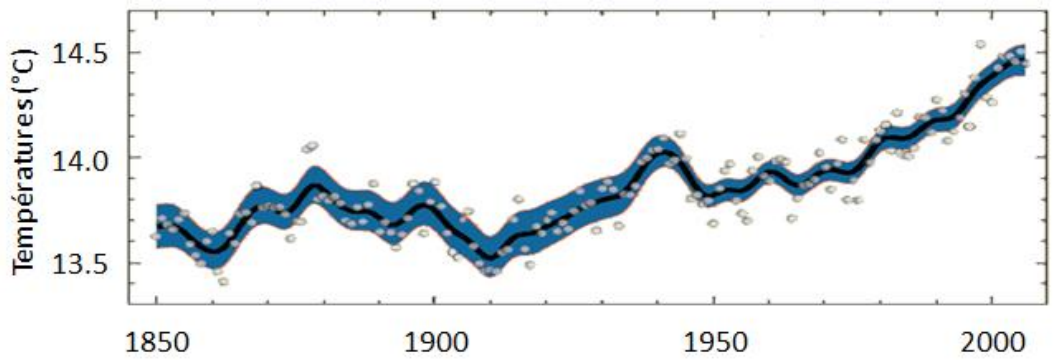

Figure 1-3. Evolution de la température moyenne à la surface du globe entre 1850 et 2000 (courbes lissées : moyennes décennales, points : valeurs annuelles). D'après le GIEC (2007).

Lors de l'étude de l'évolution des sols, il est donc nécessaire de prendre en compte les dynamiques temporelles des propriétés étudiées et des facteurs contrôlant ces dynamiques, qui varient et interagissent à des pas de temps différents (Figure 1-4).

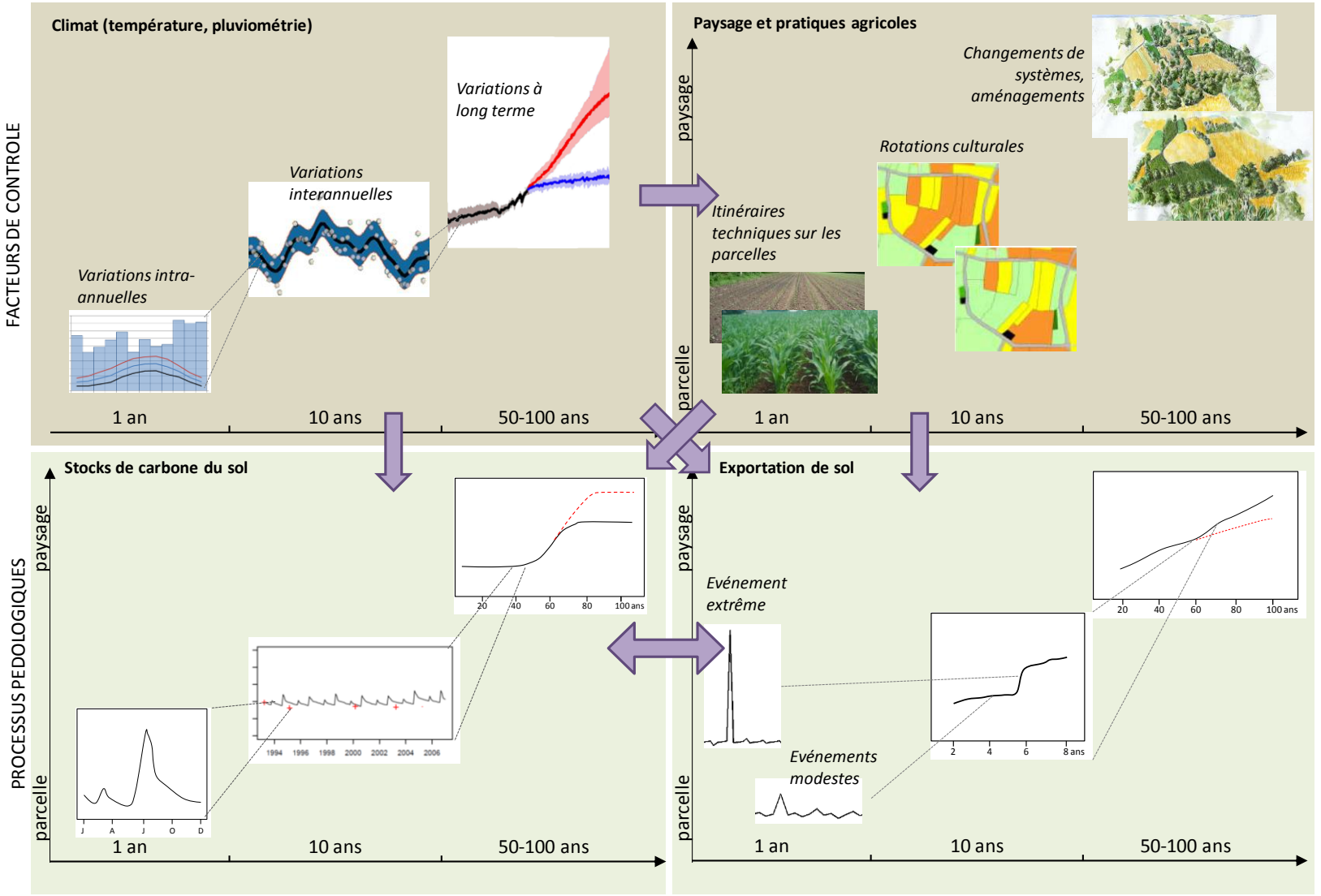

Figure 1-4. Représentation schématique des dynamiques temporelles des stocks de carbone et de la redistribution des sols, ainsi que des facteurs contrôlant ces dynamiques (climat, paysage, pratiques agricoles)

Le climat est un facteur de contrôle important concernant les dynamiques d'évolution des sols. Dans une étude visant à simuler l'évolution des sols, et plus particulièrement les dynamiques de la matière organique et de la redistribution des sols, il est donc nécessaire de prendre en compte les variabilités intra et interannuelles du climat, les événements extrêmes mais aussi le cumul d'événements plus modestes et les grandes tendances de variation du climat.

1.3.2 Dynamique temporelle de la mosaïque paysagère

L'hétérogénéité spatiale des mosaïques paysagères résulte largement des hétérogénéités temporelles liées aux activités humaines dans les paysages agricoles (Burel and Baudry, 2000). Les mosaïques paysagères sont caractérisées par une variabilité intra et interannuelle, mais elles sont également soumises à des variations sur de plus longues durées (Figure 1-4).

A l'échelle intra-annuelle, la mise en œuvre des itinéraires techniques sur les parcelles conduit à une hétérogénéité de l'état de surface des sols (pouvant affecter la sensibilité à l'érosion) et contrôle la dynamique des apports de C au sol par la gestion des résidus végétaux et la fertilisation. A l'échelle interannuelle, les rotations des cultures et leur organisation dans l'espace contrôlent l'hétérogénéité spatiale de la mosaïque paysagère, et de ce fait les relations spatiales entre les zones sources d'érosion et les zones de dépôt, de même que la répartition spatiale des apports de matières organiques par les résidus végétaux et par la fertilisation.

L'évolution des mosaïques paysagères peut également se dérouler graduellement, sur des temps plus longs. C'est le cas par exemple des changements de système de culture, en réponse à des évolutions du contexte politique, économique ou socio-technique, qui nécessitent parfois plusieurs années pour se mettre en place. C'est également le cas des opérations d'aménagement foncier, d'implantation de haies ou de bandes enherbées et des agrandissements de parcelles en lien avec les agrandissements d'exploitations agricoles. Ce type d'aménagement du paysage peut avoir des effets à différents pas de temps. L'implantation de haies ou de bandes enherbées demande du temps, et leur impact sur les sols n'est pas immédiat. Au contraire, l'arasement d'une haie peut avoir un effet rapide, provoquant une réduction des stocks de C par diminution des apports de matière organique par la biomasse aérienne et souterraine, et une augmentation de l'érosion des sols si la haie était dans une situation de forte pente par exemple.

1.3.3 Echelles temporelles et temps de réponse de la dynamique du carbone et de l'érosion des sols

Considérant la dynamique du C dans les sols, on estime que 75% du C incorporé dans le sol se dégraderaient en quelque mois (Arrouays et al., 2002). Environ 65% du C restant auraient un temps de résidence moyen de 40 ans, alors que 15% du C résideraient dans les sols en moyenne 4 ans et 20% plus de 1 000 ans (Balesdent and Recous, 1997). La dynamique du C dépend aussi fortement de la dynamique des apports de matière organique par la végétation ou par des pratiques de fertilisation organique, pouvant être ponctuels ou réguliers (Arrouays et al., 2002). Les durées à considérer pour l'étude de l'évolution du C du sol peuvent varier du mois au millénaire, que l'on considère le C labile, décomposable ou résistant.

En ce qui concerne l'érosion des sols, le pas de temps clef est celui de l'événement, pluvieux ou aratoire. Différents types d'événements pluvieux, caractérisés par leur durée, leur cumul pluviométrique et leur intensité, peuvent provoquer l'érosion des sols. En France, les phénomènes érosifs les plus spectaculaires, provoquant par exemple la création de ravines par concentration des

écoulements, sont le résultat d'événements pluvieux extrêmes (événements intenses hivernaux ou orages estivaux) impactant des sols nus ou peu couverts (Le Bissonnais et al., 2002b). Cependant, des événements pluvieux moins intenses et la répétition d'événements pluvieux modestes peuvent également conduire à des redistributions de sols par érosion diffuse non négligeables (Figure 1-5). Le travail du sol est aussi un facteur de redistribution des sols (par exemple Van Muysen et al., 2006). La redistribution du sol se fait au pas de temps de l'événement aratoire et peut être plus ou moins importante en fonction de l'outil utilisé (Van Muysen et al., 2000). Si l'effet d'un seul événement aratoire n'est pas spectaculaire, leur répétition, année après année, peut provoquer des déplacements de sol importants (Van Oost et al., 2005b).

Figure 1-5. Exemple de deux phénomènes érosifs en Bretagne : érosion concentrée et formation de ravine (gauche, Naizin), érosion diffuse et dépôt de sol en amont d'une haie (droite, Bazouges-la-Pérouse)

1.4 Estimation de l'évolution des sols à l'échelle du paysage : approches par modélisation dynamique et spatialisée

La modélisation se définit comme *une opération par laquelle on établit le modèle d'un système complexe, afin d'étudier plus commodément et de mesurer les effets sur ce système des variations des éléments qui le composent* (CNRTL Centre National des Ressources Textuelles et Lexicales). Dans le cadre de l'étude des sols à l'échelle des paysages, l'utilisation d'outils de modélisation se justifie par trois arguments majeurs :

- la nécessité d'intégrer les différents facteurs d'évolution des sols, ainsi que leurs interactions spatiales et temporelles ;
- le besoin de surmonter des contraintes techniques et matérielles, en simulant ce qui est difficile à mettre en œuvre expérimentalement. Ces difficultés peuvent découler de l'étude d'un territoire vaste (nécessitant de nombreuses mesures et observations), de durées

d'observation trop longues ou de la présence de paramètres difficiles à contrôler ou à estimer (climat, activités humaines…) ;

- la volonté de construire et d'évaluer des scénarios d'évolution des facteurs influant sur les dynamiques d'évolution des sols (pratiques agricoles, organisation spatiale du paysage…), par exemple dans le but de déterminer des solutions pour la protection des sols dans un contexte de changement global.

Les paragraphes qui suivent exposent les deux principales approches utilisées en modélisation en axant plus particulièrement sur les simulations des dynamiques du C et de la redistribution des sols : les approches empiriques, très dépendantes des données expérimentales, et les approches mécanistes ou à base physique, orientées sur la description des processus. Il faut cependant noter qu'il existe un continuum d'approches entre ces deux pôles (Jorgensen and Bendoricchio, 2001). Même si ces approches diffèrent par leur conception, elles reposent toutes sur des modèles mathématiques et nécessitent des données expérimentales (acquises en laboratoire ou lors d'expérimentations et d'observations de terrains), afin de calibrer et de valider les modèles mis en place.

1.4.1 Approches de modélisation empirique

Les modèles empiriques considèrent un système dans son intégralité, sans chercher à détailler les processus qui déterminent ses variations. Ils visent à simuler la réponse d'un système en se basant sur des relations statistiques ou mathématiques, construites à partir de jeux de données expérimentales. Les règles établies sont ensuite extrapolées, dans l'espace et/ou le temps.

Smith et al. (2000) ont par exemple estimé les variations des stocks de C dans les sols du Royaume-Uni (0-30 cm) selon différentes pratiques agricoles, en utilisant des relations statistiques établies par Smith et al. (1997) à partir de suivis à long-terme répartis dans toute l'Europe.

Si l'on considère l'érosion des sols, l'équation universelle des pertes de sol (USLE, Universal Soil Loss Equation; Wischmeier and Smith, 1978) est l'un des modèles empiriques les plus largement utilisés au monde (Jetten and Favis-Mortlock, 2006 ; Kinnell, 2010). Elle a été calibrée aux Etats-Unis et modélise l'érosion des sols dans sa globalité, sans que les processus soient détaillés, en se basant sur cinq facteurs décrivant l'érosivité de la pluie, l'érodibilité du sol, la pente, les pratiques culturales et la couverture végétale du sol. Cette équation a par la suite été modifiée, donnant naissance à des modèles tels que dUSLE (Flacke et al., 1990) ou RUSLE (Renard et al., 1991). RUSLE et dUSLE sont basés sur la même équation que USLE, mais le mode de calculs des paramètres de l'équation a été amélioré dans RUSLE, alors que dUSLE permet de prendre en compte la variabilité de la pente par le biais d'un MNT. Bonilla et al. (2010) ont par exemple utilisé RUSLE pour estimer l'impact de différents types d'occupation du sol sur l'érosion, à l'échelle d'un département chilien.

1.4.2 Approches de modélisation mécaniste

Les modèles mécanistes visent à expliquer les évolutions d'un système, en détaillant les processus de manière explicite (Thornley and France, 2007). Contrairement aux modèles empiriques, ces modèles ont des structures fixes : leur formalisme, le nombre de processus qu'ils modélisent ainsi que leur hiérarchie ne varient pas d'une étude à l'autre (Viaud et al., 2010).

Dans le cadre de la modélisation de la dynamique du C dans les sols, Smith et al. (1998) identifient deux grands types de modèle mécaniste : ceux orientés « organismes » et ceux orientés

« processus ». Les modèles orientés organismes représentent de façon explicite la dynamique des communautés microbiennes impliquées dans les processus de dégradation de la matière organique (Blagodatsky and Smith, 2012 ; Moorhead et al., 2012). Les modèles orientés processus s'attachent à décrire des flux et des transformations de matière ou d'énergie ; les organismes sont pris en compte mais de manière implicite et sont considérés comme non limitant pour la dégradation de la matière organique. Ce groupe rassemble un grand nombre de modèles dits compartimentaux. Les modèles les plus couramment utilisés sont CENTURY (Parton et al., 1987), RothC (Coleman and Jenkinson, 1996) et DNDC (Li et al., 1994). Ces modèles ont été calibrés à partir d'études expérimentales à l'échelle de la parcelle, puis appliqués à des étendues spatiales plus vastes (paysage, région, pays…) pour modéliser les évolutions des matières organiques dans les sols (par ex. Falloon and Smith, 2002 ; Falloon et al., 2006 ; Sleutel et al., 2006).

De nombreux modèles mécanistes ont été élaborés pour modéliser la redistribution des sols. Ces modèles diffèrent par les types de processus pris en compte (érosion hydrique diffuse et/ou concentrée, érosion aratoire, érosion éolienne, dépôts des sédiments), l'extension spatiale à laquelle ils sont destinés et le pas de temps qu'ils considèrent. En ce qui concerne l'érosion hydrique, ces modèles sont par exemple basés sur des équations décrivant la genèse du ruissellement et sa concentration en sédiments. Le MMF model (Morgan, 2001) a été créé pour modéliser l'érosion hydrique, le dépôt et les pertes de sol au pas de temps annuel et à l'échelle spatiale de la parcelle. Bakker et al. (2008) ont utilisé WATEM/SEDEM pour estimer l'impact des changements d'occupation du sol dans différents bassins-versants européens. Le modèle PESERA est un modèle spatialement distribué, conçu pour quantifier l'érosion hydrique à l'échelle européenne (Grimm et al., 2002 ; Kirkby et al., 2004)

Il faut cependant noter que la description de nombreux processus au sein des modèles mécanistes repose sur des relations établies de manière empirique. C'est le cas pour les modèles simulant la dynamique du C, lorsque par exemple les constantes de dégradation de la matière organique sont définies à partir de suivis à long terme ou d'expérimentations (Falloon and Smith, 2000). De même, du fait de la complexité des mécanismes impliqués dans l'érosion hydrique des sols, même les modèles les plus mécanistes comportent encore des relations empiriques. En effet, certains facteurs sont basés sur l'équation USLE (Jetten and Favis-Mortlock, 2006), ou sont déduits d'analyses statistiques. Le modèle ANSWER (Beasley et al., 1981), même s'il détaille les processus en jeux dans l'érosion des sols (genèse du ruissellement, détachement des particules), est en partie basé sur l'équation USLE.

Le choix du modèle dépend de l'objectif de l'étude. Dans le cadre de la modélisation de l'évolution des sols à l'échelle du paysage, il faut s'assurer que le modèle soit apte à simuler les processus au sein de chaque élément du paysage, ainsi que les interactions entre ces éléments (Jorgensen and Bendoricchio, 2001). Dans le cadre d'une modélisation spatiale et temporelle, il faut aussi veiller à choisir un modèle en adéquation avec les extensions et les résolutions spatiales et temporelles que l'on s'est fixées (modèle spatialement distribué ou non, pas de temps horaire, journalier ou annuel, modèle adapté pour des simulations à l'échelle de la parcelle, du versant, de la région, etc.).

Les modèles empiriques offrent l'avantage d'être aisés d'application, car ils nécessitent peu de paramètres. Les modèles empiriques simulant la dynamique du C dans les sols sont principalement adaptés pour des études à des échelles régionales, voire nationales, et sont utiles pour déterminer

les impacts majeurs des changements d'occupation du sol ou de pratiques agricoles (Viaud et al., 2010). Les modèles empiriques d'érosion des sols sont surtout utilisés pour localiser les sources de sédiments (Merritt et al., 2003). Ils sont également utiles pour modéliser des pertes en sol moyennes à l'échelle d'une parcelle (Huang, 1995). Cependant, leur utilisation s'avère limitée lorsqu'il s'agit d'intégrer des processus, des connectivités et des interactions, reconnus comme des moteurs d'évolution des sols dominants à l'échelle du paysage (Kirkby et al., 1996 ; Viaud et al., 2010).

Les modèles mécanistes sont plus à même de modéliser l'évolution des sols dans les paysages, car ils permettent de prendre en compte différents processus contrôlant les dynamiques du C ou de la redistribution des sols. Ces modèles sont parfois complexes à calibrer et à mettre en œuvre, car ils nécessitent un grand nombre de paramètres, parfois difficilement accessibles. De plus, les fortes variabilités spatiales des propriétés des sols rendent leur calibration difficile. C'est par exemple le cas des modèles prenant en compte l'évolution des croûtes de battances et l'infiltration sur les sols battants (Le Bissonnais et al., 1998b). D'une manière générale, le principal problème rencontré avec les modèles mécanistes est due à la complexité des phénomènes impliqués : plus l'on veut représenter fidèlement la réalité, plus on doit intégrer de mécanismes, mais sans pour autant avoir une vision claire de leurs interactions.

Certains pensent que les modèles empiriques ne seraient pas adaptés à l'étude de l'impact des changements de pratiques agricoles sur les écosystèmes agricoles, à cause de la trop grande simplification des processus modélisés (Thorsen et al., 2001). Cependant, d'autres argumentent que les modèles empiriques peuvent être plus justes que des modèles mécanistes, mais uniquement s'ils sont utilisés dans le domaine où ils ont été calibrés (Ferro and Minacapilli, 1995). Il est donc peu probable que l'utilisation de modèles empiriques soit adéquate dans le cadre de l'étude de l'évolution des sols à l'échelle du paysage, en prenant en compte l'impact de l'occupation du sol et des pratiques agricoles, les propriétés des sols pouvant varier fortement dans l'espace et dans le temps, et dépasser le domaine de variation du modèle.

Face à ces constats, Harris et Boardman (1990) ont proposé pour la prédiction de l'érosion des sols une approche intermédiaire dite à base-experte, et considérée comme plus applicable sur un territoire agricole. Cette approche se base sur l'utilisation de données expérimentales, analysée sur la base d'une connaissance acquise par expertise. Les modèles mécanistes STREAM (Cerdan et al., 2002b) et LandSoil (Ciampalini et al., in press) sont en partie conçus selon ce concept. La genèse du ruissellement est par exemple modélisée à partir de règles établies par expertise et sur la base de données expérimentales.

1.5 Conclusion partielle

L'étude des sols à l'échelle du paysage permet de prendre en compte la variabilité spatio-temporelle des sols et la dynamique des processus contrôlant l'évolution des sols, i.e. les flux d'eau et de matière (Sommer, 2006).

La modélisation est particulièrement adaptée pour étudier l'évolution des sols à l'échelle des paysages, car elle permet de représenter plusieurs processus ainsi que leurs interactions et d'intégrer ces processus dans l'espace et dans le temps. Utilisés en simulation, les modèles permettent également de tester différents scénarios mettant en jeu des facteurs de changement des sols, et d'évaluer leurs impacts sur l'évolution des sols, notamment dans un contexte de changement global.

En ce qui concerne les outils de modélisation, il semble que les modèles mécanistes soient plus adaptés à la modélisation de l’évolution des sols à l’échelle du paysage que les modèles empiriques, puisqu'ils permettent de représenter explicitement les interactions spatiales et temporelles entre les processus pédologiques étudiés, et entre les éléments du paysage. Il faut cependant veiller à ce que les modèles puissent être adaptés à la zone d’étude choisie, qu’ils intègrent les principaux facteurs d’évolution des sols (C et redistribution), et qu’ils permettent des simulation de l’évolution des sols à moyen terme ou long terme en prenant en compte les différents éléments d’un paysage (sols, topographie, occupation du sol, pratiques agricoles).

Les modélisations intégrées à l’échelle du paysage doivent également permettre de prendre en compte les dynamiques temporelles des propriétés du sol, mais aussi celles des facteurs contrôlant leurs variations.

Chapitre 2.
Matériel et méthodes : description de la zone d'étude et de la démarche de modélisation de l'évolution des sols

Ce chapitre a pour objectif de présenter la zone d'étude et les modèles de dynamiques spatiales utilisés pour simuler l'évolution des sols en fonction des changements de structure du paysage et de climat. Seuls les éléments généraux de matériel et méthodes nécessaires à la compréhension de l'ensemble des chapitres sont présentés ici. Les méthodes spécifiques seront présentées au sein des chapitres concernés.

2.1 Description de la zone d'étude

2.1.1 Le site atelier de Pleine-Fougères

Le site atelier de Pleine-Fougères (48° 36' N, 1° 32' W) est situé dans le nord de l'Ille-et-Vilaine, au sud de la baie du Mont-Saint-Michel (Figure 2-1a). Il fait partie de la Zone Atelier Armorique, qui s'inscrit dans le réseau «Zones Ateliers» de l'Institut Écologie et Environnement du CNRS, ainsi que dans les réseaux européens et internationaux LTER-Europe (European Long-Term Ecosystem Research Network) et ILTER (International Long Term Ecological Research). Le site a une superficie de 1000 ha et s'étend sur trois communes : Pleine-Fougères, Vieux-Viel et Trans-la-Forêt. Il présente une grande complexité du point de vue du matériau parental des sols, du relief et du paysage, qui se traduit par une diversité d'occupation du sol, de pratiques agricoles et d'aménagement du paysage. Les sols du site atelier sont donc susceptibles de présenter une grande diversité, particulièrement au niveau de leur organisation dans le paysage, de leurs épaisseurs et de leurs stocks de C organique.

2.1.2 Contexte climatique

Le site atelier de Pleine-Fougères présente un climat océanique tempéré, caractérisé par de faibles amplitudes thermiques, avec des étés frais et des hivers doux. L'humidité de l'air est importante, les pluies fréquentes mais peu abondantes (Figure 2-2). Les précipitations annuelles moyennes sont de 782 mm, la température annuelle moyenne est de 12°C.

2.1.3 Contexte géologique

2.1.3.1 Contexte géologique régional

Le site atelier de Pleine-Fougères se situe au cœur du domaine mancellien[5], qui appartient au domaine nord du Massif armoricain (Figure 2-3). Le domaine mancellien est bordé au sud par le cisaillement Nord-armoricain, à l'ouest par la faille Granville-Cancale et à l'est par les couches transgressives[6] du Cambrien inférieur puis du Mésozoïque du bassin de Paris (Figure 2-3 et Figure 2-4).

L'histoire géologique du Massif armoricain est caractérisée par de longues périodes sédimentaires, entrecoupées d'épisodes tectoniques, métamorphiques, plutoniques et volcaniques (Lardeux et al., 2002 ; Thomas, 2005). Le Massif armoricain a subi deux orogénèses, marquant encore fortement la géologie bretonne actuelle et permettant de délimiter trois grands domaines géologiques (domaines nord, centre et sud-armoricains, Figure 2-4).

[5] du latin Mancellia, région du Maine.
[6] couches sédimentaires formées lors de transgressions marines.

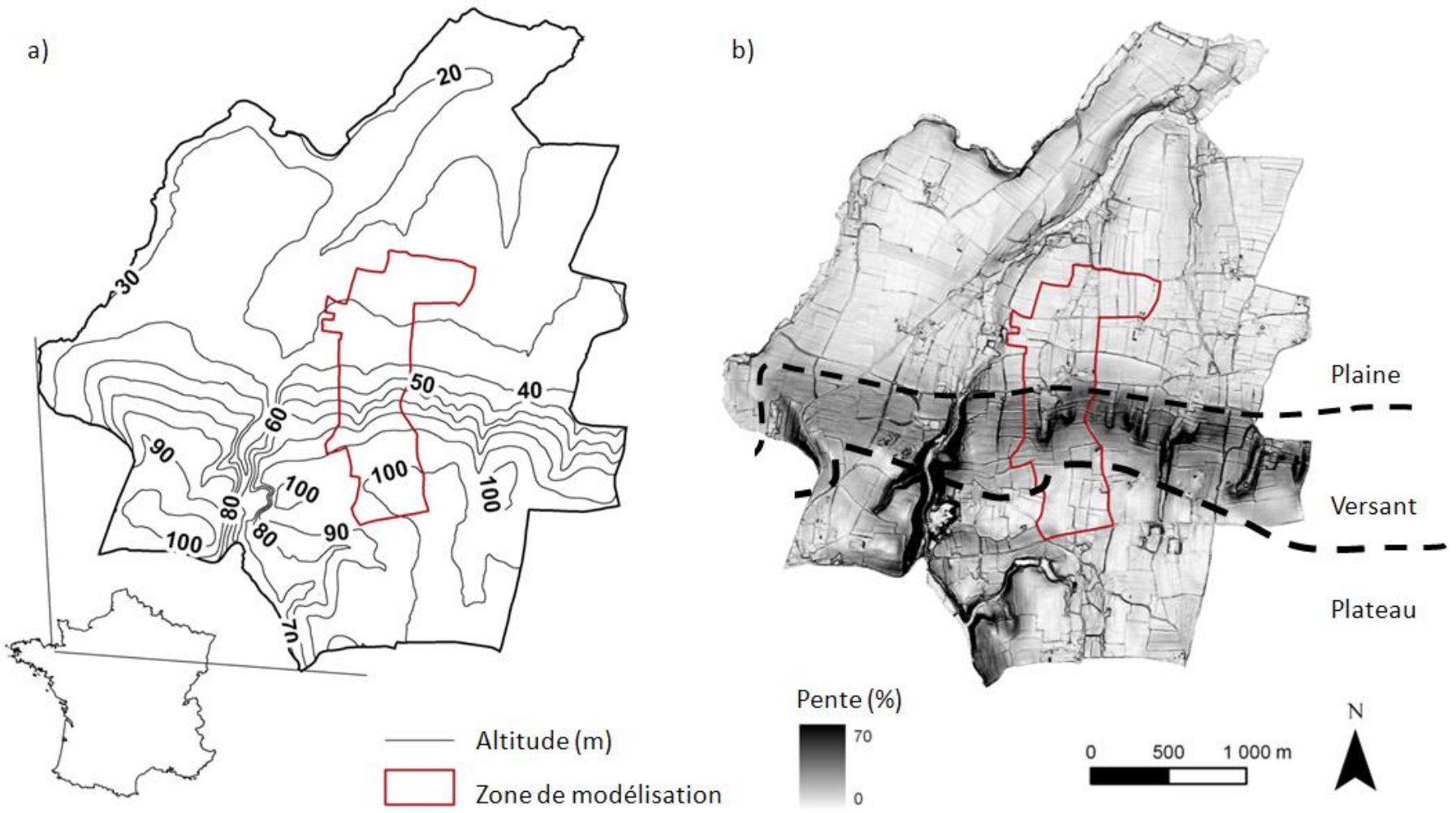

Figure 2-1. Localisation et topographie du site atelier de Pleine-Fougères et de la zone de modélisation (a : altitude, b : pente et délimitation des grands ensembles topographiques).

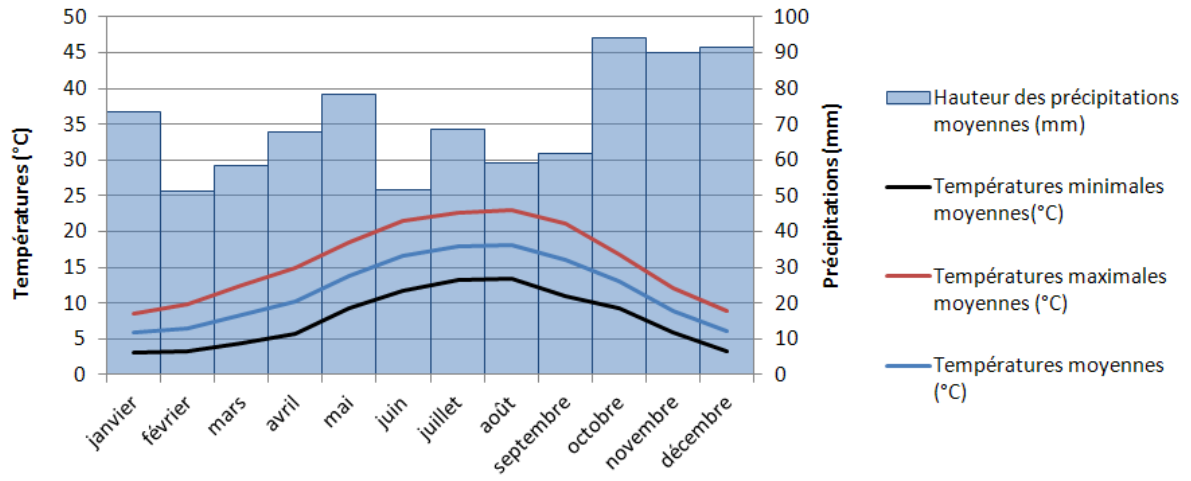

Figure 2-2. Diagramme ombrothermique (Météo France, station de Pontorson).

La première orogénèse (cadomien, 650-540 Ma) a donné naissance à la chaîne cadomienne dont on trouve encore des traces dans le domaine Nord-armoricain, notamment sous la forme de granitoïdes qui constituent le batholite[7] du domaine mancellien (e.g. granodiorites du Massif de Bonnemain, leucogranites du Massif de Dinan, Figure 2-4). Le domaine mancellien est constitué par des matériaux Briovériens, recoupés par le batholite cadomien. Les matériaux briovériens sont des ensembles sédimentaires volcano-détritiques ou détritiques terrigènes[8] issus d'un socle cristallin précambrien et déposés sur un subtratum icartien[9] (non observable dans le domaine mancellien). Ces sédiments ont été déformés pendant l'orogénèse cadomienne, formant des plis serrés orientés en moyenne à 45° (NE). Le batholite, occupant plus de 10 000km², s'est ensuite mis en place en provoquant un métamorphisme thermique des matériaux briovériens (formations de cornéennes et de schistes tachetés). Tous ces matériaux ont ensuite subi un long processus d'érosion, et la fin du cycle cadomien est marqué par et la transformation de la chaîne cadomienne en pénéplaine.

L'orogénèse hercynienne (ou varisque) entraine ensuite une extension du domaine mancellien (direction E-W à ENE-WSW), ce qui provoque la création de failles et l'intrusion de filons de dolérite et de quartz. S'ensuit alors une période de stabilité qui va persister pendant tous le Cénozoïque (Tertiaire et Quaternaire), et pendant laquelle le domaine mancellien reste émergé (à la différence des régions voisines qui subissent plusieurs transgressions marines). Les climats chauds et très humides du Tertiaires favorisent une altération massive des roches sur des épaisseurs pouvant avoisiner une cinquantaine de mètres, ce qui engendre l'affaissement du massif armoricain et le décapage des altérites précédemment formées.

Le Quaternaire voit se succéder des périodes glaciaires et interglaciaires, favorisant la mise en place de dépôts continentaux. Ils sont constitués en majorité de sables et de lœss (généralement non calcaires en Bretagne), déposés en plusieurs phases pendant le Weichsélien[10] (Lautridou and

[7] Intrusion de roches plutoniques, en forme de dôme ou de culot, recoupant des roches encaissantes (dictionnaire encyclopédique Larousse 1979)

[8] matériau formé en totalité ou en partie de débris arrachés à une terre émergée par érosion (Dictionnaire de Géologie, 2005)

[9] Division du Précambrien français (limite Archéen-Protérozoïque)

[10] de Weichsel, nom allemand d'un fleuve de Pologne. Nom donné à la dernière glaciation ayant eu lieu en Europe du Nord à la fin du Pleistocène ($^{-1}$ 600 ka à $^{-1}$0 ka). Equivalent du Würm dans les Alpes.

Antoine, 2003). Ces lœss ont une épaisseur variable, généralement inférieure à 4 m (Lebret and Lautridou, 1991) mais pouvant atteindre 6 m (Egal, 2004). Cependant, leur extension spatiale est mal connue. En effet, ils ne figurent sur les cartes géologiques que s'ils atteignent une épaisseur supérieure à 2 m, alors qu'ils apparaissent sur les cartes pédologiques même si leur épaisseur est souvent inférieure à 60 cm. Or, ces matériaux peuvent constituer le matériau parental des sols et influencer leurs propriétés. Les sols limoneux possèdent par exemple une bonne capacité de rétention de l'eau, mais sont sensibles à la battance et à la compaction en période humide. Les lœss bretons font partie de la grande bande lœssique recouvrant une grande partie de l'Europe du Nord (Lebret and Lautridou, 1991 ; Figure 2.5). Ces limons ne sont pas homogènes en termes de granulométrie, de composition et d'épaisseur. Ils sont majoritairement d'origine éolienne, provenant de l'érosion du fond de la Manche entre -112 ka et -15 ka suite à une baisse du niveau marin. Cependant, certains matériaux limoneux sont également autochtones et proviennent de produits d'altération des roches sous-jacentes (Lautridou, 1985 ; Pages and Le Calvez, 1980). Au niveau du domaine mancellien, ils sont également appelés ''limons à doublets '', en raison de leur agencement en couches centimétriques superposées, de couleur jaune-brun. Leur granulométrie est dominée par la fraction limoneuse (2-50 µm), qui représente entre 65 et 70% de la fraction totale (Lautridou, 1985). Le rapport limons grossiers (20-50 µm) sur limons fins (2-20 µm) dépasse en général 2,2, et le rapport argiles fines (moins de 0.2 µm) sur argiles totales (moins de 2 µm) dépasse 0,5. La période suivant le dépôt de ces formations superficielles (Flandrien) est marquée par différentes incursions marines successives et irrégulières qui commencent vers – 9 ka et provoquent le dépôt de tangues. Ceci a eu pour effet majeur le colmatage de la baie du Mont-Saint-Michel.

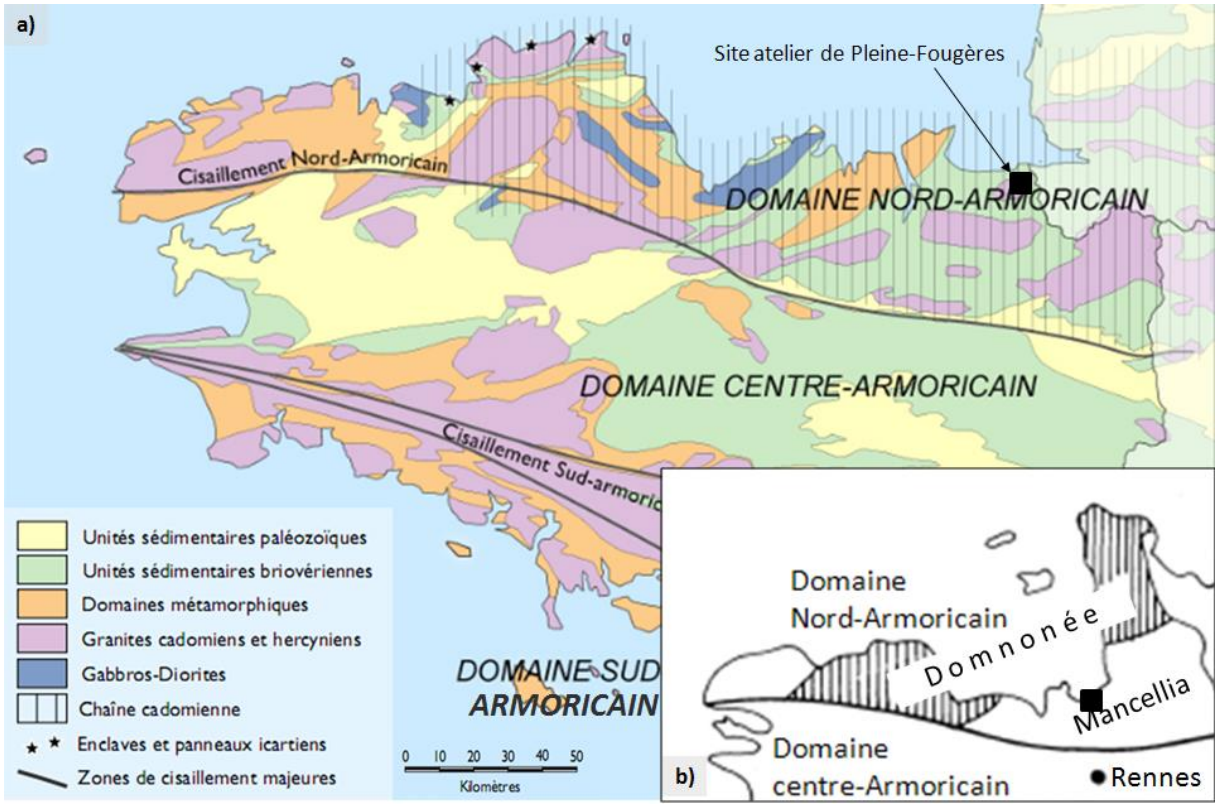

Figure 2-3. Carte géologique simplifiée de la Bretagne (a, UMR 6118, Université de Rennes 1, 2008) et localisation du domaine mancellien au sein du domaine Nord-armoricain (b, Bogdanoff et al., 1996).

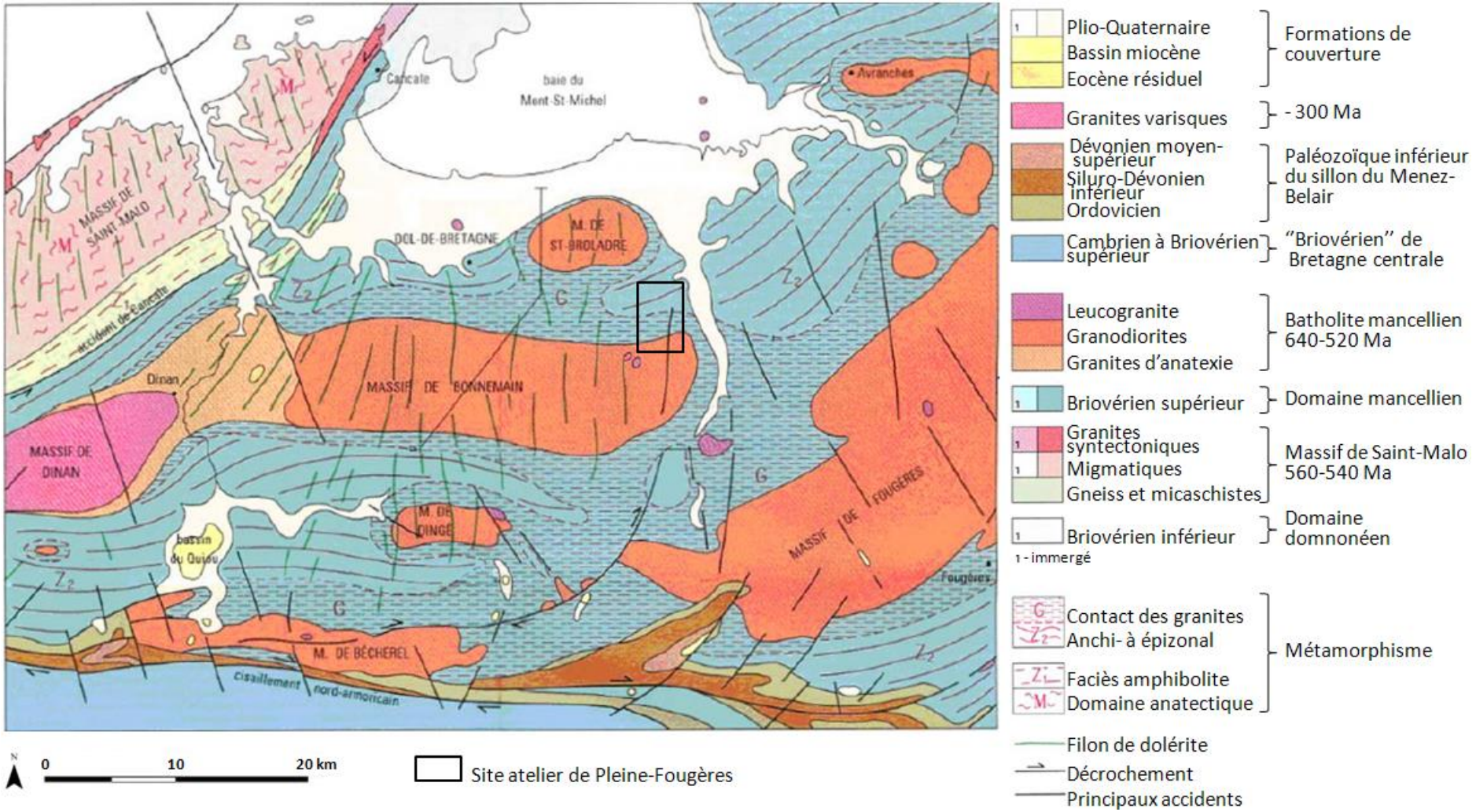

Figure 2-4. Schéma structural du domaine mancellien, extrait de la carte géologique de la France au 1:50 000, feuille de Dol-de-Bretagne (Bogdanoff et al., 1997).

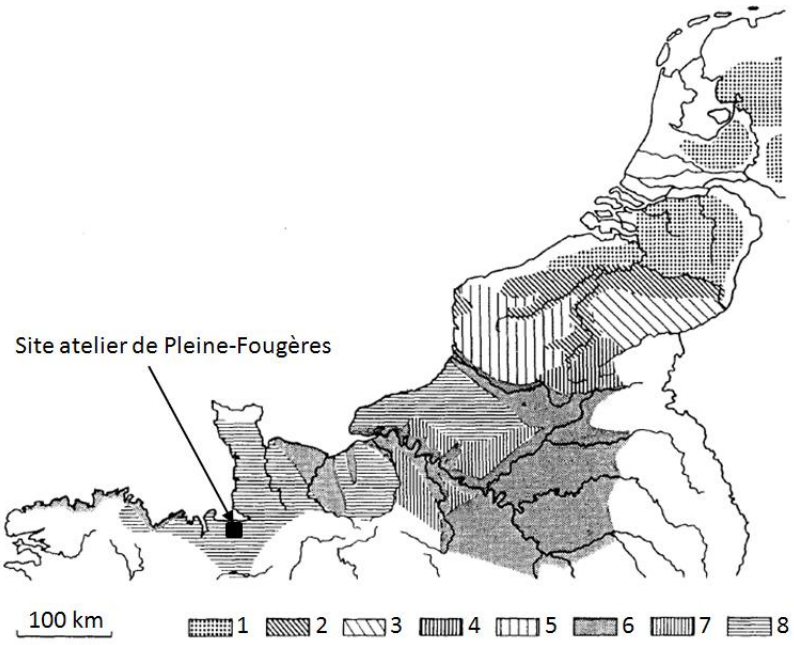

Figure 2-5. Cartographie des différents faciès de loess et de sables dans l'Europe de l'Ouest. 1 : sables de couverture, 2 : zone de transition, 3 : loess de Belgique (loess calcaire, limons à doublets, limons lités, fentes de gel), 4 : loess du nord-est de la France (loess calcaire sur limons lités, fentes de gel), 5 : loess du nord-ouest de la France (loess lités, fentes de gel), 6 : loess calcaire du Bassin Parisien, 7 : loess de l'est de la Normandie (limons à doublets sur loess calcaires), 8 : limons à doublets et limons bruns (Ouest de la Normandie et Bretagne) (Lebret and Lautridou, 1991).

2.1.3.2 Géologie locale du site d'étude

Le site atelier de Pleine-Fougères se situe au Nord du Massif de Bonnemain (Figure 2-4). Le site d'étude regroupe les principaux matériaux constituant le domaine mancellien (Figure 2-6a) : au sud les granodiorites intrusives du Massif de Bonnemain (batholite mancellien), au nord le schiste briovérien encaissant, et entre les deux des matériaux briovériens métamorphisés au contact des granodiorites (cornéennes et schistes tachetés). La granodiorite du site atelier de Pleine-Fougères est une granodiorite blanche à biotite, correspondant au type « Louvigné-du-Désert » (Jonin, 1981). L'âge de cette granodiorite a été estimé à 617 ± 12 Ma (Jonin and Vidal, 1975). Ces granodiorites ont une capacité d'altération forte (Lautridou et al., 1984). Le matériau briovérien est un schiste tendre de couleur verdâtre, s'altérant rapidement (2 à 3 ans au niveau des affleurements). Il présente des alternances de bancs massifs de grès grauwackeux et de siltites (massives ou finement litées). Les matériaux métamorphisés, schistes tachetés et cornéennes à cordiérite et biotite, sont plus difficilement altérables. Les cornéennes, en contact avec les granodiorites, sont des roches cristallines particulièrement résistantes.

La carte géologique montre la présence d'un filon de quartz au sud de la zone, ainsi que des zones de dépôts de limons éoliens au nord et au sud de la zone (Figure 2-6a). Cependant, les observations sur le terrain ainsi que la cartographie prédictive du matériau parental des sols de Bretagne (Figure 2-6b) donnent à penser que l'extension spatiale des limons est plus importante et recouvre une grande partie du site (son épaisseur étant très variable). Ces limons, jaunes à brun-jaunes, sont non carbonatés, lités (limons à doublets) et contiennent majoritairement du quartz, des argiles (illites et kaolinites), des vermiculites et des chlorites (Bogdanoff et al., 1996). La proportion de sables fins ne dépasse pas 15%.

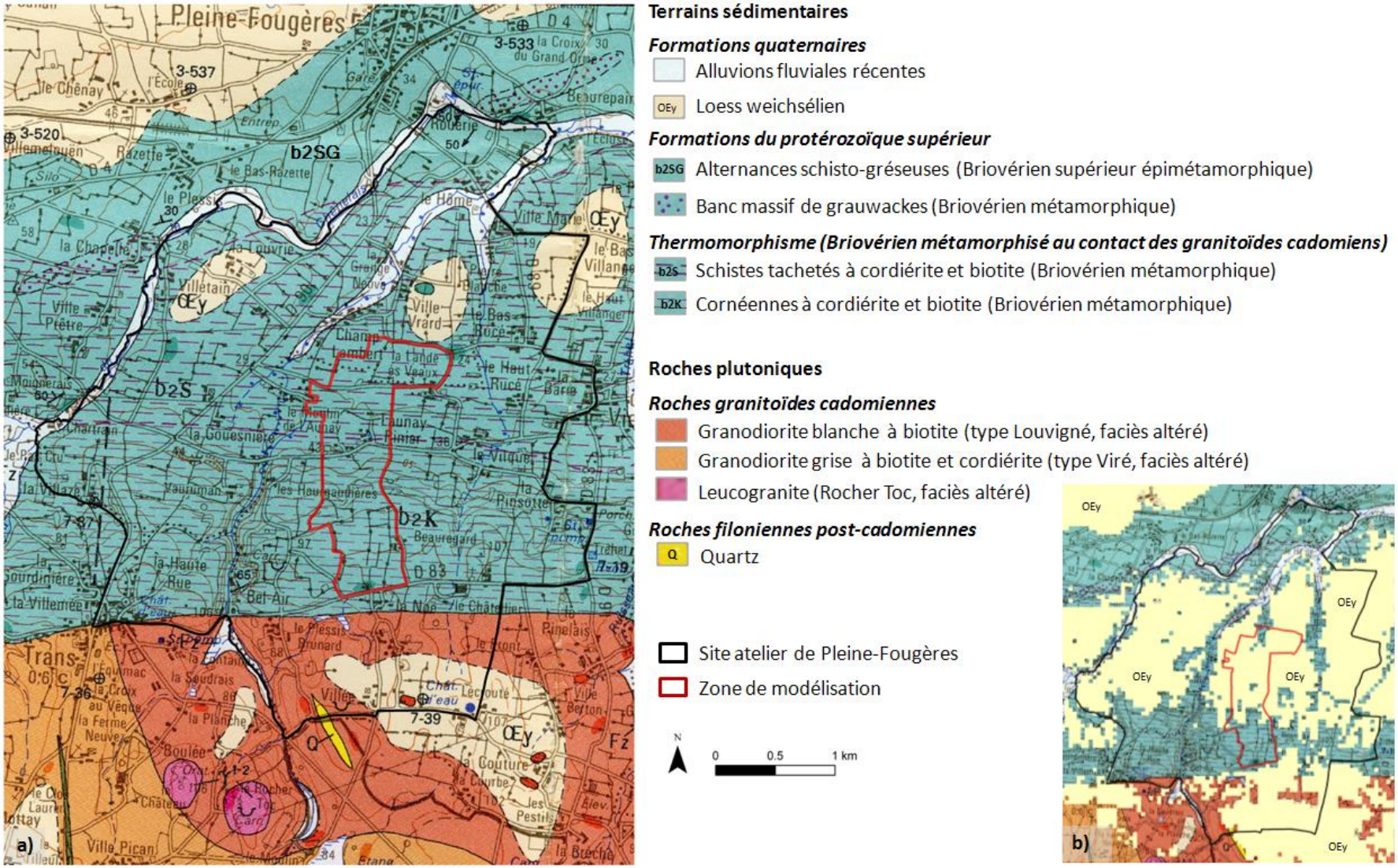

Figure 2-6. Géologie locale du site atelier de Pleine-Fougères. a) Extrait de la carte géologique de la France au 1 :50 000, feuille de Dol de Bretagne (Bogdanoff et Julien, 1996), b) extension des limons éoliens (cartographie prédictive du matériau parental, Lacoste et al., 2011 ; Annexe 1).

2.1.4 Géomorphologie

La topographie et l'implantation du réseau hydrographique actuel du site atelier de Pleine-Fougères sont fortement corrélées au type de substrat géologique, son histoire, son mode de formation et sa capacité à résister à l'altération. Le modèle actuel résulte d'une altération différentielle des matériaux, créant un paysage où s'opposent des reliefs abrupts (granodiorites et matériaux métamorphiques) et des reliefs plus mous (schistes et grès briovériens, roches assez tendres facilement entamés et déblayés par érosion). D'une manière générale, les reliefs sont modestes dans le domaine mancellien, dont le point culminant est atteint au niveau est des granodiorites du Massif de Bonnemain. Ce sommet du batholite est compris dans le site atelier de Pleine-Fougères. Les matériaux tendres du Briovérien sont façonnés en collines arrondies et sont parcourus de nombreux cours d'eau. Les dépôts de limons au Weichsélien se surimposent aux matériaux précédemment décrits, en colmatant la paléotopographie (Bogdanoff et al., 1996). Les limons éoliens ont été déposés par des vents dominants de secteur Ouest à Ouest/Nord-Ouest, et leur épaisseur actuelle est donc premièrement liée à l'orientation des pentes. A l'échelle d'un versant, on observe un phénomène de redistribution post-dépôts de ces limons, sous l'effet de l'érosion, avec une épaisseur de limon croissante de l'amont vers l'aval (Curmi, 1979).

La topographie du site atelier de Pleine-Fougères est de deux ordres. La topographie générale (variation de relief sur une distance de l'ordre de la centaine de mètres) est corrélée aux variations de substrat géologique (Figure 2-1b et Figure 2-6) : le sud de la zone d'étude comporte un plateau sur granodiorites et cornéennes, alors qu'au nord du site, séparée par un versant à plus forte pente, s'étend une plaine sur schiste briovérien. Le plateau présente un relief en creux, lié aux capacités d'altération variables de la granodiorite. Les cornéennes sont plus dures que les schistes tachetés, ce qui a provoqué la formation d'un glacis[11] montant vers les granodiorites. La limite nord de ce glacis correspond le plus souvent à la frontière entre les cornéennes et les schistes tachetés, alors que sa limite sud correspond à la frontière entre les granodiorites et les cornéennes. La zone a une altitude moyenne de 55 m, avec un minimum de 9 m au niveau de la plaine et un maximum de 110 m au niveau du plateau. Les pentes sont en moyenne de 6% sur l'ensemble de la zone ; elles sont respectivement de 4, 13 et 8% en moyenne au niveau de la plaine, du versant et du plateau. Le site est traversé par trois ruisseaux, affluents du Couesnon, orientés Nord-Sud et s'écoulant vers le Nord. Le ruisseau de Chênelais borde la partie Ouest du site atelier, le ruisseau de Tréhel borde sa partie Est, et le ruisseau du Petit Hermitage descend depuis la forêt de Villecartier (située sur le plateau de granodiorite au sud du site atelier) et sépare le site en son milieu.

Le site atelier de Pleine-Fougères présente également une microtopographie (variation de relief sur une distance de l'ordre du mètre), induite par des aménagements anthropiques (haies, talus, fossés, routes et chemins, Figure 2-7a et b) et qui se surimpose à la topographie générale.

2.1.5 Contexte pédologique

2.1.5.1 Pédogénèse

Des études sur la formation des sols ont été menées dans le pays de Fougères, dans un contexte géologique similaire à celui du site atelier de Pleine-Fougères (Van Vliet-Lanoë, 1990 ; Van Vliet-Lanöe et al., 1995). Le pays de Fougères, situé au sud-est de Pleine-Fougères, fait également

[11] Forme de relief non structurale consistant en une surface plane et peu inclinée (quelques degrés). (Dictionnaire de géologie, 2005)

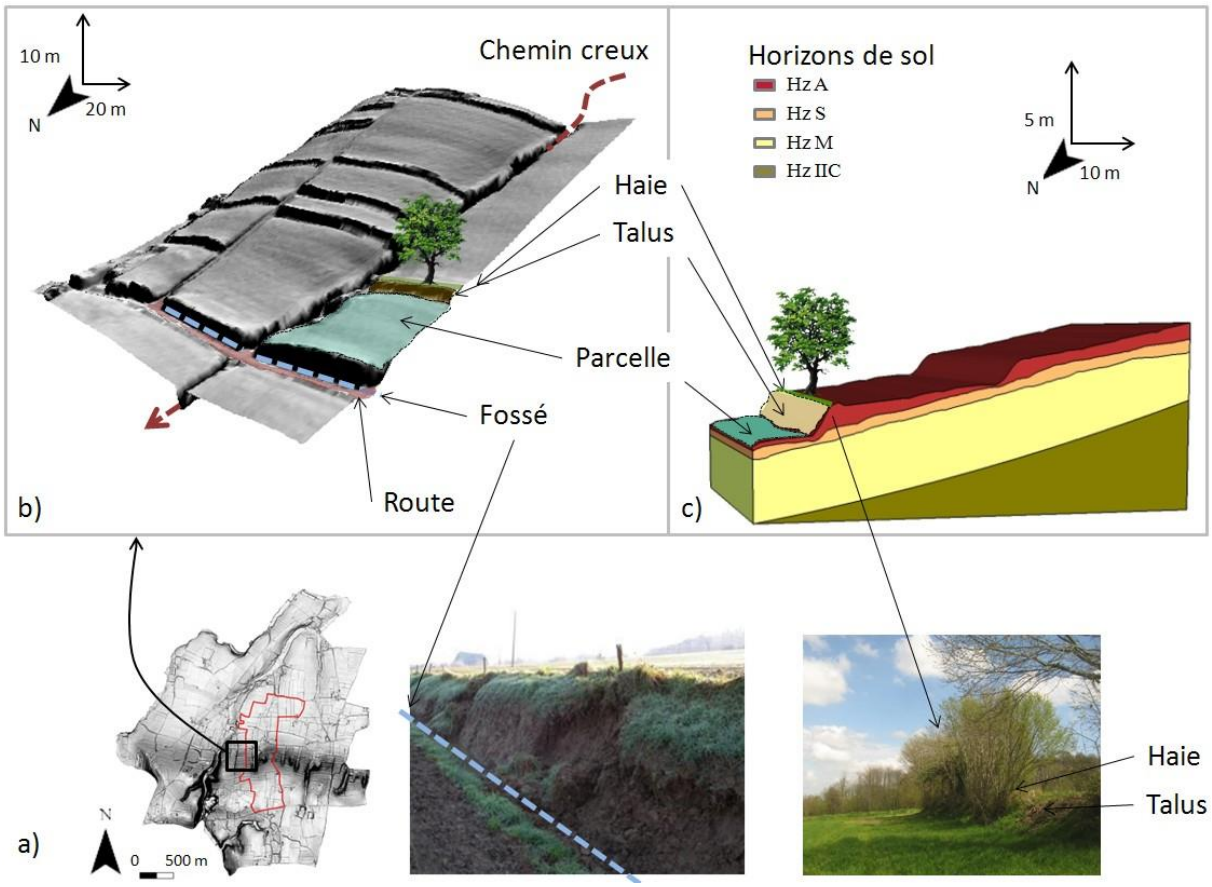

Figure 2-7. Description d'un versant du site atelier de Pleine-Fougères (a : localisation du versant au sein du site, b : représentation du versant en 3 dimensions, c : organisation des sols au niveau du versant. Photographies : illustration d'un fossé au pied d'un talus et d'une haie sur talus. Hz : horizon)

partie du domaine mancellien et présente les mêmes types de matériaux géologiques (granodiorites, dépôts lœssiques du Quaternaire). La cartographie des sols de cette zone montre que la distribution actuelle des sols est fortement corrélée à la topographie du substrat. Des observations pédostratigraphiques au niveau des limons éoliens du plateau granitique de Fougères ont permis de mettre en évidence l'intensité des phénomènes morphogénétiques et pédogénétiques pendant le Weichsélien et l'Holocène (période de réchauffement suivant le Weichsélien). Pendant le Weichsélien, la sédimentation et l'érosion restent faibles, malgré les dépôts de lœss qui est un matériau meuble et donc facilement remobilisable. La pédogénèse des sols développés dans les limons éoliens aurait débuté à l'Holocène[12] par des phénomènes d'éluviation des horizons supérieurs (formations d'horizons E et Bt), suivis par une brunification et une ferrolyse des horizons éluviés nouvellement formés. Quelques phénomènes plus anciens ont été recensés, consistant en une acidification et une podzolisation. Ces podzols se comportent à l'Holocène comme un matériau parental, et un enrichissement en aluminium a été noté dans d'anciens horizons éluviés. Cependant, la plupart des sites ayant été remaniés par l'activité humaine, il s'est révélé difficile de déterminer la chronologie des événements de la pédogénèse. L'Holocène est néanmoins une période stable, sans phénomène d'érosion majeur, ce qui permet l'installation d'un couvert végétal permanent

[12] Partie supérieure de l'ère Quaternaire, dont on fixe le début aux environs de 10 000 ans BP (Dictionnaire de géologie, 2005).

(biostasie). La pédogénèse se déroule sans perturbations majeures, et ceci jusqu'à la fin de la période Romaine. La fin du Haut Moyen-âge (IX-XI^{e} siècles) est marquée par un commencement de perturbation de la pédogénèse par l'activité humaine, menant à des dépôts minéraux et organiques dans les vallées de petits affluents (dépôts colluviaux) (Follain, 2006a). Pour cette région européenne au climat océanique tempéré, il s'avère que les phénomènes érosifs sont peu marqués dans des conditions périglaciaires, et absentes pendant les périodes interglaciaires sans occupation humaine (Van Vliet-Lanöe et al., 1995).

2.1.5.2 Les sols du site atelier de Pleine-Fougères

Les sols du site atelier de Pleine-Fougères se sont donc développés sur des matériaux géologiques d'origines et de caractéristiques très variables (Figure 2-6) : roches plutoniques (granodiorites), matériaux métamorphisés (cornéennes et schistes briovériens), matériaux encaissant briovériens (schiste tendre), limons éoliens du Quaternaire (Lacoste et al., 2011 ; Lemercier et al., 2011 ; Van Vliet-Lanoë, 1990 ; Van Vliet-Lanöe et al., 1995). La Figure 2-8 présente la répartition spatiale des différents types de sols présents sur le site : Brunisols, Luvisols, Rankosols, Colluviosols et Fluviosols (Référentiel Pédologique, 2008). Ces sols ont des épaisseurs variées, comprises entre 17 et 550 cm pour 371 sondages effectués, 65% des sols observés ayant une épaisseur supérieure à 80 cm (Figure 2-9a). Les horizons organo-minéraux (horizons A[13]) présentent également une large gamme d'épaisseur, comprises entre 3 et 250 cm, avec 51% des profils (sur un total de 415) présentant un horizon A d'une épaisseur supérieure à 30 cm (Figure 2-9b). L'organisation des sols, du point de vue de leur épaisseur totale et de l'épaisseur des horizons A, est liée d'une part au matériau parental des sols et d'autre part aux structures linéaires anthropiques (particulièrement les haies, avec ou sans talus ; Figure 2-7c). On trouve effectivement les sols les plus épais sur limons éoliens ou alluvions, et les sols les moins épais sur cornéennes et généralement sous forêt. Des épaississements d'horizons A sont généralement observés à l'amont de haies, notamment lorsque celles-ci sont dans des positions favorables au piégeage des particules de sol déplacées par érosion (Burel et al., 1993 ; Follain, 2006a). Ce type d'épaississement s'observe lorsque des haies se trouvent dans des situations globalement perpendiculaires à la pente, alors que des haies à la pente ont tendance à canaliser le ruissellement et à favoriser l'érosion hydrique. Ce phénomène est cependant complexe et dépend principalement de la topographie à l'échelle du versant et aux abords des haies (Follain et al., 2009).

L'hydromorphie des sols est également en relation avec la topographie du site, le matériau parental et les cours d'eau (Figure 2-10a). Les sols les plus hydromorphes se situent à proximité des cours d'eau, ou au niveau des zones de plus faibles pentes. Les sols bien drainés sont surtout développés sur cornéenne (sols peu épais du plateau) ou sur les schistes ne présentant pas de dépôt éoliens.

[13] Horizons « organo-minéraux » ou « hémi-organiques », c'est-à-dire contenant en mélange de la matière organique et de la matière minérale, situé à la base des horizons holorganiques s'ils existent, sinon à la partie supérieure du solum (Référentiel Pédologique, 2008)

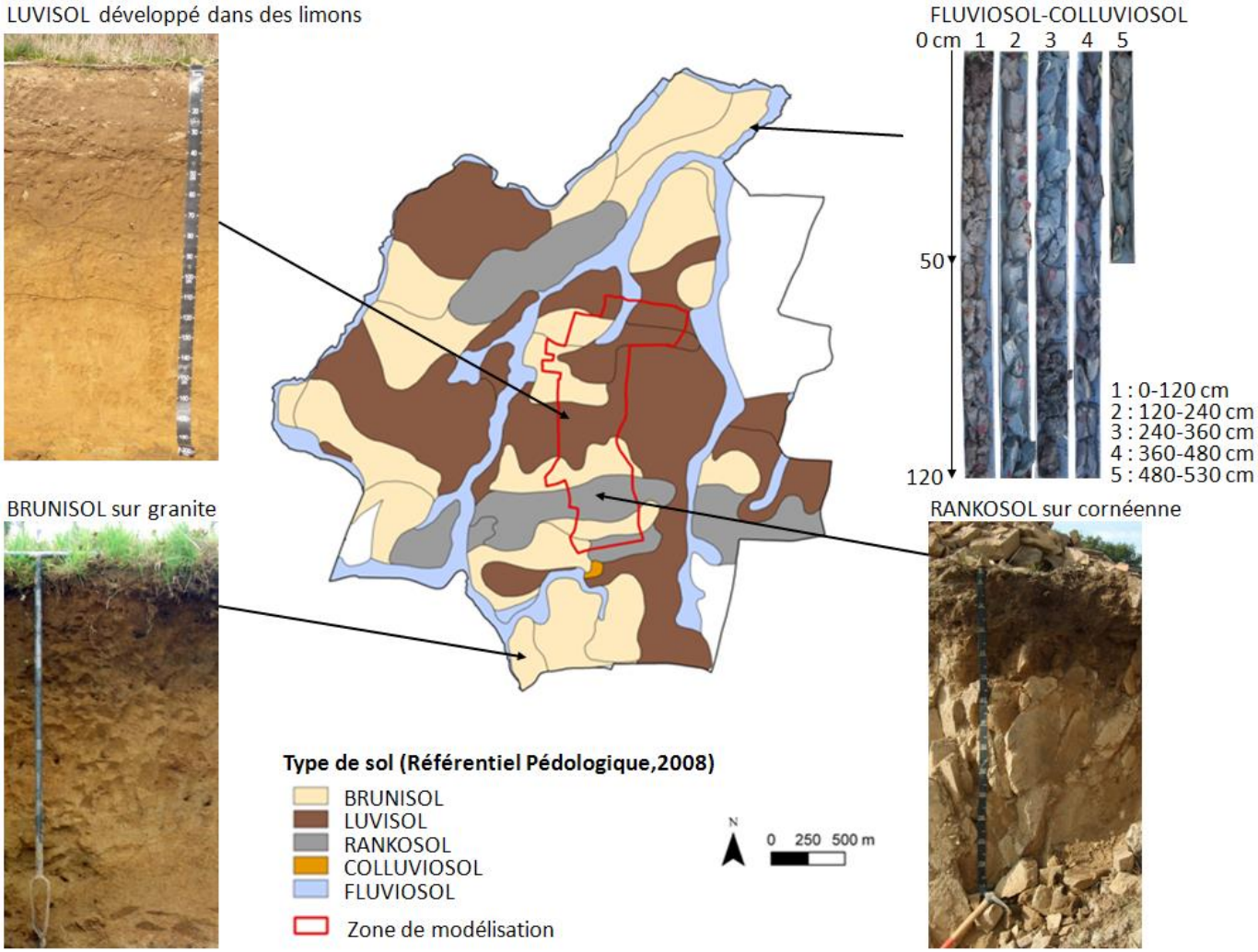

Figure 2-8. Principaux types de sol du site atelier de Pleine-Fougères (Walter, comm. Pers.).

Les sols du site atelier de Pleine-Fougères ont en majorité une texture de type limon moyen sableux[14], ce qui leur confère une forte sensibilité à la battance (Baize, 2000). Ils contiennent en moyenne 13% d'argile, 21% de limons fins, 42% de limons grossiers, 16% de sables fins et 8% de sables grossiers[15]. La Figure 2-11 montre les courbes de fréquence volumique cumulée obtenues par granulométrie laser (granulomètre Cillas 1180, Université de Rennes1) sur 60 échantillons répartis sur le site atelier de Pleine-Fougères. Ces courbes montrent une large prédominance de la fraction limoneuse (avec en moyenne 5% d'argile, 40% de limons fins, 31% de limons grossiers, 23% de sables fins et moins de 1% de sables grossiers). Ce type de courbe granulométrique cumulée est à mettre en relation avec celle des limons éoliens du nord-ouest de l'Europe, qualifiée de sigmoïde dissymétrique par Lautridou (1985). Si l'on calcule les indices granulométriques proposés par Lautridou (1985) pour identifier les types de limons, on obtient une fraction limoneuse représentant en moyenne 63 à 71% de la fraction totale, un rapport limons grossiers sur limons fins de 0,81 à 2,12 selon la méthode d'analyse utilisée (texture par laser ou décantation), et un rapport argiles fines sur argiles totales de 0,03 (granulométrie laser). Ce dernier résultat apparait sous-estimé, allant de pair avec la sous-estimation des argiles par la méthode de granulométrie laser par rapport à la méthode par décantation. Cependant, ces résultats (proches de ceux rencontrés pour des limons éoliens) semblent confirmer que les sols du site atelier de Pleine-Fougères se sont en partie développés dans les dépôts éoliens du Weichsélien, mais qu'une partie de la fraction limoneuse provient certainement de l'altération des roches sous-jacentes.

Les sols du site atelier de Pleine-Fougères ont une teneur moyenne en C organique de 12 g kg^{-1} si l'on considère une épaisseur de sol de 105 cm (Figure 2-12). Elle est en moyenne de 16 g kg^{-1} pour les horizons de surface (0-30 cm) et de 8 g kg^{-1} pour les horizons profonds (30-105 cm). Leur densité apparente moyenne est de 1,4 (sur 0-105 cm). Elle est de 1,3 pour les horizons de surface (0-30 cm) et de 1,5 pour les horizons profonds (30-105 cm).

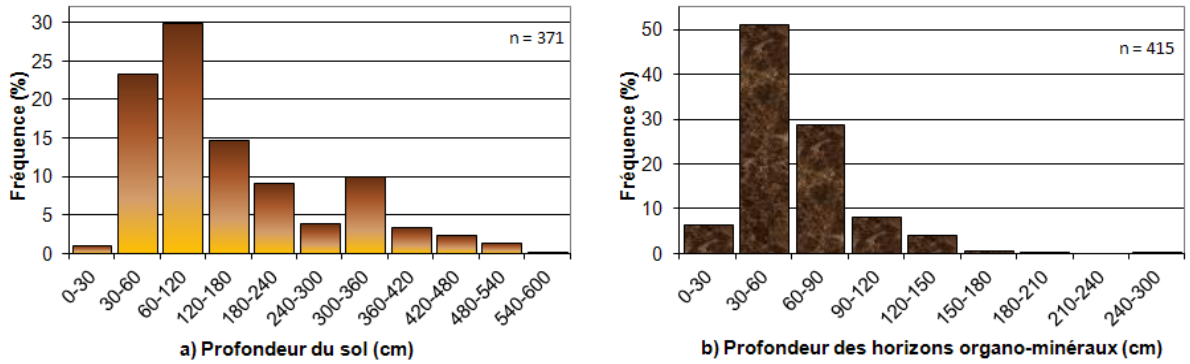

Figure 2-9. Epaisseur des sols et des horizons organo-minéraux du site atelier de Pleine-Fougères (profils de sols effectués dans le cadre du programme ANR LandSoil, voir partie 2.3 pour plus d'informations).

[14] Classe LMS du diagramme des textures de la chambre d'agriculture de l'Aisne, correspondant à la classe Lsa (limon sablo-argileux) du diagramme des textures GEPPA (Baize et Jabiol, 1995)

[15] Texture déterminée la méthode par décantation (granulométrie cinq fractions, Laboratoire d'analyse des sol d'Arras)

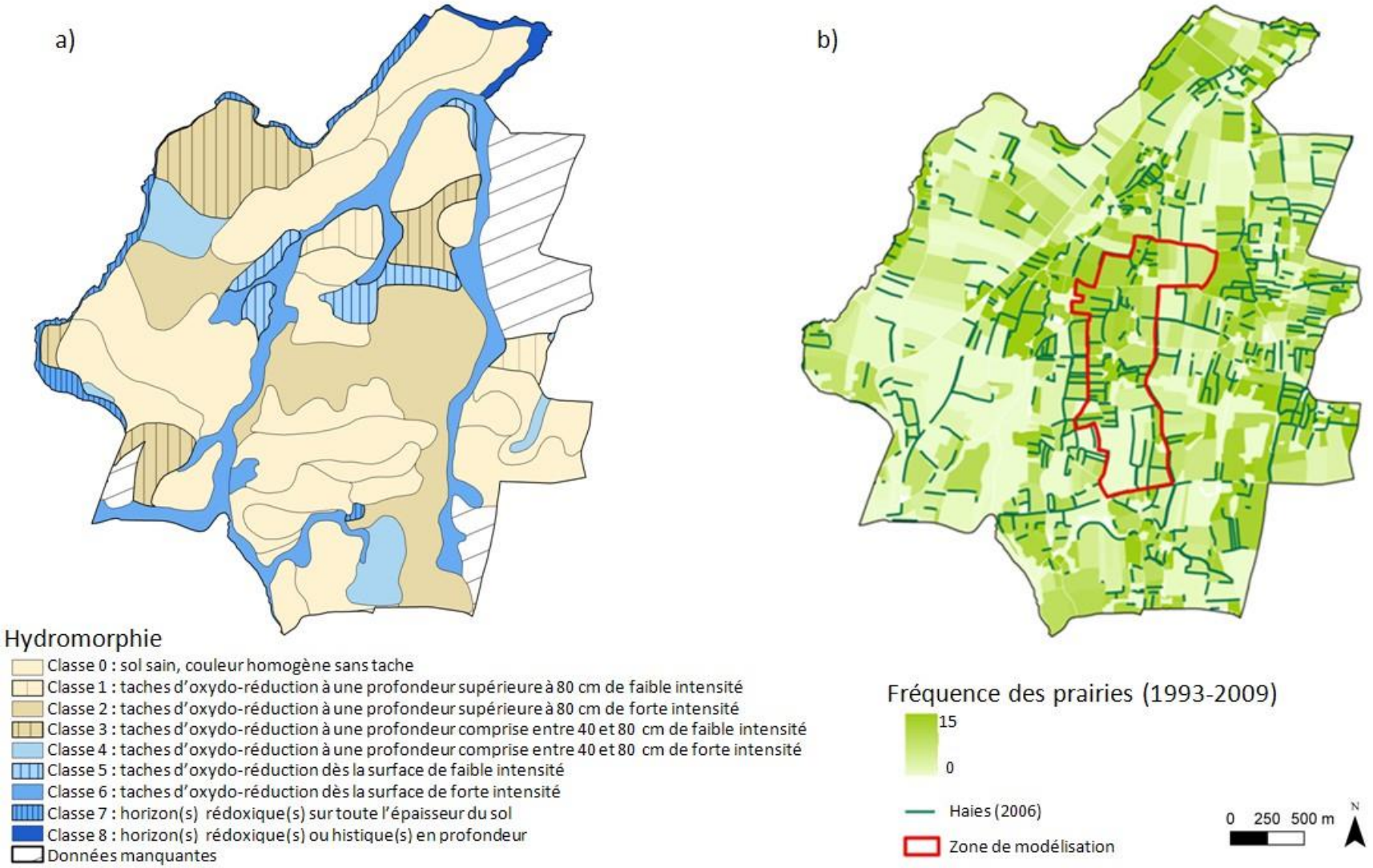

Figure 2-10. Hydromorphie des sols et fréquence d'occupation en prairie. a) cartographie d'après la carte pédologique réalisée par Walter (comm. pers.). Classe d'hydromorphie d'après Rivière et al. (1992) ; b) données d'occupation du sol acquises par photo-interprétation (source : Zone Atelier Armorique)

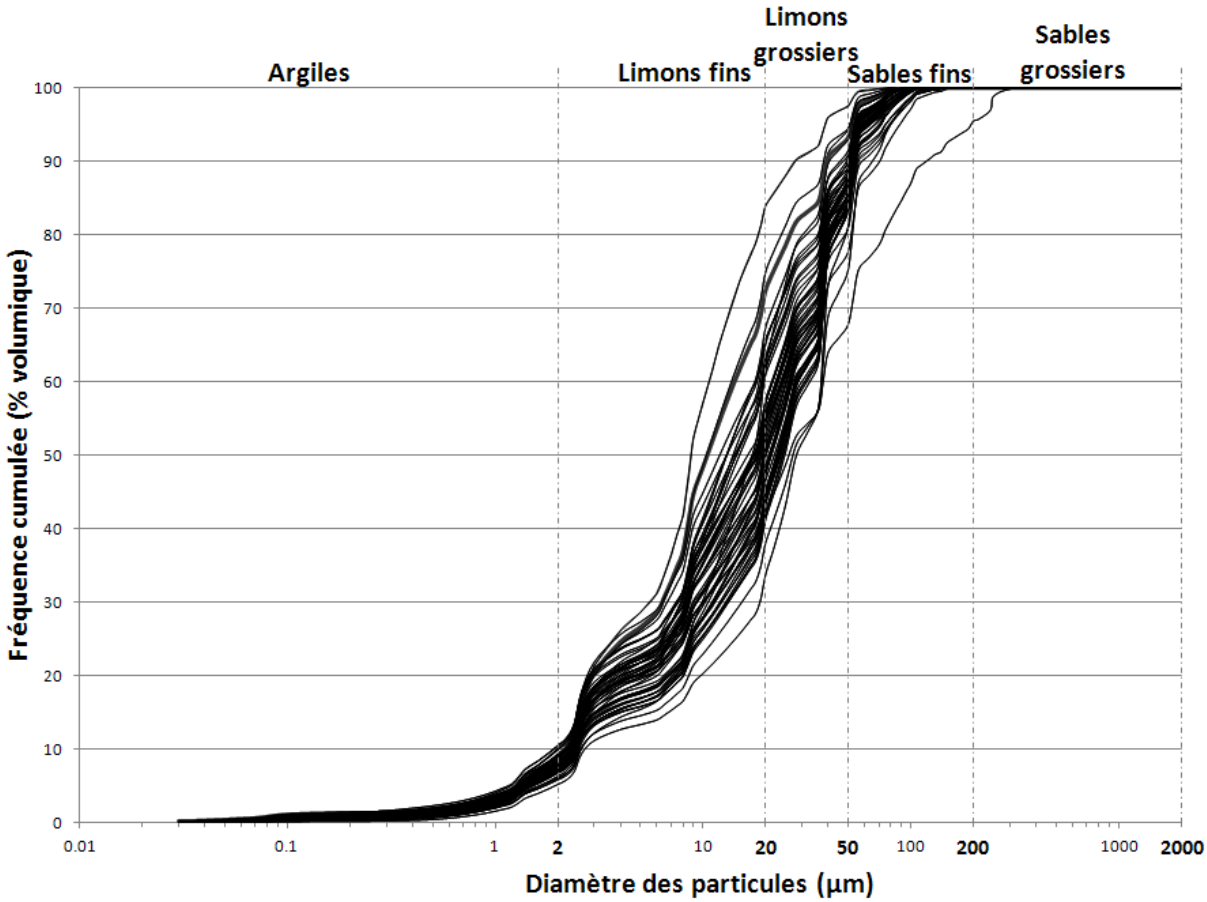

Figure 2-11. Fréquence cumulée de la taille des particules obtenue par granulométrie laser pour 60 échantillons de sol prélevés entre 0 et 60 cm de profondeur sur le site atelier de Pleine-Fougères (destruction de la matière organique à l'eau oxygénée et dispersion à l'hexamétaphosphate de sodium).

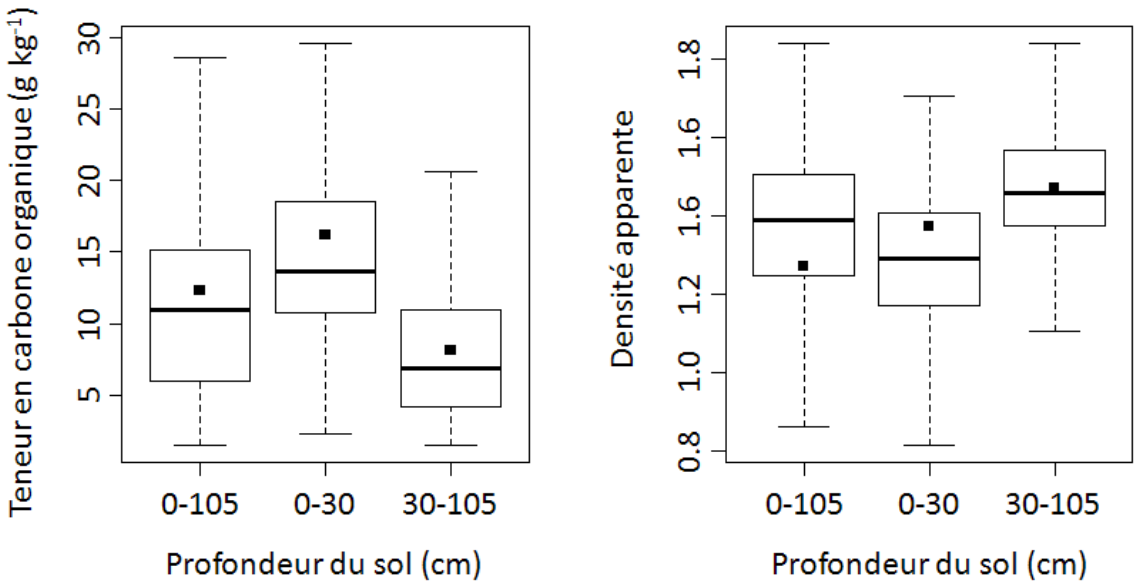

Figure 2-12. Teneurs en C organique et densité apparente des sols du site atelier de Pleine-Fougères (moyennes représentées par des carrés noirs ; échantillons prélevés dans le cadre du programme ANR LandSoil, voir partie 2.3 pour plus de détails)

2.1.6 Structure du paysage et occupation du sol

Le site atelier de Pleine-Fougères est une zone bocagère majoritairement orientée vers la polyculture et l'élevage laitier (Annexe 2). Le site est caractérisé par un gradient paysager allant d'un bocage dense avec des parcelles relativement petites et bordées de haies dans la partie est du site (communes de Trans-la-Forêt et Vieux-Viel), à un bocage lâche avec des parcelles de plus grande taille dans la plaine au nord-ouest du site (commune de Pleine-Fougères). La densité de haies est actuellement de 90 m ha^{-1} en moyenne à l'échelle du site, et la taille moyenne des parcelles est de 1 ha (maximum de 8 ha). Les haies bordant les parcelles sont le plus souvent constituées de chênes (*Quercus robur*) émondés en ragosses, avec parfois quelques châtaigniers émondés (*Castanea sativa*) et des chênes en haut jet, mais aussi des cépées de châtaigniers et des prunelliers (*Prunus spinosa*). Elles sont souvent plantées sur talus.

Le parcellaire et les structures paysagères sur le site ont fortement évolué au cours du temps (Figure 2-13). La densité de bocage a varié au cours des siècles, avec un maximum atteint entre 1850 et 1950 (Marguerie et al., 2003). Des documents d'archive comme le cadastre napoléonien (levé en 1834 au niveau du site atelier de Pleine-Fougères) ou des photos aériennes permettent de retracer l'évolution du parcellaire et, dans certains cas, des réseaux de haies. Selon ces documents, le découpage parcellaire était plus important au 19ème siècle : d'après le cadastre napoléonien (conservé aux archives départementales d'Ille-et-Vilaine) la taille moyenne des parcelles était de 0,4 ha en 1834. Cependant le cadastre napoléonien ne permet pas d'identifier la nature des limites de parcelles. Ces limites peuvent être des limites physiques matérialisées par un muret ou une haie (avec ou sans talus), des limites d'usage séparant deux propriétaires, ou des limites séparant deux cultures (Archives municipales de Rennes, 2005). Il est donc difficile d'estimer l'étendue du bocage à la fin du XIXème. Néanmoins, la comparaison du parcellaire napoléonien avec celui de 1952 (obtenu à partir de photos aériennes) suggère que la majorité des parcelles devaient être limitées par des haies. Le parcellaire de 1952 montre en effet une répartition de parcelles proche de celle de 1834, avec des parcelles de 0,6 ha en moyenne (maximum de 6 ha) et une forte densité de haies (250 m ha^{-1} en moyenne). On peut également observer que de nombreuses parcelles étaient plantées d'arbres en 1952, majoritairement des vergers de pommiers, dont il reste encore aujourd'hui quelques traces. Le parcellaire et les structures paysagères ont fortement évolué depuis les années 1960, en lien avec l'évolution des techniques agricoles et les aménagements fonciers. La commune de Pleine-Fougères a été remembrée en 1992-1993, ce qui explique que le bocage y soit aujourd'hui moins dense. Les communes de Vieux-Viel et Trans-la-Forêt n'ont pas été remembrées, mais des haies ont été localement arasées. La connaissance de l'évolution du parcellaire est importante pour comprendre l'organisation actuelle des sols, notamment les caractéristiques des horizons organo-minéraux, car celle-ci a souvent été influencée par la présence d'anciennes structures, encore présentes ou non (Follain et al., 2009).

L'activité agricole dominante est l'élevage bovin laitier, associé à des successions culturales incluant le maïs (*Zea mays*), des céréales (blé d'hiver (*Triticum aestivum*), avoine (*Avena sativa*), orge (*Hordeum vulgare)*) et des prairies temporaires ou permanentes. Les prairies sont réparties sur la totalité du site (Figure 2-10b), mais les prairies permanentes sont préférentiellement localisées près des cours d'eau, sur les sols les plus hydromorphes. Les prairies temporaires (majoritairement du ray grass italien, *Lolium multiflorum*) sont plus généralement situées au niveau des sols bien drainés (par exemple sur le plateau) ou sur les plus grandes parcelles (résultat du remembrement agricole ou de l'arasement ponctuel de haies).

Figure 2-13. Evolution du parcellaire et du bocage sur le site atelier de Pleine-Fougères (1834-2009). Sources : cadastre napoléonien (1834, archives départementales d'Ille-et-Vilaine), photographies aériennes (1952 et 2009, IGN).

2.2 Modélisation couplée de la redistribution des sols et de la dynamique du carbone organique

L'objectif est de simuler l'évolution des épaisseurs de sol et des stocks de C organique dans les horizons organo-minéraux (horizons A) sous l'effet de l'évolution de la structure du paysage et du climat, à l'échelle d'un paysage agricole. La modélisation repose sur deux modèles : un modèle simulant la redistribution des sols (LandSoil) et un modèle simulant la dynamique du C organique.

2.2.1 LandSoil : modèle de redistribution des sols à l'échelle du paysage

Le modèle LandSoil est un modèle à base expert, développé par Ciampalini et al. (in press) à partir du modèle Stream (Cerdan et al., 2002a ; Cerdan et al., 2002b ; Souchere et al., 2003 ; Souchere et al., 1998) et du modèle WaTEM/SEDEM (Govers et al., 1994). LandSoil est un modèle spatialisé, qui fonctionne à la résolution temporelle de l'événement pluvieux, et qui représente les processus d'érosion hydrique et aratoire à l'échelle du paysage (versant ou bassin versant). La formation de sol n'est pas considérée dans le modèle.

Les principales spécificités du modèle sont la prise en compte des états de surface du sol (faciès, rugosité, couverture végétal) pour caractériser son aptitude à l'infiltration ou au ruissellement et à l'émission de charges solides, ainsi que la prise en compte de la structure du paysage (topographie, parcellaire, travail du sol, structures anthropiques, fossés, haies...) pour définir la circulation du ruissellement et les redistributions de sol.

2.2.1.1 Entrées et sorties du modèle LandSoil

Pour modéliser la redistribution des sols à l'échelle du paysage, LandSoil nécessite les données d'entrée suivantes :

(i) Données météorologiques au pas de temps de l'événement pluvieux.
Un événement pluvieux est défini comme une pluie sans interruption de plus de 3h. Chaque événement pluvieux est caractérisé par 4 variables :
- le cumul pluviométrique au cours de l'événement (mm)
- la durée efficace de l'événement pluvieux (h)
- l'intensité maximale calculée à 6 min (mm h^{-1})
- le cumul des pluies antécédentes sur 24h (mm)

(ii) Données topographiques :
- altitude (Modèle Numérique d'Altitude, MNA, au format raster)

(iii) Données pédologiques :
- profondeur initiale des sols (m), au format raster
- cartographie de la variation spatiale de la capacité d'infiltration des sols (variation en % du taux initial, facultatif), au format raster

(iv) Données sur l'organisation du paysage :
- parcellaire, au format vecteur
- cartographie des types de limites de parcelles (fossé, route, dérayure, limite simple), au format vecteur

(v) Données sur les occupations du sol et les pratiques culturales au pas de temps mensuel :
- rotations culturales et variations d'état de surface du sol associées
- type et fréquence du travail du sol

Après chaque événement (pluvieux ou aratoire), les sorties du modèle LandSoil sont les suivantes pour toute maille élémentaire :

(i) altitude actualisée(m)
(ii) profondeur du sol actualisée (m)

2.2.1.2 Modélisation de l'érosion hydrique

La modélisation de l'érosion hydrique (diffuse ou linéaire) repose sur le calcul du flux total (volume d'eau ruisselé auquel est associée une teneur en matières en suspension) au pas de l'événement pluvieux. La démarche globale de modélisation de l'érosion hydrique est présentée dans la Figure 2-14.

2.2.1.2.1 Le ruissellement

A chaque événement pluvieux, une capacité d'infiltration et une pluie d'imbibition sont déterminées pour chaque pixel du bassin versant modélisé (Cerdan et al., 2002b). La capacité d'infiltration, i.e. le taux d'infiltration atteint lorsque le sol est à saturation (régime constant), est définie selon les paramètres d'état de surface du sol (facies, rugosité et couverture végétale du sol) à partir d'un tableau de règles de correspondance (Table 2-1). Par exemple, les sols ayant développé une croûte de battance et présentant une rugosité et une couverture végétale faibles ont une capacité d'infiltration faible, alors que les sols avec une forte rugosité et un état de surface fragmentaire ont une capacité d'infiltration élevée. La pluie d'imbibition (quantité d'eau nécessaire pour déclencher le ruissellement) est définie à partir d'un tableau de règles de correspondance, reliant la capacité d'infiltration et la pluie antécédente dans les 48h précédant l'événement considéré (Table 2-2). Les tableaux de règles doivent être paramétrés pour le site d'étude.

Un bilan élémentaire Infiltration / ruissellement (B) est calculé sur chaque pixel, à partir de la hauteur de pluie et de sa durée :

$$B = RR - PI - (IR \times D_{ef}) \quad (1)$$

Avec :

RR = hauteur d'eau au cours de l'événement pluvieux (mm)

PI = pluie d'imbibition (mm)

IR = capacité d'infiltration (mm h^{-1})

D_{ef}= durée efficace de l'événement pluvieux (durée pendant laquelle l'intensité de l'événement pluvieux est supérieure à 2 mm h^{-1}, h)

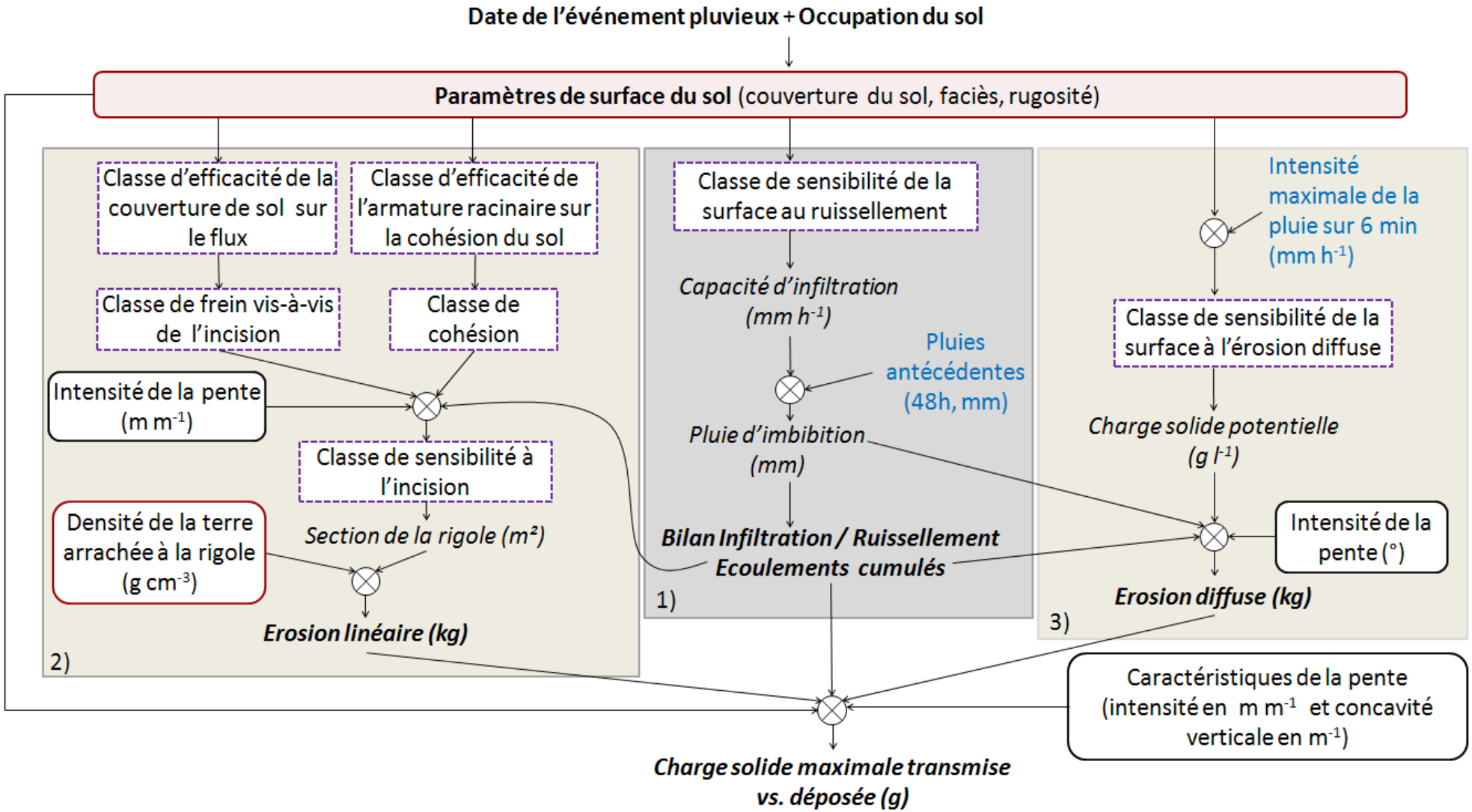

Figure 2-14. Représentation schématique de la modélisation de l'érosion hydrique par le modèle LandSoil (1 : calcul du bilan infiltration vs. ruissellement, 2 : simulation de l'érosion linéaire, 3 : simulation de l'érosion diffuse).

Table 2-1 Détermination des taux d'infiltration des sols selon les combinaisons de paramètres de surface du sol.

		Facies			
Rugosité[a]	Couverture végétale[b]	F0	F11	F12	F2
0 - 1 cm	< 20 %	10	10	5	2
	21-60 %	20	10	5	2
	> 61 %	50	20	10	5
1 - 2 cm	< 20 %	20	10	5	2
	21-60 %	50	20	10	2
	> 61 %	50	20	10	5
2 - 5 cm	< 20 %	50	20	10	5
	21-60 %	50	20	10	5
	> 61 %	50	50	20	10
5 - 10 cm	< 20 %	50	20	10	5
	21-60 %	50	50	20	10
	> 61 %	50	50	50	10
> 10 cm	< 20 %	50	20	20	10
	21-60 %	50	50	50	10
	> 61 %	50	50	50	10

[a] La rugosité de la surface du sol est définie par la différence de hauteur entre les points les plus bas et les points les plus hauts des micro dépressions du sol (Ludwig et al., 1995).

[b] Les classes de couverture du sol sont définies par le pourcentage de surface du sol recouvert par les cultures en place ou par leurs résidus.

[c] Quatre états de fermeture du sol sont définis. F0 : état initial fragmentaire ; F11 : état fragmentaire altéré avec formation d'une croûte de battance structural ; F12 : apparition locale d'une croûte de dépôt ; F2 : croûte de dépôt généralisée. Ces faciès ont été décrits en détail par (Bresson et Boiffin, 1990).

Table 2-2 Détermination des pluies d'imbibition selon la capacité d'infiltration et les pluies antécédentes.

	Pluies antécédentes* (mm)			
Capacité d'infiltration (mm h^{-1})	0	0 - 15	16 - 40	> 40
50	20	15	12	8
20	15	12	8	5
10	12	8	5	2
5	8	5	2	1
2	5	2	1	0

* quantité de pluie pendant les 48h précédent l'événement pluvieux

Le chemin du ruissellement à l'échelle du bassin est déterminé à partir de la topographie sur la base d'un modèle de drainage unidirectionnel (Jenson and Domingue, 1988 ; Souchere et al., 1998). La direction du ruissellement est modifiée par la direction du travail du sol et par les structures linéaires du paysage telles que les fossés, haies et dérayures (Souchere et al., 1998).

Le volume ruisselé (volume cumulé entrant dans un pixel) est calculé en tout point du bassin par itérations successives, de l'amont du bassin à l'exutoire, selon l'Equation (2) (Cerdan et al., 2002b) :

$$V = aB10^{-3} + \Sigma V_i \quad (2)$$

Avec :
V = ruissellement cumulé quittant le pixel (m^3)
a = taille du pixel (m^2)
B = ruissellement produit par le pixel (mm)
V_i = ruissellement provenant d'un pixel amont (m^3)

2.2.1.2.2 L'érosion diffuse

Lorsque le ruissellement se produit au cours d'un événement pluvieux, LandSoil modélise l'érosion diffuse des sols, i.e. la remobilisation de particules du sol détachées par effet splash sous l'action des gouttes d'eau. La concentration du ruissellement en sédiment (γ, g l^{-1}) est définie à partir d'un tableau de règles de correspondance, reliant les paramètres de surface du sol et l'intensité maximale de l'événement pluvieux (Table 2-3). L'intensité maximale de l'événement est calculée à partir de données météorologiques au pas de temps de 6 min.

La perte de sol par érosion diffuse (Mi, kg) est calculée pour chaque pixel en intégrant la concentration en sédiment (γ) au volume ruisselé (V). L'influence de la pente sur la perte en sol à l'échelle du pixel est prise en compte en intégrant une fonction S_f, basée sur le modèle WEPP (Laflen et al., 1991). Ceci permet de moduler la perte de sol le long de la pente. La perte de sol (Mi) est alors calculée selon l'Equation 4.

$$Mi = [\gamma + \gamma (S_f - S^*)] V \quad (4)$$

Avec :
$S_f = 1.05+0.85e^{-4\sin\vartheta}$. S_f est un facteur de pente sans dimension, θ étant la pente locale (°).
S^* = pente moyenne de la parcelle après avoir appliqué la fonction S_f (°)

2.2.1.2.3 L'érosion linéaire

La modélisation de l'érosion linéaire est basée sur des relations empiriques portant sur les relations entre les propriétés de surface et la taille des ravines produites (Souchere et al., 2003). La sensibilité à l'érosion linéaire (Ω) est calculée selon l'équation (5).

$$\Omega = friction \times cohésion \times V \times S \quad (5)$$

Avec :
friction = (classe)
cohésion = (classe)
V = ruissellement (m^3)
S = l'intensité de la pente (m m^{-1})

Table 2-3 Détermination de la concentration en sédiments du ruissellement selon les combinaisons de paramètres de surface du sol et d'intensité maximale de l'événement pluvieux.

Rugosité[a]	Coverture végétale[b]	Intensité maximal ($mm\ h^{-1}$)	Facies[c]			
			F0	F1	F12	F2
0 - 1 cm	< 20 %	0 - 10	0	2	0	2
		40 - 10	0	5	2	5
		> 40	2	10	5	10
	21-60 %	0 - 10	0	0	0	0
		40 - 10	0	2	0	2
		> 40	2	5	2	5
	> 61 %	0 - 10	0	0	0	0
		40 - 10	0	2	0	2
		> 40	2	5	2	5
1 - 2 cm	< 20 %	0 - 10	0	0	0	0
		40 - 10	2	10	5	10
		> 40	5	15	10	15
	21-60 %	0 - 10	0	2	0	2
		40 - 10	0	5	2	5
		> 40	2	10	5	10
	> 61 %	0 - 10	0	2	0	2
		40 - 10	0	5	2	5
		> 40	2	10	5	10
2 - 5 cm	< 20 %	0 - 10	0	0	0	0
		40 - 10	2	10	5	10
		> 40	5	15	10	15
	21-60 %	0 - 10	0	2	0	2
		40 - 10	0	5	2	5
		> 40	2	10	5	10
	> 61 %	0 - 10	0	2	0	2
		40 - 10	0	5	2	5
		> 40	2	10	5	10

[a] La rugosité de la surface du sol est définie par la différence de hauteur entre les points les plus bas et les points les plus hauts des micro dépressions du sol (Ludwig et al., 1995).

[b] Les classes de couverture du sol sont définies par le pourcentage de surface du sol recouvert par les cultures en place ou par leurs résidus.

[c] Quatre états de fermeture du sol sont définis. F0: état initial fragmentaire ; F11: état fragmentaire altéré avec formation d'une croûte de battance structural ; F12: apparition locale d'une croûte de dépôt ; F2: croûte de dépôt généralisée. Ces faciès ont été décrits en détail par Bresson et Boiffin (1990).

Les paramètres de friction et de cohésion reposent sur des combinaisons de paramètres de surface du sol (type d'occupation du sol et rugosité du sol). Il n'y a modélisation d'érosion linéaire que si le ruissellement concentré atteint un certain seuil, défini par une aire drainée minimum de 0,6 ha et une longueur de flux minimum de 80 m (Ludwig et al., 1996).

La section (*Kr, m²*) de la ravine est ensuite déterminée par l'équation (6).

$$Kr = \Phi\Omega \quad (6)$$

Avec :

Φ = le volume ruisselé amont par ravine ($m^2\ m^{-3}$)

Ω = classe de sensibilité à l'érosion linéaire

La perte de sol par pixel (E, kg) est alors définie par l'Equation (7).

$$E = \rho\lambda Kr \quad (7)$$

Avec :

Kr = section de la ravine (m^2)

ρ = masse volumique apparente du sol arraché à la ravine ($kg\ m^{-3}$)

λ = classe dimension du pixel (m)

2.2.1.2.4 Dépôt

Le transport de sédiments dans les volumes ruisselés est limité par une concentration maximale en sédiments transmise par un pixel. La charge solide maximale est définie par trois critères indépendants (Table 2-4) : l'occupation du sol, la couverture végétale et la topographie locale (définie par la courbure verticale et la pente). Un dépôt de sol est simulé si la concentration en sédiments est supérieure à la valeur fixée de charge solide maximale.

Table 2-4 Détermination de la charge solide maximale transmise par un pixel par le ruissellement.

Critère	Valeur seuil	Charge solide maximale transmise ($g\ l^{-1}$)
Occupation du sol	Prairie permanente	5
Couverture végétale	> 60 %	10
Pente	< 5 %	
et		10
Concavité verticale	> 0,055	

2.2.1.3 Modélisation de l'érosion aratoire

La redistribution de sol liée au travail du sol est calculée au pas de temps de l'événement aratoire. L'érosion aratoire est modélisée par l'équation (8).

$$Qs = -K_t S \quad (8)$$

Avec :

Qs = le flux de sédiment ($kg\ m^{-1}$)

K_t = le coefficient d'érosion aratoire ($kg\ m^{-1}$)

S = l'intensité de la pente ($m\ m^{-1}$)

Les coefficients d'érosion aratoire sont à adapter au type de terrain (caractéristiques du sol, topographie) ; ainsi qu'au type de travail du sol.

2.2.1.4 Calibration du modèle LandSoil pour la modélisation de la redistribution des sols de la zone atelier de Pleine-Fougères

Par héritage du modèle STREAM, les paramètres et tableau de règles par défaut implémentés dans le modèle LandSoil ceux définis pour les Luvisols limoneux du Pays de Caux. Un travail spécifique a été réalisé pour adapter ces paramètres à l'utilisation de LandSoil sur la zone atelier de Pleine-Fougères : il sera présenté dans le chapitre 3.

2.2.2 Modèle de dynamique du C à l'échelle du paysage

Le modèle permet de représenter la dynamique du C dans les 3 dimensions de l'espace : l'évolution des stocks de C est modélisée en toute localisation du paysage et pour les différents horizons contenant de la matière organique. Le modèle comprend un module "paysage" permettant de gérer les entrées de C à l'échelle du paysage, un module de dynamique du C et un module de redistribution du sol.

La dynamique des stocks de C organique dans le sol repose sur le modèle RothC 26-3 (Coleman and Jenkinson, 1996). RothC est conçu pour simuler le turnover du C dans l'horizon de surface d'un sol non saturé en eau. Il a été calibré initialement pour les prairies, la forêt, et les cultures en climat européen tempéré, et validé sur des données de plusieurs essais à long terme (Coleman et al., 1997). Il a également été testé dans divers autres contextes (Yang et al., 2003).

Pour la modélisation à l'échelle du paysage, trois modifications ont été apportées au modèle RothC (Viaud et al., 2011) : (i) l'ensemble des horizons organo-minéraux (horizons A) est représenté, et non plus uniquement l'horizon de surface, (ii) la variation des stocks est spatialisée à l'échelle d'un paysage, (iii) la variation des épaisseurs de sol en lien avec l'érosion est prise en compte.

2.2.2.1 Entrées et sorties du modèle de dynamique du carbone

Les données d'entrée suivantes sont nécessaires :

(i) Données météorologiques au pas de temps mensuel :
- précipitations (mm)
- évapotranspiration potentielle ETP (mm)
- température moyenne mensuelle (°C)

(ii) Données topographiques :
- Altitude initiale sous la forme d'un MNA au format raster

(iii) Données pédologiques en toute localisation du paysage:
- épaisseur du sol (cm)
- teneur en argile (%)
- hydromorphie (3 classes : faible, moyenne forte)
- teneur en C initiale au sein de chaque horizon (g kg^{-1})
- masse volumique apparente de chaque horizon (g cm^{-3})

(iv) Données sur les pratiques culturales au pas de temps mensuel :
- parcellaire au format vecteur
- successions de culture pour chaque parcelle

- itinéraire technique pour chaque parcelle et chaque occupation du sol (dates de semis et de récolte, date et profondeur du travail du sol, rendements, gestion des résidus aériens, présence ou non d'une interculture).

(v) Apports de matière organique au pas de temps mensuel :

- teneur en C dans les résidus de culture (résidus aériens et racines, %)
- quantités de C organique apportées par des effluents organiques
- qualité de la matière organique apportée par les résidus de culture (matériau végétal décomposable vs. résistant)
- qualité de la matière organique apportée par les effluents organiques (matériau végétal décomposable vs. résistant)

Il n'y a pas de module de croissance de culture implanté dans le modèle, mais un module simplifié permettant d'estimer les apports de C organique à chaque pas de temps et leur distribution dans le profil à partir de la connaissance des occupations du sol, des pratiques culturales (profondeur de travail du sol, apport d'amendements organiques), et des rendements.

Les sorties du modèle sont les suivantes :

(i) Stocks de C organique dans chaque compartiment du modèle, par horizon et en toute localisation du paysage

(i) Stocks totaux de C organique par horizon et en toute localisation du paysage (t ha^{-1})

(ii) Teneur en C par horizon et en toute localisation du paysage (g kg^{-1})

2.2.2.2 Modélisation de la dynamique du carbone

Le modèle est basé sur le modèle RothC-26.3, dédié à la modélisation 1D de la dynamique du C dans les horizons de surface (généralement 0-30 cm) de sols agricoles bien drainés (Coleman and Jenkinson, 1996). RothC est un modèle compartimental, à pas de temps mensuel. Les stocks initiaux de C et les apports sont répartis dans cinq compartiments conceptuels (Figure 2-15): matériel végétal décomposable (DPM), matériel végétal résistant (RPM), biomasse microbienne (BIO), matière organique humifiée (HUM) et matière organique inerte (IOM). Le compartiment IOM est le seul ne participant pas au turnover de la matière organique. C'est un compartiment de petite taille, stable, très résistant à la décomposition par les micro-organismes.

Le stock de C de chaque compartiment conceptuel DPM, RPM, BIO, HUM, IOM est initialisé pour chaque horizon de sol à partir du stock de C total de cet horizon, renseigné en entrée du modèle. Le stock de C dans le compartiment IOM est d'abord calculé d'après la relation empirique établie par Falloon et al. (1998) :

$$IOM = 0{,}049.SOC^{1{,}139} \quad (9)$$

Avec *SOC* = stock de C organique de l'horizon considéré (tC ha^{-1})

L'initialisation des stocks dans les autres compartiments se fait en utilisant le modèle en mode inverse (Parshotam, 1996), en faisant l'hypothèse que les stocks de C dans le sol sont à l'équilibre par rapport aux entrées. La dynamique du C dans chaque compartiment est représentée par une cinétique d'ordre 1, définie par une constante de décomposition k (en an^{-1}), spécifique à chaque compartiment et fixée aux valeurs suivantes (Jenkinson et al., 1987 ; Jenkinson et al., 1992) :

- DPM : k_{DPM} = 10,0
- RPM : k_{RPM} = 0,3
- BIO : k_{BIO} = 0,66
- HUM : k_{HUM} = 0,02.

La décomposition est modulée par la température et l'humidité du sol (qui ont un effet sur les biotransformations), la texture du sol (et plus particulièrement la teneur en argile du sol, les argiles ayant un effet de protection physique de la matière organique du sol), et la couverture du sol. Ainsi, la quantité de C (q) restant après un intervalle de temps δt dans un compartiment *i* est donnée par l'équation 10.

$$q(\delta t) = C_i(t).e^{abcki\delta t} \qquad (10)$$

Avec :
$C_i(t)$ = stock de C présent dans le compartiment *i* au temps t
a = facteur température
b = facteur humidité
c = facteur de couverture du sol
ki = constante de décomposition du compartiment i (basée sur des vitesses annuelles de décomposition)
δt = 1 mois

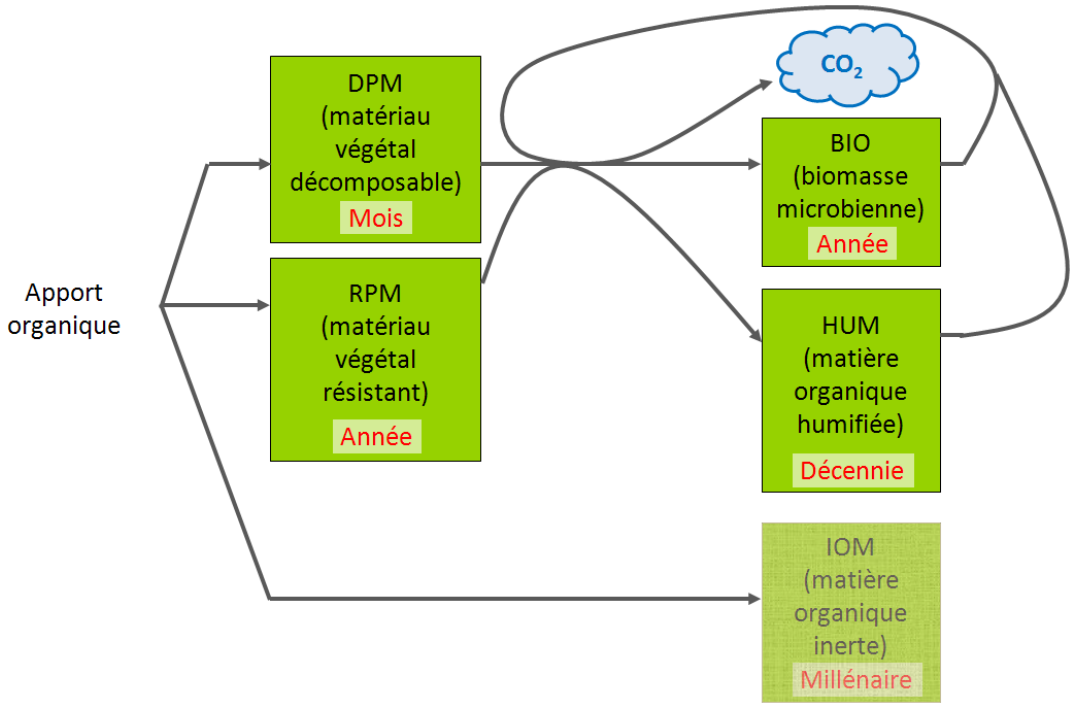

Figure 2-15. Représentation schématique de la modélisation de la dynamique du C organique des sols par le modèle RothC au sein d'un horizon de sol (en rouge : temps de résidence de la matière organique pour un compartiment donné) (d'après Coleman and Jenkinson, 1996)

Le C décomposé dans chaque compartiment est minéralisé sous forme de CO_2 ou vient alimenter les compartiments BIO et HUM. Le modèle ajuste la fraction minéralisée sous forme de CO_2 et celle libérée sous forme de la somme (BIO+HUM) en fonction de la teneur en argile du sol et selon l'équation suivante :

$$x = 1{,}67(1{,}85 + 1{,}60\ e^{-0.0786\alpha}) \qquad (11)$$

Avec :
x = le ratio CO_2 / (BIO+HUM),
a = teneur en argile du sol

Donc la quantité *x/(x+1)* évolue sous forme de CO2. La quantité restante *1/(x+1)* alimente les compartiments BIO et HUM.

2.2.2.3 Représentation du paysage

Comme pour le modèle LandSoil, le paysage est représenté par une grille régulière à mailles carrées (format raster). Dans chaque maille, le profil de sol est représenté comme une succession d'horizons. La limite entre les horizons peut être variable d'un pixel à l'autre. La base des horizons A est considérée comme étant la limite du système. La dynamique du C organique est modélisée au pas de temps mensuel pour chaque horizon considéré (Figure 2-16), selon le formalisme schématisé par la Figure 2-15. La température (T) est calculée à l'échelle du profil à partir de la température de surface (McCann et al., 1991). L'humidité (H) est considérée comme invariable sur tout le profil. Les épaisseurs d'horizon sont réactualisées au pas de temps annuel en prenant en compte les variations d'altitude et d'épaisseur de sol simulées par LandSoil. Les transferts verticaux et la dilution du C organique dus au travail du sol et à la redistribution par les processus d'érosion sont pris en compte. La densité apparente du sol (DA) n'évolue qu'en lien avec la redistribution verticale de sol.

2.2.3 Couplage des modèles LandSoil et RothC pour la modélisation de l'évolution des sols

La modélisation de l'évolution des sols (redistribution des sols et variation des stocks de C) repose sur le couplage des modèles LandSoil et RothC. La Figure 2-17 présente une vue d'ensemble de la méthode utilisée. Les deux modèles nécessitent des entrées décrivant le sol et la topographie de la zone d'étude à l'état initial, ainsi que le climat et les pratiques agricoles au long de la période de simulation. LandSoil simule la redistribution des sols au pas de temps de l'événement (pluvieux ou aratoire). A chaque événement simulé, LandSoil produit une cartographie réactualisée de l'épaisseur des sols et de la topographie sous forme d'un modèle numérique d'altitude (MNA). Le modèle de dynamique du C simule la dynamique du C au pas de temps mensuel. Le couplage entre les deux modèles est un couplage faible : tous les 10 ans, le MNA réactualisé est utilisé en entrée du modèle de dynamique du C. Les limites des horizons organo-minéraux sont réactualisées en fonction des redistributions de sol. Il n'y a pas de rétroaction du modèle de dynamique du C vers le modèle LandSoil, i.e. que l'impact de l'évolution des stocks de C sur la sensibilité des sols à l'érosion n'est pas pris en compte dans cette étude.

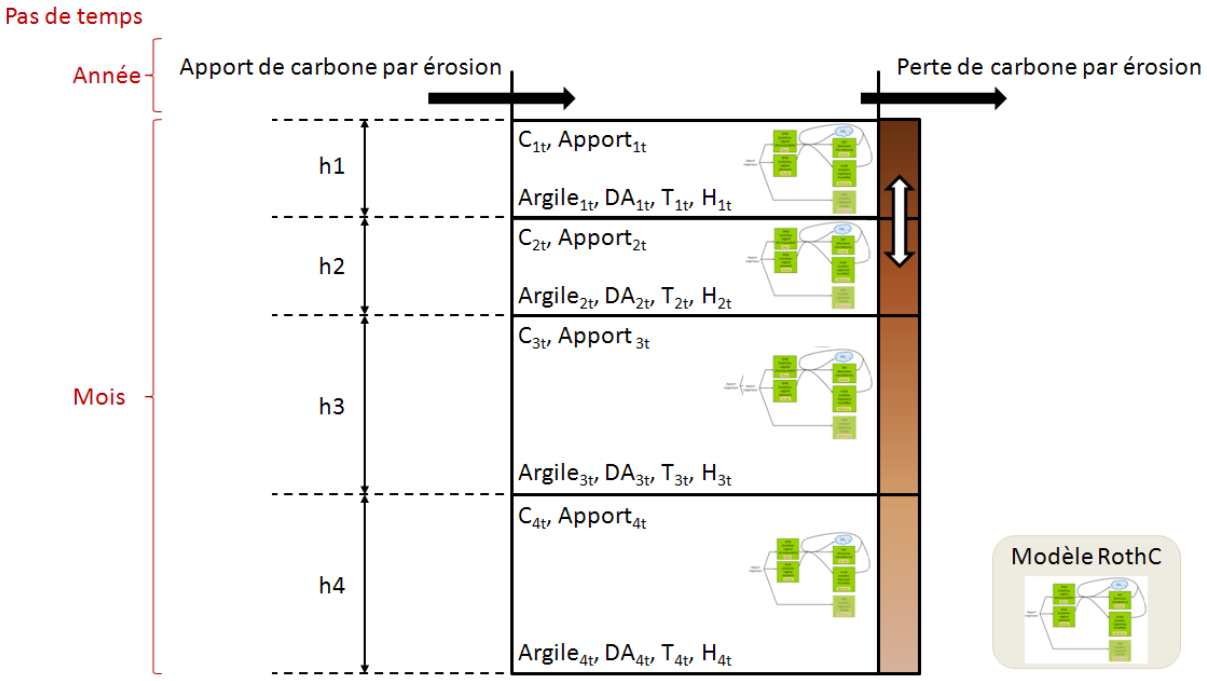

Figure 2-16. Modélisation de la dynamique du C organique des sols à l'échelle d'un profil de sol, le modèle RothC étant appliqué pour chaque horizon. A un instant t et pour chaque horizon hi considéré, les entrées du modèle sont le stock initial de C (C_{it}) et l'apport de C ($Apport_{it}$). Les paramètres de modèle sont la teneur en argile ($Argile_{it}$), la densité apparente (DA_{it}), la température (T_{it}) et l'humidité (H_{it}). (d'après Viaud et al., 2011). Voir Figure 2-15 pour les détails du modèle RothC.

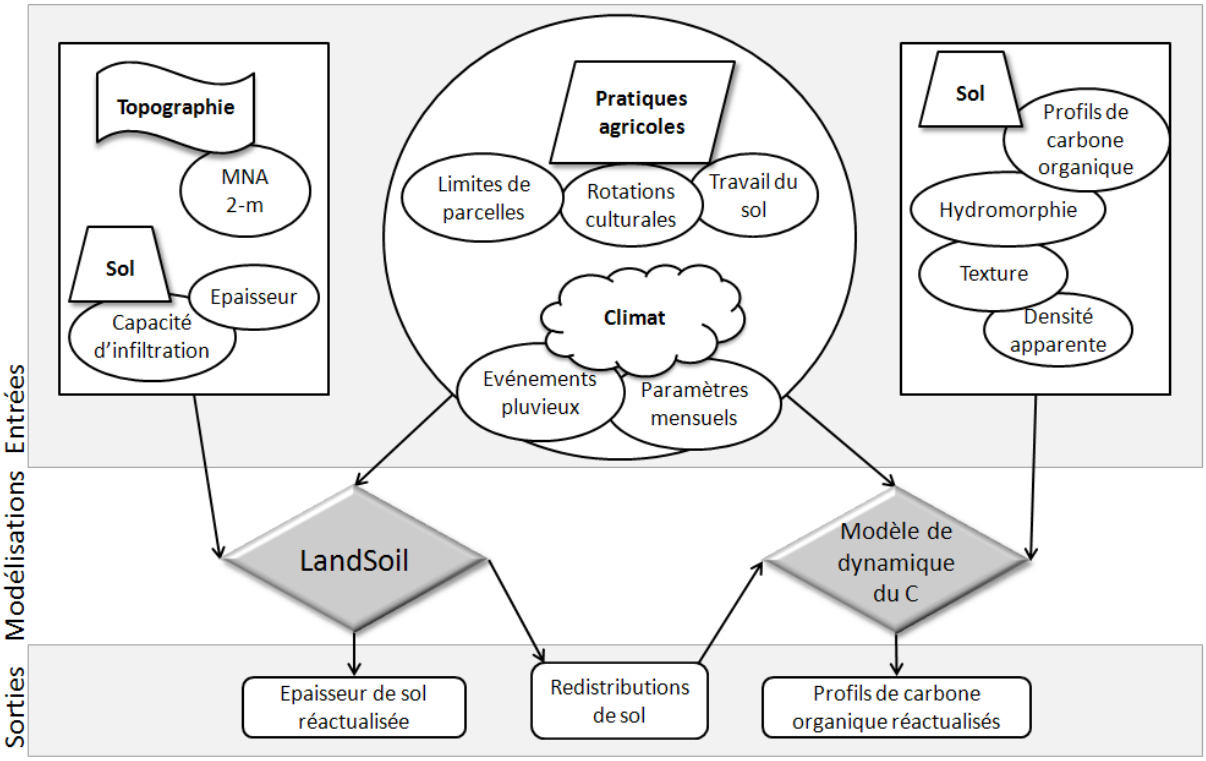

Figure 2-17. Représentation schématique de la méthode de modélisation de l'évolution des sols : couplage des modèles de redistribution des sols (LandSoil) et de dynamique du C organique.

2.2.4 Plan de simulation

La modélisation de l'évolution des sols se fait selon des scénarios faisant varier la structure du paysage et le climat.

Les scénarios concernant le paysage sont au nombre de sept et présentent deux facteurs de variation : l'occupation du sol et l'aménagement du paysage. Un scénario constitue le scénario de référence, caractérisé par une occupation du sol et une structure du paysage identique à l'actuelle (scénario stationnaire). Les six scénarios suivants font varier soit uniquement l'occupation du sol, soit uniquement l'aménagement, soit ces deux composantes du paysage simultanément. Trois de ces scénarios sont conçus pour préserver les sols, i.e. pour favoriser le stockage du C et limiter l'érosion. Ils sont basés sur l'augmentation des prairies et sur la densification du bocage. Les trois derniers scénarios reflètent au contraire une situation de dégradation des sols, i.e. limitant le stockage du C et favorisant l'érosion. Ils sont basés sur l'augmentation des cultures d'hiver et sur la suppression du bocage. Les pratiques agricoles sont associées à un type de culture et restent constantes quel que soit le scénario considéré.

Ces sept scénarios seront croisés avec deux scénarios d'évolution du climat : le scénario stationnaire, suivant la tendance climatique actuelle, et le scénario A1B, traduisant un réchauffement climatique global suivant les hypothèses du GIEC (2007).

Les quatorze scénarios résultant du croisement paysage/climat permettront d'estimer les rôles respectifs du climat, de la composition et de l'aménagement du paysage sur l'évolution des sols, tant au niveau du stockage de C que de l'érosion des sols. Ces scénarios sont détaillés dans le chapitre 5.

2.3 Caractérisation des sols du site atelier de Pleine-Fougères pour l'initialisation des modèles

L'objectif général de cette thèse est de modéliser l'évolution des sols, en termes d'épaisseur et de stocks de C, dans des conditions de changement global. Cette étude se fait dans un contexte de paysage réel, et non dans celui d'un paysage virtuel comme cela a pu être le cas dans des études précédentes (e.g. Sorel, 2008). Ceci nécessite donc une connaissance préalable des sols de la zone d'étude, i.e. une connaissance de l'état initial des sols, qui servira de donnée d'entrée aux modèles d'évolution des sols. Les deux modèles retenus pour l'érosion et la dynamique du C requièrent en entrée des cartographies continues et exhaustives des propriétés des sols suivantes :

- épaisseur des sols (LandSoil et modèle C)
- profondeur des horizons A (modèle C)
- teneurs en C dans les horizons A (modèle C)
- teneurs en éléments grossiers (modèle C)
- densité apparente dans les horizons A (modèle C)
- hydromorphie des sols (modèle C)

Le site atelier de Pleine-Fougères ne disposait pas de caractérisation exhaustive des sols. Une première étape a donc consisté en l'acquisition de données pédologiques, visant à réaliser des cartographies à haute résolution spatiale des propriétés d'intérêt pour la modélisation. La stratégie d'échantillonnage et de caractérisation des sols a été définie pour être adaptée à la méthode de cartographie numérique des sols et aux entrées nécessaires aux modèles d'évolution des sols. Deux niveaux d'échantillonnage ont été définis : un échantillonnage à l'échelle du site atelier, et un

échantillonnage au voisinage des haies pour caractériser finement l'influence de ces structures sur l'organisation des sols.

2.3.1 Principes de la cartographie des propriétés des sols

Selon la propriété du sol, sa cartographie consiste en une représentation en deux dimensions (profondeur du sol, profondeur des horizons A) ou en trois dimensions (densité apparente, teneurs en éléments grossiers, teneurs ou stocks de C organique). La démarche de cartographie s'est appuyée sur des méthodes récentes de cartographie numérique des sols (ou DSM pour Digital Soil Mapping).

Les méthodes de cartographie numérique permettent la cartographie exhaustive de propriétés de sol à partir d'interpolations spatiales ou d'identifications des relations existant entre le sol et ses facteurs de formation. Ces relations sont connues de longue date : elles ont été identifiées par Dokoutchaiev (1900), puis formalisées par Jenny (1941). En 2003, McBratney et al. intègrent et synthétisent les travaux précédents, en proposant le modèle SCORPAN, où une propriété du sol est une fonction du Sol, du Climat, des Organismes vivants (faune, flore, activité humaine), de la Topographie, du matériau Parental, de l'Age et de la positioN spatiale.

Ces méthodes se sont largement développées au cours des 40 dernières années, grâce à l'amélioration des outils informatiques, des systèmes d'informations géographiques, des méthodes d'acquisition de données exhaustives, telles que la télédétection, et bien sûr des algorithmes permettant de résoudre les équations du modèle SCORPAN, et donc de prédire les propriétés des sols à partir de ces données exhaustives (Bui, 2007). La généralisation des modèles numériques de terrain (MNT) a largement contribué à l'avancée des méthodes de cartographies numériques des sols. La cartographie numérique présente plusieurs avantages : elle est reproductible, les informations utilisées par le cartographe sont clairement identifiées, et la qualité des cartes produites peut être estimée par le calcul d'incertitudes de prédiction (Walter et al., 2007).

Dans le cas de cette étude, une méthode d'apprentissage automatique (machine learning) a été utilisée pour identifier les relations entre les propriétés du sol et certaines variables du modèle SCORPAN (Breiman, 2001). La méthode retenue est une méthode d'apprentissage supervisée, combinant des arbres de régression et de classification[16]. Ce type de méthode est particulièrement adapté pour des sites d'étude où le jeu de calibration est restreint (Friedman and Meulman, 2003). Une méthode similaire avaient déjà été appliquée avec succès pour la prédiction du matériau parental des sols de Bretagne (Lacoste et al., 2011 ; Annexe 1). Ces méthodes, comme toute méthode de cartographie numérique, nécessitent deux jeux de données, l'un de calibration et l'autre de validation.

Cette démarche est originale car elle allie la cartographie 3D des sols à la haute résolution spatiale.

2.3.2 Stratégie d'échantillonnage

2.3.2.1 Stratégie d'échantillonnage à l'échelle du site atelier

Le choix de la méthode d'échantillonnage dépend des caractéristiques du site d'étude, de l'existence de données exhaustives, de l'utilisation prévue des données acquises (type de carte à produire,

[16] La méthode de cartographie des sols est détaillée dans le chapitre 4.

résolution de la carte, méthode de cartographie, etc.), mais aussi du temps et des moyens disponibles (humains et financiers)(Gruijter et al., 2006 ; Hengl et al., 2003 ; McKenzie et al., 2008 ; Minasny and McBratney, 2006a).

Certaines données auxiliaires exhaustives en relation avec les variables d'intérêt étaient disponibles pour le site de Pleine-Fougères. Dans ce cas, l'utilisation de l'échantillonnage en Hypercube latin conditionné est conseillé pour définir un échantillonnage de calibration (Lagacherie et al., 2007 ; Minasny and McBratney, 2006a). L'échantillonnage en hypercube latin (LHS) est un échantillonnage aléatoire stratifié, basé sur la méthode des chaînes de Markov-Monte Carlo contraintes (McKay et al., 1979 ; Xu et al., 2005). C'est une méthode qui permet de réaliser un échantillonnage parcimonieux, en couvrant l'ensemble de la gamme de variation de chaque variable auxiliaire et en stratifiant de façon optimale les distributions marginales. Traditionnellement utilisé en expérimentation numérique (e.g. Pistone and Vicario, 2010 ; Pronzato and Mueller, 2012), l'échantillonnage par LHS est particulièrement adapté pour définir des jeux de calibration pour des méthodes de prédiction des sols par apprentissage (McBratney et al., 2003 ; Minasny and McBratney, 2007 ; Minasny and McBratney, 2006a). Le LHS fonctionne de la manière suivante : prenons k variables auxiliaires X1, …, Xk. La distribution de chaque variable *X* est divisée en *n* intervalles de probabilités égales (strates). Pour chaque variable, un échantillon est sélectionné aléatoirement dans chaque strate. On obtient donc *n* strates par variable *X*. Ces strates sont assemblées aléatoirement par paires pour chaque couple de variable *X*. On appelle « carré Latin » le croisement des strates de deux variables. En croisant tous les carrés latins obtenus, on définit finalement *n* échantillons aléatoires couvrant les *n* strates de chaque variable *X*, et donc respectant les distributions de ces variables. Cependant, cette méthode ne peut être appliquée directement pour échantillonner des points à partir de variables auxiliaires exhaustives sur un terrain réel. En effet, les échantillons sélectionnés par LHS peuvent ne pas être présents dans la réalité. Par exemple, si l'on considère l'altitude et le substrat comme variables auxiliaires, l'échantillonnage en LHS peut sélectionner un point ayant pour altitude 20 m et pour substrat géologique le granite. Si cette situation existe d'un point de vue probabiliste, ce n'est pas le cas sur le terrain en ce qui concerne le site atelier de Pleine-Fougères où on ne trouve du granite qu'à une altitude supérieure à 60 m. Pour pallier ce problème, un algorithme modifié a été proposé par Minasny et McBratney (2006a) : l'échantillonnage en hypercube latin conditionné (cLHS). Le cLHS permet de sélectionner les sites de la zone d'étude en respectant les carrés latins, mais en ne sélectionnant que les couples effectivement présents sur la zone d'étude.

Pour la validation, Brus et al. (2011) conseillent d'utiliser un jeu de données indépendant du jeu de calibration, sélectionné par échantillonnage aléatoire stratifié. Cette solution est préférée à la validation croisée ou à la division du jeu de données initiales en un jeu de calibration et un de validation car elle permet d'estimer la qualité de la carte produite indépendamment de tout biais.

Deux types d'échantillonnages ont été mis en œuvre sur le site atelier de Pleine-Fougères (Figure 2-18) :

a) deux échantillonnages en cHLS ont été réalisés pour la calibration des modèles de spatialisation des propriétés des sols. Quatre variables ont été retenues pour servir de variables auxiliaires dans l'échantillonnage en hypercube latin conditionné : l'altitude, un indice d'hydromorphie des sols climato-topographique (Beven and Kirkby, 1979 ; Gascuel-Odoux, 1998 ; Merot et al., 1995 ; Merot et al., 2003), les émissions naturelles de potassium et la fréquence d'occupation du sol en prairie. Deux jeux de calibration ont été sélectionnés indépendamment,

constitués respectivement de 70 et 130 points. Des descriptions de sol et des prélèvements d'échantillon pour analyses ont été effectués au niveau des 70 points. Des descriptions de sols seules ont été réalisées au niveau des 130 points. Les échantillonnages obtenus après la campagne de terrain montrent une bonne correspondance avec les échantillonnages initialement prévus et couvrent bien la distribution des variables auxiliaires choisies (Figure 2-19 et Figure 2-20). Les écarts observés entre les échantillonnages attendus et réalisés sont dus au fait que certains points sélectionnés ne pouvaient pas être échantillonnés en pratique (propriété privée, zone anthropisée, etc.) ;

b) deux échantillonnages aléatoires stratifiés selon une maille carrée de 300 m ont permis de définir deux jeux de validation de respectivement 49 et 58 points. Des descriptions de sol et des prélèvements d'échantillons pour analyse ont été effectués au niveau des 49 points. Au niveau des 58 points seules des descriptions de sol ont été réalisées.

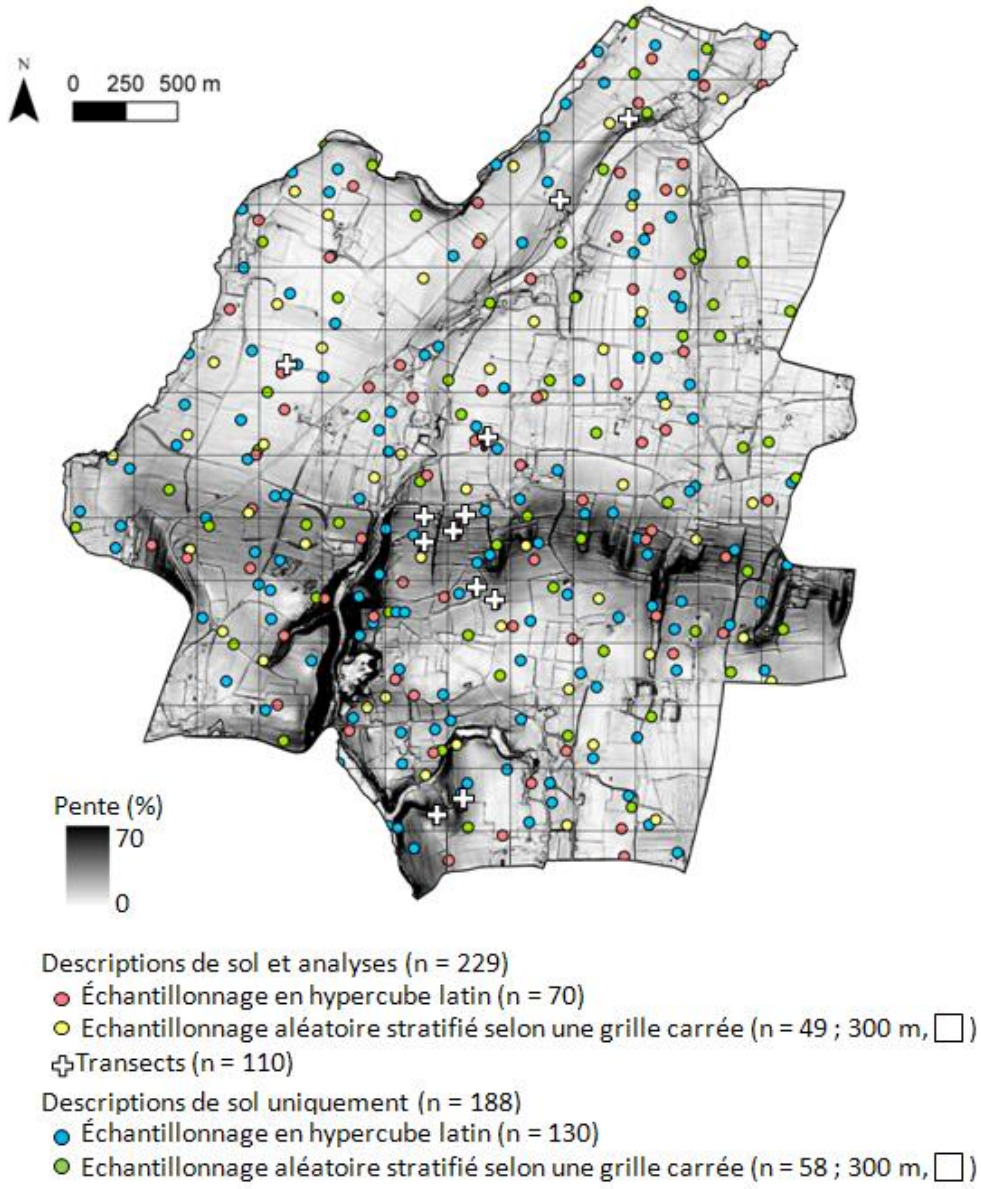

Figure 2-18. Localisation des sites de description et prélèvements de sol pour analyses au sein du site atelier de Pleine-Fougères, selon les trois stratégies d'échantillonnage retenues.

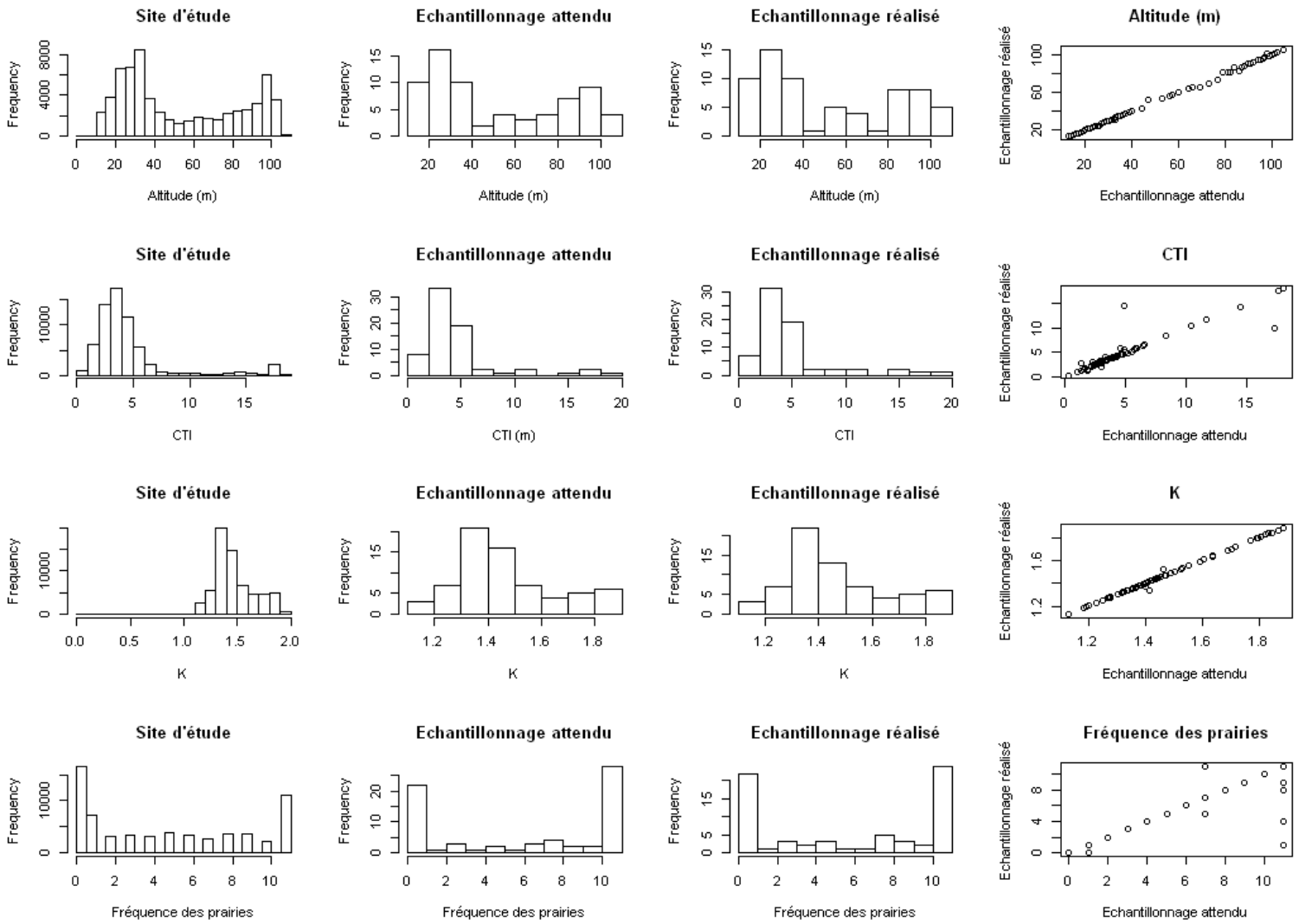

Figure 2-19. Comparaison des distributions des variables auxiliaires utilisées dans le cLHS et des distributions des points échantillonnés (jeux de 70 points). L'échantillonnage attendu est l'échantillonnage théorique obtenu par la procédure de cLHS, l'échantillonnage réalisé est celui obtenu par la campagne de terrain.

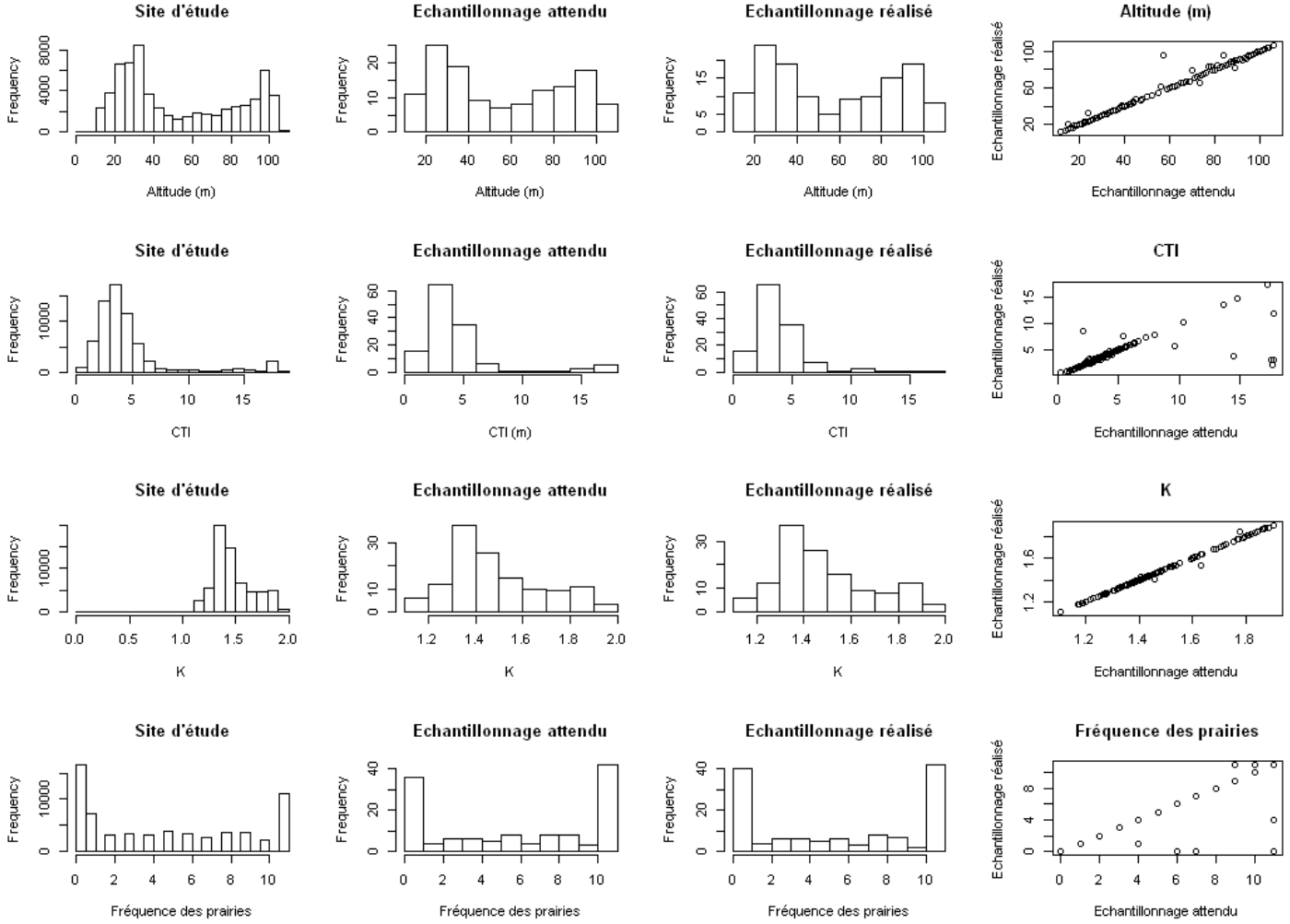

Figure 2-20. Comparaison des distributions des variables auxiliaires utilisées dans le cLHS et des distributions des points échantillonnés (jeux de 130 points). L'échantillonnage attendu est l'échantillonnage théorique obtenu par la procédure de cLHS, l'échantillonnage réalisé est celui obtenu par la campagne de terrain.

2.3.2.2 Description des sols et analyses

Une campagne de terrain a été menée entre mars 2009 et avril 2010. Des profils de sol ont été décrits et échantillonnés pour les différents plan d'échantillonnage présentés précédemment, de manière à caractériser les variables d'intérêt : épaisseur des sols, épaisseurs des horizons A, hydromorphie, teneur en C, densité apparente, teneur en éléments grossiers, teneur en argile.

2.3.2.3 Caractérisation de l'épaisseur des sols, des horizons A, et de l'hydromorphie

Pour tous les points d'échantillonnage (200 points de calibration, 107 points de validation), des sondages ont été réalisés à l'aide d'une tarière hélicoïdale classique (longueur de 1,20 m), équipée si nécessaire de rallonges. Les variables suivantes ont été déterminées de manière experte par observation du sol : type de sol selon le Référentiel Pédologique français (AFES, 2008), épaisseur totale de sol, épaisseur et couleur des différents horizons (charte Munsell), hydromorphie (présence de signes d'engorgement temporaire ou permanent), texture (pourcentage d'argile, de limon et de sables), pourcentage de matière organique et teneur en éléments grossiers. Par « épaisseur du sol » on entend ici l'épaisseur du sol depuis la surface jusqu'au substrat géologique s'il pouvait être atteint (horizon R du Référentiel pédologique) ou jusqu'à l'horizon d'altération de ce même substrat (horizon C du Référentiel Pédologique ; AFES, 2008).

2.3.2.4 Mesure de la densité apparente, de la teneur en éléments grossiers et de la teneur en carbone

La densité apparente du sol, la teneur en éléments grossiers et la teneur en C ont été mesurées sur les points d'échantillonnage destinés à la description des sols et aux analyses (70 points de calibration, 49 points de validation), ainsi que sur les points situés sur les transects.

Des prélèvements de sol non remaniés ont été réalisés à l'aide d'une tarière à mat racinaire (cylindre de 8 cm de diamètre et de 15 cm de hauteur) pour l'échantillonnage à l'échelle du site atelier, ou d'une carotteuse hydraulique pour l'échantillonnage en transects (cylindre de 7.5 cm de diamètre et de 1 m de hauteur), jusqu'à atteindre l'horizon C ou la profondeur maximale de prélèvement (105 cm pour la tarière à mat racinaire, 11 m en théorie pour le carotteur).

La Figure 2-21 illustre la méthode adoptée pour la discrétisation verticale du profil, en prenant pour exemple trois profils de sol. Des échantillons de sol ont été systématiquement collectés sur les épaisseurs 0-7,5 cm et 7,5-15 cm, puis tous les 15 cm jusqu'à la base des horizons A (cas b et c), sauf en cas de changement d'horizon (cas a). Dans ce cas, la limite entre deux échantillons a été placée à la limite entre deux horizons.

Chaque échantillon est séché à l'air et tamisé à 2mm. La masse et le volume des éléments grossiers sont déterminés sur le refus du tamis. Un sous-échantillon de 5 g de terre fine est prélevé, séché à 105°C, puis pesé pour la détermination de la teneur en eau et de la densité apparente. Un autre sous-échantillon est broyé à 10 μm, pour la détermination de la teneur en C. Les teneurs en C ont été déterminées par le Laboratoire d'Analyse des Sols INRA d'Arras pour les 70 profils de sols sélectionnés par cHLS et les 49 profils de l'échantillonnage aléatoire stratifié (combustion sèche selon la norme NF ISO 10694, analyseur élémentaire Thermo Finnigan EA 1112).). Pour les échantillons des transects, la teneur en C a été déterminée par spectrométrie de réflexion diffuse (Aïchi et al., 2009).

Des mesures de granulométrie cinq fractions ont été réalisés sur 60 échantillons répartis sur la zone d'étude (analyses réalisées au Laboratoire d'Analyse des Sols INRA d'Arras).

La réalisation de la cartographie à partir des données d'échantillonnage fait l'objet d'un chapitre spécifique (Chapitre 4).

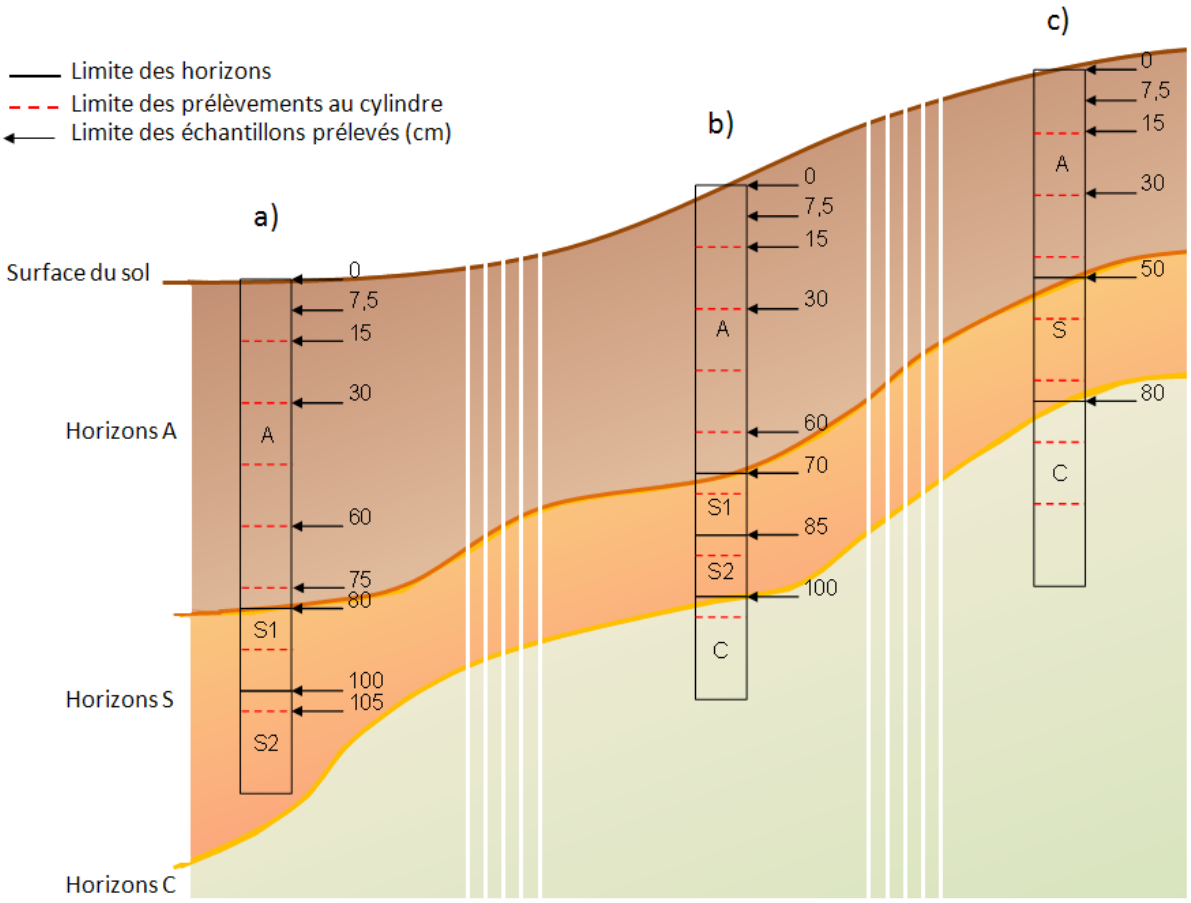

Figure 2-21. Représentation schématique de la méthode d'échantillonnage des sols sur le site atelier de Pleine-Fougères.

2.4 Conclusion partielle

Ce chapitre a présenté la zone d'étude ainsi que les modèles utilisés pour simuler l'évolution des sols dans un contexte de changement global.

Le site atelier de Pleine-Fougères présente une large diversité de substrat géologique, de matériau parental des sols, de types de sol, de topographie et d'organisation du paysage. Deux modèles sont utilisés pour modéliser l'évolution des sols de la zone atelier de Pleine-Fougères. Le modèle LandSoil, adapté du modèle STREAM, permet de modéliser l'érosion et le dépôt des sédiments, sous l'effet des pluies et/ou du travail du sol. Le modèle de dynamique du C, adapté de RothC modélise le turnover du C organique des sols. Le couplage de ces deux modèles permet la modélisation de l'évolution à l'échelle du paysage, en prenant en compte les pratiques agricoles, la structure du paysage et le climat.

Chapitre 3.
Calibration and test of LandSoil model for soil redistribution modeling

Our purpose was to use LandSoil to model soil redistribution at the landscape scale, for the study area of Pleine-Fougères (PF). LandSoil general structure is based on the STREAM model (Cerdan et al., 2002b). STREAM has been calibrated for the loamy soils of Upper Normandy (Cerdan et al., 2002b) by aggregating 15 years of laboratory and field experiments carried out in the Pays de Caux region (Boiffin and Monnier, 1986a; Chaplot and Le Bissonnais, 2000; Fox and Le Bissonnais, 1998; Gallien et al., 1995; Le Bissonnais et al., 1998a; Le Bissonnais et al., 1998b; Le Bissonnais et al., 1995; Lecomte, 1999; Lecomte et al., 1997; Martin et al., 1997). From these experimental data, expert rules were defined to model runoff and soil erosion. These rules were based on properties such as soil surface characteristics, soil infiltration rate, residual water storage after the previous event (Ws), sediment concentration in runoff, etc. The values of these parameters were implemented in STREAM and considered as default values. The calibrations for the STREAM model, defined from the Pays de Caux experiments, provided the default values implemented in the LandSoil model.

The aim of this chapter was to calibrate LandSoil to model the redistribution of loamy soils in northern Brittany. These soils are mainly developed in Aeolian loams which were laid over northern Europe during the last Quaternary glacial period (~ 28 - 13 Ka BP), and present local variability due to heterogeneous initial deposits, subsequent redistribution or mixing with underlying bedrock (Lautridou, 1985). The calibration of LandSoil has been conducted in two steps, which are laid out in the two parts of this chapter.

First, LandSoil was calibrated at the scale of event data, with rainfall events data for which runoff and the associated sediment concentrations were measured at field scale (Section 3.1). Secondly, LandSoil was used to model soil redistribution close to hedges (Section 3.2). These simulations were done for a longer period (1960-2009), and their results were compared to soil redistribution estimates based on ^{137}Cs data. This second part allowed evaluating LandSoil calibration for the loamy soils of the PF study area and LandSoil ability to model soil redistribution close to hedges, which is a complex issue in hedgerow landscapes. Section 3.4. compares the soil redistribution rates assessed in Section 3.2 to additional soil redistribution rates estimated for the PF study area.

3.1 Calibration of LandSoil for soil redistribution at the scale of rainfall events

3.1.1 Material and methods

3.1.1.1 Description of calibration sites

Two experimental fields were used to calibrate LandSoil for soil redistribution at the scale of rainfall events. These fields, named Champ-Noël and Barre-Thomas were located in Brittany, south of the PF study area (Figure 3-1, see Chapter 2 for more details on the PF study area). The calibration sites supported various experiments of runoff measurements, whose data were published and are available (Cros-Cayot, 1996; Gascuel-Odoux et al., 1996; Heddadj and Gascuel-Odoux, 1999; Huang et al., 2002; Le Bissonnais et al., 2002a). The main characteristics of calibration sites and the PF study area are compared in Table 3-1. These calibration sites are at a distance of 45 km from the PF study area and have similar temperate oceanic climate, which was classified as Cfb by the Köppen classification (Köppen, 1936; Peel et al., 2007). This classification was based on precipitation and temperature. The Cfb climate is defined as a wet and hot temperate climate, with a temperate summer. It is characterised by the following properties: mean temperatures for the three colder

months range from -3 to 18°C; mean temperatures for the four hotter months are above 10°C but under 22°C. Summer and winter seasons are well defined; precipitation occurs every month and there is no dry season. This kind of climate is linked to soft relief, which allows a great deal of air intrusion from the Atlantic Ocean and a climate homogenisation. Both calibration sites and the PF study area have the same mean annual temperature (12°C), but the PF study area has higher mean annual rainfall (782 mm versus 659 mm for the calibration sites). Summer months have higher mean monthly rainfall in the PF study area, with slightly lower mean monthly temperature (Figure 3-2).

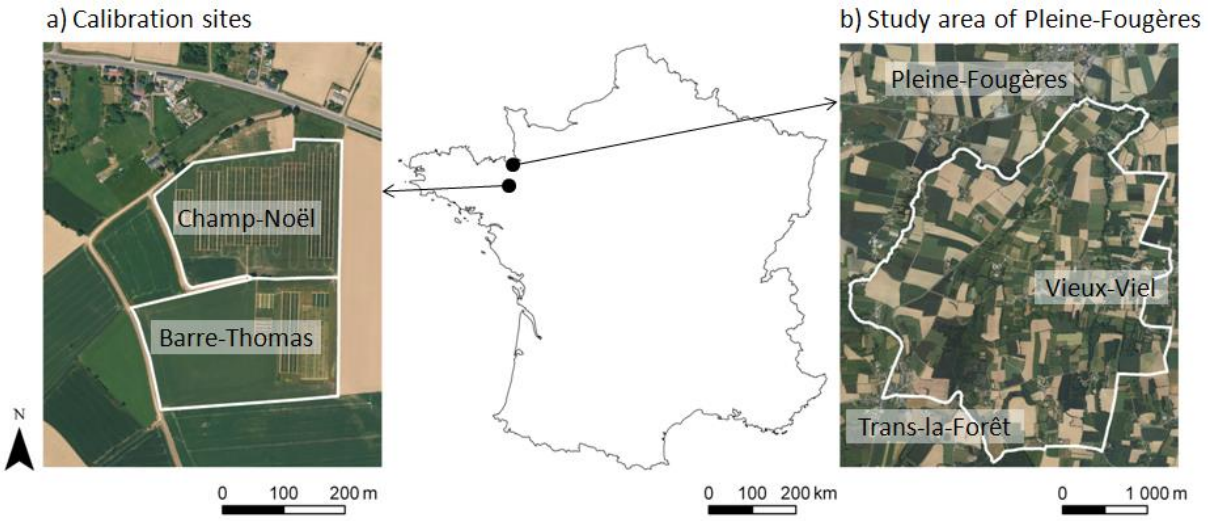

Figure 3-1. Location in France of the calibration sites (a) and the PF study area (b)

Table 3-1. Characteristics of the calibration sites for LandSoil (Champ-Noël and Barre-Thomas) and for the PF study area

Characteristics	Champ-Noël/ Barre-Thomas	Pleine-Fougères
Location	Brittany, France	Brittany, France
Coordinates (outlet)	48.115° N 1.728°W	48.505° N 1.565°W
Topography	Convexo-concave hillslope	Plateau, hillslope, lowland
Area (ha)	12	1000
Average field size (ha)	6	1
Soil parent material	Aeolian loam on tender schist	Aeolian loam, tender and hard schist, granite
Soil classification (World Base Reference, 2006)	Eutric Luvisol Colluvic	Cambisols, Haplic Luvisols, Leptosols, Colluvic Cambisols, Fluvisols
Soil surface texture		
% silt	69-74	33-76
% clay	14-17	8-25
% sand	11-15	13-52
% organic carbon	1-2	1-8
Average precipitation (mm yr^{-1})	659[a]	782[b]
Mean annual temperature (°C)	12	12
Main land use	Rotation winter wheat/maize	Mixed crops and dairy farming

[a] Daily meteorological data from 1997 to 2010 (Pontorson station)

[b] Daily meteorological data from 1990 to 2010 (Rennes station)

Calibration sites are located on convexo-concave hillslopes, about 200 m long, with a mean slope of 3%. This topography is similar to numerous fields of the PF study area. Soils of the calibration sites are Eutric Luvisol Colluvic, developed on the same parent materials as soils of the PF study area: Quaternary Aeolian loam deposits with an average thickness of 2 m (Trautmann et al. 1999), covering Brioverian schist (Figure 3-3). Soils of both calibration sites and the PF study area have a predominant silt fraction (mean value: 71% and 63% respectively of the total fine earth fraction) and moderate organic carbon content (1- 2% and 1-8%, respectively), which lead to a high sensitivity to soil surface sealing (Baize, 2000; Figure 3.4). However, the soils of the PF study area show higher texture variability than the soils of the calibration sites, with for example the silt fraction ranging from 33 to 76%. Crop rotations in calibration sites are also present in the PF study area. For all these reasons, the calibration sites turned out to be pertinent sites to calibrate LandSoil for soil redistribution modelling in the PF study area.

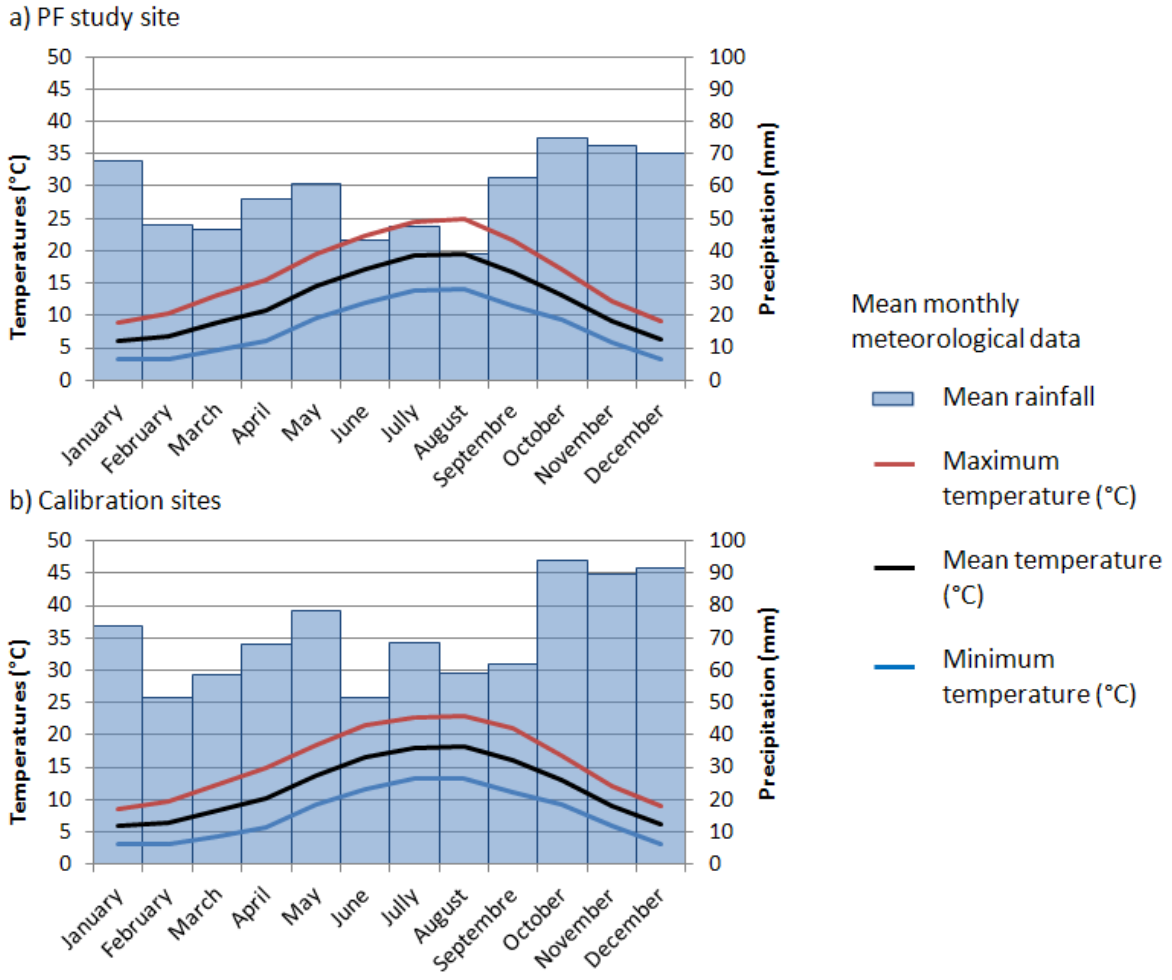

Figure 3-2. Climographs of the PF study area (a, meteorological data from 1997 to 2010, Météo-France, Pontorson station) and of the calibration sites (b, meteorological data from 1990 to 2010, Météo-France, Rennes station).

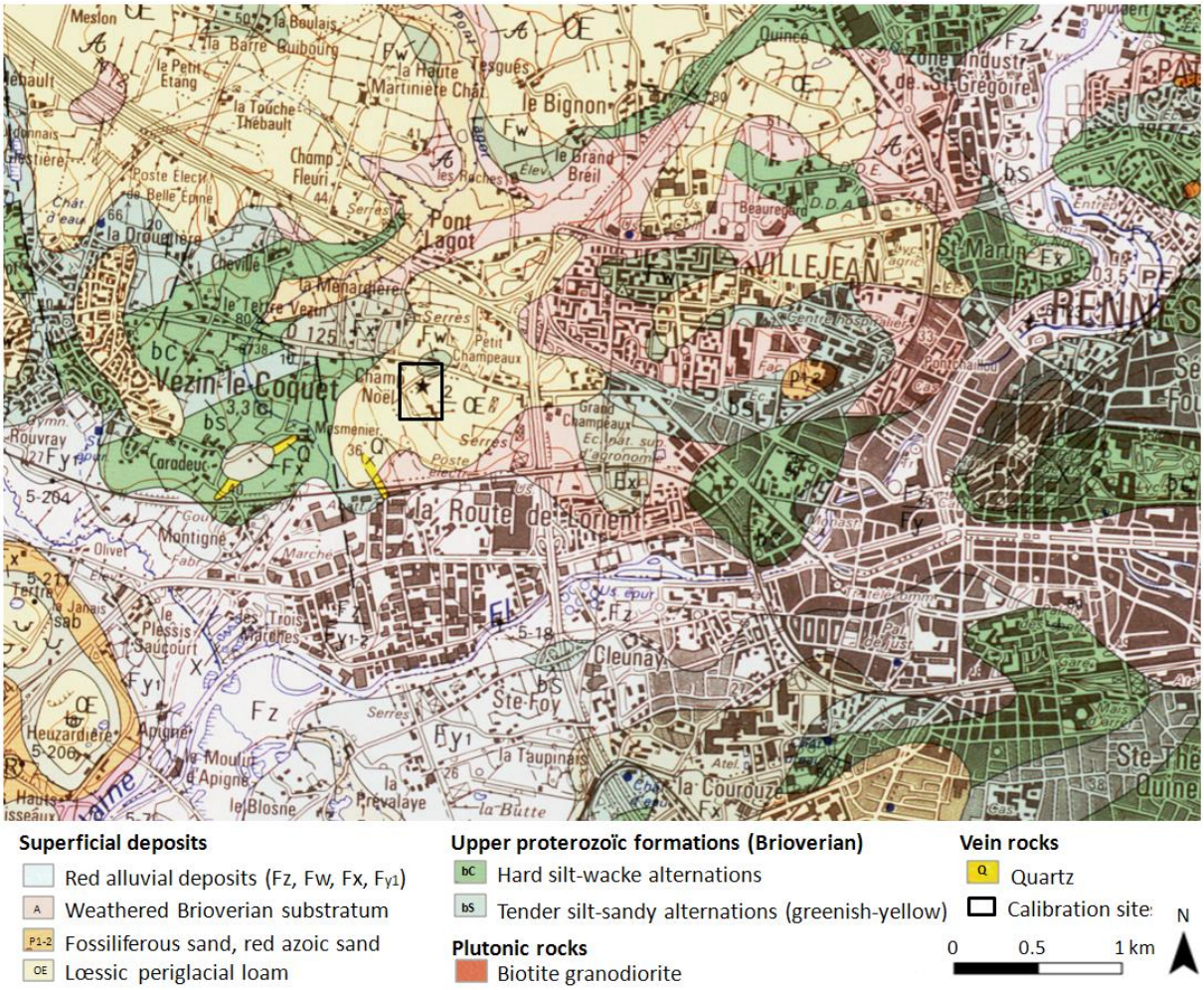

Figure 3-3. Local geology of the calibration sites. Extract from the French geological map (1:50 000ème), Rennes sheet (Trautmann et al., 1999, Trautmann et al., 2000)

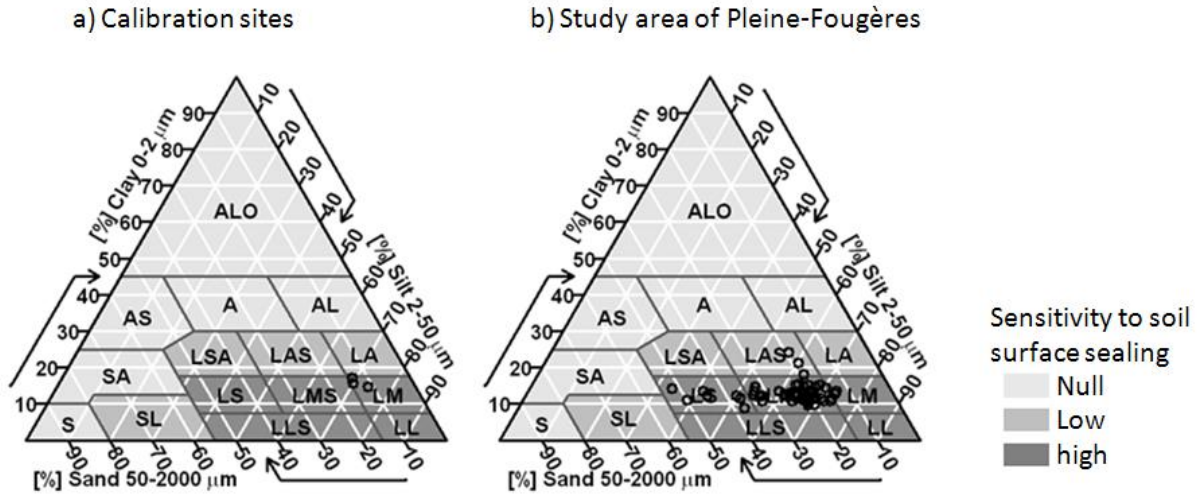

Figure 3-4. Texture of surface layer (0 – 30 cm) and associated sensitivity to surface sealing (Baize, 2000) for the calibration sites and the PF study area

3.1.1.2 LandSoil calibration from experimental data

LandSoil is an expert-based model allowing soil redistribution modelling at the time scale of rainfall events (see Chapter 2 for LandSoil description). Runoff modelling is based on Equation 1, which determines water infiltration versus water runoff:

$$B = RR - Ws - (IR \times D_{ef}) \quad (1)$$

with:

B = water infiltration (if B is <0) or water runoff (if B is >0)

RR = total rainfall (mm)

Ws = residual water storage after the previous event (mm)

IR = infiltration rate (mm h^{-1})

D_{ef} = effective duration, time during which rainfall intensity is higher than 2 mm h^{-1} (h)

The values of soil infiltration rate (IR) are determined following expert rules based on three soil surface parameters: soil roughness, vegetation cover and soil surface crusting (Cerdan et al., 2002b; Le Bissonnais et al., 2005). Ws (amount of rainfall needed to reach soil saturation) is derived from the value of IR, according to the amount of 48 h antecedent rainfall. Once the amount of runoff is calculated (Equation 1), sediment concentration in runoff is determined according to soil surface characteristics and the value of rainfall maximal-intensity. Consequently, various data are necessary to (i) determine the values for three parameters (infiltration rate, Ws and sediment concentration in runoff) on the calibration sites from existing experimental data, and (ii) replace these values in LandSoil decision rules and compare them with LandSoil default values.

3.1.1.3 Calibration of imbibition rain from rainfall simulation on field plots

Ws was estimated from rainfall simulation experiments on the calibration sites, where sufficient data were available. The rainfall simulations were conducted on field plots ranging from 1 to 4 m² (mean value: 2.5 m²), during 15 to 120 min (mean value: 60 min), for rainfall intensity ranging from 15 to 50 mm h^{-1} (mean value: 35 mm h^{-1}). These simulated rainfalls were in the range of the natural rainfalls observed in the PF study area. Plots were isolated from the whole fields and runoff was collected, to measure runoff volume and its sediment concentration.

To calculate Ws values, available data were the duration and the intensity of simulated rainfall data and the duration before runoff starts. Ws was calculated as follow:

$$Ws = I \times D_{br} \quad (2)$$

with:

I = rainfall intensity (mm h^{-1})

D_{br} = duration before runoff start (h)

Data were also needed to set these values of Ws back in the LandSoil decision tree: soil surface parameters and soil infiltration rate (*IR*). We used data from 12 of these experiments to calculate Ws values on calibration sites (data from Dupre, 1997; Gascuel-Odoux and Heddadj, 1999; Jaunatre, 1997; Le Cornet, 1999; Lion, 1997; Moinerais, 2003; Segal, 1996).

3.1.1.4 Calibration of infiltration rate (IR) and sediment concentration in runoff from experiments under natural rainfall at field scale

Infiltration rate (IR) and sediment concentration in runoff were estimated on calibration sites from experiments under natural rainfall events. IR was derived from Equation (1) for rainfall events with

available necessary information, namely rainfall descriptors and runoff amounts. The amounts of runoff for each natural rainfall were estimated at the field scale by Cros-Cayot (1996), using an experimental device composed of four sets of three collectors located evenly in the field (one set in the upper part of the field, two sets in the slope, one set in the lower part). All the measurements were done under maize (crop and then stubble field), with the collectors placed between maize rows in such a way that each collector intercepts the whole runoff occurring in the maize row from the upper part of the field so that the hydrologic contributory areas of the collectors did not overlay. For each rainfall event and each collector, the total runoff and its associated sediment concentration were measured. The necessary data to set these values of infiltration rain and sediment concentration in the LandSoil framework were rainfall maximum intensity and soil surface parameters: these data were available for 31 natural rainfall events from May 1994 through March 1995 and were used to calculate infiltration rates and sediment concentrations in runoff.

3.1.1.5 Disaggregation of hourly rainfall data to LandSoil modelling time scale

The most accurate and available meteorological data are in general hourly data, either from meteorological stations or from specific weather surveys associated to experimental studies. Rainfall characteristics derived from such data are hourly parameters: hourly amount of rainfall, hourly duration of rainfall, and hourly rainfall intensity. However, modelling soil redistribution with LandSoil requires more precise rainfall parameters: calculation of effective duration (D_{ef}) and rainfall maximum intensity; derived from 6-minute interval rainfall data. LandSoil is very sensitive to these parameters (Souchere et al., 2005). Nevertheless, 6-minute interval meteorological data were only available for a period from July 2005 through December 2009 (Figure 3-7). These four years, with annual rainfalls ranging from 530 to 760 mm (mean value: 680 mm), are representative of a longer period (1990-2009), where annual rainfalls ranged from 500 to 850 mm (mean value: 690 mm). The goal was to determine a linear relationship between rainfall parameters at these two time-scale meteorological data (hourly and 6-minute intervals), and then use them to convert hourly data into 6-minute data likely to be used by LandSoil. For both hourly and 6-minute data, a rainfall event was considered as a rainy period with no rainfall interruption longer than 3 hours, i.e. two rainfall events were separated by a dry period of at least 3 hours. The R stats package[17] was used to calculate the linear regression between hourly and 6-minute rainfall parameters. The linear regression was obtained using the least squares method, i.e. by minimizing the sum of the prediction squared errors made by the model. The regression between hourly and 6-minute rainfall parameters was estimated using the correlation coefficient R^2 (calculated with the R stats package) and Lin's concordance coefficient (CCC; Lin, 1989) calculated with the R epiR package (Stevenson, 2012). R^2 and CCC are calculated by the following Equations.

$$R^2 = \frac{\sum_{i=1}^{n}(x_i - \hat{x}_i)^2}{\sum_{i=1}^{n}(x_i - \bar{x})^2} \quad (2)$$

$$ccc = \frac{2S_{xy}}{S_x^2 + S_y^2 + (\bar{x} - \bar{y})^2} \quad (3)$$

Where $S_x^2 = \frac{1}{n}\sum_{i=1}^{n}(x_i - \bar{x})^2$, $S_y^2 = \frac{1}{n}\sum_{i=1}^{n}(y_i - \bar{y})^2$, $S_{xy} = \frac{1}{n}\sum_{i=1}^{n}(x_i - \bar{x})(y_i - \bar{y})$

With y_i = the predicted value of x_i at location$i$, $\bar{x}$ = the mean value of x and n = the number of locations.

[17] R Development Core Team (2012). R. version 2.15.0 (2012-03-30)

R^2 indicates how well two datasets are correlated (linear correlation), whereas CCC measures the agreement between two variables (fitting with the y = x line).

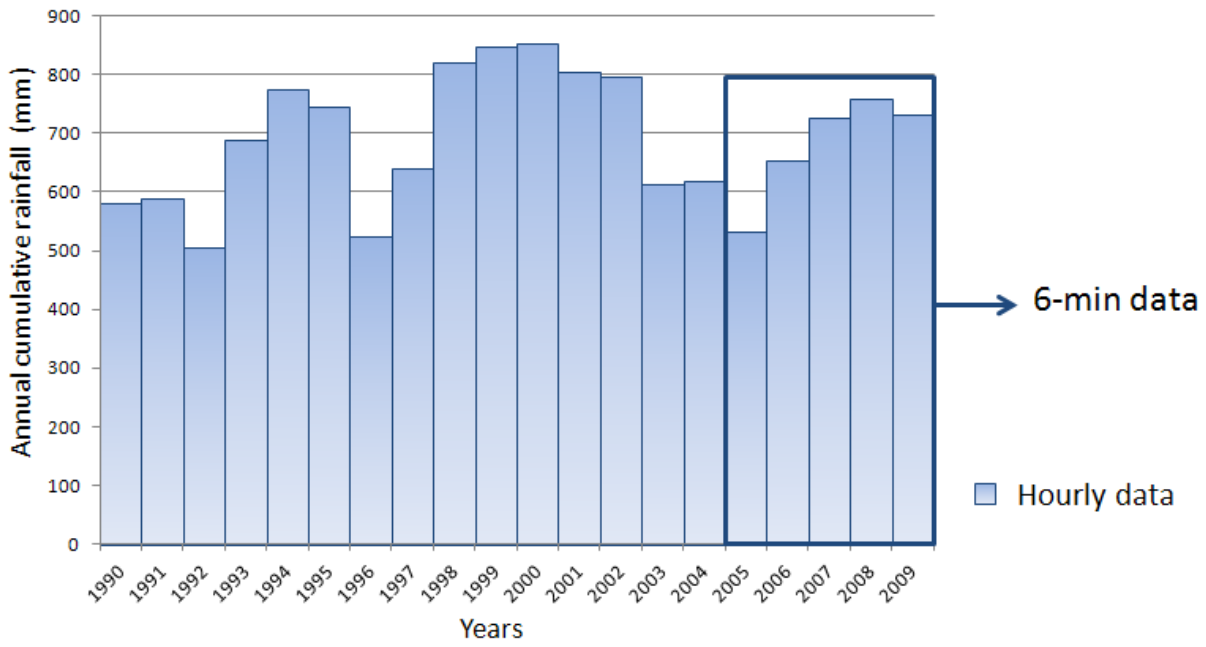

Figure 3-5. Annual rainfall from 1990 to 2009 calculated from hourly meteorological data and position of existing 6-minute interval data (meteorological data for the Rennes station, Météo-France)

3.1.2 Results

3.1.2.1 Calibration of residual water storage after the previous event

Estimates of Ws were derived from 12 simulated rainfall experiments on the calibration sites. For each class of infiltration rate (IR), median values of Ws were estimated and represented as a logarithmic function of IR (Figure 3-8 and Equation 4).

$$Ws = 4.17\ ln(IR) - 5.48 \qquad (4)$$

with:

Ws = residual water storage after the previous event (mm)

IR = infiltration rate (mm h^{-1})

By comparison, default values implemented in LandSoil appeared also to follow a logarithmic function, but with systematic higher Ws values for a given IR (Figure 3-8). Values of Ws were calculated using Equation 4 for each class of infiltration rate defined in LandSoil (Table 3-2).

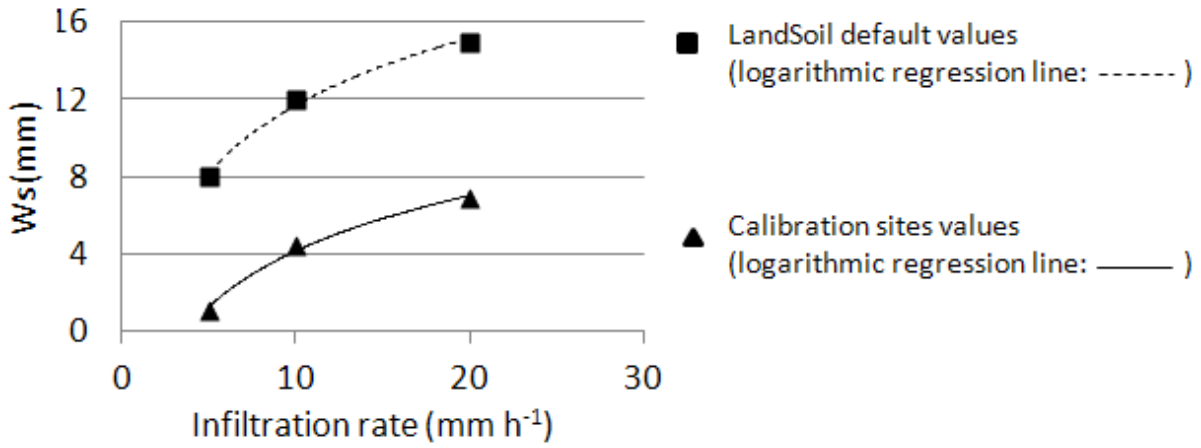

Figure 3-6. Relation between Ws and infiltration rate for calibration sites and default values of the LandSoil model. For the calibration sites, Ws values are median values for each class of infiltration rate.

Table 3-2. Comparison between Ws values from calibration sites (in bold) and Ws default values of the LandSoil model. Ws is expressed considering antecedent rainfall and infiltration rate according to classes defined in LandSoil.

	Antecedent 48-h rainfall (mm)			
Infiltration rate (mm h^{-1})	0	0 - 15	16 - 40	> 40
50	20 - **11**	15 - ***7***	12 - ***4***	8 - ***1***
20	15 - ***7***	12 - ***4***	8 - ***1***	5 - ***0***
10	12 - ***4***	8 - ***1***	5 - ***0***	2 - ***0***
5	8 - ***1***	5 - ***0***	2 - ***0***	1 - ***0***
2	5 - ***0***	2 - 0	1 - ***0***	0 - ***0***

3.1.2.2 Calibration of soil infiltration rates

Infiltration rates were derived from experiments under natural rainfall described by Cros-Cayot (1996). Results are summarized in Table 3-3. They are expressed according to the classes of soil surface parameter, as implemented in LandSoil. Existing data on calibration sites only allowed infiltration rate estimates for three combinations of soil surface parameters. Table 3-3 also gives the default values of IR used in LandSoil, which are on average twice as high as those estimated from the calibration sites.

3.1.2.3 Calibration of sediment concentrations in runoff

Sediment concentrations in runoff were estimated from experiments under natural rainfall (Cros-Cayot, 1996). Results are summarized in Table 3-4. They are expressed according to the classes of soil surface parameters and rainfall maximum intensity, as expressed in LandSoil. Existing data on calibration sites allowed calculating sediment concentration for six combinations of soil surface parameters. Table 3-4 also gives the default values of sediment concentration used in LandSoil and shows no significant difference.

Table 3-3. Comparison of infiltration rate (mm h^{-1}) derived from existing experiments (in bold) on the calibration sites (Cros-Cayot, 1996) and default values of the LandSoil model, according to soil surface characteristics

Soil roughness[a]	Vegetation cover[b]	Crusting stage[c]			
		F0	F11	F12	F2
0 - 1 cm	< 20 %	10	10	5	2
	21-60 %	20			
	> 61 %	50	20	10	5 - ***2.49****
1 - 2 cm	< 20 %	20	10	5	2
	21-60 %	50	20	10	
	> 61 %				5
2 - 5 cm	< 20 %	50	20	10	5
	21-60 %			10 - ***3.15****	5 - ***2.49****
	> 61 %		50	20	10
5 - 10 cm	< 20 %	50	20	10	5
	21-60 %		50	20	10
	> 61 %			50	
> 10 cm	< 20 %	50	20	20	10
	21-60 %		50	50	
	> 61 %				

[a] Soil surface roughness state is defined by the elevation difference between the deepest part of micro depressions and the lowest point of their divide (Ludwig et al., 1995).

[b] Vegetation cover classes are defined as the percentage of soil surface covered by canopy or litter

[c] Soil surface crusting stage. F0= initial fragmentary structure; F11= altered fragmentary state with structural crusts; F12= local appearance of depositional crusts; F2= continuous state with depositional crusts. Soil surface crusting stages were described (Bresson and Boiffin, 1990).

*****Combination of soil surface parameters for which infiltration rates have been measured in calibration sites (values in bold).

3.1.2.4 Disaggregation of hourly rainfall data into 6-minute data

Between July 2005 and December 2009, 1 181 rainfall events were described with their associated hourly and 6-minute parameters. Figure 3-7 (a, b and c) shows the relation between rainfall parameters calculated from 6-minute and hourly data. Rainfall amounts from both datasets were well correlated (R^2 = 1, CCC = 1, Figure 3-7a). Effective rainfall duration and rainfall maximum intensity calculated from hourly data were underestimated compared to those calculated from 6-minute data (Figure 3-7b and c).

Effective rainfall duration and rainfall maximum intensity calculated from 6-minute data were expressed by fitting a multiple linear regression model to rainfall parameters calculated from hourly data. To predict the effective duration for 6-minute data (Def_{6min}), four hourly parameters were found significant: hourly total duration (DT_h), hourly effective duration (Def_h), hourly total rainfall (RR_h) and hourly maximum intensity ($Imax_h$). The relation was well fitted (R^2 = 0.93) and is given by Equation (5).

Table 3-4. Comparison of sediment concentration (g l^{-1}) measured in calibration sites (in bold, Cros-Cayot, 1996) and used as default values in LandSoil according to soil surface characteristics (soil surface crust, roughness and vegetation cover)

Soil roughness[a]	Vegetation cover[b]	Maximum raifall intensity (mm h^{-1})	Crusting stage[c]			
			F0	F1	F12	F2
0 - 1 cm	< 20 %	0 à 10 mm/h	0	2	0	2 - ***1.99****
		10 à 40 mm/h		5	2	5
		> 40 mm/h	2	10	5	10
	21-60 %	0 à 10 mm/h	0	0	0	0 - ***0.48****
		10 à 40 mm/h		2	0	2
		> 40 mm/h	2	5	2	5
	> 61 %	0 à 10 mm/h	0	0	0	0 - ***1.41****
		10 à 40 mm/h		2	0	2 - ***2.41****
		> 40 mm/h	2	5	2	5 - ***3.69****
1 - 2 cm	< 20 %	0 à 10 mm/h	0	0	0	0
		10 à 40 mm/h	2	10	5	10
		> 40 mm/h	5	15	10	15
	21-60 %	0 à 10 mm/h	0	2	0	2
		10 à 40 mm/h		5	2	5
		> 40 mm/h	2	10	5	10
	> 61 %	0 à 10 mm/h	0	2	0	2
		10 à 40 mm/h		5	2	5
		> 40 mm/h	2	10	5	10
2 - 5 cm	< 20 %	0 à 10 mm/h	0			
		10 à 40 mm/h	2	10	5	10
		> 40 mm/h	5	15	10	15
	21-60 %	0 à 10 mm/h	0	2	0	2
		10 à 40 mm/h		5	2 - ***1.76****	5
		> 40 mm/h	2	10	5	10
	> 61 %	0 à 10 mm/h	0	2	0	2
		10 à 40 mm/h		5	2	5
		> 40 mm/h	2	10	5	10

[a] Soil surface roughness state is defined by the elevation difference between the deepest part of micro depressions and the lowest point of their divide (Ludwig et al., 1995).

[b] Vegetation cover classes are defined as the percentage of soil surface covered by canopy or litter

[c] Soil surface crusting stage. F0= initial fragmentary structure; F11= altered fragmentary state with structural crusts; F12= local appearance of depositional crusts; F2= continuous state with depositional crusts. Soil surface crusting stages were described (Bresson and Boiffin, 1990).

*****Combination of soil surface parameters for which infiltration rates have been measured in Champ-Noël (values in bold).

$Def_{6min} = 0.09\ DT_h - 0.06\ Def_h + 0.31\ RR_h - 0.28\ Imax_h + 0.07$ $R^2 = 0.93$ (5)

where:
Def_{6min}= predicted 6-minute effective duration (h)
DT_h= hourly total duration (h)
Def_h= hourly effective duration (h)
RR_h = hourly total rainfall (mm)
$Imax_h$ = hourly maximum intensity (mm h^{-1})

To predict the maximum intensity from 6-minute data ($Imax_{6min}$), five hourly parameters were significant: hourly total duration (DT_h), hourly effective duration (Def_h), hourly total rainfall (RR_h), hourly maximum intensity (PA_h) and antecedent rainfall amounts during the 48 hours preceding the rainfall event. The relation was also well fitted ($R^2 = 0.81$) and is given by Equation (6).

$Imax_{6min} = -0.02\ DT_h + 0.83\ Def_h - 0.63\ RR_h + 4.65\ Imax_h + 0.02\ PA_h + 0.98$ $R^2 = 0.77$ (6)

where:
$Imax_{6min}$= predicted 6-minute maximum intensity (mm h^{-1})
DT_h= hourly total duration (h)
Def_h= hourly effective duration (h)
RR_h=hourly total rainfall (mm)
$Imax_h$= hourly maximum intensity (mm h^{-1})
PA_h= antecedent rainfall amounts (mm)

Figure 3-7 (d and e) shows the relation between rainfall parameters calculated from 6-minute and those predicted from hourly rainfall parameters by Equations 5 and 6. The correlations between both datasets were improved compared to previous ones (Figure 7b and c). For effective rainfall duration, R^2 improved from 0.63 to 0.93 and CCC from 0.68 to 0.96 (Figure 7d). For maximum rainfall intensity, R^2 improved from 0.73 to 0.76 and CCC from 0.31 to 0.86 (Figure 7e).

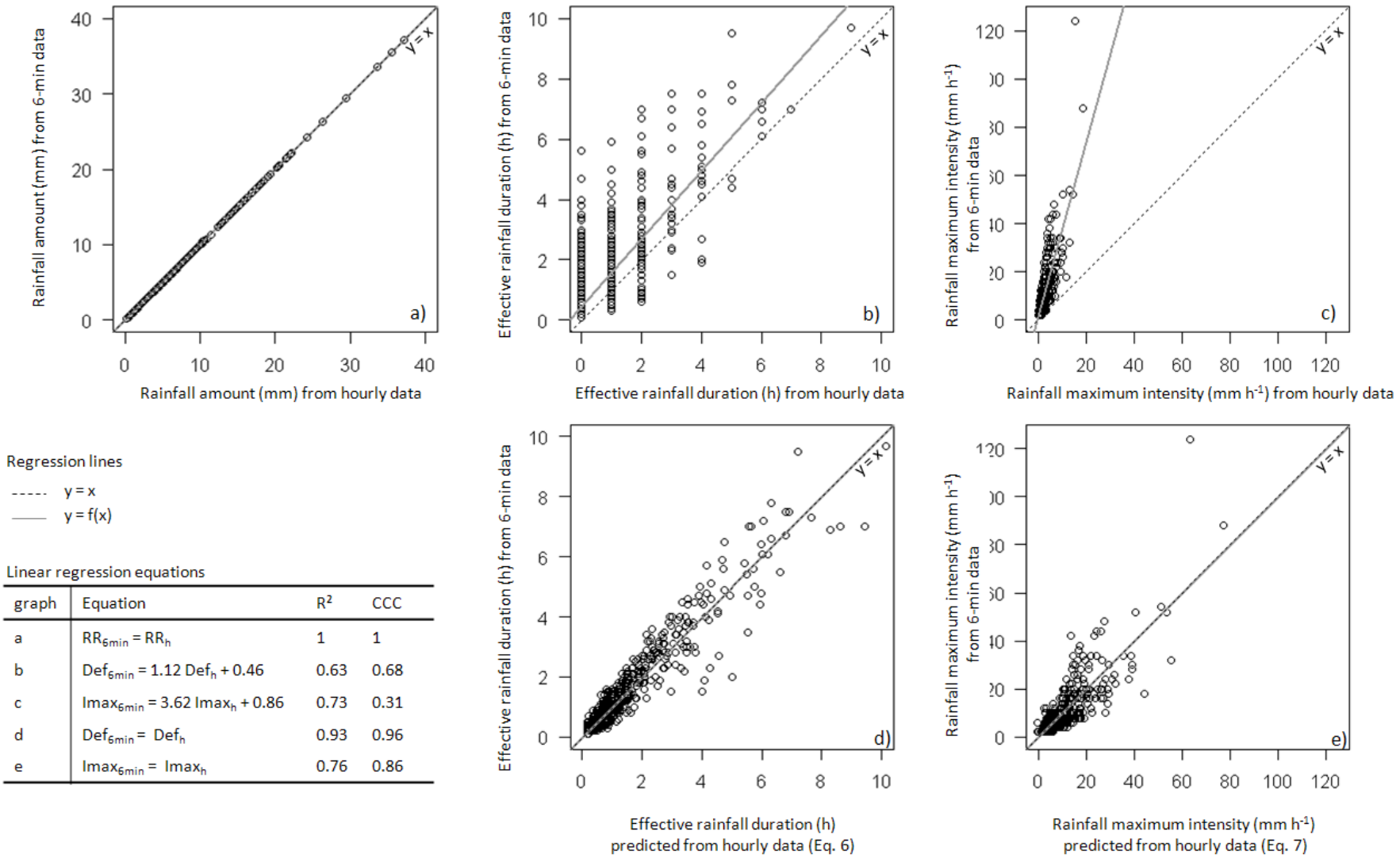

Linear regression equations

graph	Equation	R^2	CCC
a	$RR_{6min} = RR_h$	1	1
b	$Def_{6min} = 1.12\ Def_h + 0.46$	0.63	0.68
c	$Imax_{6min} = 3.62\ Imax_h + 0.86$	0.73	0.31
d	$Def_{6min} = Def_h$	0.93	0.96
e	$Imax_{6min} = Imax_h$	0.76	0.86

Figure 3-7. Comparison of rainfall events parameters calculated from 6-minute and hourly meteorological data (2005-2009, Météo-France, Rennes Station). a, b and c : raw 6-minute and hourly data, d and e: raw 6-minute data and predicted hourly data (Equations 5 and 6). RR= rainfall amount, Def= effective duration, Imax= maximal intensity. R^2= regression coefficient, CCC= Lin's concordance coefficient.

3.1.3 Discussion and choice of parameters for soil redistribution modelling in the study area of Pleine-Fougères

The purpose of this section was to calibrate LandSoil in order to model the redistribution of loamy soils in the context of the PF study area. Three parameters used in LandSoil were estimated from existing data on calibration sites located near Rennes: residual water storage after the previous event (Ws), infiltration rate and sediment concentration in runoff. Ws was estimated in this study from experimental data under simulated rainfall at plot scale, while infiltration rate and sediment concentration in runoff were estimated under natural rainfall at field scale. This allows taking into account field variability, integrating the different soil properties present in the field, and gives results more representative of the whole field (Le Bissonnais et al., 1998a).

Ws is the amount of infiltrated water before the beginning of runoff. Previous studies have shown that Ws variations are due to initial soil water content and soil crusting stage (e.g. Le Bissonnais et al., 1992). Infiltration rate variations are also related to soil crusting stage (Boiffin and Monnier, 1986a; Le Bissonnais et al., 1992) which depends on rainfall characteristics, soil texture, soil organic-carbon content and agricultural practices (namely tillage and crop residues management ; King and Le Bissonnais, 1992). For example, soils with high clay and organic-carbon content are less prone to crusting (Le Bissonnais et al., 1995). Using experimental data from the calibration sites, we found that Ws ranged from 0 to 11 mm on calibration sites, while it ranged from 0 to 20 mm h^{-1} for the model default values. For soil infiltration rate, we found that values ranged from 1 to 25 mm h^{-1}, while they ranged from 2 to 50 mm h^{-1} for the model default values. Soils of the calibration sites and the PF study area have similar properties regarding soil parent material, soil texture and soil organic-carbon content. Crop rotations and farming practices were also similar in both situations. When comparing topsoil texture of the calibration sites, the PF study area and the sites from which the LandSoil default values were derived (Le Bissonnais et al., 1998a), we found that silt fraction ranged from 69 to 74%, 33 to 76% and 57 to 61%, respectively; clay fraction ranged from 14 to 17%, 8 to 25% and 11 to 13%, respectively; sand fraction ranged from 11 to 15%, 13 to 52% and 25 to 27%, respectively; and soil organic carbon content from 1 to 2%, 1 to 8% and 1 to 2%, respectively. We assumed similarity of Ws at both sites, and Ws considered for soil redistribution modelling in the PF study area were estimated from calibration sites (Table 3-2). We assumed that soils of the PF study area had infiltration rate values between those estimated from the calibration sites (1 to 25 mm h^{-1}) and those used as initial values in LandSoil (2 to 50 mm h^{-1}, Table 3-3). Section 3.2 should help to choose the best range of infiltration rate for further use of LandSoil in the PF study area. For the sediment concentration in runoff, estimates from measurement in calibration sites showed values similar to those used as default values in LandSoil and were therefore assumed. The soil parameters used to model soil redistribution in further work are summarized in Appendix 3.

3.2 Use of 137Cs measurements and spatially distributed erosion model to assess long-term soil redistribution in a changing hedgerow landscape

This second part of Chapter 3 aims (i) to assess LandSoil ability to simulate soil redistribution in hedgerow landscapes, and (ii) to have a better estimate of the range of infiltration rate adapted to the loamy soils of the PF study area. This site presents different soil parent materials: granodiorites, tender Brioverian schists, spotted schists, hornfels, and heterogeneous Quaternary Aeolian loam deposits. These deposits have variable composition and thickness. The resulting soils have a silt loam texture with a silt fraction accounting for 60 to 70% of fine earth (see Chapter 2 for details). However, these soils present quite different characteristics, and more specifically different infiltration rates. To take into account these specificities and cover the variability of loamy soils observed in North-Western France (Brittany and Normandy), three ranges of infiltration rate were used: 1 to 25 mm h^{-1} (IR_1), 1.5 to 37.5 mm h^{-1} (IR_2) and 2 to 50 mm h^{-1} (IR_3). These ranges were defined from the results of Section 3.1. IR_1 was defined for loamy soils in Brittany, IR_3 is related to loamy soils of Normandy, and IR_2 corresponds to intermediate values of soil infiltration rates.

Section 3.2 is a submitted paper.

Combining ^{137}Cs measurements and a spatially distributed erosion model to assess soil redistribution in a hedgerow landscape of northwestern France (1960 – 2010)

LACOSTE Marine[1,2,*], MICHOT Didier[2,1,3], VIAUD Valérie[1,2], EVRARD Olivier[4],WALTER Christian[2,1,3],

[1]INRA, UMR1069, Sol Agro et hydrosystème Spatialisation, F-35000 Rennes, France
[2] AGROCAMPUS OUEST, UMR1069, Sol Agro et hydrosystème Spatialisation, F-35000 Rennes, France
[3] Université européenne de Bretagne, France
[4] Laboratoire des Sciences du Climat et de l'Environnement (LSCE/IPSL), UMR 8212 (CEA/CNRS/UVSQ), F-91198 Gif-Sur-Yvette Cedex, France

* Corresponding author at: [1]INRA, UMR1069, Sol Agro et hydrosystème Spatialisation, 65, rue de St-Brieuc CS 84215, 35042 Rennes Cedex – France. Tel.: +332.23.48.70.47.
E-mail address: marine.lacoste@rennes.inra.fr (M. Lacoste).

Abstract

Erosion is one of the main threats to the soils and it is associated with numerous environmental and economic impacts. At the landscape scale, soil redistribution patterns induced by water and tillage erosion are complex, and landscape structures play an important role on their spatial distribution. In this study, soil redistribution patterns, caused by both water and tillage erosion, were estimated in the vicinity of hedges in an agricultural landscape. Two complementary methods were employed: ^{137}Cs conversion models and a spatially-distributed soil erosion model (LandSoil model). Both methods proved that hedges affected soil redistribution patterns, leading to soil deposition or limiting soil erosion uphill from hedges, even if soil erosion rates were always higher than soil deposition rates. Depending on the method, the mean soil redistribution rates varied between -15.9 and -4.7 t ha^{-1} yr^{-1} for all the study sites, -4.8 t ha^{-1} yr^{-1} or 2.2 t ha^{-1} yr^{-1} in positions uphill from hedges, while the rates reached -4.8 to -11.2 t ha^{-1} yr^{-1} in positions located downhill from hedges. The impact of tillage on the soil redistribution in the vicinity of hedges was found to be more important than water processes because 87% of the soil net redistribution was linked to tillage. This confirmed the importance to take landscape structures into account and to work at the landscape scale rather than at the plot scale to better estimate soil redistribution in agricultural areas.

Keywords: soil redistribution; ^{137}Cs; spatial modelling; hedge; agricultural landscape

1. Introduction

In 2006, the European Commission identified soil erosion as one of the major threats on soils. Soil erosion may affect all soil functions (Boardman and Poesen, 2006), also described as soil ecosystem services (Dominati et al., 2010): life and human activity physical support, food and fibre production, water filter, oxygen production, carbone storage and climate regulation, etc. Soil erosion has been recognised to have direct consequences both on-site (because of the soil loss from fields), and off-site: during the last decades, a significant increase in environmental issues such as eutrophication, pollution of water bodies and reservoir sedimentation has been observed in Europe, as a result of soil erosion on agricultural land (Boardman and Poesen, 2006). In numerous cases soil erosion leads to a significant reduction in soil thickness. If soil thickness decline is not compensated

by soil formation, soil erosion may induce the loss of soil nutrients (Bakker et al., 2004) or soil organic carbon (Papiernik et al., 2005; Papiernik et al., 2009), and threaten the sustainability of crop production (Bakker et al., 2004). Methods and models have been developed to estimate soil redistribution by erosion and to understand the effect of several parameters on this redistribution (climate, soil properties, land use and agricultural practices, landscape structure, etc.). Before the 1990s, studies focused mostly on water erosion, because this was the most obvious process contributing to soil exportation out of cultivated fields (Govers et al., 1996). However, it is now recognized that tillage erosion is also an important process to consider, especially when studying soil loss and deposits within individual fields (Govers et al., 1994). Regarding erosion rates, tillage erosion can have an equivalent or even a higher impact than water erosion on soil redistribution (Govers et al., 1999; Lobb et al., 2007; Van Oost et al., 2005b; Chartin et al., 2013). Both water and tillage erosion depend on topography, but have distinct impacts on soil redistribution regarding spatial patterns (Li et al., 2007). Water erosion is maximal on steep mid-slopes and where water concentrates, whereas tillage induces maximum erosion at convexities and deposition at concavities (Govers et al., 1996; Li et al., 2007; Thiessen et al., 2009; Van Oost et al., 2005b). Moreover, there are linkages and interactions between water and tillage erosion (Li et al. 2007).

Runoff and soil erosion have been studied at different scales, from plots to catchments, and it appears that both landscape management and structure have an impact on soil erosion and sedimentation in agricultural land. The impacts of land use on soil redistribution have been shown in many studies, whatever the spatial extent considered. Cerdan et al. (2010) compiled European studies of soil erosion conducted at plot scale and showed that spring crops and vineyards were the most sensitive land uses to soil erosion. From a long-term survey of soil erosion at the catchment scale, Prasuhn (2012) showed that potatoes were the crop inducing the most serious soil erosion. Consequently, land use change has an impact on soil redistribution dynamics. Vannière et al. (2003) examined the impact of historical human occupation on soil redistribution at the hillslope scale. They explained the recorded variations in soil erosion by the changes in agricultural activities. Bakker et al. (2008) estimated that the past land-use change (de-intensification or intensification) in four European landscapes directly impacted soil erosion and sediment export to the rivers. Besides land use, the farming practices, and particularly the tillage practices, impact the soil redistribution. Van Muysen et al. (2000) showed that soil distribution depends on tillage speed and depth. Prasuhn (2012) observed that conventional plough tillage induced higher soil erosion rates than reduced tillage practices. However, it has been shown that these factors (land use and farming practices) were not sufficient to understand soil redistribution at landscape and catchment scales. Bakker et al. (2008) underlined that the spatial pattern of land use change strongly impacted soil redistribution and export out of the studied catchments. In this context, the spatial distribution and the connectivity between areas producing soil erosion and the zones where deposition takes place should be taken into account in the framework of studies conducted at the landscape or catchment scale (Cerdan et al., 2012; Delmas et al. 2012). Vegetated filter strips are part of the anthropogenic structures that impact connectivity inside a landscape, with an effect on water and sediments transfer (Bracken and Croke, 2005; Evrard et al., 2008; Gumiere et al., 2011). More particularly, linear structures such as hedges have been recognised as key elements of the landscape to prevent or limit erosion (Baudry et al., 2000; Boardman and Poesen, 2006; Kiepe, 1995b; Skinner and Chambers, 1996). During the last decades, important changes in landscape structure and soil use have been observed in Western Europe: land use homogenisation, removal of linear structures such as hedges and loss of connectivity between landscape elements were outlined to be the main observed

changes (Burel and Baudry, 1990; Deckers et al., 2005; Petit et al., 2003). Such changes in landscape modify soil redistribution dynamics (Evrard et al., 2010) and should be taken into account in soil redistribution modelling.

The ability of empirical models (e.g. USLE) to integrate the dominant processes of soil redistribution at the catchment scale is uncertain (Kirkby et al., 1996), whereas process-based models require numerous input data, which are generally not available and difficult to measure (Takken et al., 1999). In such a context, spatially-distributed and expert-based models (e.g. STREAM; Cerdan et al., 2002b) can offer an alternative solution, especially when dealing with connectivity issues in landscapes (Gumiere et al., 2010). Such models focus on the dominant processes to avoid over-parameterisation and the associated uncertainties, and model simulations rely on decision rules derived by expert judgment from databases of field measurements carried out in a specific region. However, validation of such models remains an important issue in areas where experimental data, i.e. runoff and erosion measurements, are missing. This issue can be addressed by using ^{137}Cs. ^{137}Cs is an artificial radionuclide (half-life of 30 years) produced by the thermonuclear bomb tests conducted during the 1960s as well as, in certain regions of the world (i.e., mainly in Europe), by the Chernobyl accident in 1986. ^{137}Cs is now stored in soils, and its stock decreases by radioactive decay and by fine sediment transfer due to water and tillage erosion. ^{137}Cs has been widely used as a tracer of soil redistribution and it proved to be useful in soil erosion studies conducted around the world (Ritchie and McHenry, 1990; Zapata, 2003a). Several studies showed a good correlation between soil redistribution obtained from ^{137}Cs inventories and field measurements (Kachanoski, 1987; Mabit et al., 2002; Porto and Walling, 2012; Porto et al., 2001; Porto et al., 2003a; Porto et al., 2003b) and ^{137}Cs has been used previously to validate or calibrate erosion models (Bacchi et al., 2003; Li et al., 2007; Li et al., 2008; Li et al., 2000; Porto et al., 2003b; Quine, 1999; Tiessen et al., 2009; Walling et al., 2003). The use of ^{137}Cs estimates of soil redistribution relies on several hypotheses, especially that the distribution of local fallout was uniform (Walling and Quine, 1992). Such a statement could be uncertain in complex hedgerow landscapes, especially close to hedges (Follain et al., 2009). Moreover, Parsons and Foster (2011) underlined that the conditions necessary to the use of ^{137}Cs as a soil redistribution indicator are most often not verified. Another limitation is that ^{137}Cs is not a spatially integrative measurement and its high cost may limit sampling at landscape scale.

In this study, we aim to combine two methods to estimate the spatial and temporal soil redistribution dynamics near hedges from 1960 to 2009, in a rural hedgerow landscape. A new model simulating soil redistribution at the landscape scale (LandSoil, Ciampalini et al., 2012) and ^{137}Cs measurements have been used to this end. The results of both methods will be compared and discussed.

2. Materials and methods

2.2. Study sites

The study sites were selected within the study area of Pleine-Fougères (NW France, 48° 505’ N, 1° 565’ W), which belongs to the European Long-Term Ecosystem Research Network, and covers an area of 10 km² (Fig. 1). This area is characterised by a high soil spatial heterogeneity. Soil types are mainly Cambisols and Luvisols, but Leptsosols and Fluvisols from alluvial and colluvial deposits are also found (IUSS Working Group WRB, 2007). These soils exhibit features reflecting variable redoximorphic conditions, soil and A-horizon thickness, and soil parent material (granite, hard and soft schist with a heterogeneous cover of superficial deposits such as aeolian loam, alluvium and

colluviums). Main topographical features may be associated with the presence of different geological substrates: granite under the plateau (south of the study area), Brioverian schists under plains (north of the area), metamorphic schists at the transition between granite and soft schist under hillslides. In addition, the presence of linear anthropogenic structures at field boundaries (hedges, banks, ditches, lanes and roads) delineates large microtopographical changes. Landscape evolution has been driven by former agricultural policies and local farming practices, consisting in the enlargement of fields in order to facilitate the use of large machinery. Numerous hedges have been removed during a land consolidation programme conducted in the early 1990s, and some are still selectively removed by farmers. The result is that hedge density decreased from 250 m ha^{-1} in 1952 to 90 m ha^{-1} in 2000 (unpublished data, derived from analysis of aerial photographs using Geographical Information Systems). The main land uses are annual crops (maize (*Zea mays*), winter wheat (*Triticum aestivum*)) and temporary or permanent grasslands (mostly Italian ryegrass, *Lolium multiflorum*). Hedges mainly consist of grass strips planted with trees such as oaks (*Quercus robur)*, chesnuts (*Castanea sativa)* and blackthorns (*Prunus spinosa*).

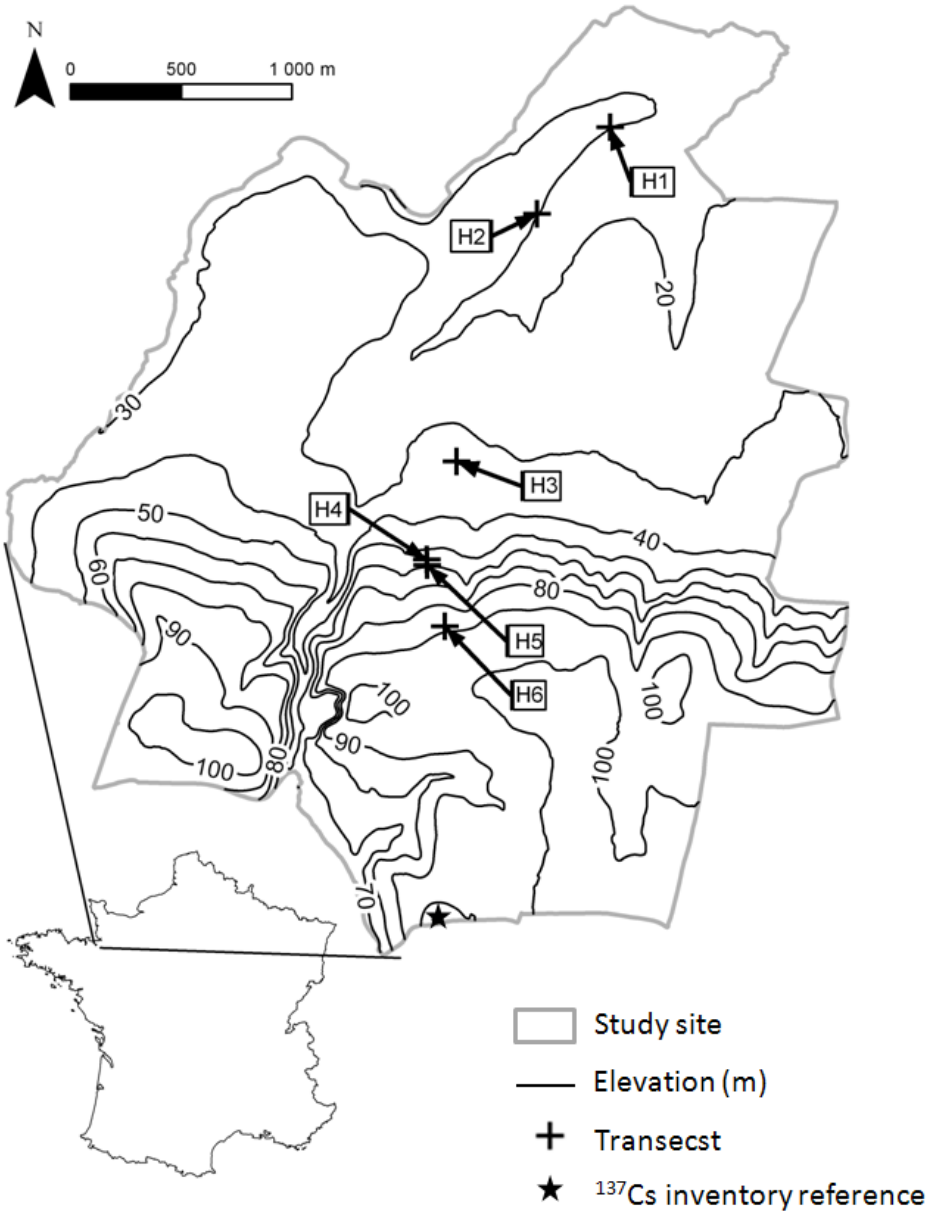

Figure 3-8. Location of the transects in the study area of Pleine-Fougères

Six 30-m long transects, perpendicular to six hedges (one transect per hedge) and parallel to the slope have been determined (Table 3-5). They have been chosen to document the variability observed across the study area in terms of soil depth, local slope and drainage area. Five transects were intersecting currently existing hedges, whereas one transect was selected along a hillslope where the hedge was removed in 1970. The field size around the transects ranged from 0.3 to 3 ha (mean value = 1 ha). We ensured that each transect was representative of soil redistribution along the hedge by conducting a slingram electromagnetic survey (EM31). Along each transect, eight locations were sampled at increasing distances from the hedge: one point in the hedge bank, four points uphill from the hedge at 20, 10, 5 and 2 m and three points downhill of the hedge (at 2, 5 and 10 m). A field survey was carried out in 2009. Soils were described at every sampling point using auger (soil type, soil thickness, A-horizon thickness, colour, texture, gravel content, soil organic carbon content) and a precise toposequence of soil horizons was drawn. Soil redistribution along transects was inferred from comparison between the observed A-horizon thickness and the tilled layer thickness.

2.3. Estimating soil redistribution rates based on ^{137}Cs measurements

For each hedge, two soil profiles were sampled for ^{137}Cs measurements in March 2010: samples were systematically collected at 5 m uphill and downhill from the hedge, respectively. Undisturbed soil cores were sampled with a 7.5 cm diameter hydraulic core sampler (SEDIDRILL 80) to document the total A-horizon thickness (up to 90 cm). All cores were cut into sections of variable length: the first section corresponded to the uppermost 30 cm (i.e. the ploughed mixed layer), whereas the deeper sections were cut into 5 cm sections. All samples were dried at 105°C, weighed and sieved to 2 mm. ^{137}Cs activity was then measured for 102 samples, at 661 keV using Germanium gamma-ray detectors (Germanium hyperpure – GeHP, N-type, coaxial model) for 80,000 to 300,000 s.

Total ^{137}Cs inventory (^{137}Cs surface activity; A_S in Bq m^{-2}) of each core was then calculated according to Eq. (1):

$$A_S = \sum_{i=1}^{n} A_i \times \frac{M_i}{S} \qquad (1)$$

where A_i is the ^{137}Cs concentration in each sub-sample *i* of the core containing ^{137}Cs (Bq kg^{-1}); M_i is the mass (kg) of the soil fine fraction of each sub-sample *i*; S is the surface area (m^2) of the soil core; n is the number of sections in the soil core.

In order to estimate whether soil deposition or erosion occurred in the investigated area, ^{137}Cs inventories were compared to an additional soil core, used as reference and sampled at an undisturbed site, i.e. in a pasture located to the south of the study area (a flat part of the plateau), where we considered that soil redistribution was very unlikely to occur during the past 60 years. Soil redistribution rates (t ha^{-1} yr^{-1}) were calculated using the ^{137}Cs conversion models developed by Walling and He (2001). The use of these models relies on four hypotheses (Walling and Quine, 1992): (i) the ^{137}Cs fallout is locally and spatially uniform, (ii) the fallout is rapidly and irreversibly fixed onto soil particles; (iii) the subsequent redistribution of fallout is due to the movement of soil particles; and (iv) estimates of soil erosion can be derived from measurements of ^{137}Cs inventories. Regarding the irreversible binding issue, Kato et al. (2012) observed after the Fukushima Daiichi nuclear accident that the bulk of radiocaesium was absorbed in the upper 2.0 cm in the soil profile.

Table 3-5. Characteristics of sampling locations for ^{137}Cs inventories and modelling area

Hedges								^{137}Cs sampling sites		
Study site	Date of hedge removal (where applicable)	Orientation	Soil parent material	Topographic location	Local slope (%)	Uphill slope length (m)	Modeling area extent (ha)	Position relative to the hedge*	Soil thickness (cm)	A-hz thickness (cm)
H1	-	NE-SW	Brioverian schist	plain	3.3	10.9	1.68	$H1_{up}$	40	40
								$H1_{down}$	21	21
H2	1970	NE-SW	Brioverian schist	plain	3.0	10.3	1.68	$H2_{up}$	55	40
								$H2_{down}$	70	36
H3	-	E-W	Brioverian schist	plain	1.3	5.6	2.47	$H3_{up}$	70	64
								$H3_{down}$	60	53
H4	-	E-W	Aeolian loam	hillside	6.9	7.0	1.64	$H4_{up}$	500	90
								$H4_{down}$	490	30
H5	-	E-W	Aeolian loam	hillside	6.5	24.0	0.91	$H5_{up}$	550	70
								$H5_{down}$	500	30
H6	-	E-W	Hornfels	upper hillside	4.0	30.1	1.21	$H6_{up}$	50	38
								$H6_{down}$	30	30

* up: sampling site uphill from the hedge, down: sampling site downhill from the hedge

In this study we applied four ^{137}Cs conversion models: two proportional models (PM) and two mass-balance models (MBM). PM are based on the premise that ^{137}Cs fallout inputs are completely mixed within the plough layer, and that the soil loss is directly proportional to the amount of ^{137}Cs removed from the soil profile since the beginning of the ^{137}Cs accumulation. PM-1954 considers ^{137}Cs fallout since 1954, whereas PM-1963 takes ^{137}Cs into account since 1963 (when the major fallout occurred). MBM are more complex. The simplified mass balance model (MBM1) takes into account the progressive decrease of ^{137}Cs content in the plough layer because of the mixing with soil which lowers concentration of ^{137}Cs. Additionally, MBM2 takes into account the variation in ^{137}Cs fallout over time (based on the annual ^{137}Cs fallout measured in the northern hemisphere) and the ^{137}Cs redistribution before its incorporation in soil by ploughing. Both MBM1 and MBM2 consider the major ^{137}Cs fallout since 1963. These ^{137}Cs conversion models have been implemented in software developed by Walling and He (2001).

2.4. Modelling soil redistribution over a 50-year period (1960-2010)

The LandSoil model (Ciampalini et al, 2012) was used to simulate soil redistribution between 1960 and 2009. This model is based on a combination of the STREAM runoff and soil erosion model (Cerdan et al., 2002a; Cerdan et al., 2002b; Souchere et al., 2003; Souchere et al., 1998) and the WaTEM/SEDEM tillage erosion model (Van Oost et al., 2000, Van Rompaey et al., 2001, Verstraeten et al., 2002). LandSoil is an expert-based model designed to simulate soil redistribution at a fine spatial resolution scale (1–10 m), a medium-term temporal scale (10–100 yrs.), and for study areas ranging from the field to the catchment. LandSoil is spatially-distributed, event-based, and aims to simulate soil erosion (interrill, concentrated and tillage erosion) and deposition. The model assumes that surface characteristics (soil surface crusting, surface roughness, vegetation cover (crops and residues) and residual water storage after the previous event) are the main drivers of runoff and infiltration at the field scale. A soil infiltration rate value (IR), i.e. a constant soil infiltration rate reached during prolonged rainfall which determines the production of runoff during a rainfall event, is assigned to each combination of these soil surface characteristics (Le Bisonnais et al., 1998;2005). For instance, soils with thick depositional crusts and low vegetation cover were assigned with low values of IR, whereas soils with high roughness and fragmentary structure have higher IR values. In the same way, the model assumes that surface characteristics and the maximum intensity of rainfall are the main drivers of sediment concentration in runoff. This concentration is also determined for each combination of the soil surface characteristics and rainfall maximum intensity (Cerdan et al. 2002e). To estimate the soil water erosion, the IR parameter is combined with the potential sediment concentration in runoff and with landscape properties (mainly the slope intensity). An adaptation of the rules to the local context (types of crops planted and climate) is required before running the model (Evrard et al., 2009; Evrard et al., 2010).

Several studies have estimated IR on loamy soils from Western France using plot measurements under rainfall simulation or field scale monitoring networks under natural rainfalls. Soils considered in these studies differed slightly by texture and carbon content, but showed large variations of IR associated with the variations of soil surface characteristics throughout time: Cros-Cayot (1996) and Lacoste (2012a) found IR ranging from 1 to 25 mm h^{-1} depending on surface characteristics. In different sites characterised by similar soil types, Le Bissonnais et al. (1992) and Evrard et al. (2008) estimated variations between 2 to 50 mm h^{-1}. To take into account this variability, three ranges of IR variation were considered (Table 3-6): 1 to 25 mm h^{-1} (IR_1), 1.5 to 37.5 mm h^{-1} (IR_2) and 2 to 50 mm h^{-1} (IR_3). Concerning hedges, previous studies found a wide range of IR under hedges, according to

hedge composition, thickness and climate of the study area (Table 3-7). In this study, IR under hedges was fixed at 150 mm h^{-1}. Regarding the soil concentration in runoff, the default values were determined after Cerdan et al. (2002b and 2002e) and ranged from 0 to 25 g L^{-1}. These default values have been estimated for loamy soils with similar characteristics as those of the soils in our study area, and local studies confirmed the relevance of their use in our study (Gascuel-Odoux et al, 1996; Lacoste, 2012).

LandSoil simulates soil deposition in two cases: for a given pixel, (i) soil deposit is modelled when water infiltration is higher than runoff, and (ii) when the sediment transport by water erosion is limited. For this second case, the maximum sediment concentration is controlled by several threshold functions based on the local topography and soil cover (Cerdan et al, 2002b). These functions include profile curvature (concavity > 0.055 m^{-1}), slope gradient (< 5 %), land use (permanent grassland and wood) and vegetation cover (> 60 %).

Table 3-6. The three ranges of variation of soil infiltration rate (mm h^{-1}) used to model soil redistribution. IR are classified according to parameters of soil surface (values for $IR_1 – IR_2 – IR_3$)

Soil roughness[a]	Vegetation cover[b]	Crusting stage[c]			
		F0	F11	F12	F2
0 - 1 cm	< 20 %	5 - 7.5 - 10	5 - 7.5 - 10	2.5 - 3.75 - 5	1 - 1.5 - 2
	21-60 %	10 - 15 - 20			
	> 61 %	25 - 37.5 - 50	10 - 15 - 20	5 - 7.5 - 10	2.5 - 3.75 - 5
1 - 2 cm	< 20 %	10 - 15 - 20	5 - 7.5 - 10	2.5 - 3.75 - 5	1 - 1.5 - 2
	21-60 %	25 - 37.5 - 50	10 - 15 - 20	5 - 7.5 - 10	
	> 61 %				2.5 - 3.75 - 5
2 - 5 cm	< 20 %	25 - 37.5 - 50	10 - 15 - 20	5 - 7.5 - 10	2.5 - 3.75 - 5
	21-60 %			5 - 7.5 - 10	2.5 - 3.75 - 5
	> 61 %		25 - 37.5 - 50	10 - 15 - 20	5 - 7.5 - 10
5 - 10 cm	< 20 %	25 - 37.5 - 50	10 - 15 - 20	5 - 7.5 - 10	2.5 - 3.75 - 5
	21-60 %		25 - 37.5 - 50	10 - 15 - 20	5 - 7.5 - 10
	> 61 %			25 - 37.5 - 50	
> 10 cm	< 20 %	25 - 37.5 - 50	10 - 15 - 20	10 - 15 - 20	5 - 7.5 - 10
	21-60 %		25 - 37.5 - 50	25 - 37.5 - 50	
	> 61 %				

[a] Soil surface roughness state is defined by the elevation difference between the deepest part of micro depressions and the lowest point of their divide (Ludwig et al., 1995).

[b] Vegetation cover classes are defined as the percentage of soil surface covered by canopy or litter

[c] Soil surface crusting stages from Bresson and Boiffin (1990). F0 = initial fragmentary structure; F11 = altered fragmentary state with structural crusts; F12 = local appearance of depositional crusts; F2 = continuous state with depositional crusts.

The LandSoil model was run for all rainfall/tillage events that occurred from 1960 to 2009 in the areas where ^{137}Cs inventories were available (Table 3-5). The modelling areas included one field uphill and one downhill from the hedges where transects were investigated, and the field boundaries (hedges, banks and ditches).

The following inputs were provided to LandSoil to model soil redistribution:

(i) Initial elevation: a 2-m LiDAR DEM (light detection and ranging digital elevation model), produced in 2009, was used. It allows taking into account fine topographic variations close to the hedges.

(ii) Crop rotations and associated soil surface characteristics (soil surface crusting, surface roughness, and vegetation cover). We used aerial photographs, taken during summer in 1966, 1968 and from 1993 to 2009, to create crop transition matrices (based on Markov chain) and allocated a main crop per field for each year from 1960 to 2009. Crop rotations consisted of a succession of maize, winter cereals and temporary grassland. Monthly soil surface characteristics were attributed to each crop from expert knowledge and field survey data.

(iii) Soil tillage operation data (direction of tillage and coefficient of tillage erosion). Two tillage transport coefficients (KTILL) are used by LandSoil to model soil redistribution by tillage: KTILLmax for describing soil redistribution parallel to the tillage direction and KTILLmin for characterising soil redistribution perpendicular to the tillage direction. For years with maize or winter cereals sowing, the sequence of tillage operations consisted in the use of mouldboard plough (25 to 30 cm depth), chisel, rotary harrow and air seeder. For years where grassland was established, the sequence of tillage operations consisted in the use of chisel and air seeder. Van Muysen et al. (2006) showed that the KTILL of a sequence of tillage operations can be predicted by summing the KTILL of all individual tillage operations. They also calculated that the mean annual $KTILL_{max}$, associated with mechanized agriculture, is in the order of 781 kg m^{-1} yr^{-1}. Mean annual KTILL coefficients were defined based on the results of previous studies (Table 4). Values for $KTILL_{max}$ and $KTILL_{min}$ reached respectively 631 and 376 g m^{-1} for the years with maize or winter wheat sowing, and 291 and 139 g m^{-1} for the years with grassland sowing.

Table 3-7. Comparison of infiltration rates for hedges available from the literature

Reference	Study site	Hedge type, wide	Infiltration rate (mm h^{-1})
Alegre and Rao, 1996	Loreto, Peru	Contour hedgerow (*Inga edulis*), 0.5 m	500
Anderson et al , 2009	Missouri, USA	Contour strip (*Agrostis gigantea* , *Bromus* spp., *Lotus Corniculatus* L., *Quercus palustris* Muench, *Quercus bicolor* Willd., *Quercus macrocarp* Michx), 4.5 m	17
Bharati et al., 2002	Iowa, USA	Grass strip (*Panicum virgatum* L.), 7.1 m ; Shrub strip (*Cornus stolonifera* Michx., *Physocarpus opulifolius* L.), 2 rows ; Tree strip (*Populus X euramericana* 'Eugenei', *Fraxinus pennsylvanica* Marsh. , *Acer saccharinum* L., *Juglans nigra* L.), 5 rows	90-450
Kiepe et al, 1995	Kenya	Contour hedgerows of *Cassi siamea* Lam.	69-135
Perret et al., 1996	Reunion Island	*Caliendra* hedges	225
Rachman et al., 2004	Iowa, USA	Grass strip, 0.75-1 m	144-208
Richet et al. 2006	Normandy, France	Grass strip, 0.75-1 m	120-200
Souiller et al., 2002	Loire-Atlantique, France	Grass strip, 3 m^2	83-123 (mean value: 106)

(iv) Rainfall event characteristics: rainfall amount (mm), rainfall maximum intensity (mm h^{-1}), effective rainfall duration (h) and rainfall amount during the 48-h before the event (mm). These parameters were defined from predictive 6-minute meteorological data from 1960 to 2009, estimated from hourly meteorological data from Lacoste (2012a). Hourly data were provided by the INRA unity Agroclim for the Rennes Station.

Table 3-8. Tillage erosion coefficients available from the literature and chosen in this study (in bold)

Reference	Implement	Soil bulk density (g cm^{-3})	Tillage depth (cm)	Tillage speed (m s^{-1})	$KTILL_{max}$ (kg m^{-1})	$KTILL_{min}$ (kg m^{-1})
Values for ligth cultivators plus seeders					*60*	*n.a.*
Li et al., 2007	Air seeder	1.27	3	2.23	18	n.a.
Li et al., 2007	Light cultivator	1.25	8	2.23	42	n.a.
Mean values for chisel ploughs					*274*	*139*
Govers et al. , 1994	Chisel plough	1.35	12	1.25	111	n.a.
Poesen et al., 1997	Duckfoot chisel	1.58	15	0.65	282	139
Quine et al, 1999	Duckfoot chisel	1.38	19	2.3	657	n.a.
Tiessen et al. 2007	Chisel plough	1.37	16.2	1.92	64.4	n.a.
Van Muysen et al., 2001	Chisel plough	1.25	20	2.02	258	n.a.
Mean values for mouldboards					*297*	*237*
Lindstrom et al. , 1992	Mouldboard	1.35	24	2.1	330	363
Montgomery et al. 1999	Mouldboard	1.31	23	1	n.a.	110
Revel et al. 1993	Mouldboard	1.35	27	1.8	263	n.a.
Values used for a full tillage sequence for maize or wheat sowing (mouldboard, chisel, light cultivator and air seeder)					*631**	*376**
Values used for a full tillage sequence for grassland sowing (chisel, light cultivator and air seeder)					*292**	*139**

From LandSoil outputs, we computed for each 2-m pixel of the modelled areas the soil redistribution rates and the proportion of soil redistribution by water erosion processes compared to the absolute net soil redistribution.

2.5. Comparing soil redistribution rates derived from ^{137}Cs and from modelling

For the two methods, negative values of soil redistribution rate correspond to soil erosion rates, whereas positive values are soil deposition rates. The soil redistribution rates estimated by ^{137}Cs were located and valid for the sampling points alone, whereas those estimated from LandSoil modelling were grid maps, spatially explicit across the fields located uphill and downhill from the studied hedges. To facilitate comparison between both estimation methods, soil redistribution rates derived from LandSoil modelling were averaged over 10*10 meters windows centred on the ^{137}Cs sampling points. The redistribution rates showed in the results refer to these two spatial extents: points for the ^{137}Cs-derived estimations and 10*10 meters windows for the LandSoil modelling. These results were compared to the soil redistribution rates obtained from the ^{137}Cs survey using the correlation coefficient R^2 (Eq. 2) and Lin's concordance coefficient (Eq. 3).

$$R^2 = \frac{\sum_{i=1}^{n}(x_i - \hat{x}_i)^2}{\sum_{i=1}^{n}(x_i - \bar{x})^2} \qquad (2)$$

$$ccc = \frac{2S_{xy}}{S_x^2 + S_y^2 + (\bar{x}-\bar{y})^2} \quad (3)$$

Where $S_x^2 = \frac{1}{n}\sum_{i=1}^{n}(x_i - \bar{x})^2$, $S_y^2 = \frac{1}{n}\sum_{i=1}^{n}(y_i - \bar{y})^2$, $S_{xy} = \frac{1}{n}\sum_{i=1}^{n}(x_i - \bar{x})(y_i - \bar{y})$

In both equations *x* and *y* are estimates of soil redistribution rate by ^{137}Cs and LandSoil, respectively, y_i and x_i are estimate of soil redistribution rate for the sampling site *i*, $\bar{x}$ is the mean value x and *n* is the number of sampling sites.

R^2 indicates how well two datasets are correlated (linear correlation), whereas CCC measures the agreement between two variables. CCC combines measurements of both precision and accuracy to determine how far the observed data deviate from the line of perfect concordance (i.e. the 45°-line on a square scatter plot).

3. Results

3.1. Soil redistribution rates based on ^{137}Cs measurements

Fig. 2 gives an example of the soil redistribution patterns observed along the transects crossing the hedges H4 and H5, and the associated ^{137}Cs concentration distributions with depth. These two hedges were located in the centre of the study area, on the hillside, on deep soils developed in aeolian loams. For both H4 and H5, we observed soil deposition uphill from the hedge (characterised by an A-horizon thicker than the ploughed horizon), and soil erosion downhill from the hedge (characterised by a thinner A-horizon).

The reference ^{137}Cs inventory was 1590 Bq m^{-2}. The results of ^{137}Cs inventories calculated uphill and downhill from each hedge were compared in Table 5. Except for H4 and H5, ^{137}Cs inventories measured uphill and downhill from the hedges were lower than the reference ^{137}Cs inventory. Except for the hedge H3, ^{137}Cs inventories uphill from all the other hedges differed from the ones calculated for downhill positions and ranged from 123 Bq m^{-2} (H6) to 1010 Bq m^{-2} (H2). For three hedges (H1, H4 and H5), ^{137}Cs inventories were higher in uphill positions. For three hedges (H2 and H6) the opposite result was observed. For the hedge H3, ^{137}Cs inventories were similar in both positions (difference of 8 Bq m^{-2} between both positions).

The soil redistribution rates estimated from the four ^{137}Cs conversion models were well correlated, with an R^2 ranging from 0.94 to 1 and CCC ranging from 0.80 to 0.97 (Table 5). The largest difference between model estimates was obtained for $H2_{up}$ (where the hedge was removed in 1970), with a difference of 41 t ha^{-1} yr^{-1}. According to ^{137}Cs inventories, the mean soil redistribution rate was estimated to -12.60 t ha^{-1} yr^{-1}, the mean soil erosion rate was estimated to -15.89 t ha^{-1} yr^{-1}, and the mean soil deposition rate to 3.82 t ha^{-1} yr^{-1}. Among the six sampling sites, four were estimated to be erosion sites, both for positions uphill and downhill from the hedge (H1, H2, H3 and H6). For transects across hedges H4 and H5, positions uphill from the hedge were estimated to be deposition sites, whereas positions downhill from the hedge were estimated to be erosion sites. Focusing of the 5 currently existing hedges, the mean soil redistribution rate was estimated to -4.77 t ha^{-1} yr^{-1} for the positions uphill from the hedges, and to -11.15 t ha^{-1} yr^{-1} for the positions downhill from the hedges.

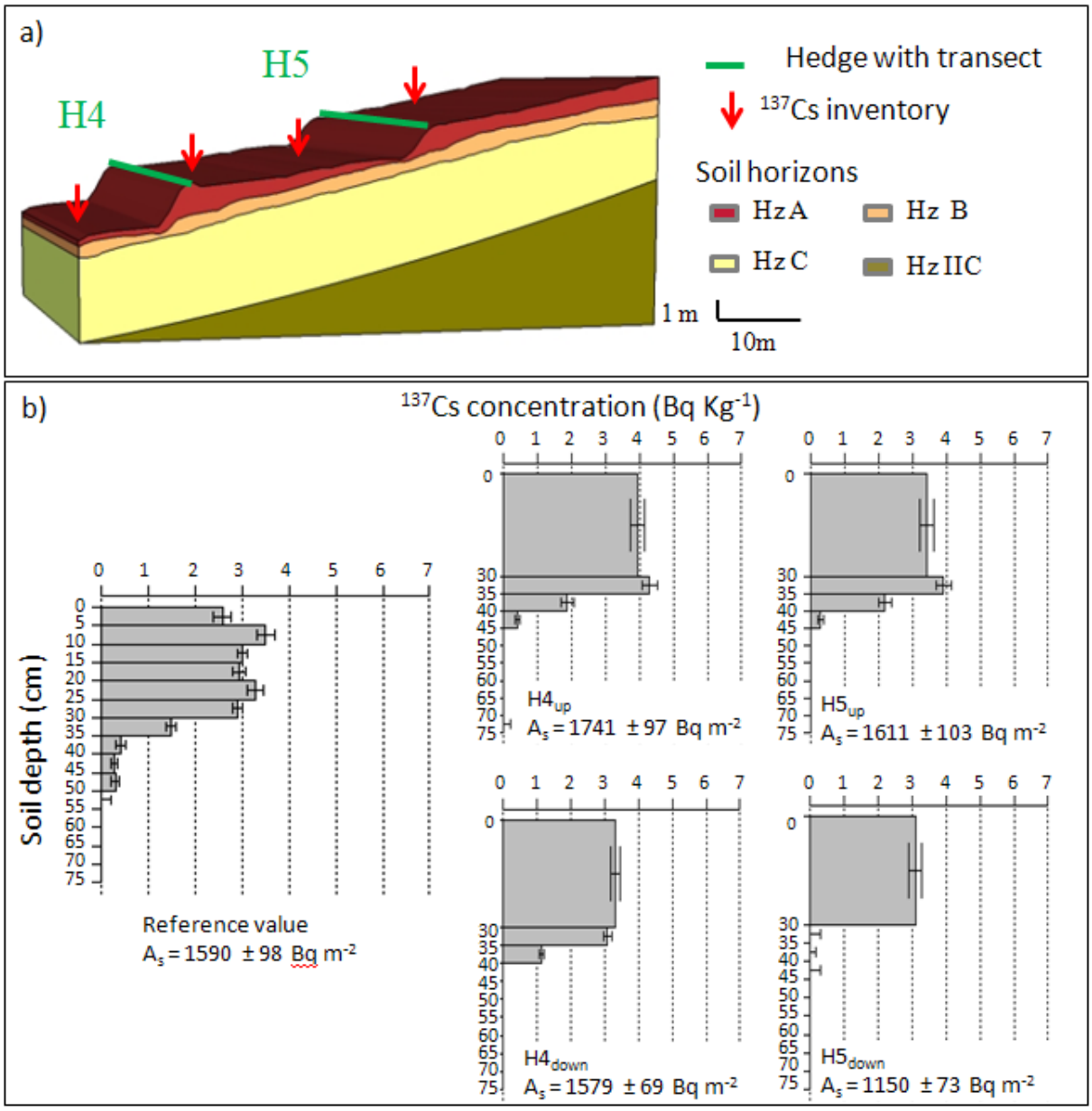

Figure 3-9. Soil distribution patterns in the vicinity of hedges H4 and H5. a) Location of transects in the hillside, b) Vertical distribution of 137Cs for reference value and 137Cs inventories on H4 and H5. Hz A: organo-mineral horizon, Hz B: structural horizon, Hz M: Aeolian loam, Hz C: eroded rock.

3.2. Soil redistribution rates over 50 years based on soil redistribution modelling with the LandSoil model

Soil redistribution rates obtained with LandSoil are summarized in Table 6. The soil redistribution rates estimated using the three sets of soil infiltration rates were strongly correlated, with an R^2 ranging from 0.96 to 1 and CCC ranging from 0.91 to 0.99. The largest differences between estimates were obtained for $H4_{down}$ and $H5_{down}$, with a difference of 3.3 t ha^{-1} yr^{-1}. Overall mean soil redistribution rates showed that the model usually predicted erosion along the simulated transects. The mean soil redistribution rate was estimated at -1.20t ha^{-1} yr^{-1}, the mean soil erosion rate at -4.73 t ha^{-1} yr^{-1}, and the mean soil deposition rate at 2.34 t ha^{-1} yr^{-1}. Among the six sampling sites, LandSoil modelled soil deposition uphill from hedges and soil erosion downhill from hedges for five hedges (H1, H3, H4, H5 and H6). The opposite pattern was modelled for the hedge H2 (i.e. the area uphill

from hedge experienced soil deposition and area downhill from hedge experienced soil erosion). H2 corresponds to the situation where the hedge was removed in 1970. Focusing of the 5 currently existing hedges, the mean soil redistribution rate was estimated at 2.18 t ha^{-1} yr^{-1} for the positions uphill from the hedges, and at -4.84 t ha^{-1} yr^{-1} for the positions downhill from the hedges.

Table 3-9. Statistics of soil redistribution rates derived from the four ^{137}Cs conversion models

Location	^{137}Cs inventory	Soil redistribution rate estimation (t ha^{-1} yr^{-1})			
	(Bq m^{-2})	minimum	mean	median	maximum
$H1_{up}$	1412	-8.71	-7.61	-7.93	-5.87
$H1_{down}$	1274	-15.95	-13.88	-14.24	-11.10
$H2_{up}$	438	-88.48	-65.70	-63.49	-47.35
$H2_{down}$	1448	-6.96	-5.94	-6.18	-4.45
$H3_{up}$	1285	-16.41	-13.83	-13.73	-11.43
$H3_{down}$	1293	-15.93	-13.44	-13.37	-11.09
$H4_{up}$	1741	5.19	6.64	6.82	7.73
$H4_{down}$	1579	-5.29	-2.47	-2.08	-0.46
$H5_{up}$	1611	0.85	1.00	0.95	1.23
$H5_{down}$	1150	-25.32	-20.70	-19.80	-17.86
$H6_{up}$	1326	-12.92	-10.05	-10.28	-6.73
$H6_{down}$	1449	-6.88	-5.25	-5.37	-3.40

Negative values: soil erosion, positive values: soil deposition.

Table 3-10. Statistics of soil redistribution rates from 1960 to 2009 derived from LandSoil model, considering 3 infiltration rates (IR_1, IR_2 and IR_3)

Location	Soil redistribution rate (1960-2009, t ha^{-1} yr^{-1})						Proportion of water redistribution in total soil redistribution (%)
	minimum	mean	median	maximum	Mean tillage redistribution	Mean water redistribution	
$H1_{up}$	1.42	1.54	1.46	1.73	1.78	-0.24	10
$H1_{down}$	-6.53	-5.61	-5.89	-4.41	-5.28	-0.33	5
$H2_{up}$	-5.16	-4.20	-4.17	-3.26	-3.72	-0.48	7
$H2_{down}$	2.64	3.12	3.24	3.49	3.35	-0.23	7
$H3_{up}$	0.78	0.96	0.89	1.22	1.34	-0.38	18
$H3_{down}$	-1.01	-0.52	-0.39	-0.17	-0.13	-0.40	64
$H4_{up}$	2.80	3.47	3.66	3.95	3.76	-0.40	8
$H4_{down}$	-8.24	-6.75	-7.06	-4.96	-6.25	-0.51	7
$H5_{up}$	2.42	3.15	3.41	3.63	3.58	-0.42	9
$H5_{down}$	-8.26	-6.78	-7.08	-4.99	-6.26	-0.52	7
$H6_{up}$	1.62	1.77	1.76	1.94	1.86	-0.09	10
$H6_{down}$	-5.24	-4.53	-4.67	-3.67	-4.18	-0.35	7

Negative values: soil erosion; positive values: soil deposition.

Relative contribution of water and tillage erosion processes to soil redistribution is given in Table 6. Contribution of water redistribution to absolute net soil redistribution ranged from 7 to 64% (mean value: 13%). Considering soil redistribution due to the single tillage operations only, the mean soil redistribution rate was estimated at -0.84 t ha^{-1} yr^{-1}, the mean soil erosion rate at -4.30 t ha^{-1} yr^{-1}, and the mean soil deposition rate at 2.61 t ha^{-1} yr^{-1}. LandSoil only modelled water erosion in the vicinity of the hedges, and the mean soil erosion rate was estimated at -0.36 t ha^{-1} yr^{-1}.

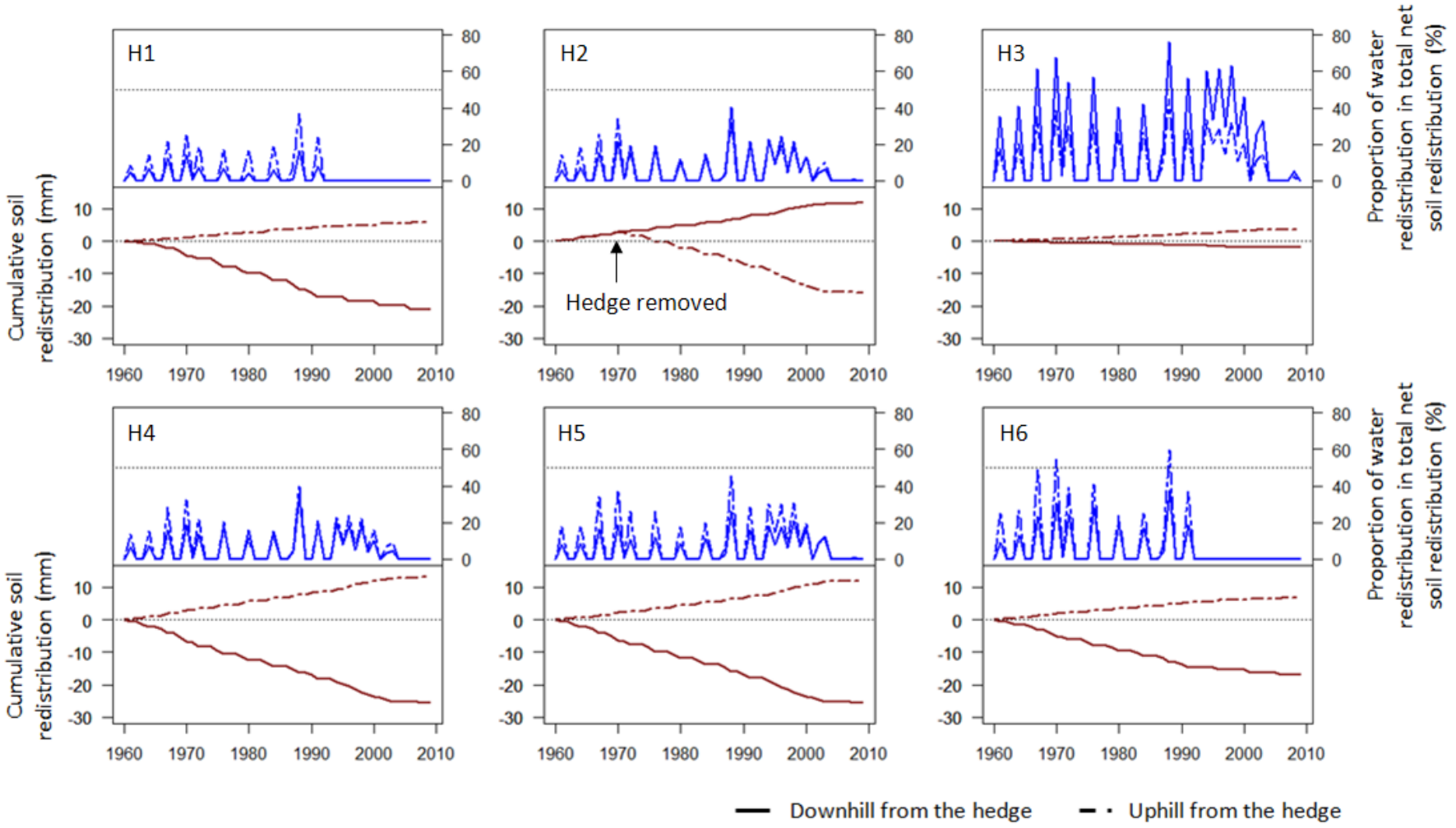

Figure 3-10. Soil redistribution modelling between 1960 and 2009: cumulative soil redistribution (lower half of graphs) and annual proportion of water redistribution in absolute net soil redistribution (upper half of graphs). Both were calculated by averaging soil redistribution on 10*10 m windows centred ^{137}Cs measurements.

Fig. 3 shows the annual variations of the contribution of water erosion processes to absolute soil redistribution between 1960–2009, and the cumulative soil redistribution. Depending on the year, the transect and the position from the hedge, the contribution of water erosion processes to absolute soil redistribution ranged from 0 to 76%. The contribution of water redistribution to absolute soil redistribution remained lower than 50% for five hedges (H1, H2, H4 and H5), and reached 50% and more for two hedges (H3 and H6). For all hedges except H3, the contribution of water erosion processes to absolute soil redistribution was similar or higher for positions located uphill of hedges than for positions situated downhill from hedges. For H3 the opposite pattern was obtained from the model. For all hedges except H2, results showed no change in soil redistribution dynamics: positions uphill from hedges always proved to be deposition sites, whereas positions downhill from hedges were erosion sites. For hedge H2, both positions uphill and downhill from the hedge were deposition sites before the hedge removal in 1970, and then the position uphill from hedges became an erosion site, whereas the position downhill from hedges was a deposition site. The intra and inter-annual variations of the modelled soil redistribution were due to the combination of meterological conditions (extreme rainfall events) and soil cover linked to land use.

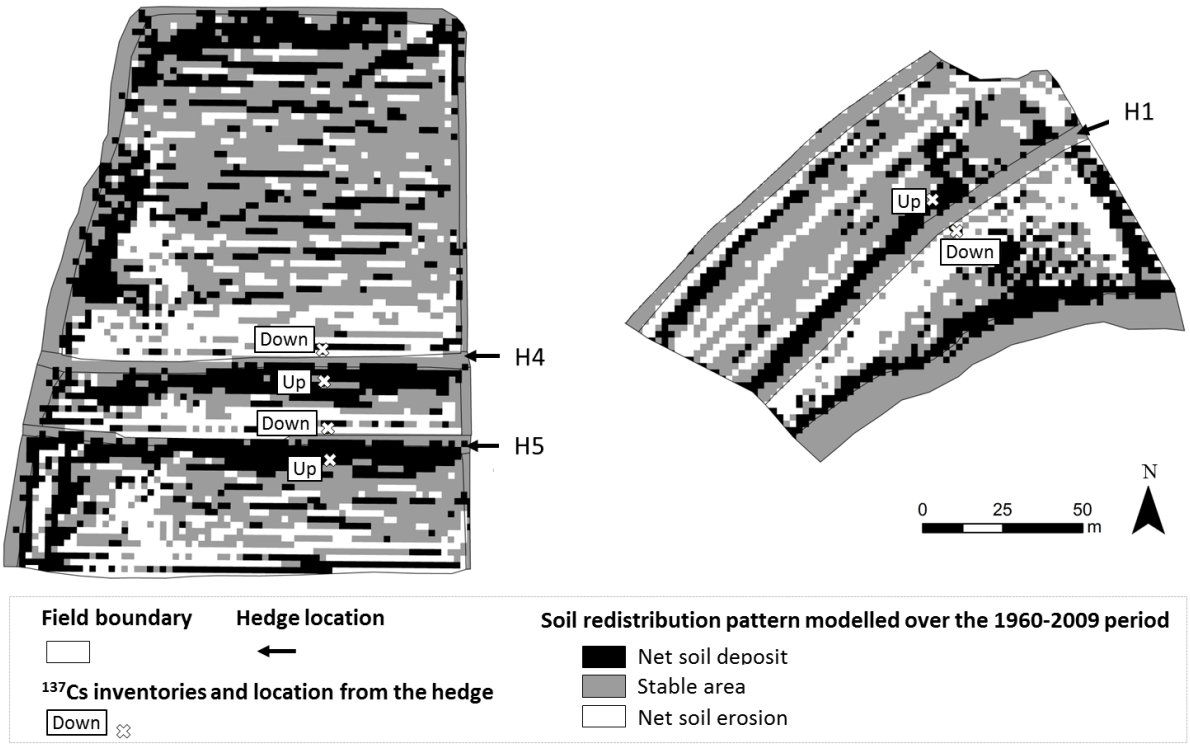

Figure 3-11. Maps of soil redistribution pattern simulated by LandSoil in the vicinity of hedges H1, H4 and H5 from 1960 to 2009 (Net soil deposit: areas where a net soil deposit was modelled, Stable area: areas where soil redistribution modelling resulted in unchanged soil thickness, Net soil erosion: areas where a net soil loss was modelled).

Fig. 4 and Fig. 5 show the spatial distribution of the soil redistribution simulated by LandSoil for the hedges H1, H3 and H4. For the three hedges shown in Fig. 5, LandSoil modelling results showed (i) soil deposition uphill from the hedge; (ii) soil erosion downhill from the hedge, and (iii) higher soil redistribution at the field boundaries rather than within the fields. For the modelling areas shown in Fig. 4, the mean soil redistributions across the entire fields ranged from -0.07 to -0.42 t ha^{-1} yr^{-1}, whereas it ranged from -8.26 to 3.95 t ha^{-1} yr^{-1} in the vicinity of the hedges. Fig. 6 shows the relative contribution of water erosion processes to the net soil redistribution. For the three hedges H1, H4

and H5, tillage redistribution tended to be dominant at the vicinity of the hedge. Water redistribution was nevertheless dominant within the fields.

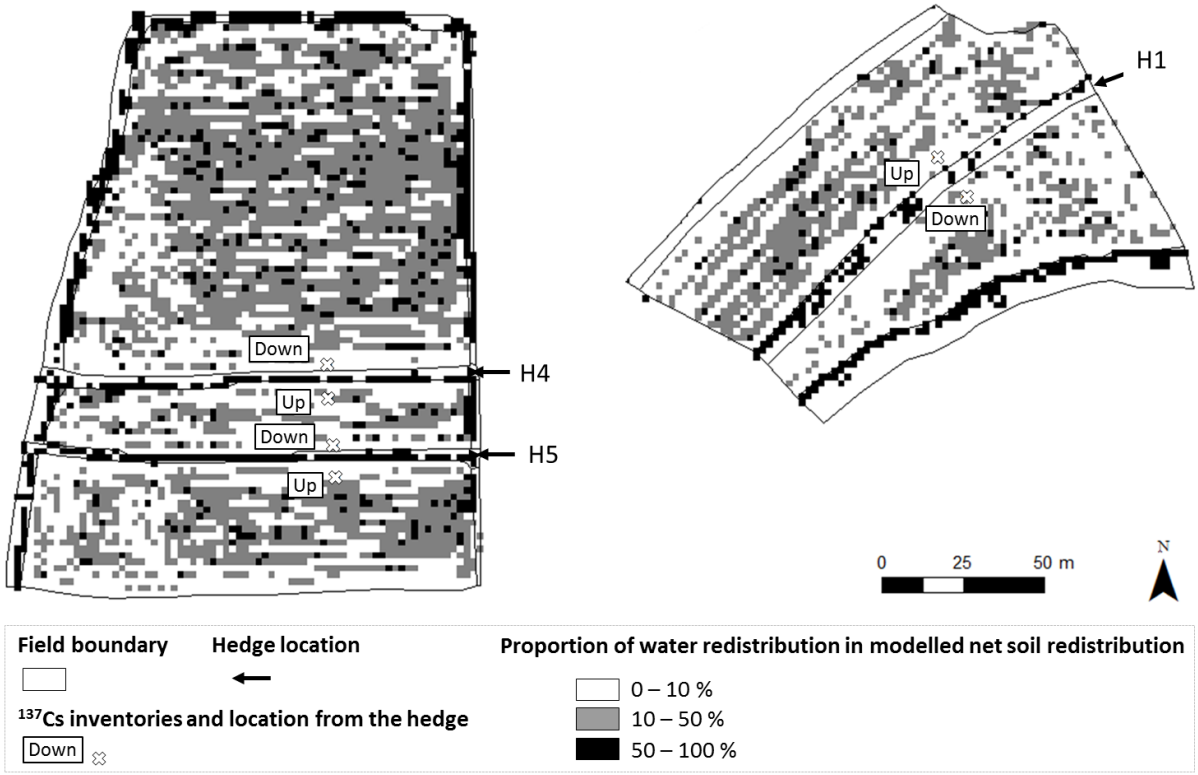

Figure 3-12. Spatial distribution of the proportion of water redistribution in absolute net soil redistribution estimated by the LandSoil model in the vicinity of hedges H1, H4 and H5

3.3. Comparison of soil redistribution rates from ^{137}Cs measurements and LandSoil model

The correlation coefficient R^2 and Lin's concordance coefficient (CCC) were calculated to compare the soil redistribution rates estimated from ^{137}Cs inventories and from LandSoil. Considering all the study sites, R^2 and CCC reached 0.17 and 0.12, respectively. Considering only the positions uphill from the hedges, R^2 and CCC amounted to 0.99 and 0.15, respectively. Finally, considering only the positions downhill from the hedges, R^2 and CCC was equal to 0.29 and 0.17, respectively.

Fig. 6 compares the soil redistribution rates modelled from ^{137}Cs inventories and LandSoil. The rates overlap only for two transects in uphill hedge positions (H4 and H5), and two transects in downhill hedge positions (H4 and H6). The two methods predicted a different dominant redistribution process for three hedges. For the hedges H3, H6 and H1, positions uphill from the hedges were estimated to be erosion sites by ^{137}Cs inventories conversion models, whereas they were estimated to be deposition sites by LandSoil model. The same pattern was observed for the hedge H2 (for the position downhill from the hedge).

Soil redistribution rates estimated from ^{137}Cs inventories conversion models were higher for all study sites, except for hedge H5 (uphill from the hedge) and the hedges H6 and H4 (downhill from the hedge). Hedge H2, removed in 1970, showed the largest estimate differences: for the position uphill from the hedge both methods estimated soil erosion, but the mean soil erosion was estimated to -4.2 t ha^{-1} yr^{-1} by LandSoil and -66 t ha^{-1} yr^{-1} from the ^{137}Cs inventories.

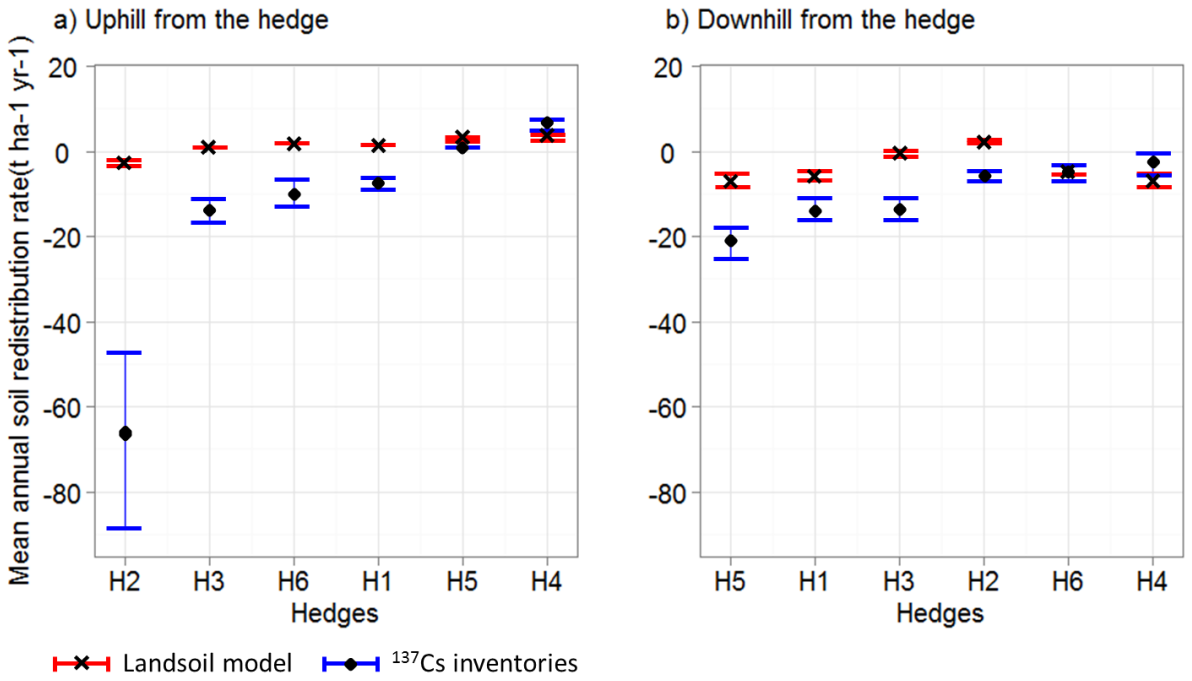

Figure 3-13. Comparison of soil redistribution rates obtained from ^{137}Cs measurements and predicted by LandSoil (black cross and black points figure mean soil redistribution rates predicted by LandSoil model and ^{137}Cs inventories, respectively).

4. Discussion

4.1. Methods to estimate soil redistribution patterns and rates

4.1.2. Soil redistribution estimated from ^{137}Cs inventories

In a hedgerow landscape, hedges obstruct winds, so the diffusion of ^{137}Cs in the landscape by the wind may not be uniform. Moreover, the canopy of trees constituting the hedge is prone to intercept ^{137}Cs before soil deposition (Kato et al., 2012), which could be another explanation to the non-uniform ^{137}Cs fallout. The ^{137}Cs reference inventory that we used was located to the south of the study area (Fig. 1), inside a flat cultivated field without hedges at its boundaries. It could mean that this reference inventory that we compared to ^{137}Cs inventories on transects was not representative of the initial ^{137}Cs fallout for the whole study area, and specifically for the study sites. If the reference inventory was not representative of the initial ^{137}Cs fallout, soil redistribution patterns and modelled rates using ^{137}Cs conversion models could be biased. This could explain why the patterns of soil redistribution modelled by ^{137}Cs inventory conversion models were not always consistent with known soil redistribution at hedge proximity in such a landscape. For example, soil erosion was estimated uphill from the hedge H1, whereas the survey of A-Horizon thickness (thicker in positions uphill from the hedges than in positions downhill from the hedge) suggested the occurrence of soil deposition. Moreover, previous studies showed that positions uphill from hedges were more prone to soil deposition (Follain, 2006a; Follain et al., 2006b; Walter et al., 2003a). However, such soil deposition could have occurred prior to ^{137}Cs fallout, and positions uphill from the hedges could have become, during the last decades, areas where soil erosion was prevailing over soil deposition. Another solution to have a better estimate of soil redistribution using ^{137}Cs inventories would be to find a more representative reference ^{137}Cs inventory, a local reference profile for each hedge, sampled in

the proximity of each of those landscape features. However, it seems difficult to find such a location, without soil redistribution, in an agricultural landscape. An estimate of the soil redistribution dynamics in the vicinity of hedges could be done without using a ^{137}Cs reference inventory, by comparing for each transect the uphill/downhill ^{137}Cs inventory. For the hedge H1 for example, the ^{137}Cs inventory uphill from the hedge was higher than the ^{137}Cs inventory downhill from the hedge. This is insufficient to conclude that soil deposition occurred uphill from H1, but we may assume that soil erosion was higher downhill from H1. Regarding the hedge H2, which was removed in 1970, the soil redistribution estimate using the ^{137}Cs inventories can be biased because of the possible soil redistribution in the fields by farmers during the hedge removal.
Another possible issue was the choice of the conversion model. In this study, two PM models (PM-1954 and PM-1963) and two mass balance models (MBM1 and MBM2) have been applied. However, the soil redistribution rates estimated from these four models were very similar and very well correlated (Table 5).

4.1.2. Soil redistribution estimated by LandSoil model

LandSoil is an expert-based model, which allows minimizing the number of parameters to calibrate. However, parameters requiring calibration remain, and these parameters are a source of uncertainties:

(i) Parameters linked to soil redistribution by water processes

Three main parameters have to be examined to simulate soil redistribution by water: infiltration rate, potential sediment concentration in runoff, and factors of soil deposition (or factors controlling the maximum sediment concentration in runoff). In this study, we used three ranges of soil infiltration rates to take soil variability into account, but because of the limited contribution of water erosion processes to soil redistribution in the hedge vicinity, they were no significant differences between the results produced with the three IR ranges. , The default values used in LandSoil for potential sediment concentration in runoff (Cerdan et al, 2002b and 2002e) were consistent with the available data in our study area (Gascuel-Odoux et al., 1996; Lacoste, 2012). Finally, the maximum sediment concentration in runoff was controlled with threshold functions based on four factors: profile curvature, slope gradient, land use and vegetation cover. The thresholds values for these factors have been determined by Cerdan et al (2002b and 2002e) using data on runoff and soil redistribution under natural rainfall on loamy soils of Northern France. No data were available in our study area to calibrate these thresholds but, given the observed similarities between the study sites, we assumed that these values were valid in our study site. The threshold values for topographic parameters (curvature and slope), estimated for a 5x5 m DEM, have only been adapted for a 2x2 m DEM.

(ii) Parameters linked to soil redistribution by tillage processes

Regarding soil redistribution by tillage, the most important parameters to calibrate are the tillage erosion coefficients. In this study, sequences of tillage operations have been estimated from surveys among farmers. The resulting tillage erosion coefficients have been estimated from previous studies (Table 4).

(ii) Other source of uncertainties

All the input data could be source of uncertainties. In this study, the most sensitive data was the DEM. In fact, a 2-m resolution DEM was used, to take into account the fine topography at hedge

vicinity. However, such a DEM may be noisy and needs to be pre-processed. A non-controlled DEM could lead to mis-modelling the drainage network, and consequently the soil erosion and deposition areas.

The soil redistribution patterns modelled by LandSoil were consistent with previous knowledge of soil redistribution in such a landscape, i.e. soil deposition uphill from hedges and soil erosion downhill from hedges (Baudry et al., 2000). H2 was the only hedge where an opposite pattern was modelled. H2 was also the only hedge removed during the simulation process, and in such conditions this result is consistent: soil previously deposited uphill from the hedge could be eroded and redistributed downhill from the hedge. Models such as LandSoil provide quantitative estimations of the spatial variability of soil redistribution and its variability over time by dynamic modelling. LandSoil also allows distinguishing and quantifying the contribution of the different processes taking part in soil redistribution (in this study water and tillage redistribution). These types of models could be particularly interesting to better understand the impacts of landscape structure on soil redistribution processes or to estimate soil variation in time according to various global change scenarios.

4.1.3. Soil redistribution dynamics in agricultural landscapes

Scale issues

Soil erosion has been studied on a range of temporal and spatial scales. Results showed that there is no simple relationship between erosion rates when up- or downscaling (Chaplot and Poesen, 2012; Delmas et al., 2012; Le Bissonnais et al., 1998a). At the scale of Europe, Delmas et al (2012) showed that soil erosion rates decrease from the field to the catchment scale. Moreover, Le Bissonnais et al. (1998a) showed that the size of the plot used for soil erosion measurement have an impact on the results. Therefore, comparisons of studies should be conducted carefully. In this study, soil redistribution rates are given at the plot scale (100 m²), located in the vicinity of hedges. However, both methods used to estimate these rates integrate soil redistribution on larger spatial extents: (i) ^{137}Cs inventories take into account all soil particle movements at a given point without scale restriction. In our hedgerow landscape, we can assume that the spatial extent of soil redistribution is limited by the hedges located at the field boundaries (mean field size around the studied transects = 1 ha). Therefore, ^{137}Cs inventories provided a way to estimate soil redistribution rates from point-to-field scales; (ii) the LandSoil model was run at the field scale so that it also allowed assessing the soil redistribution rates from plot-to-field scales. According to ^{137}Cs inventories, the mean soil redistribution rate was estimated to -12.6 t ha^{-1} yr^{-1}, the mean soil erosion rate was estimated to -15.9 t ha^{-1} yr^{-1}, and the mean soil deposition rate to 3.8 t ha^{-1} yr^{-1}. Considering LandSoil estimates, the mean soil redistribution rate was estimated to -1.2 t ha^{-1} yr^{-1}, the mean soil erosion rate was estimated to -4.7 t ha^{-1} yr^{-1}, and the mean soil deposition rate to 2.3 t ha^{-1} yr^{-1}.

These rates are close to those estimated in previous studies. Cerdan et al. (2010) estimated from a synthesis of existing field measurements on medium-sized plots (>3 m and <200 m in length) that the mean soil erosion rate in Europe was -1.2 t ha^{-1} yr^{-1} considering all land uses, and -3.6 t ha^{-1} yr^{-1} considering only arable land. Verheijen et al. (2009) synthesized studies at plot-to-field scales and estimated that soil erosion rates in Europe ranged from -3.2 to -19.8 t ha^{-1} yr^{-1}. In our study, the two used methods estimated that erosion processes were more pronounced than deposition processes. This result was also described by Van Oost et al. (2005b), who studied soil redistribution at the field scale.

Tillage vs. water erosion

In this study, the mean soil redistribution rate due to tillage operation was estimated by the LandSoil model to -0.84 t ha^{-1} yr^{-1} considering all situations, to-4.30 t ha^{-1} yr^{-1} considering erosion sites and to 2.61 t ha^{-1} yr^{-1} considering deposition sites. Considering the soil redistribution due to water processes, the LandSoil model estimated that soil erosion was prevailing at the observed location (erosion rates ranged from -0.09 to -0.52 t ha^{-1} yr^{-1}, mean value = -0.36 t ha^{-1} yr^{-1}). Therefore, these results show that (i) tillage operations were the main processes inducing soil redistribution at the observed locations, and (ii) it could be inferred that water processes mainly induce soil erosion in the vicinity of hedges. This first result was shared by Quine et al. (1994) and Van Oost et al. (2005b), who showed that soil erosion at the field scale was mainly due to tillage operations during the last decades (i.e. contemporary erosion). According to Verheijen et al. (2009), tillage erosion rates in Europe ranged from 3.0 to 9.0 t ha^{-1} yr^{-1}(studies at plot-to-field scale), which is consistent with our results. . At the field scale, Cros-Cayot (1996) estimated water soil erosion to 1.55 t ha^{-1} yr^{-1} for loamy soils in Brittany. Verheijen et al. (2009) reported that previous studies estimated that sheet erosion due to water runoff ranged from 0.1 to 8.8 t ha^{-1} yr^{-1} in Europe.

Impacts of linear anthropogenic structures

Both methods were associated with uncertainties and it turns out to be difficult to directly compare their respective results. Soil redistribution rates were not well correlated (overall R^2 = 0.17), estimates of soil redistribution patterns were not always consistent, and for most of the sampling sites soil redistribution rates estimated from ^{137}Cs inventories were higher than those estimated from LandSoil.

However, both methods showed that hedges had an impact on soil redistribution. For positions uphill from the hedges, we modelled either soil accumulation or soil erosion with a lower rate than the one modelled for positions downhill from hedges. Focusing of the 5 still existing hedges, the mean soil redistribution rates estimated by LandSoil and ^{137}Cs inventories were 2.2 and -4.5 t ha^{-1} yr^{-1} respectively for the positions uphill from the hedges, and -4.8 and -11.2 t ha^{-1} yr^{-1} respectively for the positions downhill from the hedges. This result was consistent with those of previous studies: hedges act as a trap for soil particles in runoff and can enhance runoff infiltration (Baudry et al., 2000); moreover, hedges act as a zero flux line regarding tillage erosion processes (Govers et al., 1996). Both processes result in the differentiation of soil redistribution on both sides of hedges. The impacts of hedges on soil redistribution at the landscape scale have been modeled by Follain et al. (2006b). They concluded that hedges have an impact on soil redistribution and landscape topography evolution. In hedge-less landscape, soil can be redistributed over longer distances, which induces landscape leveling. In contrast, in a hedged landscape, hedges contribute to bank creation in soil deposit areas (uphill from hedges). It has also been shown that hedges have an impact on soil horizon structure, particularly regarding the A-horizon thickness (Follain et al., 2009). It comes out that, at the field-to-landscape scale, hedges are a factor of heterogeneity when dealing with soil redistribution (Fig. xxx; Follain et al., 2006b; Lacoste, 2012): they impact soil redistribution within fields but they also impact soil export from the fields and from landscapes or catchments. Hedges should therefore be taken into account in studies dealing with soil redistribution. Nevertheless, it could be difficult to take them explicitly into account in studies conducted in large areas (landscape-to-region or country). One solution could be to use a connectivity index as describe by Cerdan et al. (2012).

5. Conclusions

This study aimed to estimate soil redistribution patterns and rates in a hedgerow landscape for areas close to hedges. We compared two methods, one derived from ^{137}Cs survey and the other based on a spatially distributed soil redistribution model (LandSoil). Soil redistribution rate estimates obtained with ^{137}Cs survey were higher than those obtained with LandSoil, but both were consistent with other values found in previous studies. Estimates from both methods showed that soil erosion processes were dominant in the vicinity of the hedge. Depending on the method, mean soil redistribution rate varied between -4.8 t ha^{-1} yr^{-1} and 2.2 t ha^{-1} yr^{-1} in positions uphill from hedges, whereas they reached -4.8 to -11.2 t ha^{-1} yr^{-1} in positions downhill from hedges. Both methods modelled hedges as anti-erosive landscape elements: estimates of soil redistribution uphill from the hedges showed either soil redistribution or lower soil erosion than positions downhill from hedges. Estimates from LandSoil were consistent with previous studies on soil redistribution in relation to landscape structure, and showed its ability to model soil redistribution in complex hedgerow landscapes. At the field scale, the estimates of soil redistribution by LandSoil showed that soil redistribution was more important at the vicinity of field boundaries. Moreover, the impact of tillage on the soil redistribution in the vicinity of the hedges was found more important than water processes (an average of 87% of the soil net redistribution was due to tillage). However, soil redistribution processes varied in space and in time, and water erosion processes were dominant within the fields. Further work will focus on the impacts of landscape structure on soil redistribution in the context of global change.

Acknowledgements

The authors acknowledge the ANR VMCS and the LandSoil project (landscape design for soil conservation under soil use and climate change, http://www.inra.fr/landsoil/; ANR-08-VULN-006) for scientific and financial support, the Z.A. Armorique (LTER-Europe, http://osur.univ-rennes1.fr/zoneatelier-armorique/) for LiDAR and land-use data provision, and are grateful to G. Dutin and I. Lefèvre for technical assistance.

3.3 Soil redistribution at the scale of the pF study area

Additional soil redistribution measurements have been conducted at the scale of the PF study area:

(i) Eight other transects have been studied and supported 137Cs inventories, allowing a larger representation of the study area. These transects were not used for soil redistribution estimate with LandSoil because of uncertainties concerning soil use and landscape structure evolutions in their environment. However, soil redistribution rates were estimated using the same conversion models as described in this study. They ranged from -0.5 to -91.9 t ha-1 yr-1 for erosion rates and from 0.9 to 34.8 t ha-1 yr-1 for deposition rates (Appendix 4). These results also estimated that soil erosion was the dominant process of soil redistribution, over soil deposition. Net soil deposition or minor soil erosion was predicted uphill from the hedges; whereas soil erosion was predicted downhill form the hedges. These results were consistent with the anti-erosion function of hedges. In Section 3.2, we estimated soil redistribution rate by 137Cs inventories and by modelling with LandSoil. Depending to the method, mean soil redistribution mean soil erosion ranged from -65 t ha-1 yr-1 or -2.5 t ha-1 yr-1, while soil deposition rate ranged from 0.5 to 6.6 t ha-1 yr-1. These soil redistribution rates were consistent with those estimated at the scale of the PF study area.

(ii) Soil redistribution rates have been estimated over longer periods for two soil pits, using the OSL dating (Optically Simulated luminescence; Appendix 5). The basis of the A-horizon, sampled at 100 cm and 130 cm, have been dated at 9,620 yr BP (± 98) and 5,390 yr BP (± 470), which correspond to the first human settlements (Follain, 2006a). Soil deposition rates were estimated ranging from 0.4 to 82 t ha-1 yr-1 according to the specific pit and the considered time period (defined from the OSL age). Higher soil accumulation rates were found for the surface horizon, which may imply that soil redistribution processes, both erosion and deposition, increased since the first human settlements and the forest clearing induced by the development of agriculture.

3.4 Chapter conclusion

The aims of Chapter 3 were (i) to calibrate LandSoil at the scale of rainfall events for its use on the PF study area (Section 3.1), (ii) to test LandSoil ability to model soil redistribution close to hedges over a few decades (Section 3.2). Even if no calibration data were available on the PF study area, pre-existing data was available on sites with similar properties (calibration sites in Brittany), which allowed calibration of LandSoil parameters (residual water storage after the previous event, infiltration rate and sediment concentration in runoff). Moreover, the comparison of LandSoil results with another method for soil redistribution estimate (based on ^{137}Cs) allowed assessing LandSoil ability to model soil redistribution close to hedges, even though no measures of soil erosion were available on the PF study area. LandSoil can be used to model soil redistribution in hedgerow landscapes. In Section 3.3, we used three ranges of value for soil infiltration rate to model soil redistribution with LandSoil. One was obtained for loamy soils in Brittany (Section 3.2 of this chapter), another for the loamy soils of Normandy, and the last was an intermediate range of values. One goal was to compare soil redistribution results from LandSoil to those from the ^{137}Cs method, in order to determine the best suitable range of soil infiltration to model soil redistribution in the study

area. As we saw in the Section 3.3, we need to be careful when comparing the results for the methods. It is not easy to use this comparison of results to choose a range of soil infiltration. Moreover, soil redistribution due to water processes was not dominant in the hedge vicinity, and the results obtained with LandSoil using the three ranges of values were very well correlated and not significantly different.

LandSoil will be used for further work in the perspective of soil redistribution modelling in the PF study area under global change conditions (Chapter 5). According to the characteristics of the soils in the PF study area and taking into account the future computation time, the intermediate soil infiltration rate will be used to model soil evolution under climate and soil use change in the PF study area. All the soil parameters used to model soil redistribution in further work are summarized in Appendix 3.

Chapitre 4.
3D soil mapping to produce input data for soil evolution modelling at the landscape scale

Initialization is an important step in any modelling process. This chapter aims to expose the methods we used to produce adequate soil input data for the soil evolution models at the landscape scale. These models have been described in Chapter 2.

The soil redistribution model and the soil organic matter (SOM) model required the following maps as input data:

- Soil thickness map,
- A-horizon thickness map,
- 3D soil organic carbon (SOC) stocks map,
- 3D soil bulk density map.

These maps were produced with a 2-m resolution, by combining different digital soil mapping methods such as conditioned Latin Hypercube Sampling (cLHS), depth functions (especially for the 3D maps) and learning methods. The predictive confidence interval was assessed for each map, using a method based on fuzzy clustering.

This chapter is divided in two sections:

- Section 4.1 is a submitted research article. It presents the methodology used to model the 3D organization of soil at the landscape scale. This section mainly focuses on the predictive method and on the accuracy of the resulting maps. Only the results corresponding to SOC content, bulk density maps and the resulting SOC stocks maps are presented in the paper. The predictive maps of soil thickness and A-horizons thickness are shown in Appendix 6.
- Section 4.2 has been published as a conference proceeding (Lacoste et al., 2012b). It describes the spatial organization of SOC stocks at the landscape scale relative to the landscape structures (distance from the hedges, land use) and to other soil properties (soil drainage conditions).

4.1 Initialization of SOC stocks for soil evolution modelling at the landscape scale

This section is a research article published in Geoderma (Lacoste et al., 2014).

High resolution 3D mapping of soil organic carbon in a heterogeneous agricultural landscape

Marine Lacoste[a,*], Budiman Minasny[c], Alex McBratney[c], Didier Michot[a,c] ,Valérie Viaud[a] , Christian Walter[a,c]

[a] INRA, AGROCAMPUS OUEST, UMR1069, Sol Agro et hydrosystème Spatialisation, F-35000 Rennes, France
[b] Faculty of Agriculture, Food & Natural Resources, The University of Sydney, NSW 2006, Australia
[c] Université Européenne de Bretagne, France

[*] Corresponding author. Tel.: +33223487047; fax: +332 23 48 54 30.
E-mail address: Marine.Lacoste@rennes.inra.fr (M. Lacoste).

Abstract:
Soil organic carbon (SOC) is a key element of agroecosystems functioning and has a crucial impact on global carbon storage. At the landscape scale, SOC spatial variability is strongly affected by natural and anthropogenic processes and linear anthropogenic elements (such hedges or ditches). This study aims at mapping SOC stocks distribution in the A-horizons for a depth up to 105 cm, at a high spatial resolution, for an area of 10 km² in a heterogeneous agricultural landscape (North-Western France). We used a data mining tool, Cubist, to build rule-based predictive models and predict SOC content and soil bulk density (BD) from a calibration dataset at 8 standard layers (0-to-7.5 cm, 7.5-to-15 cm, 15-to-30 cm, 30-to-45 cm, 45-to-60 cm, 60-to-75 cm, 75-to-90 cm and 90-to-105 cm). For the models calibration, 70 sampling locations were selected within the whole study area using the conditioned Latin hypercube sampling method. Two independent validation datasets were used to assess the performance of the predictive models: (i) at landscape scale, 49 sampling locations were selected using stratified random sampling based on a 300-m square grid; (ii) at hedge vicinity, 112 sampling locations were selected along transects perpendicular to 14 purposively chosen hedges. Undisturbed samples were collected at fixed depths and analysed for BD and SOC content at each sampling location and continuous soil profiles were reconstructed using equal-area splines. Predictive environmental data consisted in attributes derived from a light detection and ranging digital elevation model (LiDAR DEM), geological variables, land use data and a predictive map of A-horizon thickness. Considering the two validation datasets (at landscape scale and hedge vicinity), root mean square errors (RMSE) of the predictions, computed for all the standard soil layers (up to a depth of 105 cm), were respectively 7.74 and 5.02 g kg^{-1} for SOC content, and 0.15 and 0.21 g cm^{-3} for BD. Best predictions were obtained for layers between 15 and 60 cm of depth. The SOC stocks were calculated over a depth of 105 cm by combining the prediction of SOC content and BD. The final maps show that the carbon stocks in the soil below 30 cm accounted for 33% of the total SOC stocks on average. The whole method produced consistent results between the two predicted soil properties. The final SOC stocks maps provide continuous data along soil profile up to 105 cm, which may be critical information for supporting carbon policy and management decisions.

Keywords: soil organic carbon, soil bulk density, depth functions, data mining, LiDAR DEM, 3D mapping

1. Introduction

Soil organic carbon (SOC), identified as an important pool in the global carbon cycle (Grace, 2004), is a key variable in influencing many agronomical, environmental and political issues. SOC directly controls soil fertility and soil structure, and small changes in SOC can have a large impact on the atmospheric carbon dioxide concentrations (Johnston et al., 2004). SOC assessment and dynamics have been studied at different scales, from field to global scale. The choice of the scale depends on the problem to deal with (impact of cropping practices and spreading, impact of land management and land use, setting up of agricultural policies, etc.), but it has been argued that the most relevant scale to address the issue for the environment and agroecosystem issues was the landscape scale (Viaud et al., 2010). This scale enables to take into account the interaction between SOC dynamics, natural and anthropogenic processes, for instance the relation between SOC storage and soil erosion. In most studies on SOC assessment and modelling, only the topsoil is considered, i.e. the soil layer up to 30 cm and more rarely to 50 cm (e.g. Mishra et al., 2010; Ungaro et al., 2010; Zhang et al., 2010). However, it has been shown that an important amount of carbon is also stored at greater depth (Meersmans et al., 2009a). It appears therefore necessary to produce SOC data not only for the topsoil, but also for the underlying layers. Previous studies dealing with SOC prediction in depth (up to 1 m or more) applied depth functions (Meersmans et al., 2009a), mainly combined with geostatistical methods (mostly kriging; Kempen et al., 2011; Mishra et al., 2009; Vasques et al, 2010) or with machine learning methods such as neural networks (Malone et al., 2009; Minasny et al. 2006c). In these studies, SOC stocks are always calculated by multiplication of SOC content and soil bulk density (BD), and the BD is always estimated by pedotransfer functions. Statistical methods have several advantages, such as simplicity and ease of interpretation. Moreover, geostatistical methods unequivocally take into account spatial correlation between soil observations. However, they also present disadvantages: they require fairly dense soil datasets and the effects of the different drivers of SOC dynamics are hardly include in statistical models. Machine learning methods allow, using either limited or large datasets. Machine learning methods offer useful tools to predict soil properties from spatially exhaustive environmental predictors and limited or large soil datasets, by describing without preconceived ideas the complex relationship between soil properties and covariates known as *scorpan* factors. These *scorpan* factors were first formalized by Jenny (1941), latter by McBratney et al. (2003) and comprise climatic, biological, topographic, geological, temporal and spatial factors. However, depending on the tool used for machine learning, these relationships may be quite difficult to interpret. Moreover, a major limitation of the learning methods is the computation of an error map. However, different methods have been proposed to produce such a map (e.g. Lemercier et al., 2011; Malone et al., 2011; Solomatine and Shrestha, 2009).

In this study, we aim to map SOC stocks in a heterogeneous agricultural landscape, with a high resolution (grid spacing of 2 m), and to quantify the uncertainties of the final 3D map. This fine resolution is required to take into account the linear elements of the landscape (e.g. hedges, mainly on bank, and ditches). To achieve this goal, we propose to map both SOC content (g kg^{-1}) and soil BD (g cm^{-3}) in 3D (i.e. from soil surface to a depth up to 105 cm). These maps are then combined to produce a map of SOC stocks. The following steps were achieved: (i) selection of soil sampling locations, (ii) fitting of equal-area spline functions to SOC content and soil BD data to obtain continuous soil profiles, and extraction of soil properties for eight standard soil layers, to be used as calibration and validation datasets, (iii) creation of 2D rule-based models based on spatially exhaustive environmental covariates, to predict SOC content and BD for the eight standard soil layers from the surface to a depth of 105 cm, (iv) reconstruction of continuous soil profiles of SOC content

and soil BD using a spline function, (v) production of prediction interval established by fuzzy clustering for each predictive map of SOC content and soil BD (one map per standard layer), (vi) mapping of SOC stocks (tC ha^{-1}) and the associate uncertainties from the soil surface and up to 105 cm by combining SOC content and soil BD maps.

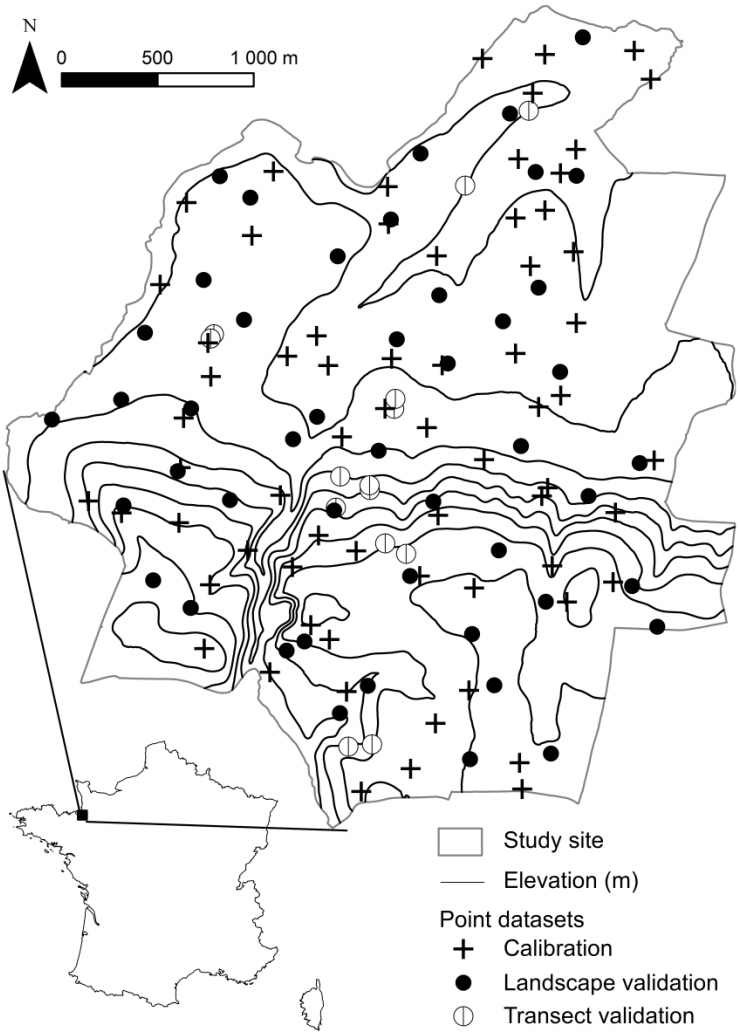

Figure 4-1. Location of the study area in France and the soil sampling locations within the study area.

2. Material and methods

2.1. Study area

The study area (NW France, 48° 36' N, 1° 32' W), was part of the European Long-Term Ecosystem Research Network, and covers an area of 10 km² (Figure 4-1). Landscape scale was considered here as an intermediate integration level between the field and the physiographic region (Turner, 1989; Burel and Baudry, 2003). Its exact extent, however, depends on the ecological process under study and on the spatial range of the biophysical and anthropogenic processes driving it (Forman, 1995). In Western Europe, considering the spatial scale for the biophysical and pedological processes controlling soil organic matter dynamics and given the average size of farms, the extent of the landscape can be considered to range from 1 to 100 km² and would correspond to small watersheds (Viaud et al., 2010). Our study area was characterized by high soil heterogeneity at short distances.

The soil types encountered are mainly Cambisols and Luvisols, but also Leptsosols and Fluvisols (IUSS Working Group WRB, 2007). These soils present varying redoximorphic conditions, soil and A-horizon thickness (for 17 to 550 cm and from 3 to 250 cm, respectively), and soil parent material (granite, hard and soft schist with a heterogenic cover of superficial deposits such as Aeolian loam, alluvium and colluvium). The general topography is highly correlated with the geological formations: plateau on granite (south of the site), plain on soft schist (north of the site), hillside on hard schist at the transition between granite and soft schist. However, the study site presents a marked micro-topography, mainly due to the presence of hedges (often on banks) and ditches at the field boundaries. The hedge density differs from less than 90 to 200 m ha^{-1} according to past land consolidation initiatives. Land use comprises mainly annual crops (corn, wheat, barley) and temporary or permanent grasslands, but the study area also includes wood plots and natural areas.

2.2. Soil data

We used three independent datasets based on the following sampling strategy:

(i) Calibration dataset: designed to calibrate the predictive models. We selected 70 sampling locations using conditioned Latin hypercube sampling (cLHS), a sampling method described as efficient for calibration purposes (Lagacherie et al., 2007; Minasny and McBratney, 2006a). This method is a stratified random procedure that provides an efficient way of sampling variables from their multivariate distributions (Minasny and McBratney, 2006a). cLHS allows selecting locations with a good representation of the study area according to environmental covariates. As covariates we used elevation, a topographic wetness index (Eq.1; Beven and Kirkby, 1979; Merot et al., 2003), natural gamma emission of potassium and grassland frequency over 15 years (from 1993 to 2007).

$$wi = \ln\left(\frac{A_{sm}}{DG}\right) \quad (1)$$

Where *wi* is the topographic wetness index, A_{sm} the specific multidirectional upslope contributing area and *DG* represents the downslope gradient.

Figure 4-2 shows that the distribution of the variables resulting from cLHS sampling was similar to their distribution over the whole study area.

(ii) Landscape validation dataset: designed to assess the models performance at the landscape scale. We selected 49 sampling locations by using stratified random sampling, a sampling method efficient for validation issues (Brus et al., 2011). The strata were defined by a 300-m square grid, so all strata have an equal area of 9 ha. In each stratum, one sampling location was selected by random sampling.

(iii) Transects validation dataset: designed to assess the models performance at the hedge vicinity. We selected 14 hedges by expert knowledge to represent the whole study area by taking into account soil parent material, A-horizon and soil thickness, field size and local slope up to hedges. All selected hedges were perpendicular to the slope and 8 sampling locations were defined along each transect: 1 site under the hedge, 4 sites upslope the hedge (2, 5, 10, and 20 m from the hedge) and 3 sites downslope the hedge (2, 5 and 10 m from the hedge). In total, 112 sampling locations were selected.

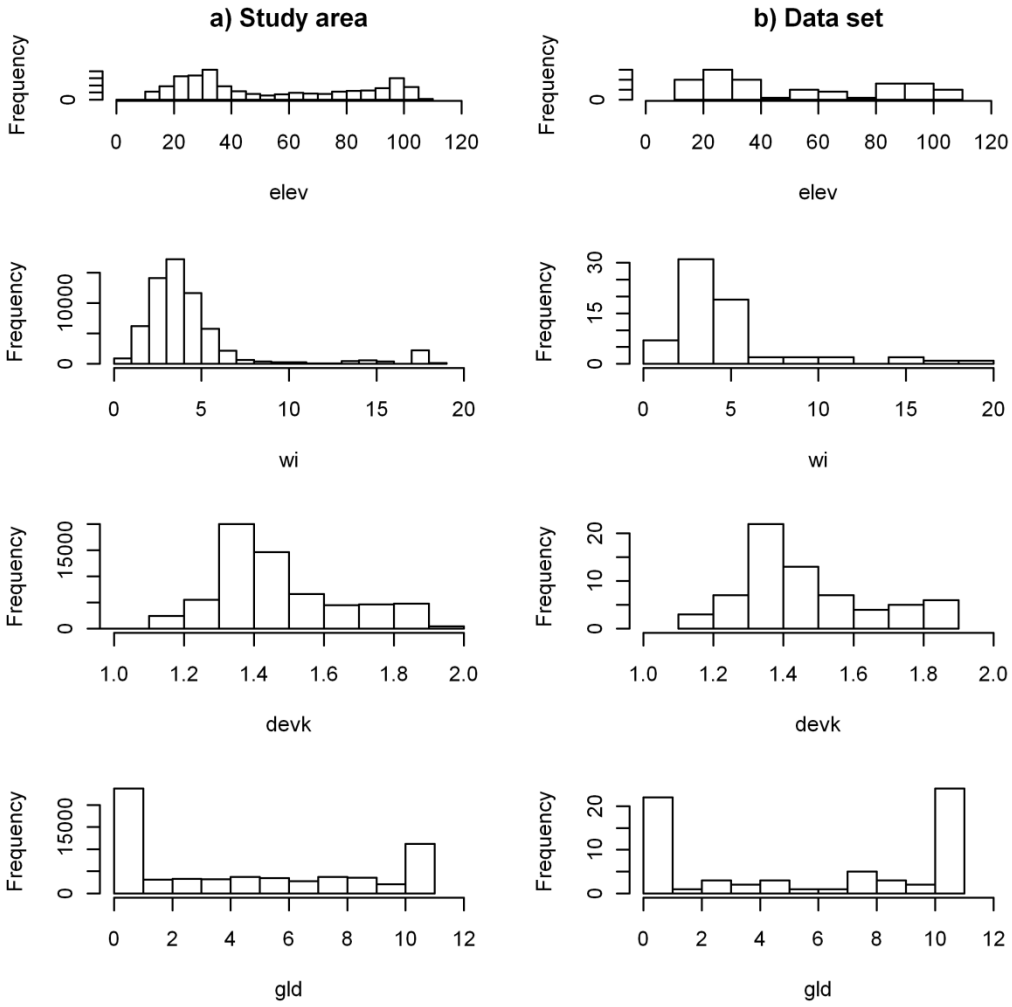

Figure 4-2. Comparison of the distribution of the environmental data used for the cLHS (a) entire study area, (b) calibration dataset (see Table 4-1 for the covariates names and units).

Sampling locations were placed either in agricultural or in natural areas. For the calibration and the landscape validation dataset, sampling was done using a manual root auger with a diameter of 8 cm; for the transect validation dataset, it was done with a 7.5 cm diameter mechanical auger. Both methods allow sampling soil core (continuous soil profiles) up to 105 cm. Each core was cut to provide undisturbed soil increment of known volume. Two soil increments were consistently sampled (0-to-7.5 cm and 7.5-to-15 cm), and then the soil cores have been cut into 15 cm soil increments until the bottom limit of the A horizons. When an A-horizon limit was found inside a 15 cm soil increment, this increment was cut again on this limit to provide soil samples belonging to only one A-horizon. The A-horizons were distinguished in the field from other soil horizons by colour observation (Munsell value and chroma < 5 on wet samples). For the calibration and landscape validation dataset, SOC content (g kg^{-1}) was determined by dry combustion (Thermoscientific Finnigan EA 1112 Flash elemental analyzer). For the transect validation dataset, SOC content was estimated using diffuse reflectance spectroscopy within the visible and near-infrared spectral ranges, combined with a partial least squares regression model (Aïchi et al, 2009). Initially, this model has been calibrated and validated on a regional database (SOC content analysed by dry combustion), for a spatial area where our study area where included. For this study, this model has been re-calibrated

by adding the calibration dataset we used in this study (SOC content from dry combustion) to the regional database. BD of the fine earth was measured (g cm^{-3}) for all the soil datasets (calibration and validation datasets): soil samples with a known volume were dried at 105°C and sieved at 2 mm; the resulting fine earth and gravels were weighed, and the volume of the gravels was measured. Soil sampling and measurements were done between May 2009 and October 2010.

2.3. Environmental covariates

Nineteen environmental variables were selected to be used as covariates in the SOC content and BD models (Table 4-1). Eleven covariates were derived from a 2 m LiDAR DEM (light detection and ranging digital elevation model): elevation, difference of elevation between a 20 m and a 5 m DEM (the 5 m and 20 m DEM were resampled from the 2 m LiDAR DEM), local hillslope gradient, profile and tangential curvatures, elevation above the nearest stream, topographic wetness index (Eq. 1, Beven and Kirkby, 1979; Merot et al., 2003), horizontal and vertical overland flow distances (Freeman, 1991; O'Callaghan and Mark, 1984), multiresolution indexes of ridge top and valley bottom flatness (Gallant and Dowling, 2003).

Table 4-1. Environmental covariates used to predict SOC and BD

Name	Description (units)	Soil forming factor	Type	Mean	(minimum, maximum)
Terrain attributes derived from the DEM					
elev	Elevation (m)	r	Q	52.5	(11, 110)
dif.elev	Difference between the elevation from the 20m DEM and the 5m DEM (m)	r	Q	0	(-14, 14)
slope	Local hillslope gradient (%)	r	Q	3.6	(0, 71)
vcurv	Profile (vertical) curvature ($m.100m^{-1}$)	r	Q	0	(-61, 61)
hcurv	Tangential (horizontal) curvature ($m.100m^{-1}$)	r	Q	0	(-44, 39)
zc	altitude above the channel network (m)	r	Q	3.1	(0, 35)
wi	Modified topographic wetness index	r	Q	10.2	(3, 15)
hof	horizontal overland flow distance (m)	r	Q	138.8	(1, 890)
vof	vertical overland flow distance (m)	r	Q	7	(0, 56)
mrrtf	multiresolution index of ridge top flatness	r	Q	1.2	(0, 6)
mrvbf	multiresolution index of valley bottom flatness	r	Q	1.5	(0, 6)
Geological data					
spm	Predictive map of soil parent material (50 m grid)	p	C	14 classes	
geol	Bedrock lithological units (1/50 000)	p	C	4 classes	
Gamma-ray spectrometry (airborne geophysical survey)					
devk	Deviation from mean K emissions of the corresponding lithogeological unit (Bonijoly et al., 1999)	p	Q	0	(-0.5, 0.5)
Land use/ landscape					
gld	grassland frequency on 15 years	o	Q	6	(0, 15)
frt	forest frequency on 15 years	o	Q	1	(0, 15)
lowh	distance to the lowest hedge (m)	o	Q	24.9	(0, 265)
highh	distance to the highest hedge (m)	o	Q	29.6	(0, 307)
Soil data					
hza	Predictive map of the A horizon (cm)	s	Q	48.4	(3, 241)

r = relief, *p* = parent material, *s* = soil properties, *o* = organisms, Q = quantitative, C = categorical

These attributes have been computed using the open source GIS (Geographical Information System) SAGA v.2.0.5 (System for Automated Geoscientific Analyses, http://www.saga-gis.org/en/index.html). All terrain attributes were originally derived from a 2 m LiDAR DEM, but such DEM shows locally noisy variations, which could lead to irrelevant terrain attributes. To deal with this issue, the terrain attributes were derived from DEM resampled at 5, 10 and 20 m from the 2 m LiDAR

DEM and then used as covariates. The difference of elevation between a 20 m and a 5m DEM was considered to identify local soil deposit or erosion. The geology of the study area was described by two maps: a 1:50,000 map of lithological units (Chantraine et al. 2002) and a predictive map of soil parent material (50 m grid spacing; Lacoste et al., 2011). This predictive map includes superficial deposits, i.e. Aeolian loam, colluvial and alluvial deposits. Gamma-ray spectrometry was based on existing airborne geophysical surveys interpolated by ordinary kriging at 250 m resolution (Bonijoly et al., 1999). Deviation from mean K emission of the related lithological unit, defined using the exhaustive lithological map produced by Chantraine et al. (2002), was considered in order to detect thick covers of superficial deposits, especially Aeolian loam. Land use and landscape were described by four attributes: grassland and forest frequencies over 15 years (from 1993 to 2007), distances to the nearest hedge (uphill and downhill from the hedge). Finally, we used one attribute to describe the soil: the A-horizon thickness, provided by a predictive map produced by Lacoste (2012a) with data collected at the same time of the one used to predict SOC stocks and soil BD, using the Cubist algorithm Quinlan (1992, 1993, 1994) to create a predictive model based on the same covariates as described in the Table 4-1.

2.4. Prediction and mapping methods

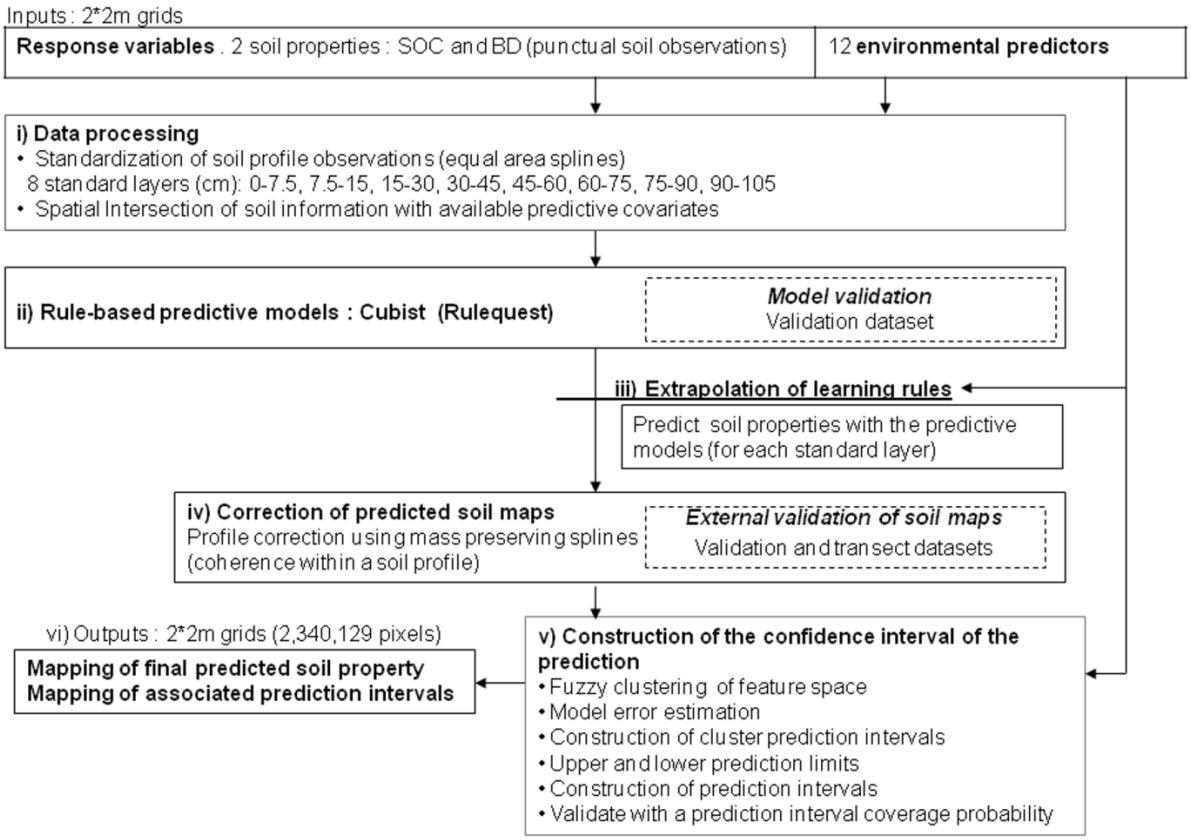

Figure 4-3. Overview diagram of the method implemented to produce 3D continuous predictive maps of SOC content and BD at the landscape scale.

The method used to predict and map the total SOC stocks up to 105 cm involved six main steps (Figure 4-3):

i) *Preparation of the calibration and validation datasets.*

The first step achieved depth standardization of the soil profile observations provided by soil core sampling. Continuous SOC content and BD profiles (from the soil surface to a maximum depth of 105 cm) were produced by fitting equal-area spline functions to the soil observations. The equal-area spline function we used was a generalization of the quadratic equal-area spline model of Bishop et al. (1999) and was described by Malone et al. (2009). We fitted the spline function to the measured values for each soil property (SOC content and BD). The spline function depends on a smoothing parameter lambda (λ). For this parameter λ, we tested the following values: 10, 1, 0.1, 0.01, 0.001, 0.0001 and 0.00001 (the higher the value λ, the smoother is the fitted profile). For each profile, we recorded the value λ that produced the fitted profile with the highest fit quality, according to the root mean square error (RMSE). For each variable (SOC content and BD), we chose the λ value that occurred most frequently among profiles. Eight standard soil layers were defined: 0-to-7.5 cm, 7.5-to-15 cm, 15-to-30 cm, 30-to-45 cm, 45-to-60 cm, 60-to-75 cm, 75-to-90 cm, 90-to-105 cm. The two first layers were described to consider rapid SOC content and BD changes with depth in grasslands or in fields with minimum tillage (Follain et al, 2007; Viaud et al., 2010). From the fitted spline, we derived the mean value of SOC content and BD within the 8 defined depth increments (i.e. the eight standard soil layer). These fitted values were used as calibration or validation data, and spatially intersected with the available spatially exhaustive environmental covariates.

ii) Creation of predictive models based on the calibration dataset and the spatially exhaustive environmental covariates.

Models were created separately both for SOC content and BD, and for each standard soil layers. We used Cubist v.2.04. , a commercial software tool distributed by Rulequest© (http://www.rulequest.com/) and based on the tree model algorithm M5 developed by Quinlan (1992, 1993, 1994). Cubist is a rule-based regression algorithm, allowing the creation of a predictive model based on conditions rules (partition of the calibration space according to the associate environmental covariates) and linear predictive rules (prediction of the variable of interest by combining the environmental covariates values). Cubist has been used in various fields with good results and is recognized as an efficient tool in term of computation time (Walton, 2008). Cubist creates an explicit model and gives the relative importance of the predictors, allowing an easy model interpretation.

iii) Models performance

First, the models constructed by Cubist were evaluated on the calibration dataset, from which they were generated (internal evaluation). Second, the models were evaluated on the two independent datasets not used to create the models, taken separately (external evaluation on the landscape and transect validation datasets) and together. Four different error indexes were calculated both for the internal and external evaluation: (i) the Mean Absolute Error (MAE, Eq.2), (ii) the Root Mean Square Error, which is a measurement of the average error (or accuracy) of the prediction (RMSE, Eq.3), (iii) the coefficient of determination, which measures the agreement between measured and predicted data (R^2, Eq.4), and (iv) the Lins's Concordance Correlation Coefficient (ρ_c, Eq.4) which evaluates the degree to which pairs of observations fall on the 45° line through the origin (Eq. 5; Lin, 1989, 2000).

The value of this index is scaled between −1 and 1, with a value of 1 representing complete agreement between all paired sites.

$$MAE = \frac{1}{n}\sum_{i=1}^{n}|y_i - x_i| \quad (2)$$

$$R^2 = \frac{\sum_{i=1}^{n}(y_i - \bar{x})}{\sum_{i=1}^{n}(x_i - \bar{x})} \quad (3)$$

$$RMSE = \sqrt{\frac{\sum_{i=1}^{n}(y_i - x_i)}{n}} \quad (4)$$

$$\rho_c = \frac{2S_{xy}}{S_x^2 + S_y^2 + (\bar{x} - \bar{y})^2} \quad (5)$$

Where $S_x^2 = \frac{1}{n}\sum_{i=1}^{n}(x_i - \bar{x})^2$, $S_y^2 = \frac{1}{n}\sum_{i=1}^{n}(y_i - \bar{y})^2$, $S_{xy} = \frac{1}{n}\sum_{i=1}^{n}(x_i - \bar{x})(y_i - \bar{y})$

For all these four equations, $\bar{x}$ and $\bar{y}$ are the mean value for populations *x* (measured) and *y* (predicted) of size *n*, x_i and y_i are paired ith values from the population *x* and *y.*

iv) Production of spatially exhaustive maps of SOC content and BD.

Predictive maps of SOC content and BD have been produced separately for every standard soil layer by applying the learning rules created by Cubist to the entire study area (2,340,129 pixels), where spatially exhaustive covariates were available. For each of the standard soil layer (from the soil surface to a depth of 105 cm), the predictive models have been applied for every pixels of the study area.

v) Reconstruction of continuous soil profiles from the predictive SOC content and BD values and depth correction.

Continuous SOC content and BD profiles (from the soil surface to a depth of 105 cm) were produced for each pixel of the study area, by fitting equal-area spline functions to the SOC content and BD values predicted by the Cubist learning rules. This profile reconstruction step allowed obtaining smoothed continuous soil profiles, used to create continuous 3D maps. The influence of the soil profile reconstruction on soil properties values was assessed by comparing the values of the four error indexes previously described calculated from (i) the predicted values for the standard soil layers (without soil profile reconstruction) and all the measured values from the two validation datasets considered together, and (ii) the new predicted values extracted from the continuous soil profile for the standard soil layers and the two validation datasets considered together. The coherence between SOC content profiles and A-horizon thickness was controlled using a predictive map of A-horizon thickness available for the study area (Lacoste, 2012). It allowed correcting the continuous soil profiles, by removing SOC content and BD values where SOC contents values were predicted under the A-horizon limits.

vi) Mapping of SOC stocks

SOC stocks were computed by combining predictions of SOC content, soil BD and soil gravel content. Predictions of soil gravel content were produced with the same field datasets and covariates we used to product the predictive maps of SOC contents and soil BD (Lacoste, M., 2012). For a soil layer *i*, the SOC stock are given by Eq. 6:

$$SOC_{stock.i} = (SOC_{content.i} \times BD_i \times (1 - Gr_i/100) \times t_i)/10 \quad (6)$$

Where $SOC_{stock.i}$ is the SOC stock in tC ha^{-1}, $SOC_{content.i}$ the SOC content in g kg^{-1}, BD_i the fine earth BD in g cm^{-3}, GR_i the volume percentage of gravel (%) and t_i the thickness of the depth increment *i* (cm). For every pixel in the study area, total SOC stocks (0-to-105 cm) were estimated by summation of the stocks for all the intermediate soil increments.

vii) Construction of the prediction interval of predictive maps.

The prediction intervals were calculated for each standard soil layer, using the method fully described by Malone et al. (2011). This method presented the major advantage to not require the identification and the determination of the contribution of each source of uncertainty to the overall prediction uncertainty. It was based on the assumption that pixels in the same feature space (determined by the covariates values) will share similar distribution of errors. This method was implemented as follows for each standard soil layer: (i) clustering of the feature space of the environmental covariates associated to the two validation datasets, using a fuzzy k-means routine with extragrades ; (ii) determination of the error distribution model for each cluster, based on the residuals determined by comparing the values of predicted and measured soil properties ; (iii) for each cluster, calculation of prediction intervals with a 95% confidence level (95% of the real soil properties values should fall within these bounds) ; (iv) partition of the whole study area according to the defined clusters ; (v) computation of the prediction interval for each pixel using the error distribution models defined for each cluster. The prediction interval obtained or each standard soil layers were combined to produce a final prediction interval until a depth of 105 cm.

```
Rule 1: [112 cases, mean 8.112288, range 1.116017 to 20.19062, est err 2.3599148]
        If
                Gld in {1, 2, 3, 4, 5, 6, 8, 10, 11, 12, 13, 14, 15}
        Then
                SOC = 8.1774597 – 0.78 mrvbf + 0.03 hza + 1.5 dif.elev
Rule 2: [118 cases, mean 8.9629173, range 1.116017 to 16.52321, est err 2.1300650]
        If
                Smp in {1, 2, 3}
        Then
                SOC = 3.8902728 + 0.0084 hza
Rule 3: [7 cases, mean 12.0846968, range 6.084407 to 20.19062, est err 6.4643254]
        If
                Smp in {6,14}
                High <= 6.929646
        Then
                SOC = 9.8467357
Rule 4: [12 cases, mean 20.6772995, range 6.774977 to 31.96915, est err 2.8409903]
        If
                Smp in {6, 14}
                Gld in {0, 9}
                High > 6.929646
        Then
                SOC = 27.0501001 – 0.212 highh – 3.49 vcurv – 0.018 lowh
```

Figure 4-4. Example of the Cubist model used for the prediction of SOC content in the 30-to-45- cm soil layer.

3. Results

3.1. Models description

3.1.1. Example of one model used to predict SOC content: the case of the 30-to-45 cm standard soil layer

We obtained an explicit model for each soil property and for each standard soil layer. Figure 4-4 gives an example of the rules obtained to predict SOC content for the 30-to-45 cm standard soil layer. This particular model included four linear predictive rules (introduced by "then"), applied to different partitions of the study area determined by condition rules (introduced by "if").

3.1.2. Fitting performance evaluation: internal and external validations

Table 4-2. Fitting performance for the SOC content predictive models

Standard soil layers (cm)		0-7.5	7.5-15	15-30	30-45	45-60	60-75	75-90	90-105	all layers
Evaluation on the calibration dataset	MAE (g kg^{-1})	3.02	4.06	2.12	1.29	0.73	1.01	7.49	0.94	2.31
	RMSE (g kg^{-1})	5.35	6.11	3.06	1.63	0.90	1.60	7.97	0.94	4.05
	R^2	0.79	0.38	0.55	0.73	0.85	0.46	0.71	0.11	0.80
	ρ_c	0.87	0.47	0.72	0.80	0.92	0.65	0.26	0.10	0.88
Evaluation on the validation dataset	MAE (g kg^{-1})	6.85	5.07	2.97	2.33	2.77	1.50	13.62	7.64	4.08
	RMSE (g kg^{-1})	12.64	9.17	4.29	3.55	4.56	2.22	13.89	7.84	7.74
	R^2	0.12	0.01	0.03	0.05	0.08	0.51	0.29	0.25	0.31
	ρ_c	0.28	0.05	-0.15	0.21	0.14	0.55	0.03	0.16	0.52
Evaluation on the transect dataset	MAE (g kg^{-1})	3.26	3.72	2.42	1.54	1.50	2.04	12.48	2.42	3.07
	RMSE (g kg^{-1})	4.60	6.06	3.98	2.16	1.93	2.97	13.19	3.23	5.02
	R^2	0.77	0.48	0.72	0.84	0.85	0.60	0.25	0.51	0.71
	ρ_c	0.84	0.55	0.82	0.91	0.92	0.72	0.09	0.58	0.82

Table 4-2 and Table 4-3 show the results of the fitting performance for the models used to predict SOC content and BD, respectively. The four errors indexes described in part 2.4. are given for each standard soil layer (allowing an estimation of the model performance according to the considered depth) and for the soil standard layers all together (allowing an overall assessment of the model performance). Considering the evaluation on the calibration dataset (internal validation), the SOC content models showed an overall MAE of 2.31 g kg^{-1}, RMSE of 4.05 g kg^{-1}, R^2 of 0.80 and ρ_c of 0.88 (Table 4-2). For the evaluation on the landscape validation dataset (external validation), these models showed an overall MAE of 4.08 g kg^{-1}, RMSE of 7.74 g kg^{-1}, R^2 of 0.31 and ρ_c of 0.52. Finally, for the evaluation on the transect validation dataset (external validation), these models showed an overall MAE of 3.07 g kg^{-1}, RMSE of 5.02 g kg^{-1}, R^2 of 0.71 and ρ_c of 0.82. When considering together the two datasets used for external validation (landscape and transect validation datasets), these SOC content models showed an overall MAE of 3.35 g kg^{-1}, RMSE of 5.92 g kg^{-1}, R^2 of 0.60 and ρ_c of 0.73. Considering the four error indexes and the three evaluation datasets, the best predictions of SOC

content were obtained for the middle of the soil profiles (depth between 15 and 75 cm), and the worst prediction in the deeper horizons (depth of 75 cm and below).

Table 4-3 Fitting performance for the BD predictive models.

Standard soil layers (cm)		0-7.5	7.5-15	15-30	30-45	45-60	60-75	75-90	90-105	all layers
Evaluation on the calibration dataset	MAE (g kg^{-1})	0.08	0.10	0.05	0.08	0.05	0.06	0.05	0.06	0.07
	RMSE (g kg^{-1})	0.11	0.12	0.06	0.11	0.06	0.08	0.08	0.07	0.09
	R^2	0.79	0.56	0.85	0.32	0.74	0.66	0.80	0.66	0.77
	ρ_c	0.84	0.69	0.89	0.49	0.81	0.63	0.64	0.73	0.86
Evaluation on the validation dataset	MAE (g kg^{-1})	0.13	0.13	0.12	0.10	0.07	0.08	0.04	0.12	0.11
	RMSE (g kg^{-1})	0.17	0.18	0.16	0.13	0.10	0.13	0.05	0.17	0.15
	R^2	0.08	0.03	0.01	0.09	0.47	0.05	0.38	0.27	0.26
	ρ_c	0.21	-0.15	0.00	0.25	0.56	-0.03	0.47	-0.27	0.49
Evaluation on the transect dataset	MAE (g kg^{-1})	0.27	0.13	0.11	0.11	0.11	0.20	0.18	0.17	0.15
	RMSE (g kg^{-1})	0.31	0.17	0.15	0.16	0.17	0.26	0.22	0.21	0.21
	R^2	0.08	0.09	0.15	0.03	0.08	0.30	0.10	0.02	0.23
	ρ_c	0.02	0.05	-0.12	-0.03	0.08	0.16	0.11	-0.01	0.49

Considering the evaluation on the calibration dataset (internal validation), the BD models showed an overall MAE of 0.07 g cm^{-3}, RMSE of 0.09 g cm^{-3}, R^2 of 0.77 and ρ_c of 0.86 (Table 4-3). For the evaluation on the landscape validation dataset (external validation), these models showed an overall MAE of 0.11 g cm^{-3}, RMSE of 0.15 g cm^{-3}, R^2 of 0.26 and ρ_c of 0.49. Finally, for the evaluation on the transect validation dataset (external validation), these models showed an overall MAE of 0.15 g cm^{-3}, RMSE of 0.21 g cm^{-3}, R^2 of 0.23 and ρ_c of 0.49. When considering together the two datasets used for external validation (landscape and transect validation datasets), these BD models showed an overall MAE of 0.14 g cm^{-3}, RMSE of 0.19 g cm^{-3}, R^2 of 0.23 and ρ_c of 0.38. Considering the influence of the depth on the BD models performance, errors indexes showed in Table 4-3 didn't allowed determining a clear distribution pattern, except for the evaluation on the transect validation dataset which have higher values of MAE and RMSE for the very topsoil layer (0-to-7.5 cm) and for the deeper soil layers (60-to-95 cm).

Table 4-4 shows the SOC content and BD models performances assessed using the transect validation dataset, according to the distance to the hedge and the depth. Considering all the standard soil layers (without depth distinction), both predictions of SOC content and BD had low RMSE variation according to the distance to the hedge: RMSE for SOC content models range from 3.11 to 4.36 g kg^{-1}, and RMSE for BD models range from 0.12 to 0.21 g cm^{-3}. Highest RMSE values were found for locations 2 m downhill from the hedges for the SOC content models (4.36 g kg^{-1}), and for locations just under the hedge for the BD models (0.21 g cm^{-3}). The evolution with depth of the performance of SOC content models and BD models slightly varied according to the distance to the hedge: the SOC content models showed a better performance in the middle of the soil profile (between 7.5 cm and 60 cm), with poorer performance for topsoil and deep layers, and the BD models showed a higher RMSE values under the hedges (2 m downhill and uphill from the hedge, and just under the hedges), especially for the very topsoil layer (0-to-7.5 cm).

Table 4-4. RMSE for SOC content and BD prediction, according to the distance to the hedge, calculated on transect validation dataset (SOC content/BD).

Distance to the hedge	Standard soil layers (cm)								
(m, -: downhill, +:uphill)	0-7.5	7.5-15	15-30	30-45	45-60	60-75	75-90	90-105	all layers
-10	5.5 / 0.24	4.99 / 0.15	2.32 / 0.13	3.49 / 0.21	3.14 / 0.18	5.15 / 0.42	7.78 / 0.22	4.21 / 0.19	3.30 / 0.15
-5	5.46 / 0.32	5.68 / 0.15	7.01 / 0.11	2.35 / 0.09	2.05 / 0.18	3.21 / 0.01	7.23 / -	5 / -	3.50 / 0.14
-2	11.24 / 0.37	9.06 / 0.2	7.7 / 0.13	2.87 / 0.13	3.16 / 0.11	4.76 / 0.17	0.79 / -	2.24 / -	4.36 / 0.15
0	6.29 / 0.39	5.18 / 0.2	2.92 / 0.25	2.53 / 0.21	2.51 / 0.22	1.28 / 0.3	2.82 / 0.34	2.47 / 0.29	2.77 / 0.21
2	4.47 / 0.38	4.6 / 0.17	4.23 / 0.12	1.53 / 0.09	2.39 / 0.14	3.74 / 0.21	7.64 / 0.22	5.72 / 0.21	3.24 / 0.15
5	5.18 / 0.32	4.09 / 0.09	4.74 / 0.06	1.34 / 0.08	1.59 / 0.1	3.61 / 0.18	6.83 / 0.23	4.42 / 0.19	3.00 / 0.12
10	4.13 / 0.26	3.02 / 0.13	2.64 / 0.1	2.72 / 0.16	2.21 / 0.18	4.44 / 0.27	9.34 / 0.12	4.57 / 0.12	2.91 / 0.14
20	3.43 / 0.29	2.89 / 0.12	2.38 / 0.1	2.47 / 0.15	2.98 / 0.18	6.12 / 0.22	9.33 / 0.15	4.37 / 0.18	3.11 / 0.14

3.1.3. Relative importance of the covariates in the predictive models rules

Table 4-5. Relative importance (%) of the environmental covariates used in the SOC content predictive models rules and resolution of the DEM and its derived attributes used as covariates (see Table 4-1 for the covariates names and units).

	Standard soil layers								
Models properties	0-7.5	7.5-15	15-30	30-45	45-60	60-75	75-90	90-105	All layers
Relative importance of covariates used in condition rules (%)									
gld	100	27	100	50	100	23	-	-	50
vof	-	18	-	-	-	-	100	-	15
spm	-	-	-	55	-	-	-	-	7
hof	-	-	-	-	47	-	-	-	6
vcurv	-	-	-	-	41	4	-	-	6
highh	-	-	-	8	31	-	-	-	5
slope	-	-	30	-	-	-	-	-	4
hcurv	-	-	-	-	-	4	-	-	1
Relative importance of covariates used in linear predictive rules (%)									
hof	100	91	84	-	60	-	95	20	56
slope	-	16	86	-	31	19	95	20	33
dif.elev	59	54	100	45	-	19	5	-	35
hza	41	-	30	92	-	58	-	-	28
vof	41	55	-	-	-	11	100	-	26
mrrtf	59	-	-	-	-	-	95	40	24
elev	59	-	-	-	59	38	-	20	22
hcurv	-	54	70	-	-	49	-	-	22
Wi	-	19	100	-	19	-	-	-	17
vcurv	-	-	-	5	59	2	-	60	16
zc	-	53	-	-	-	-	-	60	14
highh	-	20	30	5	18	-	-	20	12
lowh	-	19		5	59	3	-	-	11
mrvbf	41	-	-	45	-	-	-	-	11
devk	-	-	-	-	-	30	-	-	4
Resolution of the LIDAR DEM and its derived attributes (m)									
	5	20	20	5	5	5	5	5	

Table 4-6. Relative importance (%) of the environmental covariates used in the BD predictive models rules and resolution of the DEM and its derived attributes used as covariates (see Table 4-1 for the covariates names and units).

	Standard soil layers								
Model properties	0-7.5	7.5-15	15-30	30-45	45-60	60-75	75-90	90-105	All layers
Relative importance of covariates used in condition rules (%)									
vof	60	60	-	-	-	-	-	-	15
gld	-	-	20	-	-	-	-	-	3
Relative importance of covariates used in linear predictive rules (%)									
elev	51	-	-	60	-	40	40	-	24
devk	-	-	60	60	20	-	10	-	19
wi	51	48	-	-	40	-	-	-	17
mrvbf	-	-	-	60	-	-	10	60	16
vof	4	44	-	40	20	-	-	-	14
mrrtf	2	48	20	-	-	-	-	-	9
zc	36	-	-	-	-	20	-	-	7
vcurv	-	-	54	-	-	-	-	-	7
hof	-	32	-	20	-	-	-	-	7
slope	-	48	-	-	-	-	-	-	6
Resolution of the LIDAR DEM and its derived attributes (m)									
	10	10	20	5	20	5	5	20	

Table 4-5 and Table 4-6 give the relatives importance of the covariates used to create the SOC content and BD models, respectively. They also show the resolution of the DEM and its derived terrain attributes used as covariates in the models. Considering SOC content models (Table 4-5), grassland frequency (*gld*) was the most used covariate in the condition rules. This attribute was considered as a stratifier for all the standard soil layers, except the two deeper ones. Other covariates appeared also important in the condition rules, namely vertical overland flow distance (*vof*), soil parent material (*spm*) or vertical curvature (*vcurv*), but mostly for one or two standard soil layers. A larger panel of covariates was integrated in the linear predictive rules. Amongst the covariates exerting a high influence in the predictions were the horizontal overland flow distance (*hof*), the *slope* and the difference between the elevation from the 20 m and the 5 m DEM (*dif.elev*). BD models involved less covariate in the construction of both the condition and linear predictive rules (Table 4-6). The condition rules used only the vertical overland flow distance (*vof*) and the grassland frequency (*gld*) in the models for the first 3 standard soil layers (from 0 cm to 30 cm depth). In the linear predictive rules, important covariates were the elevation (*elev*), the deviation from the mean K emissions (*devk*), the topographic wetness index (*wi, Eq.1*), the multiresolution index of valley bottom flatness (*mrvbf*) and the vertical overland flow distance (*vof*).

For the OC content models, the terrain attributes with a 5 m resolution were mostly used in the predictive rules, except for two standard soil layers (7.5-to-15 cm and 15-to-30 cm) were a 20 m resolution was used. For the BD models, the choice of the optimal terrain attribute resolution was less uniform: terrain attributes were used with a resolution of 10 m for the two surface layers (0-to-7.5 cm and 7.5-to-15 cm), 5 m for three standard layers (30-to-45 cm, 60-to-75 cm and 75-to-90 cm), 20 m for the three remaining standard layers (15-to-30 cm, 45-to-60 cm and 90-to-105 cm).

3.2. Soil profile reconstruction

The following values of error indexes compare the soil data not used to create the predictive model (landscape plus transect validation datasets, taking into account all the soil layers) with the SOC content and BD predicted values, calculated before and after the spline reconstruction process. For SOC content prediction, MAE changed with the soil profile reconstruction from 3.35 g kg^{-1} to 3.43 g kg^{-1}, RMSE decreased from 5.92 to 5.66 g kg^{-1}, R^2 improved from 0.60 to 0.66, and ρ_c improved from 0.73 to 0.75. For BD prediction, MAE stayed at 0.14 g cm^{-3} with the soil profile reconstruction, RMSE stayed at 0.19 g cm^{-3}, R^2 improved from 0.23 to 0.24, and ρ_c decreased from 0.38 to 0.34. Figure 4-5 shows that this profile reconstruction step allowed smoothing the soil profiles and removing extreme predictions, without compromising prediction accuracy.

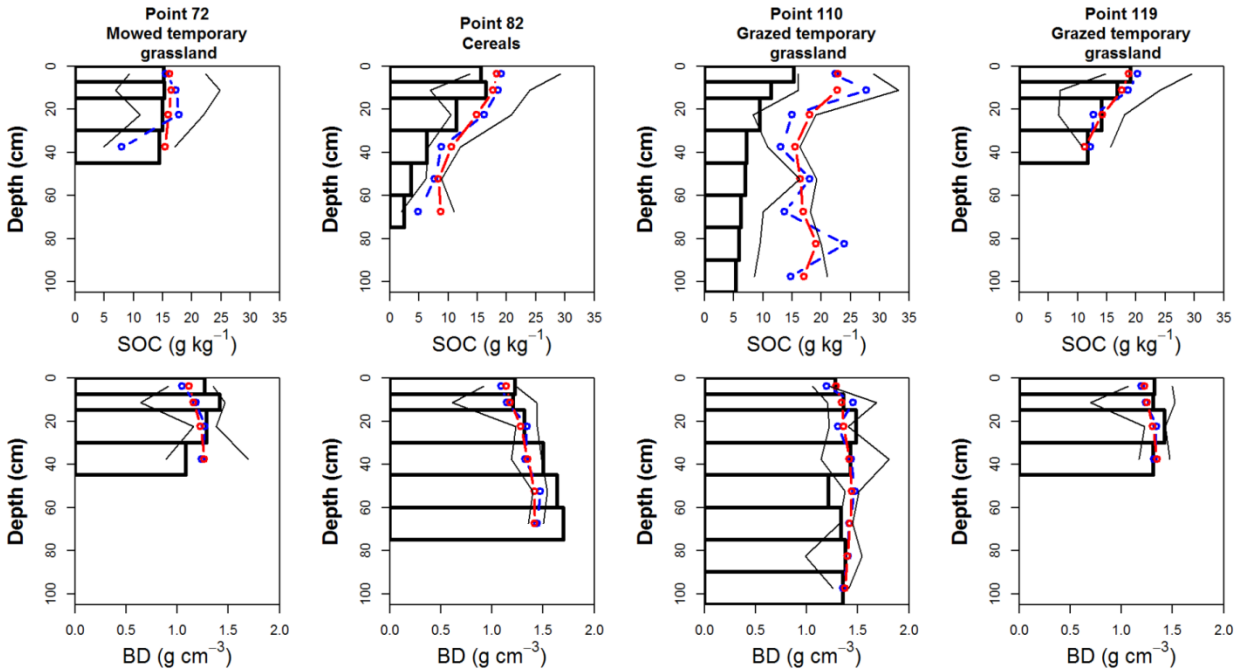

Figure 4-5. Examples of soil profile reconstruction considering four randomly selected sampled soil profiles (histogram: validation data derived from measurements for the standard layers, dashed blue line: predictions from Cubist (raw values), solid red line: predictions after the reconstruction of soil profiles using the mass preserving splines, solid black lines: upper and lower prediction limits of the prediction interval).

3.3. Description of the SOC content and BD predictions

Table 4-7. Descriptive statistics of the SOC content and BD values for the calibration dataset, landscape and transect validation datasets, and for the predictions.

	minimum	1st quartile	median	mean	3rd quartile	maximum	standard deviation
SOC content (g kg^{-1})							
Calibration dataset	1.71	6.74	11.26	12.86	15.84	63.26	9.03
Landscape validation dataset	0.04	7.96	13.05	14.30	18.93	65.53	9.22
Transect validation dataset	1.51	5.61	10.41	11.22	13.82	74.89	8.97
Predicted values	1.08	7.42	10.27	11.41	14.45	60.47	5.23
Soil BD (g cm^{-3})							
Calibration dataset	0.60	1.25	1.39	1.35	1.48	1.70	0.19
Landscape validation dataset	0.42	1.19	1.32	1.31	1.46	2.29	0.23
Transect validation dataset	0.70	1.28	1.39	1.37	1.49	1.71	0.17
Predicted values	0.80	1.32	1.40	1.38	1.46	1.57	0.11

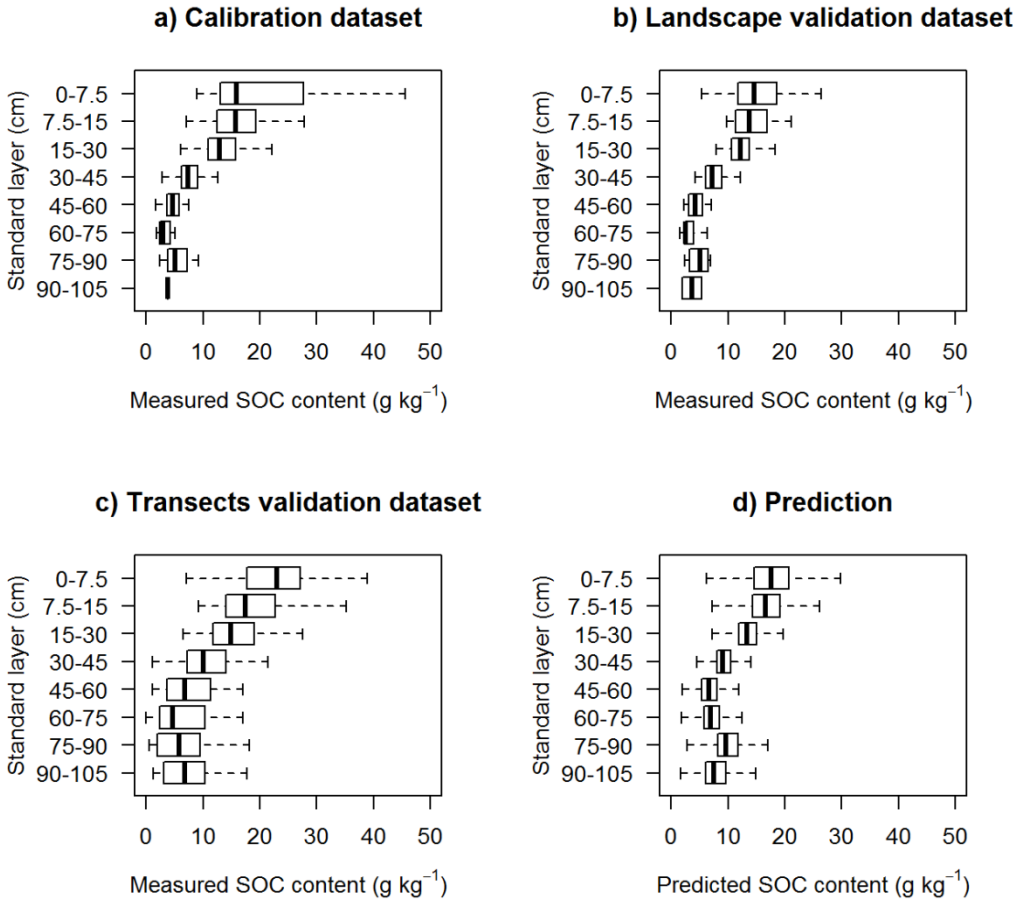

Figure 4-6. Distribution of the SOC content with depth according to standard soil layers for calibration dataset (a), landscape validation dataset (b), transect validation dataset (c) and the prediction of SOC content (d).

Table 4-7 gives the descriptive statistics of the measured SOC content and fine earth BD for the calibration, landscape and transect validation datasets, and the descriptive statistics of the predicted SOC content and fine earth BD. Measured values of SOC content ranged from 1.7 to 63 g kg^{-1} (mean value = 13 g kg^{-1}) for the calibration dataset, 0.1 to 66 g kg^{-1} (mean value = 14 g kg^{-1}) for the landscape validation dataset, and 1.5 to 75 g kg^{-1} (mean value = 11 g kg^{-1}) for the transect validation dataset. SOC content predictions ranged from 1 to 61 g kg^{-1} (mean value = 11 g kg^{-1}). We observed the same trend in SOC content distribution with depth in the calibration dataset, landscape validation dataset, transect validation dataset and the predicted values of SOC content (Figure 4-6). Surface horizon (0-to-7.5 cm) was proved to be on average the most concentrated horizon in SOC content. However, the deeper horizons also presented significant SOC content concentration.

Measured values of BD ranged from 0.6 to 1.7 g cm^{-3} (mean value = 1.4 g cm^{-3}) for the calibration dataset, from 0.4 to 2.3 g cm^{-3} (mean value = 1.3 g cm^{-3}) for the landscape validation dataset, and from 0.7 to 1.7 g cm^{-3} (mean value = 1.4 g cm^{-3}) for the transect validation dataset. BD predictions ranged from 0.8 to 1.6 g cm^{-3} (mean value = 1.4 g cm^{-3}). These four different datasets revealed the same general trend in BD distribution with depth (Figure 4-7): BD increased with depth until 60 cm before slightly decreasing again. The transect validation dataset showed a more dispersed distribution for the deeper layers (Figure 4-7c).

Figure 4-8 shows the relation between SOC content and BD, for the measured values (calibration, landscape and transect validation datasets, Figure 4-8a) and for the predicted values (Figure 4-8b, 1,000 randomly selected points). The pattern observed in the measured data (BD decrease with an increasing SOC content) also was also found in the predicted data and followed the same trend (R^2 = 0.51 for the measured data and R^2 = 0.54 for the predicted data).

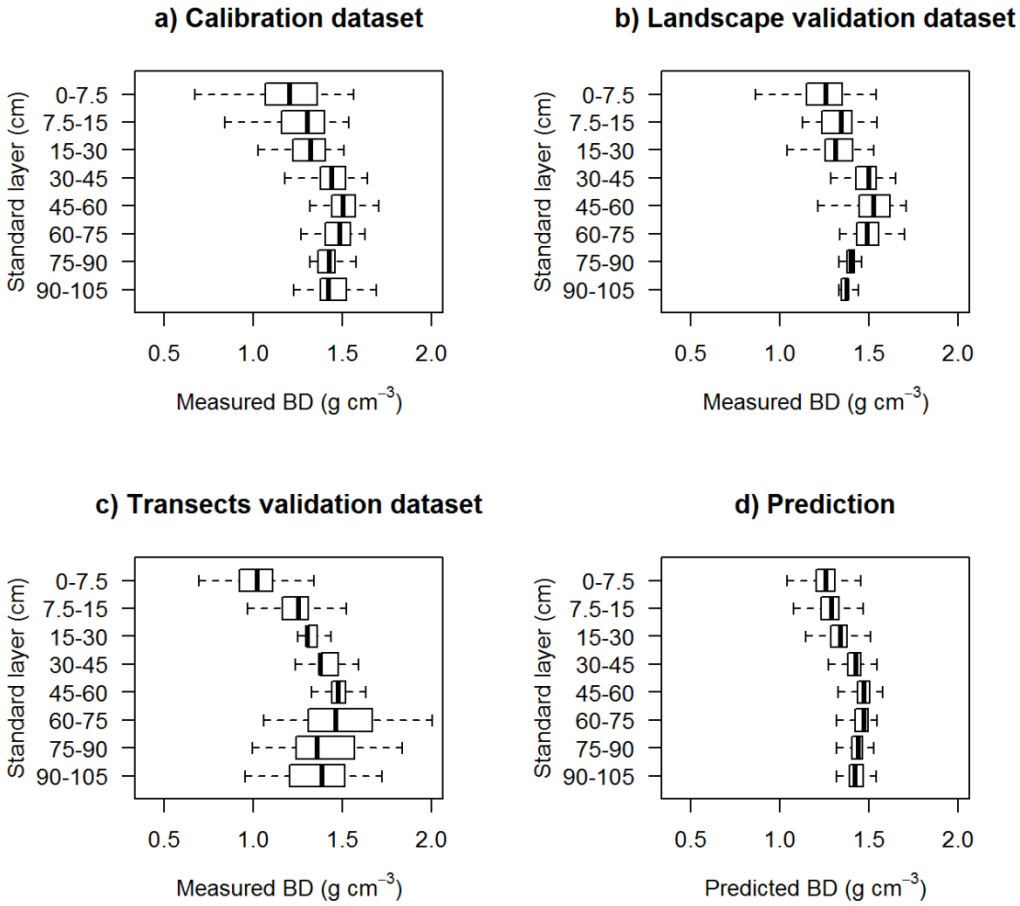

Figure 4-7. Distribution of the BD with depth according to standard soil layers for calibration dataset (a), landscape validation dataset (b), transect validation dataset (c) and the prediction of BD (d).

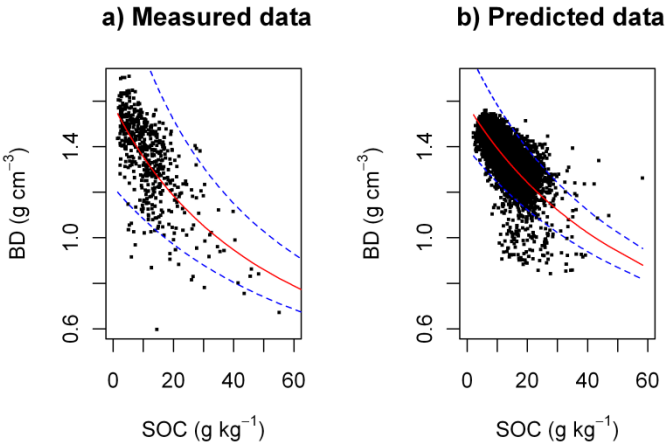

Figure 4-8. Relation between BD and SOC content in measured (calibration and validation datasets) and predicted data. Solid red line = trend line BD = 1/(0.01 SOC + 0.63), blue dashed lines = 95% confidence interval.

3.4. Example of spatial variation for topsoil predictions

Figure 4-9 shows the SOC content and BD predictions and prediction interval maps for the surface soil layer (0-to-7.5 cm). SOC content prediction for this layer ranged from 5 to 60 g kg^{-1} (mean value = 18 g kg^{-1}), whereas prediction of BD ranged from 0.6 to 1.5 g cm^{-3} (mean value = 1.2 g cm^{-3}). The spatial variability of SOC content prediction was mainly driven by land use and more precisely by the grassland frequency (*gld*, Table 4-5): higher SOC content was predicted for fields with a high frequency of grassland. Other covariates were also used to predict SOC content for this topsoil layer: the horizontal overland flow distance (*hof*), the difference between the elevation from the 20m DEM and the 5m DEM (*dif.elev*), the multiresolution index of ridge top flatness (*mrrtf*) and elevation (*elev*). The spatial variation of predicted BD was also driven by the vertical overland flow distance (*vof*), the elevation (*elev*) and the wetness index (*wi*).

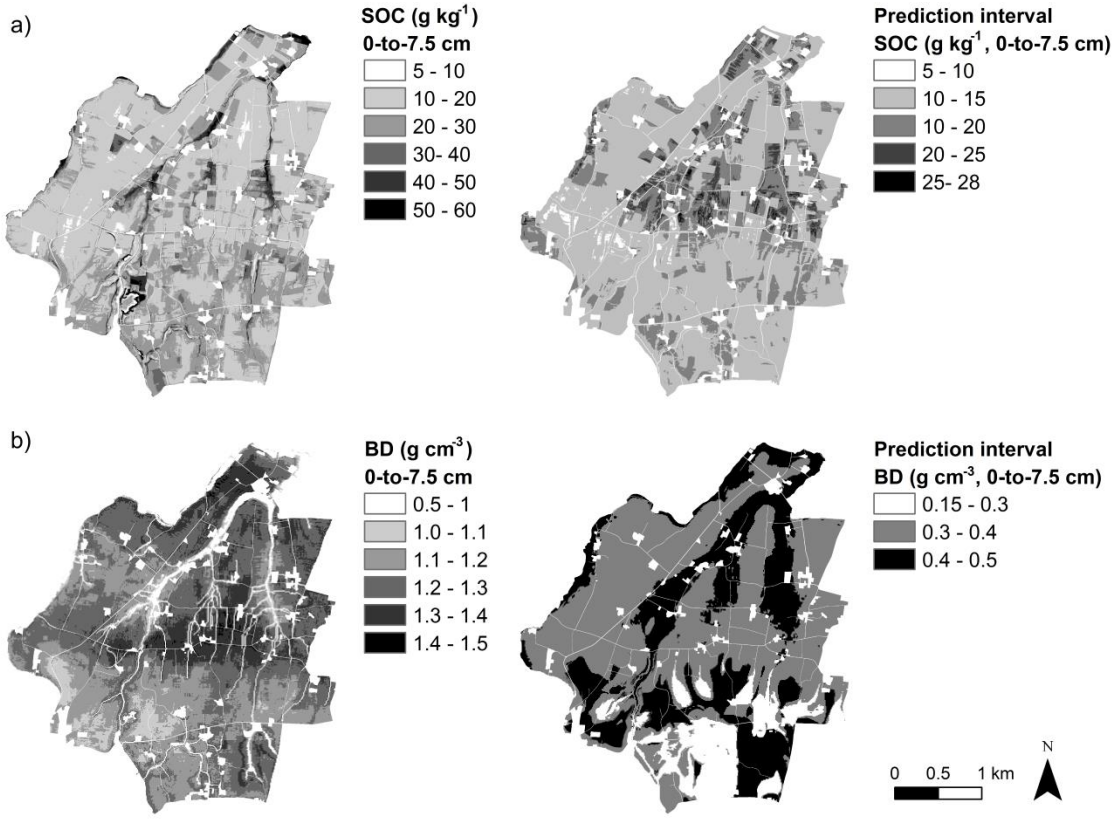

Figure 4-9. Predictive maps of SOC content and BD for the 0-to- 7.5 cm soil layer. (a) SOC content and its prediction interval, b) BD and its prediction interval.

3.5. Estimation of SOC stocks

Figure 4-10 gives example of the spatial distribution of SOC stocks at the landscape scale. The total predicted SOC stocks (0-to-105 cm) ranged from 5 to 360 tC ha^{-1} (mean value = 89 tC ha^{-1}, Fig. 10a). In the tillage layer (0-to-30 cm), SOC stocks ranged from 3 to 175 tC ha^{-1} (mean value = 58 tC ha^{-1}, Fig. 10b). We estimated the mean SOC stocks for the 0-to-30 cm layer at 44 t ha^{-1} under cultivated fields, 67 t ha^{-1} under grasslands and 30 t ha^{-1} under forest. SOC stocks were significant in the deeper horizons (Figure 4-10c, 30-105 cm), taking values up to 85% of total SOC stocks (mean value = 32 t ha^{-1}, counting for 33% of the total SOC stocks), mostly in situation of soil accumulation uphill from

hedges. Detailed maps (Figure 4-10) show that SOC stocks also vary within fields, mostly according to distance to the hedges and local topography.

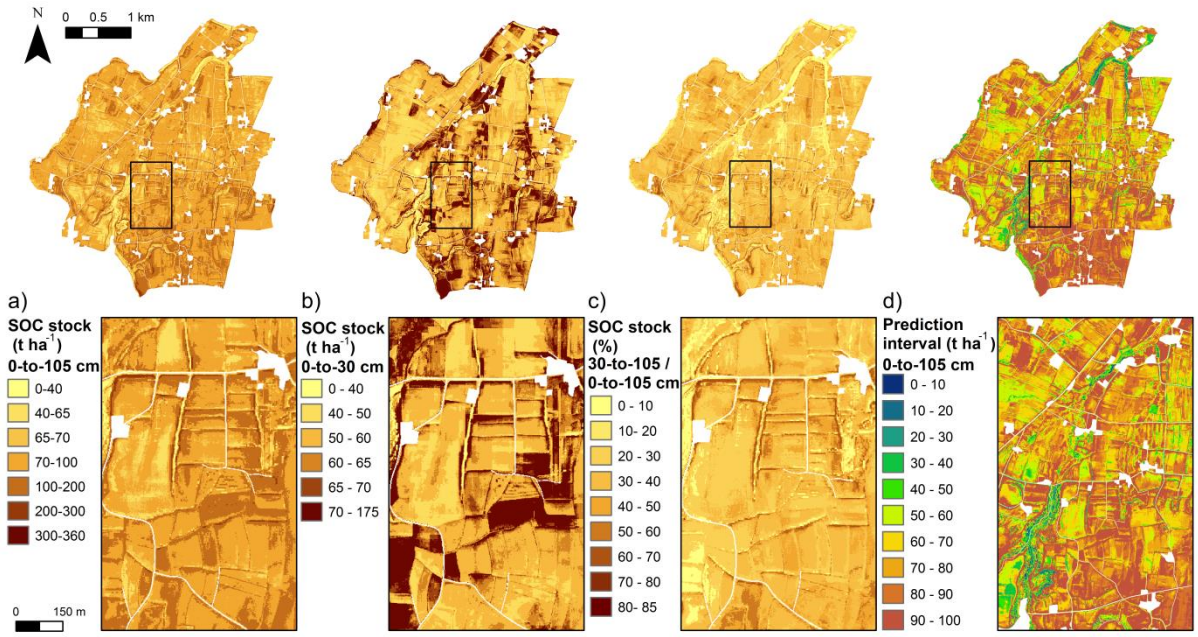

Figure 4-10. Predictive maps of SOC stocks over the 10 km² study area with a local zoom on a 60 ha area (square maps are details of the study area): a) total SOC stocks (0-105cm), b) SOC stocks within the tillage horizon (0-30 cm), c) SOC stocks in deep horizons (30-105 cm), in proportion of the total SOC stock , d) prediction interval of the prediction of the total SOC stocks (0-to-105 cm soil layer, tC ha-1).

4. Discussion

4.1. The predictive process

4.1.1. Use of a machine learning tool

First, we choose to use a machine learning tool, Cubist, to produce a high resolution predictive map of SOC stocks, by combining SOC contents and soil BD predictive maps. Machine learning was a useful method here to define the existing relationships between soil properties from a limited soil dataset and spatially exhaustive covariates. Cubist is a powerful tool where considering the computation time (model creation in less than 1 second, extrapolation to 2.3 million pixels in less than 5 minutes using a computer Intel® Core™2 CPU, 1.83 GHz, 2.00 GB RAM). Cubist also allows an easy interpretation of the predictive models, by the creation of useful outputs such as the detailed learning rules, or the importance of the covariates in the models. This makes more explicit the distribution of soil properties at the landscape scale.

4.1.2. Use of 2 m LiDAR DEM

The use of the DEM from LiDAR allowed taking into account the variations at short distance of the two soil properties we predicted, which was relevant for the typical landscape of our study area. However, this 2 m DEM was proved to be too noisy, and its derived terrain attributes became irrelevant. To deal with this problem we introduced as covariates the terrain attributes calculated from a DEM resampled at 5 m, 10 m and 20 m. For the SOC content prediction, the best model for each standard layer was created using mostly the terrain attributes at the 5 m resolution, except for two horizons (7.5-to-15 cm and 15-to-30 cm, Table 4-5). This result could be explained by tillage mixing of SOC content in these two topsoil layers, so there may be no need of very fine auxiliary

information (i.e. with resolution <20 m here) for the prediction of SOC content in these layers. In our landscape, SOC content showed a high variability in the very topsoil layer (0-to-7.5 cm), mostly because of fresh organic matter supply in areas close to hedges. In deep soil layers and for our study area, high SOC content could be mostly the result of soil erosion and accumulation processes, in strong link with linear structures within the landscape (e.g. the ditches or the hedges; Follain et al., 2009). Actually, the impact of soil redistribution (soil erosion and deposit) on the SOC storage is subject to discussion. The conclusion depends on which scale and processes are taken into account. For example, Lal and Pimentel (2008) argued that soil erosion leads to SOC loss, but Van Oost et al. (2007, 2008) maintained that it leads to SOC storage. The impact of soil erosion depends on (i) the fate of the SOC in the eroded soil (exportation or deposition out of the area of interest) and (ii) the evolution of the SOC mineralization (at the eroded sites, during soil transportation by the erosion processes and at the deposit sites, in soil horizon at different depth). Van Oost et al. (2006) modelled the impact of soil erosion on SOC stocks, by testing various hypothesis on SOC dynamic during soil transportation and on SOC dynamic in the deep soil horizons (after burying). They concluded that soil erosion could conduce both to SOC loss or storage. Doetterl at al. (2012) estimated that soil erosion processes could lead to carbon stabilization in areas where of soil deposit, but also in areas of erosion. The net balance would contribute to net carbon storage. However, they didn't take into account the priming effect observed in other studies (e.g. Fontaine et al.). Moreover, the carbon dynamic in the deep soil layers seems to be highly dependent on the spatial distribution of the fresh organic matter, the stable carbon and the microorganisms responsible for SOC mineralization (Rumpel and Koegel-Knabner, 2011). Berhe (2012) also underlined that the SOC mineralization rate could vary according to the location in landscape. Concerning the impact of linear landscape features (hedges) on SOC storage, Follain et al. (2006b) demonstrated that (i) the combination of diffusive transport and water erosion could significantly modify the topography and soil redistribution over a few centuries, (ii) hedges modify soil distribution and landforms by favouring deposition in the uphill position and soil erosion in the downhill position in agreement with field observations. Actually, such soil accumulation and A-horizon thickening uphill from hedges have been observed in the type of landscape we studied (Follain, 2006a; Follain et al. 2009; Lacoste, 2012). Moreover, SOC storage due to hedges has been described in previous studies, due to (i) a local effect under the hedge due to tree activity, and (ii) an anti-erosive effect at the hillslope scale (Follain et al., 2007; Walter et al., 2003a). Then, SOC content attested high spatial variability in the very topsoil layer and in deep soil layer, and this could explain why finer predictors (terrain attributes with a 5 m resolution) were used for SOC content predictions in this soil layers. According to the BD predictions, the choice of the terrain attributes resolution for each standard layer was not so consistent and more difficult to explain (Table 4-6). Terrain attributes at coarser resolution (10 and 20 m) were mostly preferred to those at fine resolution (5 m) to be used as predictors.

4.1.3. Creation of independent predictive models (for each standard soil layer and for each soil properties)

The creation of the predictive models was made independently for each of the standard soil layer: there was no initial guarantee of consistency for the predictions within soil profiles. The reconstruction of the soil profiles by fitting the spline function to the predicted values of SOC content and BD was a relevant solution to deal with this problem. This method was shown to be able to remove part of the inconstancies in the predictions, without altering the accuracy of the prediction (Figure 4-5). Moreover, the predicting process we used was proved to maintain the existing relation

between the soil properties (SOC content and BD, Figure 4-8). Finally, SOC content and BD were both predicted until the depth of 105 cm, for every pixels of the study area. But A-horizon were characterised by highly variable thickness (from 3 to 250 cm), and at some locations the soil was shallower than 105 cm, and deeper at others. To deal with this depth problem, we used a predictive map of A-horizons thickness, also produced with Cubist (Lacoste et al., 2012b). This predictive map of A-horizons thickness was used to correct the SOC content and BD maps, removing values in the soil layers not predicted as A-horizon. However, it remained a problem concerning the A-horizons deeper than 105 cm, mostly predicted under or close to some hedges (from 0 to 5 m uphill from hedges), where soil accumulation was possible, or where Aeolian loam was the soil parent material. SOC content and BD were not predicted in soils at depths over 105 cm and then, we possibly underestimated SOC stocks in soils deeper than 105 cm.

4.2. Importance of environmental predictors

According to SOC content predictions, we found a strong influence of land use (frequency of grassland), hydrologic terrain attributes (horizontal and vertical flow distances) and some topographic attributes (slope, difference between the 20 m and the 5 m DEM; Table 4-5). Other studies have also demonstrated a strong influence of topography on the distribution of SOC content (Florinsky et al., 2002; Grimm et al., 2008; Kheir et al., 2010; Kravchenko et al., 2006a; Kravchenko et al., 2006b; Malone et al., 2009; Vasques et al., 2010). This could be explained by dependences between the spatial differentiation of SOC content, soil redistribution (soil erosion and deposit) and soil waterlogging, highly linked to landscape morphology (Arrouays et al., 1998; Florinsky et al., 2002; Moore et al., 1993; Walter et al., 2003b). Regarding BD, the best predictors were topographic terrain attributes (elevation and multiresolution index of ridge top flatness), the deviation from the mean K emissions and a hydrographic terrain attribute (the modified topographic wetness index). In our landscape, these covariates allowed identifying the global position in the landscape (plateau, hillslope, plain) and the position from local topographical object such as hedges on bank or ditches, but also the soil parent material and the waterlogging and drainage condition which were highly linked to the landscape geomorphology.

4.3. Predictive models performance

4.3.1. Overall performance

Regarding SOC content and without distinction of depth (overall performance on soil profiles), the predictive models showed a MAE of 2.31 g kg^{-1}, a RMSE of 4.05 g kg^{-1} , a R^2 of 0.80, and a ρ_c of 0.88 for evaluation on the calibration dataset. For evaluation on the two datasets used for external evaluation and taken together, these models showed a MAE of 3.36 g kg^{-1}, a RMSE of 5.92 g kg^{-1} , a R^2 of 0.60, and a ρ_c of 0.73. These values proved that the models reached to explain SOC content values from the calibration dataset, according to the environmental covariates we used. The predictive models were also quite efficient to predict SOC content values for new locations, not used in the model creation step. This attested that: (i) our calibration dataset, even limited (70 sampling location for a study area of 10 km^2), was representative of the SOC content value at the scale of our study area (this idea was also supported by the results in Table 4-7), and then, the sampling method we used, i.e. cLHS, was proved to be efficient to design a sampling population able to capture the SOC content variation at the landscape scale; (ii) the environmental covariates we used were efficient to explain the SOC content values at landscape scale, and at a fine resolution; (iii) the machine learning

tool we used was able to capture the relationship between the SOC content values and the environmental covariates.

In comparison to previous study, our predictive models present quite better performance. For example, Florinsky et al. (2002) used a regression equation with a R^2 of 0.37 to predict SOC content in A-horizons in an agricultural area in the middle part of Canada. Malone et al. (2009) produced SOC content maps for soil depth up to 1 m in an agricultural area of Western Australia. Their models fit the measured values with an R^2 of 0.44, but cross-validation on the training datasets results in R^2 value of 0.10. Moreover, Malone et al. (2009) argues that, for quantitative soil spatial models, R^2 over 0.50 are unusual and values of 0.50 or less are common.

Regarding BD and without distinction of depth (overall performance on soil profiles), the predictive models showed a MAE of 0.07 cm^{-3}, a RMSE of 0.09 cm^{-3}, a R^2 of 0.77, and a ρ_c of 0.86 for evaluation on the calibration dataset. For evaluation on the two datasets used for external evaluation and taken together, these models showed a MAE of 0.14 g cm^{-3}, a RMSE of 0.19 g cm^{-3}, a R^2 of 0.23, and a ρ_c of 0.38. The good models performance showed in internal validation proved that these models reached to explain SOC content values from the calibration dataset, according to the environmental covariates we used. Nevertheless, the predictive models showed poorer performance according to external evaluation. Results given by Table 4-7 indicate that distribution of BD for the calibration dataset was in accordance with those of the other datasets (landscape and transect validation datasets), which suggests that the calibration dataset was quite well representative to the BD values for the study area. This could imply that the poor models performance in external evaluation could be due to a lack of covariates to explain the BD variations. In fact, some variables important to explain BD variation were hard to take into account, e.g. the type of tillage (depth and tool used) or the history of farming practices (e.g. the time elapsed since the last tillage, the use of tool which could lead to soil compaction). Other studies mainly predict BD using pedotransfer functions based on SOC content, depth and clay, silt and sand content. Martin et al. (2009) found that the best predictor was the soil concentration in organic carbon. As we see that there was a strong relation between SOC content and BD in our data (Figure 4-8). A two steps method may be an interesting way to improve the BD prediction: a predictive map of SOC content could be produced in a first step, and then, in a second, used among the covariates step to predict BD.

However, our results were consistent with some previous studies. Martin et al. (2009) compared seven predictions of BD at the French national scale in agricultural or natural areas, five produced with PTFs with a R^2 ranging from 0.29 to 0.37 and two produced with a boosted regression tree with a R^2 ranging from 0.83 to 0.94. Tranter et al. (2007) compared BD predictions across Australia using neural networks, multiple linear regression and regression trees (Cubist), and obtained R^2 ranging from 0.39 to 0.48, 0.41 to 0.50 and 0.20 to 0.43, respectively. These same models had an RMSE ranging from 0.13 to 0.16, 0.15 to 0.18 and 0.16 to 0.19 g cm^{-3}, respectively.

4.3.2. Variation of models performance with depth and distance to the hedges

We used two validation datasets for the evaluation of the SOC content and BD predictive models: the landscape validation dataset and the transect validation dataset, which were two independent datasets. The landscape validation dataset incorporated sampling locations distributed in the whole study area, whereas the transect dataset was concentrated on locations close to hedges. In fact, we assessed that the SOC content and BD distributions in space and depth differed regarding the locations inside the study area, and especially according to the hedges proximity. For the SOC content, the predictive models showed a better performance for the evaluation on the transect

validation dataset than for the evaluation on the landscape validation dataset (Table 4-2). This could attest that the prediction SOC content at hedges proximity (until 20 m uphill from hedges and 10 m downhill from hedges) was better that the general SOC content prediction at the Landscape scale. This could be explained by the fact that SOC distribution close to hedges may mostly be due to fresh organic matter supply from the hedge and soil redistribution (Walter et al., 2003a). Yet, no information about fresh organic matter supply was contained in the covariates used in the he predictive models creation (Table 4-1). Moreover, these covariates used in the predictive models were mostly linked to soil redistribution (slope, overland flow distance, difference in elevation for the 5 m and 20 m DEM, etc., Table 4-5). The SOC content prediction at the scale of the study area could be improved by using covariates including data on soil organic improver. For the BD, the predictive models showed a slightly lower performance for the evaluation on the transect validation dataset than for the evaluation on the landscape validation dataset (Table 4-3). This involved that the performances of the BD predictive model were equivalent for locations close to hedges or at the scale of the study area.

In our study, we found better predictions of SOC content for layers in the middle of the soil profile (between 15 and 60 cm, Table 4-2). These results differ from other studies: for Malone et al. (2009), the accuracy of carbon prediction decreased for each depth interval; Kempen et al. (2011), predicting SOC stocks up to a depth of 90 cm for agricultural soils in the Netherlands, found highest prediction accuracy for the topsoil layer (0-30 cm), with higher errors in the 30-60 cm soil layer. Our results could be explain in three points: (i) poorer models performance for the very topsoil layer (0-to-7.5 cm) and in the deeper soil layers could be due to a larger SOC content range for this layer (Figure 4-6), which make harder to explain the SOC form the covariates ; (ii) better performance in the bottom part of the tilled soil layer (15-to-30 cm) could be due to a lower range of the SOC content value, because of the soil mixing during soil tillage; and finally (iii), poorer performance in deeper soil horizon could be due to a decrease of data for these layers, both in calibration or in landscape and transect validation datasets (deep A-horizons were not observed for every soil profiles), and so on , to a greater difficulty to create predictive soil models and to estimate their performance. Concerning the prediction of SOC content, our results indicated that the predictions were not influenced by the distance to hedges, except at 2 m downhill from the hedge where the RMSE was higher, especially for the 0-to-30 cm soil layers. This could be explained by a larger range of SOC values and a higher spatial variation, due to the hedge and the topography influence on SOC content close to hedges (Follain et al, 2007, Walter et al, 2003a). Finally, the models showed a good predictive performance in areas close to hedges (Table 4-4).

Concerning the BD predictions, the highest prediction error was found for the evaluation on the transect validation dataset, and especially for the topsoil horizons and the deeper soil horizons. In comparison with the other datasets, the transect validation dataset was characterized by the larger range of BD values. This can explain the poor predictive performance we obtained. Similar results were observed in De Vos et al. (2005) when predicting BD for forest soil. Regarding the BD predictions, our results attested that the distance to the hedges didn’t have strong influence on the predictive performance, except for the topsoil layer (0-to-7.5 cm) and for location close the hedges (2 m downhill and uphill from the hedge and just under the hedge) where the RMSE values were slightly higher (Table 4-4). This result could be explained by the fact that (i) hedges have a specific impact on soil properties and moreover on soil BD (Walter et al; 2003a), so they induce a larger variability of BD values which make harder the BD prediction close to hedges, and (ii) there is no soil tillage at hedges

vicinity, so there is no soil homogenisation and the BD values for the 0-to-7.5 cm soil layer were very different from the BD values for the below soil layers (Figure 4-7).

4.4. SOC distribution at the landscape scale

Our results are consistent with previous estimations of SOC stocks in French soils (Arrouays et al., 2002), except for the forest. For Arrouays et al. (2002), the mean SOC stocks for the 0-to-30 cm layer was estimated at 40 t ha^{-1} under cultivated fields, 65 t ha^{-1} under grassland and 70 t ha^{-1} under forest. From our results, we estimated the mean SOC stocks for the 0-to-30 cm soil layer to 44 t ha^{-1} under cultivated fields, 67 t ha^{-1} under grasslands and 30 t ha^{-1} under forest. The lower SOC stocks under forest could be explained in our study area by the fact that forest were encountered mostly on shallower soils from hard schist or in hard slopes, whereas deep soils were used for grasslands and cultivated fields. Consequently, in our study area, the soil carbon storage capacity was lower under forest than under the cultivated fields or grassland.

5. Conclusion

The method we implemented to map the 3-dimensional spatial distribution of SOC stocks at the landscape scale is innovative in three main aspects. First, we chose to model and map the SOC content and the BD from soil surface up to a depth of 105 cm, with a resolution of 2 m to deal with our heterogeneous study site. According to our knowledge, there is no previous digital soil mapping study at such a high resolution. Second, we used the cLHS to select our calibration dataset: this sampling method has been proposed for data mining and digital soil mapping (Minasny and McBratney, 2006a), but there is no example in the literature of its use in a real mapping study. Finally, the combination of depth functions (equal area splines) and machine learning method turn out to be efficient to produce continuous 3D maps of SOC content and BD, which are essential data to understand the soil functions and even more to prospect soil evolution.

Acknowledgements

This research was financially supported by the French National Research Agency, “Vulnerability program: environments, climates and societies (VMCS)”, Project “LandSoil” n. ANR-08-VMCS-006-01. The authors thank the Zone Atelier Armorique for LiDAR and land-use data provision, and are grateful to G. Dutin for technical assistance.

4.2 SOC stocks distribution at the landscape scale in relation with landscape elements and soil properties

This section is a published conference proceeding (Lacoste et al., 2012b).

High resolution 3D mapping for soil organic carbon assessment in a rural landscape

M. Lacoste, D. Michot, V. Viaud & C. Walter
INRA, AGROCAMPUS OUEST, UMR1069, Sol Agro et hydrosystème Spatialisation, F-35000 Rennes, France
B. Minasny & A. McBratney
Faculty of Agriculture, Food & Natural Resources, The University of Sydney, NSW 2006, Australia

Abstract:
Soil organic carbon (SOC) stocks were mapped at 2 m resolution in a complex agricultural landscape (NW France). Soil properties were described and measured for 200 points selected with conditioned Latin hypercube sampling, and used to reconstruct continuous soil profiles via equal-area splines. Calibration data were extracted from these profiles for 8 standard layers up to 105 cm, and used in a data mining tool (Cubist) to build rule-based predictive models and predict SOC content and bulk density. Predictive environmental data consisted in radiometric emissions, geological variables and topographic attributes (from LIDAR DEM). The predictive maps were evaluated with two independent datasets, focusing on landscape scale or hedgerow proximity. The respective RMSE for these datasets were 7.47 and 4.77 g kg^{-1} for SOC content, 0.11 and 0.21 g cm-3 for bulk density (BD). The best predictions were obtained for depths between 15 and 60 cm. The SOC stocks below 30 cm accounted for an average of 33% of the total SOC stocks.

1. Introduction
Soil organic carbon (SOC), identified as an important pool in the global carbon cycle, is a key variable in influencing many agronomical, environmental and political issues. SOC directly controls soil fertility and soil structure, and small changes in SOC can have a large impact on the atmospheric carbon dioxide concentrations. SOC assessment and dynamics have been studied at different scales, from field to global scale. The choice of the scale depends on the problem to deal with (impact of cropping practices and spreading, impact of land management and land use, setting up of agricultural policies, etc.), but it has been shown that the most relevant scale to address the issue for the environment and agroecosystem was the landscape scale (Viaud et al., 2010). This scale enables to take into account the interaction between SOC dynamics, natural and anthropogenic processes, for instance the relation between SOC storage and soil erosion. In most studies on SOC assessment and modelling only the topsoil is taken into account, i.e. mainly up to 30 cm and more rarely to 50 cm (e.g. Mishra (Mishra et al., 2010). However, an important amount of carbon is also stored at greater depth (Meersmans et al., 2009a). It appears therefore necessary to produce SOC data not only for the topsoil, but also for the underlying layers. Previous studies dealing with SOC prediction in depth (up to 1 m or more) applied depth functions (Meersmans et al., 2009b), mainly combined with geostatistical methods (mostly kriging; e.g. Kempen et al., 2011) or with machine learning methods such as neural networks (Malone et al., 2009). In these studies, SOC stocks are always calculated by multiplication of SOC content and soil bulk density (BD), and the BD is always estimated by pedotransfer functions. Machine learning methods offer useful tools to predict soil properties from exhaustive environmental predictors and limited soil datasets, using the relations of these soil properties with predictors known as scorpan factors. These scorpan factors are a generalization of Jenny's factor and were described by McBratney et al. (2003). They comprise climatic, anthropogenic, biological, environmental, topographic, geological, temporal and spatial factors.

In this study we propose to map SOC content (g kg^{-1}) and soil BD (g cm^{-3}) in 3D (i.e. in surface and for different depths up to 105 cm), at the landscape scale and at a fine resolution (grid spacing of 2 m). This fine resolution is required to take into account the linear elements of the landscape (mainly hedges). To achieve this goal the following steps were achieved: (i) selection of soil data using the conditioned Latin hypercube sampling (cLHS), (ii) fit of equal-area spline functions to SOC content data and extraction of data at defined depth to be used at calibration dataset, (iii) creation of rule-based models based on environmental covariates, to predict SOC content and BD at each standard depth, (iv) reconstruction of continuous soil profiles using a spline function, (v) construction of confidence interval of prediction based on fuzzy clustering, (vi) map of the final maps of SOC content, BD and SOC stocks (tC ha^{-1}) up to 105 cm. After a brief presentation of the accuracy of the predictions, we discussed the impact of hedges, soil waterlogging and land use on SOC stocks distribution at the landscape scale.

2. Material and methods

2.1. Study area

The study site (NW France, 48° 36′ N, 1° 32′ W) is part of the European Long-Term Ecosystem Research Network, and covers an area of 10 km^2. This site is characterised by high soil heterogeneity at short distances. The soil types encountered are mainly Cambisols and Luvisols, but also Leptsosols and Fluvisols from alluvial and colluvial deposits. These soils present varying redoximorphic conditions, soil and A-horizon depths and soil parent material (granite, hard and soft schist with a heterogenic cover of superficial deposits such as Aeolian loam, alluvium and colluviums). The general topography is highly correlated with the geological formations: plateau on granite (south of the site), plain on soft schist (north of the site), hillside on hard schist (transition between granite and soft schist). However, the study site presents a marked micro-topography, mainly due to the presence of hedges at field boundaries. The hedge density differs according to the politics of agricultural landscape management, passed or actual. The main land uses are annual crops (corn, wheat, barley) and temporary or permanent grasslands, but the study area also included wood plots and natural areas.

2.2. Method

We used three independent datasets: (i) 70 calibration points selected using conditioned Latin hypercube sampling (Minasny and McBratney, 2006a), (ii) 47 points selected by stratified random sampling using a square grid (landscape scale validation: validation dataset), (iii) 112 points along transects perpendicular to hedges (hedge proximity validation: transect dataset). We acquired SOC content and BD data for each site up to 105 cm (soil sampling and measurements in 2009/2010). Eleven topographic attributes derived from a 2 m LIDAR DEM were used as environmental covariates, plus Gamma-ray spectrometry, geological maps, and land use data. SOC content and BD were predicted and mapped for 8 standard layers (0-7.5 cm, 7.5-15 cm, 15-30 cm, 30-45 cm, 45-60 cm, 60-75 cm, 75-90 cm, 90-105 cm) using a six steps method (Figure 4-11), fully described in Lacoste et al. (2014).

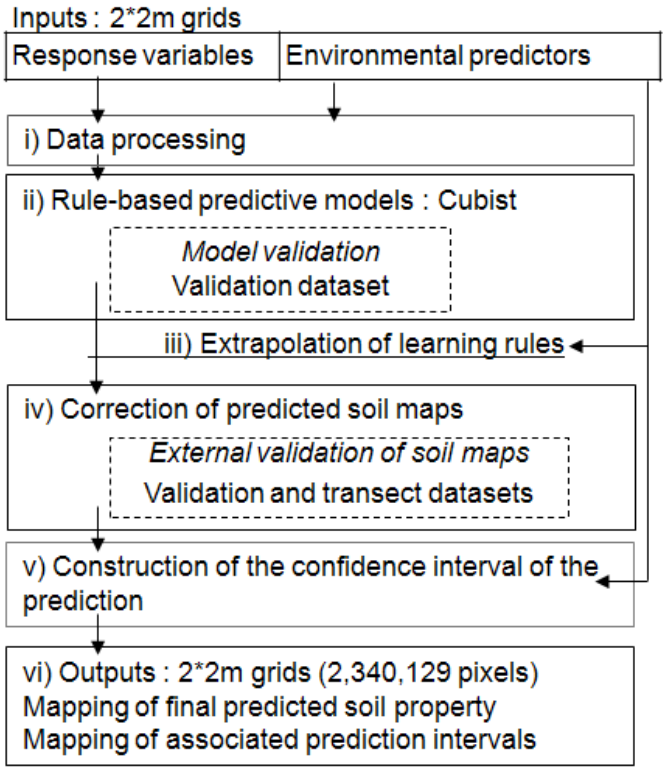

Figure 4-11 Overview diagram of the 6-steps method implemented to produce 3D continuous predictive maps of SOC content and BD at the landscape scale.

3. Results

3.1. Description of the predictions

Values of SOC content ranged from 1.7 to 62 g kg^{-1}, 1.5 to 75 g kg^{-1} and 0.1 to 66 g kg^{-1} for the calibration, validation and transect datasets respectively. Measured values of BD ranged from 0.7 to 1.7 g cm^{-3} for both calibration and validation datasets, and from 0.6 to 1.7 g cm^{-3} for transect dataset. BD predictions ranged from 0.8 to 1.6 g cm^{-3}.

Predicted SOC stocks (up to 105 cm of depth) ranged from 5 to 360 tC ha^{-1} (mean value = 89 tC ha^{-1}). In the tillage layer (0-30 cm), SOC stocks ranged from 3 to 175 tC ha^{-1} (mean value = 58 tC ha^{-1}). We estimated the mean SOC stocks in topsoil (0-30 cm) at 44 tC ha^{-1} under cultivated fields, 67 tC ha^{-1} under grasslands and 30 tC ha^{-1} under forest. SOC stocks in the deeper horizons (30-105 cm), took a mean value of 32 tC ha^{-1}, counting for 33% of the total SOC stocks (maximum value = 227 tC ha^{-1} counting for 85% of the total SOC stocks).

3.2. Accuracy of the predictions

Respectively, predictions of SOC content and BD had an overall mean absolute error (MAE) of 3.89 g kg^{-1} and 0.15 g cm^{-3} for the validation dataset, 3.25 g kg^{-1} and 0.15 g cm^{-3} for the transect validation. Table 4-8 shows accuracy of predictions for each standard layers. Distance to hedges had no strong influence on prediction accuracy.

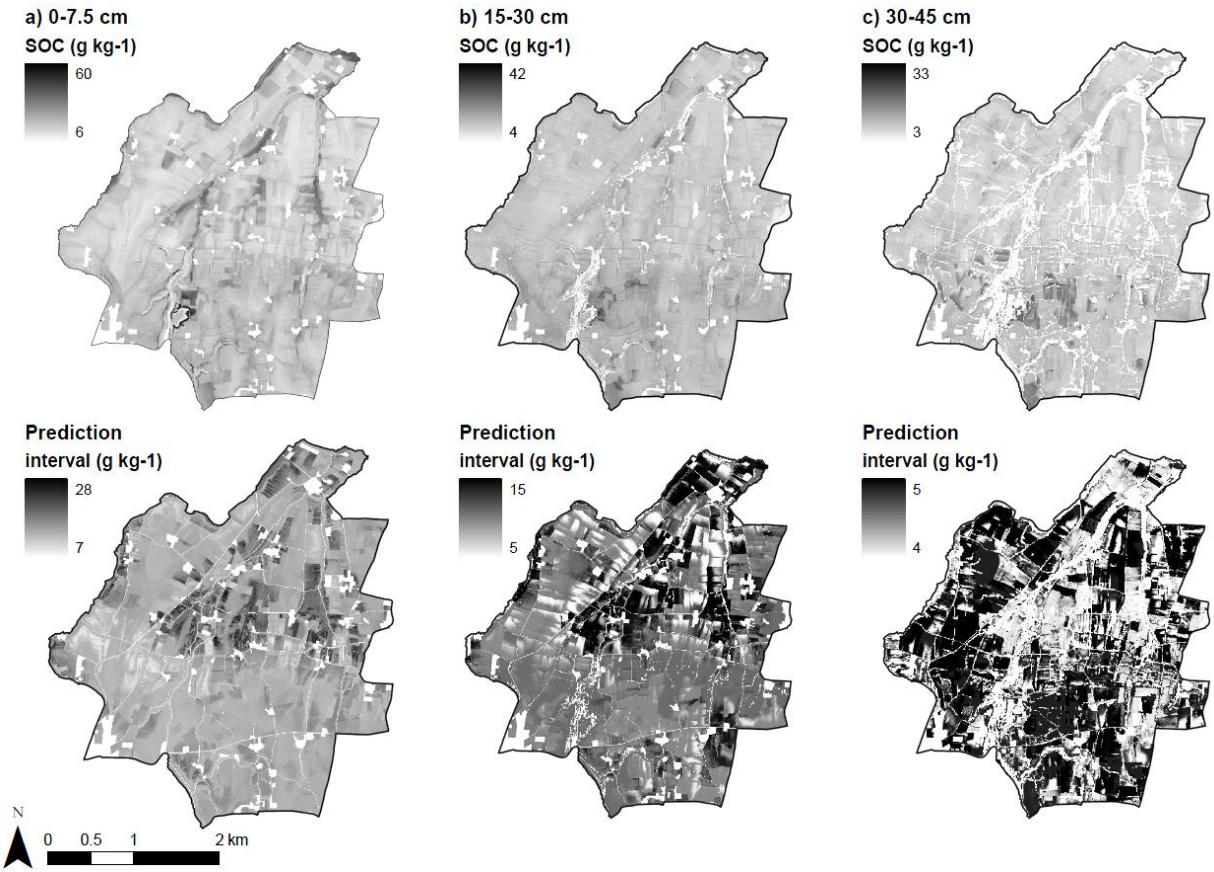

Figure 4-12 Examples of SOC content predictions and their associate prediction interval of error for three standard layers

Table 4-8 Absolute error of predictions for each standard layer according to the validation dataset

Standard layers (cm)	Absolute error of predictions SOC content (g kg^{-1})/Soil bulk density (g cm^{-3})		
	1st Quartile	Median	3rd Quartile
0 –7.5	1.10 / 0.05	3.34 / 0.13	6.30 / 0.17
7.5 –15	1.43 / 0.05	2.97 / 0.11	4.09 /0.19
15 – 30	1.08 / 0.06	1.85 / 0.09	2.71 / 0.17
30 – 45	0.91 / 0.04	2.05 / 0.08	3.36 / 0.14
45 – 60	1.65 / 0.03	2.27 / 0.08	4.10 / 0.13
60 – 75	3.03 / 0.02	4.03 / 0.05	4.57 / 0.11
75 – 90	6.09 / 0.02	7.53 / 0.05	9.78 / 0.08
90 – 105	8.64 / 0.03	9.63 / 0.07	10.62 / 0.13

3.3. Examples of predictive SOC content maps

Figure 4-12 shows SOC content predictive and confidence interval maps for three standard layers. Both predictions and prediction intervals had lower range of variations for deeper standard layers.

3.4. Digital soil assessment of SOC sequestration at landscape scale

3.4.1. Impact of hedge proximity on SOC stocks

Table 4-9 describes the variation of predicted SOC stocks regarding to the distance to hedges. At more than 10 m from the hedge, the proportion of SOC stocks in deeper soil layers (> 30 cm) were slightly lower in comparison with total SOC stocks. The total SOC stocks decrease when the distance to the hedge increases.

Table 4-9 Impact of hedge proximity on SOC stocks

Distance from the hedge (m)	SOC total stock (t ha^{-1}) (*)		
	1st Quartile	Median	3rd Quartile
0 – 2	73.90 (56)	91.20[a] (66)	113.20 (77)
2 – 5	73.20 (57)	89.40[b] (66)	110.60 (77)
5 – 10	74.00 (58)	89.70[c] (66)	109.40 (77)
> 10	73.17 (60)	84.29[d] (67)	97.45 (75)

* Proportion of SOC topsoil stock on total SOC stocks (%)

The index letter within a column indicates significant difference using the Student test at the 5% threshold.

3.4.2. Impact of soil waterlogging on SOC stock predictions

Table 4-10 describes the variation of predicted SOC stocks regarding to the intensity of soil waterlogging. Soils with moderate waterlogging were predicted with the higher SOC stocks. In comparison with total SOC stocks, the proportion of SOC stocks in topsoil layers (< 30 cm) was higher for soils with high waterlogging.

Table 4-10 Impact of conditions of the soil hydromorphy on SOC stocks

Waterlogging intensity	SOC total stock (t ha^{-1}) (*)		
	1st Quartile	Median	3rd Quartile
Null	75.75 (59)	86.64[a] (65)	100.20 (73)
Low	73.39 (58)	83.42[b] (63)	94.46 (73)
Moderate	70.58 (60)	89.54[c] (65)	106.80 (74)
High	71.64 (64)	84.56[d] (74)	98.48 (81)

* Proportion of SOC topsoil stock on total SOC stocks (%)

The index letter within a column indicates significant difference using the Student test at the 5% threshold.

3.4.3. Impact of land use on SOC stocks

Table 4-11 describes the variation of predicted SOC stocks regarding to land use, i.e. the number of years in grassland. Fields with a higher grassland frequency were mainly pasture grassland and were predicted with higher SOC stocks. In comparison with total SOC stocks, the proportion of SOC stocks in topsoil layers (< 30 cm) was higher for soils with higher grassland frequency.

Table 4-11 Impact of grassland frequency on SOC stocks

Number of year in grassland (1993-2008)	SOC total stock (t ha^{-1}) (*)		
	1st Quartile	Median	3rd Quartile
1 – 5	69.53 (59)	80.57[a] (65)	93.75 (74)
6 – 10	77.38 (59)	88.68[b] (64)	101.70 (72)
11 – 15	78.37 (63)	89.92[c] (68)	104.10 (78)

* Proportion of SOC topsoil stock on total SOC stocks (%)

The index letter within a column indicates significant difference using the Student test at the 5% threshold.

4. Discussion

4.1. Predictive maps accuracy

We found that the more accurate predictions of SOC content were for the middle of the soil profile (between 15 and 60 cm, Table 4-8). Cases of poor prediction may have different origin. In the first soil layers (0-7.5 and 7.5-15 cm), it may be explained by the high variability of SOC content. The deeper layers (> 60 cm) presented as well a higher variability in SOC content, but also fewer soil data and calibration points: the combination of these two points made the learning process more difficult. For BD, the highest prediction error was found for the topsoil horizons. Deeper soil layers showed the lowest variability of BD because of lower influence of tillage practices and stronger influence of soil parent material.

4.2. Digital soil assessment of SOC sequestration at landscape scale

Concerning the impact of hedge proximity (Table 4-9), our predicted maps showed higher SOC storage closer to the hedge, with SOC stocks slightly more important in deep layers (> 30 cm). This could be explained first by direct carbon inputs from the hedge, and second by soil accumulation uphill to hedges (when they are perpendicular to the main slope direction).

When we consider the influence of soil waterlogging on SOC stocks (Table 4-10), the predictive maps showed higher SOC stocks in soils with moderate waterlogging, and lower SOC stocks in soils with high waterlogging. Soils with moderate waterlogging were mostly in situation of plain with soft slope, while soils with high waterlogging corresponded to soils close to the streams, with stronger slope. The same influence of topography combine to soil waterlogging condition was shown by Eglin et al. (2008). However, unlike Eglin et al. (2008), the predictions of SOC stocks showed higher stocks in soils with null waterlogging.

Regarding the impact of grassland frequency on SOC stocks (Table 4-11), SOC stocks were positively correlated to grassland frequency, and higher proportion of topsoil SOC stocks were observed within fields with high frequency of grassland (11 to 15 years between 1993 and 2008). Our results were consistent with those made by the French research institute INRA (Arrouays et al., 2002), except for the forest. In the INRA report, the mean SOC stocks in agricultural soils, for the 0-30 cm layer, was estimated at 40 tC ha^{-1} under cultivated fields, 65 tC ha^{-1} under grassland and 70 tC ha^{-1} under forest. We estimated the mean SOC stocks for the 0-30 cm layer at 44 tC ha^{-1} under cultivated fields, 67 tC ha^{-1} under grasslands and 30 tC ha^{-1} under forest.

5. Conclusion

The method we implemented to model the 3-dimensional spatial distribution of SOC stocks at the landscape scale is innovative in three main aspects. First, we chose to model and map the SOC content and the BD at the resolution of 2 m to deal with our complex study site. According to our knowledge, there is no digital soil mapping study at such a high resolution. Second, we used the cLHS to select our calibration dataset: this sampling method has been proposed for data mining and digital soil mapping (Minasny and McBratney, 2006a), but there is no example in the literature of its use in a real mapping study. Finally, the combination of depth functions (equal area splines) and machine learning method turn out to be efficient to produce continuous 3D maps of SOC content and BD, which are essential data to understand the soil functions and even more to prospect soil evolution.

Acknowledgements

This work was supported by the ANR VMCS. The authors thank the Zone Atelier Armorique for LIDAR and land-use data provision, and are grateful to G. Dutin for technical assistance.

4.3 Chapter conclusion

In this chapter we first explained the method used to produce the soil input data required for the initialization of the soil evolution models. We produced 3D maps at high spatial resolution (2 m) of several soil properties: SOC content, soil bulk density, and the resulting SOC stocks. Then we assessed the relation between the SOC stocks distribution in the landscape and some relevant landscape elements (land use, soil waterlogging, and distance from the hedge).

The final maps showed a mean average error of 0.15 g cm^{-3} for the soil bulk density, 3 g kg^{-1} for the SOC content and 25 t ha^{-1} for the SOC stocks. The errors of prediction showed a high spatial variability, and were higher for areas close to hedges, where the soils also showed a high variability.

Finally, the mean SOC stocks were estimated at 89 tC ha^{-1} for the whole study area (44 t ha^{-1} under cultivated fields, 67 t ha^{-1} under grasslands and 30 t ha^{-1} under forest). The SOC distributions in space were closely related to the land use and landscape structure. We predicted higher SOC stocks in areas close to hedges, in fields frequently in grasslands, and for in soils with moderate waterlogging.

The maps were used as input data to soil evolution models (Chapter 5).

Chapitre 5.
Landscape-scale modelling of erosion processes and soil carbon dynamics under land use and climate change

This chapter aimed to model soil evolution over several decades (from 2010 to 2100), at the landscape scale and in the context of global change. Global change includes changes in climate and landscape structure (land use and landscape management). Two soil evolution processes were considered: soil redistribution and soil organic carbon (SOC) dynamics. Soil redistribution was modelled using LandSoil, a spatially-distributed and event-based model. Evolution of SOC stocks was modelled using a spatially-distributed version of the RothC model. The study area and the two models have been described in Chapter 2.

This chapter is organized into two sections, each of them written as an article:

- Section 5.1 aims to describe soil evolution for a business-as-usual scenario, and to discuss the interactions between redistribution processes and SOC dynamics.
- Section 5.2 considers soil evolution under contrasted scenarios of global change. Thirteen scenarios of global change have been compared to the business-as-usual scenario.

5.1 Impact de la redistribution du sol sur les stocks de carbone

This section is a research article to be submitted.

Model-based evaluation of soil redistribution impact on soil organic carbon stocks in a hedgerow landscape under temperate climate

LACOSTE Marine[1,*], VIAUD Valérie[1], MICHOT Didier[2, 3], WALTER Christian[2,3]

[1]INRA, UMR1069, Sol Agro et hydrosystèmes Spatialisation, F-35000 Rennes, France
[2] AGROCAMPUS OUEST, UMR1069, Sol Agro et hydrosystèmes Spatialisation, F-35000 Rennes, France
[3] Université européenne de Bretagne, France
*Corresponding author: marine.lacoste@rennes.inra.fr

Abstract:
For a long time soil organic carbon (SOC) has been considered as an important parameter of soil fertility. Now SOC stocks are also regards as a factor of climate mitigation. However, there is a need of knowledge about the vertical and horizontal SOC transfers. We modelled the SOC stocks evolution at the landscape scale, by taking into account the soil redistribution by tillage and water processes. We used a spatially SOC dynamic model (adapted from RothC), coupled to a soil redistribution model (LandSoil). We modelled the SOC dynamic in an agricultural landscape dedicated to dairy farming, with a mix of intensive or semi-intensive cropping and grasslands. Our study site also integrated interstitial landscape elements, such as hedges. We found that soil redistribution, and more specifically soil exportation out of the study site, accounted for 1% of the total SOC stocks loss (equivalent to 1 kgC ha^{-1} yr^{-1}). The major process of soil redistribution was soil tillage; but most of the soil loss was due to soil erosion by water, while soil redistribution by tillage mostly induced soil redistribution inside the cultivated fields. Deep SOC stocks were significant and account for 25% on average considering the whole study site.

Keywords: Soil organic matter; tillage erosion; water erosion; agricultural landscape; agroecosystems.

1. Introduction
Soils are a crucial resource providing a range of ecosystem services (Dominati et al., 2010), but they are subjected to numerous pressures. In 2006, the European Commission has identified soil erosion and loss of soil organic carbon (SOC) as two of the main degradation processes of soils in Europe (European Commission, 2006).
SOC directly impacts soil physical, chemical and biological properties, and thereby controls soil fertility. Soils are closely related to the global carbon cycle and represent one of the main environmental carbon pool (Grace, 2004). Therefore small changes in SOC stocks and dynamics can significantly modify C transfer to other environmental compartments, like the hydrosphere and the atmosphere. For instance, larger SOC mineralization can have a large impact on the atmospheric carbon dioxide concentrations (Johnston et al., 2004), that is why SOC management could play an important part in climate change mitigation (Lal, 2004). SOC dynamic and evolution is highly dependent to the land use and the soil organic matter (SOM) management by farmers, which includes the types of crop rotation, the tillage practices , fertilization practices and the crop residues management. Most often, studies consider SOC stocks for the topsoil horizon (0-30 cm), but some

authors underlined the importance to take into account deeper soil horizons (Chan et al., 2009; Meersmans et al., 2009a; Quine and Zhang, 2002; Stallard, 1998).

Soil erosion includes soil transfer by wind, by water (rill and interrill erosion) and by soil tillage (Van Oost et al., 2005b). It can result in spectacular soil losses (like mudslides), but also less visible phenomenon which can lead to an irreversible soil degradation (Arrouays et al., 2002). The eroded soil can be trapped in some landscape area, which forms soil deposition areas (Follain, 2006a), or exported out of the watershed by rivers, which is a disturbance factor for ecosystems.

Several studies have examined the relationship between SOC dynamics and erosion processes, using field and modelling approaches, and shown that soils with higher SOC content are less prone to erosion (e.g. Quinton et al., 2006). At the landscape scale, soil erosion affects SOC spatial distribution, due to horizontal transfers, deep burial in depositional sites or exportation out of the catchment of C-enriched sediments (Lal, 2003). Moreover, soil erosion impacts the SOC dynamic of the eroded or buried soil particles (Lal, 2003; Van Oost et al., 2007). However, the balance of the soil redistribution impacts on SOC stocks at the landscape scale is discussed and whether erosion is a source or a sink of carbon is currently under debate (Lal and Pimentel, 2008; Van Oost et al., 2007). Even though ongoing researches aim to determine the SOC dynamics in eroded soil particles (e.g. Balesdent et al., 2000; Bol et al., 2009; Doetterl et al., 2012; Schmidt et al., 2011), few data are available to calibrate the SOC dynamic models. At the landscape scale, soil redistribution can impact important soil volumes. For example, several studies showed that important quantities of soil could be deposited uphill from hedges in hedgerow landscapes, whereas the soils were eroded downhill from the hedges (Follain, 2006a; Salvador-Blanes et al., 2006). These soils redistribution impacts the SOC spatial distribution in the landscape (Lal, 2003; Walter et al., 2003b). Soil landscape modelling allows taking into account (i) the spatial variability of the soil properties (SOC stocks, soil texture, soil thickness) and of the drivers of soil change (soil agricultural practice, topography, landscape structure...), and (ii) the transfers of matter and water between the landscapes elements (Pennock and Veldkamp, 2006; Sommer, 2006; Van Oost et al., 2000; Viaud et al., 2010; Yoo et al., 2009).

The purpose of this study was to quantify the impact of soil redistribution on SOC stocks evolution at the landscape scale. We modelled SOC dynamics in a complex hedgerow landscape for a 100-year period, under business-as-usual (BAU) climate and land use, with and without considering soil redistribution by erosion processes.

2. Material and methods

2.1. Study site

The study site is a 84 ha agricultural catchment, part of the European Long-Term Ecosystem Research and French "Zones Ateliers" networks (NW France, 48° 505’ N, 1° 565’ W) (Figure 5-1). The site is characterised by a plateau on metamorphic schist in the south (mean elevation 100 m) and a plain on Brioverian schist in the north (mean elevation 30 m), connected by a hillslope with a 13 % average slope. Hard and soft schists are locally covered by Quaternary Aeolian loam deposits with variable thickness. Soils are heterogeneous in terms of parent material, depth, and drainage conditions. The main soil types are Cambisols and Luvisols, but also Leptsosols and Fluvisols (WRB, 2007). Drainage conditions vary from well-drained soils on the plateau to poorly-drained soils with permanent redoximorphic conditions next to streams. Soil thickness ranges from 15 to 778 cm (mean value 113 m), and soil organic horizons (A-horizons) thickness ranges from 3 to 220 cm (mean value 48 cm).

Most of the catchment area is used for dairy farming. The average field size is 1.2 ha. The land use is mainly annual crops, with maize (Zea mays) and winter wheat (Triticum aestivum), and temporary or permanent grasslands (mostly Italian ryegrass, Lolium multiflorum). The study site also included woodland plots (9 % of the whole study site), and urban areas, such as roads (3 %) and build-up areas (2 %). The site is characterised by a hedgerow landscape. Hedges located at field boundaries are mainly grass stripes associated with trees such as oaks (Quercus robur), chesnut trees (Castanea sativa), and blackthorns (Prunus spinosa). The hedge density is currently 120 m ha^{-1}, but it has significantly decreased since the 50's together with agriculture modernization and land consolidation programs (Baudry and Jouin, 2003).

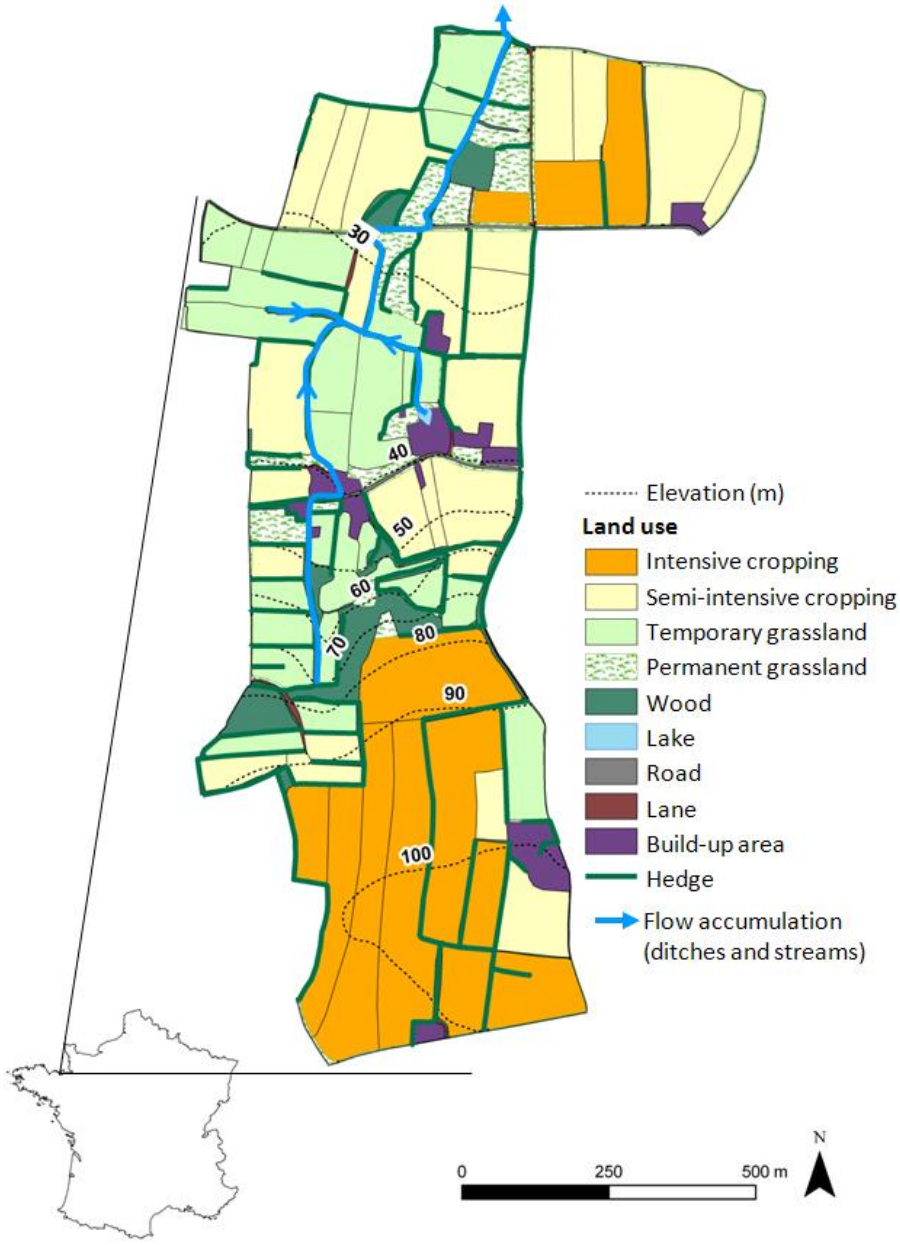

Figure 5-1. Location of the study area, map of the topography and current land use (intensive cropping: crop rotations with maize and cereals as main crops, semi-intensive cropping: crop rotations with equal proportion of maize/ cereals and temporary grasslands, temporary grassland: crop rotations with grasslands as main land use).

2.2. Soil process models

Two models were combined to evaluate the impact of soil redistribution on soil carbon stocks: a soil erosion model and a SOC dynamics model. Figure 5-2 gives an overview of the modelling process.

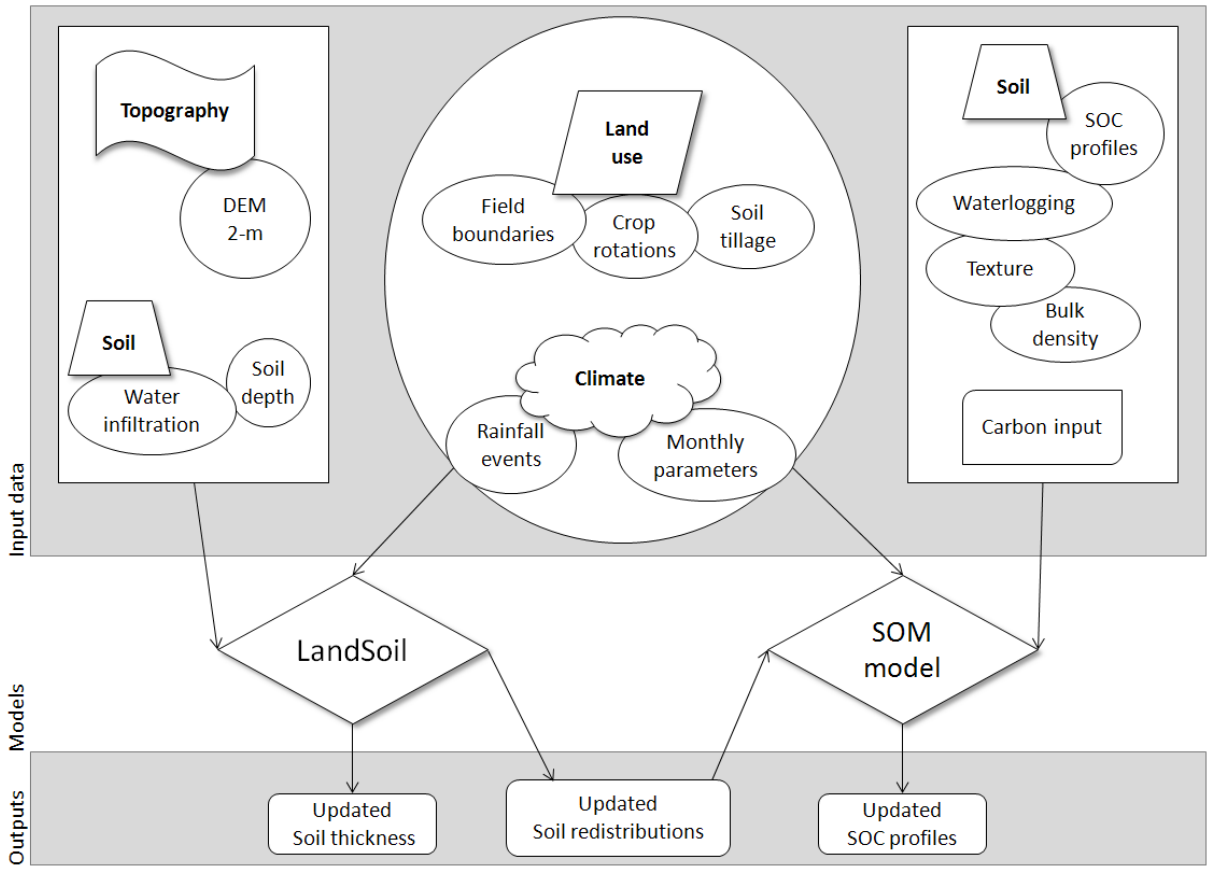

Figure 5-2. Modelling process overview. Inputs and outputs of the erosion and SOM models.

2.2.1. Soil redistribution model

Soil redistribution was modelled with the LandSoil model (Ciampalini et al., in press). LandSoil is an expert-based runoff and erosion model operating at small catchment scale. It is based on both the STREAM soil erosion model (Cerdan et al., 2002a; Cerdan et al., 2002b; Souchère et al., 2003; Souchère et al., 1998) and the WaTEM/SEDEM tillage erosion model (Govers et al., 1994). LandSoil is spatially-distributed, event-based and allows the simulation of water (interrill and rill erosion) and tillage erosion. The basic hypothesis of the model is that soil surface characteristics are the major factors controlling runoff and soil erosion/deposition processes in agricultural landscapes. Soil surface characteristics include surface crusting, soil roughness and vegetation cover (Cerdan et al., 2002b). A value for steady-state infiltration rate (IR) and residual water storage after the previous event (WS) is assigned to each combination of soil surface characteristics (Bresson and Boiffin, 1990; Le Bissonnais et al., 2005). IR and WS determine the production of runoff by a rainfall event, according to the following equation:

$$B = RR - WS - (IR \times D) \quad (1)$$

Where B is the runoff/infiltration balance (mm), R is the rainfall amount (mm), WS is the residual water storage after the previous rainfall event (mm), IR is the steady-state soil infiltration rate (mm h^{-1}) and D the effective duration of the runoff event.

The resulting runoff is routed at the catchment scale, taking into account the topography and the main linear features in the landscape (ditches, tillage directions) (Ciampalini et al., in press). Empirical relationships with soil surface properties are used to estimate sediment concentration in runoff and to model rill and interrill water erosion (Cerdan et al., 2002b).The effect of tillage operations on soil redistribution is modelled based on tillage erosion coefficient (Ktill). The model considers two main ploughing directions, contour (Ktill.c) and downslope (Ktill.s).

Input variables of the model include (1) a digital elevation model (DEM), (2) a map of the initial thickness of the soil in a raster format, (3) a vector layer representing the fields, the linear features, such as field borders, and the associated land use, tillage practices and soil surface characteristics, (4) and rainfall events characteristics. The model outputs are an updated map of soil thickness and an updated DEM.

2.2.2. SOC dynamics model

SOC dynamics was modelled with a variant of RothC 26.3 (Coleman and Jenkinson, 1996) applied to landscape scale. RothC is dedicated to modelling SOC dynamics in well-drained topsoils (first 30 cm). C stocks and inputs are divided into five conceptual compartments: DPM (Decomposable Plant Material), RPM (Resistant Plant Material), BIO (microbial Biomass), HUM (Humified Organic Matter) and IOM (Inert Organic Matter). These compartments differ in mean residence time of organic matter.

In each compartment SOM decomposition is assumed to follow a first-order kinetic. SOM decomposition depends on a decomposition constant rate, specific to the compartment, and modified by soil water content, soil temperature and soil cover according to the following equation:

$$q_j = Y e^{-abk_j t} \quad (2)$$

Where qj is the amount of SOM decomposing during time t in compartment j, kj is the decomposition rate constant of j, a is the rate modifying factor depending on soil temperature, and b is the rate modifying factor depending on soil water content.

RothC has been modified to model SOM dynamics in the whole A-horizons and in any locations of a landscape. Landscape is represented as a regular square grid. The SOM model divides the soil profile into several layers, which number and thickness are defined by the user. We assumed a single decomposition rate kj in any compartment at any depth of the soil profile, corresponding to potential mineralization, with specific rate modifying factors depending on depth. Soil temperature in each soil layer was calculated from air temperature using the (Kasuda and Archenbach, 1965) equation:

$$T_{soil} = T_{mean} - T_{amp}.e^{(-depth.(\sqrt{\frac{\pi}{365}/\alpha})}.\cos(\frac{2\pi}{365}.(t - t_{shift} - \frac{depth}{2}.(\frac{365}{\pi}/\alpha))) \quad (3)$$

Where Tmean is the mean annual air temperature, Tamp is the annual amplitude of the air temperature (maximum air temperature minus minimum air temperature), d is the depth below the soil surface (typically the mean depth of the soil compartment considered), α is the diffusivity of the soil (set to 5.37 10-3 cm2 s^{-1} after Kasuda and Archenbach (1965)), tnow is the current time (day), and tshift is the day of the year of the minimum air temperature.

The RothC modifying factor related to soil moisture is reduced by a factor 0.6 (empirical calibration) in poorly-drained soil layers.

Two processes able to change soil distribution in the soil profile are considered: tillage and erosion/deposition processes. Soil movement by bioturbation is ignored. The SOC model is combined

to the LandSoil model to consider the impact of soil redistribution on SOC transfer and SOC dynamics. The DEM updated every year by the LandSoil model is used as input in the SOC model. On a yearly time step, the updated DEM is subtracted from the previous DEM. In deposition areas, the SOC content of the deposited soil particles is set to average SOC content in the eroded areas. Decomposition rate constants of eroded particles are similar to those of the soil. Impact of changes in SOC stocks on soil sensitivity to erosion is not considered in the LandSoil model.

The SOM model runs on a monthly time step in each location of the landscape. The model does not include a crop model. C inputs to the soil are computed from crop yields and C contents in aerial and belowground plant residues. All aerial residues are assumed to enter the surface soil layer and belowground plant residues are distributed in the soil profile according to root distributions specified by the model user. Input variables of the model include soil properties (initial SOC stocks, bulk density, clay content, and drainage conditions) in each soil layers and in any location of the landscape, climate data, land use over the simulation period, farm practices (tillage, winter crops, residues management, organic amendment, sowing and harvest dates), climate (monthly rainfall, temperature and evapotranspiration), root distribution in the soil profile, C content in plant residues, and DEM. Outputs give yearly SOC stocks and contents for the considered soil layers and for each conceptual compartment.

2.3. Simulation of soil evolution

2.3.1 Simulation design

Soil evolution was modelled from 2010 to 2100 for BAU climate and land use. Two soil evolution predictions have been conducted: the SOC model was run once coupled with the soil redistribution model (the resulting predicted SOC were named SOC_{SR}), and once without coupling (the resulting predicted SOC were named SOC_{NSR}). This would allow assessing the impact of soil redistribution on SOC stocks evolution. Both models were run for a 2-m spatial resolution.

2.3.2. Input data

2.3.2.1. Climate

Climate over the simulation period (2010-2100) was considered as constant and similar to that observed over the period 1980-2010. Hourly climate data for the period 2010-2100 were simulated stochastically from the available dataset, considering similar variability and trend (US INRA Agroclim). Available data were hourly precipitation (mm h−1), potential evapotranspiration (PET, mm h−1), and temperature (°C).

The characteristics of the rainfall events (total rainfall (mm), effective rainfall duration (h), maximum intensity over 6 minutes (mm h^{-1}) and rainfall amount during the preceding 48 hours (mm)), required as input for the LandSoil model, were derived from the hourly climate data. Each rainfall occurrence was distinguished as a single event when separated by at least a 3-hour dry period. Effective duration is defined as a rainy period, which intensity not lower than 2 mm h^{-1}. Because of LandSoil constitution, the effective duration and the maximum intensity have to be calculated from 6-minute meteorological data. We used multiple linear regressions to estimate these two parameters from hourly rainfall parameters as described by Lacoste (2012a). 635 rainfall events were specified, with a mean rainfall amount of 9 mm (minimum: 2.6 mm, maximum: 50 mm), a mean effective duration of 2.8 h (minimum: 0.4 h, maximum: 9h), a mean 6-min maximum intensity of 15

mm h^{-1} (minimum: 3 mm h^{-1}, maximum: 107 mm h^{-1}), and a mean 48-h antecedent rainfall amount of 6 mm (minimum: 0 mm, maximum: 63 mm).

The hourly climate data were aggregated at a monthly time step for use as input in the SOM model. From 2010 to 2100, the mean monthly temperature, monthly precipitations and monthly PET respectively ranged from -1 to 21°C (mean value: 11°C), from 2 to 181 mm (mean value: 59 mm), and from 7 to 126 mm (mean value: 49 mm). The driest periods occur in summer (particularly August), and the wettest periods occur during late autumn and winter months (particularly November and December, Figure 5-3a). Temperature exhibits a similar pattern (Figure 5-3b).

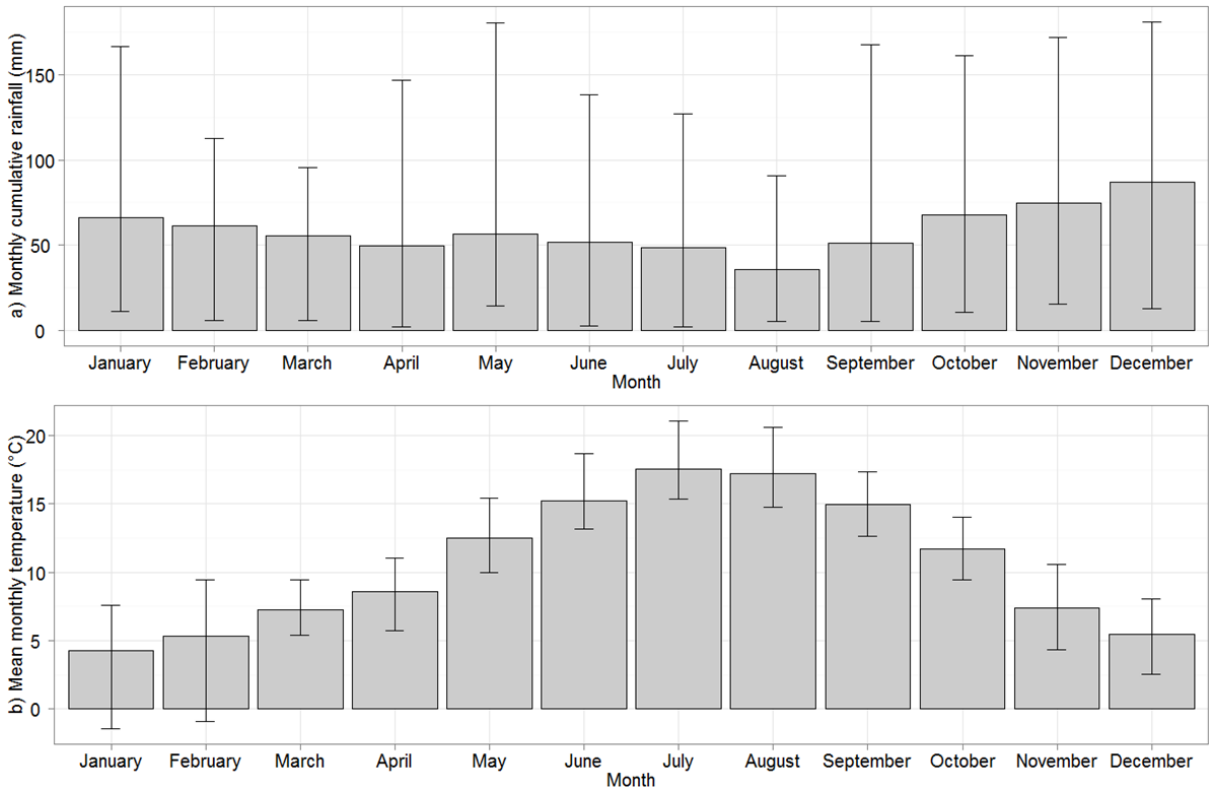

Figure 5-3. Inter-annual variations of monthly cumulative rainfalls (a) and monthly mean temperatures (b). Block bars show mean values, error bars show minimum and maximum values.

2.3.2.2. Soil and topography

The initial topography was described using a 2-m LiDAR DEM, produced in 2009. LandSoil required the range of the parameters controlling runoff: according to a previous study (Lacoste et al., in prep), steady-state infiltration rate assigned to the soils ranged from 1.5 to 37.5 mm h^{-1} and residual water storage after the previous event ranged from 0 to 11 mm. Hedges were key elements concerning water flows and soil redistribution in the study area, with a high impact on soil infiltration rate. In this study, IR under hedges was set to 150 mm h^{-1} (Richet et al., 2006). Soil bulk density was set to 1.3 g kg^{-1}.

In the vertical dimension the soil profile was divided into 8 increments (or less if soil thickness was less than 105 cm): 0-to-7.5, 7.5-to-15, 15-to-30, 30-to-45, 45-to-60, 60-to-75, 75-to-90, 90-to-105 cm. Initial soil thickness (LandSoil input), and SOC stocks and bulk density for each soil increment (SOM model inputs) were described as 2-m resolution maps. The soils maps were produced from soil

sampling data collected in 2010, and using machine learning methods (Lacoste et al., 2014). Soil waterlogging data were extracted from a soil map (Walter, unpublished data). Clay content was considered as uniform and was set to 12%.

2.3.2.3. Land use and crop management

The field pattern, hedgerows network and crop rotations over the simulation period were considered similar to those currently observed in the study site. Five land cover types were considered: silage maize, winter cereals, temporary grasslands, permanent grasslands, and woodlands. The location of woodland plots remained constant over the simulation period.

Crop rotations for the period 2010-2100 were simulated stochastically over the field pattern using a 1st-order Markov chain (Sorel et al., 2010) and starting from the crop pattern observed in 2010. The Markov chain was calibrated using land use maps derived from photo-interpretation and available for the period 1993-2010. Three main crop rotations were identified, all including maize and cereals but distinguished by the number of years with grasslands: (1) intensive crop rotations corresponding with temporary grasslands established for less than 4 years (29% of the study area); (2) semi-intensive crop rotations with temporary grasslands established for 4 years on average (31% of the study area); (3) extensive crop rotations corresponding to temporary grasslands established for 8-years on average (20% of the study area).

Crop management practices (type and depth of tillage, organic amendment, sowing and harvest date, residue management) were inferred from the results of existing farm surveys on the study site (Thenail, 2002 and unpublished data ZA Armorique). The study area included 13 cattle farms with homogeneous crop management practices: one crop management was associated to each crop. Crop management per crop was constant over the simulation period. Before maize or winter wheat sowing, tillage operations combined most often tillage with reversible plough (25-cm depth), chisel cultivator and rotary harrow. A chisel cultivator is used before grassland establishment (Table 5-1). Winter crops are established between wheat and maize. Annual C inputs by crop residues were calculated from regional statistical data (AGRESTE, 2010) on crop yields and references on C content in crop residues (Boiffin et al., 1986; Bolinder et al., 1997). The total amount of farmyard manure produced in the study area was calculated from data on herd size and animal production levels (CORPEN, 1999; CORPEN, 2001). Only maize is fertilized with organic amendment. Direct input of organic amendment in grazed grasslands was estimated according to (INRA, 2008) (Table 5-1).

2.2.3. Results analysis

The predictions of soil evolutions have been described in three steps: first the prediction of the soil redistribution has been detailed, then the predictions of SOC stocks and contents and, finally, the impact of soil redistribution on SOC evolution have been exposed.

Soil redistribution refers to soil movement resulting either from erosion or soil deposition in a specific location. Positive values of redistribution account for soil deposition, while negative values account for soil erosion. Results have been analysed considering the whole soil redistribution, and differentiating tillage and water erosion processes.

Four variables have been used to describe SOC: SOC stocks for the 0-to-30-cm and 0-to-105-cm soil layers, and SOC contents for the 0-to-7.5-cm and 0-to-30-cm soil layers.

Variations of SOC stocks or contents due to soil erosion were calculated with the following equation:

$$\Delta SOC = SOC_{NSR} - SOC_{SR} \quad (4)$$

Where ΔSOC is the variation of SOC content or stock, SOC_{SR} is the SOC content or stock predicted when the soil redistribution was modelled and, SOC_{NSR} is the SOC content or stock predicted when the no soil redistribution was modelled.

Table 5-1. Description of the parameters used to characterise the agricultural practices for the soil evolution modelling.

	Crop management				Organic fertilization		Soil tillage		
Soil use	Date of sowing	Date of harvest	Mean yield (t ha^{-1})	Aerial residue management	Type	Quantity (tC ha^{-1})	Tillage operations	$K_{till.s}$ (kg m^{-1})	$K_{till.c}$ (kg m^{-1})
Winter cereal	October	July	7.4	straw removal	None	None	reversible plough (25-cm depth), chisel cultivator, rotary harrow, air seeder	629	376
Maize	April	October	11.7	removal (silage maize)	Farmyard manure	2.4	reversible plough (25-cm depth), chisel cultivator, rotary harrow, air seeder	629	376
Grazed temporary grassland	August-October	May-June	8	removal during grazing	C excreted during grazing	1.1	chisel cultivator and air seeder	291	139
Mowed temporary grassland	August-October	May-June	8	removal (mowing)	Farmyard manure	0.2	chisel cultivator and air seeder	291	139
Grazed permanent grassland	-	-	6	removal during grazing	C excreted during grazing	1.1	chisel cultivator and air seeder	291	139
Mowed permanent grassland	-	May-June	6	removal (mowing)	None	None	chisel cultivator and air seeder	291	139

3. Results

3.1. Soil redistribution

Table 5-2 summarizes the soil redistribution rates modelled with LandSoil from 2010 to 2100.
Soil redistribution processes in the study area involved net erosion, with net soil exportation out of the landscape: the mean soil redistribution rate was -0.14 t ha^{-1} yr^{-1} and the net soil exportation is 372 t (equivalent to 0.05 t ha^{-1} yr^{-1}) over the simulation period. The areas with net soil erosion accounted for 22% of the study area, with a mean soil erosion rate of -3.95 t ha^{-1} yr^{-1}; the areas with net soil deposition accounted for 19% of the study area, with a mean soil erosion rate of 4.50 t ha^{-1} yr^{-1}. The mean soil redistribution rates was -0.31 t ha^{-1} yr^{-1} for the intensive cropping areas, -0.17 t ha^{-1} yr^{-1} for the semi-intensive cropping areas, -0.05 t ha^{-1} yr^{-1} for the temporary grasslands and 0.01 t

ha^{-1} yr^{-1} for the permanent grasslands. On average, all the cultivated areas were sources of sediments, except the permanent grasslands, which were sinks of sediments. Only deposition process was simulated for the woods and the hedges.

Table 5-2. Statistics of the soil redistribution rates predicted per pixel with the LandSoil model over the period 2010-2100 (D1: 1st decile, Q1: 1st quartile, Q3: 3rd quartile, D9: 9th decile). Negative values are soil erosion rates; positive values are for soil deposition rates. Differences between means tested with Student's t-test (α = 0.05).

	D1	Q1	Median	Mean	Q3	D9
Soil redistribution rate (t ha^{-1} yr^{-1})						
Whole study site	-3.75	-1.44	-0.09	-0.14 [a]	1.00	3.65
Intensive cropping	-3.73	-1.77	-0.42	-0.31 [b]	0.91	3.34
Semi-intensive cropping	-3.73	-1.45	-0.18	-0.17 [a]	1.11	3.58
Temporary grassland	-5.04	-1.44	-0.06	-0.05 [c]	1.30	5.01
Permanent grassland	-2.86	-0.71	0.00	0.09 [d]	0.74	3.05
Wood	0.00	0.00	0.14	1.13 [e]	1.82	4.48
Hedges	0.00	0.00	0.00	0.55 [f]	0.00	1.05
Areas of soil erosion	-0.83	-1.18	-2.05	-3.95 [g]	-3.95	-8.28
Areas of soil deposition	0.83	1.22	2.25	4.50 [h]	4.88	10.37
Soil redistribution rate by tillage (t ha^{-1} yr^{-1})						
Whole study site	-3.12	-0.95	0.00	0.00 [a]	0.87	3.20
Intensive cropping	-3.37	-1.40	-0.08	0.00 [a]	1.20	3.60
Semi-intensive cropping	-3.53	-1.24	0.00	0.01 [a]	1.27	3.65
Temporary grassland	-4.89	-1.34	0.00	0.00 [a]	1.33	4.96
Permanent grassland	-2.88	-0.74	0.00	0.00 [a]	0.63	2.84
Wood	0.00	0.00	0.00	0.00 [a]	0.00	0.00
Hedges	0.00	0.00	0.00	0.00 [a]	0.00	0.00
Areas of soil erosion	-10.66	-5.39	-2.82	-5.20 [b]	-1.79	-1.37
Areas of soil deposition	1.46	2.10	3.34	5.75 [c]	6.50	12.75
Soil redistribution rate by water (t ha^{-1} yr^{-1})						
Whole study site	-0.58	-0.35	-0.18	-0.14 [a]	0.00	0.01
Intensive cropping	-0.67	-0.60	-0.35	-0.31 [b]	-0.18	-0.01
Semi-intensive cropping	-0.47	-0.30	-0.22	-0.18 [c]	-0.10	0.00
Temporary grassland	-0.32	-0.20	-0.06	-0.06 [d]	0.00	0.03
Permanent grassland	0.00	0.00	0.00	0.09 [e]	0.00	0.00
Wood	0.00	0.00	0.00	0.55 [f]	0.00	1.05
Hedges	0.00	0.00	0.13	1.31 [g]	1.82	4.48
Areas of soil erosion	-0.63	-0.43	-0.25	-0.24 [h]	-0.10	0.00
Areas of soil deposition	-0.52	-0.31	-0.15	0.42 [i]	0.00	1.48

When considering the whole study site, redistribution associated to tillage was equal to zero for all land use classes. However, every land use class showed soil tillage erosion and deposition, both with quite equivalent rate. For example, for the whole study site, 25% of the pixels showed an erosion

rate of at least -0.95 t ha^{-1} yr^{-1}, and 25% of the pixels showed a deposition rate of at least -0.87 t ha^{-1} yr^{-1}. Moreover, soil erosion areas had a mean soil erosion rate of -5.20 t ha^{-1} yr^{-1}, and soil deposition areas had a mean soil deposition rate of 5.75 t ha^{-1} yr^{-1}. Soil redistribution by water was predicted with a mean soil redistribution rate of -0.14 t ha^{-1} yr^{-1} for the whole study site. The water processes produced mostly soil erosion in the cultivated fields (mean soil redistribution rates were -0.31, -0.18 and -0.06 t ha^{-1} yr^{-1}, for the intensive cropping, semi-intensive cropping and temporary grassland, respectively). For the permanent grasslands, the woods and the hedges, only water deposition was predicted (mean soil redistribution rates were 0.09, 0.55 and 1.31 t ha^{-1} yr^{-1}, respectively). Water processes had a minor part in the net soil redistribution in comparison to tillage processes. On average, the net soil redistribution due to water processes accounted for 19% for the whole landscape, 24% for the intensive cropping areas, 19% for the semi-intensive cropping areas, 10% for the temporary grasslands, 5% for the permanent grassland. For the areas of soil erosion or soil deposition, the soil net redistribution due to water processes was equivalent (10% on average).

The major soil redistributions were located at the actual field boundaries or where former field boundaries were located (Figure 5-4). Soil deposition was mostly predicted in areas uphill from the actual hedges, while soil erosion was mostly predicted in areas downhill from the actual hedges. Soil redistribution was also predicted in the fields, far from the field limits, but in a more spread out pattern.

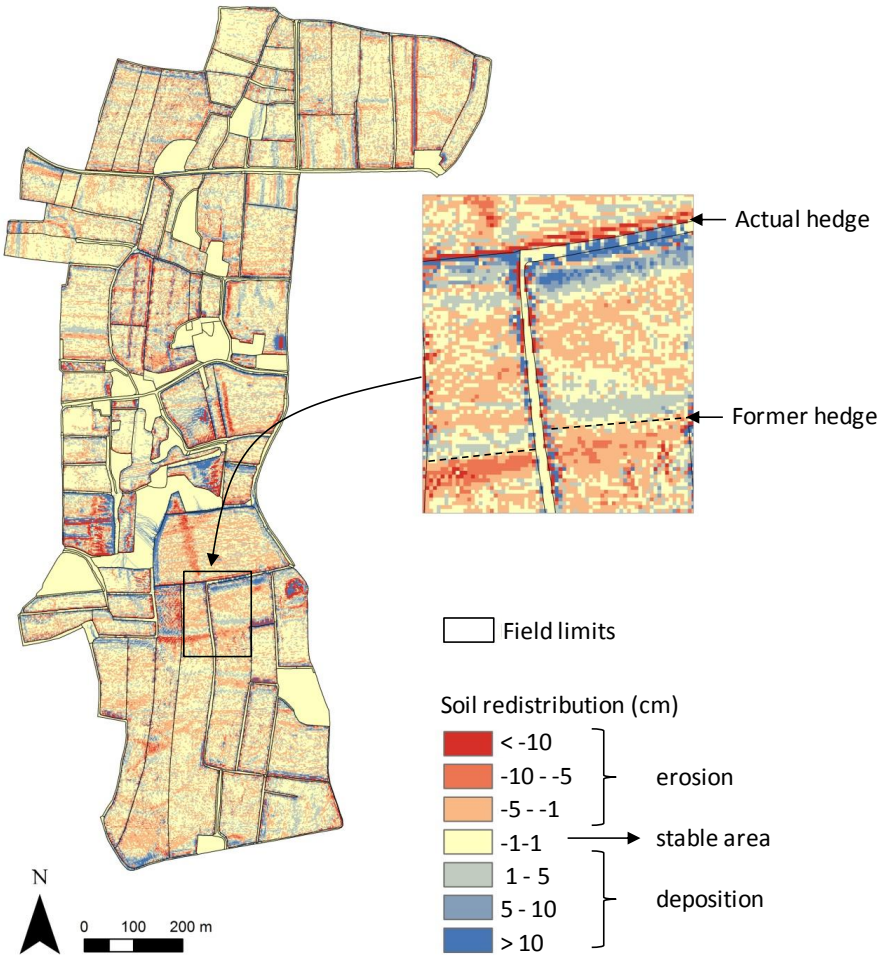

Figure 5-4. Simulated evolution of soil thickness over the period 2010-2100.

3.2. Soil organic carbon stocks

The SOC_{SR} stocks in the 0-to-105-cm soil layer showed a large range of values, with a mean value of 70 tC ha^{-1} for the whole study site, 70 tC ha^{-1} for the cultivated fields (71 tC ha^{-1} for the intensive cropping, 68 tC ha^{-1} for the temporary grasslands, 73 tC ha^{-1} for the permanent grasslands), 57 tC ha^{-1} for the wood and 68 tC ha^{-1} for the hedges (Figure 5-5a). The SOC_{SR} stocks in the 0-to-105-cm soil layer were higher than SOC_{SR} stocks in the 0-to-30 cm soil layer in all the land use classes except for the woods. The SOC_{SR} stocks in the 0-to-30 cm soil layer had a mean value of 53 tC ha^{-1} for the whole study site, 53 tC ha^{-1} for the cultivated fields (52 tC ha^{-1} for the intensive cropping, 52 tC ha^{-1} for the temporary grasslands, 55 tC ha^{-1} for the permanent grasslands), 53 tC ha^{-1} for the woods and 52 tC ha^{-1} for the hedges.

The same pattern was predicted for the SOC_{SR} content in the 0-to-7.5-cm and 0-to-30-cm soil layers (Figure 5-5b). The permanent grasslands were predicted with the higher SOC_{SR} content in the 0-to-7.5-cm soil layer (mean value: 32 gC kg^{-1}).

The SOC_{SR} stocks deeper than 30cm accounted for 25% for the whole landscape, 27% under the intensive cropping fields, 24% under the semi-intensive cropping fields, 23% under the temporary grasslands, 20% under the permanent grasslands, 8% under the woods and 23% under hedges.
The SOC_{SR} stocks and contents were higher in areas of soil deposition than in areas of soil erosion (Table 5-3).

Table 5-3. Statistics of SOC_{SR} stocks and contents simulated in 2100 by the SOC model coupled with the redistribution model, according to soil deposition vs. erosion areas (D1: 1st decile, Q1: 1st quartile, Q3: 3rd quartile, D9: 9th decile). Differences between means tested with Student's t-test (α = 0.05).

	Soil layer (cm)	D1	Q1	Median	Mean	Q3	D9
Areas of soil deposition							
SOC_{SR} stocks	0-30	48.9	50.9	53.7	53.9 [a]	56.6	59.3
	0-105	60.9	65.7	71.0	72.4 [b]	77.6	85.7
SOC_{SR} content	0-7.5	18.3	20.6	23.3	23.4 [c]	25.3	28.2
	0-30	14.7	15.5	16.4	16.6 [d]	17.6	18.9
Areas of soil erosion							
SOC_{SR} stocks	0-30	45.7	48.3	51.2	51.3 [e]	54.5	57.2
	0-105	56.4	61.4	66.9	67.4 [f]	72.8	80.0
SOC_{SR} content	0-7.5	16.8	19.0	22.0	21.8 [g]	23.8	26.0
	0-30	13.2	14.4	15.3	15.4 [h]	16.5	17.5

3.3. Impact of soil redistribution on SOC stocks

The total SOC stock in the 0-to-105-cm soil layer in the whole study site was 4317 tC at the beginning of the simulation. In 2100 and for the same soil layer, SOC_{SR} was 3252 tC and SOC_{NSR} was 3260 tC. Both SOC_{SR} and SOC_{NSR} decreased during the simulation period, but an additional loss of 8 tC was predicted when the soil redistribution model was coupled to the SOM model (SOC_{SR}). It accounted for 1% of the SOC_{SR} loss over the simulation period, which was equivalent to 1 kgC ha^{-1} y^{-1}.

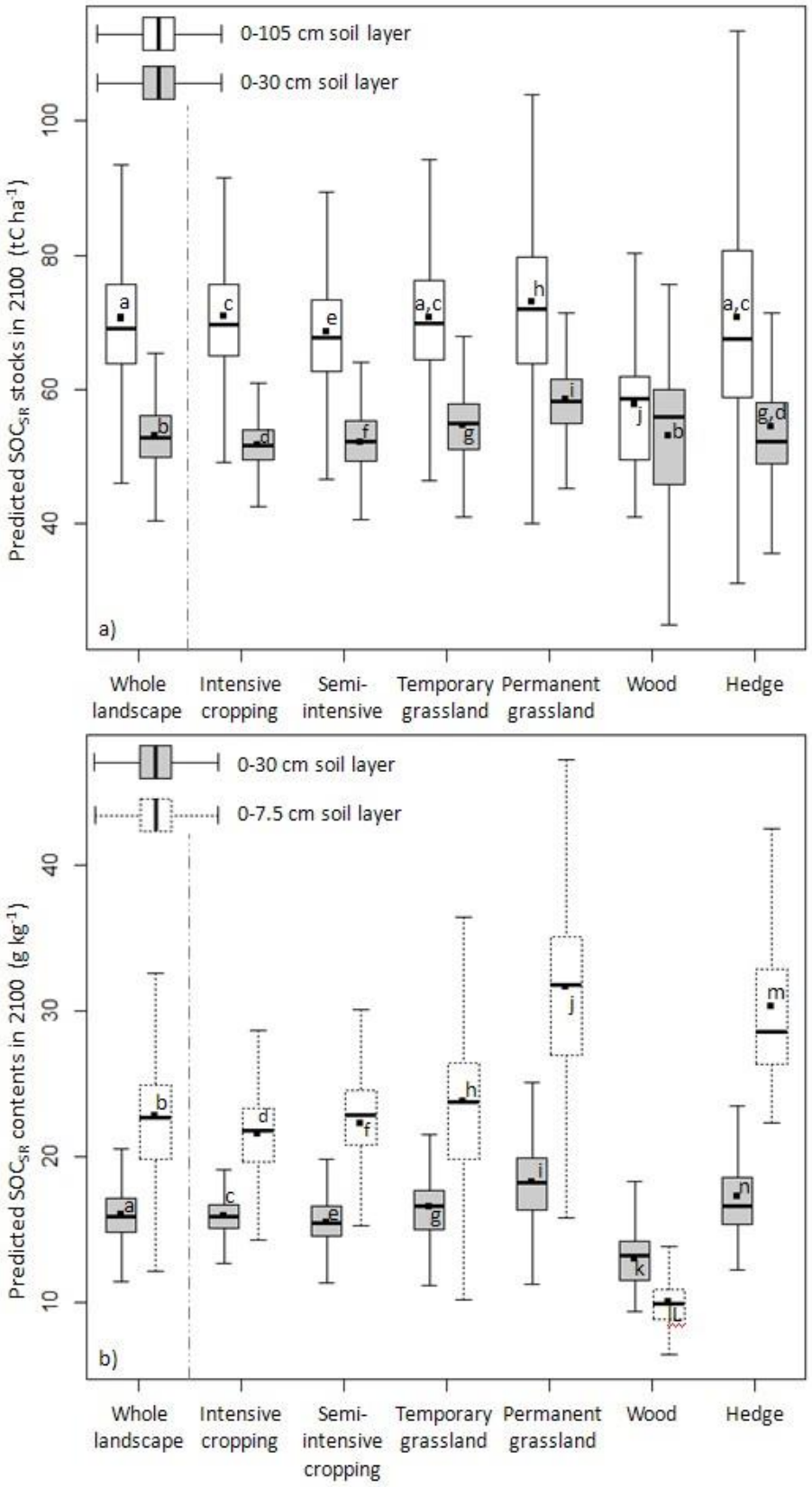

Figure 5-5. SOC$_{SR}$ stocks (a) and contents (b) simulated in 2100 by the SOC model coupled with the redistribution model, for the whole landscape and according to land use. The bottom and top of the box are the 25th and 75th percentile; the whiskers are the lowest datum still within 1.5 inter-quartile range (IQR) of the lower quartile, and the highest datum still within 1.5 IQR of the upper quartile; the black dot is the mean and the black line is the median. Differences between means tested with Student's t-test (α = 0.05).

Figure 5-6 shows the evolutions of ΔSOC stocks and contents from 2010 to 2100 for the whole study site. Evolution of ΔSOC stocks and contents were linear. On average, ΔSOC stocks and contents were positive, which means that the predicted SOC_{NSR} stocks and contents were higher than the predicted SOC_{SR} stocks and contents. However, ΔSOC showed a large range of values, with positive and negative values. This shows that soil redistribution induces both SOC loss and storage, especially for the ΔSOC stocks in the 0-to-105-cm soil layer and the ΔSOC contents in the 0-to-7.5-cm soil layer.

Figure 5-7 shows ΔSOC stocks and contents at the end of the simulation period in 2100, according to soil use. Regarding the whole landscape, mean ΔSOC stocks were 0.59 and 0.65 tC ha^{-1} for the 0-to-30 and 0-to-105 cm soil layers respectively; mean ΔSOC contents were 0.33 and 0.15 g kg^{-1} for the 0-to-7.5 and 0-30-to-cm soil layers, respectively. For the whole landscape, the intensive and the semi-intensive cropping, mean ΔSOC stocks were higher for the 0-to-105-cm soil layer than for the 0-to-30-cm soil layer. For the temporary and permanent grasslands, the opposite pattern was predicted. Greater ΔSOC stocks were simulated for the temporary grasslands (mean ΔSOC stocks: 1.07 and 0.97 tC ha^{-1} for the 0-to-30 and 0-to-105 cm soil layers respectively); lower values of ΔSOC stocks were simulated for the permanent grasslands (mean ΔSOC stocks: 0.43 and 0.21 tC ha^{-1} for the 0-30 and 0-105 cm soil layer, respectively). Mean ΔSOC contents were always higher for the 0-to-7.5-cm soil layer than for the 0-to-30-cm soil layer. Greater ΔSOC contents were also obtained for the temporary grasslands (mean values of ΔSOC contents: 0.83 and 0.36 tC ha^{-1} for the 0-to-7.5 and 0-to-30 cm soil layer respectively); lower ΔSOC contents were obtained for the semi-intensive cropping (mean ΔSOC contents: 0.07 and 0.16 tC ha^{-1} for the 0-7.5 and 0-30 cm soil layer respectively).

The ΔSOC stocks and contents in 2100 in the areas of soil deposition or erosion are given in Table 5-4. On average, negative values of ΔSOC stocks and contents were obtained for the areas of soil deposition; positive values of ΔSOC stocks and contents were obtained for the areas of soil erosion. For areas of soil deposition, the higher ΔSOC stocks and contents were obtained for the 0-to-105-cm soil layer. For areas of soil erosion, the same pattern was obtained for ΔSOC stocks, but for the ΔSOC content slightly higher values were obtained for the 0-to-7.5-cm soil layer (rather than for the 0-to-30-cm soil layer).

Table 5-4. Statistics of ΔSOC stocks and contents in 2100, in deposition and erosion areas. (D1: 1st decile, Q1: 1st quartile, Q3: 3rd quartile, D9: 9th decile). Differences between means tested with Student's t-test (α = 0.05).

	Soil layer (cm)	D1	Q1	Median	Mean	Q3	D9
Areas of soil deposition							
ΔSOC stocks	0-30	-2.7	-1.4	-0.4	-0.8 [a]	0.3	0.8
	0-105	-10.2	-5.2	-2.3	-4.2 [b]	-0.8	0.0
ΔSOC content	0-7.5	-1.1	-0.6	-0.2	-0.1 [c]	0.2	0.8
	0-30	-1.2	-0.7	-0.3	-0.4 [d]	0.0	0.2
Areas of soil erosion							
ΔSOC stocks	0-30	0.3	0.8	1.5	2.5 [e]	2.9	5.5
	0-105	1.2	1.9	3.0	5.0 [f]	5.4	10.2
ΔSOC content	0-7.5	0.1	0.4	0.7	1.1 [g]	1.3	2.6
	0-30	0.1	0.3	0.5	0.8 [h]	1.0	1.9

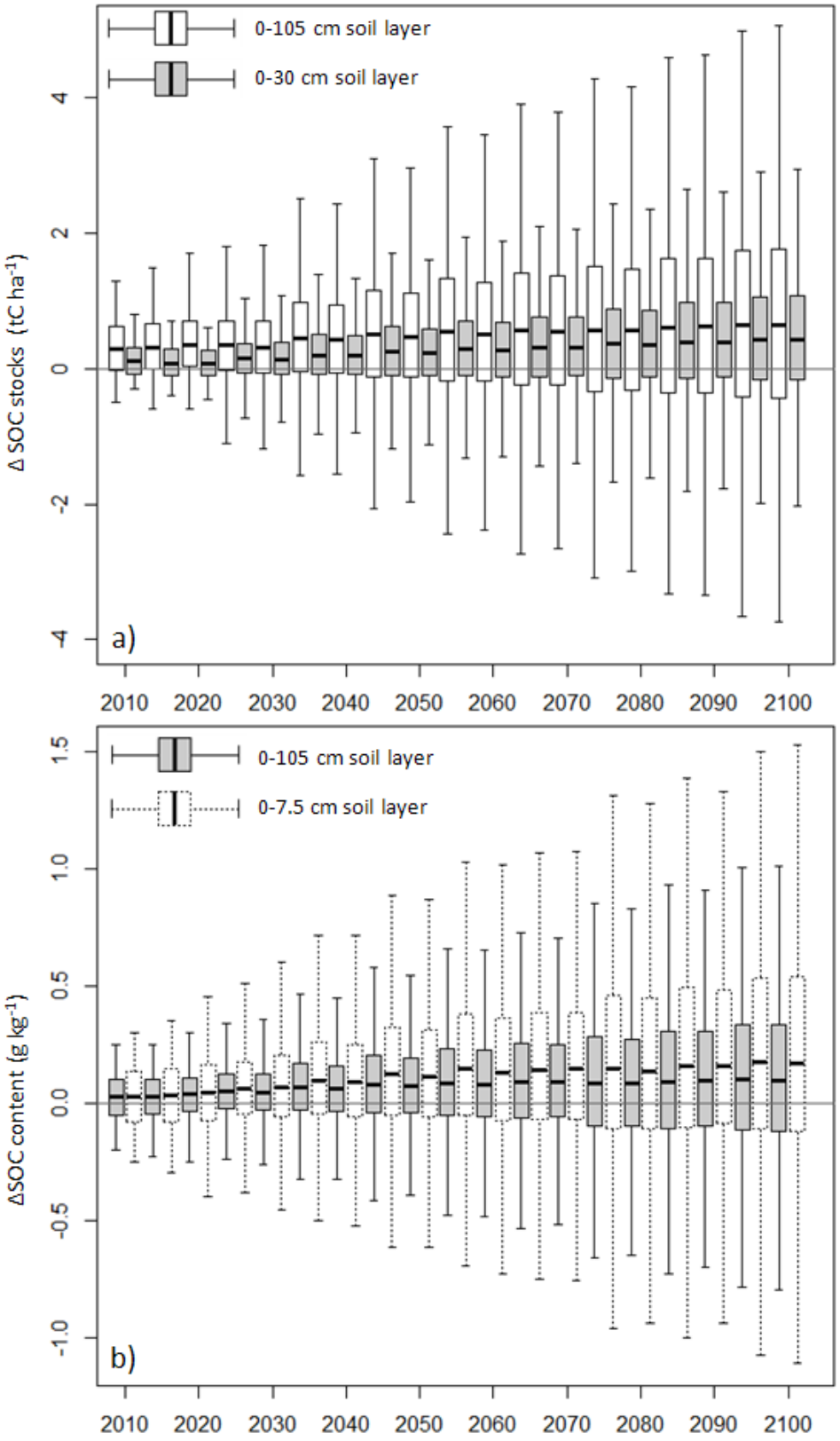

Figure 5-6. Evolution of (a) ΔSOC stocks in the 0-to-30-cm and 0-to-105-cm soil layers, (b) ΔSOC contents in the 0-to-7.5-cm and 0-to-30-cm soil layers. The bottom and top of the box are the 25th and 75th percentile; the whiskers are the lowest datum still within 1.5 inter-quartile range (IQR) of the lower quartile, and the highest datum still within 1.5 IQR of the upper quartile; the black line is the median.

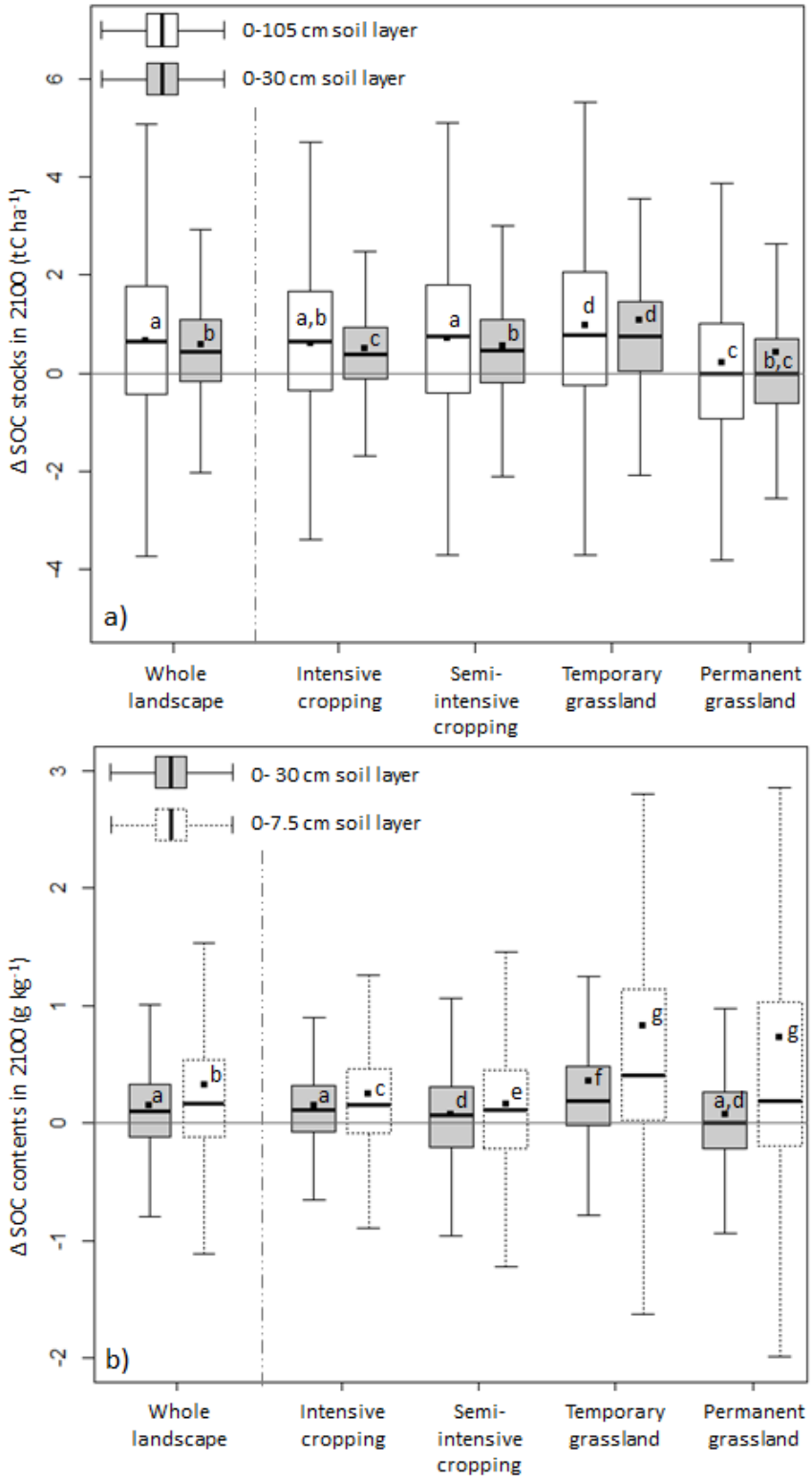

Figure 5-7. Difference in (a) ΔSOC stocks in the 0-to-30-cm and 0-to-105-cm soil layers, (b) ΔSOC contents in the 0-to-7.5-cm and 0-to-30-cm soil layers, for the whole landscape and according to land use. The bottom and top of the box are the 25th and 75th percentile; the whiskers are the lowest datum still within 1.5 inter-quartile range (IQR) of the lower quartile, and the highest datum still within 1.5 IQR of the upper quartile; the black dot is the mean; the black line is the median. Differences between means tested with Student's t-test (α = 0.05).

4. Discussion

4. 1. Soil redistribution patterns and rates

Considering soil redistribution, soil erosion processes were slightly greater than soil deposition processes: the mean soil redistribution rate was predicted to -0.14 t ha-1 yr-1 for the whole study site, with 372 t of soil exported out of the study site during the modelling period (Table 5-2). Moreover, soil erosion occurred on a slightly larger area than soil deposition (22 and 19%, respectively). Predictions of soil erosion were more important under intensive cropping (mean soil redistribution: -0.31 t ha^{-1} yr^{-1}), where both tillage and water erosion were modelled. Fields with intensive cropping, semi-intensive cropping and permanent grasslands were predicted as sources of soil sediment, while fields with permanent grasslands, woods and hedges acted in the landscape as a sink of soil sediments. This landscape was well managed to prevent from soil loss: fields with intensive cropping were mostly located far from the outlet of the study site, hedges perpendicular to the slope were maintained, woods and permanent grasslands were located where the slope was more intense and, finally, grasslands (temporary and permanent) were located around the study site outlet and in the vicinity of the preferential water flows (streams and ditches, Figure 5-1).

The main soil redistribution process was soil tillage, accounting for 81% of the net soil redistribution for the whole study site. Water redistribution processes was more important for intensive cropping (24% of the net soil redistribution), which is explained by the fact that the bare soil period was longer for this crop rotation type. However, even if tillage redistribution was more important, the mean soil redistribution rate by tillage was equal to zero for the whole study site. The areas of soil deposition and erosion showed very similar soil redistribution rate by tillage (-5.20 and 5.75 t ha^{-1} yr^{-1}, respectively). These results showed that soil erosion and soil deposition by tillage were equivalent in this landscape, both in spatial extent and in intensity, and balanced at the landscape scale. It results that the net soil loss at the landscape scale was mainly due to water processes. Water redistribution was not important, because of the spatial organization of the cropping systems. In fact, intensive cropping was located in the areas of lowest slope and, as we said before, grasslands were located in areas of highest slope. Finally, these results showed that the soil eroded in the fields was deposited in the hillslopes. These results were consistent with those obtained by Delmas et al. (2012) in an agricultural catchment in Normandy (part of the European loess belt): they estimated than the mean soil erosion was 3.3 t ha^{-1} yr^{-1} in the fields, but only 0.57 to 0.7 t ha^{-1} yr^{-1} at the hillslopes scale, and 0.16 t ha^{-1} yr^{-1} at the catchment scale.

The mean soil erosion rate was estimated at -3.95 t ha^{-1} yr^{-1}, and the mean soil deposition rate at 4.50 t ha^{-1} yr^{-1}. These results were consistent with previous studies. For example, Cerdan et al. (2010) estimated from a synthesis of existing plot measurements that the mean soil erosion rate in Europe was -1.2 t ha^{-1} yr^{-1} considering all land use classes, and -3.6 t ha^{-1} yr^{-1} considering only arable land. Verheijen et al. (2009) synthesized studies which estimated soil erosion rate in Europe and concluded that they ranged from -3.2 to -19.8 t ha^{-1} yr^{-1}.

Like other studies (e.g. Van Oost et al., 2005b), we found that soil redistribution by tillage was more important than soil redistribution by water. Soil redistribution rates by water and tillage suited with other studies. According to Verheijen et al. (2009) tillage erosion rates for Europe ranged from 3.0 to 9.0 t ha^{-1} yr^{-1} and sheet erosion due to water runoff ranged from 0.1 to 8.8 t ha^{-1} yr^{-1}, and the mean soil erosion rate was estimated at -0.36 t ha^{-1} yr^{-1}. Cros-Cayot (1996) estimated water soil erosion at 1.55 t ha^{-1} yr^{-1} for loamy soils in Brittany.

4.2. SOC stocks

At the end of the simulation period, the mean SOC_{SR} stocks for the 0-105 cm soil layer were estimated at 70 tC ha^{-1} for the whole study site, 53 tC ha^{-1} under the cultivated fields and 58 tC ha^{-1} under forests. The mean SOC_{SR} stocks for the 0-30 cm soil layer were estimated at 70 tC ha^{-1} for the whole study site, 53 tC ha^{-1} under the cultivated fields and 58 tC ha^{-1} under forests. On average, the deep SOC_{SR} stocks, stored under 30 cm, account for 25% for the whole landscape. Lower deep SOC_{SR} stocks were predicted for the permanent grasslands and woods. For permanent grasslands, this results can be explained by the fact that tillage was not frequent, so the SOC was not diluted in the ploughed soil layer. In the study site, the woods were located in the shallower soils (often less than 30 cm deep), so the SOC was little stored under 30 cm. The SOC_{SR} stocks were higher for the soil deposition areas than for the soil erosion areas, both for the 0-30 and the 0-105 cm. This result was consistent with those obtained by Yoo et al. (2006). High variability in SOC stocks and contents in 2100 was due to the high variability in the initial SOC data.

4.3. Impacts of soil redistribution on SOC stocks evolution

We estimated than 8 tC were lost by soil redistribution during the modelling period, which was equivalent to 1 kgC ha^{-1} y^{-1} and account for 1% of the SOC_{SR} stocks loss. The question if soil erosion is a factor of C loss or storage in landscape is still discussed (Lal and Pimentel, 2008; Van Oost et al., 2007; Van Oost et al., 2008). In previous study, Quinton et al. (2006) estimated that water erosion induced a loss of carbon at the scale of United-Kingdoms, ranging from 0.12 to 0.46 Tg C y^{-1}, which was equivalent to 8 to 29 kg ha y^{-1}. Gaiser et al. (2008) estimated that the mean carbon losses through erosion in were up to 0.45 tC ha^{-1} y^{-1} (state scale in Germany, under conventional tillage). Van Oost et al. (2006) showed that soil erosion by water could result in a net carbon sink or source, according to the hypotheses made on C mineralization in the eroded soil particles and the dynamic of the buried C, and the fate of the eroded sediments. According to different hypotheses on these parameters, they estimated averages fluxes of carbon at the field scale and estimated either C net sink ranging from 2.2 to 27.7 kgC ha^{-1} an^{-1}, or C net source ranging from 0.8 to 18.9 kgC ha^{-1} an^{-1}. Doetterl et al. (2012) estimated that the soil erosion was a net C sink, the because of the stabilization of C in former subsoil at eroding positions and partial preservation of buried C in pools of intermediate turnover at depositional positions. However, they underlined that the sink strength was limited and that the fate of exported soil could change the magnitude and sign of the erosion-induced C exchange.

We estimated that most of the soil eroded during the modelling period was redistributed in the landscape. At the catchment scale, Starr et al. (2000) estimated that a minimum of 73% of the sediment carried by water flows were deposited in the landscape. The SOC loss that we estimated was due to water redistribution and soil exportations out of the study site by water flows. Even if tillage processes may not cause direct soil loss because of the hypothesis made in the soil evolution model we used, they were responsible of the major SOC redistribution in the landscape. In fact, the fate of the eroded soil is important when dealing with SOC evolution. In our study site, most of the eroded soil was buried in deposition areas rather than exported. But the soil deposition rate was low, which induced a low C burial during the simulation period, and therefore a low quantity of C whose dynamic of mineralization was slowed down by C burial. This explains why we simulated a net loss of C, and not C storage.

4.4. Methodology

The fully soil redistribution and SOM model we used allowed assessing soil evolution at the landscape scale, by explicitly taking into account the different elements of the landscape, the spatial variability of soils and topography, and the areas of soil erosion and deposition. These are crucial points, given that soil redistribution and SOC distribution in the landscape are highly related to the topography and the connectivity between the landscape elements (fields, uncultivated areas, hedges...) (Yoo et al., 2006).

Further improvements of the modelling process of the coupled evolution of soil redistribution and SOC dynamics need to focus on four main issues: (i) the retroaction of SOC content change on soil erosion; (ii) the SOC dynamic in deep soil layer; (iii) the quantification of C mineralization during and after the soil erosion by water; (iv) the selective removal of soil particles by runoff. Even if ongoing studies are dealing with these subjects, few data are available to calibrated SOC dynamics and soil redistribution models to allow an adequate consideration of these three last parameters, especially for landscape scale models.

5. Conclusion

We modelled the SOC stocks evolution at the landscape scale, by taking into account the soil redistribution by tillage and water processes. We used a spatially SOC dynamic model (adapted from RothC), coupled to a soil redistribution model (LandSoil). We model the SOC dynamic in an agricultural landscape dedicated to dairy farming, with a mix of intensive or semi-intensive cropping and grassland. Our study site also integrated interstitial landscape elements, such as hedges. We found that soil redistribution, and more specifically soil exportation out of the study site, accounted for 1% of the total SOC stocks loss. The major process of soil redistribution was soil tillage; but most of the soil loss was due to soil erosion by water, while soil redistribution by tillage mostly induced soil redistribution inside the cultivated fields. Deep SOC stocks were significant and accounted for 25% on average considering the whole study site.

Acknowledgements

The authors acknowledge the ANR VMCS and the LandSoil project (landscape design for soil conservation under soil use and climate change, http://www.inra.fr/landsoil/) for scientific and financial support, the Z.A. Armorique (LTER-Europe, http://osur.univ-rennes1.fr/zoneatelier-armorique/) for LiDAR and land-use data provision, and the US INRA Agroclim - especially Frédéric Huard - for climate data provision.

5.2 Impacts de l'occupation du sol, de la structure du paysage et du climat sur l'évolution du sol

This section is a research article to be submitted.

Landscape-scale modelling of erosion processes and soil carbon dynamics under land use and climate change

M. LACOSTE [1*], V. VIAUD[1], D. MICHOT [2,3], C.WALTER[2,3]

[1]*INRA, UMR 1069, Sol Agro et hydrosystèmes Spatialisation, F-35000 Rennes, France*
[2]*AGROCAMPUS OUEST, UMR 1069, Sol Agro et hydrosystèmes Spatialisation, F-35000 Rennes, France*
[3] *Université européenne de Bretagne, France*
*Correspondance: Marine Lacoste. E-mail: marine.lacoste@rennes.inra.fr

Summary

Soil organic carbon (SOC) sequestration and soil redistribution are highly linked to soil properties, land use, farming system and climate. In a global change context, landscape and climate changes are expected, and will most probably impact soil evolution. We modelled soil evolution from 2010 to 2100 in a 1-km² hedgerow landscape, under different scenarios of landscape and climate changes. These scenarios combined contrasted land use (mixed dairy and hedgerow landscape, intensive cropping, grassland landscape), hedge networks (hedges planting or removal), and climates (business-as-usual or climate change). Two models were combined to evaluate the impact of changes in land use and climate on soils: a soil redistribution model, the LandSoil model, and a SOC model based on RothC-26.3. The results indicate that the major factor of soil degradation (including both soil erosion and decrease in SOC stocks) was land use change: the landscape with the more intensive agricultural system showed an increase in soil erosion, resulting in a net soil exportation of 4 000 t more than for the reference business-as-usual landscape, and a significant decrease in SOC stocks (-19 tC ha^{-1}). The second factor of importance was climate change, and finally hedgerow network. Sensitivity to climate change differed between landscapes, and the more sensitive ones were those with continuous cereals cropping. From our results, hedgerow landscape was proved to be well adapted for soil protection in a context of climate change, focusing on both carbon storage and soil erosion. However, this kind of landscape was very sensitive to cropping intensification and should be protected, especially in a global change context.

Keywords: soil evolution; soil redistribution; carbon storage; climate change; land use; agroecosystems.

Introduction

Soils provide ecosystem services essential to human life and well-being, including food production, physical support, filtering and buffering, nutrient cycling, and climate regulation (Dominati et al., 2010). Soils are currently undergoing rapid evolution: they are subjected to anthropogenic pressures, deriving mainly from changes in land use and climate regime, which may affect their properties and functions (Millennium Ecosystem Assessment, 2005). Erosion and decrease in soil organic carbon content (SOC) have been identified as the two main pressures on European soils (European Commission, 2006). Erosion directly induces a loss of soil (Cerdan et al., 2010), carbon and nutrients (Bakker et al., 2004; Papiernik et al., 2005; Papiernik et al., 2009), and can lead to irreversible soil degradation. Decrease in SOC loss impacts soil physical, chemical and biological properties and consequently soil fertility (Tiessen et al., 1994) and environmental quality (Lal, 2009).

In Europe, farming practices, land use and landscape structure have been significantly changing since the end of the World War II, under the evolution of social and economic context (Antrop, 2005). SOC dynamics is highly dependent on land use and management practices. Cropping systems determine the input of organic matter to the soil. They also affect SOC in terms of composition and dynamics (Kaur et al., 2008). SOC dynamics is also be affected by cropping practices such as tillage (Viaud et al., 2011) and soil amendment (Kogel-Knabner, 2005). Similarly soil erosion, is also controlled by land use (Cerdan et al., 2010) and land management practices, such as tillage (Le Bissonnais et al., 2005; Van Muysen et al., 2006) or crop residue management (Gilley et al., 2000).

Climate change is now recognized as a major driver of future rural landscape changes (Alcamo et al., 2007), and it also impacts soil properties and their evolution. IPCC predictions in the northern hemisphere for the 21st century indicate significant increase in temperature and rainfall, with more extreme events (IPCC, 2007). Plant photosynthesis will probably increase under climate change to an extent sufficient to increase litter input to the soil, although this may potentially be counteracted by increased soil organic matter decomposition (Smith et al., 2006). Moreover, soil evolution could increase or help to mitigate the climate change. Actually, soils are closely related to the global carbon cycle, representing one of the main environmental carbon pool (Grace, 2004). Small changes in SOC stocks and dynamics can modify the transfer to other environmental compartments, like the hydrosphere (by soil erosion) and the atmosphere: larger SOC mineralization can have a large impact on the atmospheric carbon dioxide concentrations (Johnston et al., 2004). For these reasons, SOC management could play an important part in climate change mitigation (Lal, 2004).

Development and adoption of farming and landscape management practices to prevent soil erosion and SOC loss is still on-going. But in agricultural landscapes, drivers of erosion processes and SOC dynamics at different temporal and spatial scales result in a variability in land use and climate change impact on soils. How soil could change depending on the location in the landscape remains highly uncertain. Depending on the cropping systems, land use changes, local soil characteristics and local trade-off between temperature increase and changes in precipitations, the balance between organic matter input to the soil and mineralization may shift and result in storage or loss. Considering these uncertainties, the potential combined impact of land use and climate change could be quantified using integrated model of soil redistribution and SOC dynamics at landscape scale, testing different scenarios of changes and the interplay between SOC dynamics and erosion. Studies at the landscape scale allow taking into account horizontal and vertical transfers of water, matter and nutrients, interactions between soil properties and soil evolution processes, and interactions between the different landscape elements (Pennock and Veldkamp, 2006). Dynamic and spatially distributed modelling at the landscape scale allows dealing with both spatial and temporal variability of the soils and its factors of evolution.

The purpose of this study was to assess the impacts of land use and climate change on soil evolution within an agricultural area, focusing on SOC dynamics and soil redistribution processes. We modelled these two soil processes under different scenarios of land use, landscape structure and climate, by coupling two dynamic and spatially distributed models.

Material and methods

Study site

The study site is a 84 ha agricultural catchment, located in Brittany (NW France, 48° 505’ N, 1° 565’ W) and included in a European Long-Term Ecosystem Research and in the French "Zones Ateliers"

networks (Figure 5-8). The geomorphology of the site is characterised by a plateau on metamorphic schist in the south (mean elevation 100 m) and a plain on Brioverian schist in the north (mean elevation 30 m) connected by a hillslope with a 13 % average slope. Hard and soft schists are locally covered by Quaternary Aeolian loam deposits with variable thickness. Soils are heterogeneous in terms of parent material, depth, and drainage conditions. The main soil types are Cambisols and Luvisols, but also Leptsosols and Fluvisols (WRB, 2007). Drainage conditions vary from well-drained soils on the plateau to poorly-drained soils with permanent redoximorphic conditions next to streams. Soil thickness ranges from 15 to 778 cm (mean value 113 m), and A-horizons thickness ranges from 3 to 220 cm (mean value 48 cm).

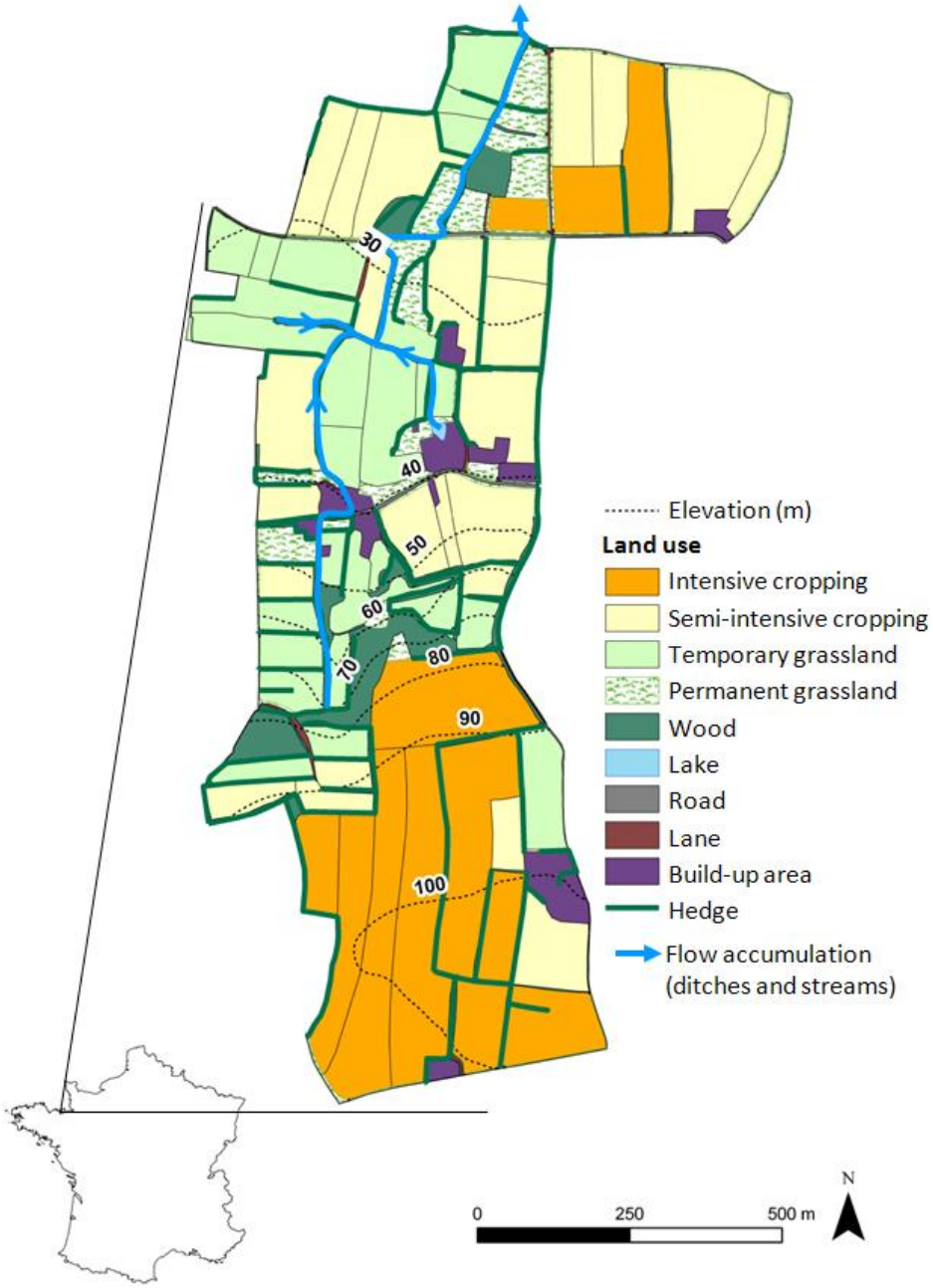

Figure 5-8. Location of the study area, topography and current land use (intensive cropping: crop rotations with maize and cereals as main crops, semi-intensive cropping: crop rotations with much as maize and cereals, as grassland, temporary grassland: crop rotations with grasslands as main land use).

Land use in the catchment is mainly dedicated to agriculture with dairy farming and 3 main crop rotations differing in the duration of grasslands: intensive crop rotations with silage maize (Zea mays) and winter wheat (Triticum aestivum) as main crops, semi-intensive crop rotations with as much maize and wheat as temporary grasslands (mostly Italian ryegrass, Lolium multiflorum), and temporary or permanent grasslands. The average field size is 1.2 ha. The study site also includes woodland plots (9 % of the whole study site), and urban areas, such as roads (3 %) and build-up areas (2 %). The site is characterised by a hedgerow landscape. Hedges located at field boundaries are mainly grass strips associated with trees such as oaks (*Quercus robur*), chesnut trees (*Castanea sativa*), and blackthorns (*Prunus spinosa*). The hedge density is currently 120 m ha^{-1} but has significantly decreased since the 50's together with agriculture modernization and land consolidation programs.

Soil process models

Two models were combined to evaluate the impact of changes in land use and climate on soils: a soil redistribution model and a SOC model. Figure 5-9 gives an overview of the modelling process.

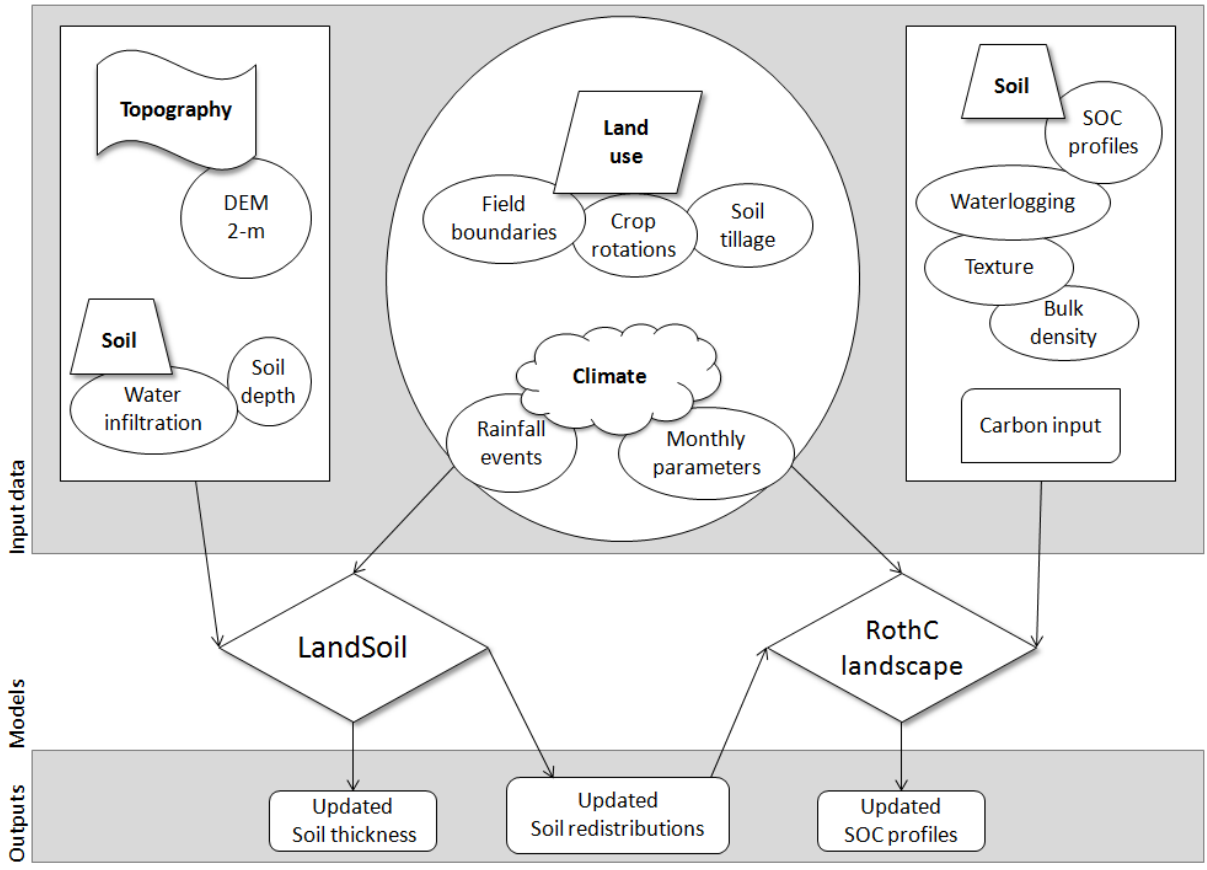

Figure 5-9. Modelling process overview.

Soil redistribution model

Soil redistribution was modelled with the LandSoil model (Ciampalini et al., 2012). LandSoil is an expert-based runoff and erosion model based on both the STREAM soil erosion model (Cerdan et al., 2002a; Cerdan et al., 2002b; Souchere et al., 2003; Souchere et al., 1998) and the WaTEM/SEDEM tillage erosion model (Govers et al., 1994). It allows the simulation of interrill, concentrated and

tillage erosion. It is a spatially distributed model dimensioned for fine spatial (1–10 m) and temporal (rainfall event) resolution scales. It includes a detailed representation of the agricultural landscape that takes into account soil surface properties, hydrologic pathways and anthropogenic elements. The model assumes that soil surface characteristics are the major factors controlling runoff and soil erosion/deposition processes in agricultural landscapes. Soil surface characteristics include surface crusting, soil roughness and vegetation cover evaluated at field scale (Cerdan et al., 2002b). A value for steady-state infiltration rate (IR) and residual water storage (W) after the previous rainfall event (PI) are assigned to each combination of soil surface characteristics (Bresson and Boiffin, 1990; Le Bissonnais et al., 2005). IR and W determine the production of runoff by a rainfall event, according to the following equation:

$$B = RR - W - (IR \times D_{ef}) \quad (1)$$

where B is the runoff vs. infiltration balance (mm), RR the rainfall amount (mm), W the residual water storage after the previous rainfall event (mm) and Def the effective duration of the rainfall event (h).

The effect of tillage on soil redistribution is modelled considering a tillage erosion coefficient (Kt). Two Kt are used: Kts models soil redistribution for up and downslope tillage, while Ktc models soil redistribution for contour tillage.

Input variables of the LandSoil model include a map of the initial soil thickness in a raster format, a digital elevation model (2-m LiDAR DEM), a field map with the locations of the ploughed fields and the associated Ktill, land use and associated soil surface characteristics, and rainfall events characteristics (total rainfall (mm), effective rainfall duration (h), maximum intensity over 6 minutes (mm h^{-1}) and rainfall amount during the preceding 48 hours (mm)). Outputs at event-step (rainfall or tillage event) are the updated map of soil thickness and an updated DEM.

SOC dynamics model

SOC dynamics was modelled with a variant of the model RothC 26.3 (Coleman and Jenkinson, 1996) applied to landscape scale. RothC is dedicated to modelling SOC dynamics in well-drained topsoils (first 30 cm). C stocks and inputs are divided into five conceptual compartments: DPM (Decomposable Plant Material), RPM (Resistant Plant Material), BIO (microbial Biomass), HUM (Humified Organic Matter) and IOM (Inert Organic Matter). These compartments differ in mean residence time of organic carbon. In each compartment SOC decomposition is assumed to follow a first-order kinetic. SOC decomposition depends on a decomposition constant rate, specific to the compartment, and modified by soil water content, soil temperature and soil cover, according to the following equation:

$$q_j = Y e^{-abk_j t} \quad (2)$$

Where q_j is the amount of SOC decomposing during time t in compartment j, k_j the decomposition rate constant of compartment j, a the rate modifying factor depending on soil temperature, and b the rate modifying factor depending on soil water content.

RothC has been modified to model SOC dynamics in the whole A-horizons and in any locations of the landscape. The landscape is represented as a regular square grid. The model divides the soil profiles into several layers, whose number and thickness are defined by the user. We assumed a single decomposition rate k_j in any compartment at any depth of the soil profile, corresponding to

potential mineralization, with specific rate modifying factors *a* and *b* depending on depth. Soil temperature in each soil layer was calculated from air temperature using the equation proposed by (Kasuda and Archenbach, 1965):

$$T_{soil} = T_{mean} - T_{amp}.e^{(-depth(\sqrt{\Pi/365/\alpha})\cdot} \cdot \cos(2\pi/365.\left(t - t_{shift} - \frac{depth}{2}.(365/\pi/\alpha)\right) \quad (3)$$

Where *Tmean* is the mean annual air temperature, T_{amp} is the annual amplitude of the air temperature (maximum air temperature minus minimum air temperature), *d* is the depth below the soil surface (typically the mean depth of the soil compartment considered), α is the diffusivity of the soil (set to 5.37 10-3 cm² s^{-1}, (Kasuda and Archenbach, 1965)), t_{now} is the current time (day), and t_{shift} is the day of the year of the minimum air temperature.

The RothC modifying factor related to soil water content *b* is reduced by a factor 0.6 (empirical calibration) in poorly-drained soil layers.

Two processes able to change soil distribution in the soil profile are considered: tillage and erosion/deposition processes. Soil mixing by bioturbation is ignored. The SOC model is combined to the LandSoil model to consider the impact of soil redistribution on SOC transfer and dynamics. The updated DEM produced by the LandSoil model is used every year as input in the SOC model. On a yearly time step, the updated DEM is subtracted from the previous DEM. In deposition area the SOC content of the deposited soil particles is set to average SOC content in the eroded areas. Decomposition rate constants of eroded particles are similar to those of the soil. Impact of changes in SOC stocks on soil sensitivity to erosion is not considered in the LandSoil model.

The SOC model runs on a monthly time step in each location of the landscape. The model does not include a crop model. C inputs to the soil are computed from crop yields and C contents in aerial and belowground plant residues. All aerial residues are assumed to enter the surface soil layer and belowground plant residues are distributed in the soil profile according to root distributions specified by the model user. Input variables of the model include soil properties (initial SOC stocks, bulk density, clay content, and drainage conditions) in each soil layers and in any location of the landscape, land use over the simulation period, farm practices (tillage, winter crops, residues management, organic amendment, sowing and harvest dates), climate (monthly rainfall, temperature and evapotranspiration), root distribution in the soil profile, C content in plant residues and DEM. Outputs give yearly maps SOC stocks and contents for the considered soil layers and for each conceptual compartment

Simulation of soil evolution

Simulation design

A simulation design was built considering two factors, landscape (7 levels) and climate (2 levels), requiring 14 simulation runs.

Landscape factor

The landscapes differed according to land use and hedgerow network.

Three contrasted land use were considered: (1) business-as-usual land use, corresponding to land use matching observations in the catchment over the past 15 years, (2) intensive cropping with winter cereals in all the fields, (3) permanent grasslands in all the fields.

For the business-as-usual land use, crop rotations for the period 2010-2100 were simulated stochastically over the field pattern using a 1st-order Markov chain (Walter et al., 2003b; Sorel et al., 2010) and starting from the crop pattern observed in 2010. The Markov chain was calibrated using land use maps derived from photo-interpretation and available for the period 1993-2010. Three main crop rotations were identified, all including maize and cereals but distinguished by the number of years with grasslands: (1) intensive crop rotations corresponding with temporary grasslands established for less than 4 years (29% of the study area); (2) semi-intensive crop rotations temporary grasslands established for 4 years on average (31% of the study area); (3) extensive crop rotations corresponding to temporary grasslands established for 8-years on average (20% of the study area) . Crop management practices (type and depth of tillage, organic amendment, sowing and harvest date, residues management) were inferred from farm surveys available on the study site (Thenail, 2002 and unpublished data ZA Armorique). The study site area includes 13 cattle farms with homogeneous crop management practices: one crop management was therefore associated to each crop. Crop management per crop was constant over the simulation period (Figure 5-5).

Table 5-5. Description of the parameters used to characterise the agricultural practices in the scenarios.

	Crop management				C inputs		Soil tillage		
Soil use	Establishment	Harvest	Mean yield (t ha^{-1})	Crop residues management	Type	Quantity (tC ha^{-1})	Tillage operations before establishment	$K_{till.s}$ (kg m^{-1})	$K_{till.c}$ (kg m^{-1})
Winter cereal	October	July	7.4	ploughing	-	-	reversible plough (25-cm depth), chisel cultivator, rotary harrow and air seeder	629	376
Maize	April	October	11.7	ploughing	Organic amendment (manure)	2.37	reversible plough (25-cm depth), chisel cultivator, rotary harrow and air seeder	629	376
Temporary pasture grassland	August-October	May-June	8	ploughing	C excreted during grazing	1.1	chisel cultivator and air seeder	291	139
Temporary grassland for cutting	August-October	May-June	8	ploughing	Organic amendment (manure)	0.2	chisel cultivator and air seeder	291	139
Permanent pasture grassland	-	-	6	ploughing	C excreted during grazing	1.1	chisel cultivator and air seeder	291	139
Permanent grassland for cutting	-	May-June	6	ploughing	-	-	chisel cultivator and air seeder	291	139

Before maize and winter wheat sowing, tillage operations combined most often tillage with reversible plough (25-cm depth), chisel cultivator and rotary harrow. A chisel cultivator is used before grassland establishment. Winter crops are established between wheat and maize. Annual C inputs by crop residues were computed from regional statistical data on crop yields (AGRESTE, 2010) and references on C content in crop residues (Boiffin et al., 1986b; Bolinder et al., 1997). The total amount of farmyard manure produced in the study area was calculated from data on herd size and animal production levels (CORPEN, 1999; CORPEN, 2001). Only maize is fertilized with farmyard manure. Direct manure input in grazed grasslands was estimated according to (INRA, 2008). For the

scenario intensive cropping (winter cereals in all the fields), continuous winter wheat cropping was considered in all the fields of the landscape, including the field located next to the stream. Crop management practices and crop yields were considered similar to those observed for wheat in the business-as-usual scenario. Similarly, in the scenario "permanent grasslands", crop management practices were considered similar to those observed for permanent grasslands in the business-as-usual scenario.

Three types of hedgerow networks were considered: (1) current hedgerow network, (2) maximum hedgerow network corresponding to hedgerows on all the field boundaries, (3) no hedgerows.

Contrasted land use and contrasted hedgerow network resulted in 7 combinations (Table 5-6), classified in three types of scenarios: business-as-usual (BAU), accentuation and protection scenarios. The constant scenario (scenario 1) was used to model soils evolution in a landscape similar to the present landscape. The accentuation scenarios (scenarios 2 to 4) were used to model soils evolution in a landscape leading to soil degradation (according to soil erosion and soil organic carbon content). The protection scenarios (scenarios 5 to 7) were used to model soils evolution in a landscape leading to soil protection. Accentuation and protection scenarios were used each in three combinations, which cross land use and hedgerow network identical or different from the constant scenario. Scenarios 2 and 5 were used to estimate the influence of changes in hedgerow network on soil evolution. Scenarios 3 and 6 were used to estimate the influence of land use changes on soil evolution. Scenarios 4 and 7 were used to estimate the combined influence of changes in land use and hedgerow network on soil evolution.

Table 5-6. Characteristics of the 7 levels of the landscape factor used in the simulation design (BAU: business-as-usual).

Scenarios	BAU	Accentuation scenarios			Protection scenarios		
	1	2	3	4	5	6	7
Landscape structure							
Land use	BAU	BAU	Intensive cropping increased	Intensive cropping increased	BAU	Permanent grasslands increased	Permanent grasslands increased
Hedgerow network	BAU	Hedges removed	BAU	Hedges removed	Hedges planting	BAU	Hedges planting
Land use proportion (%)							
Intensive cropping	28	29	84	88	27	0	0
Semi-intensive cropping	30	31	0	0	29	0	0
Temporary grassland	20	21	0	0	19	0	0
Permanent grassland	6	7	0	0	6	84	81
Wood	4	5	4	5	4	4	4
Hedges	5	0	5	0	10	5	10
Grass strips	2	1	2	1	0	2	0
Roads and lanes	3	4	3	4	3	3	3
Build-up areas	2	2	2	2	2	2	2

Climate factor

Two climate scenarios were considered: a BAU scenario and a climate change scenario. BAU climate over the simulation period (2010-2100) was considered as similar to the climate observed over the period 1980-2010: hourly climate data for the period 2010-2100 were simulated stochastically from the available dataset 1980-2010, considering similar variability and trend.

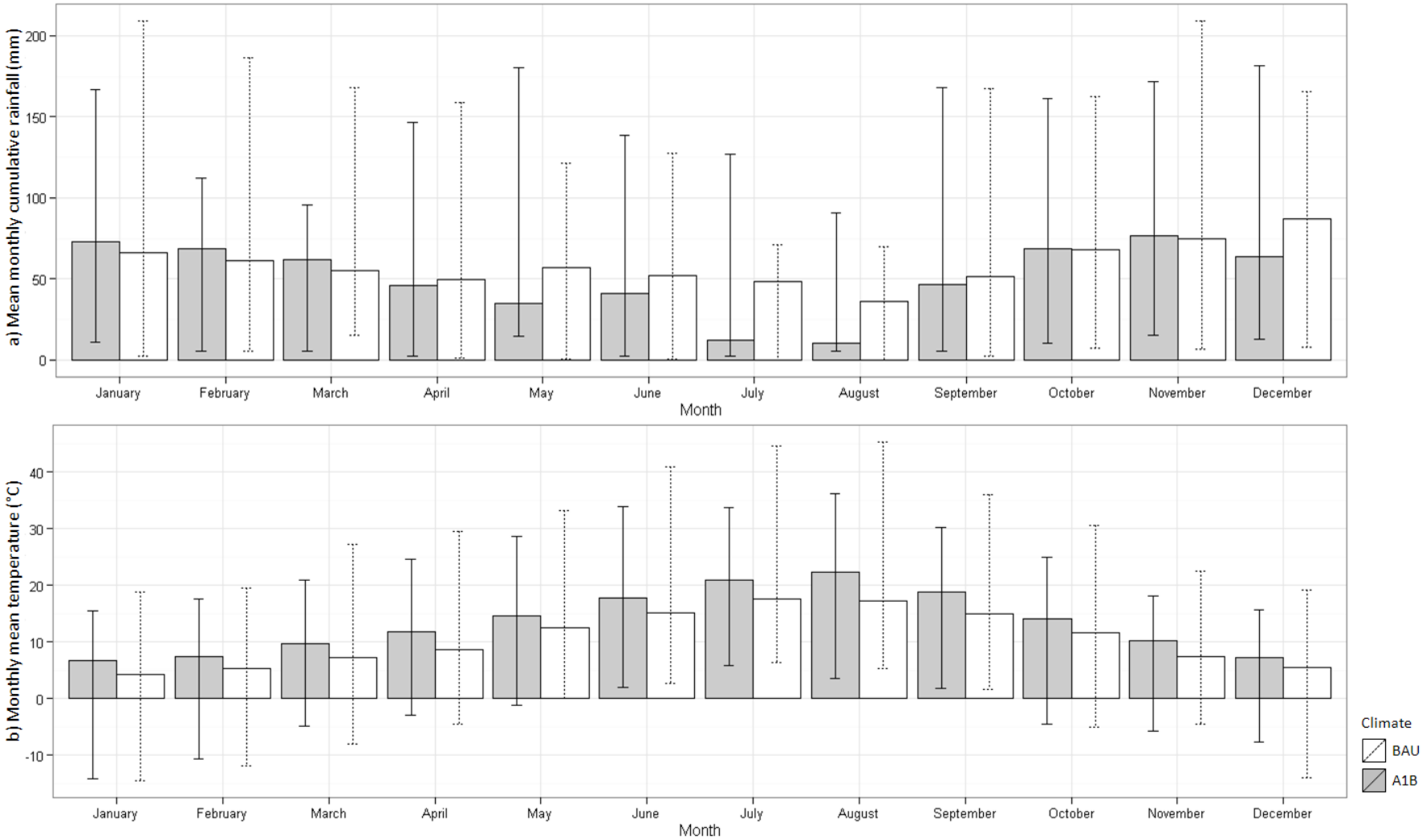

Figure 5-10. Inter-annual variations of monthly cumulative rainfalls (a) and monthly temperatures (b). The white bars represent business-as-usual climate (BAU) and the grey bars represent A1B climate. Error bars represent minimum and maximum values.

The climate change scenario was predicted by the Meteo-France atmospheric model ARPEGE/climate (Gibelin and Dequé, 2003) from the A1B emission scenarios defined by the IPCC (2000), and regionalized for the studied area by the quantile-quantile bias correction method (Deque, 2007). In comparison to the BAU climate, the A1B climate showed mean annual precipitation decreased by 12% (range: -67 to +53%), and mean annual temperature increased by 2.9 °C (range: -0.1 to 5.3°C).

The characteristics rainfall events (total rainfall (mm), effective rainfall duration (h), maximum intensity over 6 minutes (mm h^{-1}) and rainfall amount during the preceding 48 hours (mm)) required as input for the LandSoil model were derived from the hourly climate data. Each rainfall occurrence was distinguished as a single event when separated by at least a 3-hour dry period. Effective duration is defined as a rainy period, which intensity is not lower than 2 mm h^{-1}. The effective duration and the maximum intensity have to be calculated from 6-min meteorological data. We used multiple linear regressions to estimate these two parameters from hourly rainfall parameters as described in Lacoste (2012a). 635 and 1139 rainfall events were specified for the BAU and the A1B climate scenarios, respectively, with a mean rainfall amount of 9 and 12 mm, and maximum intensity of 15 and 25 mm.h^{-1} on average over the simulation period (Table 5-7).

Table 5-7. Characteristics of rainfall events causing runoff (period 2010-2100).

Climate parameters	Climate	
	BAU	A1B
Number of rainfall events	635	1139
Rainfall (mm)	9 (2.6-50)	12 (2.6-122)
Duration (h)	2.8 (0.4-9)	2.4 (0.4-27)
Maximum intensity (mm h^{-1})	15 (3-107)	25 (4-141)
48 h-antecedent rainfall (mm)	6 (0-63)	9 (0-102)

Mean values (range between brackets).

The hourly climate data were aggregated at a monthly time step for use as input in the SOC model (Figure 5-10). Over the period 2020-2050, mean monthly temperature is 10.8°C and 12.8°C respectively for the BAU and the A1B climate scenarios, and mean monthly precipitation is 58.9 and 55.3 mm respectively for the BAU and the A1B climate scenarios. Over the period 2070-2100, mean temperature is 10.7°C and 14.3°C respectively for the BAU and the A1B climate scenarios, and mean monthly precipitation is 58.6 and 46.1 mm respectively for the BAU and the A1B climate scenarios. Major differences between BAU and A1B climate scenarios are observed in summer.

Model simulation

The model was run for the period 2010-2100. The initial topography was described using a 2-m resolution LiDAR DEM, produced in 2009. LandSoil required the range of the parameters controlling runoff: according to previous study (Lacoste et al., 2012b), steady-state infiltration rate (IR) assigned to the fields ranges from 1.5 to 37.5 mm h^{-1} and residual water storage after the previous event ranges from 0 to 11 mm. IR under hedges was set to 150 mm h^{-1} (Richet et al., 2006). Soil bulk density was set to 1.3 g kg^{-1}.

In the vertical dimension the soil profile was divided into 8 increments (or less if soil thickness was less than 105 cm): 0-to-7.5, 7.5-to-15, 15-to-30, 30-to-45, 45-to-60, 60-to-75, 75-to-90, 90-to-105 cm. Initial soil thickness (LandSoil input), and SOC stocks and bulk density in each soil increment (SOM model inputs) were described as 2-m resolution maps. The soils maps were produced from soil

sampling data collected in 2010, and using machine learning methods (Lacoste et al., 2014). Clay content was considered as uniform and was set to 12%.

Result analysis

The scenario BAU landscape under BAU climate (BAU-1) was considered as the reference scenario; the simulation results of the other scenarios were analysed relatively to this reference scenario.

Soil redistribution

Soil redistribution refers to soil movement resulting either from erosion or soil deposition in a specific location. Positive values reflect net soil deposition, while negative values reflect net erosion. Results have been analysed for total soil redistribution, and soil redistribution due to only tillage or water processes.

Five indicators of soil evolution by redistribution processes were computed:

1 Average soil redistribution rates per pixel, due to water (SRw) and tillage erosion (SRt) processes respectively, over the simulation period 2010-2100 (%),

2 Cumulative quantity of soil exported out of the study site during the simulation period 2010-2100 (in t),

3 Cumulative quantities of soil eroded (NSero) and deposited (NSdep) in the whole study area and over the simulation period 2010-2100; ΔNSero and ΔNSdep describe the difference in as compared to the reference scenario BAU-1,

4 Proportion of study site areas in erosion or deposition (in %). A stable area was defined as an area with a net change in soil thickness lower than 1 cm (from 2010 to 2100),

5 Difference in soil thickness (in cm) compared to the reference scenario BAU-1 (ΔSoil-thickness).

Soil organic carbon stocks

SOC response to land use and climate scenarios was analysed by 4 variables, computed in 2100:

1 and 2: difference in SOC stocks (ΔSOC stocks) in the 0-to-30-cm and 0-to-105-cm soil layers compared to the BAU-1 scenario,

3 and 4: difference in SOC content (ΔSOC content) in the 0-to-7.5-cm and 0-to-30-cm soil layers compared to the BAU-1 scenario,

Results

Soil redistribution

Non-zero redistribution rates were predicted for all scenarios, except the scenarios involving landscapes 6 and 7 (under both the BAU and A1B climates). In comparison to the reference scenario, all scenarios increased the soil redistribution within the landscape boundaries and the soil exportation out of the study site, except the scenarios BAU-5, BAU-6, BAU-7, A1B6 and A1B7. Soil redistribution between scenarios differed both in quantity and in spatial pattern (Table 5-8). The predicted changes in soil redistribution were more pronounced for the erosion processes than for the deposition processes. Soil exportation out of the study site was predicted for all scenarios under BAU climate, except landscapes 6 and 7 (Figure 5-11).

Table 5-8. Cumulated soil erosion and soil deposition, and areas of soil erosion and soil deposition simulated over the simulation period 2010-2100.

Scenario		Net final eroded soil (NSE_{ro}, t)	Net final deposited soil (NSD_{ep}, t)	Area of soil erosion (%)	Area of soil deposition (%)
Landscape	Climate				
1	BAU	10 657	10285	22	19
	A1B	12 046	10 905	27	19
2	BAU	11 756	11238	23	20
	A1B	13 116	11 575	28	20
3	BAU	25 784	23 382	38	26
	A1B	33 676	25 887	53	21
4	BAU	27 693	23 422	40	26
	A1B	35 489	23 550	55	21
5	BAU	10 221	10 014	21	18
	A1B	11 645	10 930	26	18
6	BAU	0	0	0	0
	A1B	0	0	0	0
7	BAU	0	0	0	0
	A1B	0	0	0	0

The comparison of the landscape scenarios BAU-1, BAU-3 and BAU-6 allowed assessing the impacts of within-field land use on soil redistribution. NSEro increased by +15 127 t for BAU-3 and decreased by -10 657 t for the BAU-6, which was equivalent to a +142% and -100% change, respectively. Similar trends pattern were predicted for NSDep: it increased by +13 098 t for BAU-3 and decreased by -10 285 t for the BAU-6, which was equivalent to a +127% and -100% change, respectively. The quantity of soil exported out of the study increased by +2 029 t for BAU-3 and decreased by -372 t for the BAU-6, which was equivalent to a +545% and -100% change, respectively (Figure 5-11). For BAU-3, the areas of soil erosion and deposition increased by +16 and +7% respectively; while for the BAU-6, the areas of soil erosion and deposition decreased by +22 and +19%. The net soil redistribution due to water erosion processes increased by +13% for BAU-3, and decreased by -100% for the BAU-6 (Figure 5-11).

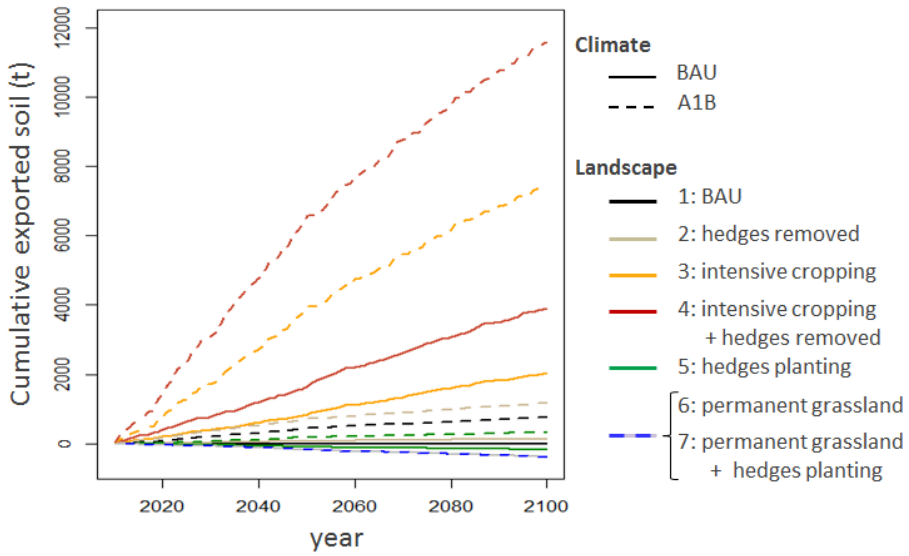

Figure 5-11. Cumulative quantities of soil exported out of the study site over the period 2010 -2100 for the 14 climate-landscape scenarios.

The comparison of the landscape scenarios BAU-1, BAU-2 and BAU-5 allowed assessing the impact of the hedgerow network on soil redistribution. In comparison to BAU-1, soil redistribution was increased by BAU-2 and decreased by BAU-5, and the impacts of BAU-2 were slightly higher than those of BAU-5. ΔNSEro was +1 099 t for BAU-2 and -436 t for the BAU-5, which was equivalent to a 10% and 4% change respectively. Similarly, ΔNSDep was 954 t for BAU-2 and -270 t for BAU-6, which was equivalent to a 9% and 3% change respectively. Soil exportation increased by 145 t for BAU-2 and decreased by 165 t for the BAU-6 respectively, which was equivalent to a 1% change in both cases (Figure 5-11). The areas of soil erosion and deposition changed by 1%, for both for BAU-2 and BAU-6 (increase for BAU-2 and decrease for BAU-6). Redistribution rates due to water erosion processes decreased by -1% for BAU-2, and increased by +4% for the BAU-5.

Interactions between change in land use and change in hedgerow network can be investigated by the comparison of landscapes 2, 3 and 4. Soil exportation out of the study site was predicted to 517 t for BAU-2, 2 401 t for BAU-3 and 4 271 t for BAU-4. The proportion of eroded soil that is deposited within the study site was 96% for BAU-2, 91% for BAU-3 and 85% for BAU-4.

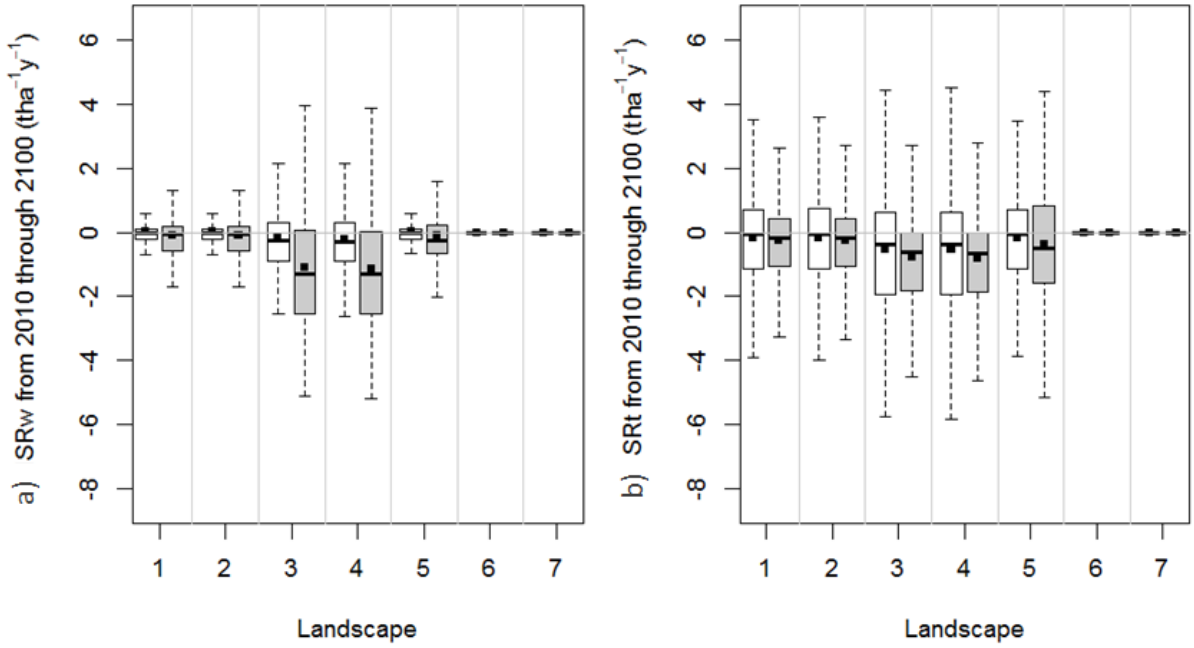

Figure 5-12. Average soil redistribution rates per pixels, due to (a) water erosion processes (SR_w) and (b) tillage (SR_t), over the simulation period (2010-2100). Negative values denote erosion, positive values denote deposition. The bottom and top of the box are the 25th and 75th percentile; the whiskers are the lowest datum still within 1.5 inter-quartile range of the lower quartile, and the highest datum still within 1.5 IQR of the upper quartile; the black dot is the mean and the black line is the median. The white box-plots represent the business-as-usual climate scenario; the grey box-plots represent the A1B climate scenario. The landscape scenarios are presented on the X-axis (see Table 5-8 for details).

The comparison of the landscape scenarios under the BAU and A1B climates allowed assessing the impact of climate on soil redistribution, and the vulnerability of the landscapes to climate change. All the landscapes were sensitive to climate change, except landscapes 6 and 7. ΔNSEro increased by 13% for the A1B-1, 12% for the A1B-2, 31% for the A1B-3, 28% for the A1B-4 and 15% for the A1B-5. ΔNSDep decreased by 6% for the A1B-1, 3% for the A1B-2, 11% for the A1B-3, 1% for the A1B-4 and 9% for the A1B-5. Net soil exportation increased by 207% for the A1B-1, 198% for the

A1B-2, 224% for the A1B-3, 180% for the A1B-4 and 246% for the A1B-5. Redistribution rates due to water erosion processes increased for all A1B scenarios, as compared to the same landscape under BAU climate. A 14% increase was predicted for A1B-1 and A1B-2, 32% for A1B-3 and A1B-4, and 11% for A1B-5. The soil redistribution by tillage was the dominant redistribution process for all scenarios, except A1B-3 and A1B-4, where soil redistribution by water reached 58% of the total soil redistribution (Figure 5-12). Figure 5-13 shows the impacts of the different scenarios on the soil thickness simulated in 2100, in comparison to the reference scenario BAU-1 (ΔSoil-thickness). The larger variation was predicted for A1B-4, with a mean ΔSoil-thickness of -1.0 cm and 10% of the site with ΔSoil-thickness upper to -10 cm.

Soil organic carbon stocks

At the end of the simulation period, the reference BAU-1 scenario showed average SOC stocks of 54 and 75 tC ha^{-1} in the 0-to-30-cm and 0-to-105-cm soil layer respectively; average SOC contents were 23 and 16 gC kg^{-1} in the 0-to-7.5-cm and 0-to-30-cm soil layer, respectively (Table 5-9). In the 0-to-30 cm soil layer 70% of the study site area had SOC contents higher than 15 gC kg^{-1} and the whole study area had SOC contents higher than 5 gC kg^{-1} in the 0-to-30-cm soil layer.

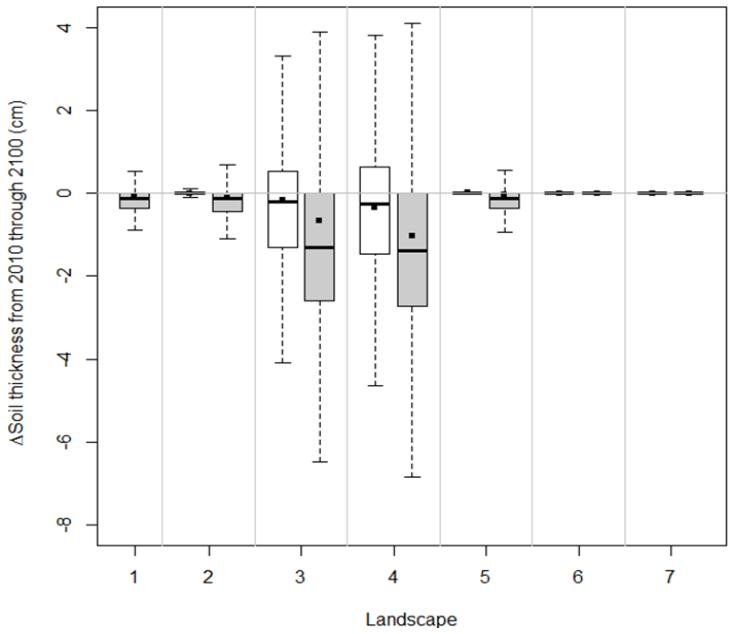

Figure 5-13. Pixel to pixel differences between the soil thickness simulated in 2100 in the different landscape-climate scenarios and the soil thickness simulated in 2100 in the reference scenario (BAU-1). The bottom and top of the box are the 25th and 75th percentile; the whiskers are the lowest datum still within 1.5 inter-quartile range of the lower quartile, and the highest datum still within 1.5 IQR of the upper quartile; the black dot is the mean and the black line is the median. The white box-plots represent the business-as-usual climate scenario; the grey box-plots represent the A1B climate scenario. The landscape scenarios are presented on the X-axis (see Table 5-8 for details).

Table 5-9. Statistics of the SOC stocks and SOC contents, simulated in 2100 in the BAU-1 reference scenario (business-as-usual landscape and climate).

	Soil layer (cm)	1st decile	1st quartile	median	mean	3rd quartile	9th decile
SOC stocks	0-30	47.42	50.12	53.44	54.05	57.46	61.87
(tC ha^{-1})	0-105	60.32	65.77	72.28	74.69	80.79	91.37
SOC content	0-7.5	16.52	19.74	22.56	22.81	25.3	30.05
(gC kg^{-1})	0-30	13.55	14.83	16.02	16.21	17.37	18.96

Figure 5-14 shows the impact of landscape-climate scenarios on SOC stocks and contents simulated at the end of the simulation period in 2100. Under the BAU climate, landscapes 2, 3 and 4 had lower SOC stocks than landscape 1, while landscapes 5, 6 and 7 allowed SOC storage. For all the landscapes under A1B climate, the final SOC stocks for the 0-to-105-cm soil layer were lower than the final stocks for the reference scenario (BAU-1).

The consideration of scenarios BAU-1, BAU-3 and BAU-6 allowed assessing the impact of the land use change on SOC stocks and contents. Land use change had a strong impact on SOC stocks: in average, SOC stocks in the 0-to-105-cm soil layers decreased by 17 tC ha^{-1} in the BAU-3 scenario under continuous wheat cropping, and decreased by 1 tC ha-1 in the BAU-6 scenarios, as compared to the BAU-1 reference scenario. Similarly, a strong impact of land use is observed regarding SOC contents in the 0-to-7.5-cm soil layer. Change to permanent grassland as little impact on SOC contents in the 0-to-30-cm soil layer (decrease of 0.6 g kg^{-1}) and led to a mean increase of 4 gC kg^{-1} in the 0-to-7.5-cm soil layer.

The comparison of the landscape scenarios BAU-1, BAU-2 and BAU-5 allowed assessing the impact of the hedgerow network on SOC stocks and contents. No impact of hedgerow was simulated on average SOC stocks and contents (Figure 5-14). Considering the scenario BAU-5, characterised by business-as-usual land use and maximum hedgerow network, SOC stocks for the 0-to-105 cm soil layer exhibited a mean increase of 1 tC ha^{-1}.The BAU-2 scenario, characterised by the same land use and no hedgerow showed a mean decrease of 1 g kg^{-1} for the SOC stocks in the 0-105 cm soil layer.

The comparison of the landscape scenarios under the BAU and A1B climates allowed assessing the impact of climate on SOC stocks and contents. All the landscapes were sensitive to climate change: SOC stocks in the 0-to-105-cm soil layer decreased by 8 tC ha^{-1} for the A1B-1, 9 tC ha^{-1} for the A1B-2, 33 tC ha^{-1} for the A1B-3, 35 tC ha^{-1} for the A1B-4 and 7 tC ha^{-1} for the A1B-5, 9 tC ha^{-1} for the A1B-6 and 2 tC ha^{-1} for the A1B-7 scenario as compared to the reference BAU-1 scenario. Similar patterns of changes were observed for SOC stocks in the 0-to-30-cm soil layer and SOC contents in the 0-to-7.5-cm and the 0-to-30-cm soil layers.

An interaction between climate and landscape was observed for SOC stocks in the 0-to-105-cm soil layer: average SOC stocks decreased by 8 tC ha^{-1} under A1B climate relative to BAU climate for the landscape scenarios 1, 2, 5, 6 and 7 (Figure 5-14), whereas they decreased by 16 tC ha^{-1} under A1B climate relative to BAU climate for the landscape scenarios 3 and 4. The same pattern was observed for the 0-to-30 cm SOC stocks and for the 0-to-7.5 and 0-to-30 cm SOC content.

Despite the decline in SOC stocks compared to the reference scenario, SOC content in the soil surface layers remained higher than 15 gC kg^{-1} for 95% and 72% of the study area, for the 0-to-7.5 and 0-to-30 cm soil layers, respectively.

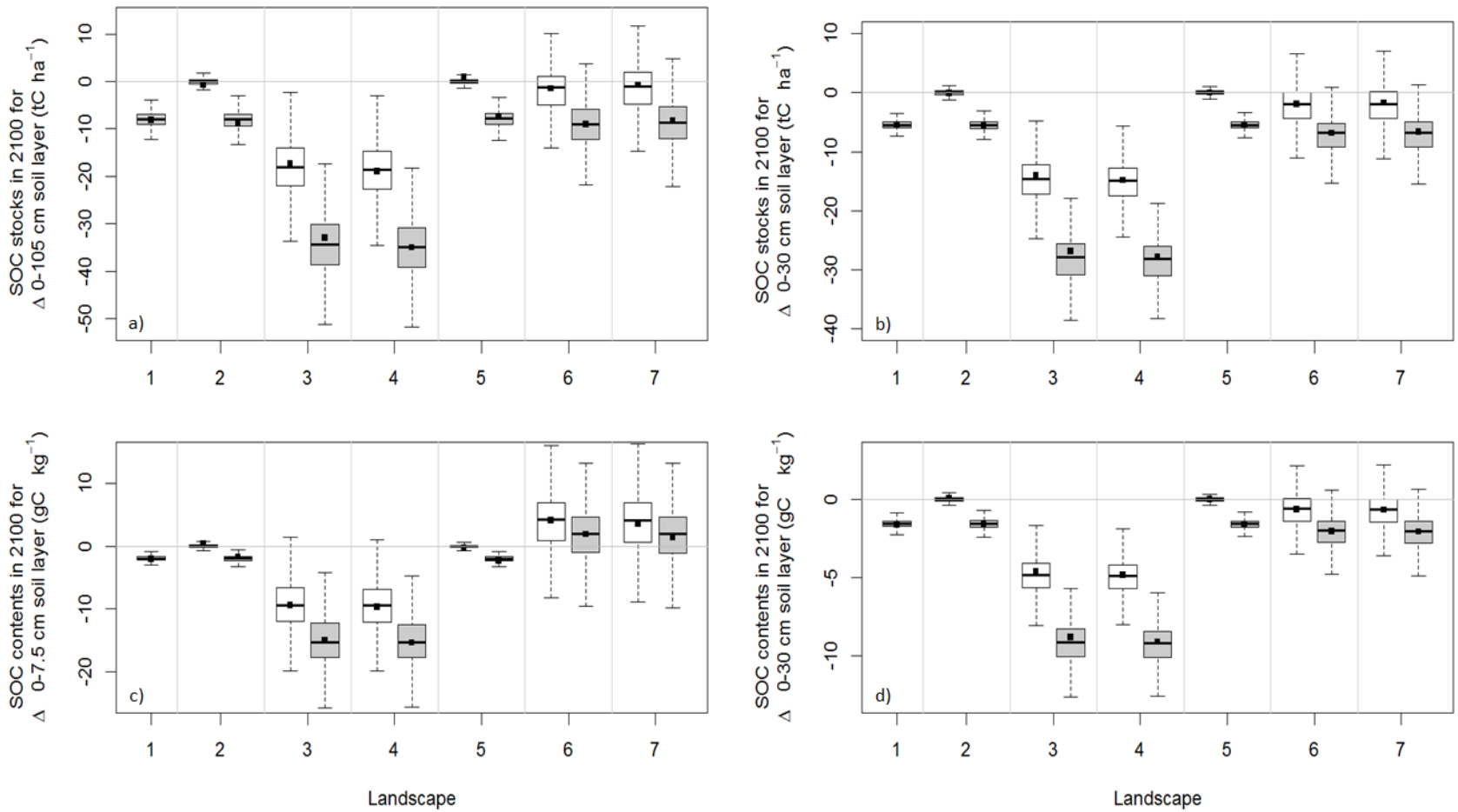

Figure 5-14. Differences in 2100 of SOC stocks (ΔSOC stocks) in the 0-to-105-cm (a) and 0-to-30-cm (b) soil layers and in SOC contents (ΔSOC contents) in the 0-to-30-cm (c) and in the 0-to-7.5-cm (d) soil layers, between each scenario and the reference scenario (BAU-1). White and grey box-plots represent respectively the BAU and the A1B climate scenarios. The landscape scenarios are presented on the X-axis (see Table 5-8 for details).

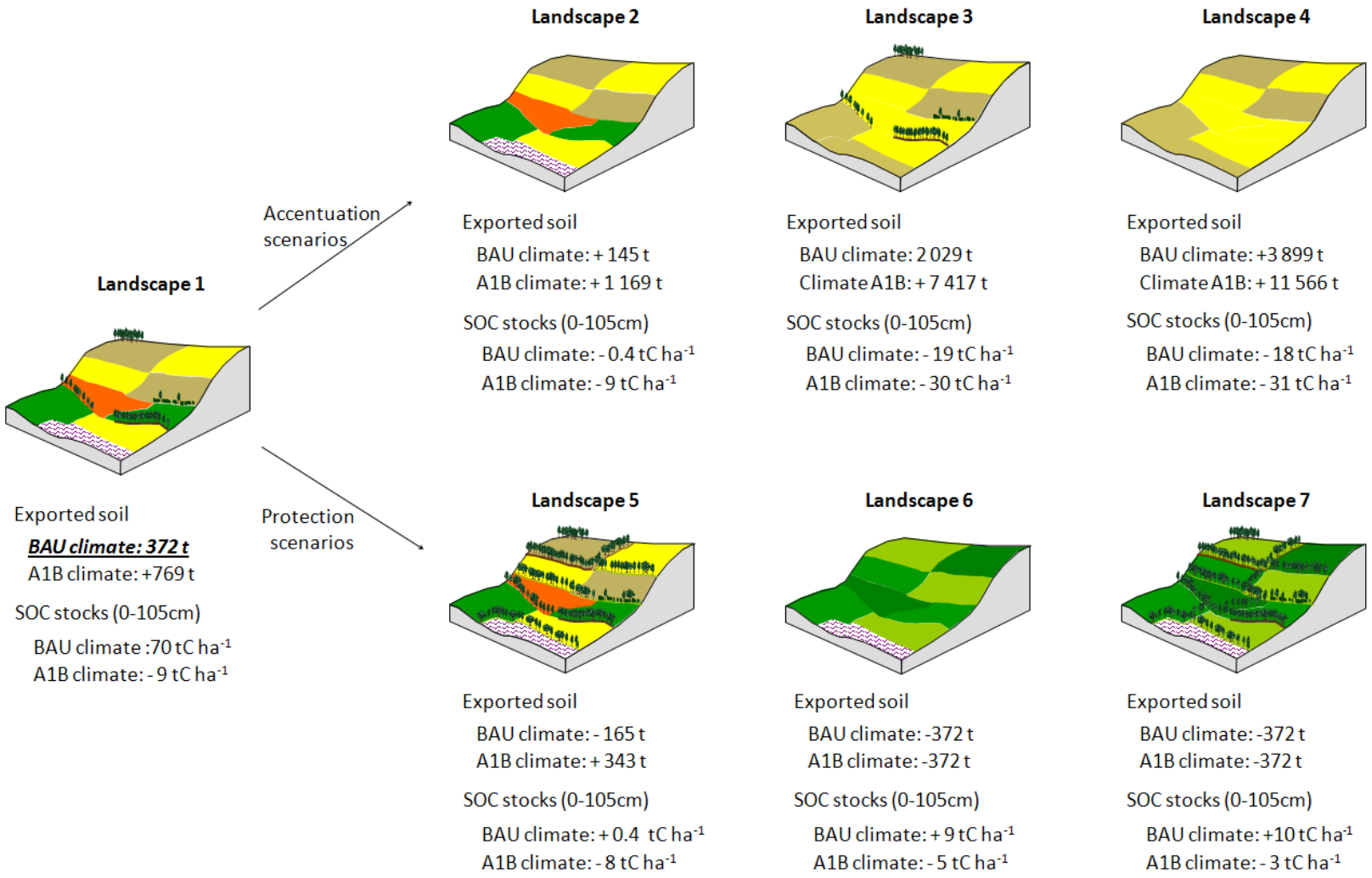

Figure 5-15. Synthesis of the simulation results (reference scenario underlined)

In comparison with the reference scenario, the percentage of the study area with SOC contents higher than 15 gC kg^{-1} decreased by 80% and 67 % for the 0-to-7.5 and 0-to-30 cm soil layers under the BAU-3 landscape scenario, by 83% and 69 % for the 0-to-7.5 and 0-to-30 cm soil layers under the BAU-4 landscape scenario, by 5% and 34 % for the 0-to-7.5 and 0-to-30 cm soil layers under the A1B-1 landscape scenario, by 92% and 71 % for the 0-to-7.5 and 0-to-30 cm soil layers under the A1B-3 landscape scenario and by 95% and 72 % for the 0-to-7.5 and 0-to-30 cm soil layers under the A1B-1 landscape scenario.

Discussion

Figure 5-15 summarizes the results of soil evolution modelling under changes in land use and climate.

Impact of land use and climate change on soil evolution

Both soil redistribution and SOC dynamics were sensitive to changes in land use and climate. Land use change in the fields had more impact on soil processes than climate change and changes in hedgerow network. Climate change induced degradation of soil properties, i.e. enhanced soil erosion and decrease in SOC stocks.

Soil redistribution

Land use in the fields had a major effect on soil redistribution, with impacts on both water and tillage redistribution processes. For instance, landscapes 3 and 4 showed the greatest soil redistribution rates, which was explained by enhanced water and tillage erosion, concomitant to longer periods of bare soil and more intense tillage.

The impact of climate on soil redistribution depended on the considered landscape, depicting interactions between climate and landscape. Landscapes 3 and 4 were more sensitive to climate change, with more soil redistribution inside the landscape and more soil exportation out of the study site. On the contrary, landscapes 6 and 7 were not sensitive to climate change: soil redistribution was not change with the climate change. Climate change had a major impact on water redistribution processes, especially in landscapes 3 and 5 (Figure 5-15). This may be explained by a longer period of bared soil due to intensive cropping, without winter cover. Climate change also slightly increased tillage erosion, showing interactions between soil redistribution by water and by tillage. Actually, soil redistribution by tillage is mainly dependent on local surface topography (curvatures): higher water redistribution induced changes in surface topography, and consequently changes in tillage erosion.

Our estimation showed a second order impact of the hedgerow network. For landscape 2, all the hedges were removed; however soil deposition still occurred in areas where the slope changes (bottomland and concave areas). Even if the proportion of deposited soil according to eroded soil was lower than for landscape 1, this soil deposition limited the impact of hedges removal. For landscape 4, no significant change in soil redistribution was estimated. Actually, the reference landscape (landscape 1) was well-designed to protect soils from erosion: hedges and grasslands were located in areas with the steepest slopes; grasslands were close to streams or ditches. The hedges added in landscape 4 were located in areas with smoother slope, less sensitive to soil erosion.

Our results showed that they were interactions between the impact of land use and the impact of the hedgerow network since soil exportations under BAU-4 were higher than the sum soil exportations under BAU-2 and BAU-3.

Overall, the main factor of soil redistribution change was the land use (associated to farming practices), then the climate, and finally the hedgerow network. This hierarchy of soil evolution factors results from comparison to the reference scenario (BAU-1).

Even for the most severe soil redistribution occurring under climate change and intensive cropping (A1B-3 and A1B-4), there was little impact of soil redistribution on soil loss out of the catchment. In fact, the maximum soil exportation (for BAU-4) was close to 12 000 t, which were equivalent to a mean soil erosion of 1 cm over the study area. However, the range of soil thickness variation was large for landscapes 3 and 4, with about 10% of the study areas with soil redistribution up to 10 cm at the end of the modelling period. The low impact of soil redistribution on soil thickness was also due to the initial characteristics of the soils of the study area, which had a mean soil thickness of 113 cm, but a large range of variation (15 to 778 cm). Nonetheless, such a soil loss may have a large impact on aquatic ecosystems (Turnpenny and Williams, 1980).

Previous studies on soil redistribution modelling under climate change showed similar results. Zhang and Nearing (2005) predicted an increased soil loss of 18 to 30% (according to tillage practice), for a mean annual precipitation decrease by 13.6% (agricultural watershed, Oklahoma). Michael et al. (2005) modelled soil erosion under climate change with less rainfall susceptible to produce runoff (-38%), but with an increase of total rainfall intensities (+23%), and showed that soil loss increased by 22 to 66% (study at the slope scale with conventional tillage, Germany).

SOC stocks and contents

A major impact of land use in the fields was simulated on SOC stocks and contents. Large decrease in SOC stocks following change to continuous wheat cropping is explained by the low C inputs to the soil by winter wheat residuals in farming systems where straw is exported from the fields, and by the absence of organic fertilization. The difference in average SOC stocks in the 0-to-30-cm soil layer between the continuous wheat scenario (BAU-3) and the permanent grassland scenario (BAU-6) (20 tC ha^{-1}) was similar to the decrease in SOC stocks following conversion from cropland to permanent grassland reported by Arrouays et al. (2002) for France (25 tC ha^{-1}). Hedgerows have little impact on SOC stocks at the landscape scale.

Climate change has a moderate impact on SOC dynamics and leads to a decrease in SOC stocks and contents in all the landscape scenarios. Considering the SOC model hypotheses, greater mineralization rates, explained by higher temperatures, were simulated under A1B climate scenario. Average decrease was 8 tC ha^{-1} under permanent grassland (A1B-6 compared to BAU-6) and 16 tC ha^{-1} under continuous wheat (A1B-3 compared to BAU-3). These values were of the same order of magnitude as those reported by Jones et al. (2009), who predicted a decrease in SOC stocks by 9 to 12 tC ha^{-1} in Europe between 1990 and 2080. The decrease in SOC stocks is contrary to the results of Brisson et al. (2010), who simulated a 4 tC ha^{-1} increase in SOC stocks under grasslands and a 3 to 4 tC ha^{-1} under maize-wheat-rate rotations in 2100. However Brisson et al. (2010) considered the indirect impacts of climate change on plant photosynthesis and on crop yields, which were not taken into account in our work, and did not model soil redistribution. Highest impact of climate change on SOC contents in the 0-to-7.5-cm and 0-to-30-cm soil layers under landscape 3 and 4 than under landscape 6 and 7 suggested the impact of soil redistribution on SOC dynamics when soil redistribution rates and soil losses were significant.

Methodology

In this study we investigated the impact of land use and climate change, and their interactions on soil evolution (soil redistribution, SOC stocks and contents), using a simulation approach based on

spatially distributed and dynamic soil models. Contrasted landscapes enabled to quantify the range of possible variations of soil processes between situations of maximum and minimum pressure on soils from anthropogenic activities, and to locate the current landscape in this variation range. This study appears innovative in two important aspects: first it provides a framework for a combined assessment of changes in anthropogenic and natural factors of soil evolution. Second, unlike other studies of soil erosion and SOC dynamics conducted at landscape scale (Dlugoss et al., 2012; Yoo et al., 2006), it fully supports soil and agroecosystem spatial heterogeneity.

For comparison purposes, the results were aggregated at landscape scale, without taking into account their spatial distribution. However, a more spatially distributed approach could be developed. It could for instance allow detailing the dynamic of soil redistribution at the vicinity of hedges, or in relation to soil variability in space, landscape structure, etc. The results could also be aggregated at the farm level to assess the impact of different farming systems on soil ecosystem services.

Soil evolution modelling could be improved by various modifications in soil processes modelling. A major enhancement would consist in the dynamic modelling of the soil surface characteristics changes, eg. surface crusting, soil roughness and vegetation cover, and the modelling of SOC change impacts on soil redistribution. Another point would be to have a better characterization of the eroded soil particle (size, SOC content...). Considering SOC dynamic, ongoing research aimed to better determine to SOC dynamics of eroded soil particles and buried SOC. However, few data were available to calibrate a SOC model for the landscape scale. It would be also crucial.

The scenarios tested could be were simples, but they appeared to be not so abstract and far removed from reality. In fact, two types of concern are facing in the present context. As the world population is growing, food safety is one of the main objective for many countries and lead to the increase of intensive cropping for food production. On the other hand, there is an increase of environmental concerns, which induced change in soil farming systems and landscape management: hedge strips and hedges planting, protection of permanent grasslands, no-till farming, etc. However, these scenarios could be improved to be better adapted to the social-economical context. Another important point would be to explore the impact of a same scenario of soil use, but considering various organisations of landscape elements in space, which could be a direct practical application of the spatially distributed models we used.

Conclusion

We modelled soil evolution from 2010 to 2100, at the scale of an agricultural landscape, under different scenarios of landscape and climate. These scenarios combined different land use (mixed dairy and hedgerow landscape, intensive cropping, grassland landscape), landscape management (hedges planting or removal), and climates (business-as-usual and climate change, with temperature and precipitations increase). We modelled soil redistribution (erosion and deposition) by water and tillage. The major factor of soil degradation was land use change: the landscape with the more intensive agricultural system showed increased soil erosion, both by tillage and water, and lower soil deposition. The second factor by importance was climate change, and finally landscape management. The landscapes didn't show the same sensitivity to climate change, and the more sensitive landscapes were those of intensive cropping. We found that the present landscape was well adapted to soil protection in a context of climate change, focusing on both carbon storage and soil erosion. However, this landscape appeared very sensitive to cropping intensification and therefore its preservation should be favoured to maintain soil ecosystem services.

Acknowledgements

This work was funded by the French National Research Agency (LandSoil progam, ANR-VUL-08-006-01). The authors thank the Z.A. Armorique (LTER-Europe, http://osur.univ-rennes1.fr/zoneatelier-armorique/) for LIDAR and land-use data provision, and the US INRA Agroclim - especially Frédéric Huard - for climate data provision.

Conclusion générale

Rappel des objectifs de la thèse

Soumis à des pressions anthropiques d'intensité croissante et dans un contexte de changement climatique, les sols évoluent à des pas de temps plus rapides que ceux de l'ordre du siècle ou du millénaire, appréhendés habituellement dans les approches de modélisation de la pédogenèse : des évolutions significatives des propriétés intrinsèques des sols ont ainsi pu être décrites à l'échelle de quelques décennies et c'est à ces échelles de temps que des variations significatives des conditions climatiques et des systèmes de production peuvent aussi se manifester. La dimension géographique de cette évolution des sols doit également être prise en compte, car les variations spatiales des propriétés intrinsèques des sols, de leur état initial, de leur position dans le paysage, mais aussi des modes de gestion, influencent fortement la réponse des sols à des forçages climatiques ou des évolutions globales des systèmes de production.

Dans ce contexte, l'objectif de ce travail était de développer une démarche de modélisation représentant l'évolution des sols au sein d'un paysage agricole complexe et sur une durée de quelques décennies, en tenant compte d'évolutions potentielles de la structure du paysage et du climat.

Principaux acquis de la thèse

Modélisation prédictive à haute résolution spatiale de la distribution 3D des sols

Les propriétés des sols varient spatialement, en fonction des différents éléments du paysage (Jenny, 1941) : topographie, matériau parental, occupation du sol, structure du paysage, pratiques agricoles, climat, etc. Dans un paysage bocager, l'épaisseur des sols, l'organisation des horizons et la distribution spatiale des stocks de carbone sont influencées par la présence de haies (Follain et al., 2007 ; Walter et al., 2003a).

Le couplage de méthodes statistiques a permis la cartographie prédictive fine en trois dimensions de plusieurs propriétés du sol nécessaires à la caractérisation des sols, et notamment à l'estimation des stocks de carbone (épaisseur des sols et des horizons organo-minéraux, densité apparente, teneurs en carbone). Ces cartographies ont reposées sur l'utilisation de méthodes d'apprentissage, permettant de relier les propriétés de sol à leurs facteurs de variations. Leur intérêt majeur est qu'elles peuvent être appliquées à des jeux de données restreints et irréguliers du point de vue de leur localisation spatiale. Cependant, il est nécessaire que le jeu de calibration utilisé représente au maximum la variabilité des déterminants de la propriété d'intérêt. Ces méthodes d'apprentissage ont donc été couplées à un échantillonnage en Hypercube Latin conditionné (cLHS) (Minasny and McBratney, 2006a), qui a permis de réaliser un échantillonnage de calibration parcimonieux, mais représentatif du site d'étude. L'utilisation d'un MNT à fine résolution spatiale (2 m), issu d'une prospection aéroportée LiDAR, a été déterminante pour la prise en compte des variations fines de la topographie, impactée à courte distance par la structure du paysage, et principalement par les haies.

La quantification de l'incertitude des cartes produites est une étape indispensable dans le cadre de la cartographie numérique des sols. L'utilisation d'un jeu de données de calibration limité a permis de concentrer des moyens pour la mise en place d'un jeu de validation indépendant, permettant une estimation rigoureuse et non biaisée de la qualité des cartes produites. Nous

montrons ainsi que les estimations de stocks de carbone dans l'espace géographique sont connues avec une précision moyenne de l'ordre de 25 t ha^{-1} et que les sources principales d'incertitude sont les estimations des teneurs en carbone. Celles-ci ont été prédites avec une erreur moyenne absolue de 3 g kg^{-1}, alors que la masse volumique a été estimée avec une erreur moyenne absolue de 0,15 g cm^3.

La cartographie prédictive des propriétés des sols a permis l'évaluation exhaustive des stocks de carbone organique du sol à l'échelle du paysage, en intégrant une épaisseur totale de 105 cm. A l'échelle du site atelier de Pleine-Fougères, les stocks de carbone du sol jusqu'à 105 cm sont en moyenne de 89 tC ha^{-1} et varient dans une large gamme de 5 à 360 tC ha^{-1}. Dans l'horizon 0-30 cm, la moyenne des stocks est de 58 tC ha^{-1} et l'étendue comprise entre 3 et 175 tC ha^{-1} : il s'agit de stocks globalement importants si on les compare à des statistiques nationales (42 tC ha^{-1} dans les 30 premiers cm de sol pour des terres arables, (ARROUAYS ET AL., 2002)). Les stocks profonds, i.e. situés à une profondeur supérieure à 30 cm, représentent en moyenne 33% des stocks totaux ; cette valeur est cependant très variable selon l'occupation du sol et la situation dans le paysage. Ainsi, la proportion des stocks de carbone profonds atteint un maximum de 83% en amont de certaines haies.

Les cartographies prédictives produites montrent une forte variabilité spatiale des stocks de carbone des sols, particulièrement en ce qui concerne les stocks profonds. Dans le modèle de prédiction dérivé des mesures de terrain, la variabilité spatiale des stocks de carbone profonds dépend majoritairement de la topographie et de la position par rapport aux haies, alors que la variabilité des stocks de surface est surtout corrélée à l'occupation du sol des parcelles cultivées. Cependant, la présence d'une haie modifie localement les stocks de carbone, de surface et de profondeur. Ceci s'explique par des apports directs de matière organique par la canopée et par les racines, mais aussi par des processus de redistribution des sols (érosion - sédimentation) (Follain et al., 2009 ; Walter et al., 2003a).

Cette description de la variabilité spatiale des stocks de carbone vient en appui aux politiques publiques qui visent à rémunérer la séquestration de carbone dans les sols, mais supposent des protocoles simples de vérification d'un stockage effectif. Nous montrons qu'une approche simplifiée est envisageable pour la quantification des stocks de surface, en se basant sur les occupations du sol, les rendements des cultures, le mode de gestion des résidus de culture et les types d'amendement organique. Des incertitudes perdureront cependant dans le cadre d'un paysage bocager. L'estimation des stocks profonds apparaît plus délicate et très dépendante de la topographie, des redistributions de sols et de la structure du paysage.

Modélisation dans l'espace et dans le temps de l'évolution des sols

Dans le cadre de ce travail, nous avons modélisé à l'échelle d'un paysage l'évolution dynamique et spatialisée des sols. Ceci a permis de prendre en compte les flux d'eau et de sédiments entre les différents compartiments du paysage, de considérer l'impact de la redistribution des sols sur l'évolution des stocks de carbone et d'intégrer des éléments dont les dynamiques temporelles varient à différents pas de temps, allant de l'événement pluvieux au siècle.

La calibration du modèle de redistribution des sols (LandSoil) pour son application à notre zone d'étude a été possible grâce à la disponibilité de mesures de terrains sur des sols comparables à ceux du site atelier de Pleine-Fougères. Cette calibration n'a pas pu être réalisée pour le modèle de dynamique du carbone, faute de données. L'utilisation de données expérimentales pour la

calibration d'un modèle permet de s'assurer de la validité du modèle dans le contexte de l'étude, mais de telles données ne sont pas toujours disponibles. Des méthodes isotopiques, intégratives des variations passées, ont montré leur intérêt pour la calibration de modèles de redistribution des sols. Cependant, l'utilisation du ^{137}Cs s'est avérée délicate dans le contexte d'un paysage bocager, les haies pouvant perturber les retombées de ^{137}Cs au sol.

L'utilisation d'un MNT à haute résolution (LiDAR) a permis de représenter les variations à courte distance de la topographie (pentes et courbures), ce qui est important pour la modélisation de la redistribution des sols en interaction avec les éléments linéaires du paysage. Cependant, un tel MNT comporte un certain « bruit », constituant une variation indésirable et non réaliste de l'altitude, auquel le modèle de redistribution des sols est très sensible. L'utilisation d'un MNT fin nécessite donc qu'il soit traité en amont des modélisations, pour ne garder que l'information pertinente. Une des corrections classiques est par exemple de supprimer toutes les objets au-dessus de la surface du sol, comme les infrastructures humaines ou la végétation (Sharma et al., 2010). Ces traitements sont cependant complexes et les méthodes pour les réaliser constituent un champ de recherche à part entière (par exemple Li et al., 2011 ; Liu, 2008).

Les scénarios de paysage que nous avons conçus sont très simplificateurs. Ils constituent cependant des situations contrastées qui ont permis d'estimer l'amplitude de variation possible de notre système, ce qui n'avait encore jamais été réalisé dans notre contexte, i.e. pour la modélisation couplée de la dynamique du carbone et de la redistribution des sols, à l'échelle d'un paysage bocager. On peut néanmoins noter que ces scénarios sont cohérents avec les grandes tendances socio-économiques actuelles. Dans un contexte d'augmentation de la population mondiale, la volonté d'assurer la sécurité alimentaire des pays se renforce et provoque dans différentes régions une intensification de la production agricole. Cette situation correspond aux scénarios défavorables à la protection des sols que nous avons implémentés. D'un autre côté, le développement de préoccupations environnementales pousse à considérer davantage la protection de l'environnement et des ressources naturelles : ceci se traduit au niveau agricole par une simplification du travail du sol, un intérêt renforcé pour les prairies, la mise en place de bandes enherbées et la préservation voire l'implantation de haies. Le paysage stationnaire que nous avons implémenté (correspondant au paysage actuel), comprend déjà des zones d'agriculture intensive et des zones de prairies : la conception des scénarios extrêmes, favorisant la dégradation ou la protection des sols, a seulement consisté en la généralisation des zones de prairies ou de cultures intensives sur l'ensemble du secteur d'étude.

Enfin, la comparaison de l'état final des scénarios à l'état final d'un scénario de référence (scenario stationnaire) a permis de s'affranchir des incertitudes sur les données d'entrée des modèles. L'initialisation est en effet un point crucial en modélisation et les incertitudes que comportent les données d'entrée se propagent jusqu'aux résultats, souvent amplifiées par les incertitudes liées à la structure même du modèle. La comparaison à un scénario de référence permet donc de gommer ces incertitudes, en supposant que les résultats des scénarios présentent tous les mêmes incertitudes puisqu'ils sont produits à partir des mêmes données d'entrée et des mêmes modèles.

Structure du paysage et sensibilité des sols au changement global

La modélisation couplée de l'évolution des sols a permis d'identifier les processus et déterminants majeurs de l'évolution des sols au sein de notre site d'étude. La Figure 5-16 présente les principaux résultats obtenus pour trois scénarios contrastés : le scénario stationnaire, un scénario menant à une

dégradation des sols et un scénario favorisant la protection des sols. Les paragraphes suivants font un bilan des processus et des déterminants majeurs de l'évolution des sols.

Redistribution des sols

La modélisation de la redistribution des sols a été menée en intégrant les processus hydriques et aratoires à l'origine de l'érosion et de l'accumulation des sols.

En ce qui concerne le paysage stationnaire, l'estimation des taux de redistribution moyens sur la période 2010-2100 montre une légère prédominance de l'érosion par rapport à l'accumulation à l'échelle de la zone d'étude (le taux de redistribution moyen ayant été estimé à -0,14 t ha^{-1} an^{-1}). Les taux de redistribution estimés sont très dépendants de l'occupation du sol et des pratiques culturales, qui influent sur les paramètres de surface de sol. Dans notre cas, ce faible taux moyen de redistribution s'explique par le fait que l'occupation du sol est très liée à la topographie du site d'étude. Les cultures intensives, créant des situations plus favorables à l'érosion, se situent sur de grandes parcelles au niveau du plateau ; les prairies et les haies sont localisées au niveau des zones les plus sensibles à l'érosion ou proches des exutoires. La redistribution des sols est majoritairement due au travail du sol, provoquant des redistributions de l'ordre de 5 t ha^{-1} an^{-1} (accumulation ou érosion). Les estimations de redistribution hydrique sont plus faibles (érosion de -0,14 t ha^{-1} an^{-1} en moyenne). Ces résultats sont cohérents avec des études antérieures, qui montrent que l'érosion aratoire peut être à l'origine de redistributions majeures de sols dans les paysages (Van Oost et al., 2005b). Cependant, l'intensité des redistributions de sols dus aux processus hydriques est très variable dans le temps, et dépend de l'effet combiné des états de surface du sol et des caractéristiques des événements pluvieux. Ces deux processus, aratoire et hydrique, provoquent à la fois l'érosion et l'accumulation des sols. La localisation des zones d'accumulation dépend de la topographie du site, i.e. des zones de rupture de pente et des zones concaves. Même si nos estimations montrent que le travail du sol est majoritairement responsable des déplacements de sol, cette redistribution reste intra-parcellaire. Les pertes nettes de sol, exporté hors du site d'étude, sont liées à l'érosion hydrique.

Stocks de carbone et impact de l'érosion sur les stocks de carbone

La variabilité spatiale et temporelle des stocks de carbone est très dépendante de l'occupation des sols et des pratiques agricoles, déterminant les apports de carbone par amendement organique et par la gestion des résidus de culture. A la fin de la période de simulation, les stocks moyens de carbone pour le scénario de référence (paysage et climat stationnaire) sont estimés à 70 tC ha^{-1} sur l'épaisseur 0-105 cm. Les stocks profonds (i.e. au-delà de 30 cm) représentent 25% des stocks totaux. Les stocks totaux diffèrent peu selon l'occupation du sol, même s'ils sont légèrement plus élevés pour les prairies permanentes. Les variations les plus importantes ont été estimées pour les teneurs en carbone dans les premiers cm de sol (épaisseur 0-7,5 cm).

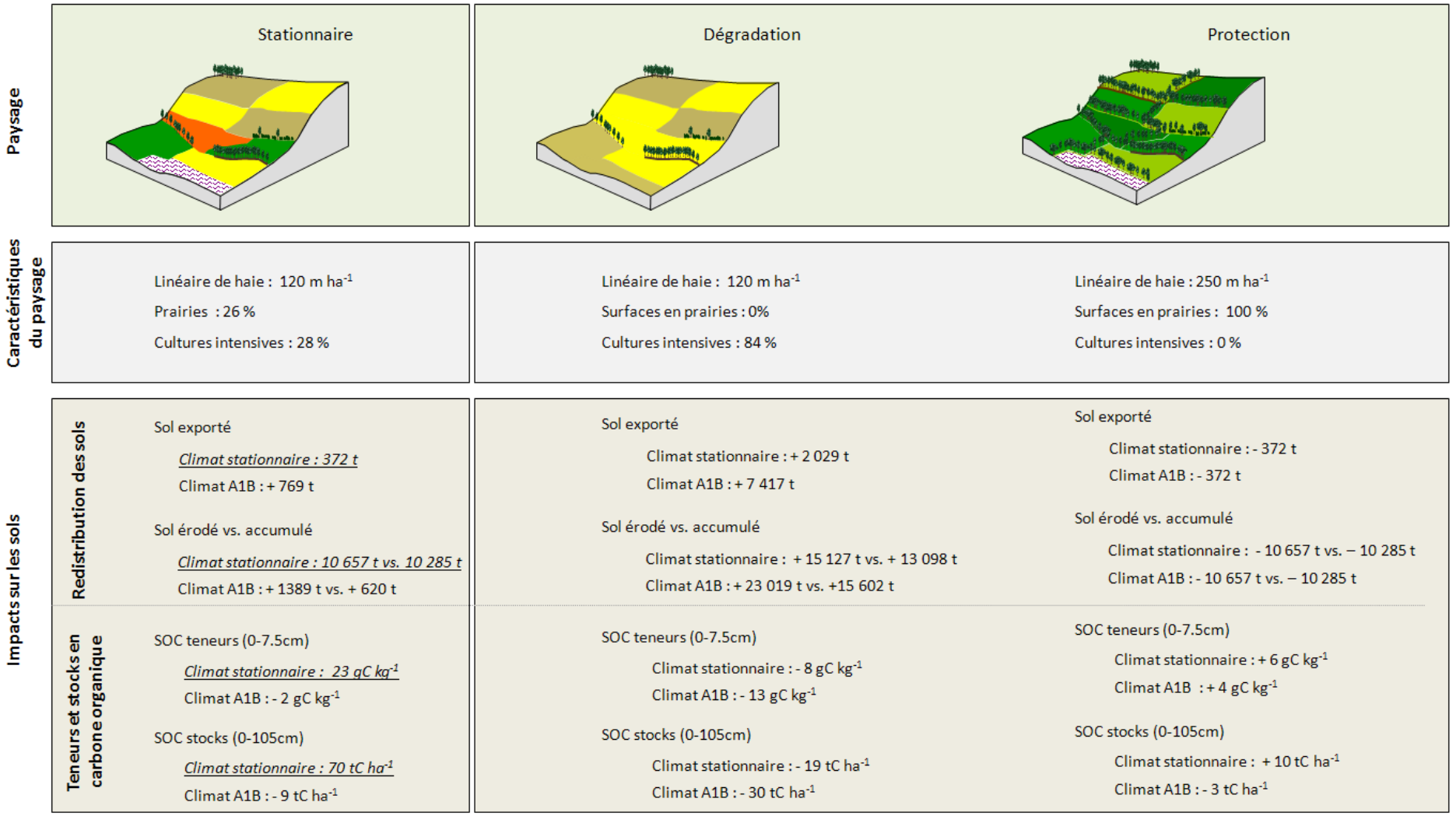

Figure 5-16. Impact de la structure du paysage et du climat sur l'évolution des sols à l'échelle d'un paysage : synthèse des résultats de simulation. Les résultats sont donnés en comparaison au scénario stationnaire (italique souligné) après 90 années de simulation. SOC : carbone organique du sol.

Nos résultats contribuent au débat sur l'effet des processus de redistribution de sol sur le stockage de carbone dans les sols. Les études antérieures sont contradictoires quant à l'impact de la redistribution des sols sur les stocks de carbone à l'échelle du paysage. Lal et Pimentel (2008) soutiennent que l'érosion conduit à perte nette de carbone. Ils sont contestés par Van Oost et al. (2007 ; 2008) qui rapportent le phénomène inverse. Dans ce travail, nous avons modélisé l'évolution des stocks de carbone en prenant ou non en compte la redistribution des sols. Nos résultats montrent que l'érosion conduit à une légère perte nette de carbone (de l'ordre de 1 kg ha^{-1} an^{-1}). Nous avons également estimé que les zones de dépôts présentaient des stocks de carbone totaux plus importants que les zones d'érosion. La perte nette de carbone est majoritairement liée à la perte nette de sol, exporté hors du site d'étude. Une accumulation en amont des haies a été modélisée, mais elle reste faible. Le carbone érodé a donc été peu enfoui par le biais de la redistribution des sols, ce qui n'a pas abouti à une réduction significative de la minéralisation du carbone.

L'impact de l'érosion sur les stocks de carbone paraît fortement conditionné par le devenir du carbone déplacé (enfouissement ou exportation) et par l'évolution de sa dynamique de minéralisation, tant au niveau des horizons profonds qu'au niveau des sites d'érosion. La minéralisation du carbone pendant son transport est également à considérer. Van Oost et al. (2006) ont modélisé l'impact de l'érosion sur les stocks de carbone en testant différentes hypothèses portant sur la dynamique du carbone des particules érodées pendant le transport et la dynamique du carbone profond. Ils concluent que l'érosion peut conduire selon les cas à un stockage ou à une perte nette de carbone. Récemment, Doetterl et al. (2012) ont estimé que les processus d'érosion menaient à la stabilisation du carbone au niveau des zones d'accumulation (le carbone y étant plus stable car protégé physiquement), mais aussi au niveau des zones d'érosion (le carbone provenant d'anciens horizons profonds étant plus stable). Le bilan conduirait à un stockage net de carbone. Cependant, ces auteurs ne prennent pas en compte le phénomène de « priming effect » démontré par diverses études (par exemple Fontaine et al., 2007) : quand le carbone profond est à nouveau en présence de matière organique fraîche (ce qui est le cas s'il est mélangé aux horizons de surface dans les zones d'érosion), les microorganismes du sol sont à même de le décomposer. La minéralisation du carbone s'en trouve donc augmentée. La stabilité de la matière organique dans les horizons de sols profonds est également dépendante de ce phénomène (Rumpel and Koegel-Knabner, 2011). Le déterminant principal de la dynamique du carbone profond semble être la distribution spatiale de la matière fraîche, du carbone stable et des microorganismes. Les processus pédologiques contrôlant leurs distributions doivent donc être pris en compte, ce qui est complexe à l'échelle du paysage. D'autres facteurs, tels que le changement de température, l'apport de nutriments, d'énergie ou la présence ou non d'oxygène, sont également à prendre en compte. Cependant, les études réalisées sont majoritairement des approches en laboratoire, ce qui rend leur généralisation difficile à l'échelle de la parcelle, et encore plus du paysage. Berhe (2012) souligne notamment que les taux de minéralisation de la matière organique varient en fonction de la position dans le paysage.

L'estimation plus fine de l'impact de la redistribution des sols sur les stocks de carbone nécessite donc de faire le bilan entre sites d'accumulation et d'érosion, enfouissement de carbone et minéralisation, tout en prenant en compte les exportations nette de sol. L'échelle du paysage est donc parfaitement adaptée pour ce type de bilan.

Effets attendus du changement climatique en interaction avec le paysage

Selon le GIEC (2007), le changement climatique devrait se manifester par une hausse de la température mondiale comprise entre 1,4 et 5,8°C, mais avec de fortes disparités selon la région considérée : une hausse de la sécheresse devrait être observée dans certaines zones, alors que d'autres régions seront confrontées à l'augmentation des précipitations et particulièrement des événements extrêmes. Le programme Climaster a conclu que le climat de l'ouest de la France avait déjà changé au cours du XX^{ème} siècle (Merot, 2011). Les simulations utilisées dans ce travail étaient issues du modèle Arpège de Météo France et régionalisées selon une méthode des Quantiles-Quantiles développée par l'INRA (Deque, 2007). Sous l'impact du changement climatique (climat A1B), l'évolution climatique simulée à Pleine-Fougères est caractérisée par une hausse sur 100 ans de la température mensuelle moyenne de 2 à 4°C, et par une baisse des précipitations mensuelles moyennes. Cependant, une augmentation de la fréquence des événements pluvieux importants susceptibles de provoquer du ruissellement est également simulée. Ces événements sont en moyenne plus brefs, mais aussi plus intenses.

La Figure 5-17 récapitule les résultats obtenus quant à la redistribution des sols et à la variation des stocks de carbone pour les différents scénarios modélisés. D'après les modélisations réalisées, le changement climatique affecte à la fois la redistribution des sols et le stockage de carbone dans les sols, mais tous les paysages ne présentent pas la même sensibilité (Figure 5-17).

En ce qui concerne les stocks de carbone, le changement climatique impacte tous les paysages avec la même amplitude en moyenne : il provoque un déstockage moyen de carbone 11 tC ha^{-1}, résultant de l'augmentation de la minéralisation due à une augmentation de la température. Il apparait donc qu'il n'y a pas d'interaction forte entre le type de paysage et le changement de climat en ce qui concerne les évolutions de stocks de carbone. De précédentes études ont estimé que le changement climatique pouvait conduire à des pertes ou à un stockage de carbone. Jones et al. (2009) estiment par exemple que le changement climatique seul, sans changement de production primaire, va entrainer des pertes de l'ordre de 9 à 12 tC ha^{-1}. Par contre, la tendance s'inverse si des changements de production primaire et des adaptations technologiques sont considérés. Le changement climatique peut avoir simultanément un effet positif et un effet négatif sur le stockage du carbone dans les sols, car il peut à la fois augmenter la production de biomasse et la minéralisation du carbone (Harrison et al., 2008). Le programme Climator conclut globalement à un effet de stockage de carbone quelle que soit la culture (Brisson and Levrault, 2012). Cependant, ces résultats proviennent de modélisations à l'échelle de la parcelle, qui n'intègrent pas les redistributions de sol. A l'échelle globale, la plupart des travaux tendent à prédire un déstockage du C du sol avec le changement climatique (Eglin et al., 2010). Néanmoins, l'évolution future des stocks de carbone et la réponse au changement climatique dépendent fortement des occupations du sol passées et donc de l'état des stocks par rapport à un état d'équilibre.

En ce qui concerne la redistribution des sols, les scénarios les plus favorables à la préservation des sols (occupation du sol en prairie permanente) n'apparaissent pas sensibles au changement climatique. En effet, étant donné que les sols ne sont pas travaillés et sont en permanence couverts, aucune redistribution de sol n'est modélisée. Pour tous les autres scénarios, le changement climatique conduit à l'augmentation de l'érosion hydrique, et donc à des augmentations des exportations nettes de sols. Ce résultat est en accord avec ceux du programme Climaster, qui prévoit une augmentation de l'aléa érosif au niveau dans l'ouest de la France en réponse au changement climatique. D'autres études ont cherché à quantifier l'impact du changement climatique sur l'érosion

à l'aide de démarches de modélisation. Par exemple, Zhang et Nearing (2005) ont prédit une augmentation des pertes de sols de 18 à 30% (selon le type de travail du sol), pour un climat caractérisé par une diminution des précipitations annuelles moyenne de 13.6% (étude réalisée à l'échelle d'un bassin versant, Oklahoma). Michael et al. (2005) ont modélisé l'érosion des sols sous un climat montrant une diminution de 38% des événements susceptibles de produire du ruissèlement, mais avec une augmentation des intensités de 23%, et ont prédit des augmentations de pertes de sols de 22 à 66% (étude sous labour conventionnel à l'échelle d'un versant, Allemagne).

Les paysages les plus simples, mais caractérisés par une agriculture plus intensive, montrent une plus grande sensibilité au changement climatique, contrairement aux paysages plus complexes (avec des associations de cultures et la présence de haies). La structure du paysage a donc une grande importance quant à la capacité d'un paysage à atténuer l'impact du changement climatique sur les sols. Le paysage actuel (paysage de bocage orienté vers l'élevage laitier, avec imbrication de prairies et de cultures) apparait être le paysage le plus résilient parmi les combinaisons testées, mis à part les paysages où les prairies constituent l'unique occupation du sol. C'est en effet le paysage qui semble le mieux à même de résister à des changements de climat : il présente des variations de stock de carbone total équivalentes aux autres scénarios (Figure 5-17a), une diminution des teneurs en carbone de surface inférieure aux paysages en agriculture intensive (Figure 5-17b) et des pertes de sol inférieures aux autres scénarios (Figure 5-17). Ceci est surtout dû à la structure de ce paysage et à son organisation dans l'espace : les cultures intensives sont localisées au niveau des zones les moins sensibles à l'érosion, alors que des haies perpendiculaires à la pente et des prairies sont situées au niveau des zones les plus sensibles (pentes fortes, exutoires). Les paysages de bocage sont très répandus, en France et de par le monde, et sont confrontés à de nombreuses dégradations, même si les préoccupations environnementales actuelles tendent à les préserver : l'intensification de l'agriculture provoque l'agrandissement des parcelles par arasement des haies, et il est fréquent que des prairies permanentes soient retournées pour augmenter les zones de production (Baudry and Jouin, 2003). Il semble donc nécessaire d'être vigilant quant à la préservation de tels paysages, dans un but de protection des sols.

Hiérarchie des facteurs d'évolution des sols

Nos résultats montrent que le facteur majeur d'évolution des sols est l'occupation des sols, suivie par le changement climatique et enfin par la présence de haies.

Concernant la redistribution des sols, une intensification de l'agriculture provoque une augmentation des exportations de sol de l'ordre de 2 000 t par rapport au scénario de référence, alors que le changement climatique induit une augmentation de 770 t (Figure 5-16). De la même manière, les stocks de carbone totaux diminuent de 19 tC ha^{-1} sous l'effet de l'intensification de l'agriculture, alors qu'ils diminuent de 9 tC ha^{-1} sous l'effet du changement de climat (Figure 5-16).

Quel que soit le processus considéré, redistribution des sols ou variation des stocks de carbone, l'effet présence versus absence de haie reste inférieur à ceux du changement de l'occupation du sol ou du climat. L'arasement et la plantation de haie diminuent ou augmentent respectivement les stocks totaux de carbone de l'ordre de 0.5 tC ha^{-1}, et les exportations de sols de l'ordre de 150 t. La proportion de sol accumulé au sein du paysage, par rapport au sol érodé, est très légèrement favorisée par la plantation de haie (1%). Il faut cependant noter que la topographie initiale reste la même quel que soit le scénario. Dans le cas du scénario sans haie, l'accumulation s'effectue toujours en partie au niveau des zones de rupture de pente.

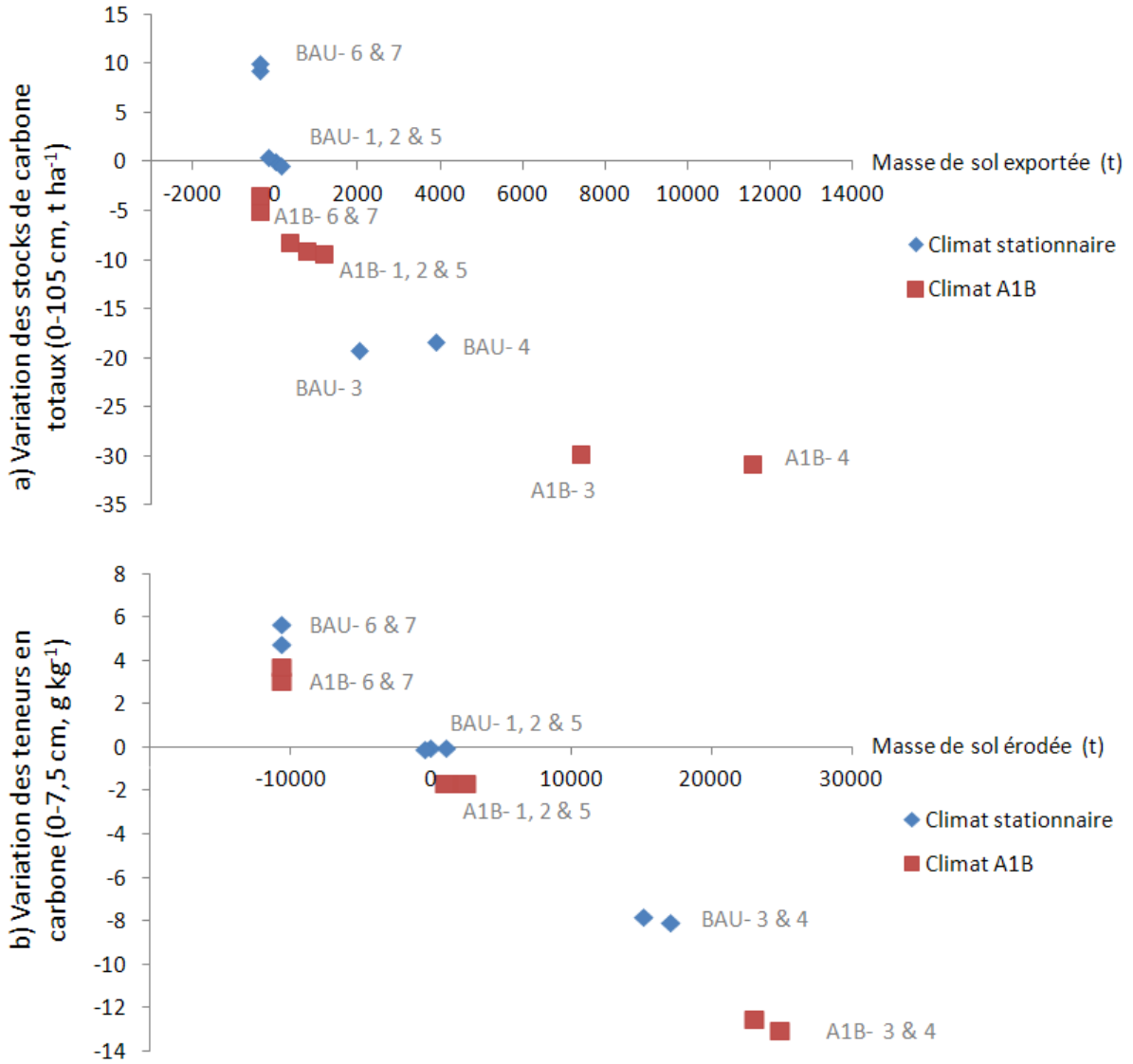

Figure 5-17. Impact du changement climatique sur les stocks carbone et les redistributions de sol. Résultats des différents scénarios donnés en comparaison au scénario de référence (BAU-1) après 90 années de simulation. Scénarios climatiques : BAU = climat stationnaire, A1B = changement climatique. Scénarios paysage : 1 = occupations du sol et haies stationnaires, 2= occupation du sol stationnaire et pas de haies, 3 = blé et haies stationnaires, 4 = blé et pas de haies, 5 = occupation du sol stationnaire et haies maximales, 6 = prairies et haies stationnaires, 7 = prairies et haies maximales.

Limites de l'étude

Difficultés liées à la modélisation à haute résolution spatiale

Malgré la disponibilité croissante de données spatialisées et les progrès en matière de temps de calcul, la modélisation des sols à haute résolution spatiale à l'échelle du paysage se heurte encore à des difficultés méthodologiques. Cette approche nécessite un effort d'acquisition de données d'entrée spatialisées. Toutes les données ne sont pas toujours disponibles et n'ont pas toutes les

mêmes résolutions spatiales, ce qui peut conduire à une augmentation des incertitudes quant aux propriétés initiales des sols.

La représentation du paysage pourrait être optimisée en adaptant la résolution spatiale à la complexité locale des éléments du paysage : l'intérêt d'une modélisation à une résolution spatiale de l'ordre du mètre est de pouvoir intégrer dans la modélisation des éléments linéaires (haies, talus, fossés, bord de champs), dont les effets sont mal représentés dans les approches classiques de représentation du paysage fondées sur des mailles de 20 à 50 m. Mais, cela conduit à des calculs sur de très nombreuses mailles (210 000 sur la zone d'étude), dans des situations voisines souvent semblables et qui pourraient être regroupées : ainsi des mailles au centre des parcelles dans un contexte topographique homogène sont considérées l'une après l'autre alors qu'elles pourraient être aisément regroupées, ce qui simplifierait l'approche et réduirait drastiquement les temps de calcul. Les pistes d'amélioration viennent d'une représentation multi-résolution des paysages agricoles, s'adaptant à la complexité du système étudié, en adaptant une résolution spatiale fine à proximité des structures sensibles et plus lâche au-delà : des développements techniques récents, s'appuyant notamment sur la théorie des ondelettes, laissent augurer des avancées dans ce mode de représentation à résolution multiple (McBratney et al., 2003 ; Strand et al., 2006).

Représentation simplifiée des sols et des processus pédologiques

Diverses simplifications ont été adoptées pour représenter les sols et les processus qui régissent le stockage de carbone et les processus d'érosion et de sédimentation.

Concernant la modélisation de la redistribution des sols, les points sensibles sont les suivants :

- la sensibilité des sols à l'érosion dépend des paramètres d'état de surface des sols, à savoir la couverture végétale, la rugosité et le faciès, est définie de manière fine par parcelle. La variabilité spatiale de la sensibilité des sols à l'érosion, à l'échelle du paysage mais aussi à l'échelle intra-parcellaire n'est donc pas prise en compte. Cela peut mener à sous-estimer ou à surestimer l'érosion selon la zone considérée. Cros-Cayot (1996) a par exemple montré que le ruissellement et l'érosion des sols variaient au sein d'une parcelle, en fonction de la topographie locale mais aussi en fonction des variations des propriétés de sols comme la texture ou la teneur de carbone ;
- l'évolution des états de surface est définie mensuellement pour une culture donnée. La rugosité et le faciès ne varient donc pas dynamiquement sous l'impact des événements pluvieux, et la couverture végétale n'évolue pas en fonction de la croissance des cultures. Ceci peut également mener à sous-estimer ou à surestimer l'érosion selon la zone et la culture considérée, surtout dans un contexte de changement climatique ;
- l'érosion sélective des particules par érosion hydrique diffuse n'est pas modélisée. Or, des études ont montré que l'érosion diffuse et la sédimentation des particules de sols étaient fortement liés à la taille des particules (par exemple Issa et al., 2006; Leguedois, 2003). A long terme, la redistribution sélective des particules de sol peut avoir un impact sur la qualité des sols et sur leur sensibilité à l'érosion, d'autant plus qu'elle implique également une érosion sélective des matières organiques (Lal, 2003). La prise en compte de ce processus semble donc importante dans le cadre de la modélisation de l'évolution des sols sur des périodes de l'ordre du siècle ;

- le modèle de redistribution des sols que nous utilisons ne permet pas de modéliser la provenance des particules de sol déplacées. Les propriétés des sols ne changent donc pas au cours de la modélisation. Le routage de ces particules permettrait de définir leur origine et leurs caractéristiques (texture, teneur en carbone) et donc de modifier les caractéristiques des sols que leur redistribution modifient.

Concernant la modélisation de la dynamique du carbone, il semble nécessaire de mieux considérer les points suivants :

- la modélisation de la dynamique du carbone dans les horizons profonds ne prend en compte que les variations d'humidité et de température, mais l'influence d'une activité biologique réduite ou l'effet de l'hydromorphie n'ont pas été intégrés. Ces processus sont cependant difficiles à modéliser à l'échelle du paysage, et les données nécessaires à la calibration des modèles sont peu disponibles à cette échelle ;
- la dynamique du carbone dans les particules érodées, pendant le transport et au niveau des sites de dépôts, est définie de la même manière que dans tout horizon de sol. Or, il semblerait que l'érosion conduise à une augmentation de la minéralisation des particules érodées, suite à la désagrégation de ces particules (Lal, 2003). Il est donc possible que nous sous-estimions l'impact de l'érosion sur les stocks de carbone.

Enfin, concernant le couplage des processus pédologiques, il apparait important de prendre en compte l'impact de la variation des stocks de carbone sur l'érosion des sols. En effet, la sensibilité des sols à l'érosion dépend en partie de leur teneur en matières organiques (Chenu et al., 2000). Il est donc probable que nous sous-estimions les redistributions des sols, étant donné que nous ne prenons pas en compte l'effet de la diminution des stocks de carbone sur l'érosion.

Validations et incertitudes

Les modèles utilisés ont été validés et appliqués dans différents contextes, mais ces validations sont réalisées sur des temps plus courts que les temps de simulation, et sur des étendues spatiales plus restreintes.

La validation des modèles se fait généralement en reconstituant des évolutions passées des sols (par exemple Ciampalini et al., in press ; Coleman et al., 1997). Cependant, on suppose dans ce cas que les processus contrôlant la dynamique des processus modélisés ne varient pas lors de modélisations prospectives, et que leur hiérarchie reste constante. Ceci n'est pas forcément le cas à l'échelle du paysage et dans un contexte de changement climatique.

D'autre part, il n'est pas aisé de valider des modèles distribués à l'échelle du paysage. Dans le cadre de l'évolution des sols, les mesures et les observations pédologiques sont peu intégratives spatialement : la validation des modèles suppose donc une répétition de mesures dans l'espace, qui peut être lourde à mettre en œuvre. Certaines mesures faites à l'exutoire d'un bassin versant peuvent permettre d'intégrer l'ensemble des processus internes à celui-ci. Par exemple la mesure des concentrations en sédiments à l'exutoire d'un bassin versant peut permettre d'estimer l'intensité de l'érosion. Cependant, ces mesures ne renseignent pas sur la redistribution des sols au sein des parcelles. Il est de plus difficile d'obtenir des données adéquates pour valider des modèles représentant des flux d'eau et de matière (Bouma et al., 1998).

La mise en relation avec des observatoires à long terme à l'échelle du paysage pourrait consister une piste pour la validation des mécanismes modélisés, en permettant de constituer des jeux de données distribués dans le temps et dans l'espace.

Un des problèmes majeurs en modélisation reste la quantification des incertitudes, particulièrement lorsqu'il s'agit d'utiliser un modèle dans un but de prédiction ou d'aide à la décision. Les modèles distribués à l'échelle du paysage nécessitent diverses données d'entrée et paramétrages qui sont sources d'incertitudes (erreurs de mesures, résolution inadaptée de l'échantillonnage, positions dans l'espace incertaines, etc.) (Heuvelink et al., 2007). La quantification de ces incertitudes peut se révéler difficile en pratique et constitue le sujet de nombreuses études (par exemple Brown and Heuvelink, 2007 ; Crosetto and Tarantola, 2001 ; Goovaerts, 2001 ; Lesschen et al., 2007 ; Malone et al., 2011 ; Marrel et al., 2008).

Scénarios de paysage

Même si les scénarios implémentés sont intéressants et reflètent certaines grandes orientations possibles des systèmes agricoles, ils demeurent caricaturaux et peuvent être raffinés.
Il serait notamment intéressant :

- de prendre en compte des variations de pratiques culturales et d'itinéraires techniques, comme par exemple le développement de techniques culturales sans labour ;
- de tester l'influence de la répartition spatiale des occupations du sol, à composition du paysage constante. Ceci permettrait d'affiner l'estimation de l'impact de l'organisation spatiale du paysage sur l'évolution des sols.
- d'affiner les scénarios en fonction du contexte politique et socio-économique, en collaboration avec les disciplines compétentes (agronomie systémique, sciences sociales).

Perspectives

Ces conclusions amènent à définir différentes perspectives de recherche.

Pour améliorer de la modélisation de l'évolution des sols, il est nécessaire:

- de lever des verrous de connaissances, afin d'améliorer la modélisation des processus pédologiques, notamment en ce qui concerne la dynamique de la matière organique dans les horizons profonds ou pendant le transport des particules de sol. Les travaux d'expérimentation ou d'observation de plus en plus nombreux sur ces thématiques, et menés dans une diversité de contextes agricoles et pédo-climatiques, fourniront des références pour calibrer les modèles d'évolution des sols ;
- d'améliorer la représentation des paysages et de leur évolution. Nous avons fait évoluer les cultures au sein des parcelles et le type de limite de parcelle (caractérisées par l'absence ou la présence de haie) mais l'organisation spatiale est restée constante en cours des simulations pour chaque paysage simulé. Une représentation plus réaliste des paysages agricoles nécessite la modélisation de l'évolution de la taille des parcelles, l'arasement ou la

plantation de haie, le mode d'allocation des cultures sur les parcelles, la gestion de la matière organique au sein de l'exploitation, etc. ;

- de mettre en place un meilleur couplage entre les processus déjà pris en compte dans cette étude (dynamique du carbone et redistribution des sols), mais aussi avec d'autres processus pédologiques et d'autres compartiments des écosystèmes : écosystèmes aquatiques, atmosphère, biosphère (faune et flore). Dans cet objectif, les plateformes de modélisation de paysage telles que le projet Paysage Virtuel à l'INRA), en cours en mise en place et qui doivent proposer une convergence quant au mode de représentation du paysage, peuvent présenter un net intérêt et permettre le couplage des différents modèles existants : dynamique des cultures, dynamique de l'azote et du carbone, flux d'eau et de nutriments, redistribution des sols, stratégies des exploitants agricoles. Il reste à faire le choix des éléments les plus pertinents à intégrer prioritairement, compte tenu de la complexité de mise en œuvre des modèles à l'échelle du paysage. Ces choix peuvent être orientés grâce aux observations réalisées au niveau des observatoires à long terme ;
- de mettre en place des démarches de validation des modèles distribués à l'échelle du paysage et de quantification de la propagation des incertitudes de prédiction aux différentes étapes de la modélisation dynamique spatiale ;
- de faire un effort de généralisation des modèles à d'autres types de paysage, réunissant d'autres types de sols, de cultures, etc. Cela est notamment réalisé dans le cadre du programme ANR LandSoil (paysage de grandes cultures sur sol calcaires, paysage de vignobles méditerranéen).

Bibliographie

AFES (Editeur), 2008. Référentiel pédologique, 405 p.

Agger, P. et Brandt, J., 1988. Dynamics of small biotopes in Danish agricultural landscapes. *Landscape Ecology*, 1 : 227-240.

Aïchi, H., Fouad, Y., Walter, C., Viscarra Rossel, R. A., Chabaane, Z.L. et Sanaa, M., 2009. Regional predictions of soil organic carbon content from spectral reflectance measurements. *Biosystems Engineering*, 104 : 442-446.

Alcamo, J., Moreno, J.M., Nováky, B., Bindi, M., Corobov, R., Devoy, R.J.N., Giannakopoulos, C., Martin, E., Olesen, J.E. et Shvidenko, A., 2007. Europe. Climate Change 2007: Impacts, Adaptation and Vulnerability. Contribution of Working Group II to the Fourth Assessment Report of the Intergovernmental Panel on Climate Change, M.L. Parry, O.F. Canziani, J.P. Palutikof, P.J. van der Linden et C.E. Hanson (Editeurs), Cambridge University Press, Cambridge, UK, p. 541-580.

Alegre, J.C. et Rao, M.R., 1996. Soil and water conservation by contour hedging in the humid tropics of Peru. Agriculture Ecosystems & Environment, 57, 17-25.

Anderson, D.W., Heil, R.D., Cole, C.V. et Deutsch, P.C., 1983. Identification and characterization of ecosystems at different integrative levels. In: R. Lowrance, R. Todd, L. Asmussen et R. Leonard (Editeurs), Nutrient cycling in agrcultural ecosystems. University of Georgia, College of Agriculture Experiment Stations, 602 p.

Anderson, S.H., Udawatta, R.P., Seobi, T. et Garrett, H.E., 2009. Soil water content and infiltration in agroforestry buffer strips. Agroforestry Systems, 75, 5-16.

Antrop, M., 2005. Why landscapes of the past are important for the future. *Landscape and Urban Planning*, 70 : 21-34.

Antrop, M., 2008. Landscapes at risk: about change in the European landscapes. In: P. Dostal (Editeur), Evolution of Geographical Systems and Risk Processes in the Global Context. Charles University, Faculty of Science, Prague, p. 57-79.

Archives Municipales de Rennes, Cadastre, mode d'emploi, 2005. En ligne, 3, Aout 2012. http://www.documents.rennes.fr/actus/documents/423CADASTREv2.pdf

Arrouays, D., Daroussin, J., Kicin, J.L. et Hassika, P., 1998. Improving topsoil carbon storage prediction using a digital elevation model in temperate forest soils of France. *Soil Science,* 163 : 103-108.

Arrouays, D., Deslais, W., Daroussin, J., Balesdent, J., Gailland, J., Dupoucy, J.L., Nys, C., Badeau V., et Belkacem, S., 1999. Stocks de carbone dans les sols de France : quelles estimations? *Comptes Rendus de l'Académie d'Agriculture de France*, 85 : 278-292.

Arrouays, D., Balesdent, J., Germon, J.C., Jayet, P.A., Soussana, J.F. et Stengel, P., 2002. Contribution à la lutte contre l'effet de serre : Stocker du carbone dans les sols agricoles de France ? Expertise Scientifique Collective, INRA Paris : 332 p.

Bacchi, O.O.S., Reichardt, K. et Sparovek, G., 2003. Sediment spatial distribution evaluated by three methods and its relation to some soil properties. *Soil and Tillage Research*, 69 : 117-125.

Baize, D. et Jabiol, B., 1995. Guide pour la description des sols. INRA Editions, Paris, 375 p.

Baize, D. (Editeur), 2000. Guide des analyses en pédologie. Techniques et Pratiques. INRA, Paris, 257p.

Bakker, M.M., Govers, G. et Rounsevell, M.D.A., 2004. The crop productivity-erosion relationship: an analysis based on experimental work. *Catena*, 57 : 55-76.

Bakker, M.M., Govers, G., van Doom, A., Quetier, F., Chouvardas, D., et Rounsevell, M., 2008. The response of soil erosion and sediment export to land-use change in four areas of Europe: The importance of landscape pattern. *Geomorphology*, 98 : 213-226.

Balesdent, J. et Recous, S., 1997. Les temps de résidence du carbone et le potentiel de stockage de carbone dans quelques sols cultivés français. *Canadian Journal of Soil Science*, 77 : 187-193.

Balesdent, J., Chenu, C. et Balabane, M., 2000. Relationship of soil organic matter dynamics to physical protection and tillage. *Soil & Tillage Research*, 53 : 215-230.

Baudry, J., Bunce, R.G.H. et Burel, F., 2000. Hedgerows: An international perspective on their origin, function and management. *Journal of Environmental Management*, 60 : 7-22.

Baudry, J. et Jouin, A. (Editeurs), 2003. De la haie aux bocages. Organisation, dynamique et gestion. INRA, Paris, 431 p.

Baudry, J. et Perichon, S., 2007. Les haies et les bocages dans le monde : éléments de comparaison. In: A. Antoine et D. Marguerie (Editeurs), Bocages et sociétés. Espace et territoires. Presses Universitaires de rennes, Rennes, p. 23-32.

Beasley, D.B., Huggins, L.F. et Monke, E.J., 1981. ANSWERS: A model for watershed planning. *Transactions of the Asae*, 23 : 938-944.

Belleguic, K., Conseil, C., Eveno, T., Lorge, S. et Baraer, F., 2012. Le changement climatique en Bretagne. Météo-France, 77 p.

Berger, G., Kaechele, H. et Pfeffer, H., 2006. The greening of the European common agricultural policy by linking the European-wide obligation of set-aside with voluntary agri-environmental measures on a regional scale. *Environmental Science & Policy*, 9 : 509-524.

Berhe, A.A., 2012. Decomposition of organic substrates at eroding vs. depositional landform positions. *Plant and Soil*, 350 : 261-280.

Beven, K.J. et Kirkby, M.J., 1979. A physically based, variable contributing area model of basin hydrology. *Hydrological Sciences Journal*, 24 : 43-69.

Bharati, L., Lee, K.H., Isenhart et T.M., Schultz, R.C., 2002. Soil-water infiltration under crops, pasture, and established riparian buffer in Midwestern USA. Agroforestry Systems, 56, 249-257.

Bishop, T.F.A., McBratney, A.B. et Laslett, G.M., 1999. Modelling soil attribute depth functions with equal-area quadratic smoothing splines. *Geoderma*, 91 : 27-45.

Blagodatsky, S. et Smith, P., 2012. Soil physics meets soil biology: Towards better mechanistic prediction of greenhouse gas emissions from soil. *Soil Biology & Biochemistry*, 47: 78-92.

Boardman, J. et Poesen, J., 2006. Soil erosion in Europe: major processes, causes and consequences. In: J. Boardman et J. Poesen (Editeurs), Soil Erosion in Europe. Chichester, p. 479-487.

Bogdanoff, S. et Julien, M., avec la collaboration de Lafond, R.L., Carn, A., et Vaginay, M. , 1996. Notice explicative, Carte géol. France (1/50 000), feuille Dol-de-Bretagne (246). Orléans : BRGM, 47 p. Carte géologique par Bogdanoff, S., Jourdan, C. et Laond, R.L. (1997)

Bogdanoff, S., Jourdan, C., et Lafond, R.L., 1997. Carte géol. France (1/50 000), feuille Dol-de-Bretagne (246). Orléans : BRGM. Notice explicative par Bogdanoff, S. et Julien, M., avec la collaboration de Lafond, R. L., Carn, A. et Vaginay, M., 1996, 47 p.

Boiffin, J. et Monnier, G., 1986a. Infiltration rate as affected by soil surface crusting caused by rainfall. In: F. Caillebaud, D. Gabriels et M. De Boodt (Editeurs), Assessment of soil surface sealing and crusting. Flanders Research Center for Soil Erosion and Soil Conservation, Ghent, p. 210-217.

Boiffin, J., Zagbahi, J.K. et Sebillotte, M., 1986b. Cropping system and organic status of soils. Application of the Henin-Dupuis model. *Agronomie*, 6 : 437-446.

Bol, R., Poirier, N., Balesdent, J. et Gleixner, G., 2009. Molecular turnover time of soil organic matter in particle-size fractions of an arable soil. *Rapid Communications in Mass Spectrometry*, 23 : 2551-2558.

Bolinder, M.A., Angers, D.A. et Dubuc, J.P., 1997. Estimating shoot to root ratios and annual carbon inputs in soils for cereal crops. *Agriculture Ecosystems & Environment*, 63 : 61-66.

Bonijoly, D., Perrin, J., Truffert, C. et Asfirne, F., 1999. Couverture géophysique aéroportée du Massif armoricain. Rapport BRGM/RR-40471-FR. 75 p.

Bonilla, C.A., Reyes, J.L. et Magri, A., 2010. Water erosion prediction using the revised universal soil loss equation (RUSLE) in a GIS framework, Central Chile. *Chilean Journal of Agricultural Research*, 70 : 159-169.

Bouma, J., Finke, P.A., Hoosbeek, M.R. et Breeuwsma, A., 1998. Soil and water quality at different scales: concepts, challenges, conclusions and recommendations. *Nutrient Cycling in Agroecosystems*, 50 : 5-11.

Bradley, R.I., Milne, R. Bell, J. Lilly, A., Jordan, C. et Higgins, A., 2005. A soil carbon and land use database for the United Kingdom. *Soil Use and Management*, 21 : 363-369.

Breiman, L., 2001. Statistical modeling: The two cultures. *Statistical Science*, 16 : 199-215.

Bresson, L.M. et Boiffin, J., 1990. Morphological characterization of soil crust development stages on an experimental field. *Geoderma*, 47 : 301-325.

Brisson, N. et Levrault, F. (Editeurs), 2012. Changement climatique, agriculture et forêt en France : simulations d'impacts sur les principales espèces. Le Livre Vert du projet Climator (2007-2010). ADEME. 336 p.

Brown, J.D. et Heuvelink, G.B.M., 2007. The Data Uncertainty Engine (DUE): A software tool for assessing and simulating uncertain environmental variables. *Computers & Geosciences*, 33 : 172-190.

Brus, D.J., Kempen, B. et Heuvelink, G.B.M., 2011. Sampling for validation of digital soil maps. *European Journal of Soil Science*, 62 : 394-407.

Bui, E., 2007. A Review of Digital Soil Mapping in Australia. In: A.B.M. P. Lagacherie et M. Voltz (Editeurs), Developments in Soil Science. Elsevier, p. 25-37.

Burel, F. et Baudry, J., 1990. Structural dynamic of a hedgerow network landscape in Brittany France. *Landscape Ecology*, 4 : 197-210.

Burel, F., Baudry, J. et Lefeuvre, J.C., 1993. Landscape structure and the control of water runoff. In: R.G.H. Bunce, M.G. Paoletti et L. Ryszkowski (Editeurs), Landscape Ecology and Agroecosystems, London, p. 47-41.

Burel, F. et Baudry, J., 1999. Ecologie du paysage. Concepts, méthodes et applications., Paris, 359 p.

Burel, F. et Baudry, J., 2003. Landscape ecology: concepts, methods and applications. Science Publishers Inc., Enfield (USA) - Plymouth (UK), 362 p.

Calvo-Iglesias, M.S., Fra-Paleo, U. et Diaz-Varela, R.A., 2009. Changes in farming system and population as drivers of land cover and landscape dynamics: The case of enclosed and semi-openfield systems in Northern Galicia (Spain). *Landscape and Urban Planning*, 90 : 168-177.

Carnet, C., 1976. Premières données sur le rôle du bocage sur la distribution des sol et la circulation de l'eau dans les sols. In: I.e.U.d.R. CNRS (Editor), Les bocages : histoire, écologie, économie, p. 159-162.

Carnet, C., Merot, P. et Ruellan, A., 1979. Approche du rôle des talus dans la distribution des sols et dans le fonctionnement hydrique et hydrologique d'un bassin versant bocager en région granitique de Bretagne. *Science du Sol*, 4: 377-397.

Cellier, P., Bleeker, A., Breuer, L., Dalgaard, T., Dragosits, U., Drouet, J.L., Durand, P., Duretz, S., Hutchings, N., Kros, J., Loubet, B., Oenema, O., Olesen, J.E., Mérot, P., Theobald, M.R., Viaud, V., de Vries, W. et Sutton, M.A., 2011. Dispersion and fate of nitrogen in rural landscapes. In: M.A. Sutton et al. (Editeurs), The European Nitrogen Assessment. Cambridge University Press, p. 229–248.

Cerdan, A., 1999. Parent material and vegetation affect soil erosion in eastern Spain. *Soil Science Society of America Journal*, 63 : 362-368.

Cerdan, O., Le Bissonnais, Y., Couturier, A. et Saby, N., 2002a. Modelling interrill erosion in small cultivated catchments. *Hydrological Processes*, 16 : 3215-3226.

Cerdan, O., Le Bissonnais, Y., Couturier, A., Bourennane, H. et Souchère, V., 2002b. Rill erosion on cultivated hillslopes during two extreme rainfall events in Normandy, France. *Soil and Tillage Research*, 67, 99-108.

Cerdan, O., Souchere, V., Lecomte, V., Couturier, A. et Le Bissonnais, Y., 2002c. Incorporating soil surface crusting processes in an expert-based runoff model: Sealing and Transfer by Runoff and Erosion related to Agricultural Management. *Catena*, 46 : 189-205.

Cerdan, O., Le Bissonnais, Y., Couturier, A., Saby, N., 2002d. Modelling interrill erosion in small cultivated catchments. Hydrological Processes, 16, 3215-3226.

Cerdan, O., Le Bissonnais, Y., Souchère, V., Martin, P. et Lecomte, V., 2002c. Sediment concentration in interrill flow: interactions between soil surface conditions, vegetation and rainfall. *Earth Surface Processes and Landforms*, 27, 193-205.

Cerdan, O., Govers, G., Le Bissonnais, Y., Van Oost, K., Poesen, J., Saby, N., Gobin, A., Vacca, A., Quinton, J., Auerswald, K., Klik, A., Kwaad, F.J.P.M., Raclot, D., Ionita, I., Rejman, J., Rousseva, S., Muxart, T., Roxo, M.J. et Dostal, T., 2010. Rates and spatial variations of soil erosion in Europe: A study based on erosion plot data. Geomorphology, 122, 167-177

Cerdan, O., Delmas, M., Négrel, P., Mouchel, J.-M., Petelet-Giraud, E., Salvador-Blanes, S. et Degan, F., 2012. Contribution of diffuse hillslope erosion to the sediment export of French rivers. *Comptes Rendus Geoscience*, 344, 636-645.

Chan, C., Kay, B.D. et Gregorich, E.G., 2009. Spatial variability in organic carbon stocks on level sites: Relation to vertical penetration of the A horizon. *Canadian Journal of Soil Science*, 89 : 455-459.

Chantraine, J., Rabu, D. et Béchennec, F., 2002. Carte géologique numérique à 1:250 000 du Massif armoricain. Version 1.1., BRGM (Bureau de Recherches Géologiques et Minières).

Chaplot, V. et Le Bissonnais, Y., 2000. Field measurements of interrill erosion under different slopes and plot sizes. *Earth Surface Processes and Landforms*, 25 : 145-153.

Chenu, C., Le Bissonnais, Y. et Arrouays, D., 2000. Organic matter influence on clay wettability and soil aggregate stability. *Soil Science Society of America Journal*, 64 : 1479-1486.

Ciampalini, R., Follain, S. et Le Bissonnais, Y., 2012. LandSoil: A model for analysing the impact of erosion on agricultural landscape evolution. *Geomorphology*, 175, 25-37.

Coleman, K. et Jenkinson, D., 1996. RothC-26.3 - a model for the turnover of carbon in soil. In: D.S. Powlson, J.U. Smith et P. Smith (Editeurs), Evaluation of soil organic matter models using existing long term data-sets. NATO ASI Series. Springer-Verlag, Heidelberg, p. 237-246.

Coleman, K., Jenkinson, D.S., Crocker, G.J., Grace, P.R., Klir, J., Korschens, M., Poulton P.R. et Richter, D.D., 1997. Simulating trends in soil organic carbon in long-term experiments using RothC-26.3. *Geoderma*, 81 : 29-44.

CORPEN, 1999. Estimation des flux d'azote, de phosphore et de potassium associés aux vaches laitières et à leur système fourrager.

CORPEN, 2001. Estimation des flux d'azote, de phosphore et de potassium associés aux bovins allaitants et aux bovins en croissance ou à l'engrais, issus des troupeaux allaitants et laitiers, et à leur système fourrager.

Cros-Cayot, S., 1996. Distribution spatiale des transferts de surface à l'échelle du versant. Contexte Armoricain, Thèse de doctorat de l'E.N.S.A.R., Rennes, 218 p.

Crosetto, M. et Tarantola, S., 2001. Uncertainty and sensitivity analysis: tools for GIS-based model implementation. International Journal of Geographical Information Science, 15(5): 415-437.

Curmi, P., 1979. Altération et différenciation pédologique sur granite en Bretagne; étude d'une toposéquence. , ENSAR, Rennes, 165 p.

De Vos, B., Van Meirvenne, M., Quataert, P., Deckers, J. et Muys, B., 2005. Predictive quality of pedotransfer functions for estimating bulk density of forest soils. *Soil Science Society of America Journal*, 69 : 500-510.

de Vries, W., Cellier, P., Erisman, J.W. et Sutton, M.A., 2011. Assessment of nitrogen fluxes to air and water from site scale to continental scale: An overview. *Environmental Pollution*, 159 : 3143-3148.

Deckers, B., Kerselaers, E., Gulinck, H., Muys, B. et Hermy, M., 2005. Long-term spatio-temporal dynamics of a hedgerow network landscape in Flanders, Belgium. *Environmental Conservation*, 32 : 20-29.

Delmas, M., Pak, L.T., Cerdan, O., Souchere, V., Le Bissonnais, Y., Couturier, A. et Sorel, L., 2012. Erosion and sediment budget across scale: A case study in a catchment of the European loess belt. *Journal of Hydrology*, 420, 255-263.

Deque, M., 2007. Frequency of precipitation and temperature extremes over France in an anthropogenic scenario: Model results and statistical correction according to observed values. *Global and Planetary Change*, 57 : 16-26.

Doetterl, S., Six, J., Van Wesemael, B. et Van Oost, K., 2012. Carbon cycling in eroding landscapes: geomorphic controls on soil organic C pool composition and C stabilization. *Global Change Biology*, 18 : 2218-2232.

Dokoutchaiev, V., 1900. Zones verticales des sols, zones agricoles, sols du Caucase. . Exposition Univelselle de 1900 à Paris, Sect. russe, ed. du Ministère des Finances, St-Pétersbourg, 56 p.

Dominati, E., Patterson, M. et Mackay, A., 2010. A framework for classifying and quantifying the natural capital and ecosystem services of soils. *Ecological Economics*, 69 : 1858-1868.

Dlugoss, V., Fiener, P., Van Oost, K. et Schneider, K., 2012. Model based analysis of lateral and vertical soil carbon fluxes induced by soil redistribution processes in a small agricultural catchment. *Earth surface processes and landforms*, 37: 193-208.

Dupre, T., 1997. Impact de la plasticulture sur les transferts superficiels. Contexte Armoricain. 32 p.

Egal, E., Thieblemenot, D., Thomas, E., Guennoc, P. et Hallegouët, B., avec la collaboration de Carn, A., Chantraine, J., Guerrot, C., Houlgatte, E., Le Berre, P., Martalet, G., Monnier, J., Tegyey, M. et Truffert, C., 2004. Notice explicative, Carte géol. France (1/50 000), feuille Saint-Brieuc (243). Orléans : BRGM, 221 p. Carte géologique par Egal, E., Thomas, E., Guennoc, P., Hallegouët, B., Houlgatte, E. et Augris, C. (2005)

Eglin, T., Walter, C., Nys, C., Follain, S., Forgeard, F., Legout, A. et Squividant, H., 2008. Influence of waterlogging on carbon stock variability at hillslope scale in a beech forest (Fougeres forest, West France). *Annals of Forest Science*, 65.

Eglin, T., Ciais, P., Piao, S. L., Barre, P., Bellassen, V., Cadule, P., Chenu, C., Gasser, T., Koven, C., Reichstein, M. et Smith, P., 2010. Historical and future perspectives of global soil carbon response to climate and land-use changes. *Tellus Series B-Chemical and Physical Meteorology*, 62 : 700-718.

European Commission, 2005. Agri-environment measures. Overview on general principles, types of measures, and application.

European Commission, 2006. Vers une stratégie thématique pour la protection des sols, Bruxelles.

Evrard, O., Vandaele, K., Bielders, C. et van Wesemael, B., 2008. Seasonal evolution of runoff generation on agricultural land in the Belgian loess belt and implications for muddy flood triggering. *Earth Surface Processes and Landforms*, 33 : 1285-1301.

Evrard, O., Cerdan, O., van Wesemael, B., Chauvet, M., Le Bissonnais, Y., Raclot, D., Vandaele, K., Andrieux, P. et Bielders, C., 2009. Reliability of an expert-based runoff and erosion model: Application of STREAM to different environments. Catena, 78, 129-141.

Evrard, O., Nord, G., Cerdan, O., Souchere, V., Le Bissonnais, Y. et Bonte, P., 2010. Modelling the impact of land use change and rainfall seasonality on sediment export from an agricultural catchment of the northwestern European loess belt. *Agriculture Ecosystems & Environment*, 138, 83-94.

Falloon, P., Smith, P., Coleman, K. et Marshall, S., 1998. Estimating the size of the inert organic matter pool from total soil organic carbon content for use in the Rothamsted carbon model. *Soil Biology & Biochemistry*, 30 : 1207-1211.

Falloon, P.D. et Smith, P., 2000. Modelling refractory soil organic matter. *Biology and Fertility of Soils*, 30 : 388-398.

Falloon, P. et Smith, P., 2002. Simulating SOC changes in long-term experiments with RothC and CENTURY: model evaluation for a regional scale application. *Soil Use and Management*, 18 : 101-111.

Falloon, P., Smith, P., Bradley, R. I., Milne, R., Tomlinson, R., Viner, D., Livermore, M. et Brown, T., 2006. RothCUK - a dynamic modelling system for estimating changes in soil C from mineral soils at 1-km resolution in the UK. *Soil Use and Management*, 22 : 274-288.

FAO, 2012. Mainstreaming climate-smart agriculture into a broader lanscape approach. Background Paper for theSecond Global Conferenceon Agriculture, Food Securityand Climate Change, Hanoi, Vietnam, 3-7 September 2012.

Ferro, V. et Minacapilli, M., 1995. Sediment delivery processes at basin-scale. *Hydrological Sciences Journal*, 40 : 703-717.

Finke, P.A. et Hutson, J.L., 2008. Modelling soil genesis in calcareous loess. *Geoderma*, 145 : 462-479.

Flacke, W., Auerswald, K. et Neufang, L., 1990. Combining a modified universal soil loss equation with a digital terrain model for computing hig-resolution maps of soil loss resulting from rain wash. *Catena*, 17 : 383-397.

Florinsky, I.V., Eilers, R.G., Manning, G.R. et Fuller, L.G., 2002. Prediction of soil properties by digital terrain modelling. *Environmental Modelling & Software*, 17 : 295-311.

Follain, S., 2006a. Effet du réseau bocage sur l'organisation des sol. Redisribution des sols et stockage en carbone organique, Thèse de doctorat de l'E.N.S.A.R., Rennes, 241 p.

Follain, S., Minasny, B., McBratney, A.B. et Walter, C., 2006b. Simulation of soil thickness evolution in a complex agricultural landscape at fine spatial and temporal scales. *Geoderma*, 133 : 71-86.

Follain, S., Walter, C., Legout, A., Lemercier, B. et Dutin, G., 2007. Induced effects of hedgerow networks on soil organic carbon storage within an agricultural landscape. *Geoderma*, 142 : 80-95.

Follain, S., Walter, C., Bonte, P., Marguerie, D. et Lefevre, I., 2009. A-horizon dynamics in a historical hedged landscape. *Geoderma*, 150 : 334-343.

Fontaine, S., Barot, S., Barre, P., Bdioui, N., Mary, B. et Rumpel, C., 2007. Stability of organic carbon in deep soil layers controlled by fresh carbon supply. *Nature*, 450 : 277-280.

Forman, R.T.T., 1995. Some general principles of landscape and regional ecology. *Landscape Ecology*, 10 : 133-142.

Fox, D.M. et Le Bissonnais, Y., 1998. Process-based analysis of aggregate stability effects on sealing, infiltration, and interrill erosion. *Soil Science Society of America Journal*, 62 : 717-724.

Friedman, J.H. et Meulman, J.J., 2003. Multiple additive regression trees with application in epidemiology. *Statistics in Medicine*, 22 : 1365-1381.

Gaiser, T., Stahr, K., Billen, N. et Mohammad, M.A.-R., 2008. Modeling carbon sequestration under zero tillage at the regional scale. I. The effect of soil erosion. *Ecological Modelling*, 218 : 110-120.

Gallien, E., Le Bissonnais, Y., Eimberck, M., Benkhadra, H., Ligneau, L., Ouvry, J.F. et Martin, P., 1995. Influence des couverts végétaux de jachère sur le ruissellement et l'érosion diffuse en sol limoneux cultivé. *Cahiers Agricultures*, 4: 171-193.

Gascuel-Odoux, C., Cros-Cayot, S. et Durand, P., 1996. Spatial variations of sheet flow and sediment transport on an agricultural field. Earth Surface Processes and Landforms, 21(9): 843-851.

Gascuel-Odoux, C., 1998. Les zones contributives de fond de vallée : localisation, structure et fonctionnement hydrodynamique. In: INRA (Editeur), Agriculture intensive et qualité des eaux. Cheverry, C., Paris, p. 129-141.

Gascuel-Odoux, C. et Heddadj, D., 1999. Maîtrise des transferts de surface dans le contexte armoricain. Rapport Bretagne Eau Pure : 95/09-020.

Gennadiyev, A.N. et Olson, K.R., 1998. Pedological cooperation between Russia and the USA, past to present. *Soil Science Society of America Journal*, 62 : 1153-1161.

Gerrits, L. et Edelenbos, J., 2004. Management of sediment through stakeholder involvement. *J. Soils Sediments*, 4 : 239-246.

Gibelin, A.L, Déqué, M., 2003. Anthropogenic climate change over the Mediterranean region simulated by a global variable resolution model. *Climate Dynamics*, 20: 327–339.

GIEC, 2007. Bilan 2007 des changements climatiques. Contribution des Groupes de travail I, II et III au quatrième Rapport d'évaluation du Groupe d'experts intergouvernemental sur l'évolution du climat. Équipe de rédaction principale, Pachauri, R.K. et Reisinger, A., GUEC, Genève, Suisse.

Gilley, J.E., Eghball, B., Kramer, L.A. et Moorman, T.B., 2000. Narrow grass hedge effects on runoff and soil loss. *Journal of Soil and Water Conservation*, 55 : 190-196.

Goovaerts, P., 2001. Geostatistical modelling of uncertainty in soil science. *Geoderma*, 103 : 3-26.

Govers, G., Vandaele, K., Desmet, P., Poesen, J. et Bunte, K., 1994. The role of tillage in soil redistribution on hillslopes. *European Journal of Soil Science*, 45 : 469-478.

Govers G., Quine, T.A., Desmet, P.J J. et Walling, D.E., 1996. The relative contribution of soil tillage and overland flow erosion to soil redistribution on agricultural land. *Earth Surface Processes and Landforms*, 10, 929-946.

Govers, G., Lobb, D.A. et Quine, T.A., 1999. Preface - Tillage erosion and translocation: emergence of a new paradigm in soil erosion research. *Soil & Tillage Research*, 51 : 167-174.

Grace, J., 2004. Understanding and managing the global carbon cycle. *Journal of Ecology*, 92 : 189-202.

Grimm, R., Jones, R. et Montanarella, L., 2002. Soil Erosion Risk in Europe, Institute for Environment and Sustainability, JRC, Ispra, 40 p.

Grimm, R., Behrens, T., Marker, M. et Elsenbeer, H., 2008. Soil organic carbon concentrations and stocks on Barro Colorado Island - Digital soil mapping using Random Forests analysis. *Geoderma*, 146 : 102-113.

Gruijter, J.d., Brus, D., Bierkens, M. et Knotters, M., 2006. Sampling for natural resource monitoring. Sampling for natural resource monitoring.

Gumiere, S.J., Le Bissonnais, Y., Raclot, D. et Cheviron, B., 2011. Vegetated filter effects on sedimentological connectivity of agricultural catchments in erosion modelling: A review. *Earth Surface Processes and Landforms*, 36, 3-19.

Harris, T.M. et Boardman, J., 1990. A rule-based expert system approach to predicting waterbone soil erosion. Soil Erosion on Agricultural Land. Wiley, Chichester.

Harrison, R.G., Jones, C.D. et Hughes, J.K., 2008. Competing roles of rising CO2 and climate change in the contemporary European carbon balance. *Biogeosciences*, 51 : 1-10.

Heddadj, D. et Gascuel-Odoux, C., 1999. Topographic and seasonal variations of unsaturated hydraulic conductivity as measured by tension disc infiltrometers at the field scale. European *Journal of Soil Science*, 50 : 275-283.

Hengl, T., Rossiter, D.G. et Stein, A., 2003. Soil sampling strategies for spatial prediction by correlation with auxiliary maps. *Australian Journal of Soil Research*, 41 : 1403-1422.

Heuvelink, G.B.M., Brown, J.D. et van Loon, E.E., 2007. A probabilistic framework for representing and simulating uncertain environmental variables. *International Journal of Geographical Information Science*, 21 : 497-513.

Hoosbeek, M.R., Amundson, R.G. et Bryant, R.B., 2000. Pedological modeling. In: M.E. Sumner (Editeur), Handbook of soil science. CRC Press, p. 77-116.

Huang, C., Gascuel-Odoux, C. et Cros-Cayot, S., 2002. Hillslope topographic and hydrologic effects on overland flow and erosion. *Catena*, 46 : 177-188.

Huang, C.H., 1995. Empirical analysis of slope and runoff for sediment delivery from interrill areas. *Soil Science Society of America Journal*, 59 : 982-990.

Huggett, R.J., 1975. Soil landscape systems: a model of soil genesis. *Geoderma*, 13 : 1-22.

IPCC, 2000. Ipcc special report emissions scenarios. summary for policymakers. Tech. rep., Intergovernmental Panel on Climate Change. IPCC, 2007. Climate Change 2007: Impacts, Adaptation and Vulnerability. Contribution of Working Group II to the Fourth Assessment. Report of the Intergovernmental Panel on Climate Change, M.L. Parry, O.F. Canziani, J.P. Palutikof, P.J. van der Linden et C.E. Hanson, Eds., Cambridge University Press, Cambridge, UK, 976p.

IPCC, 2007. Climate Change 2007: Impacts, Adaptation and Vulnerability. Contribution of Working Group II to the Fourth Assessment. Report of the Intergovernmental Panel on Climate Change. Change, M.L. Parry, O.F. Canziani, J.P. Palutikof, P.J. van der Linden et C.E. Hanson, Eds., Cambridge University Press, Cambridge, UK, 976 p.

Issa, O.M., Le Bissonnais, Y., Planchon, O., Favis-Mortlock, D., Silvera, N. et Wainwright, J., 2006. Soil detachment and transport on field- and laboratory-scale interrill areas: erosion processes and the size-selectivity of eroded sediment. *Earth Surface Processes and Landforms*, 31 : 929-939.

IUSS Working Group WRB, 2007. World Reference Base for Soil Resources 2006, first update 2007. World Soil Resources Reports No. 103. FAO, Rome.

Jaunatre, D., 1997. Influence de techniques culturales sur le ruissellement et les transferts de ppolluants à l'échelle d'un bassin versant en contexte armoricain. Mémoire de fin d'étude.

Jenkinson, D.S., Hart, P.B.S., Rayner, J.H. et Parry, L.C., 1987. Modelling the turnover of organic matter in long-term experiments at Rothamsted. INTECOL bulletin, 15: 1-8.

Jenkinson, D.S., Harkness, D.D., Vance, E.D., Adams, D.E. et Harrison, A.F., 1992. Calculating Net Primary Production and Annual Input of Organic-Matter to Soil from the Amount and Radiocarbon Content of Soil Organic-Matter. *Soil Biology & Biochemistry*, 24 : 295-308.

Jenny, H., 1941. Factors of soil formation, A system of quantitative pedology. McGraw-Hill, New-York.

Jenson, S.K. et Domingue, J.O., 1988. Extracting topographic structure from digital elevation data for geographic information system analysis. *Photogrammetric Engineering and Remote Sensing*, 54 : 1593–1600.

Jetten, V. et Favis-Mortlock, D., 2006. Modelling soil erosion in Europe. In: J. Boardman, Poesen, J (Editeur), Soil erosion in Europe. Wiley, Chichester, p. 695-716.

Johnston, C.A., Groffman, P., Breshears, D.D., Cardon, Z.G., Currie, W., Emanuel, W., Gaudinski, J., Jackson, R.B., Lajtha, K., Nadelhoffer, K., Nelson, D., Post, W. M., Retallack, G. et Wielopolski, L., 2004. Carbon cycling in soil. *Frontiers in Ecology and the Environment*, 2 : 522-528.

Jonin, M. et Vidal, P., 1975. Etude geochronologique des granitoïdes de la Mancellia, Massif Armoricain, France. *Canadian Journal of Earth Sciences*, 12 : 920-927.

Jonin, M., 1981. Un batholite fini-précambrien : le batholite mancellien (Massif armoricain, France) ; étude pétrographique et géochimique. Thèse d'État, Brest, 319 p.

Jones, A., Stolbovoy, V., Rusco, E., Gentile, AR., Gardi, C., Marechal, B. et Montanarella, L., 2009. Climate change in Europe. 2. Impact on soil. A review. *Agronomy for Sustainable Development*, 29, p. 423-432.

Jorgensen, S.E. et Bendoricchio, G., 2001. Fundamentals of ecological modelling Elvesier Science (Development in environmental modelling) , Oxford, 530 p.

Kachanoski, R.G., 1987. Comparison of measured soil Cesiun-137 losses and erosion rates. *Canadian Journal of Soil Science*, 67 : 199-203.

Kasuda, T. et Archenbach, P.R., 1965. Earth temperature and thermal diffusivity at selected stations in the united states. ASHRAE Transactions, 71.

Kato, H., Onda, Y. et Teramage, M., 2012. Depth distribution of ^{137}Cs, ^{134}Cs, and ^{131}I in soil profile after Fukushima Dai-ichi Nuclear Power Plant Accident. *Journal of Environmental Radioactivity*, 111, 59-64.

Kempen, B., Brus, D.J. et Stoorvogel, J.J., 2011. Three-dimensional mapping of soil organic matter content using soil type–specific depth functions. *Geoderma*, 162 : 107-123.

Kheir, R.B., Greve, M.H., Bocher, P.K., Greve, M.B., Larsen, R. et McCloy, K., 2010. Predictive mapping of soil organic carbon in wet cultivated lands using classification-tree based models: The case study of Denmark. *Journal of Environmental Management*, 91 : 1150-1160.

Kiepe, P., 1995. Effect of cassia-siamea hedgerow barriers on soil physical properties. *Geoderma*, 66, 113-120.

Kiepe, P., 1995b. No runoff, no soil loss: soil and water conservation in hedgerow barrier systems.

King, D. et Le Bissonnais, Y., 1992. The role of soils and cultural practices in water infiltration and runoff. An example: runoff and erosion in Northern European silty soils. *Comptes Rendus de l'Academie d'Agriculture de France*, 78 : 91-105.

King, D., 2006. Research for sustainable soil management. In: A.E. Hartemink (Editeur), The future of soil science, p. 68-70.

Kinnell, P.I.A., 2010. Event soil loss, runoff and the Universal Soil Loss Equation family of models: A review. *Journal of Hydrology*, 385 : 384-397.

Kirk, G., 2006. Views on the future of soil science. In: A.E. Hartemink (Editor), The future of soil science, p. 71-72.

Kirkby, M.J., Imeson, A.C., Bergkamp, G. et Cammeraat, L.H., 1996. Scaling up processes and models from the field plot to the watershed and regional areas. *Journal of Soil and Water Conservation*, 51 : 391-396.

Kirkby, M.J., Jones, R.J.A., Irvine, B., Gobin, A., Govers, G., Cerdan, O., Van Rompaey, A.J.J., Le Bissonnais, Y., Daroussin, J., King, D., Montanarella, L., Grimm, M., Vieillefont, V., Puigdefabregas, J., Boer, M., Kosmas, C., Yassoglou, N., Tsara, M., Mantel, S., Van Lynden, G.J. et Huting, J., 2004. Pan-European Soil Erosion Risk Assessment: The PESERA Map. European Soil Bureau Research Report, Publications of the European Communities, Luxembourg. 18 p.

Köppen, W., 1936. Das geographisca System der Klimate. In: W. Köppen et G. Geiger (Editeurs), Handbuch der Klimatologie. Gebrüder, Borntraeger, Berlin.

Kravchenko, A.N., Robertson, G.P., Hao, X. et Bullock, D.G., 2006a. Management practice effects on surface total carbon: Differences in spatial variability patterns. *Agronomy Journal*, 98 : 1559-1568.

Kravchenko, A.N., Robertson, G.R., Snap, S.S. et Smucker, A.J.M., 2006b. Using information about spatial variability to improve estimates of total soil carbon. *Agronomy Journal*, 98 : 823-829.

Lacoste, M., Lemercier, B. et Walter, C., 2011. Regional mapping of soil parent material by machine learning based on point data. *Geomorphology*, 133 : 90-99.

Lacoste, M., 2012a. Soil evolution at the landscape scale under climate and land use change, PhD thesis, Agrocampus-Ouest, Rennes, 243 p.

Lacoste, M., Michot, D., Viaud, V., Walter, C., Minasny, B. et McBratney, A.B., 2012b. High resolution 3D mapping for soil organic carbon assessment in a rural landscape. In: B. Minasny, B.P. Malone et A.B. McBratney (Editeurs), Digital Soil Assessments et Beyond. Taylor & Francis Group, London, p. 341 - 345.

Lacoste, M., Minasny, B., McBratney, A., Michot, D., Viaud, V. et Walter, C., 2014. High resolution 3D mapping of soil organic carbon in a heterogeneous agricultural landscape. *Geoderma*, 213, 296-311.

Lacoste, M., Viaud, V., Michot, D. et Walter, C., in prep. Model-based evaluation of soil redistribution impact on soil organic carbon stocks in a hedgerow landscape under temperate climate.

Laflen, J.M., Lane, L.J. et Foster, G.R., 1991. WEPP - A new generation of erosion prediction technology. *Journal of Soil and Water Conservation*, 46 : 34-38.

Lagacherie, P., McBratney, A. et Voltz, M. (Editeurs), 2007. Digital soil mapping. An Introducy perspective. Developments in Soil Science. Elsevier, Amsterdam.

Lal, R., 1997. Soil degradative effects of slope length and tillage methods on alfisols in western Nigeria .1. Runoff, erosion and crop response. *Land Degradation & Development*, 8 : 201-219.

Lal, R., 2003. Soil erosion and the global carbon budget. *Environment International*, 29 : 437-450.

Lal, R., 2004. Soil carbon sequestration impacts on global climate change and food security. *Science*, 304 : 1623-1627.

Lal, R. et Pimentel, D., 2008. Soil erosion: A carbon sink or source? *Science*, 319 : 1040-1042.

Lal, R. 2009. Challenges and opportunities in soil organic matter research. *European Journal of Soil Science*, 60: 158–169.

Lardeux, H., Audren, B., Ballèvre, M., Blais, S., Brun, J.p., Chauris, L., Chauvel, J.J., Darboux, J.R., Esteoule-Choux, J., Jegouzo, P., Marchand, J., Morzadec, M.T., Paris, F., Pelhate, A., Regnault, S., Sagon, J.P., Boillot, G., Cogné, J., Durand, S., Le Corre, C., Hallegouet, B., Lefort, J.P., Le Menn, J., Plusquelec, Y. et Thonon, P., 2002. Guide géologique de la Bretagne. Guides géologiques régionaux. Dunod, Paris, 221 p.

Lautridou, J.P., Dadet, P. et Beurrier, M., 1984. Notice explicative, Carte géol. France (1/50 000), feuille Saint-Hilaire-du-Harcouët (247). Orléans : BRGM, 26 p. Carte géologique par Dadet, P., Lautridou, J.P., Beurrier, M., Le Métour, J. (1983)

Lautridou, J.P., 1985. Le cycle périglaciaire pleistocene en Europe du Nord-Ouest, Thèse de doctorat de l'Université de Caen, 908 p.

Lautridou, J.P. et Antoine, P., 2003. La séquence du dernier cycle (Eemien-Weichselien) dans les loess de la France Septentrionale, Données récentes sur les modalités de peuplement en Europe au Paléolithique inférieur et moyen, Rennes, Université de Rennes 1.

Layer, B., 2000. Effet du système haie/talus sur l'organisation des horizons et les stocks de carbone dans des versants du Massif Armoricain, 21 p.

Le Bissonnais, Y., Singer, M.J. et Bissonnais, Y.l., 1992. Crusting, runoff, and erosion response to soil water content and successive rainfalls. *Soil Science Society of America Journal*, 56 : 1898-1903.

Le Bissonnais, Y., Renaux, B. et Delouche, H., 1995. Interactions between soil properties and moisture-content in crust formation, runoff and interrill erosion from tilled loess soils. *Catena*, 25 : 33-46.

Le Bissonnais, Y., Benkhadra, H., Chaplot, V., Fox, D., King, D. et Daroussin, J., 1998a. Crusting, runoff and sheet erosion on silty loamy soils at various scales and upscaling from m^2 to small catchments. *Soil and Tillage Research*, 46 : 69-80.

Le Bissonnais, Y., Fox, D. et Bresson, L.M., 1998b. Incorporating crusting processes in erosion models. In: J. Boardman et D.T. Favis-Mortlock (Editeurs), Modelling Soil Erosion by Water. Springer-Verlag NATO-ASI Global Change Series, Heideilberg, p. 237–246.

Le Bissonnais, Y., Cros-Cayot, S. et Gascuel-Odoux, C., 2002a. Topographic dependence of aggregate stability, overland flow and sediment transport. *Agronomie*, 22 : 489-501.

Le Bissonnais, Y., Thorette, J., Bardet, C. et Daroussin, J., 2002b. L'érosion hydrique de sols en France. Inra-Ifen.

Le Bissonnais, Y., Cerdan, O., Lecomte, V., Benkhadra, H., Souchere, V. et Martin, P., 2005. Variability of soil surface characteristics influencing runoff and interrill erosion. *Catena*, 62 : 111-124.

Le Cornet, A., 1999. Le ruisselement et le travail simplifié du sol dans le contexte armoricain.

Lebret, P. et Lautridou, J.P., 1991. The loess of West Europe. *GeoJournal*, 24 : 151-156.

Lecomte, V., Le Bissonnais, Y., Renaux, B., Couturier, A. et Ligneau, L., 1997. Erosion hydrique et transfert de produits phytosanitaires dans les eaux de ruissellement. *Cahiers Agricultures*, 6 : 157-183.

Lecomte, V., 1999. Transfert de produits phytosanitaires par le ruissellement et l'érosion de la parcelle au bassin versant—processus, déterminisme et modélisation spatiale, Thèse de doctorat de l'Ecole Nationale du Génie Rural, des Eaux et Forêts, 212 p.

Legros, J.P., 1982. L'évolution granulométrique au cours de la pédogénèse. Approche par simulation sur ordinateur. Application aux sols acides sur matériaux cristallins en zone tempérée. Thèse d'Etat. Université de Montpellier. 436 p.

Leguedois, S., 2003. Mécansimes de l'érosion diffuse des sols. Modélisation du transfert et de l'évolution granulométrique des fragments de terre érodés. Thèse de l'Université d'orléans, 156 p.

Lemercier, B., Lacoste, M., Loum, M. et Walter, C., 2011. Extrapolation at regional scale of local soil knowledge using boosted classification trees: A two-step approach. *Geoderma*, 171 : 75-84.

Lesschen, J.P., Stoorvogel, J.J., Smaling, E.M.A., Heuvelink, G.B.M. et Veldkamp, A., 2007. A spatially explicit methodology to quantify soil nutrient balances and their uncertainties at the national level. *Nutrient Cycling in Agroecosystems*, 78 : 111-131.

Li, C.S., Frolking, S. et Harriss, R., 1994. Modelling carbon biogeochemistry in agricultural soils. *Global Biogeochemical Cycles*, 8 : 237-254.

Li, S., Lobb, D.A., Lindstrom, M.J. et Farenhorst, A., 2007. Tillage and water erosion on different landscapes in the northern North American Great Plains evaluated using (CS)-C-137 technique and soil erosion models. *Catena*, 70 : 493-505.

Li, S., Lobb, D.A., Lindstrom, M.J. et Farenhorst, A., 2008. Patterns of water and tillage erosion on topographically complex landscapes in the North American Great Plains. *Journal of Soil and Water Conservation*, 63 : 37-46.

Li, S., MacMillan, R.A., Lobb, D.A., McConkey, B.G., Moulin, A. et Fraser, W.R., 2011. Lidar DEM error analyses and topographic depression identification in a hummocky landscape in the prairie region of Canada. *Geomorphology*, 129 : 263-275.

Li, Y., Lindstrom, M.J., Zhang, J. et Yang, J., 2000. Spatial variability of soil erosion and soil quality on hillslopes in the chinese loess plateau. Acta geologica hispanica, 35 : p.261-270.

Lin, H., 2011. Three Principles of Soil Change and Pedogenesis in Time and Space. *Soil Science Society of America Journal*, 75 : 2049-2070.

Lin, L.I., 1989. A concordance correlation-coefficient to evaluate reproducibility. *Biometrics*, 45 : 255-268.

Lion, E., 1997. Le ruissellement et les pratiques culturales du maïs. Mémoire. 97 p.

Liu, X.Y., 2008. Airborne LiDAR for DEM generation: some critical issues. *Progress in Physical Geography*, 32 : 31-49.

Ludwig, B., Auzet, A.V., Boiffin, J., Papy, F., King, D. et Chadoeuf, J., 1996. Etats de surface, structure hydrographique et érosion en rigole de bassins versants cultivés du Nord de la France. *Etude et gestion des Sols*, 3 : 53-70.

Lobb, D.A., Huffman, E. et Reicosky, D.C., 2007. Importance of information on tillage practices in the modelling of environmental processes and in the use of environmental indicators. *Journal of Environmental Management*, 82 : 377-387.

Ludwig, B., Boiffin, J., Chadoeuf, J. et Auzet, A.V., 1995. Hydrological structure and erosion damage caused by concentrated flow in cultivated catchments. *Catena*, 25 : 227-252.

Mabit, L., Bernard, C. et Laverdiere, M.R., 2002. Quantification of soil redistribution and sediment budget in a Canadian watershed from fallout caesium-137 (Cs-137) data. *Canadian Journal of Soil Science,* 82 : 423-431.

Malone, B.P., McBratney, A.B., Minasny, B. et Laslett, G.M., 2009. Mapping continuous depth functions of soil carbon storage and available water capacity. *Geoderma*, 154 : 138-152.

Malone, B.P., McBratney, A.B. et Minasny, B., 2011. Empirical estimates of uncertainty for mapping continuous depth functions of soil attributes. *Geoderma*, 160 : 614-626.

Marguerie, D., Antoine, A., Thenail, C., Baudry, J., Bernard, V., Burel, F., Catteddu, I., Daire, M.Y., Gautier, M., Gebhardt, A., Guibal, F., Kergreis, S., Lanos, P., Le Coeur, D., Le Du, L., Merot, P., Naas, P., Ouin, A., Pichot, D. et Visset, L., 2003. Bocages armoricains et sociétés, genèse, évolution et interactions., Des milieux et des hommes : fragments d'histoires croisées. Elsevier, Paris, p. 115-131.

Marrel, A., Iooss, B., Van Dorpe, F. et Volkova, E., 2008. An efficient methodology for modeling complex computer codes with Gaussian processes. *Computational Statistics & Data Analysis*, 52 : 4731-4744.

Martin, M.P., Seen, D. l., Boulonne, L., Jolivet, C., Nair, K. M., Bourgeon, G. et Arrouays, D., 2009. Optimizing pedotransfer functions for estimating soil bulk density using boosted regression trees. *Soil Science Society of America Journal*, 73 : 485-493.

Martin, P., Le Bissonnais, Y., Benkhadra, H., Ligneau, L., Ouvry, J.F. et Tremblay, M., 1997. Mesures du ruissellement et de l'érosion diffuse engendrés par les pratiques culturales en Pays de Caux (Normandie). *Geomorphologie: Relief, Processus, Environnement*, 2 : 143-154.

Maxted, J., Diebel, M. et Vander Zanden, M., 2009. Landscape Planning for Agricultural Non-Point Source Pollution Reduction. II. Balancing Watershed Size, Number of Watersheds, and Implementation Effort. *Environmental Management*, 43 : 60-68.

McBratney, A.B., Santos, M.L.M. et Minasny, B., 2003. On digital soil mapping. *Geoderma*, 117 : 3-52.

McCann, I.R., McFarland, M.J. et Witz, J.A., 1991. Near-surface bare soil temperature model for biophysical models. *Transactions of the Asae*, 34 : 748-755.

McKay, M.D., Beckman, R.J. et Conover, W.J., 1979. A comparison of three methods for selecting values of input variables in the analysis of output from a computer coed. *Technometrics*, 21 : 239-245.

McKenzie, N.J., Webster, R. et Ryan, P.J., 2008. Sampling using statistical methods. Guidelines for surveying soil and land resources, 319-326 p.

Meersmans, J., Van Wesemael, B., De Ridder, F., Dotti, M. Fallas, De Baets, S. et Van Molle, M., 2009a. Changes in organic carbon distribution with depth in agricultural soils in northern Belgium, 1960-2006. *Global Change Biology*, 15 : 2739-2750.

Meersmans, J., van Wesemael, B., De Ridder, F. et Van Molle, M., 2009b. Modelling the three-dimensional spatial distribution of soil organic carbon (SOC) at the regional scale (Flanders, Belgium). *Geoderma*, 152 : 43-52.

Merot, P., Ezzahar, B., Walter, C. et Aurousseau, P., 1995. Mapping waterlogging of soils using digital terrain models. *Hydrological Processes*, 9 : 27-34.

Merot, P., Squividant, H., Aurousseau, P., Hefting, M., Burt, T., Maitre, V., Kruk, M., Butturini, A., Thenail, C. et Viaud, V., 2003. Testing a climato-topographic index for predicting wetlands distribution along an European climate gradient. *Ecological Modelling*, 163 : 51-71.

Merot, P., Aurousseau, P., Gascuel-Odoux, C. et Durand, P., 2008. An innovative management of rural basin to recover the water quality? The Brittany case. *Houille Blanche*, 3 : 68-73.

Merot, P., 2011. CLIMASTER, Changement climatique dans le Grand Ouest. Quelles évolutions dans les systèmes agricoles et les ressources naturelles? Projet PSDR Grand Ouest, Serie Les 4 pages PSDR3.

Merritt, W.S., Letcher, R.A. et Jakeman, A.J., 2003. A review of erosion and sediment transport models. *Environmental Modelling & Software*, 18 : 761-799.

Michael, A., Schmidt, J., Enke, W., Deutschlander, T. et Malitz, G., 2005. Impact of expected increase in precipitation intensities on soil loss - results of comparative model simulations. *Catena*, 61 : 155-164.

Millennium Ecosystem Assessment, 2005. Ecosystems and Human Well-being: Biodiversity Synthesis. World Resources Institute, Washington, DC. 86 p.

Minasny, B. et McBratney, A.B., 2006a. A conditioned Latin hypercube method for sampling in the presence of ancillary information. *Computers & Geosciences*, 32 : 1378-1388.

Minasny, B. et McBratney, A.B., 2006b. Mechanistic soil–landscape modelling as an approach to developing pedogenetic classifications. *Geoderma*, 133 : 138-149.

Minasny, B., McBratney, A.B., Mendonca-Santos, M.L., Odeh, I.O.A. et Guyon, B., 2006c. Prediction and digital mapping of soil carbon storage in the Lower Namoi Valley. *Australian Journal of Soil Research*, 44 : 233-244.

Minasny, B. et McBratney, A., 2007. Latin hypercube sampling as a tool for digital soil mapping. In: P. Lagacherie, J.D. McNeill et M. Voltz (Editeurs), Digital soil Mapping. An introductory perspective. Developments in Soil Science. Elsevier, Amsterdam, p. 153-165.

Mishra, U., Lal, R., Slater, B., Calhoun, F., Liu, D.S. et Van Meirvenne, M., 2009. Predicting Soil Organic Carbon Stock Using Profile Depth Distribution Functions and Ordinary Kriging. *Soil Science Society of America Journal*, 73 : 614-621.

Mishra, U., Lal, R., Liu, D.S. et Van Meirvenne, M., 2010. Predicting the Spatial Variation of the Soil Organic Carbon Pool at a Regional Scale. *Soil Science Society of America Journal*, 74 : 906-914.

Moinerais, M., 2003. Impact des techniques culturales simplifiées sur les transferts hydriques, contexte armoricain. Rapport de fin d'études.

Montagne, D., Cornu, S., Le Forestier, L., Hardy, M., Josiere, O., Caner, L. et Cousin, I., 2008. Impact of drainage on soil-forming mechanisms in a French Albeluvisol: Input of mineralogical data in mass-balance modelling. *Geoderma*, 145 : 426-438.

Moore, I.D., Gessler, P.E., Nielsen, G.A. et Peterson, G.A., 1993. Soil attribute prediction using terrain analysis. *Soil Science Society of America Journal*, 57 : 1548-1548.

Moorhead, D.L., Lashermes, G. et Sinsabaugh, R.L., 2012. A theoretical model of C- and N-acquiring exoenzyme activities, which balances microbial demands during decomposition. *Soil Biology & Biochemistry*, 53 : 133-141.

Morgan, R.P.C., 2001. A simple approach to soil loss prediction: a revised Morgan-Morgan-Finney model. *Catena*, 44 : 305-322.

O'Neill, R.V., Johnson, A.R. et King, A.W., 1989. A hierarchical framework for the analysis of scale. *Landscape Ecology*, 3 : 193-205.

Pages, J. et Le Calvez, L., 1980. Analyse statistique d'une formation limoneuse en vue de préciser son origine. *Revue de statistique appliquée*, 28 : 45-60.

Papiernik, S.K., Lindstrom, M. J., Schumacher, J. A., Farenhorst, A., Stephens, K. D., Schumacher, T. E. et Lobb, D. A., 2005. Variation in soil properties and crop yield across an eroded prairie landscape. *Journal of Soil and Water Conservation*, 60 : 388-395.

Papiernik, S.K., Schumacher, T.E., Lobb, D.A., Lindstrom, M.J., Lieser, M.L., Eynard, A. et Schumacher, J. A., 2009. Soil properties and productivity as affected by topsoil movement within an eroded landform. *Soil & Tillage Research*, 102 : 67-77.

Parshotam, A., 1996. The Rothamsted soil-carbon turnover model - Discrete to continuous form. *Ecological Modelling*, 86 : 283-289.

Parsons, A.J. et Foster, I.D.L., 2011. What can we learn about soil erosion from the use of ^{137}Cs? *Earth-Science Reviews*, 108, 101-113.

Parton, W.J., Schimel, D.S., Cole, C.V. et Ojima, D.S., 1987. Analysis of factors controlling soil organic-matter levels in great-plains grasslands. *Soil Science Society of America Journal*, 51 : 1173-1179.

Peel, M.C., Finlayson, B.L. et McMahon, T.A., 2007. Updated world map of the Koppen-Geiger climate classification. *Hydrology and Earth System Sciences*, 11 : 1633-1644.

Pennock, D.J. et Veldkamp, A., 2006. Advances in landscape-scale soil research. *Geoderma*, 133 : 1-5.

Perret, S., Michellon, R., Boyer, J. et Tassin, J., 1996. Soil rehabilitation and erosion control through agro-ecological practices on Reunion Island (French Overseas Territory, Indian Ocean). Agriculture*, Agriculture, Ecosystems and Environment*, 59, 149-157.

Petersen, G.W., 2006. Soil science: multiple scales and multiple opportunities. In: A.E. Hartemink (Editeur), The future of soil science, p. 108-109.

Petit, S., Stuart, R.C., Gillespie, M.K. et Barr, C.J., 2003. Field boundaries in Great Britain: stock and change between 1984, 1990 and 1998. *Journal of Environmental Management*, 67 : 229-238.

Pistone, G. et Vicario, G., 2010. Comparing and generating Latin Hypercube designs in Kriging models. *Advances in Statistical Analysis*, 94 : 353-366.

Plénet, D., Lubet, E. et Juste, C., 1993. Évolution à long terme du statut carboné du sol en monoculture non irriguée du maïs (Zea mays L). *Agronomie*, 13 : 685-698.

Plieninger, T., 2012. Monitoring directions and rates of change in trees outside forests through multitemporal analysis of map sequences. *Applied Geography*, 32 : 566-576.

Poesen, J., van Wesemael, B., Govers, G., Martinez-Fernandez, J., Desmet, P., Vandaele, K., Quine, T. et Degraer, G., 1997. Patterns of rock fragment cover generated by tillage erosion. *Geomorphology*, 18, 183-197.

Porto, P., Walling, D.E. et Ferro, V., 2001. Validating the use of caesium-137 measurements to estimate soil erosion rates in a small drainage basin in Calabria, Southern Italy. *Journal of Hydrology*, 248 : 93-108.

Porto, P., Walling, D.E., Ferro, V. et Di Stefano, C., 2003a. Validating erosion rate estimates provided by caesium-137 measurements for two small forested catchments in Calabria, southern Italy. *Land Degradation & Development*, 14 : 389-408.

Porto, P., Walling, D.E., Tamburino, V. et Callegari, G., 2003b. Relating caesium-137 and soil loss from cultivated land. *Catena*, 53 : 303-326.

Porto, P. et Walling, D.E., 2012. Validating the use of Cs-137 and Pb-210(ex) measurements to estimate rates of soil loss from cultivated land in southern Italy. *Journal of Environmental Radioactivity*, 106 : 47-57.

Prasuhn, V., 2012. On-farm effects of tillage and crops on soil erosion measured over 10 years in Switzerland*. Soil & Tillage Research*, 120, 137-146.

Préfecture d'Ille-et-Vilaine. Arrêté préfectoral relatif au quatrième programme d'action à mettre en œuvre en vue de la protection des eaux contre la pollution par les nitrates d'origine agricole. AP-DN-28-07-2009.

Pronzato, L. et Mueller, W.G., 2012. Design of computer experiments: space filling and beyond. *Statistics and Computing*, 22 : 681-701.

Quine, T.A., Desmet, P.J.J., Govers, G., Vandaele, K. et Walling, D.E., 1994. A comparison of roles of tillage and water erosion in landform development and sediment export on agricultural land

near Leuven, Belgium. in: Olive, L. (Ed.), Variability in Stream Erosion and Sediment Transport (Proceedings of the Canberra Symposium, December 1994). *IAHS Publication*, pp. 77 – 86.

Quine, T.A., 1999. Use of caesium-137 data for validation of spatially distributed erosion models: the implications of tillage erosion. *Catena*, 37 : 415-430.

Quine, T.A. et Zhang, Y., 2002. An investigation of spatial variation in soil erosion, soil properties, and crop production within an agricultural field in Devon, United Kingdom. *Journal of Soil and Water Conservation*, 57 : 55-65.

Quinlan, J.R., 1992. Learning with continuous classes., Proceedings of the 5th Australian Joint Conference On Artificial Intelligence, p. 343-348.

Quinlan, J.R., 1993. Combining instance-based and model-based learning. In: M. Kaufmann (Editeur), Proceedings of the Tenth International Conference on Machine Learning, p. 236–243.

Quinlan, J.R., 1994. C4.5: Programs For Machine Learning. *Machine Learning*, 16 : 235-240.

Quinton, J.N., Catt, J.A., Wood, G.A. et Steer, J., 2006. Soil carbon losses by water erosion: Experimentation and modeling at field and national scales in the UK. *Agriculture Ecosystems & Environment*, 112 : 87-102.

Rachman, A., Anderson, S.H., Gantzer, C.J. et Thompson, A.L., 2004. Influence of stiff-stemmed grass hedge systems on infiltration. *Soil Science Society of America Journal*, 68, 2000-2006.

Raich, J.W. et Schlesinger, W.H., 1992. The global carbon-dioxde flux in soil respiration and its relationship to vegetation and climate. *Tellus Series B-Chemical and Physical Meteorology*, 44 : 81-99.

Renard, K.G., Foster, G.R., Weesies, G.A. et Porter, J.P., 1991. RUSLE - Revised Universal Soil Loss Equation. *Journal of Soil and Water Conservation*, 46 : 30-33.

Richet, J.B., Gril, J.J. et Ouvry, J.F., 2006. Infiltrabilité de dispositifs enherbés du Pays de Caux, premiers résultats. http://www.areas.asso.fr/content/blogcategory/31/48/.

Ritchie, J.C. et McHenry, J.R., 1990. Application of radioactive fallout Cesium-137 for measuring soil-erosion and sediment accumulation rates and patterns - A review. *Journal of Environmental Quality*, 19 : 215-233.

Ritchie, J.C., McCarty, G.W., Venteris, E.R. et Kaspar, T.C., 2007. Soil and soil organic carbon redistribution on the landscape. *Geomorphology*, 89 : 163-171.

Rivière, J.M., Tico, S. et Dupont, C., 1992. Méthode tarière Massif Armoricain. Caractérisation des sols. INRA, Rennes, 20 p.

Rodrigo, A., Recous, S., Neel, C. et Mary, B., 1997. Modelling temperature and moisture effects on C-N transformations in soils: comparison of nine models. *Ecological Modelling*, 102 : 325-339.

Ruellan, A., Dosso, M. et Fritsch, E., 1989. L'analyse structurale de la couverture pédologique. *Science du Sol*, 27 : 319-334.

Rumpel, C. et Koegel-Knabner, I., 2011. Deep soil organic matter-a key but poorly understood component of terrestrial C cycle. *Plant and Soil*, 338 : 143-158.

Salvador-Blanes, S., Cornu, S., Couturier, A., King, D. et Macaire, J.J., 2006. Morphological and geochemical properties of soil accumulated in hedge-induced terraces in the Massif Central, France. *Soil & Tillage Research*, 85 : 62-77.

Schmidt, M.W.I., Torn, M.S., Abiven, S., Dittmar, T., Guggenberger, G., Janssens, I.A., Kleber, M., Koegel-Knabner, I., Lehmann, J., Manning, D.A.C., Nannipieri, P., Rasse, D.P., Weiner, S. et Trumbore, S.E., 2011. Persistence of soil organic matter as an ecosystem property. *Nature*, 478 : 49-56.

Scott, N.A., Cole, C.V., Elliott, E.T. et Huffman, S.A., 1996. Soil textural control on decomposition and soil organic matter dynamics. *Soil Science Society of America Journal*, 60 : 1102-1109.

Segal, S., 1996. Expérimentation de techniques culturales en vue de maîtriser les transferts de surface dans le contexte armoricain. Mémoire. 57 p.

Sharma, M., Paige, G.B. et Miller, S.N., 2010. DEM Development from Ground-Based LiDAR Data: A Method to Remove Non-Surface Objects. *Remote Sensing*, 2 : 2629-2642.

Skinner, R.J. et Chambers, B.J., 1996. A survey to assess the extent of soil water erosion in lowland England and Wales. *Soil Use and Management*, 12 : 214-220.

Sleutel, S., De Neve, S., Beheydt, D., Li, C. et Hofman, G., 2006. Regional simulation of long-term organic carbon stock changes in cropland soils using the DNDC model: 1. Large-scale model validation against a spatially explicit data set. *Soil Use and Management*, 22 : 342-351.

Smith, P., Powlson, D.S., Glendining, M.J. et Smith, J.U., 1997. Potential for carbon sequestration in European soils: Preliminary estimates for five scenarios using results from long-term experiments. *Global Change Biology*, 3 : 67-79.

Smith, P., Andren, O., Brussaard, L.Z., Dangerfield, M., Ekschmitt, K., Lavelle, P. et Tate, K., 1998. Soil biota and global change at the ecosystem level: describing soil biota in mathematical models. *Global Change Biology*, 4 : 773-784.

Smith, P., Powlson, D.S., Smith, J.U., Falloon, P. et Coleman, K., 2000. Meeting the UK's climate change commitments: options for carbon mitigation on agricultural land. *Soil Use and Management*, 16 : 1-11.

Sommer, M., 2006. Influence of soil pattern on matter transport in and from terrestrial biogeosystems - A new concept for landscape pedology. *Geoderma*, 133 : 107-123.

Sorel, L., 2008. Paysages virtuels et analyse de scénarios pour évaluer les impacts environnementaux des systèmes de production agricole, Thèse de doctorat d'Agrocampus-Ouest. 211 p.

Sorel, L., Viaud, V., Durand, P. et Walter, C., 2010. Modeling spatio-temporal crop allocation patterns by a stochastic decision tree method, considering agronomic driving factors. *Agricultural Systems*, 103 : 647-655.

Souchere, V., King, D., Daroussin, J., Papy, F. et Capillon, A., 1998. Effects of tillage on runoff directions: consequences on runoff contributing area within agricultural catchments. *Journal of Hydrology*, 206 : 256-267.

Souchere, V., Cerdan, O., Ludwig, B., Le Bissonnais, Y., Couturier, A., Papy, F., 2003. Modelling ephemeral gully erosion in small cultivated catchments. *Catena*, 50 : 489-505.

Souchere, V., Sorel, L., Couturier, A., Le Bissonnais, Y. et Cerdan, O., 2005. Application du modèle STREAM à l'échelle d'un bassin versant au cours d'un cycle hydrologique, Colloque du Programme PirenSeine, Paris.

Souiller, C., Coquet, Y., Pot, V., Benoit, P., Réal, B., Margoum, C., Laillet, B., Labat, C., Vachier, P. et Dutertre, A., 2002. Capacités de stockage et d'épuration des sols de dispositifs enherbés vis-à-vis des produits phytosanitaires. Première partie : Dissipation des produits phytosanitaires à travers un dispositif enherbé ; mise en évidence des processus mis en jeu par simulation de ruissellement et infiltrométrie. *Etude et Gestion des Sols*, 9, 269-285.

Stallard, R.F., 1998. Terrestrial sedimentation and the carbon cycle: Coupling weathering and erosion to carbon burial. *Global Biogeochemical Cycles*, 12 : 231-257.

Starr, G.C., Lal, R., Malone, R., Hothem, D., Owens, L. et Kimble, J., 2000. Modeling soil carbon transported by water erosion processes. *Land Degradation & Development*, 11 : 83-91.

Strand, E.K., Smith, A.M.S., Bunting, S.C., Vierling, L.A., Hann, D.B. et Gessler, P.E., 2006. Wavelet estimation of plant spatial patterns in multitemporal aerial photography. *International Journal of Remote Sensing*, 27 : 2049-2054.

Takken, I., Beuselinck, L., Nachtergaele, J., Govers, G., Poesen, J. et Degraer, G., 1999. Spatial evaluation of a physically-based distributed erosion model (LISEM). *Catena*, 37 : 431-447.

Thenail, C., 2002. Relationships between farm characteristics and the variation of the density of hedgerows at the level of a micro-region of bocage landscape. Study case in Brittany, France. *Agricultural Systems*, 71 : 207-230.

Theocharopoulos, S.P., Florou, H., Walling, D.E., Kalantzakos, H., Christou, M., Tountas, P. et Nikolaou, T., 2003. Soil erosion and deposition rates in a cultivated catchment area in central Greece, estimated using the (137)Cs technique. *Soil & Tillage Research*, 69 : 153-162.

Thomas, E., 2005. Géologie succinte du massif armoricain (Bretagne). BRGM Bretagne. 6p.

Thornley, J.H.M. et France, J., 2007. Mathematical models in agriculture. Quantitative methods for the plant, animal and ecological sciences. CABI, 906 p.

Thorsen, M., 2001. Assessment of uncertainty in simulation of nitrate leaching to aquifers at catchment scale. *Journal of Hydrology*, 242 : 210-227.

Tiessen, H., Cuevas, E. et Chacon, P., 1994. The role of soil organic matter in sustaining soil fertility. *Nature,* 371: 783–785.

Tiessen, K.H.D., Li, S., Lobb, D.A., Mehuys, G.R., Rees, H.W. et Chow, T.L., 2009. Using repeated measurements of (137)Cs and modelling to identify spatial patterns of tillage and water erosion within potato production in Atlantic Canada. *Geoderma*, 153 : 104-118.

Tranter, G., Minasny, B., McBratney, A. B., Murphy, B., McKenzie, N. J., Grundy, M. et Brough, D., 2007. Building and testing conceptual and empirical models for predicting soil bulk density. *Soil Use and Management*, 23 : 437-443.

Turner, M.G., 1989. Landscape ecology - The effetct of pattern on process. *Annual Review of Ecology and Systematics*, 20: 171-197.

Turnpenny, A.W.H. et Williams, R., 1980. Effects of sedimentation on the gravels of an industrial river system. *Journal of Fish Biology*, 17 : 681-693.

Ungaro, F., Staffilani, F. et Tarocco, P., 2010. Assessing and mapping topsoil organic carbon stock at regional scale: a SCORPAN kriging approach conditional on soil map delineations and land use. *Land Degradation & Development*, 21 : 565-581.

Utset, A., Lopez, T. et Diaz, M., 2000. A comparison of soil maps, kriging and a combined method for spatially predicting bulk density and field capacity of ferralsols in the Havana-Matanzas Plain. *Geoderma*, 96 : 199-213.

Van Eetvelde, V. et Antrop, M., 2004. Analyzing structural and functional changes of traditional landscapes—two examples from Southern France. *Landscape and Urban Planning*, 67 : 79-95.

Van Muysen, W., Govers, G., Van Oost, K. et Van Rompaey, A., 2000. The effect of tillage depth, tillage speed, and soil condition on chisel tillage erosivity. *Journal of Soil and Water Conservation*, 55 : 355-364.

Van Muysen, W., Van Oost, K. et Govers, G., 2006. Soil translocation resulting from multiple passes of tillage under normal field operating conditions. *Soil & Tillage Research*, 87 : 218-230.

Van Oost, K., Govers, G. et Desmet, P., 2000. Evaluating the effects of changes in landscape structure on soil erosion by water and tillage. *Landscape Ecology*, 15 : 577-589.

Van Oost, K., Govers, G., Quine, T.A., Heckrath, G., Olesen, J.E., De Gryze, S. et Merckx, R., 2005a. Landscape-scale modeling of carbon cycling under the impact of soil redistribution: The role of tillage erosion. *Global Biogeochemical Cycles*, 19, 13 p.

Van Oost, K., Van Muysen, W., Govers, G., Deckers, J. et Quine, T.A., 2005b. From water to tillage erosion dominated landform evolution. *Geomorphology*, 72 : 193-203.

Van Oost, K., Quine, T.A., Govers, G. et Heckrath, G., 2006. Modeling soil erosion induced carbon fluxes between soil and atmosphere on agricultural land using SPEROS-C. Soil Erosion and Carbon Dynamics, 37-51 p.

Van Oost, K., Quine, T.A., Govers, G., De Gryze, S., Six, J., Harden, J.W., Ritchie, J.C., McCarty, G.W., Heckrath, G., Kosmas, C., Giraldez, J.V., da Silva, J.R.M. et Merckx, R., 2007. The impact of agricultural soil erosion on the global carbon cycle. *Science*, 318 : 626-629.

Van Oost, K., Quine, T.A., Govers, G. et Heckrath, G., 2006. Modeling soil erosion induced carbon fluxes between soil and atmosphere on agricultural land using SPEROS-C. Soil Erosion and Carbon Dynamics, 37-51 p.

Van Oost, K., Six, J., Govers, G., Quine, T. et De Gryze, S., 2008. Soil erosion: A carbon sink or source? Response. *Science*, 319 : 1042-1042.

Van Rompaey, A.J.J., Verstraeten, G., Van Oost, K., Govers, G. et Poesen, J., 2001. Modelling mean annual sediment yield using a distributed approach. *Earth Surface Processes and Landforms*, 26, 1221-1236.

Van Vliet-Lanoë, B., 1990. The genesis and age of the argillic horizon in Weichselian loess of northwestern Europe. *Quaternary International*, 5 : 49-56.

Van Vliet-Lanöe, B., Pellerin, J. et Helluin, M., 1995. Landform development and pedogenesis: The effects of the last glacial cycle in the forest of Fougeres (Ille et Vilaine, Brittany, France). *Zeitschrift Fur Geomorphologie*, 39 : 489-510.

Vanniere, B., Bossuet, G., Walter-Simonnet, A.V., Gauthier, E., Barral, P., Petit, C., Buatier, M. et Daubigney, A., 2003. Land use change, soil erosion and alluvial dynamic in the lower Doubs Valley over the 1st millenium AD (Neublans, Jura, France). *Journal of Archaeological Science*, 30, 1283-1299.

Vasques, G.M., Grunwald, S., Comerford, N.B. et Sickman, J.O., 2010. Regional modelling of soil carbon at multiple depths within a subtropical watershed. *Geoderma*, 156 : 326-336.

Verheijen, F.G.A., Jones, R.J.A., Rickson, R.J. et Smith, C.J., 2009. Tolerable versus actual soil erosion rates in Europe. *Earth-Science Reviews*, 94 : 23-38.

Viaud, V., Angers, D.A. et Walter, C., 2010. Toward Landscape-Scale Modeling of Soil Organic Matter Dynamics in Agroecosystems. *Soil Science Society of America Journal*, 74 : 1847-1860.

Viaud, V., Angers, D. et Walter, C., 2011. Challenges towards landscape-scale modeling of SOC dynamics in agroecosystems. International Symposium on Soil Organic matter 2011. Organic matter dynamics - from soils to oceans. Leuven, Belgium, 11-14 July 2011.

Walling, D.E. et Quine, T.A., 1992. The use of caesium-137 measurements in soil erosion surveys. Erosion and sediment transport monitoring programmes in river basins. Proceedings of the International Symposium held at Oslo, Norway, 24-28 August 1992., 143-152 p.

Walling, D.E. et He, Q., 2001. Models for converting 137Cs measurements to estimates of soil redistribution rates on cultivated and uncultivated soils (uncluding software for model implementation). A contribution to the I.A.E.A. co-ordinated research programmes on soil erosion (D1.50.05) and sedimentation (F3.10.01).

Walling, D.E., He, Q. et Whelan, P.A., 2003. Using 137Cs measurements to validate the application of the AGNPS and ANSWERS erosion and sediment yield models in two small Devon catchments. *Soil and Tillage Research*, 69 : 27-43.

Walter, C., Merot, P., Layer, B. et Dutin, G., 2003a. The effect of hedgerows on soil organic carbon storage in hillslopes. *Soil Use and Management*, 19 : 201-207.

Walter, C., Rossel, R.A.V. et McBratney, A.B., 2003b. Spatio-temporal simulation of the field-scale evolution of organic carbon over the landscape. *Soil Science Society of America Journal*, 67 : 1477-1486.

Walter, C., Lagacherie, P. et Follain, S., 2007. Integrating Pedological Knowledge into Digital Soil Mapping. In: A.B.M. P. Lagacherie et M. Voltz (Editeurs), Developments in Soil Science. Elsevier, p. 281-615.

Walton, J.T., 2008. Subpixel urban land cover estimation: Comparing Cubist, Random Forests, and support vector regression. *Photogrammetric Engineering and Remote Sensing*, 74 : 1213-1222.

Wischmeier, W.H. et Smith, D.D., 1978. Predicting Rainfall Erosion Losses. Handbook 537. US Department of Agriculture,Agricultural Research Service, Washington, DC.

Xu, C.G., He, H.S., Hu, Y.M., Chang, Y., Li, X.Z. et Bu, R. C., 2005. Latin hypercube sampling and geostatistical modeling of spatial uncertainty in a spatially explicit forest landscape model simulation. *Ecological Modelling*, 185 : 255-269.

Yang, X.M., Zhang, X.P., Fang, H.J., Zhu, P., Ren, J. et Wang, L. C., 2003. Long-term effects of fertilization on soil organic carbon changes in continuous corn of northeast China: RothC model Simulations. *Environmental Management*, 32 : 459-465.

Yoo, K., Amundson, R., Heimsath, A.M. et Dietrich, W.E., 2006. Spatial patterns of soil organic carbon on hillslopes: Integrating geomorphic processes and the biological C cycle. *Geoderma*, 130 : 47-65.

Yoo, K., Mudd, S.M., Sanderman, J., Amundson, R. et Blum, A., 2009. Spatial patterns and controls of soil chemical weathering rates along a transient hillslope. *Earth and Planetary Science Letters*, 288 : 184-193.

Zapata, F., 2003a. Field application of the Cs-137 technique in soil erosion and sedimentation studies - Introduction. *Soil & Tillage Research*, 69 : 1-2.

Zhang, X.C. et Nearing, M.A., 2005. Impact of climate change on soil erosion, runoff and wheat productivity in central Oklahoma. *Catena*, 61 : 185-195.

Zhang, Z.Q., Yu, D.S., Shi, X.Z., Warner, E., Ren, H.Y., Sun, W.X., Tan, M.Z. et Wang, H.J., 2010. Application of categorical information in the spatial prediction of soil organic carbon in the red soil area of China. *Soil Science and Plant Nutrition*, 56 : 307-318.

Listes

Liste des Tables

Liste des Figures

Annexes

Annexe 1. Cartographie Régionale du matériau parental des sols de Bretagne

Geomorphology 133 (2011) 90–99

Contents lists available at ScienceDirect

Geomorphology

journal homepage: www.elsevier.com/locate/geomorph

Regional mapping of soil parent material by machine learning based on point data

Marine Lacoste [a,b,*], Blandine Lemercier [a,b,c], Christian Walter [a,b,c]

[a] INRA, UMR1069, Sol Agro et hydrosystème Spatialisation, F-35000 Rennes, France
[b] AGROCAMPUS OUEST, UMR1069, Sol Agro et hydrosystème Spatialisation, F-35000 Rennes, France
[c] Université européenne de Bretagne, France

article info

Article history:
Received 15 December 2010
Received in revised form 7 June 2011
Accepted 20 June 2011
Available online 25 June 2011

Keywords:
Soil parent material
Digital soil mapping
Regional scale
Boosted classification tree
Pedogenesis factor

abstract

A machine learning system (MART) has been used to predict soil parent material (SPM) at the regional scale with a 50-m resolution. The use of point-specific soil observations as training data was tested as a replacement for the soil maps introduced in previous studies, with the aim of generating a more even distribution of training data over the study area and reducing information uncertainty. The 27,020-km^2 study area (Brittany, northwestern France) contains mainly metamorphic, igneous and sedimentary substrates. However, superficial deposits (aeolian loam, colluvial and alluvial deposits) very often represent the actual SPM and are typically under-represented in existing geological maps. In order to calibrate the predictive model, a total of 4920 point soil descriptions were used as training data along with 17 environmental predictors (terrain attributes derived from a 50-m DEM, as well as emissions of K, Th and U obtained by means of airborne gamma-ray spectrometry, geological variables at the 1:250,000 scale and land use maps obtained by remote sensing). Model predictions were then compared: i) during SPM model creation to point data not used in model calibration (internal validation), ii) to the entire point dataset (point validation), and iii) to existing detailed soil maps (external validation). The internal, point and external validation accuracy rates were 56%, 81% and 54%, respectively. Aeolian loam was one of the three most closely predicted substrates. Poor prediction results were associated with uncommon materials and areas with high geological complexity, i.e. areas where existing maps used for external validation were also imprecise. The resultant predictive map turned out to be more accurate than existing geological maps and moreover indicated surface deposits whose spatial coverage is consistent with actual knowledge of the area. This method proves quite useful in predicting SPM within areas where conventional mapping techniques might be too costly or lengthy or where soil maps are insufficient for use as training data. In addition, this method allows producing repeatable and interpretable results, whose accuracy can be assessed objectively.

© 2011 Elsevier B.V. All rights reserved.

1. Introduction

Soil parent material (SPM), regardless of its state of weathering or consolidation, is the material responsible for forming soil. By virtue of their composition, shape and location, both soils and SPM are geomorphological units involved in various geomorphological processes related to landscape formation and evolution (Jungerius, 1985). Most geomorphological studies that deal with soil erosion mapping or predictions make use of soil type, soil properties or SPM data extracted from soil maps (Terranova et al., 2009; Feng et al., 2010; Nigel and Rughooputh, 2010; Verachtert et al., 2010). Soil maps were typically only produced by application of conventional soil survey methods, resulting from complex mental models developed by pedologists during field surveys. However, such conventional methods are both costly and time-consuming and moreover mental models have rarely been clearly formulated and transmitted (McKenzie and Ryan, 1999). Over the past few years, digital soil mapping (DSM) methods have been developed as an alternative to conventional soil survey methods. DSM is a computer-assisted creation of digital soil maps (using soil classes or properties), whose uses and methods were compiled by McBratney et al. (2003). DSM is based on the SCORPAN model, which is a generalization of Jenny's (1941) equation that formalizes the relationships between soil properties and environmental attributes:

$$S = f(s; c; o; r; p; a; n) \quad (1)$$

with S: soil class or properties, s: internal soil data, c: climate, o: organisms, r: relief, p: parent material, a: age (time factor), and n: space. Machine learning offers a means for solving Eq. (1) and refers to knowledge discovery in databases using an algorithm to learn the relationship between a response variable and predictors (Breiman, 2001). The machine learning protocol includes approaches based on regressions and classifications (either unsupervised or supervised), both of which rely on preexisting soil and environmental datasets. As an

* Corresponding author at: INRA, UMR1069 SAS, 65 rue de Saint-Brieuc 35042 Rennes cedex, France. Tel.: +33 223 48 70 47; fax: +33 223 48 54 30.
E-mail address: Marine.Lacoste@rennes.inra.fr (M. Lacoste).

illustration, regressions have been conducted to predict soil bulk density (Martin et al., 2009), unsupervised classifications introduced to create soil maps with new soil classifications (Odeh et al., 1992) and supervised classifications to fill gaps in soil maps (Bui and Moran, 2003). Supervised classification problems have been solved by implementing neural networks (Zhu, 2000) or tree-based models (Lagacherie et al., 1995; Bui and Moran, 2003). Though neural networks appear to be very efficient, they still produce results that are more difficult to interpret than tree-based models (McKenzie and Ryan, 1999). Moreover, tree-based models can be used with just a minimal training dataset (Friedman and Meulman, 2003). Tree-based models were first developed by Breiman (Breiman et al., 1984) and later improved by: bagging (Breiman, 1996), boosting (Freund and Schapire, 1996; Friedman, 2001; Elith et al., 2008), and stochastic gradient boosting procedures (Friedman, 2002). Machine learning tools and techniques have been dramatically improved over the last several years and now may be widely used in DSM (Lim et al., 2000; Bui and Moran, 2003; Grinand et al., 2008; Martin et al., 2009), as a result of easier access to a digital elevation model (DEM) and remote sensing imagery, in conjunction with progress made in geographical information systems and statistics. DEMs are in fact a practical tool for providing exhaustive spatial information on the r factor of the SCORPAN model and has become more extensively used in soil sciences and geomorphological studies (McBratney et al., 2003; Dobos and Hengl, 2009; Hengl and MacMillan, 2009; Vogel and Marker, 2010). SPM (the p factor) is also a key factor in explaining soil distribution and has systematically played a high-profile role in tree-based models established at the regional scale (Bui et al., 2006; Bou Kheir et al., 2010; Vasques et al., 2010). Data for the p factor are generally derived from existing geological or lithological maps, and less often from soil maps, soil surveys or airborne gamma spectrometry (Table 1). Geological bedrock is often covered by superficial deposits (e.g., colluvial, alluvial and aeolian loam deposits); these materials thus represent the actual SPM and strongly influence landforms, landscape evolution and soil properties such as texture and waterlogging. Existing geological and geomorphological maps generally overlook or underestimate these materials; surface deposits tend therefore to be poorly mapped at the regional scale. The use of such existing maps as p factor data of the SCORPAN model introduces a strong bias into soil property predictions, making it necessary to produce more accurate SPM maps based on modern methods including machine learning approaches. The training data source is critical to machine learning methods. According to McBratney et al. (2003), the primary concern with DSM is the insufficient number of actual soil observations to fit the models. To the best of our knowledge, most existing studies rely on data extracted from soil maps to predict soil properties (e.g., Henderson et al., 2005; Bui et al., 2006). Then again, soil maps can be non-exhaustive and fail to cover the full range of existing SPM types within a given study area. Another problem with the use of soil maps as training data pertains to their presentation as non-homogenous mapping units (Lin et al., 2005). By definition, even with accurate soil maps, these units are not pure and the probability that the pixel value corresponds to the predicted soil map unit is less than 1. It is therefore useful to test the performance of machine learning approaches in situations where point soil data are available, since these situations also serve to even out the distribution of training data over the entire study area. The objectives of this study are thus to: i) produce a predictive map of SPM at the regional scale, with known accuracy and by collecting every existing data point; and ii) assess a learning method that produces explicit results and that is based on a point data training dataset stemming from soil survey as training data.

2. Material and methods

2.1. Study area

The study area (27,020 km^2) is located in northwestern France and comprises all of Brittany (Fig. 1). The area's climate is oceanic with a mean annual rainfall between 500 and 1500 mm, and a mean annual temperature ranging from 10.5 °C to 13 °C. The topography is generally smooth and highly correlated with the geological formations. The soil types encountered are mainly Cambisols, Luvisols, Leptosols and Stagnosols (IUSS Working Group WRB, 2007). Brittany is part of the Armorican Massif, whose geology is complex and influenced by several orogenies and marine transgression/regression alternations. The northern and southern parts of Brittany are primarily composed of igneous and metamorphic rocks (granite, gneiss and micaschist), whereas the central zone contains sedimentary rocks (mainly soft schist, sandstone and gritty schist). Brittany's geology is complicated even further by superficial deposits (alluvial, colluvial and aeolian loam deposits) overlaying the original bedrock. Aeolian loam was laid over northern Europe during the last Quaternary glacial period (~ 28–13 Ka BP) and in Brittany exhibits a trend of decreasing depth from north to south (Frechen et al., 2003; Haase et al., 2007). Additional local variability due to heterogeneous initial deposits or subsequent redistribution complicates the distribution of aeolian loam and diminishes the quality of existing geological maps of Brittany, on which only deposits thicker than 2 m are shown. The prediction of superficial deposits, especially aeolian loam, was therefore a key challenge of this study.

Table 1
Examples of soil parent material mapping sources used to predict soil classes or soil properties in previous studies.

Authors	Study area (location, area)	Predicted factor (resolution of the predicted map)	Source of the soil parent material mapping (resolution)
Legros and Bonneric (1979)	France, 624 km^2	Soil classes (1:500,000)	Geological and lithological maps
Bell et al. (1992)	USA	Soil drainage classes	Bedrock and superficial geology (1:24,000)
McKenzie and Austin (1993)	Australia, 5 km^2	Soil properties (1:10,000)	Soil survey, aerial photo
Dymond and Luckman (1994)	New Zealand	Soil series (1:15,000)	Regolith map
Lagacherie and Holmes (1997)	France, 35 km^2	Soil units (1:50,000)	Geological map
Bui et al. (1999)	Australia, 1300 km^2	Soil classes (1:250,000)	Geological map (1:250,000)
McKenzie and Ryan (1999)	Australia, 500 km^2	Soil properties	Geological map (1:100,000), gamma radiations (10,000 m^2)
Thomas et al. (1999)	France, 60 km^2	Soil classes (1:100,000)	Geological map (1:50,000)
Ryan et al. (2000)	Australia, 2.7 and 2500 km^2	Soil properties	Airborne gamma spectrometry
Zhu (2000)	Montana (USA), 40 km^2	Soil series	Geological map
Moran and Bui (2002)	Australia, 1,100,000 km^2	Soil classes (1:250,000)	Geological map (1:250,000)
Bui and Moran (2003)	Australia, 1,100,000 km^2	Soil classes (1:250,000 to 1:1,000,000)	Lithology map
Bui et al. (2006)	Australia	Soil properties (1.1 km^2)	Lithology map
Ballabio (2009)	Italy, 76 km^2	Soil properties	Lithology/structural units map
Bou Kheir et al. (2010)	Denmark, 5748 km^2	Soil organic carbon (1:50,000)	Geological map (1:25,000)
Vasques et al. (2010)	Florida (USA), 3585 km^2	Soil carbon, 30 m grid	Environmental geology map (1:250,000), surficial geology map (1:100,000)

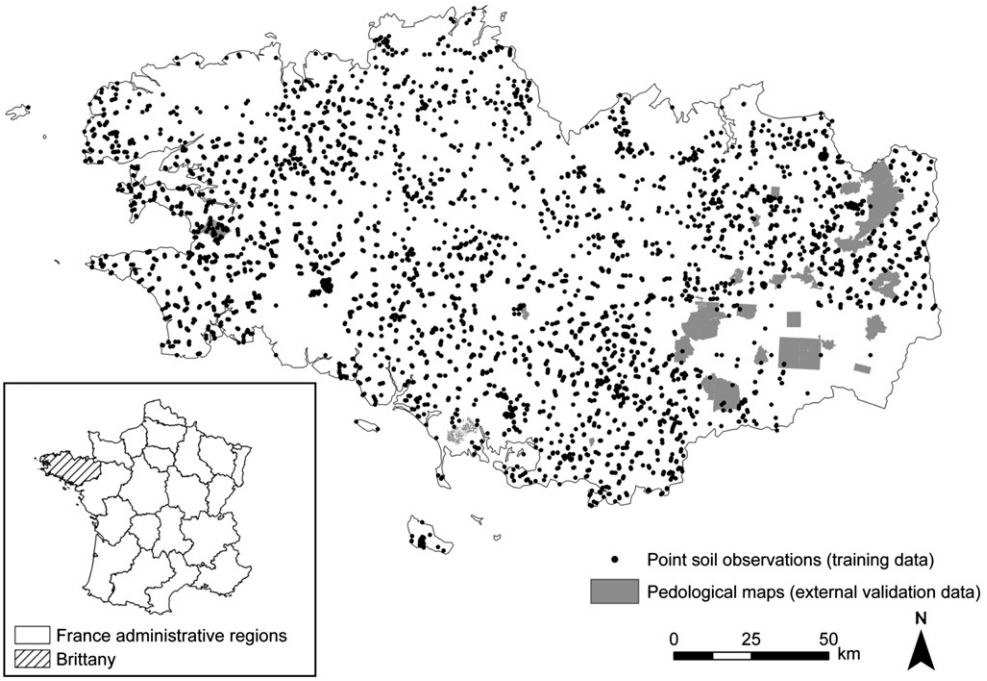

Fig. 1. Location of the study area, training data and external validation maps.

2.2. Digital datasets

2.2.1. The training dataset

The training data used were derived from 4920 point soil observations (auger borings and soil profiles described during soil surveys) distributed over the study area (Fig. 1). Soil observation locations were determined by applying a two-step method: first, pre-defined landscape units were selected using stratified random sampling; and second, soil observations were positioned on transects along hillslopes. Soil profiles were described by professional surveyors between 2000 and 2009 pursuant to a consistent field procedure. In all, 20 classes of SPM were distinguished: 11 belong to geological bedrock formations, and the other nine are superficial deposits including rare SPM types that have been aggregated into a single class (Table 2). The most common formations in the training data were granite, soft schist, modern alluvial deposits, aeolian loam deposits, colluvial deposits and micaschist, totaling 70% of the study area.

Table 2
Frequency distribution of soil parent material in the training dataset (soil descriptions at 4920 points).

SPM	Name	Frequency (%)
Granite	G	21
Soft schist	N	14
Aeolian loam	L	11
Alluvial deposits	V	10
Colluvial deposits	U	9
Micaschist	F	7
Sandstone	Q	5
Gritty schist	R	4
Medium schist	O	3
Alluvial terrace	T	3
Gneiss	I	3
Peat	H	2
Volcanic rock	Y	2
Hard schist	P	2
Quartz and puddingstone rock	X	1
Sand	S	1
Dune	D	1
Other (rare) parent material	K	0.4
Marsh	M	0.3
Rock-fall	E	0.3

2.2.2. Predictive data

Seventeen environmental predictors were selected (Table 3), with six attributes being derived directly from a 50-m DEM (IGN, 2008): elevation, local hillslope gradient, profile and tangential curvatures, sub-catchment hillslope length, and local slope direction. Four other attributes were calculated using the MNTsurf software (Squividant, 1994): hydrological distance from the nearest stream, elevation above the nearest stream, Strahler stream order (Strahler, 1952), and the Modified Compound Topographic Index (Beven and Kirkby, 1979; Merot et al., 1995; Gascuel-Odoux, 1998; Merot et al., 2003). Topographic units were defined by Lemercier (unpublished data) from the DEM and derived attributes (slope, sub-catchment hillslope length, elevation above the nearest stream, and profile and tangential curvatures) according to both multiple correspondence analysis and hierarchical ascendant classification. Geology in the study area was described by three maps: a 1/250,000 geological map showing bedrock lithological units (Chantraine et al., 2002); a 1:250,000 superficial deposits map delineating five types of deposits (aeolian loam, beach and sand dune, marine sediment, and Meso-Cenozoic sediment; Thomas, 2006); and a map of aeolian loam deposits, as determined by geostatistical analysis of the topsoil granulometric data (Walter, unpublished data). Gamma-ray spectrometry data were recorded by means of airborne geophysical surveys, with measurements being interpolated by ordinary kriging in order to produce a 250-m resolution map (Bonijoly et al., 1999). We used two attributes derived from this map: the K/Th ratio (Wilford et al., 1997) and the deviation from mean emission K of the related lithological unit defined by Chantraine et al. (2002). Lastly, land use was taken into account via a digital landscape map derived from a 250-m resolution MODIS image (Le Du-Blayo et al., 2008).

Table 3
Environmental predictors used to predict soil parent material.

Name	Description (units)	Soil forming factor	Type	Mean (range)
Terrain attributes derived from DEM				
Elev	Elevation (m)	r	Q	97 (0–382)
Slope	Local hillslope gradient (%)	r	Q	5.63 (0–146)
Vcurv	Profile (vertical) curvature (m.100 m^{-1})	r	Q	0 (−9–9)
Hcurv	Tangential (horizontal) curvature (m.100 m^{-1})	r	Q	0 (−8–6)
Catlg	Sub-catchment hillslope length: hydrological distance between the nearest and the furthest pixels from the stream (m)	r	Q	571 (0–2430)
Dist	Hydrological distance to the nearest stream	r	Q	353 (0–2483)
Aspect	Direction of the local slope (°)	r	Q	178 (−1–360)
Deniv	Elevation above the nearest stream (m)	r	Q	16 (0–302)
CTI	Modified Compound Topographic Index (Merot et al., 1995 after Beven and Kirkby, 1979)	r	Q	4 (0–27)
Strahler	Strahler stream order (Strahler, 1952)	r	C	7 classes
Topo	Landscape topographic units (Lemercier, unpublished data)	r	C	9 classes
Geological data (scale 1:250 000)				
Supdep	Superficial deposits map (Thomas, 2006)	p	C	5 classes
Loam	Estimated map of aeolian loam deposits (Walter, unpublished data)	p	C	3 classes
Geol	Bedrock lithological units (Chantraine et al., 2002)	p	C	123 classes
Gamma-ray spectrometry (airborne geophysical survey)				
Ktratio	K/Th ratio (Bonijoly et al., 1999)	p,s	Q	0.19 (−1.1–3.06)
Devk	Deviation from mean K emissions of the corresponding lithogeological unit (Bonijoly et al., 1999)	p	Q	0 (−1.94–2.11)
Land use				
Land	Digital landscape units map, defined from remotely sensed data (Modis imagery) (Le Du-Blayo et al., 2008)	o	C	20 classes

r = relief, p = parent material, s = soil properties, o = organisms, Q = quantitative, C = categorical.

2.3. Machine learning procedure

Fig. 2 provides an overview of the method employed to produce the SPM map. The learning procedure was based on the MART (Multiple Additive and Regression Trees) algorithm (Friedman, 2001). MART allows solving predictive learning problems through building classification or regression trees and using the "stochastic gradient boosting" procedure to improve prediction accuracy and avoid overfitting in comparison with a simple tree-based model (Friedman et al., 2000; Friedman and Meulman, 2003; McBratney et al., 2003; Lawrence et al., 2004; Gey and Poggi, 2006; Elith et al., 2008; Martin et al., 2009). A tree consists of a binary recursive partition of the training data, with predictors and split points being chosen to both minimize prediction errors and yield homogenous final groups in the terminal nodes. The MART algorithm iteratively builds relatively small trees from a fraction of the training data (randomly sampled without replacement) until a satisfactory and stable error rate is achieved. With the introduction of boosting, more weight is iteratively ascribed to poorly-classified training data so as to reduce classification errors. The final model is a combination of all the simple trees. MART, like other tree-based algorithms, offers a number of advantages (Friedman and Meulman, 2003). For starters, it is non-parametric, meaning that no hypothesis is required on the variable distribution and no data transformation is needed either. Moreover, it is not sensitive to missing values, outliers and data uncorrelated with the variable to be predicted, even if such data may be numerous. As opposed to other learning methods, the interactions between predictors (whether linear or not) are taken into account without any a priori knowledge. MART is capable of handling qualitative and quantitative predictors, both numerical and ordinal, equally well. Model outcomes are not sensitive to differing measurement scales from one predictor to the next. The most influential model setting parameters are: the learning rate (determination of the contribution of each tree to the final model), tree complexity (i.e. tree size, control over the number of terminal nodes), and the size of the sample fraction from the training data used to build each tree (Friedman, 2001). MART requires two

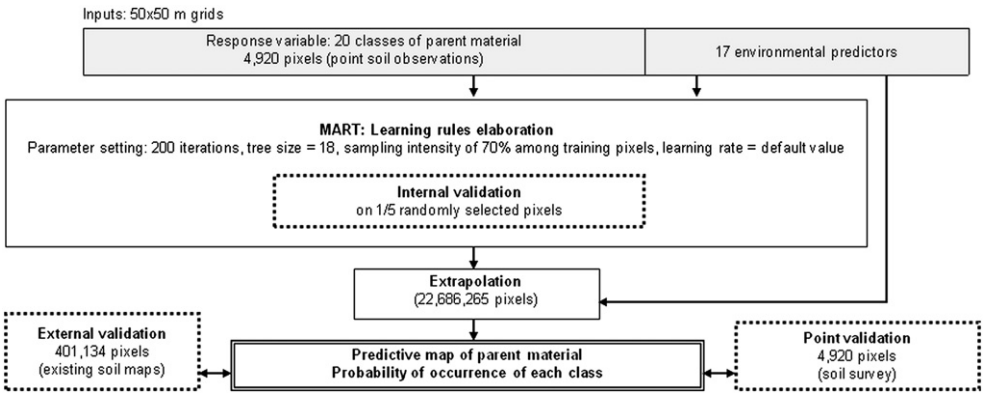

Fig. 2. Methodological overview for the predictive mapping of soil parent material.

input datasets to create the learning rules: the response variable, here SPM; and a set of predictors. The MART application, implemented in the R statistical software (R Development Core Team, 2008), was run in its classification mode. The results of a sensitivity analysis (data not shown) have led to identifying the following parameter settings: number of iterations (i.e. number of trees) = 200; number of terminal nodes in each tree = 18; and fraction of training observations randomly sampled at each iteration = 0.7; and learning rate = default value defined by Eq. (2):

$$\text{learning rate} = \max(0.01; 0.1 \cdot \min(1; \text{nrow}(x) \cdot \text{ntest}) / 10000) \quad (2)$$

with nrow(x): number of pixels in the training data, ntest: number of pixels in the test sample used for the internal validation, i.e. 1/5 of the training data.

2.4. Model interpretation and accuracy

The MART model, established from the training data, was extrapolated over the entire study area using exhaustive predictors. The prediction was performed for 22,686,265 pixels with a 50-m resolution. For each pixel, the probability of occurrence of each SPM class was estimated and the predicted SPM was derived from the class with the maximum probability.

Three validations were performed in order to evaluate prediction accuracy (Fig. 2). The internal and point validation allowed assessing model accuracy before its extrapolation over the study area. The external validation step then made it possible to assess the final SPM prediction map. Internal validation was calculated as the model was increasing in size and performed with 1/5 of the data used at each iteration. The point validation was carried out with all available point SPM data, a portion of which was used to develop the predictive SPM model. This validation enabled estimating the quality of the MART model fit (Martin et al., 2009). For the external validation step, the predictive SPM map was compared to preexisting SPM maps derived from 1:25,000 scale soil maps, located mainly in the eastern part of the study area (Fig. 1) and covering an area of 20 km^2 (corresponding to 3.7% of the study area). These maps presented all SPM classes, except for rockfalls. Error matrices generated from both point and external validations served to calculate a set of performance indices. General indications of model performance were provided by overall accuracy measures and the Kappa index, which is a chance-corrected index of the agreement between observed and predicted soil classes (Cohen, 1960; Elith et al., 2008). This Kappa index assumes values between −1 and 1. The higher the value, the better the prediction (Bergeri et al., 2002). Moreover, the level of agreement between predictions and observations was measured for each class by calculating two precision indices, the producer's and user's accuracies (Story and Congalton, 1986). According to Congalton and Green (2009), given n samples assigned to one of k predicted classes, and independently to one of the same k classes in the reference datasets, η_{ij} being the number of samples classified into category $i = \{1,2,\ldots,k\}$ in the prediction and $j = \{1,2,\ldots,k\}$ in the reference dataset, the number of samples classified into category i in the prediction is given by:

$$\eta_{i+} = \sum_{j=1}^{k} \eta_{ij} \quad (3)$$

and the number of samples classified into category j in the reference dataset is given by:

$$\eta_{+j} = \sum_{i=1}^{k} \eta_{ij}. \quad (4)$$

The producer's accuracy P_p for class j and the user's accuracy P_u for class i are calculated by:

$$P_{pj} = \eta_{ij} / \eta_{+j} \quad (5)$$

$$P_{ui} = \eta_{ij} / \eta_{i+}. \quad (6)$$

For a given SPM class, the producer's accuracy estimates the amount of overestimation, while the user's accuracy indicates the underestimation (Schmidt et al., 2008).

3. Results

3.1. Model description

3.1.1. Relative importance of predictors

Considering the overall SPM prediction (Table 4), the most influential parameter was the geological map (geol). The landscape map (land) was the only other predictor with a relative importance above 50%. Even though other predictors seem to exert little influence on the overall SPM prediction, all predictors were nonetheless used to draft the learning rules. The parameter showing minimum relative importance towards overall SPM prediction was the aeolian loam deposit estimation map (loam, 16%). Moreover, in reference to the prediction of particular SPM types, the relative importance of predictors actually changed from one SPM to the next. Table 4 lists the relative importance of predictors applied to SPM predictions. For the aeolian loam deposit prediction (Table 4), geol was still the most important predictor, although three others also exerted a relative importance in excess of 50%: the superficial deposits map (supdep), landscape map (land), and topographical unit map (topo). When considering the alluvial deposit prediction (Table 4), elevation above the nearest stream (deniv) proved to be the most influential predictor, with three other predictors exhibiting a relative importance greater than 50%: geol, land and Strahler stream orders (strahler). As for the colluvial deposit prediction (Table 4), geol was the most prominent predictor and two other predictors revealed more than 50% relative importance: land, and the profile curvature (vcurv). The predictors with more limited overall importance might therefore be weighty to predict a particular class of SPM. For instance, the vcurv variable showed 24% of overall importance, although it exhibited a relative importance of 54% in colluvial deposits prediction (Table 4).

3.1.2. Assessment of model accuracy

The various indices of SPM prediction model performance are presented in Table 5. Internal and point validations showed an overall accuracy of respectively 56% and 81%, while point validation yielded a Kappa index of 0.78, thus illustrating the good agreement between observed and predicted SPM. According to the internal validation, the best predicted SPM types (i.e. internal accuracy ≥ overall accuracy) were granite, soft schist, aeolian loam, micaschist and dune. Other SPM types, corresponding to less frequent materials, were poorly predicted (sandstone, alluvial deposits, hard schist, gritty schist, medium schist, alluvial terraces, alluvial deposits, peat, quartz and puddingstone rock). The SPM types that appeared very infrequently in the training dataset were not taken into account during the internal validation step (rockfall, quartz and puddingstone rock, marsh and other rare SPM types). The accuracy rates derived from point validation were high across all SPM classes, both the producer's and user's accuracies (with values ranging respectively from 58% to 100% and from 70% to 100%). Producer's and user's accuracies allowed estimating the levels of overestimation or underestimation in SPM predictions. For the most accurately predicted SPM types (granite, soft schist, micaschist and alluvial and dune deposits), the producer's accuracy was systematically greater than the user's, implying that the model overestimates the occurrence of these materials. All other materials were underestimated

Table 4
Relative contribution of environmental predictors for a boosted classification tree model to predict soil parent material.

SPM class	Relative importance of environmental predictors (%)																
	Geol	Land	Deniv	CTI	Topo	Elev	Devk	Supdep	Hcurv	Dist	Ktratio	Strahler	Vcurv	Aspect	Catlg	Slope	Loam
All	100	52	48	47	40	35	35	34	32	31	28	28	24	24	23	20	16
D	100	78	4	40	62	17	3	96	16	5	8	2	2	6	9	10	1
E	100	64	12	18	59	30	27	1	23	26	29	1	23	42	19	34	2
F	100	49	34	34	44	55	29	8	36	25	39	26	36	24	29	23	7
G	100	40	30	44	35	34	33	18	21	30	25	14	27	15	10	18	13
H	100	86	50	39	70	73	47	18	46	17	27	53	37	46	19	24	20
I	100	77	49	50	58	35	25	12	34	27	24	17	26	41	23	26	0
K	100	67	15	20	62	23	13	59	17	12	16	2	32	7	14	14	8
L	100	64	40	46	52	38	44	86	32	43	40	17	48	38	37	33	39
M	93	100	3	3	3	16	2	22	1	5	33	24	3	12	12	2	1
N	100	47	40	53	40	39	39	32	33	27	36	21	31	33	27	26	19
O	100	82	31	36	68	61	38	9	30	37	47	25	42	48	27	46	0
P	100	96	26	52	94	24	52	0	33	31	29	16	27	39	39	35	0
Q	100	51	46	46	48	30	47	16	35	29	32	13	26	19	26	14	14
R	100	69	44	47	59	43	33	15	47	32	36	15	46	43	41	26	15
S	100	76	27	22	88	29	23	78	18	19	38	0	17	22	21	19	22
T	100	100	96	67	81	65	76	97	68	56	53	33	54	61	51	46	46
U	100	62	27	31	46	32	34	25	42	34	25	36	54	33	26	35	7
V	98	57	100	36	40	28	37	21	34	19	27	52	33	41	36	29	9
X	100	66	47	32	69	43	42	0	26	27	38	0	35	32	24	24	18
Y	100	61	24	16	43	28	25	16	22	23	21	10	43	21	29	17	19

Table 2 defines the names of SPM classes.
Table 3 defines the names of environmental predictors.

(i.e. the user's accuracy greater than the producer's), except for alluvial deposits, which were poorly predicted yet overestimated. For aeolian loam deposits and marsh, however, the producer's and user's accuracies were equal or nearly equal (respectively 79% and 78% for aeolian loam, and both accuracies at 93% for marsh).

3.2. The predictive SPM map

The SPM model was extrapolated over the entire study area (Fig. 3). The predictive map integrates all 20 types of SPM present in the training data (Table 5). The spatial extent of the regional distribution of bedrock structures and superficial deposits appears to be consistent with existing knowledge of the study area. According to this map, superficial deposits represent 32% of the total area, with 13% aeolian loam, 9% alluvial deposits and 7% colluvial deposits. The remaining superficial deposits separately represent approximately 1% of the study area. Granite and soft schist were the most widely predicted SPM, covering respectively 24% and 22% of the study area.

3.3. Assessment of predictive SPM map accuracy

3.3.1. External validation

This predictive map was compared to SPM maps extracted from existing 1:25,000-scale soil maps (external validation). Table 5 summarizes the outcomes of this external validation step. The overall accuracy of external validation equaled 54% and the Kappa index amounted to 0.47. According to this external validation, the most accurately predicted SPM types (i.e. mean external accuracy ≥ overall accuracy) were: micaschist, granite, sandstone, soft schist, and aeolian loam. For these SPM types, which are among the most widespread throughout the study area, the producer's accuracy was systematically greater than the user's, hence making the SPM types appear to be overestimated. The other SPM types, less frequently encountered and not as well predicted, turned out to be underestimated (i.e. the user's accuracy exceeded the producer's). Error matrices (not shown here) revealed a confusion between soft schist, granite, and alluvial and colluvial deposits all at the same time.

3.3.2. Validation of the probability of occurrence as a prediction uncertainty indicator

The probabilities of occurrence associated with the predictive SPM map are shown in Fig. 3. It appears therefore that several geological structures have high probabilities of occurrence, in particular granite massifs in the northern and southern parts, as well as some volcanic massifs in the North and aeolian loam deposits also in the North. Lower probabilities were associated with areas where soft schist, gritty schist and sandstone were predominantly predicted (Fig. 3). Fig. 4 was obtained by comparing external validation accuracy and the

Table 5
Accuracy of the prediction of soil parent material class performed with a boosted tree-based classification (MART) model.

Parent material	G	N	L	V	U	F	Q	R	I	O	Y	M	T	P	H	D	S	X	K	E	Overall accuracy	Kappa index
Proportion in the predictive map (%)	24	22	13	9	7	6	5	4	3	3	2	1	1	1	1	b1	b1	b1	b1	b1	–	–
MART accuracy (%)	82	67	59	53	19	75	41	24	44	22	47	–	26	18	5	100	22	–	–	–	56	–
Internal validation (%)																						
Producer's accuracy	92	83	79	83	66	84	76	66	80	71	89	93	76	73	74	100	85	69	58	86	81	0.78
User's accuracy	84	70	78	75	79	83	87	92	88	85	91	93	82	94	87	90	100	98	100	100		
External validation (%)																						
Producer's accuracy	75	84	72	36	11	90	76	14	0	12	0	0	14	50	3	0	0	0	0	–	54	0.47
User's accuracy	70	51	57	49	17	76	63	52	0	46	2	0	24	51	8	0	0	0	3	–		
Mean accuracy (%)	73	67	65	42	14	83	69	33	0	29	1	0	19	51	5	0	0	0	2	–		
Probability of occurrence	0.7	1	0.56	0.5	0.39	0.48	0.54	0	0.48	0	0.54	1	0.44	0.5	0.42	0.53	0	0	0.5	0.3	53	–

Table 2 defines the names of SPM classes.

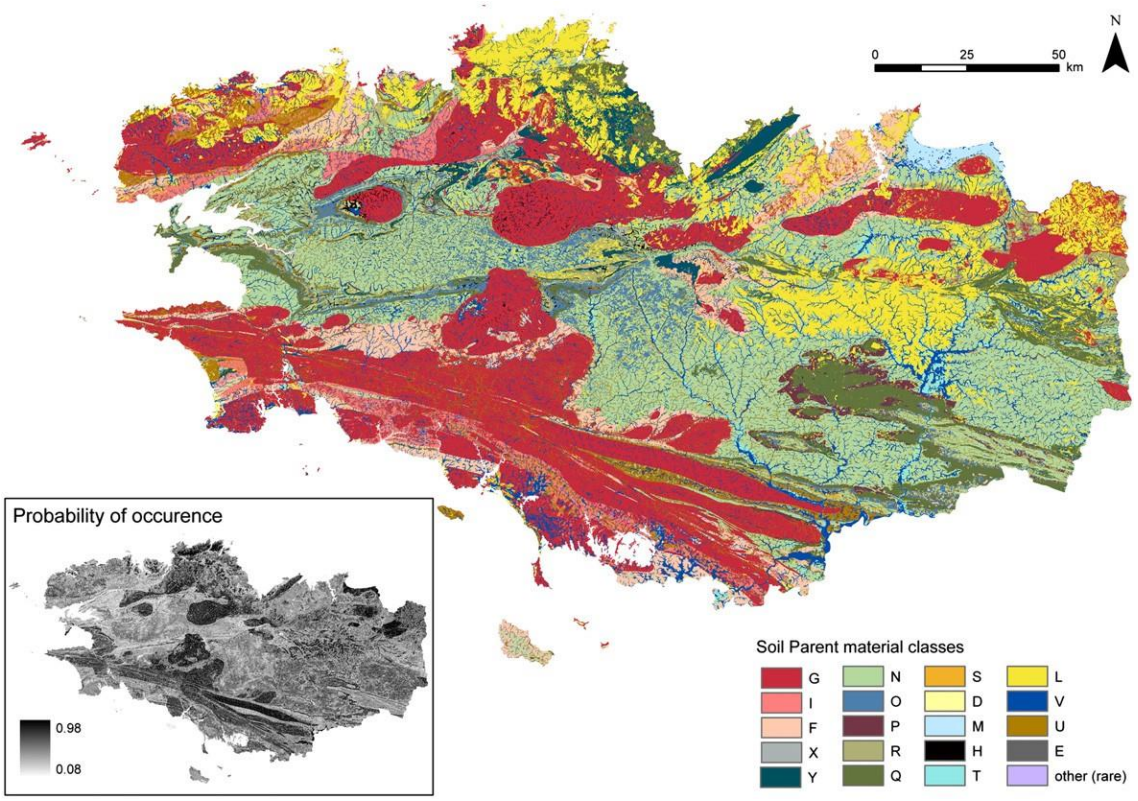

Fig. 3. Predicted soil parent material types and associated probability of occurrence. See Table 2 for soil type codes.

probability of occurrence for every pixel where SPM was predicted. The probabilities of occurrence were then divided into 10 equal classes, for subsequent association with the percentage of accurately predicted pixels (according to the external validation step).

A strong linear correlation exists between the probabilities of occurrence associated with SPM classes and external error rates (Fig. 4); consequently, probabilities of occurrence are a good indicator of prediction uncertainties and allow estimating prediction map accuracy over the entire study area. The overall probability of occurrence for the study area equaled 53% (Table 5), with the most certain predictions found for granite, aeolian loam and sandstone (Table 5 and Fig. 5).

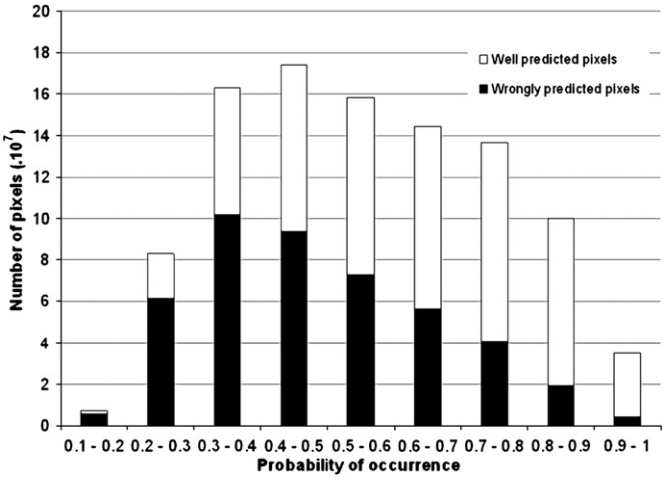

Fig. 4. Relation between the probability of occurrence of soil parent material and overall external validation accuracy.

4. Discussion

4.1. The predictive process

The procedure adopted for this study is based on machine learning and combines very different preexisting datasets in order to create a new representation of the regional distribution of SPM, including survey data, existing maps, and continuous digital datasets covering various aspects like relief, land use and gamma-ray emissions. This procedure however remains very explicit and produces repeatable results; the predictors and their respective contributions are clearly identified and error rates make it possible to assess predictive maps. Another key point using the MART procedure is that it allows us to reduce overfitting, which is a common issue in tree-based methods. First, the use of stochastic gradient boosting introduces some randomness in the boosted procedure, which was proved to shrink overfitting (Friedman, 2002; Lawrence et al., 2004). Second, the critical MART parameter to

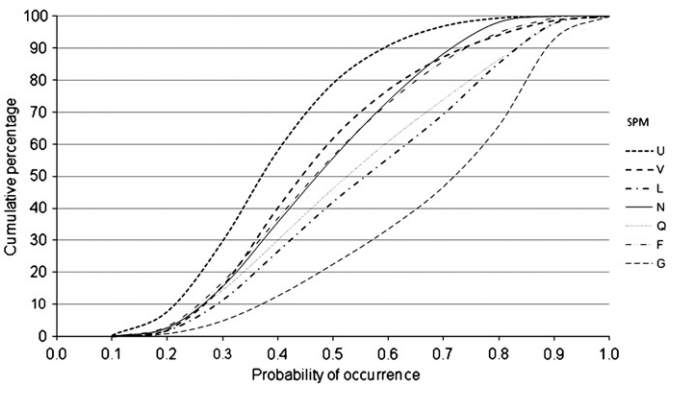

Fig. 5. Cumulative percentage of probability of occurrence for the main predicted soil parent materials.

control overfitting is the learning rate (Elith et al., 2008). It was found in our study that the best learning rate was the default value. Finally, external validation using data independent of the training data is crucial to confirm that the model does not overfit the training data.

4.2. Predictive map accuracy

As regards the overall SPM prediction, accuracy rates were 56% for internal validation, 81% for point validation, 54% for external validation, and 53% for the mean probability of occurrence. These results are consistent with previous studies based on boosted classification tree models: Moran and Bui (2002) predicted soil types using terrain attributes and remotely sensed data with an internal accuracy of 69.9%; Grinand et al. (2008) obtained overall accuracies of 69% and 35% for point and external validations respectively while predicting soil-landscape units using comparable input variables; and Lemercier et al. (in press) produced a predictive SPM map in a reduced part of our study area using 1:25,000 soil maps as training data and found overall validation rates of 73% and 49%, respectively. Another point of discussion to be raised is the sizable gap noted in overall accuracies: the internal validation, external validation and probabilities of occurrence were respectively 56%, 54% and 53%, while point validation reached 81%. Such a difference has been observed in previous studies dealing with soil class prediction or land cover classification (Muchoney and Strahler, 2002; Grinand et al., 2008). These authors explained the gap in accuracy error rates by a spatial autocorrelation of both the pixels used to fit the model and those used for point validation. This explanation is particularly well adapted to the present study, given that some pixels involved in the point validation also belonged to the training dataset, thus they cannot be considered as truly independent. Nevertheless, the difference between overall accuracies must be put into perspective with the validation dataset. The external validation dataset was composed of pixels stemming from existing detailed soil maps (1:25,000) covering a restricted part of the study area (only 3.7%) and primarily located in eastern Brittany. These maps therefore prevented performing external validation on the entire area. A more evenly distributed and larger area might have enabled a better prediction accuracy assessment via external validation. The external validation process introduced another bias since its results were dependent on the purity of the map. Walter (1990) assessed the purity of some of the 1:25,000 soil maps used in this study during external validation. Regarding SPM, the purity of soil units ranged between 86% and 100%. Two biases were introduced when using soil maps as part of the external validation step: i) the maps did not encompass the whole study area; and ii) their SPM units were not homogeneous. The probabilities of occurrence associated with SPM classes seemed however to provide a good substitute for assessing the prediction accuracy over the whole area. The predictive SPM map can be compared to preexisting data, i.e. 1:25,000 soil maps and geological maps. Fig. 6 provides an example of such a comparison in a restricted area. Moreover, the external validation is yet a comparison between the predictive SPM and preexisting SPM maps derived from the soil maps. The predictive map is more complex than the geological map, yet remains less complex than the SPM map extracted from the soil map. All three maps show the same overall bedrock structure (granite, soft schist and sandstone); however, only the predictive SPM map and the SPM map extracted from the preexisting soil maps display a similar spatial coverage of superficial deposits (aeolian loam, alluvial and colluvial deposits). The spatial organization of aeolian loam deposits has thus been considerably improved in the predictive SPM map vs. the preexisting geological map. The external validation reached 54%. The predictive SPM map and SPM map coming from preexisting soil maps present similar global structure regarding the main SPM types (granite, soft schist, and aeolian loam). The major difference between the two is that the predictive SPM shows less local variability, and underestimates SPM such as alluvial deposits, some facies of schist and uncommon SPM like peat. This is perhaps because the distribution of those SPM is really complex and could not be learned from the training data.

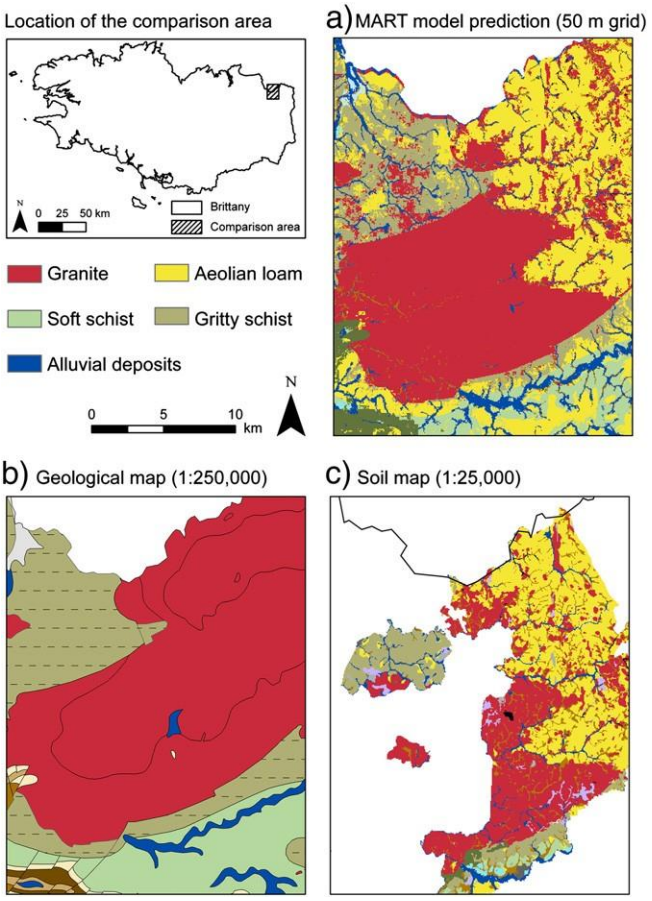

Fig. 6. Local comparison between the predicted soil parent materials based on the MART model and pre-existing data. a) Model prediction. b) Geological map. c) Soil map.

4.3. Reasons of poor predictions

The prediction accuracy may be affected by various sources of error. First of all, the MART model can only predict situations encountered in the training data, though the training area might not be representative of the complete study area. Poor predictions may be explained by the fact that some SPM types were rare, either throughout the study area or in the training data. Even if the training data used herein were well-distributed over the study area, they still represented just one soil observation for a 5-km^2 area (the training data only covered 0.04% of the study area). Moran and Bui (2002) noticed that the sampling intensity from training dataset was determinant for the prediction accuracy. His training data actually covered 25% of the corresponding study area. Lemercier et al. (in press) used 3% of the study area to compose a training dataset. The second identified source of error pertains to intrinsic characteristics of the training data. The various soil surveyors contributing to dataset composition, even those who are highly skilled, necessarily introduce subjective judgment, which locally leads for example to confusion between gritty schist and sandstone or between alluvial and colluvial deposits. Some SPM types, like colluvial and alluvial deposits, were in fact confused during the prediction due to being present in similar landscapes and under similar geomorphological conditions. Thirdly, MART does not take into account the pixel neighborhood during creation of the learning rule, which is a paradoxical situation in spatial studies. Some tests have been conducted in order to include the spatial context of pixels, by applying a filter to predictors generated

from a DEM (Moran and Bui, 2002; Grinand et al., 2008). Lastly, some poor prediction results may be related with the geological properties of the study area and the nature of SPM. The worst SPM predictions were located in areas of high geological complexity, where various facies of gritty schist and sandstone with complex spatial organization were encountered.

4.4. Relevance of the point training data approach

The above results prove that point data can constitute a dataset as efficient as soil maps for use as training data. Moreover, the model has tended to overestimate the most frequent materials, except for colluvial and alluvial deposits (which have been underestimated), and these same results were output from the internal, point and external validations of the SPM prediction. The predictive map actually turned out to be more accurate than preexisting maps. The main SPM types were all accurately predicted (granite, soft schist, micaschist and sandstone), and the map itself presented accurate predictions of superficial deposits (mostly aeolian loam deposits). The probability of occurrence proved a useful tool in assessing prediction accuracy throughout the study area; this measure served to confirm that overall prediction accuracy came close to 50% over the study area, yet some SPM types were locally more accurately predicted.

5. Conclusion

The aim of this study has been to predict SPM at the regional scale by using information derived from existing point soil observations and environmental data via application of a soil-landscape model. A boosted regression and classification tree model (MART), which is a learning machine method recently adopted in the field of soil science, was applied using point soil observations as training data. This use of point soil observations led to a more even distribution of training data within the study area than the distribution derived from soil maps and moreover enabled avoiding the introduction of soil maps with relatively pure soil units as training data. The results of this study reveal a good overall performance of the classification procedure for SPM prediction: the overall accuracy calculated on pixels used to fit the model (i.e. point validation) equaled 81%. The level of accuracy dramatically decreased for external validation based on preexisting detailed soil maps (54%). The probability of occurrence associated with predictions, which turned out to be a good indicator of the prediction accuracy, confirmed this result with a mean value of 0.53 over the entire study area. Furthermore, it appears that SPM probabilities of occurrence can be used instead of soil maps with impure soil units to assess prediction accuracy. The predictive SPM map showed a better representation of superficial deposits than preexisting data, especially for aeolian loam deposits, which were among the most accurately predicted SPM types along with granite, soft schist, sandstone and micaschist. A confusion was detected however between the predictions of alluvial and colluvial deposits. The predictive SPM map can now be used in an array of geomorphological or pedological studies requiring SPM data and/or accurate data on superficial deposit localization, such as landscape evolution studies (Yetemen et al., 2010), landslide predictions (Dewitte et al., 2010; Regmi et al., 2010) and soil erosion studies (Verachtert et al., 2010). The predictive SPM map also has potential as an environmental predictor in producing other soil property maps (e.g. soil waterlogging, bulk density, soil class, and soil texture), as required in geomorphological studies, for example when mapping soil erosion risk (Nigel and Rughooputh, 2010) or modeling sensitivity to landslides (Regmi et al., 2010).

Acknowledgments

The authors gratefully acknowledge all the soil surveyors of the study area whose data collection and digitization made this study possible. This research was performed in the framework of the "Sols de Bretagne" program that is financially supported by the French Ministry of Agriculture, the regional council of Brittany and the departmental councils of Côtes-d'Armor, Finistère, Ille-et-Vilaine and Morbihan. This work was also supported by the Landsoil program funded by ANR (Agence Nationale de la Recherche) VMCS (ANR-08-VULN-006-01).

References

Ballabio, C., 2009. Spatial prediction of soil properties in temperate mountain regions using support vector regression. Geoderma 15, 338–350.
Bell, J.C., Cunningham, R.L., Havens, M.W., 1992. Calibration and validation of a soil-landscape model for predicting soil drainage class. Soil Science Society of America Journal 56, 1860–1866.
Bergeri, I., Michel, R., Boutin, J.P., 2002. Everything (or almost everything) about the Kappa coefficient. Medecine Tropropicale 62, 634–636.
Beven, K.J., Kirkby, M.J., 1979. A physically based, variable contributing area model of basin hydrology. Hydrological Sciences Journal 24, 43–69.
Bonijoly, D., Perrin, J., Truffert, C., Asfirne, F., 1999. Couverture géophysique aéroportée du Massif armoricain. BRGM Report R 40471. 60 pp.
Bou Kheir, R., Greve, M.H., Bocher, P.K., Greve, M.B., Larsen, R., McCloy, K., 2010. Predictive mapping of soil organic carbon in wet cultivated lands using classification-tree based models: the case study of Denmark. Journal of Environmental Management 91, 1150–1160.
Breiman, L., 1996. Bagging predictors. Machine Learning 24, 123–140.
Breiman, L., 2001. Statistical modeling: the two cultures. Statistical Science 16, 199–215.
Breiman, L., Friedman, J.H., Olshen, R.A., Stone, C.J., 1984. Classification and Regression Trees. Wadsworth & Brooks, Monterey.
Bui, E.N., Moran, C.J., 2003. A strategy to fill gaps in soil survey over large spatial extents: an example from the Murray–Darling basin of Australia. Geoderma 111, 21–44.
Bui, E.N., Loughhead, A., Corner, R., 1999. Extracting soil-landscape rules from previous soil surveys. Australian Journal of Soil Research 37, 495–508.
Bui, E.N., Henderson, B.L., Viergever, K., 2006. Knowledge discovery from models of soil properties developed through data mining. Ecological Modelling 191, 431–446.
Chantraine, J., Rabu, D., Béchennec, F., 2002. Carte géologique numérique à 1:250 000 du Massif armoricain. Map.
Cohen, J., 1960. A coefficient agreement for nominal scales. Educational and Psychological Measurement 20, 37–46.
Congalton, R.G., Green, K., 2009. Assessing the Accuracy of Remotely Sensed Data, Principles and Practices (2nd ed). CRC Press, Boca Raton, Florida, United States.
Dewitte, O., Chung, C.J., Cornet, Y., Daoudi, M., Demoulin, A., 2010. Combining spatial data in landslide reactivation susceptibility mapping: a likelihood ratio-based approach in W Belgium. Geomorphology 122, 153–166.
Dobos, E., Hengl, T., 2009. Soil mapping applications. In: Hengl, T., Reuter, H.I. (Eds.), Developments in Soil Science, 33. Elsevier, pp. 461–480.
Dymond, J.R., Luckman, P.G., 1994. Direct induction of compact rule-based classifiers for resource mapping. International Journal of Geographical Information Systems 8, 357–367.
Elith, J., Leathwick, J.R., Hastie, T., 2008. A working guide to boosted regression trees. Journal of Animal Ecology 77, 802–813.
Feng, X.M., Wang, Y.F., Chen, L.D., Fu, B.J., Bai, G.S., 2010. Modeling soil erosion and its response to land-use change in hilly catchments of the Chinese Loess Plateau. Geomorphology 118, 239–248.
Frechen, M., Oches, E.A., Kohfeld, K.E., 2003. Loess in Europe — mass accumulation rates during the Last Glacial Period. Quaternary Science Reviews 22, 1835–1857. Freund, Y., Schapire, R.E., 1996. Experiments with a new boosting algorithm. Machine Learning: Proceedings of the Thirteenth International Conference, pp. 148–156. Friedman, J.H., 2001. Greedy function approximation: a gradient boosting machine. The Annals of Statistics 29, 1189–1232.
Friedman, J.H., 2002. Stochastic gradient boosting. Computational Statistics & Data Analysis 38, 367–378.
Friedman, J.H., Meulman, J.J., 2003. Multiple additive regression trees with application in epidemiology. Statistics in Medicine 22, 1365–1381.
Friedman, J.H., Hastie, T., Tibshirani, R., 2000. Additive logistic regression: a statistical view of boosting. The Annals of Statistics 28, 337–374.
Gascuel-Odoux, C., 1998. Les zones contributives de fond de vallée: localisation, structure et fonctionnement hydrodynamique. In: INRA (Ed.), Agriculture intensive et qualité des eaux. Cheverry, C., Paris, pp. 129–141.
Gey, S., Poggi, J.M., 2006. Boosting and instability for regression trees. Computational Statistics & Data Analysis 50, 533–550.
Grinand, C., Arrouays, D., Laroche, B., Martin, M.P., 2008. Extrapolating regional soil landscapes from an existing soil map: sampling intensity, validation procedures, and integration of spatial context. Geoderma 143, 180–190.
Haase, D., Fink, J., Haase, G., Ruske, R., Pecsi, M., Richter, H., Altermann, M., Jager, K.D., 2007. Loess in Europe — its spatial distribution based on a European Loess Map, scale 1: 2,500,000. Quaternary Science Reviews 26, 1301–1312.
Henderson, B.L., Bui, E.N., Moran, C.J., Simon, D.A.P., 2005. Australia-wide predictions of soil properties using, decision trees. Geoderma 124, 383–398.
Hengl, T., MacMillan, R.A., 2009. Geomorphometry — a key to landscape mapping and modelling. In: Hengl, T., Reuter, H.I. (Eds.), Developments in Soil Science, 33. Elsevier, Amsterdam, pp. 433–460.
IGN, 2008. BD ALTI®. http://www.ign.fr.

IUSS Working Group WRB, 2007. World Reference Base for Soil Resources 2006, first update 2007. World Soil Resources Reports No. 103. FAO, Rome.

Jenny, H., 1941. Factors of Soil Formation. A System of Quantitative Pedology, McGraw-Hill, New York.

Jungerius, P.D., 1985. Soils, geomorphology. In: Jungerius, P.D. (Ed.), Soils and Geomorphology. Catena Supplement 6, Cremlingen-Destedt, pp. 1–18.

Lagacherie, P., Holmes, S., 1997. Addressing geographical data errors in a classification tree soil unit prediction. International Journal of Geographical Information Science 11, 183–198.

Lagacherie, P., Legros, J.P., Burrough, P.A., 1995. A soil survey procedure using the knowledge of soil pattern established on a previously mapped reference area. Geoderma 65, 283–301.

Lawrence, R., Bunn, A., Powell, S., Zambon, M., 2004. Classification of remotely sensed imagery using stochastic gradient boosting as a refinement of classification tree analysis. Remote Sensing of Environment 90, 331–336.

Le Du-Blayo, L., Corpetti, T., Gouery, P., Bourget, E., 2008. Esquisse cartographique des pédopaysage de Bretagne. Rapport final du programme de recherche. CNRS: UMR6554 - Université de Bretagne occidentale - Brest - Université de Caen, Université de Nantes - Université de Rennes 2 - Haute Bretagne.

Legros, J.P., Bonneric, P., 1979. Modelisation informatique de la repartition des sols dans le Parc Naturel Régional du Pilat. Annales de l'Université de Savoie, Tome 4, Sciences, pp. 63–68.

Lemercier, B., Lacoste, M., Loum, M., Walter, C., in press. Extrapolation at regional scale of local soil knowledge using boosted classification trees: a two step approach, Geoderma. doi:10.1016/j.geoderma.2011.03.010.

Lim, T.S., Loh, W.Y., Shih, Y.S., 2000. A comparison of prediction accuracy, complexity, and training time of thirty-three old and new classification algorithms. Machine Learning 40, 203–228.

Lin, H.S., Wheeler, D., Bell, J., Wilding, L., 2005. Assessment of soil spatial variability at multiple scales. Ecological Modelling 182, 271–290.

Martin, M.P., Seen, D.l., Boulonne, L., Jolivet, C., Nair, K.M., Bourgeon, G., Arrouays, D., 2009. Optimizing pedotransfer functions for estimating soil bulk density using boosted regression trees. Soil Science Society of America Journal 73, 485–493.

McBratney, A.B., Santos, M.L.M., Minasny, B., 2003. On digital soil mapping. Geoderma 117, 3–52.

McKenzie, N.J., Austin, M.P., 1993. A quantitative Australian approach to medium and small scale surveys based on soil stratigraphy and environmental correlation. Geoderma 57, 329–355.

McKenzie, N.J., Ryan, P.J., 1999. Spatial prediction of soil properties using environmental correlation. Geoderma 89, 67–94.

Merot, P., Ezzahar, B., Walter, C., Aurousseau, P., 1995. Mapping waterlogging of soils using digital terrain models. Hydrological Processes 9, 27–34.

Merot, P., Squividant, H., Aurousseau, P., Hefting, M., Burt, T., Maitre, V., Kruk, M., Butturini, A., Thenail, C., Viaud, V., 2003. Testing a climato-topographic index for predicting wetlands distribution along an European climate gradient. Ecological Modelling 163, 51–71.

Moran, C.J., Bui, E.N., 2002. Spatial data mining for enhanced soil map modelling. International Journal of Geographical Information Science 16, 533–549.

Muchoney, D., Strahler, A.N., 2002. Regional vegetation mapping and direct land surface parameterization from remotely sensed and site data. International Journal of Remote Sensing 23, 1125–1142.

Nigel, R., Rughooputh, S., 2010. Mapping of monthly soil erosion risk of mainland Mauritius and its aggregation with delineated basins. Geomorphology 114, 101–114.

Odeh, I.O.A., McBratney, A.B., Chittleborough, D.J., 1992. Soil pattern recognition with fuzzy-c-means: application to classification and soil-landform interrelationships. Soil Science Society of America Journal 56, 506–516.

R Development Core Team, 2008. R: a language and environment for statistical computing. R Foundation for Statistical Computing, Vienna, Austria3-900051-07-0. http://www.R-project.org.

Regmi, N.R., Giardino, J.R., Vitek, J.D., 2010. Modeling susceptibility to landslides using the weight of evidence approach: Western Colorado, USA. Geomorphol- ogy 115, 172–187.

Ryan, P.J., McKenzie, N.J., O'Connell, D., Loughhead, A.N., Leppert, P.M., Jacquier, D., Ashton, L., 2000. Integrating forest soils information across scales: spatial prediction of soil properties under Australian forests. Forest Ecology and Management 138, 139–157.

Schmidt, K., Behrens, T., Scholten, T., 2008. Instance selection and classification tree analysis for large spatial datasets in digital soil mapping. Geoderma 146, 138–146.

Squividant, H., 1994. MNTsurf: Logiciel de traitement des modèles numériques de terrain. ENSAR, Rennes, France. 36 pp.

Story, M., Congalton, R.G., 1986. Accuracy assessment — a user perspective. Photogrammetric Engineering and Remote Sensing 52, 397–399.

Strahler, A.N., 1952. Hypsometric (area-altitude) analysis of erosional topography. Geological Society of America Bulletin 63, 1117–1142.

Terranova, O., Antronico, L., Coscarelli, R., Iaquinta, P., 2009. Soil erosion risk scenarios in the Mediterranean environment using RUSLE and GIS: an application model for Calabria (southern Italy). Geomorphology 112, 228–245.

Thomas, E., 2006. Formations superficielles de Bretagne. Essai de synthèse cartographique.

Thomas, A.L., King, D., Dambrine, E., Couturier, A., Roque, A., 1999. Predicting soil classes with parameters derived from relief geologic materials in a sandstone region of the Vosges Mountains (Northeastern France). Geoderma 90, 291–305.

Vasques, G.M., Grunwald, S., Comerford, N.B., Sickman, J.O., 2010. Regional modelling of soil carbon at multiple depths within a subtropical watershed. Geoderma 156, 326–336.

Verachtert, E., Van den Eeckhaut, M., Poesen, J., Deckers, J., 2010. Factors controlling the spatial distribution of soil piping erosion on loess-derived soils: a case study from central Belgium. Geomorphology 118, 339–348.

Vogel, S., Marker, M., 2010. Reconstructing the Roman topography and environmental features of the Sarno River Plain (Italy) before the AD 79 eruption of Somma-Vesuvius. Geomorphology 115, 67–77.

Walter, C., 1990. Estimation de propriétés du sol et quantification de leur variabilité à moyenne échelle : cartographie pédologique et géostatistique dans le sud de l'Ille et Vilaine. Ph.D. Thesis, Thesis of the University Paris VI in Soil Science, ENSA INRA, Laboratoire de Sciences du Sol, Rennes.

Wilford, J.R., Bierwirth, P.N., Craig, M.A., 1997. Application of airborne gamma-ray spectrometry in soil/regolith mapping and applied geomorphology. Journal of Australian Geology and Geophysics 17, 201–216.

Yetemen, O., Istanbulluoglu, E., Vivoni, E.R., 2010. The implications of geology, soils, and vegetation on landscape morphology: inferences from semi-arid basins with complex vegetation patterns in Central New Mexico, USA. Geomorphology 116, 246–263.

Zhu, A.X., 2000. Mapping soil landscape as spatial continua: the neural network approach. Water Resources Research 36, 663–677.

Annexe 2. Parcellaire de la zone d'étude (relevé d'occupation du sol de 2006)

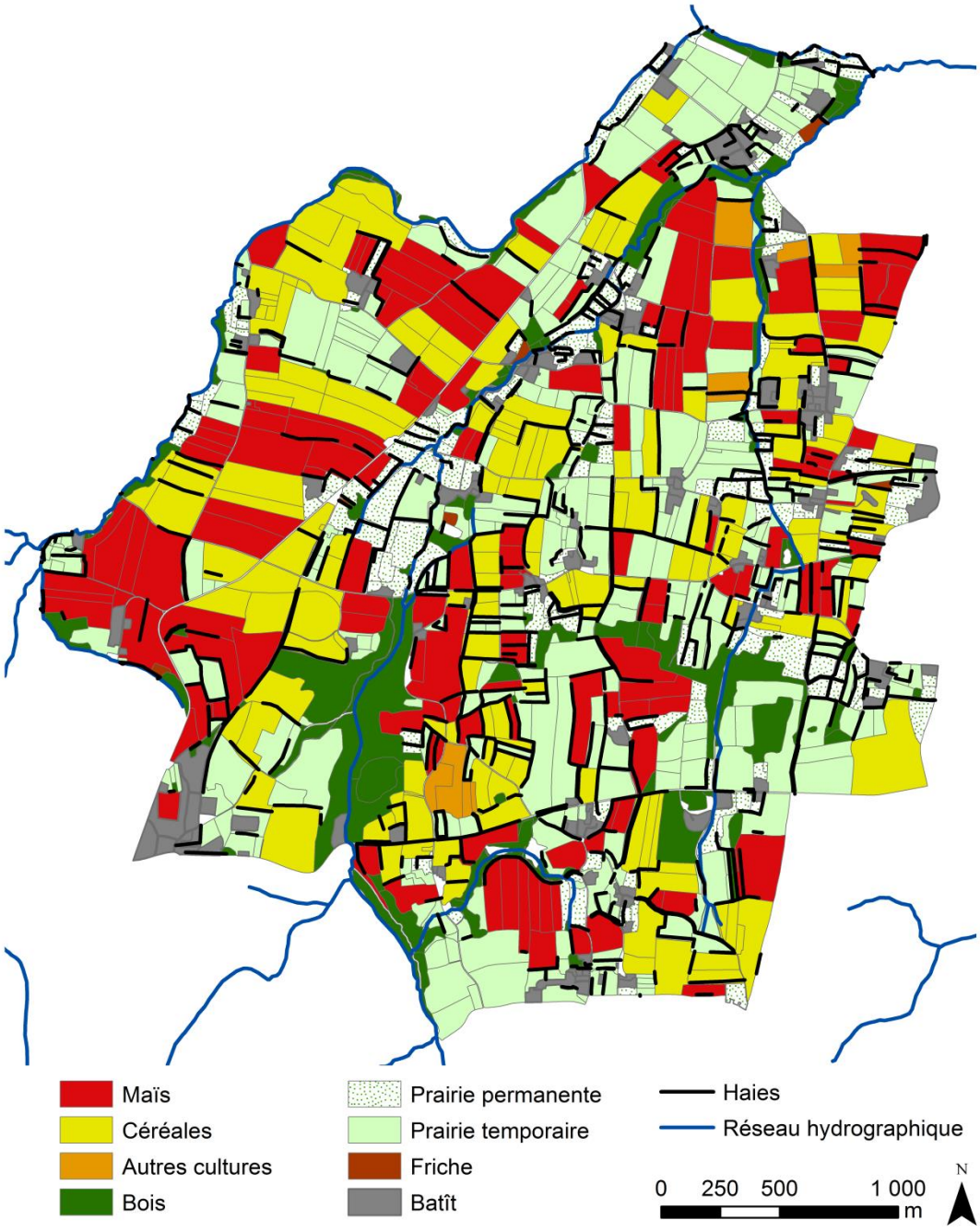

Figure 5-18. Parcellaire et occupation du sol de la zone d'étude.

Annexe 3. Parameters used in LandSoil to model soil redistribution at landscape scale for the study area of Pleine-Fougères

Three parameters used in LandSoil have been calibrated in Chapter 3:

- Infiltration rate (mm h^{-1}, Table 5-10).
- Residual water storage after the previous rainfall event (mm, Table 5-11).
- Sediment concentration in runoff (g l^{-1}, Table 5-12).

Table 5-10. Infiltration rate (mm h^{-1}).

Soil roughness[a]	Vegetation cover[b]	Crusting stage[c]			
		F0	F11	F12	F2
0 - 1 cm	< 20 %	7.5	7.5	3.75	1.5
	21-60 %	15			
	> 61 %	37.5	15	7.5	3.75
1 - 2 cm	< 20 %	15	7.5	3.7	1.5
	21-60 %	37.5	15	7.5	
	> 61 %				3.75
2 - 5 cm	< 20 %	37.5	15	7.5	3.75
	21-60 %			7.5	3.75
	> 61 %		37.5	15	7.5
5 - 10 cm	< 20 %	37.5	15	7.5	3.75
	21-60 %		37.5	15	7.5
	> 61 %			37.5	
> 10 cm	< 20 %	37.5	15	15	7.5
	21-60 %		37.5	37.5	
	> 61 %				

[a] Soil surface roughness state is defined by the elevation difference between the deepest part of micro depressions and the lowest point of their divide (Ludwig et al., 1995).

[b] Vegetation cover classes are defined as the percentage of soil surface covered by canopy or litter

[c] Soil surface crusting stages from Bresson and Boiffin (1990). F0 = initial fragmentary structure; F11 = altered fragmentary state with structural crusts; F12 = local appearance of depositional crusts; F2 = continuous state with depositional crusts.

Table 5-11. Residual water storage after the previous rainfall event (mm).

Infiltration rate (mm h^{-1})	Antecedent 48-h rainfall (mm)			
	0	0 - 15	16 - 40	> 40
50	11	7	4	1
20	7	4	1	0
10	4	1	0	0
5	1	0	0	0
2	0	0	0	0

Table 5-12. Sediment concentration in runoff (g l^{-1}).

Soil roughness[a]	Vegetation cover[b]	Maximum raifall intensity (mm h^{-1})	Crusting stage[c]			
			F0	F1	F12	F2
0 - 1 cm	< 20 %	0 à 10 mm/h	0	2	0	2
		10 à 40 mm/h		5	2	5
		> 40 mm/h	2	10	5	10
	21-60 %	0 à 10 mm/h	0	0	0	0
		10 à 40 mm/h		2	0	2
		> 40 mm/h	2	5	2	5
	> 61 %	0 à 10 mm/h	0	0	0	0
		10 à 40 mm/h		2	0	2
		> 40 mm/h	2	5	2	5
1 - 2 cm	< 20 %	0 à 10 mm/h	0	0	0	0
		10 à 40 mm/h	2	10	5	10
		> 40 mm/h	5	15	10	15
	21-60 %	0 à 10 mm/h	0	2	0	2
		10 à 40 mm/h		5	2	5
		> 40 mm/h	2	10	5	10
	> 61 %	0 à 10 mm/h	0	2	0	2
		10 à 40 mm/h		5	2	5
		> 40 mm/h	2	10	5	10
2 - 5 cm	< 20 %	0 à 10 mm/h	0			
		10 à 40 mm/h	2	10	5	10
		> 40 mm/h	5	15	10	15
	21-60 %	0 à 10 mm/h	0	2	0	2
		10 à 40 mm/h		5	2	5
		> 40 mm/h	2	10	5	10
	> 61 %	0 à 10 mm/h	0	2	0	2
		10 à 40 mm/h		5	2	5
		> 40 mm/h	2	10	5	10

[a] Soil surface roughness state is defined by the elevation difference between the deepest part of micro depressions and the lowest point of their divide (Ludwig et al., 1995).

[b] Vegetation cover classes are defined as the percentage of soil surface covered by canopy or litter

[c] Soil surface crusting stages from Bresson and Boiffin (1990). F0 = initial fragmentary structure; F11 = altered fragmentary state with structural crusts; F12 = local appearance of depositional crusts; F2 = continuous state with depositional crusts.

Annexe 4 : Estimation of soil reidstribution rate by ^{137}Cs inventories

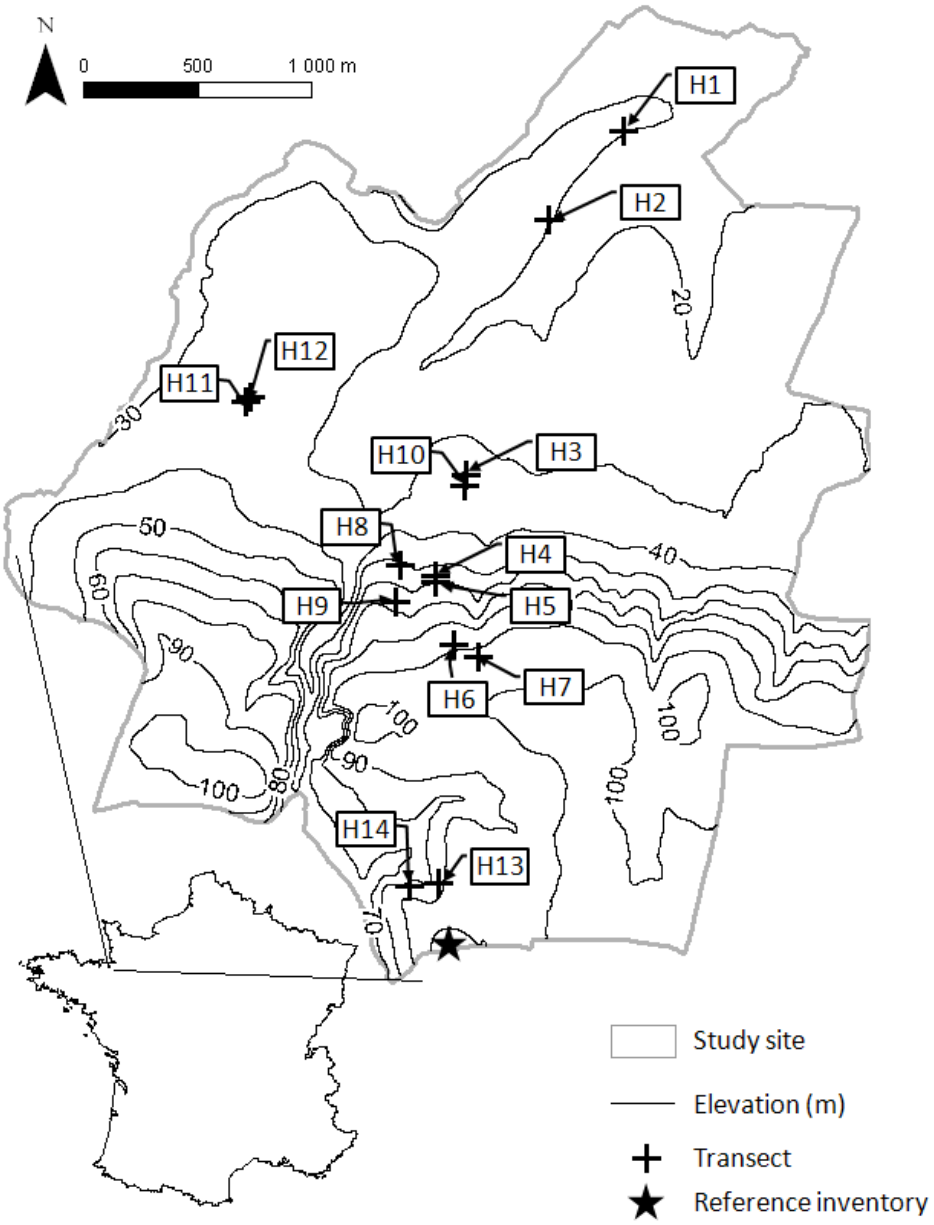

Figure 5-19. Location of the sampling sites for by ^{137}Cs inventories.

Table 5-13. Characteristics of the samples used for ^{137}Cs measurements and obtained 137Cs concentrations

Hedge	Position from the hedge	Soil layer (cm)	Analysed weight (g)	counting date	counting time (s)	Sample bulk density	Sample weight (g)	Cs-137 concentration (Bq/kg)	< 2.0 s
H1	up	0 - 30	83.90	07/04/11	93892	1.03	1364.26	4.4 +-	0.2
		30 - 35	83.63	28/03/11	170486	1.23	271.86	0.4 +-	0.1
		35 - 40	83.13	08/04/11	249247	1.42	312.59	0.3 +-	0.1
		40 - 45	82.65	29/04/11	254078	1.09	240.80	<	0.1
H1	down	0 - 30	61.34	13/04/11	91104	1.08	1428.54	3.7 +-	0.2
		30 - 35	79.48	11/04/11	170672	1.39	306.43	0.5 +-	0.1
		35 - 42	82.02	06/05/11	225825	1.33	411.67	0.4 +-	0.1
H2	up	0 - 30	86.54	21/03/11	110202	1.02	1356.50	1.3 +-	0.1
		30 - 35	82.11	24/03/11	94845	1.32	291.26	0.6 +-	0.1
		35 - 40	80.13	04/04/11	183492	1.28	282.02	<	0.2
H2	down	0 - 30	80.43	17/03/11	95360	1.04	1383.89	4.0 +-	0.2
		30 - 35	80.35	22/03/11	90124	1.12	247.63	3.0 +-	0.2
		35 - 40	80.77	25/03/11	229920	1.48	327.60	0.2 +-	0.1
		40 - 45	80.08	24/04/11	163160	1.43	316.20	<	0.2
H3	up	0 - 30	64.84	30/09/10	104046	1.18	1562.85	3.2 +-	0.2
		30 - 35	56.91	20/09/10	154486	1.29	285.89	2.5 +-	0.2
		35 - 40	59.94	23/09/10	130278	1.38	303.99	<	0.3
H3	down	0 - 30	58.99	27/09/10	141713	1.20	1587.69	3.2 +-	0.2
		30 - 35	58.87	24/09/10	241546	1.42	313.64	2.0 +-	0.1
H4	up	0 - 30	61.09	24/08/10	106126	1.13	1496.16	3.9 +-	0.2
		30 - 35	61.69	30/08/10	89022	1.21	268.35	4.3 +-	0.2
		35 - 40	62.85	31/08/10	82164	1.30	287.33	1.9 +-	0.2
		40 - 45	63.08	01/09/10	433946	1.25	277.11	0.4 +-	0.1
		70 - 75	63.64	10/09/10	231749	1.19	262.23	<	0.2
H4	down	0 - 30	71.42	06/09/10	169382	1.27	1684.25	3.3 +-	0.1
		30 - 35	69.24	27/08/10	236228	1.42	313.21	3.1 +-	0.1
		35 - 40	81.18	03/12/10		1.64	362.20	1.1 +-	0.1
H5	up	0 - 30	62.49	16/08/10	91655	1.17	1551.87	3.4 +-	0.2
		30 - 35	58.68	19/08/10	94210	1.26	277.35	3.9 +-	0.2
		35 - 40	60.43	08/08/10	96056	1.33	293.31	2.2 +-	0.2
		40 - 45	64.29	20/08/10	233426	1.35	297.48	0.3 +-	0.1
H5	down	0 - 30	69.63	17/08/10	89461	1.24	1645.35	3.1 +-	0.2
		30 - 35	68.01	23/08/10	83323	1.42	314.15	<	0.3
		35 - 40	66.58	13/08/10	227255	1.42	314.77	<	0.2
		40 - 45	65.64	26/08/10	90102	1.57	347.08	<	0.3
H6	up	0 - 30	82.35	24/05/11	92402	0.96	1278.21	4.1 +-	0.2
		30 - 35	79.28	27/05/11	229719	1.03	228.00	2.7 +-	0.1
		35 - 40	85.00	13/05/11	229800	1.16	257.18	0.3 +-	0.1
H6	down	0 - 30	80.41	12/05/11	107304	0.68	907.28	7.1 +-	0.2

Table 5.13. Continuation.

Hedge	Position from the hedge	Soil layer (cm)	Analysed weight (g)	counting date	counting time (s)	Sample bulk density	Sample weight (g)	Cs-137 concentration (Bq/kg)	< 2.0 s
H7	up	0 - 30	80.36	05/05/11	118445	1.09	1450.86	4.4 +-	0.2
		30 - 35	81.35	26/04/11	108083	1.19	262.25	4.1 +-	0.2
		35 - 40	81.16	02/05/11	169367	1.29	286.01	2.0 +-	0.1
		40 - 45	82.49	09/05/11	176623	1.26	278.31	0.6 +-	0.1
H7	down	0 - 30	81.16	27/04/11	155537	0.82	1091.27	5.5 +-	0.1
		30 - 39	92.67	14/04/11	104385	0.61	242.30	1.7 +-	0.1
H8	up	0 - 30	66.38	05/08/10	84716	0.95	1264.34	3.4 +-	0.2
		30 - 35	61.80	19/08/10	92294	1.12	248.00	3.6 +-	0.2
		35 - 40	66.09	06/08/10	86327	1.11	244.13	3.6 +-	0.2
		40 - 45	64.35	07/08/10	70734	1.30	286.67	3.9 +-	0.2
		70 - 75	60.24	27/08/10	236750	1.36	301.45	0.4 +-	0.1
H8	down	0 - 30	60.93	16/08/10	91836	0.69	915.26	4.0 +-	0.2
		30 - 35	60.18	17/08/10	89398	1.06	233.24	3.6 +-	0.2
		35 - 40	59.82	08/08/10	95967	1.12	247.43	3.9 +-	0.2
		40 - 45	58.64	20/08/10	233644	1.27	280.59	4.5 +-	0.1
		45 - 50	83.99	03/12/10		1.60	352.97	1.7 +-	0.1
H9	up	0 - 30	67.02	24/08/10	106229	0.89	1176.97	2.5 +-	0.2
		30 - 35	60.58	26/08/10	90150	1.25	275.61	<	0.3
			57.23	13/08/10	229178	1.20	265.16	<	0.2
H9	down	0 - 30	61.19	23/08/10	83141	1.03	1367.71	2.6 +-	0.2
		30 - 35	58.35	30/08/10	89313	0.87	192.55	<	0.3
H10	up	0 - 30	65.67	31/08/10	82134	1.25	1657.79	3.5 +-	0.2
		30 - 35	52.90	01/09/10	432637	1.24	273.19	4.0 +-	0.1
		35 - 40	59.67	06/09/10	170628	1.20	264.41	3.2 +-	0.1
		40 - 45	59.13	10/09/10	232515	1.27	280.96	0.3 +-	0.1
		70 - 75	59.79	16/09/10	105269	1.32	290.53	<	0.3
H10	down	0 - 30	65.72	23/09/10	100566	1.13	1492.81	3.6 +-	0.2
		30 - 35	65.06	24/09/10	242258	1.40	309.08	1.9 +-	0.1
H11	up	30 - 35	81.70	03/03/11	114363	1.31	290.27	3.8 +-	0.2
		35 - 40	81.93	11/03/11	233002	1.36	300.20	4.2 +-	0.1
		40 - 45	80.85	18/03/11	229166	1.57	346.98	4.8 +-	0.1
H11	down	0 - 30	84.13	10/03/11	104145	1.31	1734.96	2.4 +-	0.1
		30 - 35	80.61	14/03/11	187229	1.21	268.16	<	0.2
H12	up	0 - 30	87.69	16/02/11	103462	1.12	1490.60	3.2 +-	0.1
		30 - 35	81.63	17/02/11	94990	1.37	303.56	1.1 +-	0.1
		35 - 40	81.53	07/03/11	171003	1.35	298.09	<	0.2
H12	down	0 - 30	88.19	14/02/11	156230	1.09	1438.38	3.2 +-	0.1
		30 - 35	83.71	28/02/11	166057	1.34	295.36	2.3 +-	0.1
		35 - 40	79.06	04/03/11	229837	1.34	296.80	<	0.1

Table 5.13. Continuation.

Hedge	Position from the hedge	Soil layer (cm)	Analysed weight (g)	counting date	counting time (s)	Sample bulk density	Sample weight (g)	Cs-137 concentration (Bq/kg)	< 2.0 s
H13	up	0 - 30	81.05	30/05/11	103042	1.23	1629.78	1.3 +-	0.1
		30 - 35	81.82	14/06/11	169566	1.34	295.33	<	0.2
		35 - 40	82.31	16/05/11	162840	1.35	298.11	<	0.2
H13	down	0 - 30	79.97	26/05/11	88561	1.13	1499.80	1.9 +-	0.1
		30 - 35	80.63	18/05/11	173163	1.40	309.12	1.4 +-	0.1
		35 - 40	80.24	23/05/11	100346	1.33	294.74	1.5 +-	0.1
		40 - 45	81.60	17/05/11	242444	1.34	296.10	2.2 +-	0.1
H14	up	0 - 30	79.79	31/05/11	92571	1.19	1582.14	4.6 +-	0.2
		30 - 35	83.35	06/06/11	171669	1.39	307.21	3.4 +-	0.1
		35 - 40	80.52	20/05/11	258308	1.32	291.26	0.8 +-	0.1
		40 - 45	84.36	01/06/11	407097	1.35	298.06	0.5 +-	0.1
H14	down	0 - 30	80.82	09/06/11	91221	1.35	1786.48	4.8 +-	0.2
Ref.	-	0 - 5	60.88	14/10/10	84541	0.94	208.06	2.6 +-	0.2
		5 - 10	69.54	18/10/10	91174	1.54	339.15	3.5 +-	0.2
		10 - 15	68.26	22/10/10	263120	1.78	392.46	3.0 +-	0.1
		15 - 20	65.33	11/10/10	171421	1.38	304.91	2.9 +-	0.1
		20 - 25	68.79	07/10/10	113413	1.59	351.38	3.3 +-	0.2
		25 - 30	76.40	08/10/10	232042	1.80	397.90	2.9 +-	0.1
		30 - 35	74.67	04/10/10	176557	1.71	377.13	1.5 +-	0.1
		35 - 40	70.51	15/10/10	230943	1.60	353.96	0.4 +-	0.1
		40 - 45	76.20	01/10/10	240447	2.04	450.11	0.3 +-	0.1
		45 - 50	72.42	19/10/10	254203	1.82	402.92	0.3 +-	0.1
		50 - 55	70.86	25/10/10	166806	1.55	341.70	<	0.2

Table 5-14. Estimation of soil redistribution rate from ^{137}Cs inventories

Hedge	Position from the hedge	Sample weigth (g)	Cs-137 concentration (bq kg^{-1})	Cs-137 inventory (bq.m-2)	Redistribution rate (t ha^{-1} yr^{-1})			
					PM-1954	PM-1963	MBM1	MBM2
H1	up	1948.71	5.13	1411.85	-7.31	-8.71	-8.55	-5.87
	down	2146.64	4.57	1273.62	-13.00	-15.48	-15.95	-11.10
H2	up	1647.76	1.88	437.96	-47.35	-56.42	-88.48	-70.57
	down	1959.12	7.26	1447.53	-5.85	-6.96	-6.51	-4.45
H3	up	1848.74	5.69	1284.87	-12.53	-14.93	-16.41	-11.43
	down	1901.33	5.18	1292.86	-12.20	-14.54	-15.93	-11.09
H4	up	2328.95	10.50	1741.02	6.22	7.41	7.73	5.19
	down	2359.66	7.54	1578.63	-0.46	-0.54	-5.29	-3.61
H5	up	2420.01	9.78	1610.90	0.87	1.04	1.23	0.85
	down	1645.35	3.09	1150.14	-18.07	-21.53	-25.32	-17.86
H6	up	1763.39	6.97	1325.96	-10.84	-12.92	-9.71	-6.73
	down	907.28	7.06	1449.22	-5.78	-6.88	-4.96	-3.40
H7	up	2277.43	11.11	1850.57	10.72	12.78	10.53	7.08
	down	1333.57	7.16	1451.13	-5.70	-6.79	-5.58	-3.82
H8	up	2344.59	14.93	1655.25	2.69	3.21	2.39	1.77
	down	2029.49	17.70	1657.27	2.78	3.31	2.46	1.83
H9	up	1176.97	2.46	654.29	-38.46	-45.82	-49.96	-37.87
	down	1367.71	2.57	797.18	-32.58	-38.82	-38.92	-28.75
H10	up	2476.35	11.02	1786.11	8.07	9.62	10.33	6.97
	down	1801.89	5.49	1356.56	-9.59	-11.42	-12.23	-8.40
H11	up	2424.41	16.65	2199.52	25.07	29.87	39.82	28.29
	down	1734.96	2.39	940.53	-26.69	-31.80	-41.98	-30.55
H12	up	1794.16	4.24	1147.10	-18.20	-21.68	-23.66	-16.71
	down	1733.74	5.42	1178.18	-16.92	-20.16	-21.73	-15.29
H13	up	1629.78	1.30	481.28	-45.57	-54.30	-91.87	-72.55
	down	2399.76	7.01	999.46	-24.27	-28.91	-35.96	-25.83
H14	up	2478.67	9.28	1978.50	15.98	19.04	25.46	17.86
	down	1786.48	4.82	1947.73	14.72	17.54	23.45	16.44
Ref.	-	3577.98	20.58	1589.71	-	-	-	-

Annexe 5 : Estimation of soil deposition rate by OSL (Optically Stimulated Luminescence) dating

Sampling for OSL dating have ween done uphill from hedges H5 and H8 (Figure 5-19).
The estimation of the sample ages are in Table 5-15.
The estimation of soil deposition rated are given in Table 5-16. They were calculated with the following equation:

$$SDep = \frac{D_m - D_t}{MA_{OSL}}$$

Where *SDep* is the estimation of soil deposition rate, D_m is the measurment depth (mm), D_t is the tillage depth (mm) and MA_{OSL} is the medium age estimated by OSL measurment (yr).

Figure 5-20 and Figure 5-21 summerize the results of OSL dating.

Table 5-15. Estimations of OSL age

Location	Depth of measurment (cm)	OSL age (kyr)		
		Recent water content	Saturated water content	Medium water content
H5-bank	73.5	0.48 ± 0.04	0.53 ± 0.04	0.51 ± 0.04
H5-E1	47.5	0.26 ± 0.02	0.29 ± 0.02	0.28 ± 0.02
H5-E2	75	1.11 ± 0.09	1.17 ± 0.1	1.14 ± 0.09
H5-E3	53.3	0.35 ± 0.03	0.39 ± 0.03	0.37 ± 0.03
H5-E4	75.3	1.26 ± 0.12	1.34 ± 0.12	1.3 ± 0.12
H5-E5	101.3	8.94 ± 0.86	10.29 ± 0.98	9.62 ± 0.92
H8-bank	65	0.20 ± 0.02	0.24 ± 0.02	0.22 ± 0.02
H8-E1	52	0.11 ± 0.01	0.13 ± 0.02	0.12 ± 0.01
H8-E2	71	0.14 ± 0.01	0.17 ± 0.01	0.15 ± 0.01
H8-E3	86	0.48 ± 0.04	0.56 ± 0.04	0.52 ± 0.04
H8-E4	106	0.92 ± 0.07	1.01 ± 0.08	0.96 ± 0.07
H8-E5	133	4.98 ± 0.44	5.78 ± 0.5	5.39 ± 0.47
H8-E7	49	0.11 ± 0.01	0.12 ± 0.01	0.11 ± 0.01

Table 5-16. Estimations of soil deposition rate from OSL dating

Interval	Thickness (cm)	Deposition rate (mm yr^{-1})
H5-topsoil → talus	43.5	0.85
H5-topsoil → E1	17.5	0.63
H5-topsoil → E3	23.3	0.63
H5-E1 → E2	27.5	0.32
H5-E3 → E4	22.0	0.24
H5-E4 → E5	26.0	0.03
H5-E1 → E4	27.8	0.27
H5-E3 → E2	21.7	0.28
H5-E2 → E5	26.3	0.03
H5-E1 → E5	53.8	0.06
H5-E3 → E5	48.0	0.05
H8-topsoil → talus	35.0	1.59
H8-topsoil → E1	22.0	1.83
H8-topsoil → E7	19.0	1.73
H8-E1 → E2	19.0	6.33
H8-E2 → E3	15.0	0.41
H8-E3 → E4	20.0	0.45
H8-E4 → E5	27.0	0.06

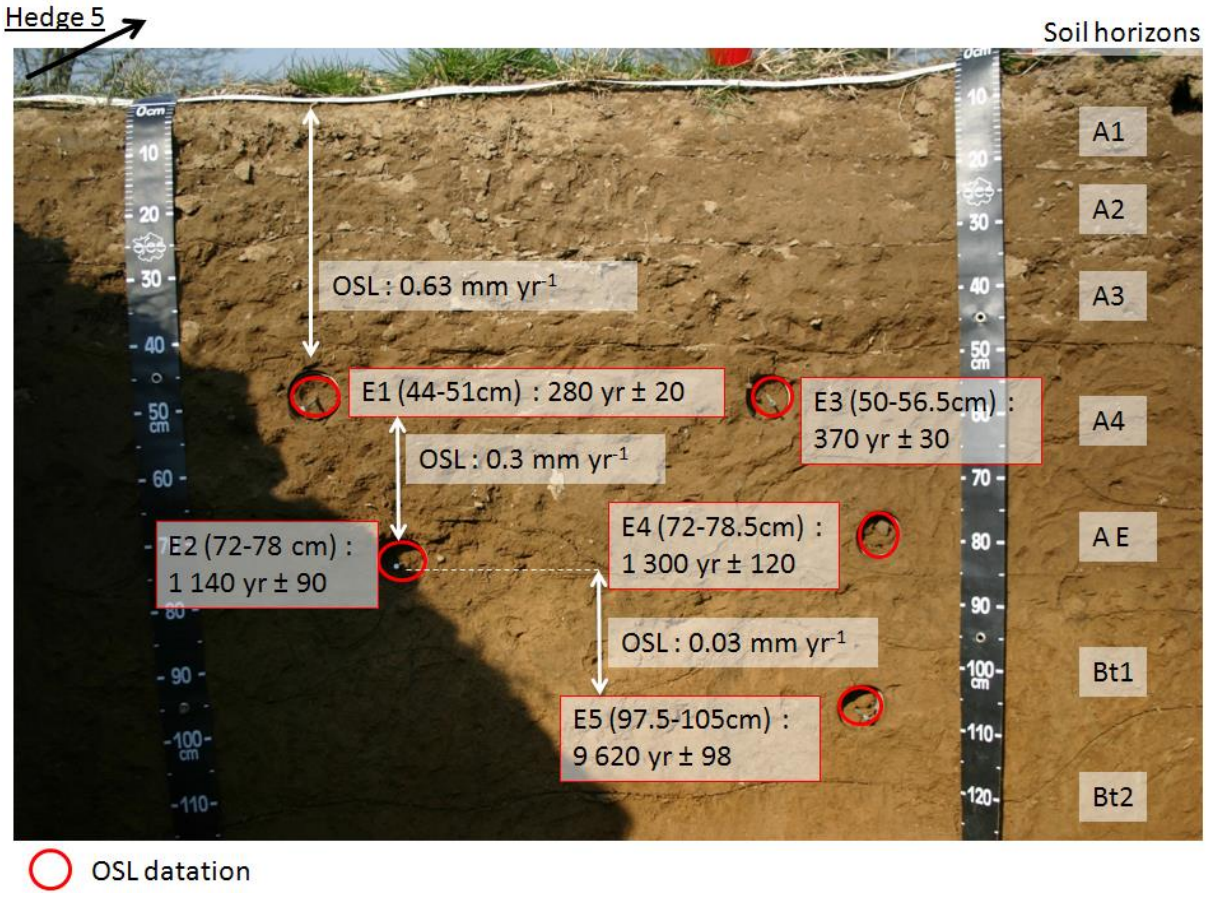

Figure 5-20. OSL dating uphill from the hedge H5

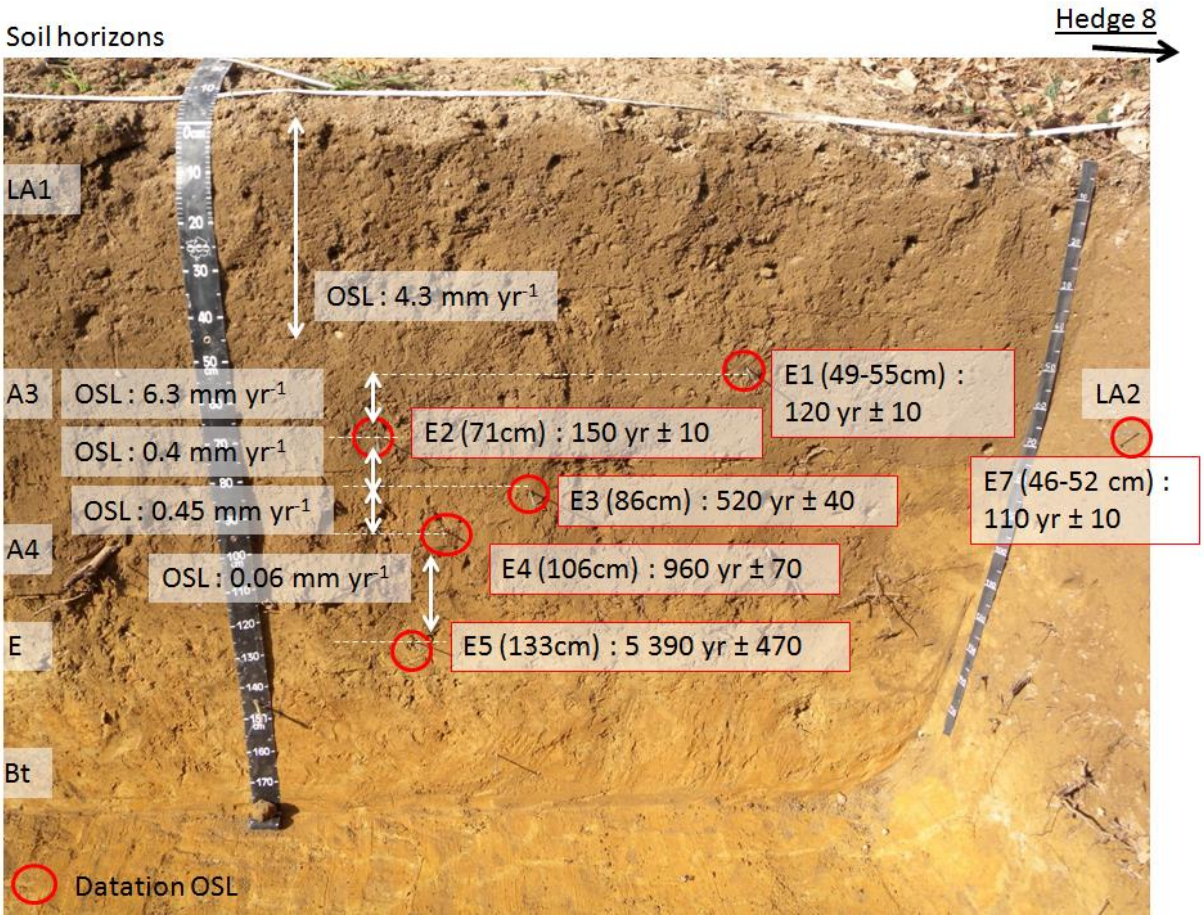

Figure 5-21. OSL dating uphill from the hedge H8

Annexe 6 : Predictive mapping of soil thickness and A-horizon thickness

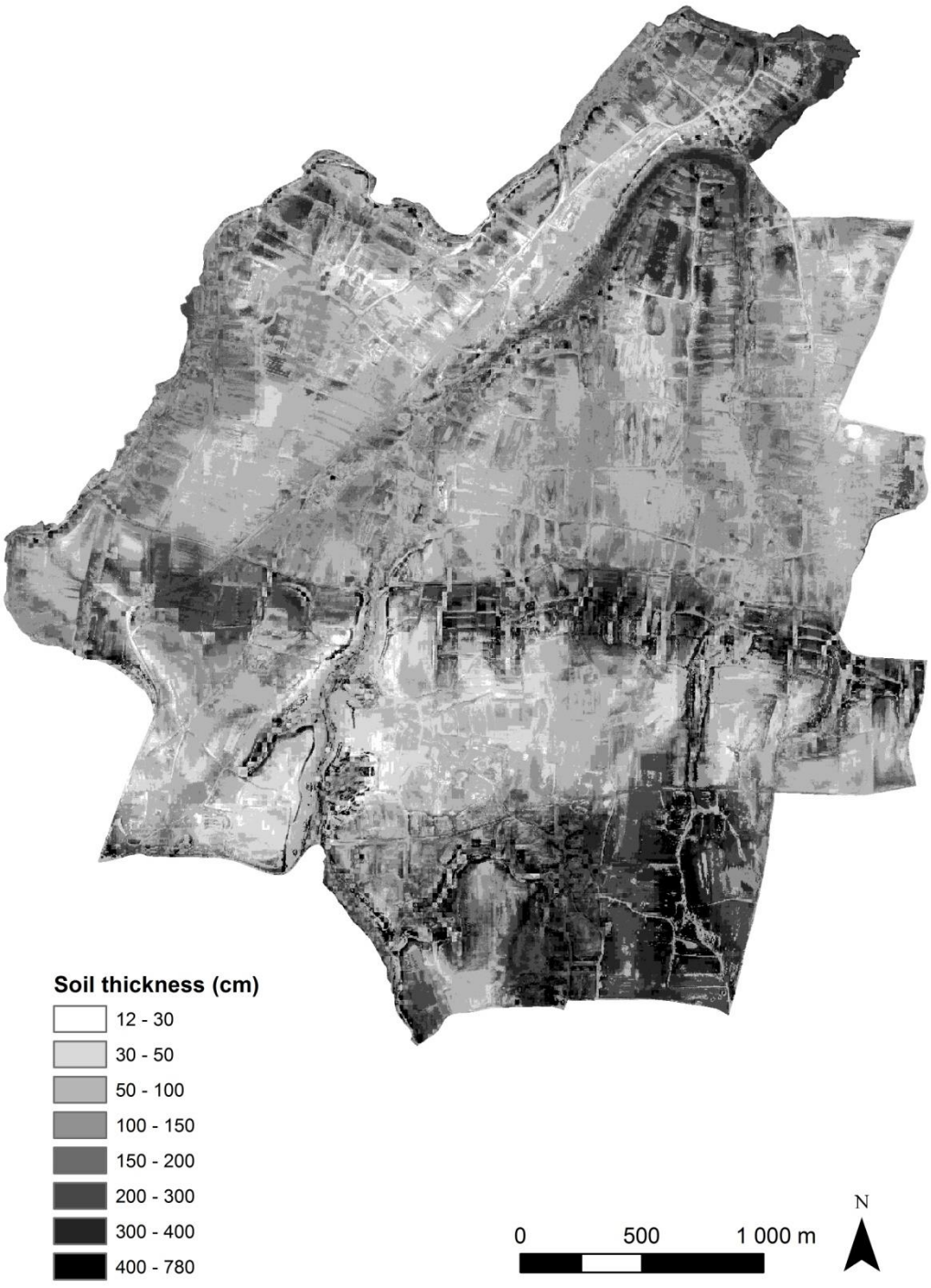

Figure 5-22. Predictive map of the soil thickness

Figure 5-23. Predictive map of the A-horizon thickness.

Table 5-17. Statistics of the calibration and validation datasets used for soil and A-horizon thickness prediction, predictions and absolute errors.

	min	1st quartile	median	mean	3rd quartile	max
Soil thickness cm)						
Calibration	30.00	70.00	130.00	165.00	231.00	530.00
Validation	30.00	77.50	110.00	157.80	220.50	530.00
Prediction	30.13	80.46	111.80	141.70	159.90	495.80
Asolute error	0.79	20.01	48.51	75.09	105.90	297.00
A-horizon thickness (cm)						
Calibration	3.00	35.00	50.00	51.84	60.00	180.00
Validation	12.00	35.00	50.00	55.60	70.00	200.00
Prediction	12.38	41.41	48.98	49.87	55.43	143.20
Asolute error	0.00	5.76	13.50	20.90	26.08	168.08

Annexe 7 : Support de la soutenance orale.

30/11/2012

vie agro santé
école doctorale de Rennes

Soil evolution at landscape scale under climate and land use change

Marine Lacoste

UMR Sol Agro et Hydrosystèmes Spatialisation - Rennes

ANR "Vulnerability: environment, climate, societies"

LandSoil program (2009-2012)

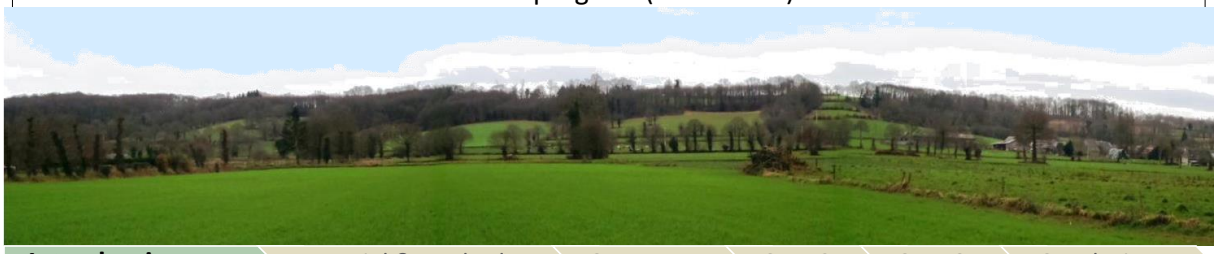

Introduction | Materiel & methods | Step 1 | Step 2 | Step 3 | Conclusion

Soils: essential and threatened resource

Soils provide essential ecosystem services

- Biomass production, climate regulation, water and air quality regulation, biodiversity support
  (Millenium Ecosystem Assessment, 2005)

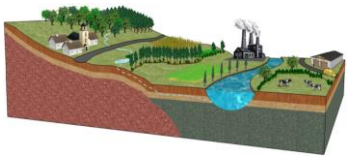

Driving factors
(Jenny, 1941; McBratney et al., 2003)

Soil degradation processes

Soil erosion
Mean soil water erosion in Europe: 1.2 t ha^{-1} yr^{-1}
(Cerdan et al., 2010)

Decrease in SOC contents
Cultivated soils in France: SOC losses up to 6 Mt
(0-30 cm soil layer, from 1990 to 2004)
(Gis Sol-BDAT, 2007)

Interactions
(Lal, 2008 ; Van Oost et al. 2007)

Climate
Precipitations
Temperatures

Human activities
Farming systems
Land use

Physical environment
Soil properties
Soil parent material
Topography

1

Spatial and temporal variability of the factors driving soil degradation

Spatial variability	Driving factors (Jenny, 1941; McBratney et al., 2003)	Temporal variability
	Climate Precipitations Temperatures	➢ Intra-annual variability, seasonal ➢ Long-term variability (several decades): climate change (Alcamo, 2007)
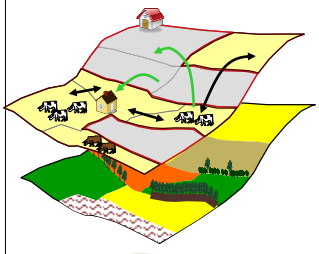	**Human activities** Farming systems Land use	➢ Intra-annual variability: crop management practices ➢ Inter-annual variability: crop rotations ➢ Long-term variability: change in farming systems, land management
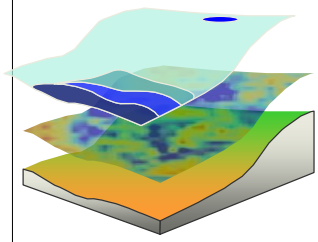	**Physical environment** Soil properties Soil parent material Topography	

Modelling is a relevant approach to address complex processes

2

Soil evolution models

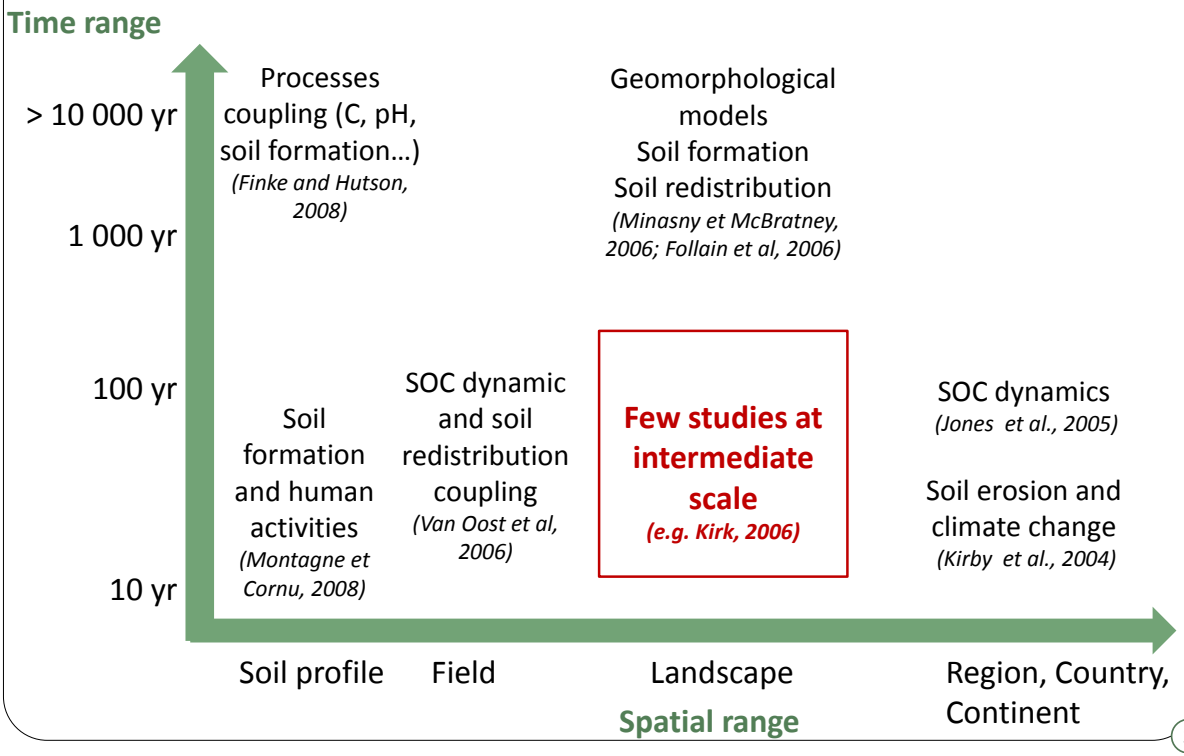

3

Relevance of the landscape scale

- **Main advantages** *(eg. Pennock et Veldkamp, 2006; Sommer, 2006)*:
  - Studies of processes at different scales (spatial and time)
  - Interactions between landscape elements (fields, hedges, grass strips)
  - Assessment of the impact of human activities
- **Used in:**
  - Ecology (biodiversity, pests) *(e.g. Burel et Baudry, 1999)*
  - Hydrology (water quality) *(e.g. Gerrits et Endelenbos, 2004; Merot et al, 2008)*
  - Transports of atmospheric contaminants (air quality) *(eg. Duretz et al., 2011, Drouet et al., 2012)*

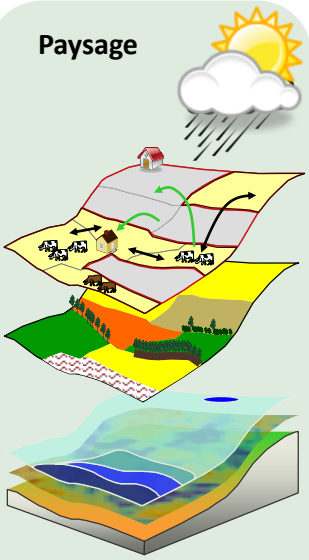

(d'après Viaud et al., 2010)

- **Less used in soil sciences:**

  Soils can have a high heterogeneity at short distance *(eg. Follain, 2006)*
  - ➢ Difficulties for model initialization at landscape scale *(Kirk, 2006)*

4

Objectives

Characterize soil redistribution and SOC dynamic at the scale of an agricultural landscape:

- For an 100 years
- Taking into account landscape structure (composition and spatial organisation) and climate.

5

Modelling process in three steps

- Spatial and dynamic models assessment at landscape scale (soil redistribution and SOC dynamic) — **Step 1**
  - ➢ LandSoil model (soil redistribution) assessment at hedges vicinity
- Soil initial state description at landscape scale — **Step 2**
- Assessment of climate and landscape change scenarios impacts on soil evolution (2010-2100) — **Step 3**

6

Soil redistribution model

LandSoil model *(Ciampalini et al, 2012)*

➢ Adapted from STREAM *(Cerdan et al., 2002)*

- Soil surface parameters (soil roughness , crusting stage, vegetation cover) control water erosion
- Soil surface parameters and soil erosion linked by expert knowledge rules
- Takes into account fields and other landscape elements (hedges)

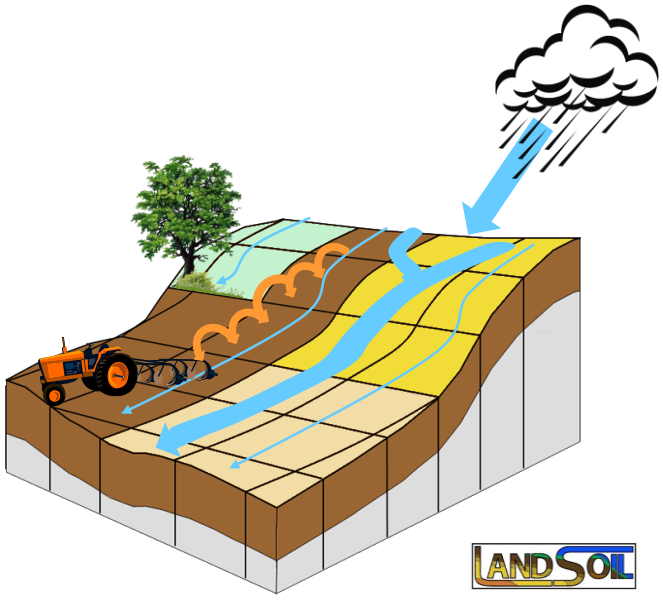

Runoff and water erosion

Tillage erosion

7

Soil redistribution model

Processes modelled :

- Water erosion
- Tillage erosion *(Govers et al., 1994)*
- Soil deposits

Time step: rainfall or tillage event

Outputs: topography and soil thickness maps

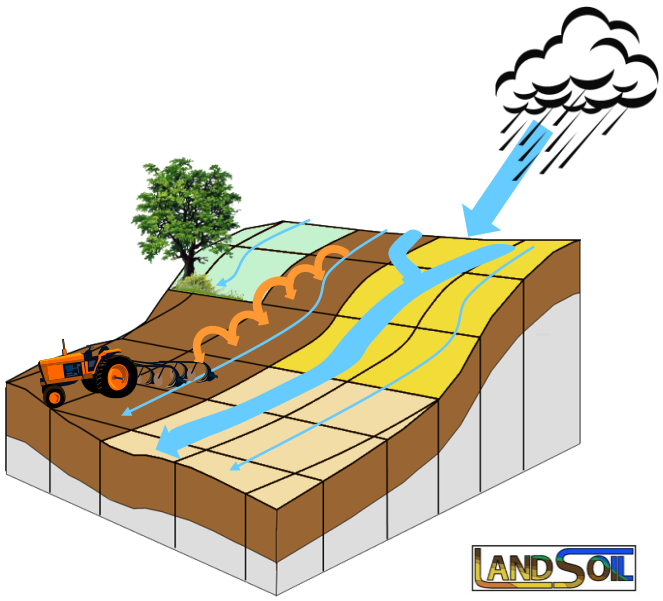

Runoff and water erosion

Tillage erosion

SOC dynamics model

RothC *(Coleman and Jenkinson, 1996),* **fully-distributed in space** *(Viaud et al., 2011)*

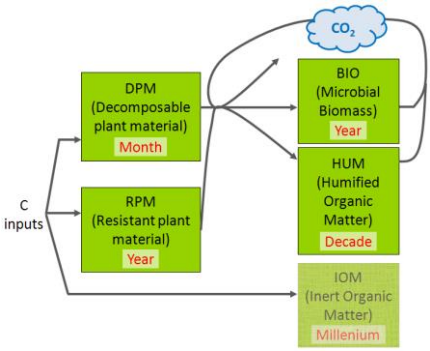

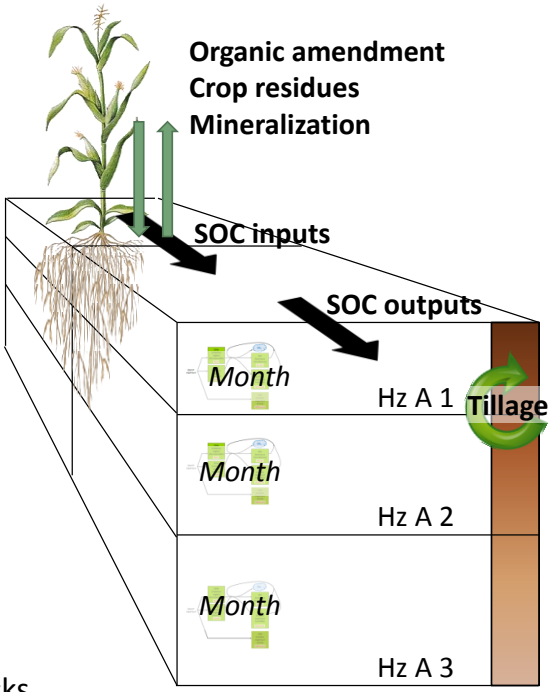

Processes modelled :

- SOC dynamics per soil horizon
- Soil lateral transfer by erosion
- Soil vertical transfer by tillage

Time step: month

Outputs: 3D maps of SOC contents and stocks

Soil evolution model: LandSoil and SOC models coupling

Landscape design:

- Square grid (2 m)
- Vertical discretization (0-105 cm)

Input data

- Climate
- Crop rotations and management practices for the simulation period
- Soil data: distributed in space and exhaustive

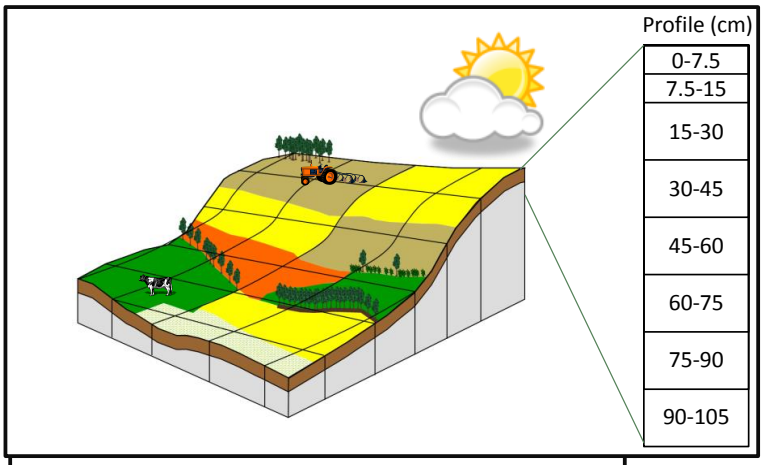

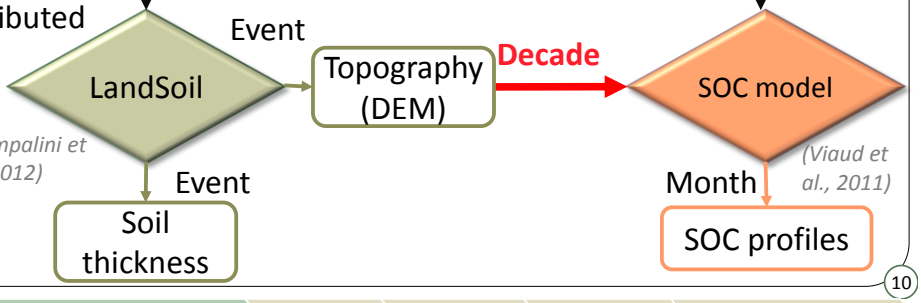

10

Study site: location

- "Zone Atelier" Armorique (LTER-Europe)
- Contrasting area with heterogeneities at short distances

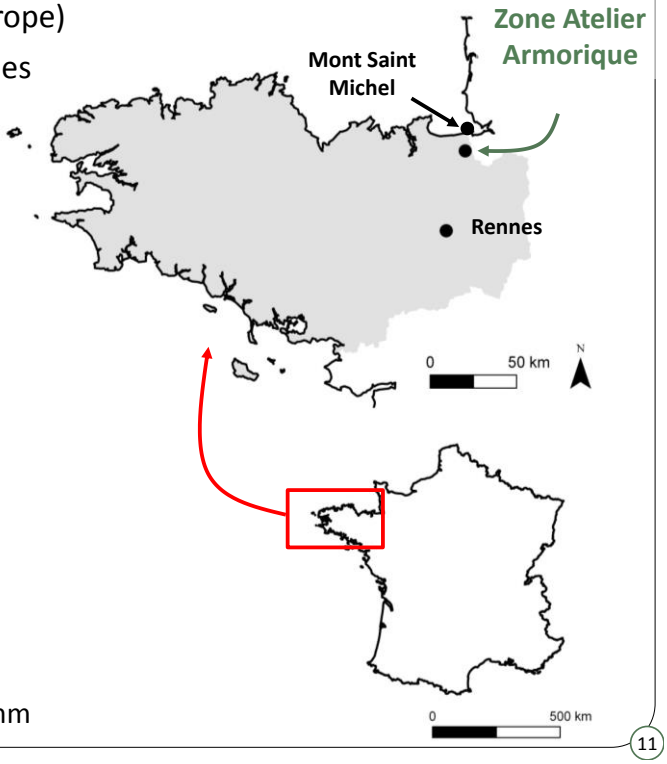

- 10 km²
- Oceanic climate
  - Mean annual temperature: 12°C
  - Mean annual precipitations: 782 mm

11

Study site: soil parent material and topography

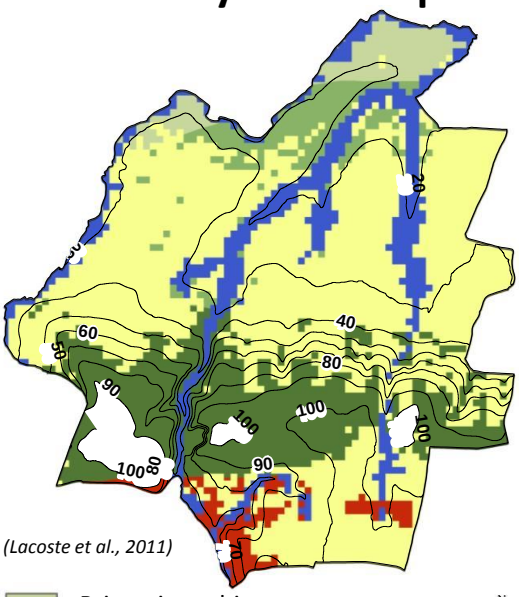

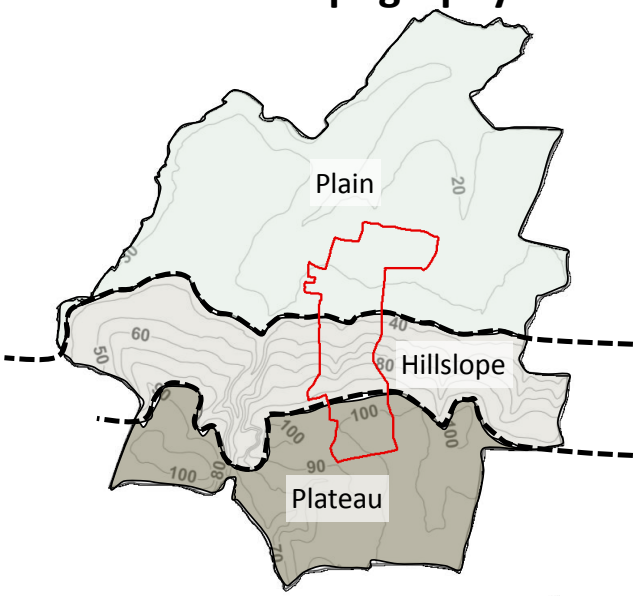

Brioverian schist
Hard schist
Hornfels
Granite
Alluvium
Quaternary Aeolian loam

0 250 500 m N

0 250 500 m N

Area for soil evolution modelling

Study site: soils spatial variability

Soil thickness: 17 to 550 cm
A-horizon thickness: 3 to 250 cm

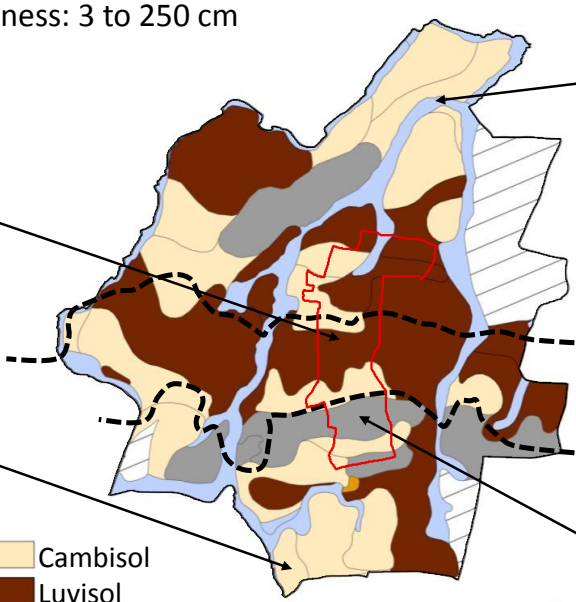

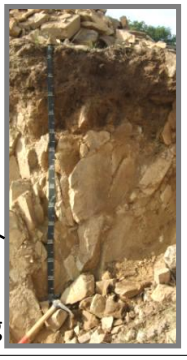

Cambisol
Luvisol
Leptosol
Colluvic cambisol
Fluviosol

0 250 500 m N

Missing data
Area for soil evolution modelling

Study site: land use and land management

- Farming systems : mixed farming (crops and dairy production)
- Land use:
  - permanent grasslands
  - crop rotations with maize, cereals and temporary grasslands
- Field size: 0.1 to 12 ha

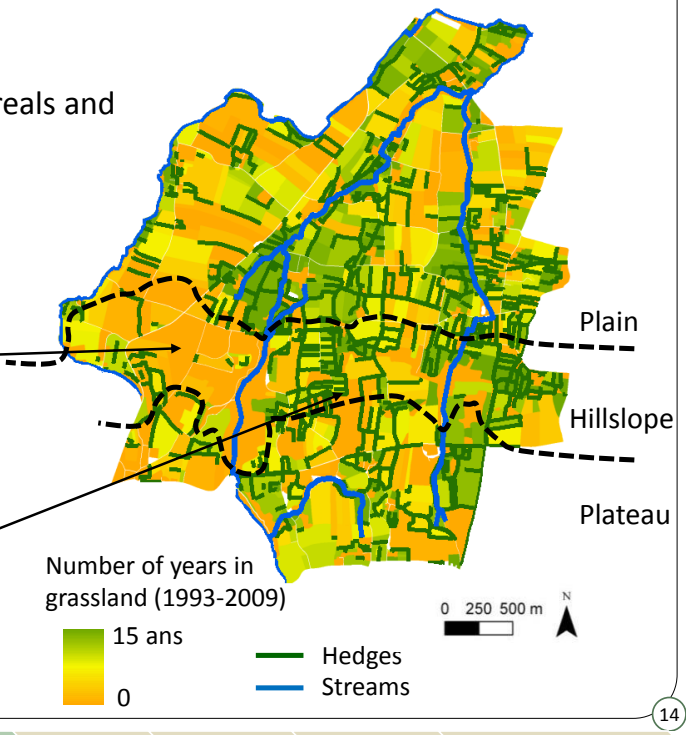

Study site: landscape structure and micro-topography

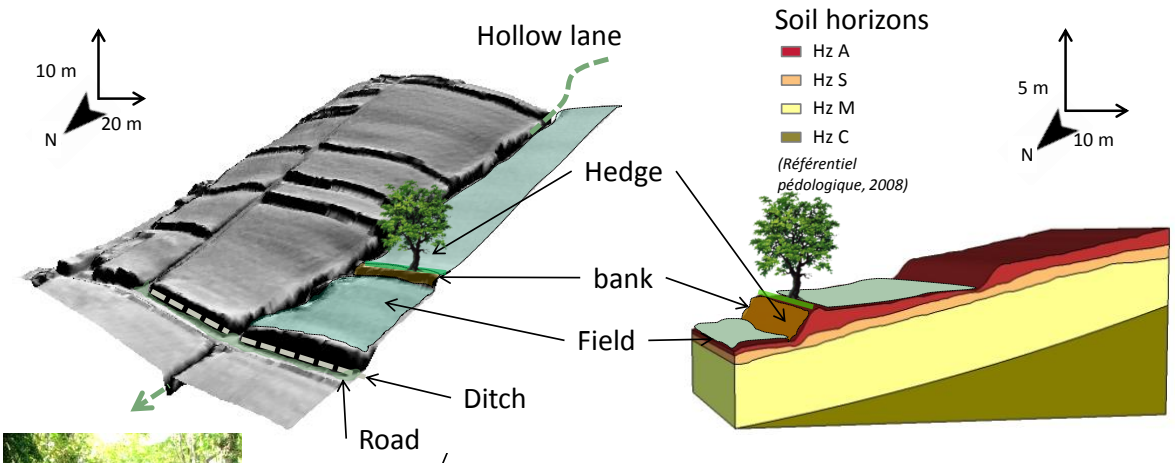

Study site: bocage evolution

- Since 1952: decrease in hedges density
- From the 1990ies: new hedges plantation

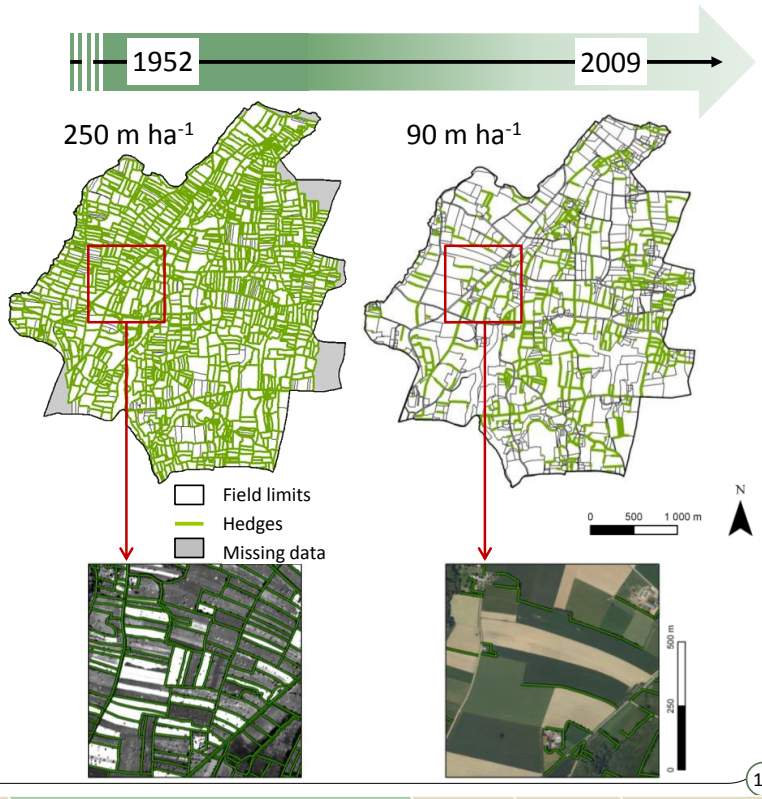

16

Step 1 : LandSoil model assessment at hedges vicinity

LandSoil model assessment at hedges vicinity (removed or still existing) :

- Comparison of soil redistribution rates (erosion and deposits) estimated by:
  - LandSoil
  - ^{137}Cs (soil redistribution indicator)
- Over the 1960-2009 period

17

Estimation of soil redistribution from ^{137}Cs

Measurements of ^{137}Cs inventories

- Sampling on 5 existing hedges: 2 profiles per hedge (5-m uphill and downhill from the hedge)
- 1 reference profile

Estimation of soil redistribution rates from ^{137}Cs inventories measurements

➢ Used of 4 ^{137}Cs models *(Walling et He, 2001)*

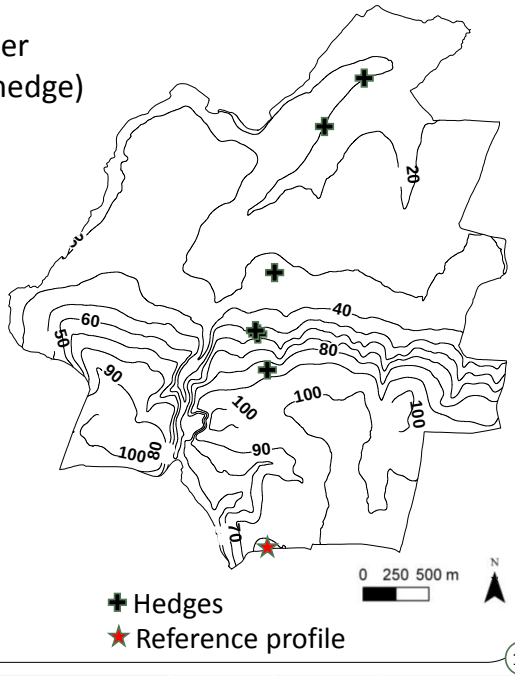

18

Comparison of soil redistribution rates estimated from LandSoil and ^{137}CS

- Point ^{137}Cs measurements
- LandSoil: simulation at field scale

➢ Results comparison in a 10 x 10-m window

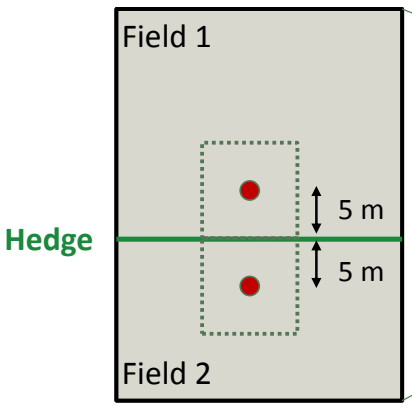

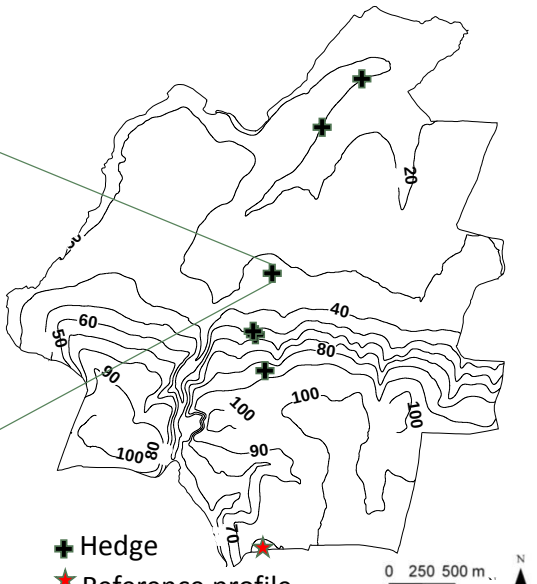

^{137}Cs profile

LandSoil modelling

Window for LandSoil and ^{137}Cs comparison

19

Soil redistribution over the 1960-2009 period, estimated from ^{137}Cs and LandSoil

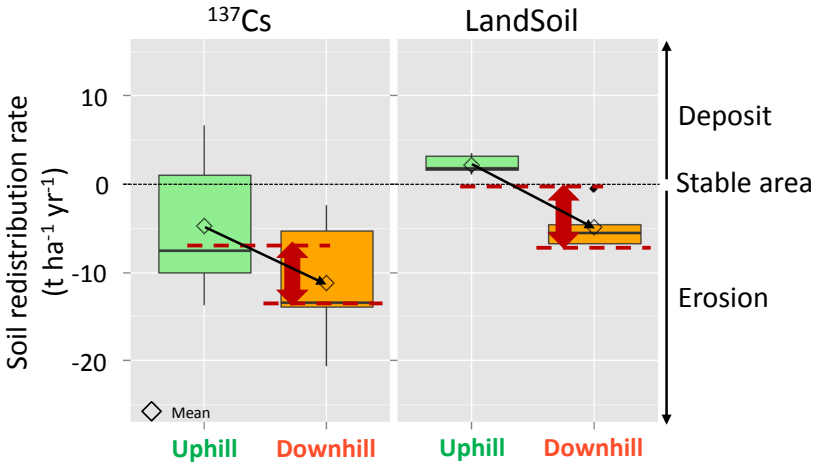

- Variations between positions uphill and downhill from the hedge: same range, same direction

Soil redistribution over the 1960-2009 period, estimated from ^{137}Cs and LandSoil

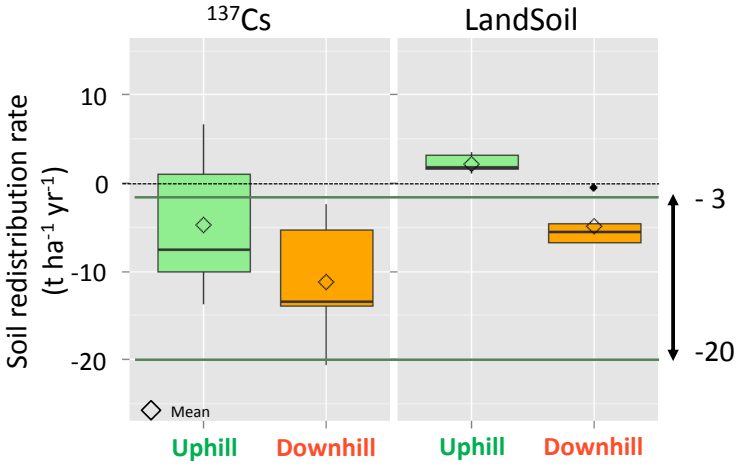

Soil erosion rate in Europe
Water and tillage erosion
(t ha^{-1} yr^{-1} ; *Verheijen et al., 2009)*

- LandSoil and ^{137}Cs estimates of soil erosion are in the range of soil erosion rates available in literature for Europe

- Soil redistribution patterns consistent
  - ➢ LandSoil can be used in hedgerow landscapes
- Coupling of soil redistribution processes: erosion (by water and tillage) and deposits
- Estimations of soil redistribution rates by LandSoil
  - On the whole: low in comparison to European estimations (mean : 1 mm for 10 years)
  - locally higher (uphill from hedges: +2 t ha^{-1} yr^{-1}, downhill: -5 t ha^{-1} an^{-1})
- The use of ^{137}Cs in hedgerow landscapes is limited (problem : homogeneity of initial ^{137}Cs fallout)

22

Step 2: description of soil initial state at landscape scale

Spatially distributed models
- ➢ High horizontal resolution (2 m)
- ➢ Vertical discretization (0-105 cm)

- 3D spatial modelling, based on purposive sampling
  - ➢ Soil and A-horizon thickness
  - ➢ SOC contents
  - ➢ Soil bulk density

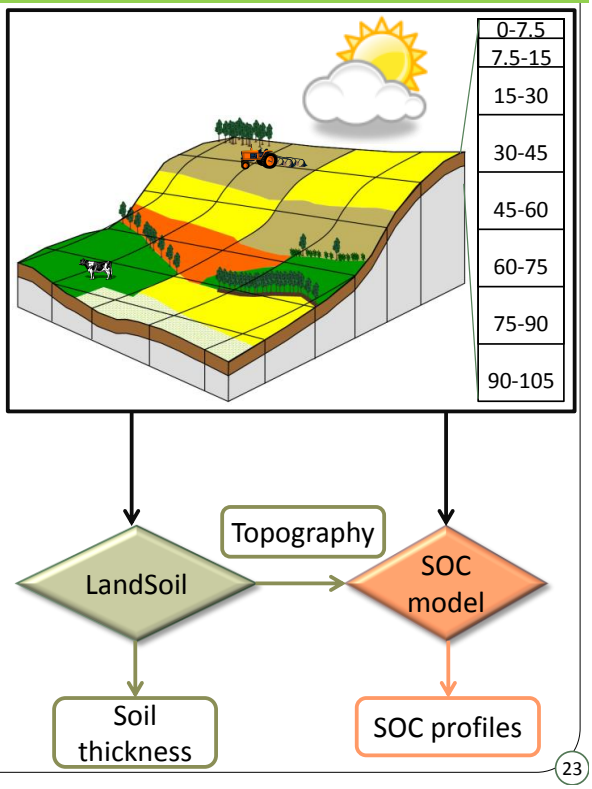

23

Soil data acquisition: sampling plan

Calibration dataset: 70 soil profiles

- Conditioned Latin Hypercube
  (*Minasny et McBratney, 2006*)
  - ➢ Good description of soil diversity at landscape scale

Validation dataset: 49 soil profiles

- Random stratified sampling (square grid, 300 m)

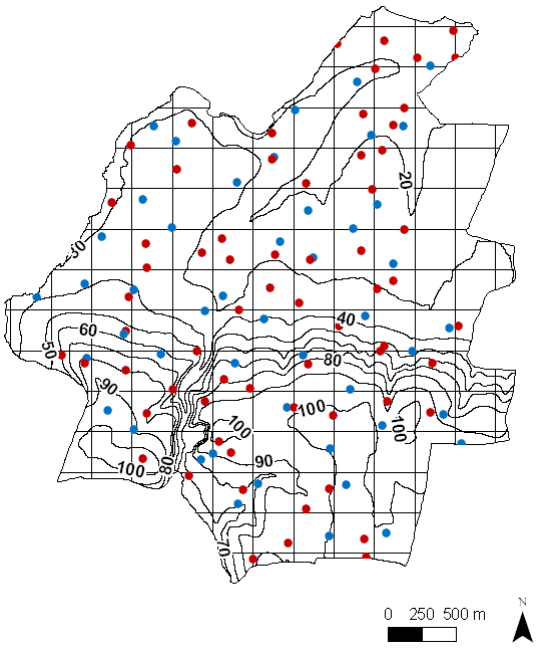

Description of soil profiles

- Soil and A-horizon thickness
- Vertical description of soil properties:
  - ➢ SOC contents, soil bulk density, soil gravel content
  - ➢ 8 soil layers down to 105 cm

24

Framework for 3D spatial prediction of soil properties

Point data to map (Calibration + validation datasets)

Exhaustive environmental predictors

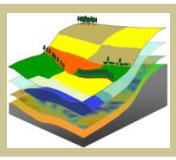

Land use
Hydrology
Soil parent material
Topography (2-m LiDAR DEM)

- **Inference model per soil layer**
  - ➢ regression and classification trees created by learning methods (Cubist ; *Quinlan, 1992*)
- **Reconstruction of continuous soil profiles with depth functions** (splines, *Bishop et al. , 1999*)
- **Uncertainties estimations** (fuzzy clustering ; *Malone et al.*, 2011)

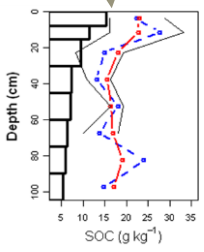

Predictive maps

Uncertainties interval maps

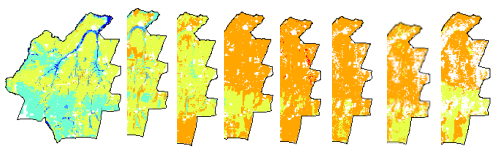

0-7.5 cm → 90- 105 cm

25

SOC stocks maps

Topsoil SOC stocks (0-30 cm) :

- on average: 58 tC ha^{-1}
- 67 % on average of total SOC stocks (0-105 cm)

0-30 cm

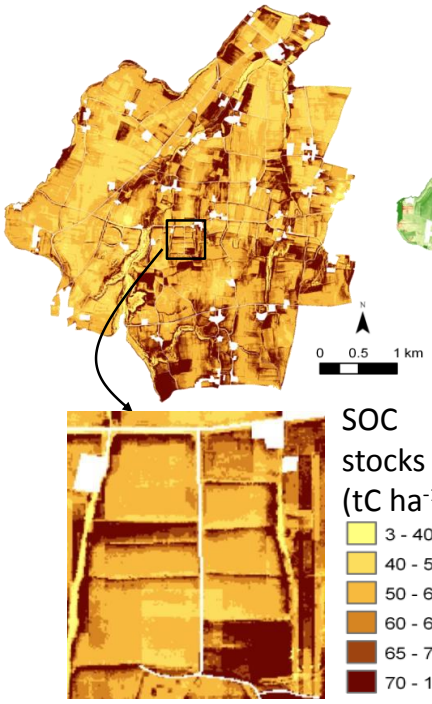

Uncertainties map

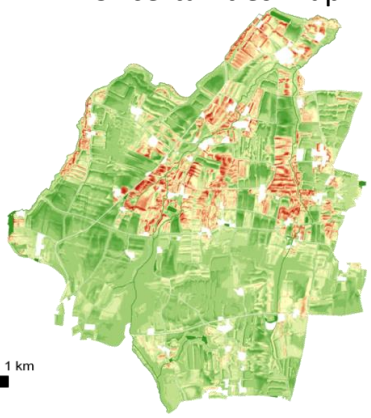

SOC stocks maps

Topsoil SOC stocks (0-30 cm) :

- on average: 58 tC ha^{-1}
- 67 % on average of total SOC stocks (0-105 cm)

- Variability of SOC stocks
  - Landscape scale: influence of land use
  - Field scale: influence of hedgerow structures and topography

0-30 cm

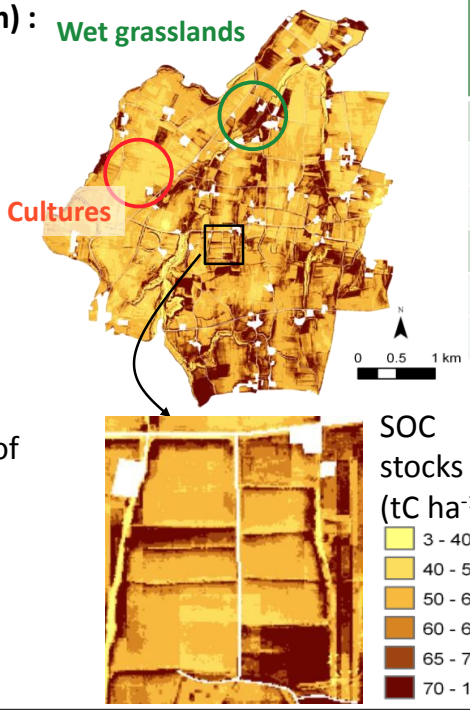

Parameters	Mean SOC stocks (tC ha^{-1})	
Years in grasslands		
< 5 years	81	−
>10 years	90	+
Distance from the hedge		
< 2 m	91	+
> 10 m	84	−

Prediction accuracy: example of SOC contents

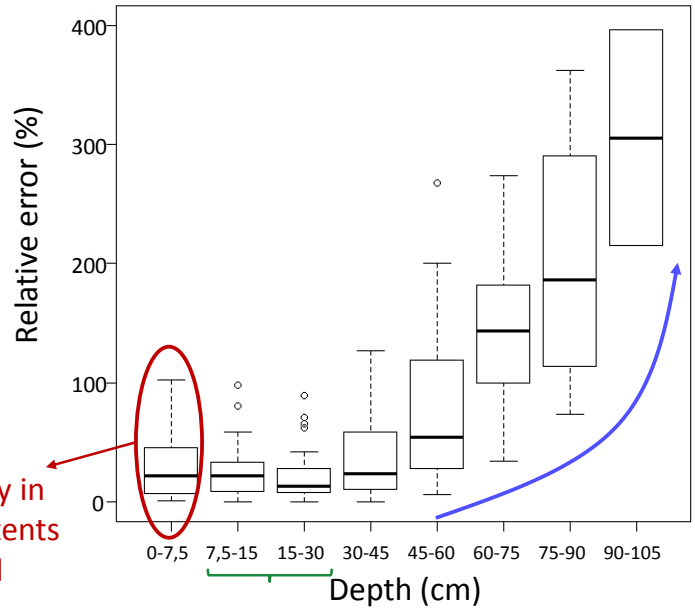

Median : 27 %

- Decrease of data (calibration and validation datasets)
- High variability in SOC contents in deep layers

High variability in SOC contents in topsoil layers

Homogenisation by soil tillage

28

- Exhaustive 3D soil mapping, at high resolution (2 m)
  - ➢ SOC contents and stocks, soil bulk density, soil gravel contents, soil and A-horizon thickness: distributions observed in landscape well modelled
  - ➢ Quantification and spatial location of uncertainties

→ Input data for soil evolution models

29

Etape 3 : Simulation of soil evolution (2010-2100)

Simulation of soil redistribution and SOC dynamic over the 2010-2100 period

- Landscape and climate change impact on soils
- Definition of the range and the rank of soil evolution factors impact

Approach: comparison of extreme scenarios to define the limits of evolution of the simulated system

30

Simulation design

- Soil modelling on a 1 km² site
- Spatial resolution: 2m
- Simulation period: 2010 – 2100

- Simulation scenarios: 2 factors
  - Climate
  - Landscape

  - Crop management practices stay unchanged

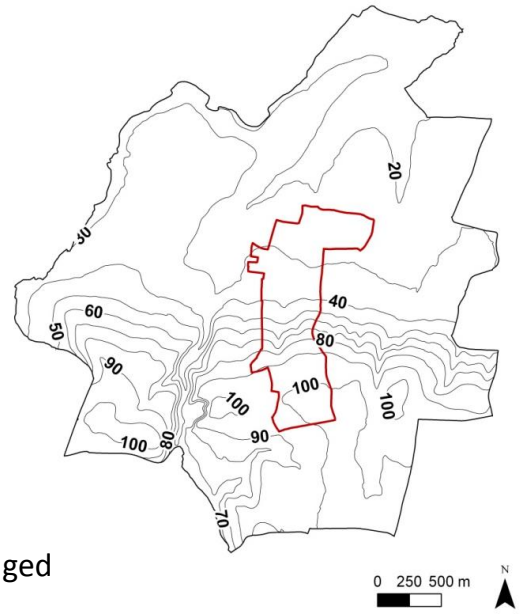

31

Description of the climate scenarios

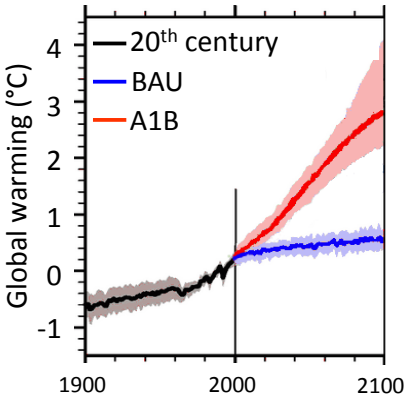

(IPCC, 2000)

Climate parameters (mean values)	Climat	
	BAU	A1B
Annual temperature (°C)	11 ↗	14
Annual precipitations (mm)	707 ↘	603
Rainfall events (defined for LandSoil)		
Number of events per year	7 ↗	13
Intensity (mm h^{-1})	15 ↗	25
Duration (h)	3 ↘	2

(source: US INRA Agroclim, Rennes station)

- A1B climate : predicted by Arpege model (Météo-France), regionalisation by the quantile-quantile method *(Deque, 2007)*
- Mean annual temperature increases
- Mean annual precipitations decrease but rainfall events are more intense

32

Description of landscape scenarios

➢ 3 levels of land use

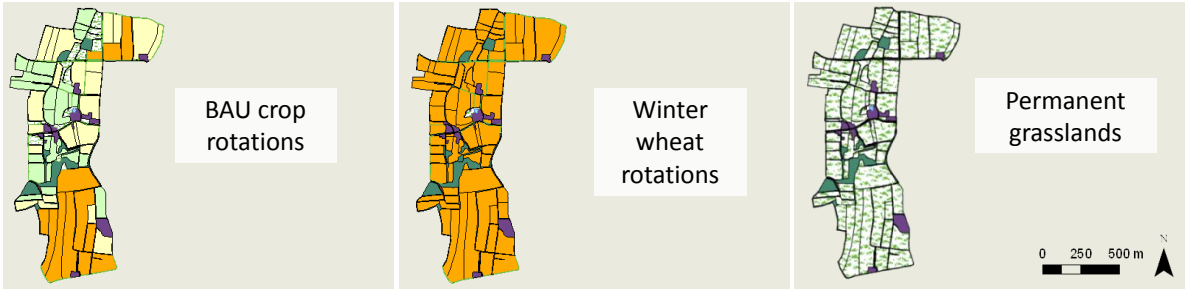

➢ 3 levels of land management: hedges

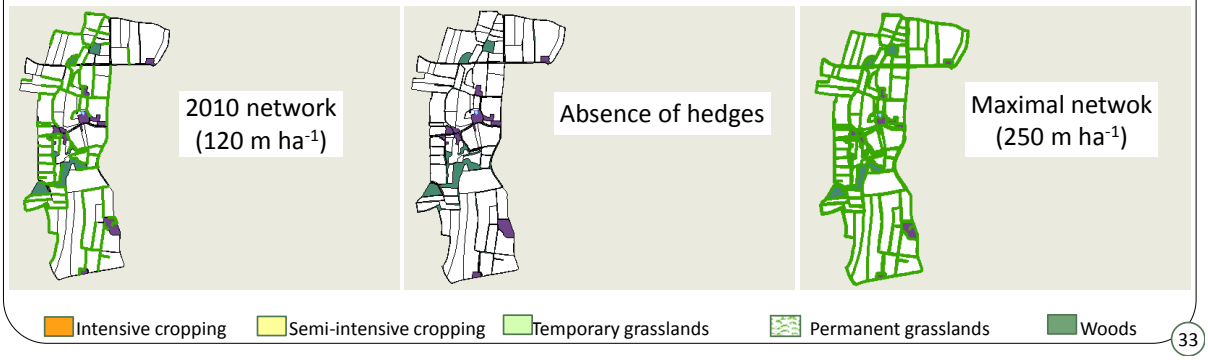

33

Selected landscape scenarios

BAU scenario
BAU land use
2010 hedges network

"Wheat without hedges" scenario
Winter wheat rotations
Absence of hedges

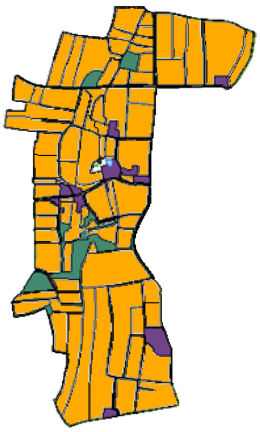

"Grasslands with hedges" scenario
Permanent grassland
Maximal hedges network

Comparison of scenarios:
Evolution scenario – BAU scenario

34

BAU scenario: soil redistribution

Soil redistribution, cumulated over the 2010-2100 period

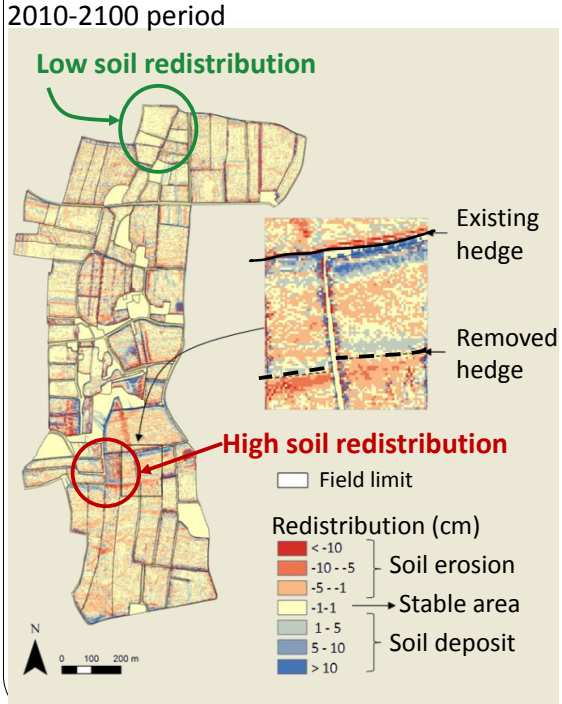

- Area of erosion: 22 %
- Area of deposit: 19 %

- Variability at landscape scale
  - ➢ High impact of land use: sink vs. sources of sediments

Land use	Soil redistribution rate (t ha^{-1} an^{-1})
Maize/wheat rotations	-0.3
Grasslands	0
Woodlands	1.1

Positive values: soil deposit
Negative values: soil erosion

35

BAU scenario: soil redistribution

Soil redistribution, cumulated over the 2010-2100 period

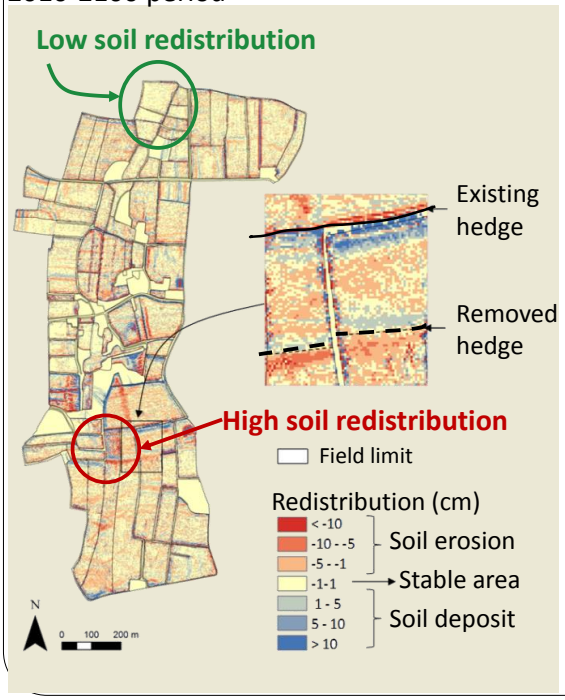

- Description of variability within fields
  - ➢ High contrasts close to hedges

10% of erosion areas > - 8 t ha^{-1} yr^{-1}

Mean : - 0,14 t ha^{-1} yr^{-1}

10% of deposit areas < +10 t ha^{-1} yr^{-1}

Positive values: soil deposit
Negative values: soil erosion

36

BAU scenario: SOC stocks evolution

SOC stocks evolution cumulated over the 2010-2100 period

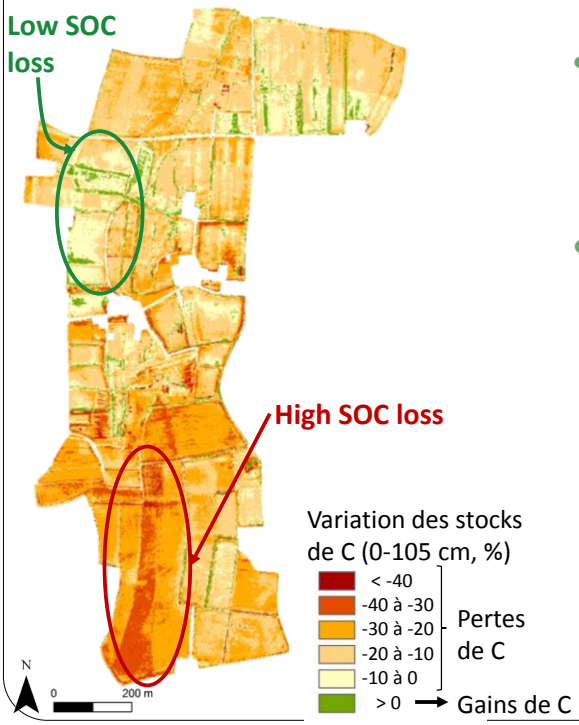

- Prediction of SOC loss: 25% of the initial SOC stocks (0-105 cm)
  - ➢ Variability at landscape scale
- SOC loss:
  - Related to land use
  - Artefact : possible discrepancy between initialization of SOC stocks and the spatial distribution of the modelled organic inputs?

37

BAU scenario: relation between soil redistribution and SOC stocks evolution

Mean SOC stocks in 2100 (0-105, tC ha^{-1})

	Min	Mean	Max
Whole modelling area	30	70	100
Erosion areas	56	67	80
Deposit areas	61	72	86

- SOC stocks in erosion areas significantly different from SOC stocks in deposit areas
- Assessment at landscape scale: 1 % of total SOC loss due to soil redistribution processes

BAU scenario: soil thickness

Variation of soil thickness in 2100 (cm)

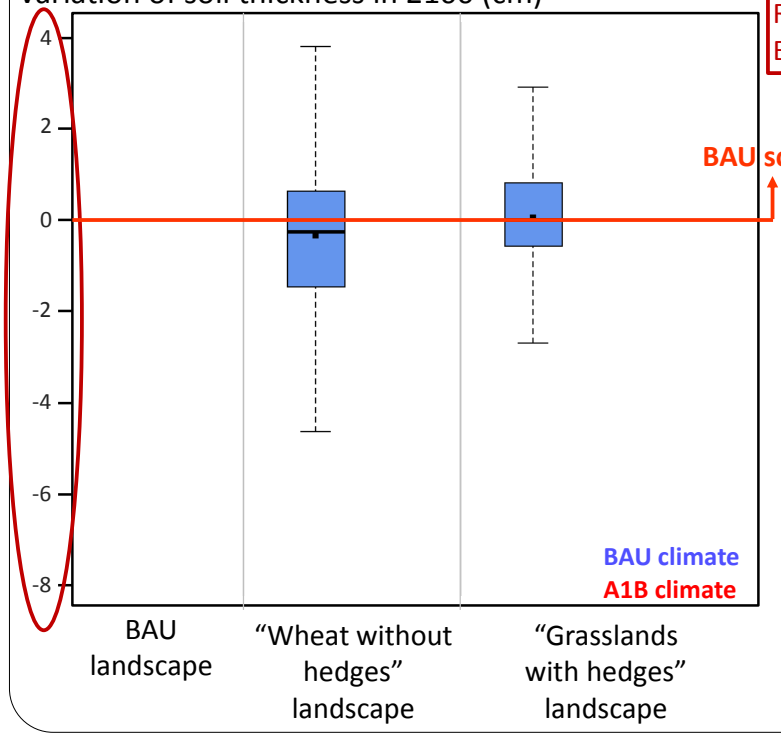

Results :
Evolution scenario – BAU scenario

- Main impact on soil redistribution: land use change
- Interactions between climate and landscape factors

BAU scenario: soil exportations

Soil exportation out of the study areas (t)

Scenario	Climate	
	BAU	A1B
BAU	-	+ 769
"Wheat without hedges"	+3 899	+11 566
"Grasslands with hedges"	-372	-372

High soil exportations

Evolution scenario: SOC stocks evolution

Variation of SOC stocks in 2100 (0-105 cm, tC ha^{-1})

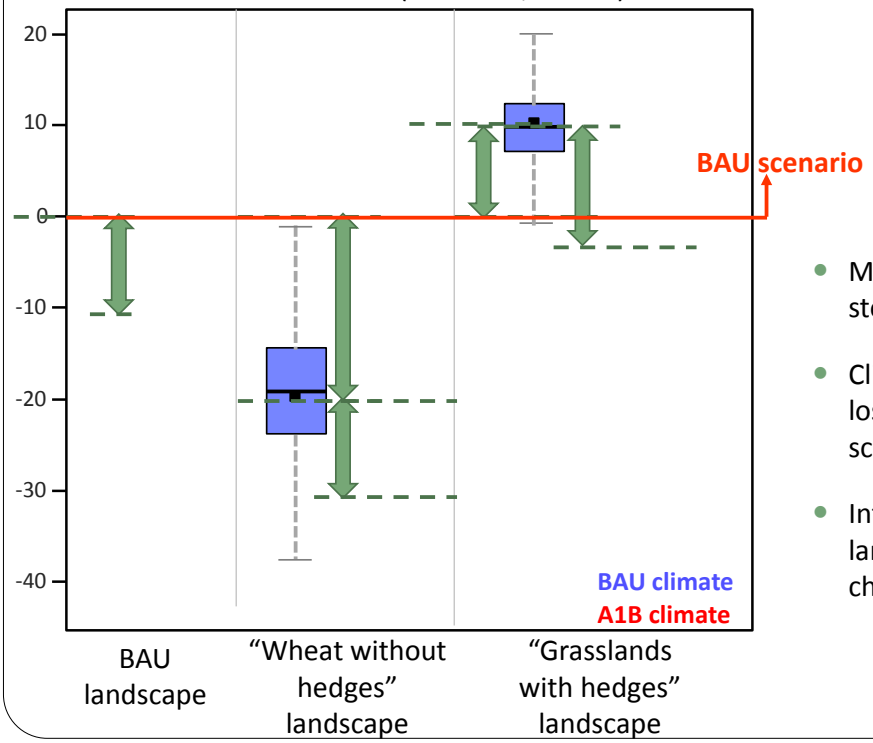

- Main impact on SOC storage: land use
- Climate change: induce loss of C for all the scenarios
- Interactions between land use and climate change was modelled

- Importance of soil evolution factors

Land use

Climate change

Land management (hedges)

- Interaction and combined effects of landscape and climate on soil evolution

42

General conclusion

Landscape sensitivity to climate change

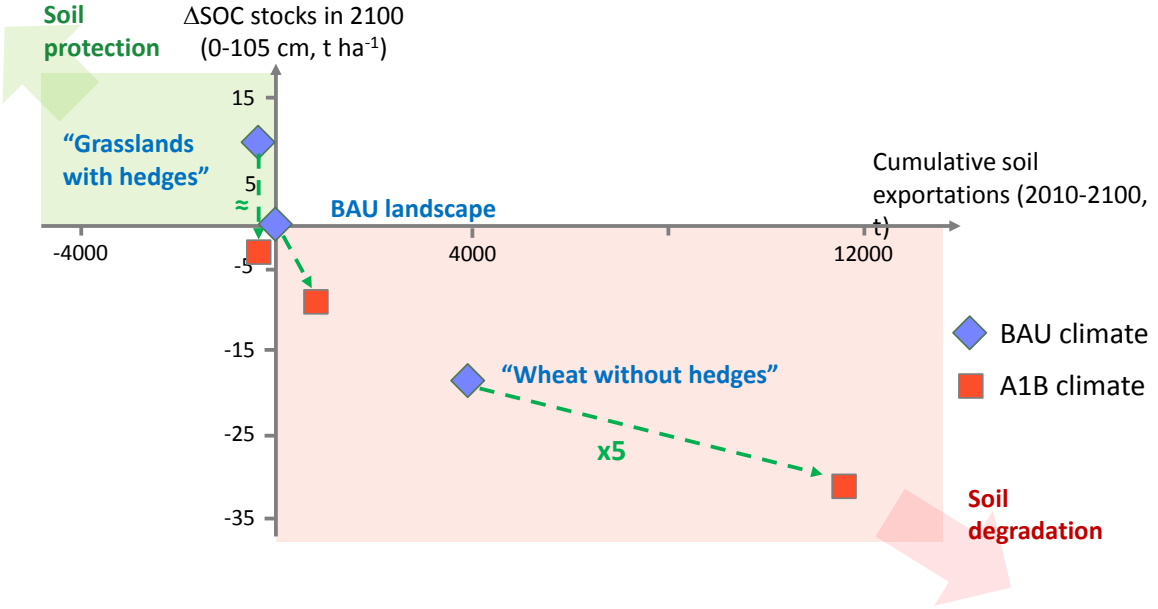

➢ Impact of climate change depend on landscape complexity

Simulation of soil evolution in heterogeneous landscape

- Interaction between climate and soil evolution
  - ➢ Importance of climate consideration
- Spatial differentiation: areas less or more sensitive to evolution
  - ➢ Importance of landscape scale simulation
- 2 soil processes modelled (SOC dynamics and soil redistributions): different response to climate and landscape change
  - ➢ Importance of coupling soil evolution processes

Approach of soil evolution simulation

LandSoil evaluation: ability to model soil redistribution close to hedges

- Comparison to ^{137}Cs
- Comparison of LandSoil results to observations
- Validity of LandSoil in hedgerow landscapes
- Limits of ^{137}Cs use in hedgerow landscape

Description of soil initial state at landscape scale: 3D mapping

- High 3D resolution
- Distribution in landscape well modelled
- Sensibility to environmental predictors
- Important factors not considered (e.g. tillage)

Simulation of soil redistribution

- Modelling method allowed taking into account:
  - Wide temporal and spatial scale (landscape, century)
  - Fine spatial and temporal resolution (2m, event / month)
  - Coupling of SOC dynamics and soil redistribution
- Simple coupling: feedback from SOC to soil redistribution not considered
- Heavy approach (time consuming)

45

Perspectives

Soil evolution modelling

- **Improve of the modelling process**
  - Feedback from SOC to soil sensitivity to erosion
  - Dynamic evolution of other soil properties (soil surface parameters, texture)
  - Scenarios construction:
    - More complex scenarios (collaboration with economist, agronomist, sociologist, actors on the ground)
    - Consideration of spatial organisation in landscape
- **Knowledge improvement**
  - C dynamics in eroded soil particles and deep soil horizons

Modelling method

- Uncertainties propagation during the modelling process
- Elaboration of models evaluation processes (long term observation network)

46

Perspectives

Use of spatially distributed models

- Participation in decision making processes: definition of strategies for soil management taking into account
  - agricultural practices
  - crop rotations
  - Spatial distribution of land use and land management elements in landscapes

47

Tank you for your attention

Thanks to the UMR SAS members and more particularly to Gilles Dutin and the field workers